# Investigations into novel antagonists of the CXCR4 chemokine receptor to prevent the migration of cancerous cells

**Isabel Hamshaw**

A thesis presented for the degree of Doctor of Philosophy
at the University of East Anglia, Norwich, UK

**January 2020**

# Abstract

Chemokines are signalling molecules that enable cell migration. The chemokine CXCL12 and its receptor CXCR4 have major roles in neutrophil homeostasis. However, CXCR4 is overexpressed on cancer cells, leading to aberrant downstream signalling. This study identifies the importance of two downstream proteins, PKC and PKD, in CXCL12-stimulated PC3 prostate cancer migration. Additionally, novel CXCR4 antagonists for *in situ* click chemistry were developed and 3D printed materials for migration assays were designed. Finally, cellular expression of ACKR3, which also binds CXCL12, and its role in migration was investigated.

Experiments used MCF-7 breast cancer cells, PC3 cells, Jurkat leukemic T-lymphocytes and THP-1 AML cells which naturally express CXCR4 and ACKR3 and SKMEL28 melanoma cells which naturally express CXCR4. PKC/PKD inhibitors, CXCR4 antagonists and CXCR4/ACKR3 antibodies were used in migration assays and calcium release assays to measure cellular responses. Immunofluorescence, flow cytometry and copper-catalysed alkyne-azide cycloaddition (CuAAC) determined CXCR4 expression and/or internalisation. Actin expression was analysed after incubation with PKC/PKD inhibitors or CXCR4 antagonists.

PKC/PKD inhibition prevented CXCL12-stimulated cell migration. The novel CXCR4 antagonists AZ6-2, IS4 and IS7 are more potent than AMD3100. IS4 is more stable than AZ6-2 and can be used in CuAAC. IS7 fluorescently labels CXCR4. ACKR3 has no effect upon cellular migration using chemotaxis assays. ACKR3 has faster turnover rates in PC3 and THP-1 cells than MCF-7 and Jurkat cells. ACKR3 internalisation in MCF-7 and Jurkat cells occurs via caveolin-dependant endocytosis. In the presence of CXCL12, ACKR3 internalisation occurs via clathrin/caveolin independent endocytosis in Jurkat cells. 3D printing can be used to print stoppers for the ORIS™ Cell Migration assay.

CXCL12-stimulated migration can be modulated by PKC/PKD inhibitors and CXCR4 antagonists. IS4/IS7 are potential future therapeutics or laboratory tools. ACKR3 turnover and internalisation vary in different cell types. 3D printing could be a useful for the development of migration assays.

# Abbreviations

| | |
|---|---|
| 7TM | 7 transmembrane α-helical domain |
| 7TMRs | 7 transmembrane receptors |
| ACKR3 | Atypical chemokine receptor 3 |
| AcOH | Acetic acid |
| ADP | Adenosine diphosphate |
| ALL | Acute lymphoblastic leukaemia |
| AML | Acute myelogenous leukaemia |
| ANOVA | Analysis of variance |
| aPKCs | Atypical PKCs |
| ASK | Apoptosis signalling kinase |
| ATCC | American type culture collection |
| ATP | Adenosine triphosphate |
| BAD | CL2 associated agonist of cell death |
| BAM22 | Bovine adrenal medulla 22 |
| BJ | Binder Jetting |
| BODIPY | Borondipyrromethene |
| BSA | Bovine serum albumin |
| BSO | Buthionine sulfoximine |
| $Ca^{2+}$ | Calcium ions |
| CAD | Computer aided design |
| CAM | Computer aider manufacture |
| CAT | Collective to amoeboid transition |
| CCL | C-C motif chemokine receptor ligand |
| CCR | C-C motif chemokine receptor |
| CDE | Clathrin-dependent endocytosis |
| $CHCl_3$ | Chloroform |
| CLL | Chronic lymphocytic leukaemia |
| CO2 | Carbon dioxide |
| cPKC | Classical PKCs |
| CPN | Carboxypeptidase-N |
| Crk | Proto-oncogene c-Crk |
| CT | Computed tomography |
| CTCF | Corrected total cell fluorescence |

| | |
|---|---|
| Cu | Copper |
| CuAAC | Copper-catalysed alkyne-azide cycloaddition |
| $CuSO_4$ | Copper sulfate |
| CXCL | C-X-C motif chemokine receptor ligand |
| CXCR | C-X-C motif chemokine receptor |
| DAG | Diacylglycerol |
| DAPI | 4′,6-diamidino-2-phenylindole |
| DCM | Dichloromethane |
| DDP4 | serine protease dipeptidyl peptidases IV |
| DIPEA | *N*,*N*-diisopropylethylamine |
| DLP | Digital Light Processing |
| DMEM | Dulbecco's modified Eagle's medium |
| DMF | *N*,*N*-dimethylformamide |
| DMSO | Dimethyl sulfoxide |
| DPX | Distyrene, plasticizer, xylene |
| EBM | Electron Beam Melting |
| ECL | Extracellular loop |
| EDT | Ethanedithiol |
| EDTA | Ethylenediaminetetraacetic acid |
| EGF | Epidermal growth factor |
| EGFR | Epidermal growth factor receptor |
| EMT | epithelial-to-mesenchymal transition |
| ER | Endoplasmic reticulum |
| ERK | Extracellular signal-regulated kinase |
| $Et_2O$ | Diethyl ether |
| EtOH | Ethanol |
| FA | Focal adhesion |
| FACS | Fluorescence-activated cell sorting |
| FAK | Focal adhesion kinase |
| FBS | Foetal bovine serum |
| FDA | Food and drug administration |
| FDM | Fused deposition method |
| Gα | G-Protein α subunit |
| GAGs | Glycosaminoglycans |

| | |
|---|---|
| GAP | guanosine triphosphatase-activating proteins |
| Gβγ | G-Protein βγ subunit |
| G-CSF | Granulocyte colony-stimulating factor |
| GDP | Guanosine diphosphate |
| GEF | Guanine nucleotide exchange factor |
| GMP | Good manufacturing practice |
| GPCR | G-Protein coupled receptor |
| GPI | Glycosysylphosphatidylinositol |
| GRK | G-protein couple receptor kinase |
| GSH | reduced glutathione |
| GSSG | Oxidized glutathione/ glutathione disulfide |
| GTP | Guanosine triphosphate |
| HDAC1 | Histone Deacetylase 1 |
| HBTU | *O*-benzotriazole-*N*,*N*,*N*′,*N*′-tetramethyl-uroniumhexafluorophosphate |
| HIF-1 | Hypoxia-Inducible Factor-1 |
| HIV | Human immunodeficiency virus |
| HPLC | High performance liquid chromatography |
| HRE | HIF-Response Element |
| IC50 | Concentration at which 50% inhibition occurs |
| ICL | Intracellular loop |
| IGF-1 | Insulin-like grown factor 1 |
| IGFR-1 | Insulin-like growth factor receptor 1 |
| IP3 | Inositol triphosphate |
| IL | Interleukin |
| JAK | Janus kinase |
| KCl | Potassium chloride |
| $K_d$ | Dissociation equilibrium constant |
| LOM | Laminated object manufacturing |
| mAb | Monoclonal antibody |
| MALDI-TOF | Matrix-assisted laser desorption/ionization-time of flight |
| MAT | Mesenchymal to amoeboid transition |

| | |
|---|---|
| MAPK | Mitogen activated protein kinase |
| MCD | Methyl-β-cyclodextrine |
| MeOH | Methanol |
| MET | Mesenchymal-to-epithelial transition |
| $MgCl_2$ | Magnesium chloride |
| MIF | Macrophage migratory inhibitory factor |
| MJ | Material jetting |
| MLC | Myosin light chain |
| MLCK | MLC kinase |
| MM | Multiple myeloma |
| MMP | Matrix metalloproteinases |
| MTS | 3-(4, 5-dimethylthiazol-2-yl)-5-(3-carboxymethoxyphenyl)-2-(4-sulfophenyl)-2H-tetrazolium |
| MSC | Mesenchymal stem cells |
| NaCl | Sodium chloride |
| NADH | Nicotinamide adenine dinucleotide |
| NADPH | Nicotinamide adenine dinucleotide phosphate |
| NEM | *N*-ethylmaleimide |
| NFκB | Nuclear factor kappa-light-chain-enhancer of activated B cells |
| NHL | Non-Hodgkin's lymphoma |
| NMP | N-Methyl-2-pyrrolidone |
| NMR | Nuclear magnetic resonance |
| nPKCs | Novel PKCs |
| N.s | Not significant |
| p38 | p38 mitogen activated protein kinase |
| PAD | Peptidylarginine deiminase |
| PBGF | Pre-B cell growth factor |
| PBS | Phosphate buffered saline |
| PDBu | Phorbol dibutyrate |
| PET | Positron emission tomography |
| PGA | Poly-glycolic acid |
| PH | Pleckstrin homology |

| | |
|---|---|
| PI | Phosphoinositide |
| PI3K | Phosphoinositide 3-kinase |
| PIP | Piperidine |
| PIP2 | Phosphatidylinositol 4,5-biphosphate |
| PKC | Protein kinase C |
| PKD | Protein kinase D |
| PLA | poly-lactic acid |
| PLC | Phospholipase C |
| PMA | Phorbol 12-myristate 13-acetate |
| Rac | Ras-related C3 botulinum toxin substrate |
| Ras | Rat sarcoma GTPase |
| RGS | Regulators of G-protein signalling |
| Rho | Ras homology GTPase |
| RhoG | Ras homolog gene family, member G |
| ROCK | Rho-associated serine/threonine kinase |
| ROS | Reactive oxygen species |
| RP-HPLC-ESI | Reversed-phase - high-performance liquid chromatography - electrospray ionization |
| RPMI | Roswell Park memorial institute medium |
| RTKs | Receptor tyrosine kinases |
| SCID | Severe combined immunodeficiency |
| SDF-1 | Stromal cell-derived factor 1 |
| SEM | Standard error of the mean |
| SH | Thiol |
| SHE | Safety, Health, Environment |
| SLA | Stereolithography |
| SLM | Selective laser melting |
| SLS | Selective laser sintering |
| SPR | Surface plasmon resonance |
| SS | disulphide |
| STAT | Signal transducer and activator of transcription |
| TEM | Trans-endothelial migration |
| TFA | Trifluoroacetic acid |
| TFF2 | Secreted trefoil factor family 2 |

| | |
|---|---|
| TGFα | Transforming growth factor α |
| TIPS | Triisopropylsilane |
| TME | Tumour microenvironment |
| TNFα | Tumour necrosis factor alpha |
| UV | Ultra violet |
| VEGF | Vascular endothelial growth factor |
| vHL | von Hippel-Lindau |
| WASP | Wiskott–Aldrich syndrome protein |
| WAVE | WASP-family verprolin-homologous protein |
| WBC | White blood cell |
| WM | Waldenström macroglobulinemia |

# Contents

# List of Tables

# List of Figures

**CHAPTER 4**

**CHAPTER 5**

**CHAPTER 6**

**CHAPTER 7**

# Publications

HAMSHAW, I., AJDARIRAD, M. & MUELLER, A. 2019. The role of PKC and PKD in CXCL12 directed prostate cancer migration. *Biochemical and biophysical research communications,* 519**,** 86-92.

(In preparation) HAMSHAW I., COMINETTI M. M. D., SEARCEY M. & MUELLER A. Identification of a Novel CXCR4 Antagonist Suitable for *in situ* Click Chemistry.

# Acknowledgments

Firstly, I would like to thank my Ph.D. supervisor Dr Anja Mueller for her continuous support, knowledge and guidance during my research. Additionally, I would also like to thank my secondary supervisor Dr Anastasia Sobolewski for her support and knowledge.

I would like to thank those I collaborated with: Professor Mark Searcey, Dr Marco M. D. Cominetti, Dr Derek Warren and Dr James M. Courtney for their knowledge, support, skills and technical assistance. I would also like to thank other members of The University of East Anglia including, Professor Maria O'Connell, Dr Leanne Stokes and Dr Rosemary Norton for their knowledge, support and assistance.

I would also like to thank my CAP 1.11 colleagues who have helped and supported me through these years of research: Dr Hui Poh Goh, Dr Gerald R. Keil, Enana Al Assaf and Wing Y. Lai. Additionally, I would like to thank Dr Marco M. D. Cominetti, Dr Gerald R. Keil, Dr Hui Poh Goh, Dr Ryan Tinson, Dr Stefan Bidula and Dr James M. Courtney for all the time and effort they put into proof reading my thesis. I would also like to thank Morvarid Ajdarirad for her work during her ERASMUS research project which contributed to my recent publication.

Special thanks goes to Dr James M. Courtney for his continuous support over the years. I would also like to say a special thank you to all the friends I made at The University of East Anglia, my friends from The University of Hull and those who have stuck with me from Aylsham High School! Special thanks goes to my family who constantly told me how proud they are. Finally, I would especially like to thank my parents, not only for their financial support (!) but for their emotional support and believing in me over the years.

# Chapter 1: Introduction

## 1.1. Chemokines

Chemokines are small 8-14 kDa peptides that belong to a large multifunctional family of chemoattractant cytokines (Rossi and Zlotnik, 2000, Teicher and Fricker, 2010). Specifically, chemokines are signalling molecules that enable directional cell migration or chemotaxis of cells to sites of infection and injury or to secondary lymphoid organs for maturation (Laing and Secombes, 2004, Teicher and Fricker, 2010). Chemokines range from 70 to 100 amino acids in length and have 20-95% amino acid sequence identity that is rich in basic amino acids such as arginine (R), lysine (K) and histidine (H) (Christopherson and Hromas, 2001, Liu et al., 2011). Initially, chemokines are produced from a pro-peptide that is reduced to the active chemokine upon cell secretion (Davis et al., 2005).

There are four different subclasses of chemokine divided into the two major; CXCL (α chemokines) and CCL (β chemokines) and the two minor; CL and CX3CL groups. These subclasses are based upon the pattern of cysteine residues at the N-terminus of the chemokine ligand with X representing any amino acid (Figure 1.1) (Allen et al., 2007, Clore and Gronenborn, 1995, de Munnik et al., 2015, Zlotnik and Yoshie, 2000). Therefore, the CCL subclass have two cysteine residues adjacent to one another while the CXCL subclass has a single amino acid between the two initial cysteine amino acids. (Christopherson and Hromas, 2001). In mammals, 17 different CXCLs chemokines have been identified and are divided into two categories: the “ELR-positive” chemokines, with the specific amino acid motif (the ELR motif Glu-Leu-Arg), immediately before the first cysteine and the “ELR-negative” chemokines, which do not have this sequence (Strieter et al., 1995). CXCL chemokines with the ELR motif immediately prior to the CXCL motif are potent chemoattractants for neutrophils, whereas those without the ELR motif are generally for directing lymphocytes (Yoshida et al., 1998).

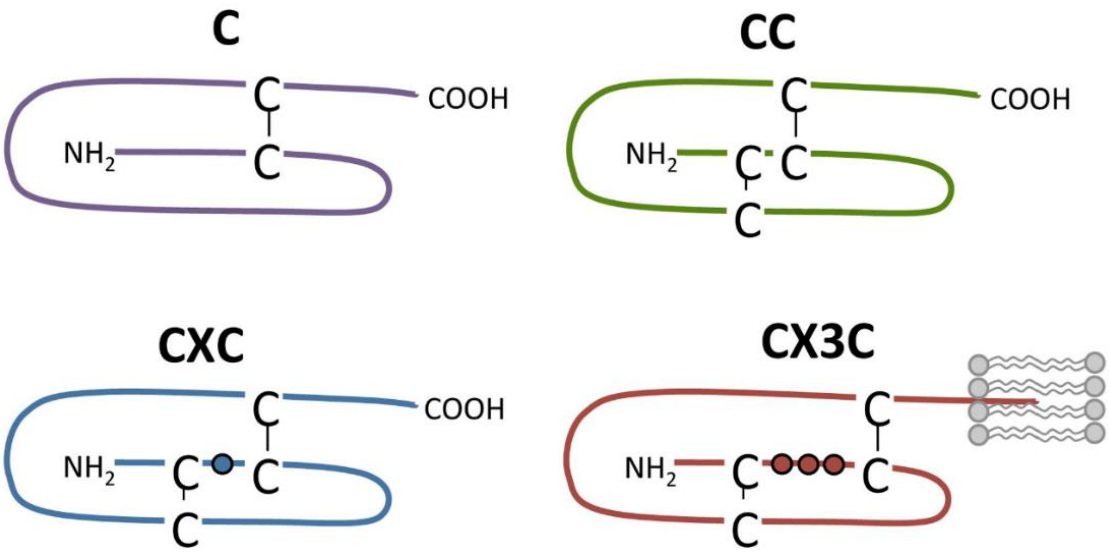


**Figure 1.1: The Different Subclasses of Chemokines (de Munnik et al., 2015).** Chemokines are divided into four different subclasses dependent upon the number and the spatial organization of cysteine residues at the N-terminus of the chemokine ligand with X representing any amino acid. CXCL and CCL belong to the major class of chemokines while C and CX3CL belong to the minor class of chemokines. Disulphide bridges are shown as black lines while the lipid transmembrane domain of CX3CL is depicted in grey.

Chemokines are also sub-grouped based upon their function as either homeostatic or inflammatory chemokines. These subgroups are dependent upon if the chemokine is stimulated by inflammation or are constitutively expressed due to homeostatic immune regulation (Oo and Adams, 2010, Zlotnik and Yoshie, 2000). Inflammatory chemokines, such as CXCL8, are secreted in high concentrations during inflammation, infection or due to tissue damage. Their secretion then enables the recruitment of immune cells such as: neutrophils, monocytes, natural killer (NK) cells and killer T cells all of which express the complimentary inflammatory chemokine receptors (Heydtmann and Adams, 2002, Peveri et al., 1988). The production of these inflammatory chemokines is stimulated by proinflammatory cytokines, for example interleukin-1. (Le et al., 2004).

In contrast, homeostatic chemokines, such as CXCL12, are constitutively produced mainly within lymphoid organs such as the bone marrow, thymus or secondary lymphoid organs. However, non-lymphoid organs, such as the skin or the mucosa, can also produce them (Oo and Adams, 2010, Zlotnik and Yoshie, 2000). Unlike the inflammatory chemokines, homeostatic chemokines do not

need to be stimulated by external stimuli (Rot and Von Andrian, 2004). These chemokines are involved in immune surveillance and leukocyte trafficking to secondary lymphoid organs for antigen presentation and maturation (Oo and Adams, 2010, Rot and Von Andrian, 2004, Zlotnik and Yoshie, 2000). However, the biological role of chemokines goes far beyond the trafficking of immune cells and are also involved in stem cell homing and proliferation, angiogenesis, neurogenesis, haematopoiesis and embryonic development (Broxmeyer et al., 1990, Mehrad et al., 2007, Raman et al., 2011, Sohni and Verfaillie, 2013).

While chemokines have roles in normal human physiology, they have also been implicated in myocardial infarction, arthritis, inflammatory diseases such as dermatitis and psoriasis, respiratory distress syndrome as well as in cancer metastasis (Baggiolini and Dahinden, 1994, Kasama et al., 1995, Kukielka et al., 1995, Nedoszytko et al., 2014, Puneet et al., 2005).

## 1.2. Chemokine Receptors

Chemokine receptors can be divided into two groups: G-protein-coupled receptors (GPCRs), which activate signalling via G proteins and atypical receptors, which activate signalling by binding to β-arrestin (Stone et al., 2017). GPCR are the largest and most diverse group of transmembrane receptors in humans. Due to the size of this family, human GPCRs are further subdivided using the GRAFS system based upon their phylogeny. These families include the Glutamate receptor family (formally class C), the Rhodopsin receptor family (formally class A), the Adhesion receptor family (formally part of class B), the Frizzled/Taste2 receptor family (formally part of class F) and the Secretin receptor family (formally part of class B). Previous classes including class D (fungal mating pheromone receptors) and class E (cyclic AMP receptors) which do not contain human receptors, thus have been removed from the GRAFS system (Schiöth and Fredriksson, 2005).

There are over 800 functional GPCRs in the human genome, 90% of which belong to the rhodopsin family (Fredriksson et al., 2003, Schiöth and Fredriksson, 2005, Wolf and Grünewald, 2015). Therefore, the rhodopsin receptor family can be further subdivided into classes α-δ (Schiöth and Fredriksson, 2005). Chemokine receptors belong to the γ rhodopsin subfamily however, they were previously subdivided into type A1 or A2 rhodopsin receptor family (Attwood and Findlay, 1994, Joost and Methner, 2002, Schiöth and Fredriksson, 2005).

Each chemokine receptor is typically 350 amino acids in length that form a seven transmembrane α-helical domain (7TM) which is connected by three intracellular loops (ICL) and three extracellular connecting loops (ECL) (Figure 1.2) (Kahler and Sticht, 2016, Steen et al., 2014). The N-terminal tail of the receptor is on the extracellular side whilst the C-terminal tail resides on the cytosolic side of the receptor (Murdoch and Finn, 2000, Palczewski et al., 2000). Within these TM domains, conserved cysteine residues exist which enables the formation of a disulphide bridge between loops (Fredriksson et al., 2003). These disulphide bridges are important for the structural integrity of the protein. The first disulphide bond occurs between the N-terminal domain and ECL3 and the second between ECL1 and ECL2 (Fredriksson et al., 2003, Kahler and Sticht, 2016).

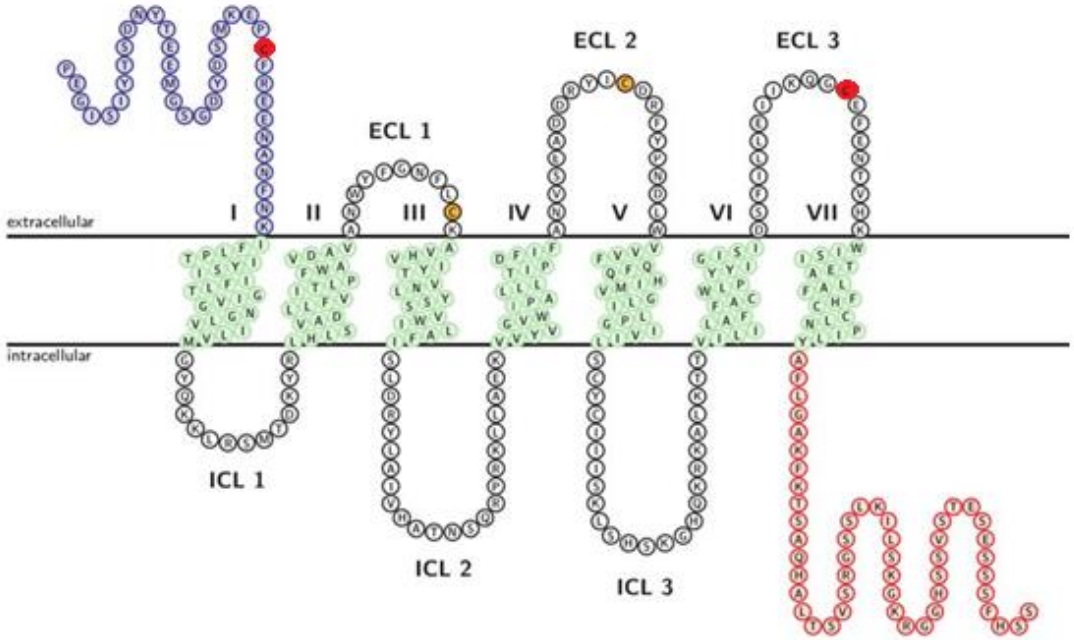


**Figure 1.2: Representation of the Chemokine Receptor CXCR4 (Kahler and Sticht, 2016).** Chemokine receptors are located in the cellular membrane. Generally, these receptors have an N-terminal domain (blue), seven transmembrane domains (green), three loops facing into the cell (ICL1-3), three loops facing out of the cell (ECL1-3) and an internal C-terminal domain (red). Specifically, CXCR4 has two disulphide bridges formed between two sets of cysteine (red and yellow) on the extracellular side of the receptor.

In humans, there are more than 50 types of chemokines with 24 receptors (Murphy, 2019). Therefore, multiple chemokines bind to the same receptor with high affinity. As such, chemokine receptors are deemed ‘promiscuous’ and

demonstrate the high degree of redundancy in the chemokine family as multiple chemokines can bind to the same receptor (Bièche et al., 2007, Salazar et al., 2013). The binding of the chemokine to its cognitive receptor initiates an intracellular cascade of events that enables secondary messages to activate chemotaxis and various other functions controlled by chemokine receptors that is discussed in more detail later (Stone et al., 2017, Teicher and Fricker, 2010).

To stop downstream cellular signalling, the receptor is phosphorylated which occurs only on certain serine and threonine residues that are predominantly found in the C-terminal tail and the third intracellular loop (Claing et al., 2002, Krupnick and Benovic, 1998, Luo et al., 2017, Marchese et al., 2008, Marchese et al., 2003). Not all chemokine receptors have the same number of phosphorylation sites. For example, the chemokine receptor CCR5 has approximately 4 phosphorylation sites while CXCR4 has over 18 phosphorylation sites (Alkhatib, 2009, Mueller et al., 2013, Oppermann et al., 1999). Generally, the ability of chemokine receptors to be activated and deactivated by various mechanism enables them to respond quickly to small environmental changes. Often the intensity and duration of receptor activation is more important than activation of a signalling pathway itself (Maudsley et al., 2005).

By understanding the differences in the structure, function and downstream signalling of different chemokine receptors, a greater understanding of their signalling pathways can occur. This will pave the way for creating therapeutics that target these signalling pathways to prevent chemokine receptor specific diseases.

## 1.3. The CXCR4 Receptor

The CXCR4 chemokine receptor is composed of 352 amino acids residues that arrange into seven transmembrane domains with three extracellular loops and three intracellular loops (Figures 1.2 and 1.3) (Federsppiel et al., 1993) originally discovered the CXCR4 receptor and found the gene to be localized on the 2q21 chromosome. Additionally, they discovered that it had 93% sequence homology with bovine neuropeptide Y. Originally, it was given the name LESTR (leukocyte-derived-seven-transmembrane-domain-receptor) as it was found to be highly expressed by white blood cells (WBC) and was thought to function in the activation of inflammatory cells (Loetscher et al., 1994). However, it did not receive much attention until it was found to be a co-receptor for the entry of HIV into $CD4^+$ T cells by binding to the gp120 envelope protein of HIV-1 whereupon

it was renamed CXCR4, in keeping with the new chemokine-receptor nomenclature (Oberlin et al., 1996). Since its discovery, CXCR4 has been found to be expressed on a wide variety of cells including: monocytes, B cells, naïve T cells, CD34+ hematopoietic progenitor cells and in a variety of tissues including the thymus, brain, spleen and stomach (Aiuti et al., 1997, Aiuti et al., 1999, Jo et al., 2000, Nagasawa et al., 1994). Specifically, it was found that the CXCR4 receptor has a major role in neutrophil homeostasis. This homeostasis occurs via the expression levels of CXCR4 increasing on old or senescent neutrophils, aiding in their clearance from the blood to the bone marrow. This causes neutrophil retention in the bone marrow and aids controlled neutrophil release (Martin et al., 2003). Additionally, it has been found that both CXCR4 and its cognate ligand CXCL12 are constitutively expressed in the central nervous system (CNS), circulatory system and immune system with knockout of CXCR4 causing severe impairments in these systems (Banisadr et al., 2003, Bleul et al., 1997, Halks-Miller et al., 1997, LaRocca et al., 2019, Ma et al., 1998, Mithal et al., 2012, Tham et al., 2001, Wong et al., 1996).

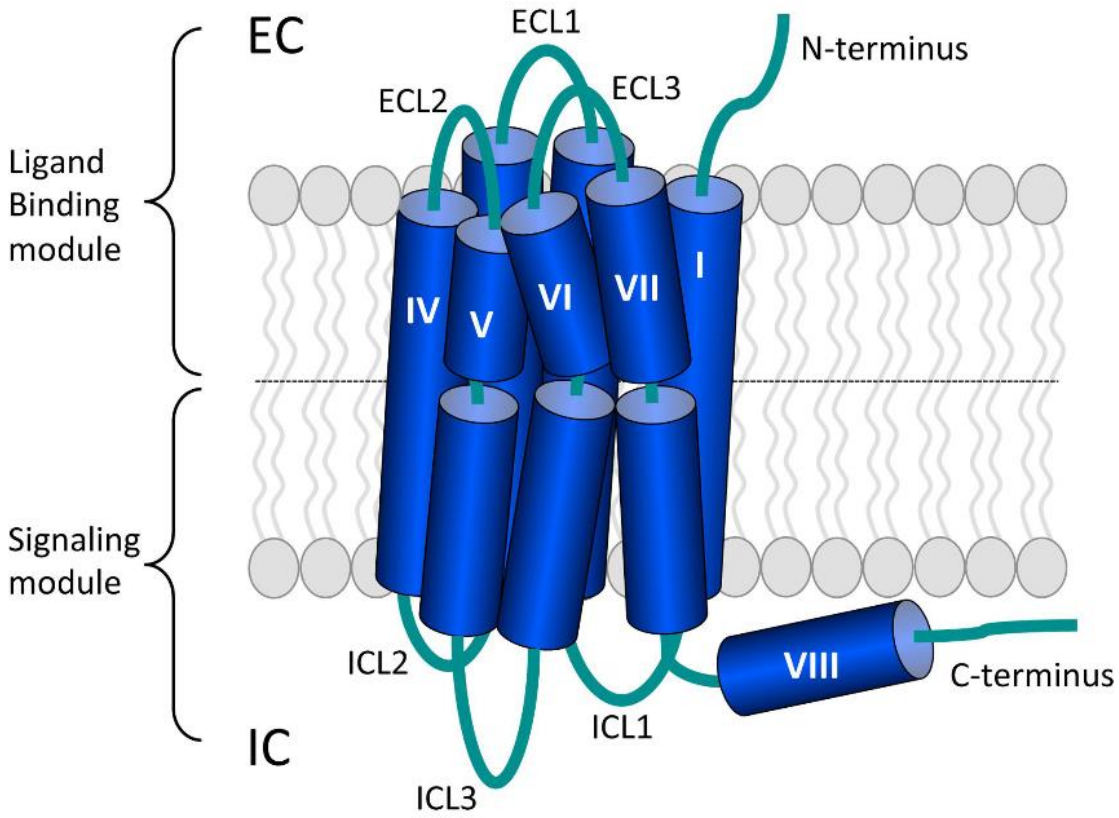


**Figure 1.3: The Structure of CXCR4 (de Munnik et al., 2015).** CXCR4 has an external N-terminal domain, seven transmembrane domains labelled I to VII, three extracellular loops labelled ECL1-3, three intracellular loops labelled ICL1-3 and an internal C-terminal domain. The seven transmembrane domains are arranged counter-clockwise and are divided into the ligand-binding module and the downstream signalling module that signals the G protein.

## 1.4. The CXCL12 Chemokine

### 1.4.1. CXCL12/SDF-1α

Originally, CXCL12 was identified as a pre-B cell growth factor (PBGF), which plays an important role in homeostatic processes (Namen et al., 1988). It was subsequently synthesised by both Tashiro et al. (1993) and Nagasawa et al. (1994). Due to this chemokine being constitutively expressed by bone marrow stromal cells, such as fibroblasts and endothelial cells, it was renamed stromal cell derived factor 1 (SDF-1) before finally being named CXCL12 in 2000 (Bleul et al., 1996, Nagasawa et al., 1994, Zlotnik and Yoshie, 2000). Other cells and tissues including the skin, heart, brain, pancreas, bile ducts, epithelial cells, endothelium, lung, liver and thymus also express CXCL12 (Dar et al., 2006, Müller et al., 2001, Yun and Jo, 2003).

CXCL12 enables leukocyte and hematopoietic precursor development and mobilisation as well as pre-B cell proliferation and survival (Aiuti et al., 1997, D'Apuzzo et al., 1997, Ma et al., 1998, Zou et al., 1998). Hence, CXCL12 gene knockout is embryonically lethal as it leads to impaired haematopoiesis exhibited as a defect in the trafficking of hematopoietic stem cells and defects in the circulatory system, CNS and vasculature (Ma et al., 1998, Ratajczak et al., 2006). Additionally, B lymphopoiesis and myelopoiesis are dramatically reduced in CXCL12 knockout mice (Nagasawa et al., 1996). During tissue injury such as hypoxia, irradiation or the presence of toxins, expression levels of CXCL12 increases. This enables the recruitment of CXCR4-positive stem cells for tissue repair (Gambaryan et al., 2011). Not only does CXCL12 bind to CXCR4, but can also bind to atypical chemokine receptor 3 (ACKR3), discussed in more detail later (Salazar et al., 2014, Sun et al., 2010).

Whilst the majority of CXCL chemokine genes are found on chromosome 4, the CXCL12 gene is located on chromosome 10q11.1. Additionally, it has only 27% amino acid sequence identity with other CXCL chemokines and only 22% sequence identity to CCL chemokines, thus can be described as a distant relation (Shirozu et al., 1995). Through solution NMR spectroscopy and X-ray crystallography, the structure of CXCL12 was determined to consist of three anti-parallel β strands with an overlaying α-helix as shown in Figure 1.4 (Murphy et al., 2007).

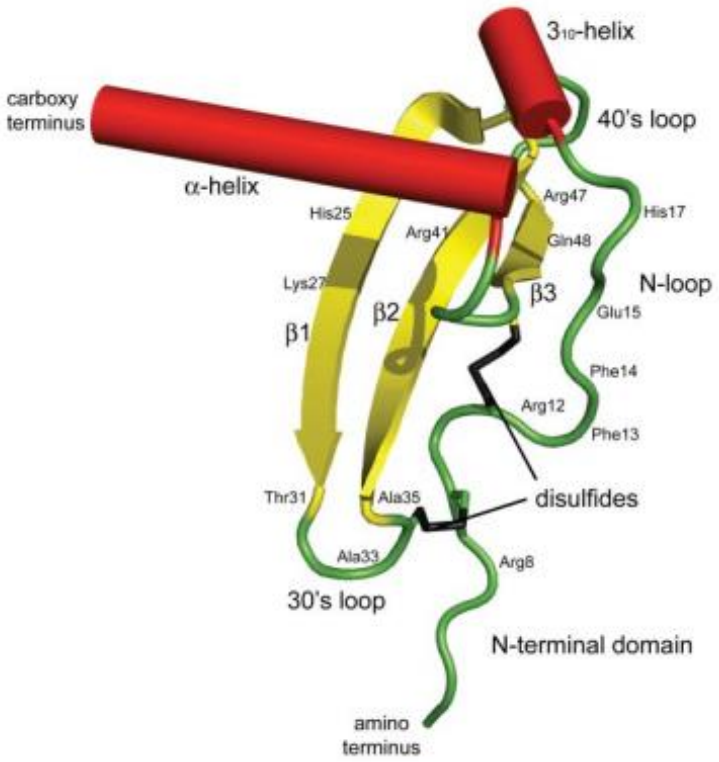


**Figure 1.4: The Structure of SDF-1/CXCL12 (Murphy et al., 2007).** CXCL12 consisted of three anti-parallel β strands (yellow) with an overlaying α-helix (red). The helical regions are displayed as cylinders or loops. CXCL12 has two conserved disulphide bridges (black) and the position of residues are labelled but are subject to mutagenesis.

### 1.4.2. CXCL12 Isoforms

Six different spliced variants (isoforms) of CXCL12 chemokine have been discovered: α, β, γ, δ, ε, ψ (Yu et al., 2006). Tashiro et al. (1993) and Shirozu et al. (1995) discovered the first two isoforms, SDF-1α and SDF-1β in both human and in mice and identified that these isoforms were alternatively spliced variants of the same gene.

These isoforms arise due to CXCL12 initially being secreted as an 89 amino acid pro-peptide. To become biologically active, CXCL12 is then subjected to the proteolytic removal of 21 amino acids from the NH2 terminal end to create SDF-1α (Davis et al., 2005, Marquez-Curtis et al., 2008). SDF-1β encodes these same 89 amino acids of the pro-protein but has an additional four amino acids creating a 93 amino acid protein residue. Therefore, SDF-1α consists of three exons only while spliced variants have an additional fourth exon attached to a C-terminal residue that differs in length depending upon the isoform (Crump et al., 1997, Pawig et al., 2015, Tashiro et al., 1993). CXCL12 is positive charged due to it

being sequenced from numerous basic amino acids, hence why they can bind to negatively charged glycosaminoglycans (GAGs) (Amara et al., 1999). However, due to splicing variants having different fourth exons, the charge of the protein is altered thus alters the strength of GAG binding (Janowski, 2009).

While SDF-1α is the smallest and most predominant isoform that can exists in all organs in a constitutive manner, it undergoes rapid proteolysis in blood and therefore is not expressed in blood cells (Davis et al., 2005, Tashiro et al., 1993).This proteolytic degraded occurs at both ends of CXCL12 with proteolysis of the N-terminus occurring slowly but ultimately switches off chemokine activity and decreases the binding affinity of CXCL12 (Davis et al., 2005, Sierra et al., 2004). Conversely, the degradation of the C-terminus is rapid and mediated by carboxypeptidase-N (CPN) (Davis et al., 2005). While C-terminus proteolysis does not inactivate SDF-1α, it decreases its activity by half (Janowski, 2009). The attachment of a longer, fourth exon during the splicing process stabilizes CXCL12 and prevents proteolytic degradation of chemokines at the C-terminus in the blood (Yu et al., 2006). Thus, SDF-1β is more resistant to blood-dependent degradation and therefore is present in highly vascularized organs such as the liver, spleen and kidneys (Davis et al., 2005). Both SDF-1α and SDF-1β enable B-cell lymphopoiesis with SDF-1α being more involved with local tissue-specific physiological processes such as maintaining the stem cell population in the bone marrow and germ cell development (Boldajipour et al., 2008, Nagasawa et al., 1994, Stumm et al., 2002, Tashiro et al., 1993, Weidt et al., 2007). Alternatively, SDF-1β is more involved with angiogenesis and is upregulated during ischemia (Stumm et al., 2002). Therefore, CXCL12 isoforms are processed post-translationally with the microenvironment dictating the production of different isoforms of CXCL12 with different binding and signalling properties (Janssens et al., 2018b).

A third alternatively spliced CXCL12 variant, SDF-1γ, was discovered in rats and later in humans (Gleichmann et al., 2000). The SDF-1γ isoform is much longer than both SDF-1α and SDF-1β, consisting of 119 amino acids. It is strongly positively charged, giving it the highest affinity for GAGs of all the isoforms. It is due to its affinity for GAGs that upon secretion it is almost never found in a disengaged state (Yu et al., 2006). Therefore, this variant is found in the heart, lungs and mature nervous system (Gleichmann et al., 2000, Yu et al., 2006).

Following this Yu et al. (2006), discovered three other splice variants. The first, SDF-1δ, has an additional 51 amino acids to the CXCL12 pro-protein and is expressed in several adult tissues but is highly expressed in foetal liver as well as the spleen and lungs. The second, SDF-1ε, has only one additional amino acid and the third SDF-1φ has an additional 11 additional amino acids. Both SDF-1ε and SDF-1φ can be found in the heart and liver while all isoforms are abundant in the pancreas. In total there are six discovered isoforms of human CXCL12 however SDF-1δ, SDF-1ε and SDF-1φ are less well characterised (Yu et al., 2006).

## 1.5. CXCR4/CXCL12 Binding

There are two major binding structures that enabling the binding of CXCR4 to CXCL12. As mentioned, the CXCL12 pro-protein consist of 89 amino acid residues, the first 21 of which are the signalling peptide that is cleaved off to create the mature CXCL12 splice variants. Therefore, Lys-22 of the pro-protein becomes Lys-1 beginning at the N-terminus in the mature CXCL12 isoform (Davis et al., 2005, Pawig et al., 2015). Crump et al. (1997) first reported the concept of the 'two site' binding model of chemokines to their receptors. The first site involves the chemokine core binding to CXCR4 to enable the docking of the chemokine to the receptor. This chemokine core is the 'RFFESH loop' of CXCL12, which corresponds to the CXCL12 amino acids residues 12–17. The second binding site enables the activation of CXCR4 signalling. This occurs via the N-terminal region of CXCL12, more precisely amino acids Lys-1 and Pro-2, binding to the receptor groove compromising of the transmembrane helices and the extracellular loops (Crump et al., 1997). While the amino acid residues responsible for binding CXCL12 have been elucidated, the CXCR4 residues involved have yet to be identified in detail due to the challenge of determining the structure of a full length membrane protein (Wu et al., 2010).

Posttranslational sulfation of Tyr-21, Tyr-12, Tyr-7 in the CXCR4 N-terminus increased the binding affinity of CXCR4 for CXCL12 due to electrostatic interactions between these acidic sulfated tyrosines to basic residues within CXCL12 (Seibert et al., 2008, Veldkamp et al., 2008). Therefore, these tyrosine residues are predicted to contribute to the first site of interaction between CXCR4 and CXCL12. Specifically, sulfated Tyr-21 interacts with the β1 strand of CXCL12 based on the crystal structure of CXCR4 bound to the broad-spectrum viral chemokine vMIP-II (Qin et al., 2015). Additionally, Qin et al. (2015) found

agreement with the two site binding hypothesis discussed above (named chemokine recognition site 1 and 2, CRS1 and CRS2). However, they found that there was an absence of a distinct boundary between these two sites, thus they introduced an intermediate region, CRS1.5. This site acts like a pivot between CRS1 and CRS2, allowing specific interactions to occur between the receptor and the ligand. Specifically, they found that the CRS1 interaction involves CXCR4 N-terminal residues 23-SMKEP-27 (Figure 1.2) packing against the chemokine N loop (residues 13-LGYQ-16) and the third β strand (β3, residues 49-QVC-51). This interaction continues toward CRS1.5, where CXCR4 receptor residues 27-PCFRE-31 bind to chemokine residues 8-PDKCC-12. In CRS2, the chemokine N terminus makes hydrogen bonds to receptor residues D97$^{2.63}$, D262$^{6.58}$ and E288$^{7.39}$ and numerous van der Waals packing interactions (Qin et al., 2015).

Additionally, it has also been found that the acidic residue Asp-187 of CXCR4 is an important ligand/receptor contact point that might be involved in the second site of interaction with the Lys-1 and Pro-2 residues of CXCL12 (Wu et al., 2010). These residues were identified from the crystal structure of CXCR4 in complex with the CXCL12 competitive antagonist IT1t. Wu et al. (2010) also cocrystallised CXCR4 with the antagonistic peptide CVX15 which identified interactions occurring between the CXCL12 N-terminus (1-KPVSLSYR-8) to CXCR4. However, the information that can be divulged from these crystal structures has several limitations due to CXCR4 being cocrystallised with antagonists and not CXCL12 and so the receptor resembles an inactive conformational state. Additionally, it was observed that the conformation of the N-terminal of the CXCR4 receptor crystallised with vMIP-II in the work by Qin et al. (2015) differs significantly from their previous work with IT1t and the cyclic peptide CVX15 (Wu et al., 2010). This suggests that while we have better insight into the specific binding sites of CXCR4, different amino acids are involved in the binding of CXCR4 to various agonists and antagonists.

Several mutagenesis studies have also been conducted to determine critical residues for CXCR4 signalling. For example, Di Maro et al. (2016) identified two residues in CXCR4, His-113 and Tyr-116, that were critical for ligand binding. However, another mutagenesis study conducted by Wescott et al. (2016) did not identify these residues but 41 other critical residues, 33 of which were confined within six of the TM helices (Figure 1. 5). These residues were mapped onto the crystal structures determined by Wu et al. (2010) and Qin et al. (2015). From this

mapping, these critical residues were categorised into: chemokine engagement, signal initiation, signal propagation, micro-switch activation and G protein coupling based upon their function and location (Wescott et al., 2016).

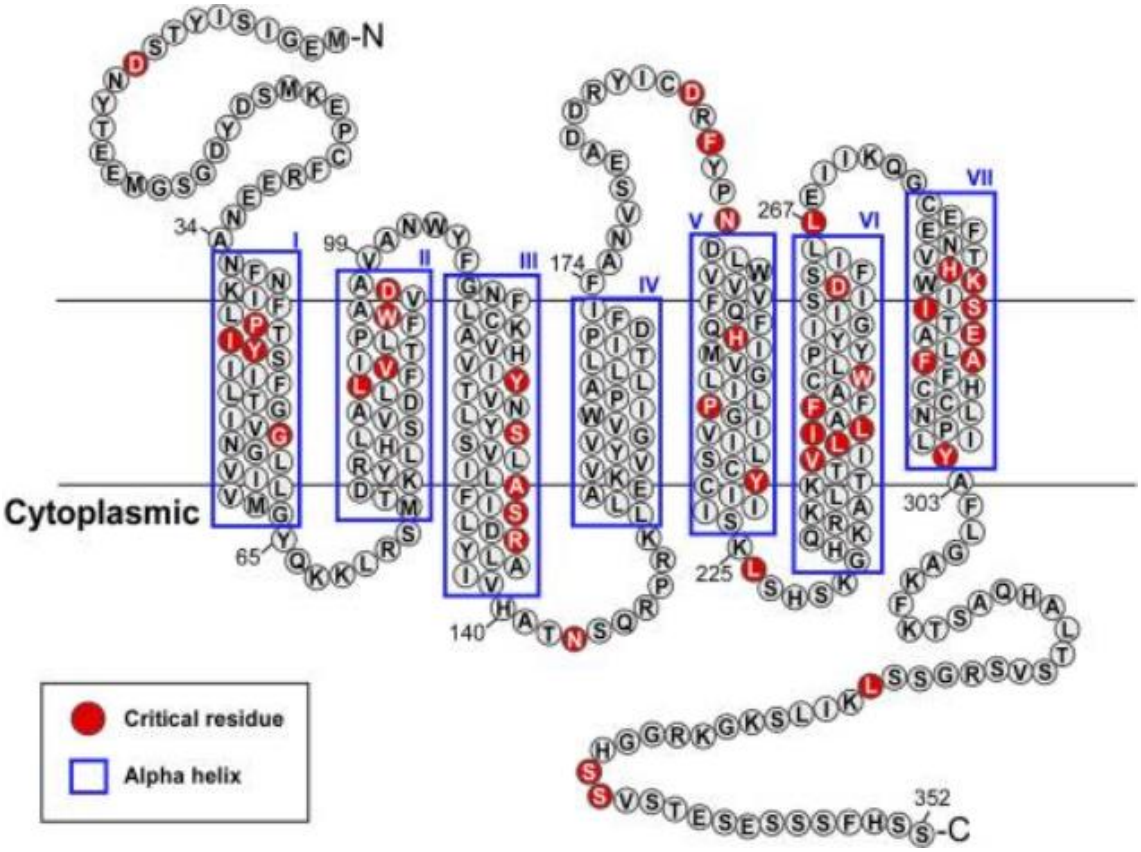


**Figure 1.5: The 41 Critical Residues for CXCL12-Mediated Signalling in CXCR4 (Wescott et al., 2016).** Mutagenesis experiments identified 41 critical residues for CXCL12-mediated signalling in CXCR4. 33 of these residues are within the TM helices except helix IV, that contains no critical residues. These residues can be categorised based on their function and location into residues that are required for: chemokine engagement, signal initiation, signal propagation, micro-switch activation and G protein coupling.

## 1.6. CXCL12 and GAGs

As mentioned previously, in addition to CXCL12 binding directly to CXCR4, CXCL12 is also able to interact with GAGs such as heparan sulfate (Amara et al., 1999). The binding of CXCL12 to GAGs helps localize the chemokine on or near to cell surfaces (Rueda et al., 2008). Therefore, when chemokines are initially secreted, they become immobilized on GAGs which are concentrated near to chemokine receptors in such a way that they form an immobilized gradient. This provides directionality to guide leukocytes towards the inflammatory site (Springer, 1994). Leukocytes will roll along the endothelial cell surface due to

weak interactions with adhesion molecules such as selectins. This rolling continues until chemokines engage their cognate chemokine receptors, on the surface of leukocytes, resulting in leukocyte arrest aided by integrin activation (Springer, 1994, Springer, 1995). This GAG-mediated mechanism is thought to help oligomerize CXCL12, prevent premature activation of leukocytes before reaching the inflammatory site and prevent CXCL12 proteolysis (Rot, 1992, Volpe et al., 2012).

## 1.7. The CXCR4/CXCL12 Signalling Axis

### 1.7.1. The Heterotrimeric G Protein

The binding of CXCL12 to CXCR4 enables the transduction of information by the activation of heterotrimeric guanine nucleotide binding proteins (G proteins) (Offermanns and Schultz, 1994). These G proteins are both bound to the chemokine receptor and are associated with the inner surface of the plasma membrane (Goldsmith and Dhanasekaran, 2007). One single chemokine receptor can activate multiple G proteins and therefore can induce several different downstream signalling pathways. Alternatively, multiple receptors can converge and activate a single G protein that will activate a very specific signalling pathway (Offermanns and Schultz, 1994). This interaction between multiple different receptors to create one specific amplified signal is defined as cross talk that will 'fine tune' a signal. G-protein activation can also produce negative, regulatory effects upon signal cascades where one receptor can negatively regulate another receptor, again to 'fine tune' the resulting signal (Selbie and Hill, 1998).

The G protein itself is composed of three subunits a 36-52 kDa α subunit, a 35-36 kDa β subunit and finally an 8-20 kDa γ subunit. There are multiple isoforms of each subunit including: 20 types of α subunits; 5 types of β subunits and finally 14 types of γ subunits (Jaakola, 2005, Liebmann and Bohmer, 2000). However, not every combination of these subunits is possible. These 20 different types of α subunits can then be organised into four families depending upon their amino acid sequence similarity and their signalling function, see Table 1.1 (Liebmann and Bohmer, 2000, Strathmann and Simon, 1991). The β subunit and the γ subunit are often tightly associated to one another and therefore are referred to as a single entity, the βγ subunit dimer (Conklin and Bourne, 1993, Hepler and Gilman, 1992, Simon et al., 1991). For clarity, G proteins are defined by their α

subunit therefore, a $G_i$ G protein heterodimer contains a $G\alpha_i$ subunit, a $G_o$ protein heterodimer contains a $G\alpha_o$ subunit and so on (Jaakola, 2005).

**Table 1.1: The G Protein Family.**

| G protein family | α Subunits Within Family | Function | Reference |
|---|---|---|---|
| **$G_s$** | $\alpha_s$, $\alpha_{olf}$ | Adenylyl cyclase stimulation, $Ca^{2+}$ channel control | (Liebmann and Bohmer, 2000, Strathmann and Simon, 1990) |
| **$G_{i/o}$** | $\alpha_{1\text{-}3}$, $\alpha_{oA}$, $\alpha_{oB}$ $\alpha_{t1\text{-}2}$, $\alpha_{gust}$, $\alpha_z$ | Adenylyl cyclase inhibition, gating of $K^+$ and $Ca^{2+}$ ion channels | (Liebmann and Bohmer, 2000, Strathmann and Simon, 1990) |
| **$G_{q/11}$** | $\alpha_q$, $\alpha_{11}$, $\alpha_{14\text{-}16}$ | Phospholipase C β and NFκB activation | (Liebmann and Bohmer, 2000, Strathmann and Simon, 1990) |
| **$G_{12/13}$** | $\alpha_{12}$, $\alpha_{13}$ | $Na^+/K^+$ exchange, Rho GTPase Activation | (Liebmann and Bohmer, 2000, Strathmann and Simon, 1990, Suzuki et al., 2009) |

In the 'classic' model for G protein signalling, see Figure 1.6, the binding of a ligand to its GPCR causes the dissociation of GDP that is bound to the α subunit. GDP is then replaced by GTP via the guanine nucleotide exchange factor (GEF).The now GTP bound α subunit can then dissociate from the receptor and from the βγ-subunit thus 'activating' the G protein (Hepler and Gilman, 1992, Johnson and Dhanasekaran, 1989, Urano et al., 2013). Following this, both the Gα subunit (see Table 1.1) and the Gβγ subunit dimer can interact with and activate different effector molecules in both a normal and in a disease state (Leopoldt et al., 1998, Liebmann and Bohmer, 2000, Strathmann and Simon, 1991, Suzuki et al., 2009). For example; the βγ subunit dimer contributes to breast cancer metastasis via the activation of Rac (Kirui et al., 2010). Additionally, the expression of $G\alpha_{12}$ has been shown to be highly up-regulated in oral squamous cell carcinoma (Gan et al., 2014). Finally, to terminate the signal, Regulators of G-protein Signalling (RGS) proteins function as guanosine triphosphatase-activating proteins (GAPs) for Gα subunits, enabling accelerated hydrolyse of GTP. Specifically for CXCR4 signalling, RGS16 acts as a negative regulator (Berthebaud et al., 2005).

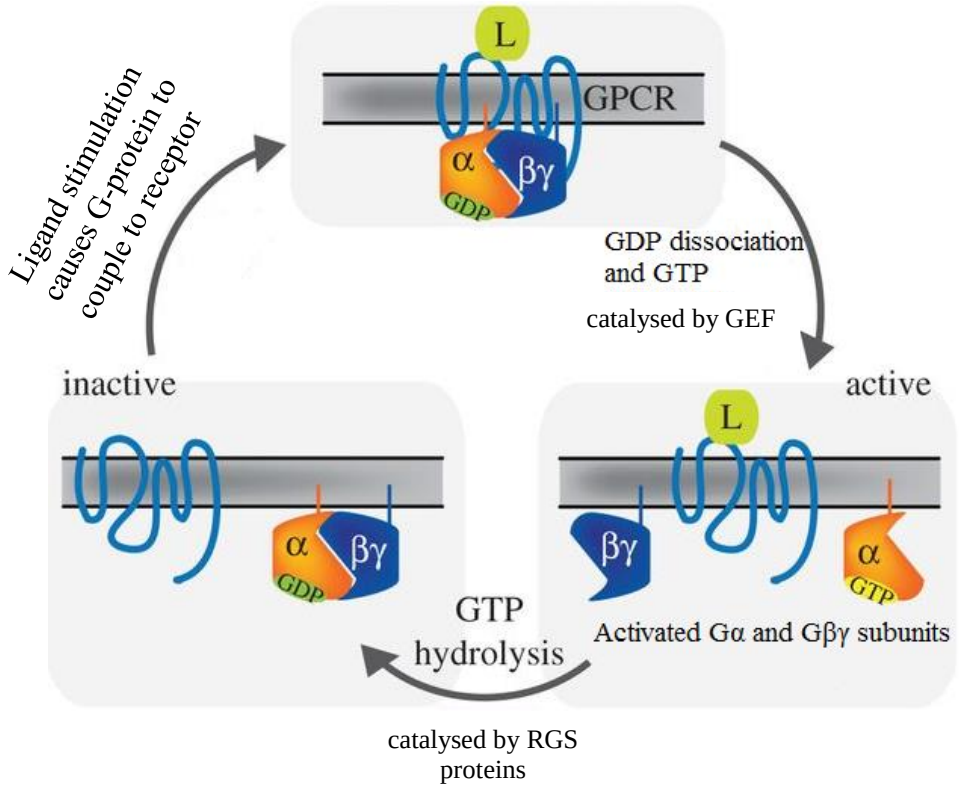


**Figure 1.6: The Classic Model for G Protein Signalling (adapted from (Urano et al., 2013).** Upon ligand stimulation (L), the G-protein couples to the GPCR and causes the α subunits of the G protein to release GDP which is then replaced by GTP, catalysed by GEF. This enables the release of the β subunit and the γ subunit, which form a Gβγ subunit dimer. This is now an activated G protein with both the Gα subunit and the Gβγ subunit dimer being able to interact with and activate different effector molecules. RGS proteins can then promote the GTP hydrolysis and terminate G protein signalling.

### 1.7.2. G Protein Signalling

While GPCRs can interact with a variety of different Gα subunits, CXCR4 mainly interacts with $G\alpha_i$ in response to CXCL12 stimulation (Vila-Coro et al., 1999). However, CXCR4 can couple efficiently to the $G\alpha_{q/11}$, $G\alpha_{12/13}$, $G\alpha_o$ and $G\alpha_s$ subtypes (Kleemann et al., 2008, Ling et al., 1999, Quoyer et al., 2013, Tan et al., 2006, Teicher and Fricker, 2010, Yagi et al., 2011). The $G\alpha_i$ subunit has an inhibitory role, inhibiting adenylyl cyclase–mediated cyclic adenosine monophosphate (cAMP) production, see Figure 1.7 (Gilman, 1987). Additionally, the $G\alpha_i$ subunit can also activate the MEK/ERK pathway, phosphoinositide 3 kinase (PI3K) and the Rac/Rho pathway all of which lead to gene transcription, cell survival, migration, adhesion and proliferation (Busillo and Benovic, 2007, Ganju et al., 2012, Neptune and Bourne, 1997, Teicher and Fricker, 2010).

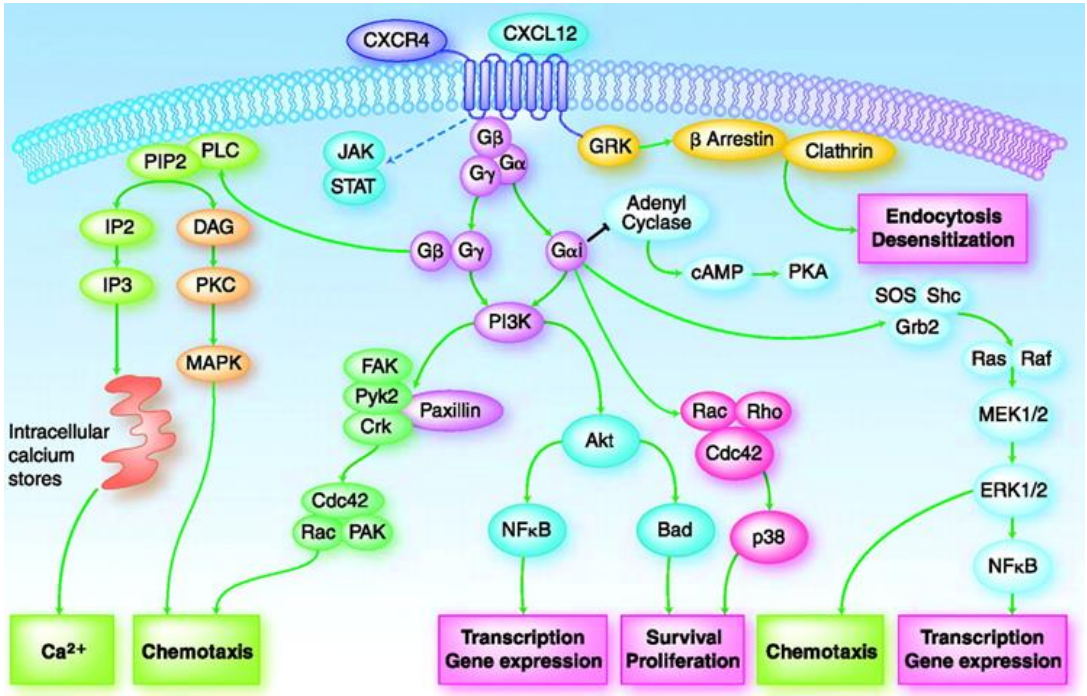


**Figure 1.7: The CXCR4/CXCL12 Signalling Axis (Teicher and Fricker, 2010).**The binding of CXCL12 to its receptor, CXCR4, releases GDP from the G protein. GTP replaces GDP, enabling the dissociation of the heterotrimer into Gβγ and Gα. This α-monomer can be divided into four distinct families: $G\alpha_s$, $G\alpha_i$, $G\alpha_q$ and $G\alpha_{12}$ with CXCR4 mainly modulating downstream signalling via $G\alpha_i$. This can activate PI3K, ERK1, ERK2, and NFκB. The activation of ERK1/2 pathway enables chemotaxis and the activation of NFκB. The $G\alpha_i$ subunit can also activate PI3K enabling chemotaxis, transcription, gene expression, survival and proliferation. Additionally, $G\alpha_i$ can also activate the Rac-Rho pathway that, via p38 enables cellular survival and proliferation. Both the Gα and the Gβγ subunits stimulate chemotaxis and proliferation via PI3K that phosphorylates and activates several proteins kinase pathways including focal adhesion kinase (FAK) and Rac. PI3K also activates serine-threonine kinase Akt then NFκB that plays key roles in transcription and gene expression, cell survival, proliferation or can inactivate the pro-apoptotic proteins Bcl-2 and BAD. The Gβγ subunit is also involved in signalling and can trigger PLC activation, which hydrolyses PIP2 into two secondary messengers, IP3 that increases intracellular calcium and DAG that activates PKC and the MAPK signalling pathway to initiate chemotaxis. Aside from G protein downstream signalling there is the JAK/STAT pathway and the GRK/β-arrestin pathways. The JAK/STAT signalling pathway can also enable protein transcription, cellular proliferation, differentiation and migration. The GRK/β-arrestin pathway on the other hand is involved mainly in receptor desensitization and receptor recycling.

The activation of the extracellular signal-regulated kinase (ERK) 1/2 pathway enables the phosphorylation and activation of other cellular proteins and the translocation of the ERK1/2 protein itself into the nucleus. Inside the nucleus, ERK1/2 can phosphorylate and activate transcription factors such as NFκB. These transcription factors enable changes in gene expression, cell cycle progression and can stimulate chemotaxis (Sun et al., 2010).

PI3K is a ubiquitously expressed kinase that phosphorylates several focal adhesion components such as proline-rich kinase-2 (Pyk-2), Crk-associated substrate (p130Cas), focal adhesion kinase (FAK), paxilin, Nck, Crk, and Crk-L enabling the reorganisation of the actin cytoskeleton to allow for cell migration (Teicher and Fricker, 2010, Wang et al., 2000). Additionally, PI3K can activate effectors such as Akt (also known as protein kinase B) and phospholipase C (PLC) (Falasca et al., 1998). Akt is a key protein in tumour development as it inactivates the pro-apoptotic protein BAD resulting in cellular survival. Additionally, Akt can inactivate GSK3β and stabilize β-catenin. This enables β-catenin to move into the nucleus and activate gene transcriptions that promote cellular proliferation (Mo et al., 2013). PI3K has several isotypes: PI3Kα, β, γ and δ. PI3K γ has proven to be involved with GPCR signalling with some speculative evidence that the PI3Kα, β and δ isotypes can also be activated by GPCRs (Murga et al., 2000, Rommel et al., 2007). PI3Ks are central to cellular migration but are also involved in other cellular processes such as, transcription, gene expression and the survival and proliferation of cells via PI3K activating the Rac-Rho pathway (Montaner et al., 2013). For this reason, PI3K is often overexpressed in cancerous cells. This overexpression can be due to mutations in the PI3K kinase itself, or due to the overexpression of upstream signalling pathways i.e. CXCR4 receptor overexpression (Chatterjee et al., 2014, Zunder et al., 2008). The Gβγ subunit can also activate PI3K leading to the phosphorylation and activation of several proteins kinase pathways including Rac enabling chemotaxis and proliferation (Curnock et al., 2002). Interestingly, Rac 1 is also activated via the $G\alpha_i$ subunit directly and specifically regulate CXCR4 expression in resting cells. This was demonstrate by Zoughlami et al. (2012) whom found that the inhibition of Rac 1 caused a decrease in CXCR4 signalling via the polybasic domain in the C-terminal of Rac 1 binding to CXCR4. This prevented CXCL12 binding and therefore prevented CXCR4 downstream signalling. Additionally, Rac 1 inhibition caused a conformational change in CXCR4 that

decreased its cell surface expression levels and decreased the capacity of CXCR4 to initiate $G\alpha_i$ protein signalling. Therefore, Rac 1 acts as an intracellular positive allosteric modulator of CXCR4 as well as being downstream of CXCR4 and causing the translation of CXCL12 stimulus into cytoskeletal remodelling and cell movement (Zoughlami et al., 2012).

As mentioned, the Gβγ subunit is also involved in signalling and aside from activating PI3K, it can also trigger PLCβ activation which hydrolyses Phosphatidylinositol 4,5-biphosphate (PIP2) into two secondary messengers: inositol triphosphate (IP3) and diacylglycerol (DAG) (Goldsmith and Dhanasekaran, 2007). IP3 is hydrophilic which allows it to detach from the membrane and bind to the IP3 channel on the endoplasmic reticulum (ER). This opens the IP3 channels enabling the influx of calcium ions ($Ca^{2+}$) from the intracellular stores and into the cytosol (Baggiolini, 2001). DAG activation in turn activates protein kinase C (PKC) and the MAPK signalling pathway to initiate chemotaxis (Goldsmith and Dhanasekaran, 2007).

Multiple signalling pathways are active at any given time to enable signalling amplification for the appropriate biological outcome to occur. In the case of CXCR4/CXCL12 signalling, such biological outcomes are changes of cell cycle progression, calcium influx, chemotaxis, transcription and post-transcriptional changes, gene expression, survival and proliferation of normal cells (Teicher and Fricker, 2010).

### 1.7.3. G Protein Independent Signalling

The activation of both the JAK/STAT pathway and the GRK/arrestin pathway shown in Figure 1.7 are in fact G protein independent signalling pathways. It has been postulated that GPCR oligomerization can initiate these signalling pathways. While CXCR4 is predominantly in a monomeric state it can form both homodimers and heterodimers with for example: CCR2, CCR7 and ACKR3 (Hayasaka et al., 2015, Levoye et al., 2009, Sohy et al., 2007). Specifically, it has been suggested that CXCR4 homodimerization results in G-protein-independent signalling through the JAK/STAT signalling pathway (Mellado et al., 2001).

The G-protein receptor kinases (GRK) pathway becomes activated as a CXCR4 desensitizing measure once the appropriate signalling response has been achieved. Thus, GRKs are recruited directly to the intracellular C terminus of CXCR4 and are discussed in more detail below (Teicher and Fricker, 2010).

### 1.7.3.1. JAK/STAT Signalling

There are four members of the JAK family: JAK1, JAK2, JAK 3 and Tyk2. As mentioned previously, the activation of JAK occurs via ligand-mediated receptor multi-dimerization where two JAKs are brought together enabling trans-phosphorylation. Specifically, the ligand CXCL12 enables the association of JAK2 and JAK3 with CXCR4 (Rawlings et al., 2004, Vila-Coro et al., 1999). The activated JAKs can then phosphorylate targets, such as STATs, which are transcription factors that reside in the cytoplasm until activated (Rawlings et al., 2004). There are seven members of the STAT family. Each member has a conserved tyrosine residue at the C-terminus that are phosphorylated by JAK. Once phosphorylated, STAT can dimerize via interaction between their conserved SH2 domain and become translocated into the nucleus. Once in the nucleus, dimerized STATs can bind to specific DNA sequences to enable the transcription of target genes (Rawlings et al., 2004). While JAK/STAT activation is G protein-independent, G protein coupling is involved in JAK/STAT-receptor complex recycling (Vila-Coro et al., 1999).

The activation of this pathway enables gene transcription, cellular proliferation, differentiation and migration. Therefore, overexpression and/or mutations in the JAK/STAT pathway can lead to tumour metastasis and cancer progression (LaFave and Levine, 2012, Marotta et al., 2011, Rawlings et al., 2004, Saxena et al., 2007).

### 1.7.3.2. GRK and Arrestin Signalling

Once activation of the receptor has occurred, desensitization or silencing must follow to turn off the GPCR signal and avoid the negative effects of sustained signalling (Shukla et al., 2011). Such negative effects include: excessive infiltrations of leukocytes into tissues leading to inflammation; autoimmune disease and tumour growth or; chemokine sensitivity to cells that are normal not responsive to chemokines (Scholten et al., 2012). Therefore, CXCR4 is rapidly phosphorylated at serine sites by GRKs. In turn, GRKs recruit β-arrestins which can bind to 7TMR which physically shield the cytoplasmic surface of the receptor preventing any additional protein binding or activation, thus the receptor is desensitized (Gurevich et al., 2012, Krupnick and Benovic, 1998, Teicher and Fricker, 2010). Specifically, β-arrestin blocks G-protein access to the 7TMR binding domains thereby reducing the ability of G-protein to dissociate into $G_{\alpha}$ and

$G_{\beta\gamma}$ subunits causing decreased downstream signals initiated by the G-proteins (L Mohan et al., 2012).

Aside from receptor desensitization, these two protein families are also involved in the trafficking of the 7TMR for internalisation, 'resensitization' and/or degradation (Reiter and Lefkowitz, 2006). Internalisation occurs via several forms of endocytosis: clathrin-dependent endocytosis (CDE); caveolin-dependent endocytosis and clathrin/caveolae-independent endocytosis. However, it has been hypothesised that CXCR4 internalisation occurs via CDE (Cheng et al., 2000, Claing et al., 2002, von Zastrow and Williams, 2012, Xu et al., 2017). 7TMR trafficking enables one of three events to occur. The first is that the 7TMRs becomes dephosphorylated, resensitized then recycled back to the membrane surface. The second is that the 7TMR becomes targeted by lysosomes for degradation. Finally, internalization of 7TMRs can enable the activation of intracellular signalling pathways (Marchese et al., 2003, Reiter and Lefkowitz, 2006). Haribabu et al. (1997) found that when CXCR4 is bound to CXCL12, the receptor is both rapidly phosphorylated and desensitized. Specifically, GRK2 is recruited to enhance the internalization of CXCR4 and therefore it has been suggested that GRK2 is the negative regulator of CXCR4 signal transduction when interacting with MEK (Jiménez-Sainz et al., 2006).

Finally, arrestins can also act as signalling scaffolds thus activating and phosphorylating other receptors and signalling proteins independently of the G protein. Such example include the activation of the proto-oncogene Src (c-Src), Akt signalling, Rho pathway, Ras signalling and the ERK pathway (Shenoy and Lefkowitz, 2003). β-arrestin 1 has been found to be both an inhibitor and an activator of PI3K pathway (Reiter and Lefkowitz, 2006, Shenoy and Lefkowitz, 2003). ERK activation is the best defined and is activated by both G protein signalling as well as β-arrestin signalling. There are several differences between these two forms of ERK activation that help distinguish its original activator. For example, β-arrestin activation has a much slower onset, is more persistent and is sequestered in the cytosol while G protein ERK activation is fast, transient and is translocated to the nucleus (Reiter and Lefkowitz, 2006).

### 1.7.4. PKC and PKD Downstream Effectors

In this research, investigations specifically focused on two of the downstream proteins of the CXCR4/CXCL12 signalling axis: Protein Kinase C (PKC) and Protein Kinase D (PKD).

### 1.7.4.1. PKC Family

PKCs are a family of serine/threonine kinase enzymes which consists of a regulatory domain and a catalytic/kinase domain attached by a hinge region. The catalytic region is highly conserved and consists of motifs required for ATP/substrate binding catalysis. In general, the regulatory domain maintains the protein in an inactive conformation and consists of an auto-inhibitory pseudosubstrate domain and two membrane targeting modules, termed C1 and C2 (Steinberg, 2008).

PKCs are classified based upon differences in their $NH_2$-terminal regulatory domain. The three subfamilies consist of: (i) classical isozymes (cPKCs: α, βI, βII which contains an additional 43 residues at the $NH_2$ terminus and γ), which are dependent on $Ca^{2+}$, DAG and phosphatidylserine for activation; (ii) novel (nPKCs: δ, ε, η, θ), which require only DAG and (iii) atypical (aPKCs: ζ, ι/λ), which require neither $Ca^{2+}$ nor DAG for activation (Newton, 2009). Conventional PKC isoforms contain a C1 domain which has an ~50 residue long sequence divided into C1A and C1B (Slater et al., 2002). C1 functions as the binding motif for DAG or phorbol 12-myristate 13-acetate (PMA) (Giorgione et al., 2006) The C2 domain functions as the binding motif for calcium-dependent anionic phospholipid binding (see Figure 1.8) (Coussens et al., 1986). Novel PKCs also have a C1 domain and a C2-like domain (although the ordering of these domains is switched compared to cPKCs) (Giorgione et al., 2006). This C2-like domain is unlike the C2 domain of cPKCs and so it cannot bind calcium (Steinberg, 2008). Atypical PKCs also lack the calcium-sensitive C2 domain. However, they do contain a C1 domain that can bind $PIP_3$, phosphatidic acid or ceramide (but not DAG or PMA) (Hirai and Chida, 2003). Additionally, aPKCs contain a protein-protein interaction PB1 (Phox and Bem 1) domain that mediates interactions with other PB1-containing scaffolding proteins including p62, partitioning defective-6 (PAR-6), and MEK5 (Qiu et al., 2000, Steinberg, 2008). The activity of aPKCs is therefore regulated by these protein-protein interactions but also by phosphorylation via phosphoinositide-dependent kinase-1 (PDK-1) (Hirai and Chida, 2003).

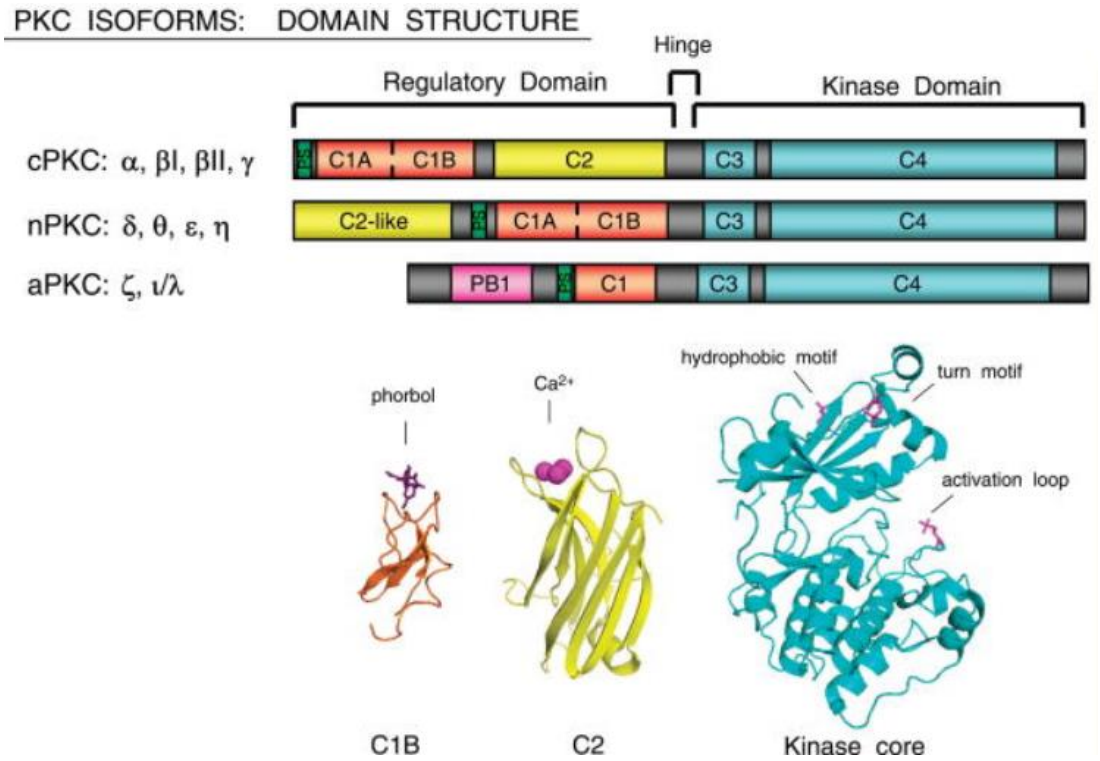


**Figure 1.8: Domain Structure of Protein Kinase C (PKC) Isoforms (Steinberg, 2008).** All PKCs have a conserved kinase domain (C3 and C4, blue), a hinge region and a more varied regulation domain (depicted in yellow, orange and pink). All PKC regulatory domains have a pseudosubstrate motif (green) at the $NH_2$ terminal of the C1 domain (orange). C1 domains are molecular sensors of phorbol 12-myristate 13-acetate (PMA)/diacylglycerol (DAG) in both cPKCs and nPKCs. Atypical PKCs do not bind PMA/DAG. The C2 domain (yellow) functions as a calcium-dependant phospholipid binding molecule in cPKCs but do not bind calcium in nPKCs. PKC isoform variable regions are depicted in grey. The ribbon diagrams show the C1B domain, the C2 domain and the kinase core.

PKC activation during CXCR4 downstream signalling generally occurs via the $G\alpha_q$ subunit activating PLCβ which hydrolyses PIP2 to produce two secondary messengers, IP3 and DAG, which can activate both cPKCs and nPKCs directly or via the release of internally stored $Ca^{2+}$ to activate cPKCs (Rebecchi and Pentyala, 2000). In addition to this, the Gβγ subunit dimer can also activate PLCβ thus IP3 and DAG, leading to both aPKCs and nPKCs activation (Camps et al., 1992, Katz et al., 1992). Atypical PKCs cannot be activated via the PLCβ pathway directly. Instead they are activated via secondary messengers, downstream of DAG such as ceramide and phosphatidic acid (Bourbon et al., 2000, Lorenzo et al., 2002). Additionally, PKCζ can also be activated via the Gα subunit activating Src which will in turn activate PKCζ and via the Gβγ subunit

dimer activating PI3K which in turn activates 3-phospoinositide-dependant protein kinase-1 (PDK-1) enabling the activation of PKCζ (Hirai and Chida, 2003). In this Mitogen-Activated Protein Kinases (MAPK) signalling pathway, PKCζ can then activate ERK leading to the transduction of signals from the cell membrane to nucleus enabling cellular proliferation and migration (Montiel et al., 2006).

Once activated, PKCs phosphorylate hydroxyl groups of serine and threonine amino acid residues on proteins, such as ERK and Src, enabling their activation (Fogh et al., 2014, Gimona et al., 2008). Overall, PKCs are involved in several signal transduction cascades including cell growth, migration via actin cytoskeleton regulation proliferation and immunological regulation (Dowling et al., 2017, Goldsmith and Dhanasekaran, 2007, Larsson, 2006). Specifically, PKCα and PKCε have been shown to control focal adhesion formation and activation of integrin, respectively (Disatnik and Rando, 1999, Gimona et al., 2008).

Some PKC isoforms are expressed in a tissue dependent manner such as PKCθ which is expressed in skeletal muscle, lymphoid organs and hematopoietic cell lines or PKCγ which is mainly found in neuronal tissue (Meller et al., 1999, Kikkawa et al., 1988) However, most PKC isoforms are ubiquitous and many cells co-express multiple PKC isoforms (Steinberg, 2008).

### 1.7.4.2. PKD Family

Similar to the PKC family, the protein kinase D (PKD) family are also a family of serine/threonine kinases. This family consists of three isoforms: PKD1 (formerly known as PKCμ), PKD2 and PKD3 (formerly known as PKCv) (Hayashi et al., 1999, Johannes et al., 1994, Sturany et al., 2001, Valverde et al., 1994). While PKDs were originally classified as PKCs due to the PKD cysteine-rich domain being homologous to the DAG binding domain of other PKC enzymes, they were renamed due to several structural difference (Figure 1.9). The first is that PKDs lack the C2 domain responsible for $Ca^{2+}$ sensitivity in cPKC subgroup (Johannes et al., 1994, Valverde et al., 1994). Additionally, the kinase domain of PKD has very low homology to the conserved kinase domain of the PKCs (Nishikawa et al., 1997, Rozengurt et al., 1995). Finally, while the $NH_2$-terminal part of PKD contains a pleckstrin homology (PH) domain it lacks the typical autoinhibitory pseudosubstrate motif present in PKCs (Figure 1.8, depicted in green) (Valverde et al., 1994). However, PKD1, PKD2 and PKD3 do share a similar structure consisting of an N-terminal regulatory domain and C-terminal kinase domain. The N-terminal domain of PKD1 and PKD2 have an

apolar region that is rich in alanine and/or proline residues which is absent in PKD3. All three isoforms contain two cysteine-rich Zn fingers, separated by long Zn-finger linker region (usually only 14–20 amino acids long in PKCs) (Rykx et al., 2003).

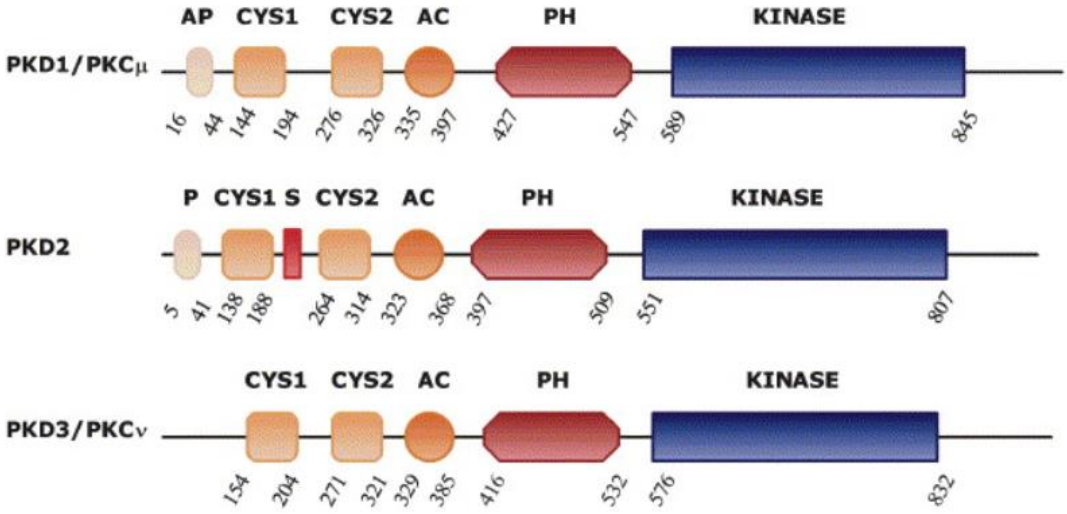


**Figure 1.9: Domain Structure of Protein Kinase D (PKD) Isoforms (Rykx et al., 2003).** All PKDs have a conserved kinase domain (KINASE, blue), a pleckstrin homology (PH) domain (red), acidic domain (AC) and two cysteine-rich Zn finger domains (CYS1 and CYS2). PKD1 additionally has an alanine and proline rich domain (AP) while PKD2 lacks this domain but has both a proline rich domain (P) and a serine-rich domain (S). PKD3 isoforms lack all three AP, P and S domains.

Activation of PKDs occurs via several biological agents including the activation of PLC and the subsequent production of DAG in a similar pathway to PKCs (Iglesias and Rozengurt, 1998, Rozengurt et al., 1995, Rozengurt et al., 2005). PKDs can also be activated by phorbol esters, growth factors and nPKCs and cPKCs themselves (Rozengurt et al., 1995, Zugaza et al., 1996). Additionally, PKD activation has been shown to occur via oxidative stress, the binding of the Gβγ dimer and through caspase-3-mediated cleavage (Endo et al., 2000, Storz and Toker, 2003, Waldron and Rozengurt, 2000).

Due to PKDs having multiple activators, the binding sites for each activator are yet to be fully elucidate. However, it has been found that PKD1 is phosphorylated on multiple sites during *in vivo* activation. Specifically, five phosphorylation sites have been identified in PKD1: two sites in the regulatory domain; two in the kinase domain and one at the C-terminus (Iglesias et al., 1998b). For example, the

binding of the Gβγ subunit dimer and other membrane lipids to PKD activates the protein by interfering with the autoregulatory role of the PH domain (Jamora et al., 1999). Also, Zn finger 2 in the regulatory domain can bind phorbol dibutyrate (PDBu) with high affinity leading to the activation of PKD1 (Iglesias and Rozengurt, 1999). However, Zn finger 1 has low affinity for PDBu (Iglesias et al., 1998a, Iglesias and Rozengurt, 1999) PKD2 also becomes activated downstream of GPCR via the activation of PLCγ (Rykx et al., 2003). Finally, PKDs can binds phorbol esters with high affinity within the cysteine-rich domain (Rozengurt, 2011).

In response to activation, PKD1 and PKD2 translocate from the cytosol to the nucleus and localize at the Golgi complex and to mitochondria. Therefore, PKD has been implicated in the regulation of multiple biological processes including: cell proliferation, migration, apoptosis and differentiation, membrane trafficking, inflammation, and cancer (Rozengurt, 2011). The exact role of PKD in cellular migration remains controversial with some groups suggesting that PKD acts as a negative regulator for cell migration while other suggest that PKD can drive cancer migration (Alpsoy and Gündüz, 2015, Eiseler et al., 2007, Peterburs et al., 2009).

## 1.8. CXCL12-Independent Activators of CXCR4

While CXCL12 is the major ligand for CXCR4, the CXCR4 receptor can also bind several other CXCL12-independent activators to initiate downstream signalling. Such CXCL12-independent activators include but are not limited to: CXCL14 (discussed in more detail later), ubiquitin, macrophage migration inhibitory factor (MIF) and secreted trefoil factor family 2 (TFF2) (Bernhagen et al., 2007), (Dubeykovskaya et al., 2009, Saini et al., 2010, Tanegashima et al., 2013a). Additionally, there is evidence that CXCR4 can be indirectly activated through cross talk between receptor-tyrosine kinases (RTKs) including but not limited to epidermal growth factor receptor (EGFR), insulin-like growth factor receptor 1 (IGFR-1) and its cognate ligand insulin-like growth factor 1 (IGF-1) (Adachi et al., 2004, Akekawatchai et al., 2005).

Ubiquitin is a highly conserved protein in eukaryotes. It has a major role in the posttranslational modification of proteins and is a natural constituent of plasma (Hershko and Ciechanover, 1998, Asseman et al., 1994). Additionally, while the mechanism of action is unknown, ubiquitin can function as an immune modulator with anti-inflammatory properties that have reduced organ injury in both disease

models and *in vivo* (Majetschak et al., 2003, Majetschak et al., 2008). Furthermore, it has been found that ubiquitin can bind to the CXCR4 receptor and promote intracellular calcium release, chemotaxis and reduce cAMP levels. However, ubiquitin has a ~2-fold lower affinity for CXCR4 than CXCL12 (Saini et al., 2010, Steagall et al., 2014).

The inflammatory cytokine MIF is involved in the regulation of the inflammatory and immune response. However, it is also a strong contributor to inflammatory diseases such as rheumatoid arthritis, systemic lupus erythematosus and systemic vasculitis (Kasama et al., 2011). Bernhagen et al. (2007) identified that both CXCR2 and CXCR4 are functional receptors for MIF. Specifically, MIF triggers the G protein subunits, $G_{\alpha i}$ which stimulated chemotaxis of monocytes and T cells and initiates calcium influx.

TFF2 contributes to the protection of the gastrointestinal mucosa from injury by strengthening and stabilizing mucin gels, stimulating epithelial repair, and decreasing inflammation (Alison et al., 1995, Hoffmann and Jagla, 2002, Oertel et al., 2001). A study by Dubeykovskaya et al. (2009) demonstrated an ability for TFF2 to activate signalling via the CXCR4 chemokine receptor resulting in increased proliferation of receptor-expressing epithelial cancer cells. Additionally, TFF2 was shown to stimulated $Ca^{2+}$ signalling in Jurkat cells through the CXCR4 receptor.

Finally, cross-talk between GPCRs and other receptors has become documented in different cellular system. For example, activation of the RTK, EGFR, normally occurs when the receptor binds to a specific ligand for example epidermal growth factor (EGF) or transforming growth factor (TGFα) (Chia et al., 1995). However, there is evidence that EGFR can be transactivated by CXCR4. Specifically, CXCL12 can induce migration in gastric cancer via Src mediated CXCR4-EGFR cross talk (Cheng et al., 2017). In a separate study by Akekawatchai et al. (2005), IGF-1R was shown to transactivate CXCR4 due to their physical association via the G protein subunits, $G_{\alpha i}$ in the breast cancer epithelial cell lines, MDA-MB-231. This interaction was shown to drive a unidirectional transactivation of the CXCR4 receptor by IGF-1 which lead to cell migration in MDA-MB-231 cells, independent of the CXCR4 chemokine ligand, CXCL12 (Akekawatchai et al., 2005).

## 1.9. Modulation of the CXCR4/CXCL12 Signalling Axis

Aside from modulating CXCR4 downstream signalling via GRKs and arrestins as discussed previously, there are several methods that can modulate the CXCR4/CXCL12 signalling axis. These include: modulating CXCL12 expression; the expression of ACKR3 receptors and via the CXCL14 chemokine (Christopherson et al., 2002, Naumann et al., 2010, Santiago et al., 2011, Salazar et al., 2014, Tanegashima et al., 2013a).

### 1.9.1. Modulation of CXCL12 Expression

As mentioned previously, CXCL12 is expressed in various human tissues by different cells with only blood cells seeming to not express CXCL12. This expression and the activity of CXCL12 is regulated by three main factors: hypoxia, atypical chemokine receptor 3 (ACKR3) scavenging, and posttranslational modifications (Christopherson et al., 2002, Naumann et al., 2010, Santiago et al., 2011).

Hypoxia is characteristically involved in inflammation via the tissue mediator HIF-1 (Hypoxia-Inducible Factor-1). HIF-1 is secreted by fibroblastic and endothelial cells and has been shown to induce CXCL12 expression and secretion due to the presence of a HIF-Response Element (HRE) on the CXCL12 gene promoter (Ceradini et al., 2004, Hitchon et al., 2002, Santiago et al., 2011). Additionally, HIF-2 has been found to be a regulator of CXCL12 expression in multiple myeloma plasma cells, contributing to *in vivo* angiogenesis (Martin et al., 2010).

Secondly, CXCL12 expression can be modulated via ACKR3 (Boldajipour et al., 2008). These receptors can act as a CXCL12 scavenger, influences the chemokines gradient, activate alternative downstream signalling pathway and decreases inflammation. ACKR3 is discussed in more detail later (Boldajipour et al., 2008, Coggins et al., 2014).

Finally, posttranslational modifications can alter the function of CXCL12. These modifications involve both chemical and enzymatic modifications such as: $NH_2$-terminal truncation, COOH-terminal truncation, citrullination, and nitration (Christopherson et al., 2002, Davis et al., 2005, Janssens et al., 2018b, Janssens et al., 2018a, Janowski, 2009, Marquez-Curtis et al., 2008, Staudt et al., 2010, Struyf et al., 2009).

NH2-terminal truncation occurs via serine proteases such as serine protease dipeptidyl peptidases IV (DDP4) and the intracellular serine protease dipeptidyl

peptidases VIII (DPP8). DPP4 cleaves at Ala or Pro residuals creating truncated CXCL12. The truncated CXCL12 is still able to bind the CXCR4 receptor however, it can no longer initiate calcium-dependent signalling or chemotaxis (Christopherson et al., 2002, Janssens et al., 2018b).

COOH-terminal truncation involves enzymes such as secreted carboxypeptidase N, the plasma membrane carboxypeptidase M, and the lysosomal Cathepsin X (Davis et al., 2005, Marquez-Curtis et al., 2008, Staudt et al., 2010). Due to the presence of lysine at the C-terminal end of CXCL12, carboxypeptidase M and N can degrade only the α-isoform of CXCL12 (Davis et al., 2005, Marquez-Curtis et al., 2008). This form of posttranslational modification does not create inactive CXCL12. Instead, it halves the activity of CXCL12 and its receptor binding affinity causing decreased chemotaxis and cell proliferation (Janowski, 2009).

In citrullination, peptidylarginine deiminase (PAD) causes the hydrolysis of the imine group of Arg into a ketone group, resulting in citrulline (Cit) formation (Struyf et al., 2009). This switch from Arg to Cit causes alterations in the structure of CXCL12, thus altering the way in which it can interact and bind with proteins such as CXCR4. This leads to the inhibition of receptor binding thus the loss of signal transduction and chemotaxis (Struyf et al., 2009).

Nitration occurs via the chemical factor peroxynitrite which causes the nitration of amino acids such as tyrosine (Janssens et al., 2018a). Tyrosine nitration reduces intracellular calcium mobilization, IP3 accumulation and ERK1/2 phosphorylation thereby decreasing cellular signalling and migration (Janssens et al., 2018b, Janssens et al., 2018a).

Finally, CXCL12 has a short half-life of ~30 minutes in the bloodstream due to proteolytic degradation by metalloproteinases (DDP4 and MMP2) and leukocyte elastases (Cathepsin G) and by binding to GAGs (Delgado et al., 2001, Lambeir et al., 2001, McQuibban et al., 2001).

### 1.9.2. Atypical Chemokine Receptor 3 (ACKR3)

RDC-1/CXCR7/ACKR3 is a seven transmembrane chemokine receptor that binds CXCL12, CXCL11 the inflammatory cytokine MIF and intermediate opioid peptides such as BAM22, produced in the adrenal cortex (Figure 1.10) (Bachelerie et al., 2014, Szpakowska et al., 2018). After several classifications and reclassifications, this receptor was finally named ACKR3 as it was considered to be an atypical chemokine receptor due to it having a modified

amino acid motif on the second extracellular loop (Bachelerie et al., 2014). Specifically, ACKR3 lacks the specific DRYLAIV motif and presents a DRYLSIT motif on the intracellular side of the receptor (Ulvmar et al., 2011). Originally this motif was thought to be essential for the receptor to couple to the G protein however, when this motif was 'corrected', replacing ICL2 of ACKR3 with that of CXCR4, thus exchanging DRYLSIT with DRYLAIV, it was found that ACKR3 still could not induce G protein signalling (Hoffmann et al., 2012).

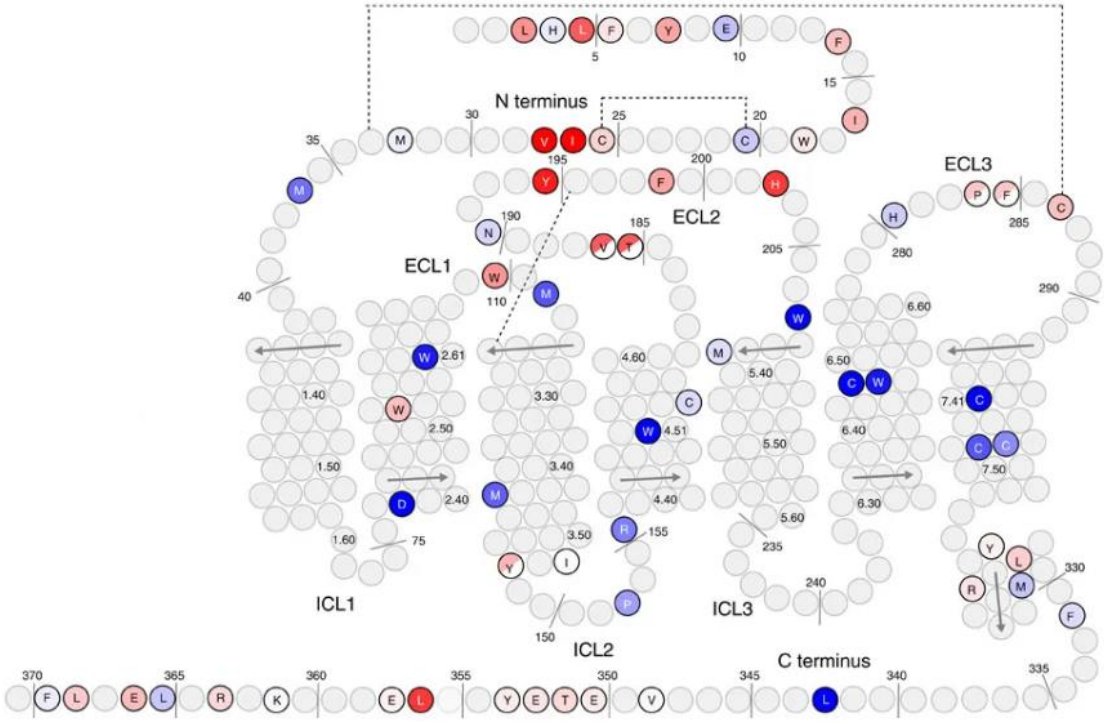


**Figure 1.10: The Structure of ACKR3 (Gustavsson et al., 2017).** ACKR3 has an external N-terminal domain, seven transmembrane domains, three extracellular loops labelled ECL1-3 and three intracellular loops labelled ICL1-3.

ACKR3 has a 10-fold higher binding affinity for CXCL12 than CXCR4, thus has been regarded as a CXCL12 scavenger or decoy receptor, sequestering CXCL12 (and CXCL11) for gradient control (Balabanian et al., 2005, Boldajipour et al., 2008, Coggins et al., 2014, Salazar et al., 2014, Zabel et al., 2009). However, ACKR3 can also initiate downstream signalling independently of CXCR4. Specifically, ACKR3 has been shown to mediate CXCL12-stimulated Akt and ERK activation via β-arrestin 2 in a ligand dependant manner (Coggins et al., 2014, Gravel et al., 2010, Rajagopal et al., 2010). This can lead to receptor internalization, cellular survival, proliferation and chemotaxis in CXCR4 negative cells (Levoye et al., 2009).

Additionally, ACKR3 can negatively modulate CXCR4 signalling by forming CXCR4/ACKR3 heterodimers thus depleting CXCR4 downstream signalling (Levoye et al., 2009, Sierro et al., 2007). This coupling has been shown to mediate a switch from $G_i$ towards a $G_q$ protein signalling, contributing to cellular adhesion as opposed to cellular motility (Scholten et al., 2012). Additionally, it has been found by Levoye et al. (2009) that the formation of the CXCR4/ACKR3 heterodimer caused an alteration in the ability of CXCR4 to induce calcium signalling, thus demonstrating the modulation ability of CXCR4 heterodimer formation. However, ACKR3 has also been found to positively modulate CXCR4 signalling with CXCR4/ACKR3 heterodimers enhancing CXCL12-stimulated intracellular calcium release and ERK1 and ERK2 activation (Sierro et al., 2007). This phenomenon was found in cell lines and animal models with forced overexpression of CXCR4 and ACKR3 and therefore it remains to be determined if this occurs in endogenously expressed cells.

ACKR3 is expressed on a variety of tissues including the heart, brain, spleen, kidneys, lungs, ovaries, testes, thyroid and placenta as well as by granulocytes, lymphocytes, monocytes, T cells and platelets. The receptor has several roles including: dendritic cell differentiation; the maturation of B cells and the switch to B memory cells; the development of the CNS; angiogenesis; neurogenesis; embryogenesis and cardiogenesis (Sánchez-Martín et al., 2011, Heuninck et al., 2019). Similar to CXCR4, ACKR3 expression is also increased in a number of cancer types including leukaemia, breast, pancreatic, colon, and lung (D'Alterio et al., 2016, Gao et al., 2015, Heuninck et al., 2019, Melo et al., 2014, Miao et al., 2007). Additionally, ACKR3 is highly expressed in tumour associated blood vessels but not by normal vasculature suggesting that this receptor has an important role in tumour angiogenesis (Wang et al., 2008). While it is agreed that ACKR3 has modulating effects upon the CXCR4/CXCL12 pathway, there are contradictory studies as to whether ACKR3 is a positive or a negative regulator of cancer metastasis. For example, Wang et al. (2008) found that ACKR3 was highly expressed on the human prostate cancer cell line PCa with increased ACKR3 expression correlating with increased aggression of the tumour due to its ability to enhance cell proliferation, cell survival, adhesion and chemotaxis. Additionally, in lung cancer it has been found that ACKR3 expression can also lead to tumour cell survival, enhanced proliferation and the enhanced progression of lung metastasis (Miao et al., 2007). Finally, Salazar et al. (2014) found that in

the breast cancer cell line MCF-7, the downregulation of ACKR3 caused a decrease in growth related to the inhibition of cell cycle progression shown via increased p21 levels and decreased levels of Cyclin B1. However, in a study by Stacer et al. (2016) mice with deleted ACKR3 receptors actually resulted in greater experimentally-stimulated breast cancer metastasis including metastatic bone cancer. From this they concluded that endothelial ACKR3 expressions supresses tumour growth, vascular intravasation and cellular survival and proliferation of the breast cancer cells.

### 1.9.3. CXCL14

CXCL14, also known as breast and kidney-expressed chemokine (BRAK), is constitutively produced in normal, non-inflammatory epithelial cells (Hromas et al., 1999, Meuter and Moser, 2008). It is ubiquitously expressed in the digestive and urinary tract, breast, brain, muscle, kidney, skin, placenta and tongue in the absence of inflammatory stimuli. During inflammation, expression of CXCL14 is downregulated, suggesting that CXCL14 plays a role in the maintenance of tissue homeostasis (Hevezi et al., 2009, Hromas et al., 1999, Kurth et al., 2001, Meuter and Moser, 2008, Schaerli et al., 2005, Sleeman et al., 2000). Specifically, a study by Meuter and Moser (2008) demonstrated that CXCL14 had a role in the recruitment of immune surveillance cells to sites of non-inflamed epithelial tissue, thus CXCL14 is involved in local chemoattractant-unrelated processes. Alternatively, studies by Dai et al. (2015) and Maerki et al. (2009) found a novel role for CXCL14 in antimicrobial defence against bacteria and fungi that cause respiratory tract or skin infections such as S*treptococcus pneumonia, Candida albicans* and *Escherichia coli* but not the Gram-negative bacteria *Pseudomonas aeruginosa*.

A study by Tanegashima et al. (2013a) found that CXCL14 could bind to CXCR4 with high affinity. CXCL12 and CXCL14 have been demonstrated to be conserved all the way back to the zebrafish and so it is suggested that they have evolved together (Huising et al., 2004). Tanegashima et al. (2013a) have therefore suggested that CXCL14 as well as ACKR3 (also been found to be conserved to the zebrafish) are proteins that can in fact modulate or fine-tune the CXCR4/CXCL12 signalling axis (Huising et al., 2004). However, other studies have found that blood monocytes, neutrophils, NK cells and dendritic cells (DCs) do in fact migrate in response to CXCL14 (Cao et al., 2000, Kurth et al., 2001, Schaerli et al., 2005, Shellenberger et al., 2004, Starnes et al., 2006).

In a study by Collins et al. (2017) it was found that CXCL14 on its own did not induce CXCR4 signalling. However, CXCL14 could synergise with CXCL12 and stimulated increased CXCR4 downstream signalling and redistribute CXCR4 at the cell surface. Therefore, it was postulated that while CXCL14 and CXCL12 were shown to not form a heterodimer, CXCL14 acts as a positive allosteric modulator of CXCR4 that enhances the potency of CXCR4 ligands rather than acting as a negative modulator of CXCR4 signalling as originally suggested by Tanegashima et al. (2013a).

Not only is the role of CXCL14 in a healthy environment still to be fully elucidated, the expression of CXCL14 and role in cancer and tumour progression is also controversial. CXCL14 has been shown to act as a natural inhibitor of CXCL12 and possessed a tumour suppressor function against carcinoma cells (Tanegashima et al., 2013a, Tanegashima et al., 2013b). Furthermore, it has been suggested that CXCL14 has anti-tumour activity by supressing tumour growth (Frederick et al., 2000, Ozawa et al., 2006, Schwarze et al., 2005). Several studies have shown that CXCL14 becomes downregulated in several human tumours to enable tumour progression (Frederick et al., 2000, Hromas et al., 1999, Ozawa et al., 2006, Shellenberger et al., 2004, Shurin et al., 2005). However, other studies support a pro-tumorigenic role of CXCL14 in both prostate and pancreatic cancer (Augsten et al., 2009, Wente et al., 2008).

## 1.11. The Progression of Cancer Metastasis

While cellular migration is necessary during gastrulation as well as in adults for tissue repair and immune surveillance, in cancer this leads to metastasis, the cause of 90% of cancer related deaths (Chaffer and Weinberg, 2011, Ridley et al., 2003). As opposed to invasion where cancer cells migrate to adjacent tissues, metastasis is defined as the spread of cancer from one organ to another non-adjacent organ (Yokota, 2000). Metastasis of a solid tumour involves multiple steps: the detachment of cancer cell(s) from the primary tumour, invasion and migration, intravasation, survival in the circulation, extravasation and finally the colonization of the micrometastasis followed by its proliferation and induction of angiogenesis at the secondary tumour site (Figure 1.11). For haematopoietic metastases which are already found within the circulatory and lymphatic system, the first steps of metastasis (cellular detachment, invasion and migration, intravasation) are not required (Trendowski, 2015). Additionally, due to their cell type, haematopoietic metastases tend not to cluster to topographical area or

organs with the exception of metastases to the CNS and endocrine system in regards to ALL. Instead, metastasis is often found throughout the lymphatic system including lymph nodes and the spleen. Specifically, in CLL metastasis occur via a lymphatic route rather than cardiovascular route with metastases found commonly within the lymph nodes, kidney, adrenals and the heart (Viadana et al., 1978).

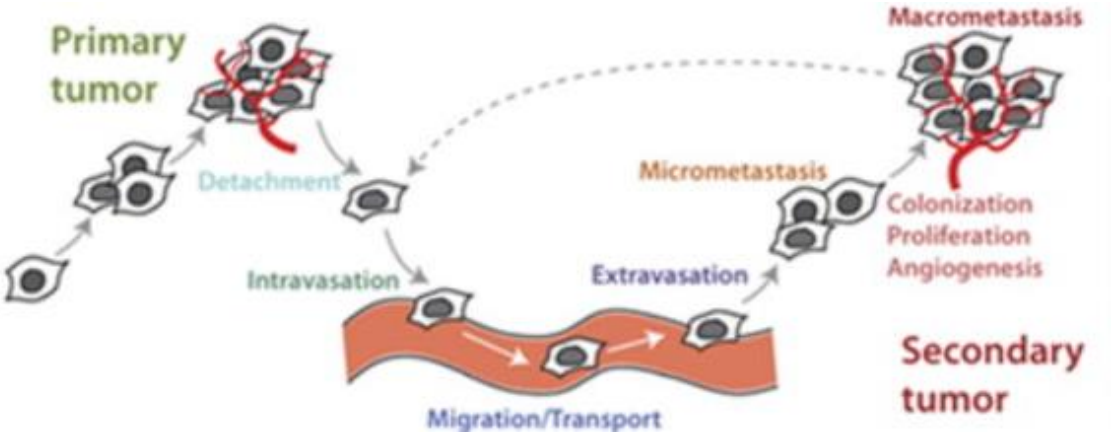


**Figure 1.11: The Progression of Cancer Metastasis (Trendowski, 2015).** Once cell(s) have detached from the primary tumour, metastasis of a solid tumour involves multiple steps: invasion and migration, intravasation, survival in the circulation, extravasation with the final step of the micrometastasis colonizing, proliferating and undergoing angiogenesis at the secondary tumour site.

### 1.11.1. Loss of E-Cadherin and Cancer Cell Detachment

To begin cancer metastasis, an adherent cancer cells needs to break away from the primary tumour to become motile and follow a chemoattractive path through the extracellular matrix to secondary sites. This process begins with the loss of cell-cell adhesion molecules such as E-cadherin (Yilmaz and Christofori, 2010). Therefore, tumour cells lose their epithelial morphology and display a mesenchymal morphology in a process called epithelial-to-mesenchymal transition (EMT) (Thiery and Sleeman, 2006). The loss of E-cadherin occurs during malignant progression in almost all epithelial cancers and therefore serves as an indicator for a poorer prognosis (Yilmaz and Christofori, 2010). Such loss of E-cadherin function can occur due to many factors such as germline or somatic gene mutations, chromosomal aberrations, transcriptional repression, DNA hypermethylation of the E-cadherin gene as well as an aberrant CXCR4/CXCL12 signalling axis (Hu et al., 2014, Yilmaz and Christofori, 2010).

### 1.11.2. Cancer Cell Migration

#### 1.11.2.1. Lamellipodium Extension in Mesenchymal Migration

Once the cell has released from the main tumour mass, it is directed to a secondary site via chemokines and growth factors which bind to cell surface receptors on the tumour cell (Condeelis and Segall, 2003). This initiates the first stage of cellular migration; the creation and extension of a large brush-like lamellipodia called the leading edge made from sheets of F-actin as demonstrated in Figure 1.12 (Olson and Sahai, 2009). Additionally, the creation of spike-like filopodia can occur. These serve as sensors to explore and potentially modify the environment as well as interact with other cell in the TME (Kurosaka and Kashina, 2008). However, their role in chemotaxis and their forward propelling movement have yet to be studied in detail (Jacquemet et al., 2015).

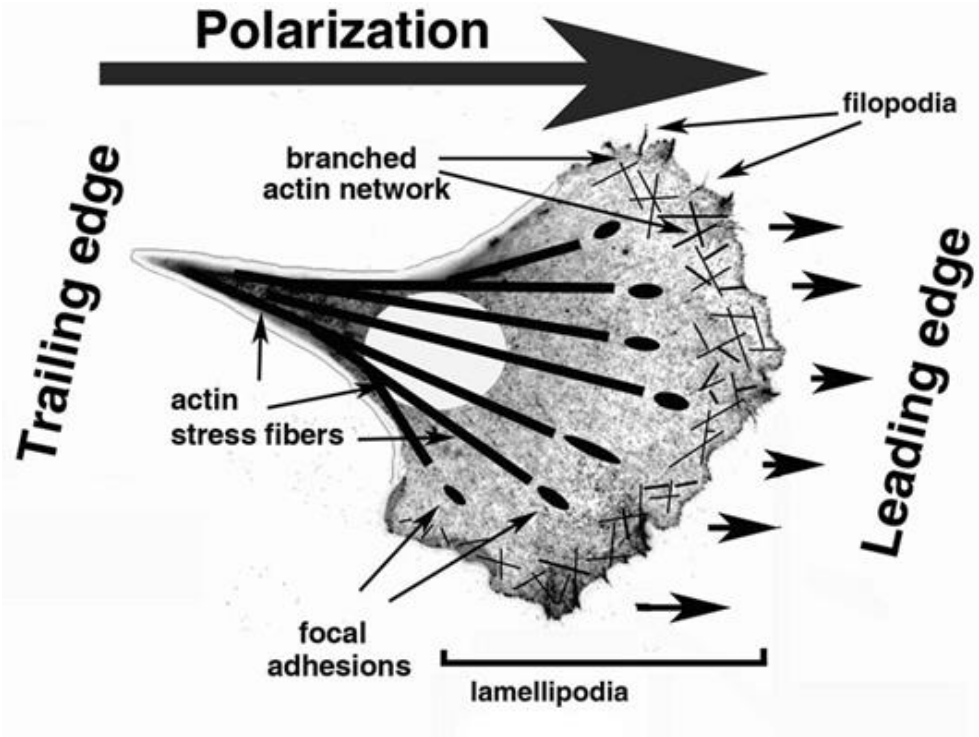


**Figure 1.12: The Cell Biology of Mesenchymal Cell Migration (Kurosaka and Kashina, 2008).** A general representation of an adherent cell during mesenchymal migration. Signalling molecules such as chemokines and growth factors create a polarization gradient that defines the leading and the trailing edge of the cell, thus the direction of cellular migration. Actin fibres enable the protrusion of the lamellipodia responsible for the directionality of the leading edge. Filopodia do not contribute to the movement of the cell but act as environmental sensor. Following protrusion extension, the cell attaches to the extracellular matrix via focal adhesions.

Actin polymerization drives lamellipodium protrusions (Condeelis and Segall, 2003). F-actin polymerisation begins with the aggregation of at least three G-actin monomers to form a stable actin nucleus structure via a process called nucleation. This can then be extended through the addition of G-actin monomers to the barbed (+) end (Ireton, 2013). F-actin filaments have fast-growing barbed (+) ends and slow-growing pointed (-) end, which orientates the polarity of the filaments and drives the directionality of cellular movement (Pollard and Borisy, 2003). This process of F-actin polymerisation is facilitated by the dimeric protein formin (Figure 1.13). Formin (consisting of F1 and F2 domains) forms a ring structure at the barbed end of the F-actin filament and both removes and blocks protein capping (Ireton, 2013). Following this, a second protein, profilin, binds and catalyses the exchange of ADP for ATP on the G-actin monomer which promotes F-actin stability, before trafficking the G-actin monomer to the barbed end, promoting extension (Ireton, 2013, Pollard and Borisy, 2003).

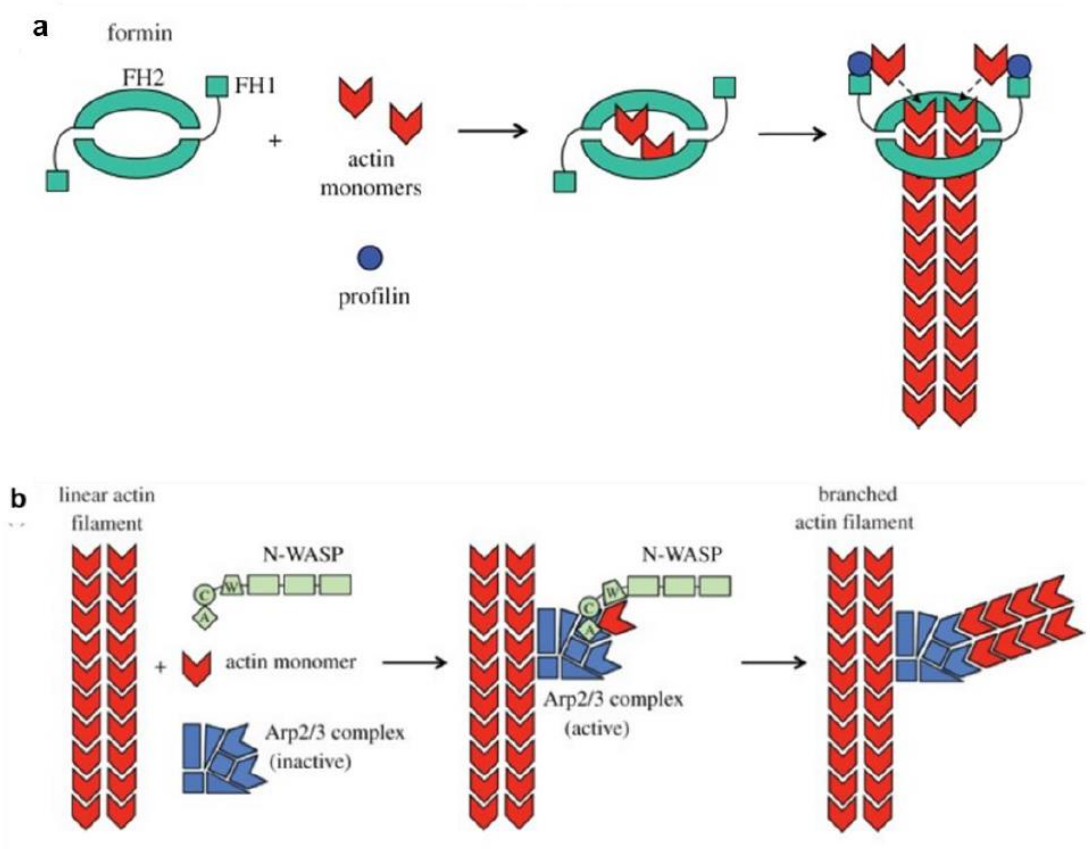


**Figure 1.13: The Molecular Mechanisms Facilitating F-Actin Polymerisation (Ireton, 2013). a)** Formin proteins function as dimers and use two domains, FH1 and FH2, to stimulate the assembly of linear actin filaments. Following this, profilin, promotes F-actin stability, before trafficking the G-actin monomer to the barbed end to promote extension. **b)** To assemble new actin filaments at the side of existing filaments, Arp2/3 and N-WASP complex and stimulate Arp2/3-mediated actin polymerization.

For directional movement to be established, the cell not only has to move in a forward direction but also weave through the ECM. Therefore, actin filaments can also be formed at a 45° angle from the original F-actin stem (Ireton, 2013). This is established via a cascade of events beginning with the Rho family of small GTP binding proteins (GTPases). These proteins are activated by guanine nucleotide exchange factors (GEFs) and inactivated by GAPs (Ridley et al., 2003). Three Rho GTPases are required for actin polymerisation: RhoG, Rac and Cdc42. RhoG acts upstream of Rac by binding and activating the Rac-GEF complex. In turn, Rac-GEF binds to and activates WAVE at the cell membrane. Cdc42 will bind a similar protein, WASP, with both WAVE and WASP targeting the Arp2/3 complex. This complex binds to the side or tip of pre-existing actin filaments, inducing the formation of new daughter filaments via actin polymerization

(Raftopoulou and Hall, 2004). These WAVE/WASP proteins can themselves regulate the activity of Rac and Cdc42 by binding to either GAPs or GEFs thus creating positive and negative feedback loops. Cdc42 is a master regulator of cellular polarization and is only active towards the front of the migrating cell and therefore by activating and inactivating this protein, lamellipodia direction can be dictated (Frugtniet et al., 2015). Sossey-Alaoui et al. (2007) found that downregulating WAVE3 in SCID mice significantly reduced the number of lung metastasis from the primary breast cancer, implicating the importance of these proteins in cancer metastasis.

#### 1.11.2.2. Formation of Focal Adhesions and Secretion of Surface Proteases

The third event in the migration of a cell is focal adhesion formation between the extending lamellipodia and the ECM creating traction. Specifically, integrins on the cell surface interact with ECM ligands such as focal adhesion kinase (FAK), α-actinin and talin (Gilmore and Burridge, 1996). Depending upon the mode of cell motility: mesenchymal, amoeboid or collective (see later), the cell may be required to secrete proteases to digest the ECM (Parri and Chiarugi, 2010). For example in fibrosarcoma which has mainly mesenchymal cell motility, Rac1 can mediate the activation of MMP2 enabling the invading tumour cell to digest type 21 collagen rich stroma and therefore enabling cellular invasion (Zhuge and Xu, 2001).

In addition to the formation of focal adhesions, specific structures called podosomes and invadopodia have been implicated in cancer cell migration (Spinardi and Marchisio, 2006, Weaver, 2006). These structures are similar to one another in that they are both small finger-like projections with central tubular invaginations that have an actin rich core that is surrounded by adhesion and scaffolding proteins such as $\beta_1$ and $\alpha_V\beta_3$ integrins and CD44 a cell surface glycoprotein (Spinardi and Marchisio, 2006, Weaver, 2006). Generally, when these structures are found in normal cell types they are referred to as podosomes and when they are found in migrating cancer cell they are referred to as invadopodia that are thought to protrude further into the ECM and are stable for hours. The functions of these structures are to enable the adhesion of the cancer cell to the ECM as well as recruiting and activating proteases such as MMP2, MMP9, and MTI-MMP to enable the degradation of the ECM, facilitating cellular migration through the tissue (Murphy and Courtneidge, 2011).

#### 1.11.2.3. Cell Body Contraction

Cellular contraction occurs via actin-myosin contraction forces. F-actin, that creates the lamellipodia, assembles together with myosin II filaments to form a complex (Ridley et al., 2003). The phosphorylation of the myosin light chain (MLC) releases the myosin heavy chain tail. This enables the myosin head to associate with the F-actin and contract or 'walk' to the actin barbed end (Olson and Sahai, 2009). Myosin phosphorylation is regulated by multiple kinases including but not limited to, MLC kinase (MLCK) and/or Rho-associated serine/threonine kinase (Rock) (Ridley et al., 2003).

#### 1.11.2.4. Tail Detachment

The final step in mesenchymal motility is the detachment of the tail. This occurs by blocking myosin II assembly via the inhibition of Rho kinase and the action of the protease calpain that can cleave focal adhesions such as talin and integrins (Potter et al., 1998, Xu et al., 2003).

### 1.11.3. Intravasation and Entrance into the Circulation

Cells that manage to migrate and break through the endothelium of the circularity system (intravasation) can then gain access to the blood circulatory system (Trendowski, 2015). Cells must then survive a specific form of apoptosis called anoikis, programmed cell death of cells that are anchorage dependant (Kim et al., 2012).

### 1.11.4. Extravasation and Colonization

Largely due to chemokine signalling, the detached metastatic cell approaches an organ suitable for secondary growth (Trendowski, 2015). The metastatic cell then undergoes a process of rolling and firm adhesion as described in Chapter 1.6. Finally cells then undergo extravasation, revert back to an epithelial morphology via mesenchymal-to-mesenchymal transition (EMT) and begin to colonize the secondary location (Chaffer and Weinberg, 2011).

### 1.11.5. Mesenchymal to Amoeboid Transition (MAT) and Collective to Amoeboid Transition (CAT)

While mesenchymal migration was described above, two other types of cellular movement exist; amoeboid and collective cellular migration, see Figure 1.14 and Table 1.2. Mesenchymal motility, is characteristically slow due to the lengthy process of actin protrusion formation and ECM digestion (Friedl and Wolf, 2003). Additionally, cells that undergo mesenchymal migration, such as fibroblasts,

adhere strongly to the external substratum, contributing to slower migration (Paňková et al., 2010). While mesenchymal cell migration has been termed ‘path generating’ due to their ability to degrade the ECM, a second mode of cellular migration, amoeboid migration, has been termed ‘path finding’ (Talkenberger et al., 2017). This description arises from amoeboid cells being more rounded and deformable than elongated mesenchymal cells. Additionally, amoeboid cells have weak ECM adhesion and low to absent proteolytic activity (Bear and Haugh, 2014). Generally, amoeboid cells are suspended in aqueous environments with successful migration involving a transition from Rac mediated mesenchymal migration to RhoA/ROCK activation of actomyosin contraction to form blebs (Morley et al., 2014). However, it has more recently been found that there are multiple ways in which amoeboid cells can migrate: using blebs or via pseudopods (Titus and Goodson, 2017). Specifically, ‘α-motility’ describe amoeboid cell crawling via pseudopodia rather than blebs. In this form of motility dynamic 3D pseudopods form at the leading edge of the migrating cell that is filled with branched actin networks assembled by the Arp2/3 complex, activated by WASP and WAVE in a similar manner to mesenchymal migration (Fritz-Laylin et al., 2017).

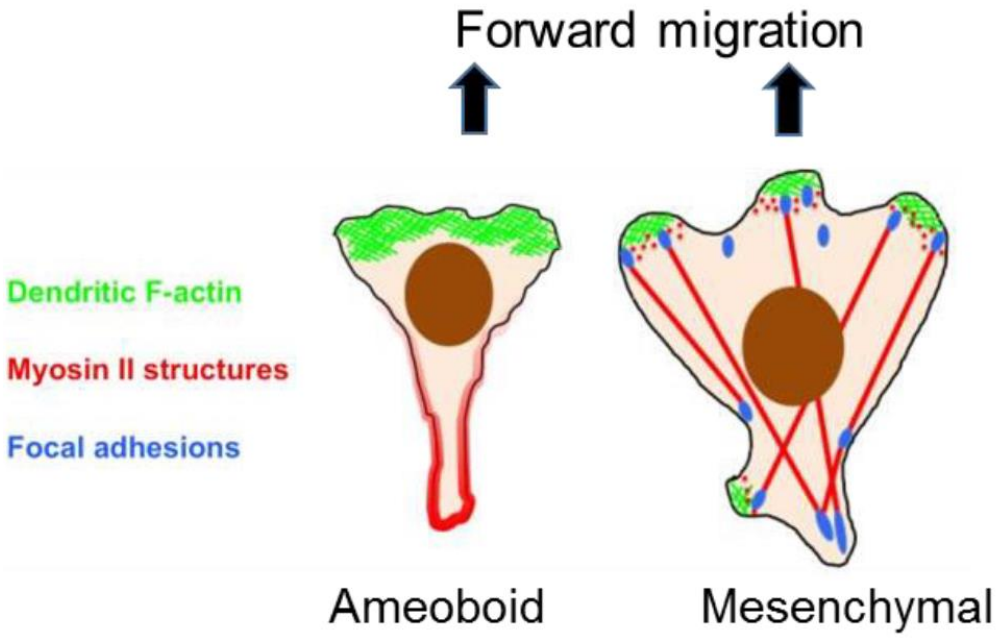


**Figure 1.14: Difference Between Amoeboid and Mesenchymal Cell Migration (Bear and Haugh, 2014).** Both mesenchymal and amoeboid cell migration is characterised by F-actin formation in the direction of migration. However, while mesenchymal migration requires the formation of focal adhesion to adhere to the substratum, amoeboid migration does not. Therefore, amoeboid cells migrate much faster than mesenchymal.

**Table 1.2: Difference Between Amoeboid and Mesenchymal Cell Migration (adapted from (Bear and Haugh, 2014).**

| | **Amoeboid** | **Mesenchymal** |
|---|---|---|
| **Migration Speed** | Fast 10 μm/min | Slow >1 μm/min |
| **Polarity** | Well defined at the front and the rear | Multiple competing lamellipodia |
| **Adhesion** | Weak | Strong |
| **Migration Mechanics** | Squeezing through pores in the ECM | Traction via adhesion to the ECM with matrix degradation if necessary |
| **Organisation of Actin Cytoskeleton** | F-actin network at the front. Corticol actomyosin mediates contractility beneath plasma membrane | F-actin in lamellipodia. Actin-myosin minifiliments mediate contraction at the leading edge and form stress fibres attached to focal adhesions |
| **Common Receptor Used for Chemotaxis** | GPCR | RTKs |
| **Example Cell Type** | Leukocytes | Fibroblasts |

Both mesenchymal cells and amoeboid cells can migrate individually however, only mesenchymal cells migrate collectively as clusters. In this form of motility, cells retain their cell-to-cell tight junctions, thus they migrate in sheets or in strands (Friedl and Mayor, 2017). This type of movement is found in distinct cancer types such as in breast cancer, prostate cancer, squamous cell carcinoma, colon cancer amongst others (Cheung and Ewald, 2016, Ilina and Friedl, 2009, Zhang et al., 2015a). Collective migration is reliant upon integrins, particularly β1-integrin mediated focal adhesions. Additionally, MT1-MMP is required at the leading edge to digest collagen and to generate an ECM track. This creates specific orientation without the need for support by stroma cells, which is required in mesenchymal motility (Friedl and Wolf, 2008, Wolf et al., 2007).

As both mesenchymal and collective migration is relatively slow, in response to environmental or epigenetic cues, such as the silencing of MMPs, cells can undergo mesenchymal to amoeboid transition (MAT) or collective to amoeboid transition (CAT) that is much faster (Parri and Chiarugi, 2010). For example, fibroblast cells utilize mesenchymal migration when in contact with the ECM but undergo MAT to form fast bleb-based amoeboids when in aqueous environments (Fritz-Laylin et al., 2017). Amoeboid motility is dependent upon RhoA and ROCK to enable its rounded morphology and is used by the majority of carcinoma cells such as colon carcinoma. This increased speed of movement is due to the cells being independent from cell-ECM contact and it does not require proteases. Instead, the cell simply squeezes through gaps in the ECM. The propulsion force that enables this movement is created via actomyosin contraction forces and therefore does not require Rac driven cell polarisation (Sahai and Marshall, 2003, Wolf et al., 2003).

## 1.10. The Role of the CXCR4 in Cancer and Cancer Metastasis

CXCR4 has a prominent role in disease including HIV infection, autoimmune disease and in cancer. Generally, CXCR4 expression is low or absent in many normal tissues however, CXCR4 is the most commonly overexpressed chemokine receptor on tumour cells. To date, aberrant CXCR4 expression has been detected in more than 30 human cancers including but not limited to: acute myeloid leukaemia (AML), breast, ovarian, melanoma, thyroid, renal, pancreatic, prostate cancer and more recently salivary gland neoplasms (Borrello et al., 2005, Koshiba et al., 2000, Mehta et al., 2007, Müller et al., 2001, Scotton et al.,

2001, Singh et al., 2004, Staller et al., 2003, Vela et al., 2015, Phattarataratip and Dhanuthai, 2017). A recent study by Kang et al. (2019) demonstrated that tumour hypoxia is causal to CXCR4 overexpression. Hypoxia is a major feature of solid tumours due to a lack of blood supply (Vaupel, 2008). Prolonged hypoxia in tumours can alter cellular behaviour and causal to tumours acquiring a more aggressive phenotype (Alqawi et al., 2007, Yamamoto et al., 2008).

Considering the normal functioning of the CXCR4/CXCL12 signalling axis in cellular survival, proliferation and chemotaxis, cancer cells that overexpress CXCR4 will have a more aggressive phenotype thus a poorer prognosis (Chatterjee et al., 2014, Johnson et al., 2004). This prognosis is due to the cancer cells 'hijacking' the CXCR4/CXCL12 signalling axis to establish pro-tumorigenic functions such as distant organ metastasis which is corroborated by the fact that CXCL12 expression is highest in common sites of metastasis such as brain, bone marrow, lungs, and liver (Sarvaiya et al., 2013). For example, Müller et al. (2001) demonstrated that the CXCR4/CXCL12 signalling axis was able to regulate breast cancer metastasis. In AML it has been found that the CXCR4/CXCL12 signalling axis is required for the survival and maintenance of immature white blood cells called blast cells that increase in number as the cancer progresses (Abraham et al., 2015). Also, mutations in the von Hippel-Lindau (vHL) tumour suppressor gene causes increased HIF-1α expression in malignant cells. HIF-1α in turn regulates NFκB, which induces CXCR4 expression in human renal cell carcinoma (RCC) cells (Staller et al., 2003). Studies of pancreatic tissue samples found that constitutively expressed CXCL12 significantly increased cancer cell migration into other areas of the pancreas (Koshiba et al., 2000). Additionally, Marchesi et al. (2004) found that several pancreatic samples displayed a 46,000 fold-increased expression of CXCR4 when compared to normal, healthy tissue. In the thyroid, the rearrangement of the RET RTK gene to generate RET/PTC oncogenes stimulated the expression of many genes including CXCR4 which enabled increased inflammation and tumour invasion (Borrello et al., 2005). Finally, it was found by Kato et al. (2003) that elevated CXCR4 expression significantly correlated to increased lymph node metastasis.

As such, CXCR4 acts as a poor prognostic marker (Akashi et al., 2008, Spoo et al., 2007, Zhang et al., 2014, Zhang et al., 2015b). For example in breast cancer, 40% of tumours have elevated levels of CXCR4 with 67% of invasive

breast tumours having increased expression and 75% of triple negative breast tumours having elevated levels of CXCR4 (Chatterjee et al., 2014).

The overexpression of CXCR4 is the most predominant cause of CXCR4 related metastasis however, a few studies have found evidence of CXCR4 mutation. For example, Crowther-Swanepoel et al. (2009) found truncated and missense mutations of CXCR4 in chronic lymphocytic leukaemia (CLL) that could affect the functioning of this receptor. Additionally, somatic mutations in CXCR4 occurs in 30-40% of patients with a B-cell malignancy called Waldenström macroglobulinemia (WM). These mutations effect CXCR4 signalling, promoting AKT and ERK1/2 signalling which leads to drug resistance in the presence of the ligand CXCL12. WM patients with CXCR4 mutations also have higher bone marrow disease due to the retention of neutrophils (Hunter et al., 2017).

Chemokines not only interact directly with tumours cells but can also interact with cells in the tumour microenvironment (TME) including: mesenchymal stem cells (MSC), monocytes/macrophages, T cells, B cells, NK cells, adipocytes, pericytes etc. (Balkwill et al., 2012). MSC can differentiate into cancer associated fibroblasts (CAFs) with both MSC and CAFs constitutively secreting CXCL12 enabling their recruitment to the CXCR4 expressing tumour (Eck et al., 2009). This creates high intra-tumour CXCL12 levels that in turn attract other pro-tumorigenic cells including pro-tumorigenic tumour associated macrophages (TAMs), vascular cells and stromal cells. These cells secrete growth factors, cytokines, chemokines and proangiogenic factors further promoting tumour growth (Mantovani et al., 2017).

The CXCR4/CXCL12 signalling axis can also induce angiogenesis, enabling vessel production and therefore tumour growth. These processes are stimulated by hypoxia that causes the upregulation of vascular endothelial growth factor (VEGF), the most potent regulator of angiogenesis. In turn, VEGF can induce the expression of CXCL12, which recruits other pro-tumorigenic CXCR4 expressing cells (Liang et al., 2007). CXCL12 can also induce the production of MMP1 and tumour necrosis factor (TNF) that increased the inflammatory process and induce tumour cell migration (Porcile et al., 2005).

## 1.12. Currently Used and Experimental CXCR4 Antagonists

Considering the roles that the CXCR4/CXCL12 signalling axis has in promoting tumour progression and metastasis, the inhibition of this pathway can potentially lead to reduced malignancy. Investigations into inhibitors of this

pathway has led to the discovery of several inhibitors including: non-peptide CXCR4 antagonists such as the bicyclam derivative AMD3100; small-peptide CXCR4 antagonists such as T140 and its derivative TN14003; CXCR4 antibodies; antagonists for CXCL12 and CXCR4 nanobodies amongst others (Table 1.3) (Chatterjee et al., 2014, Walenkamp et al., 2017). With this in mind, only two CXCR4 antagonistic compounds are available for therapeutic use: AMD3100 and CTCE-9908.

AMD3100 (also known as Mozobil™ or Plerixafor) is a bicyclam chemical compound that was originally found to have good anti-HIV activity by competitively binding to CXCR4 and therefore preventing the binding of CXCL12 (Figure 1.15) (Fricker et al., 2006). While AMD3100 treatment in HIV patients was discontinued due to cardiac toxicity, patients with non-Hodgkin's lymphoma (NHL) and multiple myeloma (MM) that were treated with AMD3100 and granulocyte colony-stimulating factor (G-CSF) had significantly increase mobilization of CD34+ hematopoietic stem cells from the bone marrow to peripheral blood (DiPersio et al., 2009a, DiPersio et al., 2009b, Cojoc et al., 2013). Therefore, in 2008 the US FDA approved the use of AMD3100 for autologous stem cell transplantation in MM and NHL patients. During this procedure, AMD3100 is used to mobilize healthy stem cells from the bone marrow to the blood whereupon these stem cells are harvested. These harvested healthy cells can then be given back to the patient (DiPersio et al., 2009b, Liles et al., 2003). There is also evidence that AMD3100 can sensitize cancer cells to conventional chemotherapy and radiotherapy as well as helping to overcome TME driven immunosuppression (Barker et al., 2015, Domanska et al., 2012, Moding et al., 2013, Uy et al., 2017, Walenkamp et al., 2017). Additionally, AMD3100 can be radiolabelled for use in PET and CT imaging. Nimmagadda et al. (2010) chelated the transition metal $^{64}$Cu with AMD3100 and demonstrated its ability to image lung metastasis from MDA-MB-231 primary breast tumours via PET. Not only can imaging be used to identify primary and secondary metastatic tumours, but it can aid in staging and the selection of patients for beneficial CXCR4-directed radionuclide therapy as seen in both MM and small cell lung cancer patients via [$^{68}$Ga]Pentixafor-PET/CT (Lapa et al., 2016, Lapa et al., 2017). Research is also looking into using AMD3100 as a method of tumour specific delivery of nanomaterials. It was shown that by using AMD3100, there was enhanced delivery of the nanomaterial to CXCR4 overexpressing tumours

demonstrating their application in nanomaterial based drug delivery of materials such as photosensitizers, anticancer drugs as well as for the diagnosis and staging of tumours as an imaging agent (Ko et al., 2018). Despite the success of AMD3100 in the clinic, it does have its drawbacks. The compound has a very short half-life of 3.5-5 hours hence multiple doses are required daily. Additionally, it must be administered via injection which increases unnecessary patient hospitalisation and has several side effects including pain at the injection site, headache, bloating, nausea and diarrhoea (Parameswaran et al., 2011, Liles et al., 2003, DiPersio et al., 2009a). Finally, it is only a weak partial agonist of CXCR4 therefore, the development of other CXCR4 inhibitors is paramount (Uy et al., 2017).

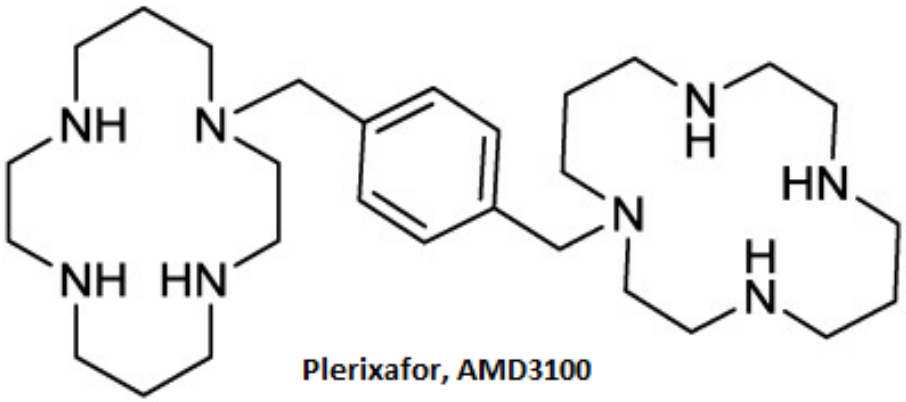


**Figure 1.15: The Structure of Plerixafor, AMD3100 (Debnath et al., 2013).** AMD3100 is a bicylam compound composed of two cyclam rings linked through an aromatic linker.

The second CXCR4 peptide antagonist that was approved was CTCE-9908. Less is known about this compound except that it is a 17 amino acid analogue of CXCL12 which has been granted approval by the FDA for the treatment of osteosarcoma (Wong et al., 2014).

Aside from these two compounds, the search for other CXCR4 antagonists focuses mainly on peptide derivatives including MSX-122, the highly potent CXCR4 antagonist T140 (no longer in clinical trial) and its derivative TN14003 (Debnath et al., 2013, Gaur et al., 2018, Sison and Brown, 2011). These efforts were followed by the development of antibodies specifically directed against CXCR4 (Walenkamp et al., 2017). For example, BMS-936564/MDX-1338 is a fully human anti–human CXCR4 IgG4 monoclonal antibody that completed phase I clinical trials. Specifically, BMS-936564 binds to the ECL2 of CXCR4 preventing CXCL12 binding (Kuhne et al., 2013). Additionally, the development of fully

human single-domain antibody-like scaffolds (termed *i-bodies*) with activity against human CXCR4 have been reported but have yet to enter clinical trials (Griffiths et al., 2016). Anti-CXCR4 nanobodies have also been developed, the first of which, ALX-0651, failed to complete clinical trials (Ramsey and McAlpine, 2013, Vela et al., 2015). However, there are several new anti-CXCR4 nanobody candidates for example: 238D2 and 238D4 which were shown to bind to CXCR4 with high affinity and prevent CXCL12 binding. When these nanobodies were linked together to form a biparatopic nanobody, it had increased potency related to its ability to bind to two CXCR4 receptors that were in close proximity. However, these have yet to enter clinical trials (Jähnichen et al., 2010). Peptide mimic CXCR4 agonists such as ATI-2342, NUCC-390 and NUCC-398 are also under preclinical development (Mishra et al., 2016). Other agents or strategies for interfering with the CXCR4–CXCL12 axis include the anti-CXCL12 aptamer (also called a PEGylated Oligonucleotide (Spiegelmer) NOX-A12 that is currently in clinical trials and RNA interference (Liang et al., 2005, Vater et al., 2013). A comprehensive list of some of the more recent CXCR4/CXCL12 signalling axis inhibitors that are in preclinical development or are in clinical trials for use as cancer therapeutics are listed in Table 1.3.

**Table 1.3 CXCR4/CXCL12 Signalling Axis Inhibitors Under Pre-Clinical Development, in Clinical Trials or Approved for use as Cancer Therapeutics**

| Type | Agent | Other Names | Stage of Development | Reference(s) |
|---|---|---|---|---|
| Non-Peptide CXCR4 Antagonist | Plerixafor | AMD3100, Mozobil | In Clinical Use | (DiPersio et al., 2009a) |
| Non-Peptide CXCR4 Antagonist | AMD3465 | | Completed phase II clinical trials 2017 | (Bodart et al., 2009) |
| Small-peptide CXCR4 Antagonist | MSX-122 | | Phase I clinical trials suspended 2008 but may be resumed | (Debnath et al., 2013) |
| Small-peptide CXCR4 Antagonist | TG-0054 | Burixafor | Completed phase II clinical trials 2018 | (Rettig et al., 2012) |
| Small-molecule CXCR4 Antagonist | X4P-001 | AMD11070, Mavorixafor | Currently undergoing phase I/II clinical trials. Estimated completion 2020 | (Portella et al., 2013) |
| Peptide CXCR4 Antagonist | TN14003 | BKT140, BL-8040, TK140 | Currently undergoing phase II clinical trials. Estimated completion 2020 | (Sison and Brown, 2011, Gaur et al., 2018) |
| Peptide CXCR4 Antagonist | CTCE-9908 | | In clinical use for osteosarcoma. | (Hassan et al., 2011, Wong et al., 2014) |
| CXCR4 Antagonist | USL311 | | Currently undergoing phase I/II clinical trials. Estimated completion 2022 | (Walenkamp et al., 2017) |
| Anti- CXCR4 IgG4 Monoclonal Antibody | MDX-1338 | BMS-936564, Ulocuplumab, Medarex | Completed phase I clinical trials 2014 | (Kuhne et al., 2013) |
| Anti- CXCR4 IgG4 Monoclonal Antibody | LY2624587 | | Completed phase I clinical trials 2012 | (Peng et al., 2016) |

| | | | | |
|---|---|---|---|---|
| Fully Human Single-Domain Antibody-like Scaffold (*i-body*) | *i-body* | | Preclinical development | (Griffiths et al., 2016) |
| Anti-CXCL12 PEGylated Oligonucleotide (Spiegelmer) | NOX-A12 | | Currently undergoing phase I/II Clinical Trials. Estimated completion 2022 | (Vater et al., 2013) |
| Polyphor | POL6326 | Balixafortide | Recruiting for phase III clinical trials. Estimated completion 2022 | (de Nigris et al., 2012) |
| CXCR4 Pepducins Antagonist | PZ-218 and PZ-210 | | Preclinical development | (O'Callaghan et al., 2012) |
| Anti-CXCR4 Nanobody | ALX-0651 | | Phase I clinical trials terminated 2012 | (Vela et al., 2015, Ramsey and McAlpine, 2013) |
| Anti-CXCR4 Biparatopic Nanobody | 238D2-238D4 | | Preclinical development | (Jähnichen et al., 2010) |
| Small molecule CXCR4 Agonist | NUCC-390 and NUCC-398 | | Preclinical development | (Mishra et al., 2016) |
| CXCR4 Agonist | ATI-2342 | | Preclinical development | (Mishra et al., 2016) |
| RNA interference (RNAi) | | | Preclinical development | (Liang et al., 2005) |

## 1.13. Potential Reasons for the Clinical Failures of GPCR Antagonists

Despite the clinical success of AMD3100 and CTCE-9908, there have been far more failures in the search for CXCR4 antagonists. These failures are owing to several causes including but not limited to: chemokine and chemokine receptor promiscuity; insufficient levels of the drug in the plasma i.e. insufficient receptor occupancy and blockade; unwanted off-target effects; poor drug-like properties; poor relevance of the target receptor to the disease; species differences between the animal models causing incorrect clinical indication and chemokine receptor and disease heterogeneity within the same species (Horuk, 2009, Pease and Horuk, 2012, Sobolik et al., 2014, Xiang et al., 2017a, Mantovani, 1999, Palleria et al., 2013, Wald et al., 2013, Wang et al., 2016).

One example of such promiscuity is that, CXCL12 binds to CXCR4 and ACKR3. Therefore, CXCL12 can still activate signalling via ACKR3, which could negate the blocking of CXCR4 via antagonists (Stacer et al., 2016). Additionally, there is positive cross talk between CXCR4 and other receptors such as CXCR2. Therefore, the activation of CXCR4 can also stimulate the upregulation of CXCR2. Hence, it is necessary to inhibit both CXCR4 and CXCR2 for clinical significance to be seen (Sobolik et al., 2014, Xiang et al., 2017b). Also, many diseases have not one, but multiple upregulated GPCRs that are independent of one another which again would require multiple GPCR antagonists. Other such inhibition combinations suggested by Sobolik et al. (2014) to reverse the aggressive phenotype of both MCF-7 and MDA-MB-231 included: MEK and CXCR4, CXCR2 and MEK or PI3K and MEK. Therefore, previous attempts with GPCR antagonists may not have considered the need for drug combinations. Hence, more research into duel antagonism is required. However, which combinations could vary patient to patient. Additionally, duel antagonism is likely to increase the risk of side effects related to the off target effects of the compound due to promiscuity. Even weak binding or low occupancy of a compound to an off-target receptor can give rise to off-target effects and create misleading data, especially when testing in animal models which could lead to a false impression of the therapeutic utility of the compounds in humans. Finally, the cost of researching duel antagonists would increase due to both/all the inhibitors being required to be tested for safety and toxicology. The costs of which would put off many pharmaceutical companies (Horuk, 2009).

For clinical efficacy there needs to be sufficient levels of the drug in the plasma to neutralise the receptor in question. Once in the blood plasma, the compound will also have to bind to the receptor with high occupancy i.e. needs to have high plasma-protein-binding properties. If there is failure of either of these two parameters, the compound will not cause sufficient clinical results (Horuk, 2009). It has been suggested that receptor occupancy needs to be greater than 90% to achieve therapeutic benefit as well as having good pharmacokinetics and slow off rates to achieve receptor blockade (Palleria et al., 2013, Pease and Horuk, 2012). This level of occupancy and desired pharmacokinetics is obviously very difficult to achieve and if the antagonist fails to sufficiently block the receptor for a sufficient amount of time, they will fail to block the activation of the desired GPCR (Horuk, 2009).

To prevent disease reoccurrence and to prevent metastasis, chronic administration of CXCR4 inhibitors is required. This in itself may lead to adverse effects not seen in short term *in vitro* experimentation and short term clinical trials (De Clercq, 2009, Peled et al., 2012, Wald et al., 2013). These adverse effects relate to CXCR4 being expressed in a vast majority of immune cells including neutrophils, macrophages and dendritic cells as well as CXCR4 being expressed on healthy tissues including the brain, heart, liver, lung spleen and kidneys. This could lead to the direct damage of these organs but additionally could have adverse effects upon immunity and immune cell mobilisation. This could lead to increased levels of leukocytes (leucocytosis), a decrease level of platelets in the blood (thrombocytopenia) or finally spleen enlargement that can result in rupture. Therefore, duel ligand delivery systems such as nanoparticle delivery might have the potential to limit this damage (Wang et al., 2016). However, these systems face the same financial difficulties as discussed previously (Horuk, 2009, Wang et al., 2016).

Finally, there is a distinct lack of animal models able to model human disease. This is due to there being vast differences in species expression of chemokine receptors as well as these receptors potentially having other functions than seen within humans (Horuk, 2009). This would cause these animal models to have different reactions to the receptor antagonists. i.e. animal models are not always predictive of human disease (Pease and Horuk, 2012). Alternatively, GPCR inhibitors that have been synthesised for human GPCRs could have limited specificity to the equivalent non-human receptor in the animal model. This could

lead to the requirement of higher doses to be used in the animal that could report false off-target effect that would not been seen in humans (Horuk, 2009). The development of transgenic animal model will greatly improve these issues. However, it has to be assumed that the human receptor is expressed in these transgenic animals and that they are functioning in a biologically similar manner to that of a human (Gurumurthy and Lloyd, 2019, Horuk, 2009). The use of animals with closer genetics such as higher primates as models then brings the problem of increase expenses (Horuk, 2009).

An alternative to blocking the CXCR4 receptor directly, would be by targeting downstream signalling proteins that are involved in CXCL12 driven metastasis. Therefore, not only is it important to continue the search for novel CXCR4 inhibitors, but also to identify which downstream proteins are vital for different cancer cell types to metastasise. For example investigations by Mills et al. (2016), discovered that Src kinase was essential for cell migration in both leukaemia and breast cancer. However, while PKC inhibitors successfully decreased migration in breast cancer cells, the same inhibitors had no effect upon the ability of leukemic cells to migrate.

## 1.14. Novel CXCR4 Antagonists Used in this Project

### 1.14.1. AZ3-2

AZ3-2 is a novel compound originally synthesised by Portella et al. (2013) as a CXCL12-derived small cyclic CXCR4 inhibitory peptide. Structure: Arg-Ala-[Cys-Arg-Phe-Phe-Cys]. Di Maro et al. (2016) modified this peptide, in an attempt to prevent its degradation in biological fluids and found that the peptide had a more promising $IC_{50}$ value. Such modifications included N-terminal acetylation, C-terminal amination and D-amino acid and L-amino acid scanning. Following this, free thiol groups were oxidized enabling the formation of disulphide bonds to help stabilise the peptide to create the final compound AZ3-2 (Figure 1.16). AZ3-2 binds to the CXCR4 receptor via its $Arg^1$ and $Arg^4$ side chains, making salt bridges with the carboxylate groups of the CXCR4 residues Asp-187 and Asp-97. Additionally, $Phe^5$ and $Phe^6$ side chains interact with Tyr-116, Leu-120, Arg-188, Phe-199, His-203, Tyr-255 and Ile-259 side chains that are in a CXCR4 pocket. Finally, hydrogen bonds are formed between $Arg^1$ and Asn-37 side chains and between the backbone amide of $Phe^6$ and the carboxylate group of Glu-288 (Di Maro et al., 2016).

a

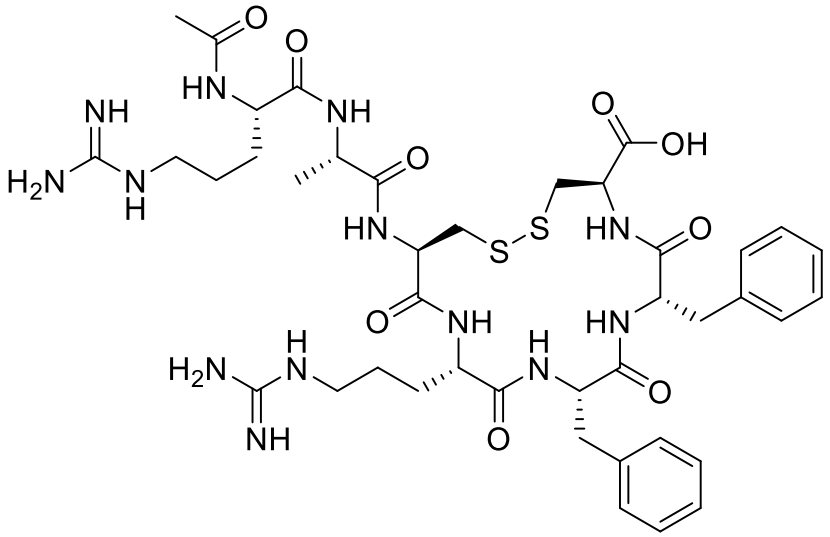

b

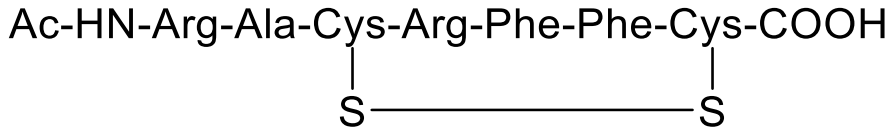


**Figure 1.16: The Structure of AZ3-2.** AZ3-2 is a seven amino acid peptide with a molecular weight of 942.13. **a)** shows the chemical structure and **b)** the amino acid sequence of AZ3-2.

### 1.14.2. AZ6-2

AZ6-2 (Figure 1.17) is another CXCL12-derived small cyclic CXCR4 inhibitory peptide synthesized by Di Maro et al. (2016). It has the same amino acid sequence and modifications as AZ3-2 however, the first cysteine amino acid is in the D configuration creating Arg-Ala-[DCys-Arg-Phe-Phe-Cys]. This configuration was found to be the most potent of the two when tested in the colon cancer cell lines HT29 and HCT116 and the leukemic cell line CEM (Di Maro et al., 2016).

a

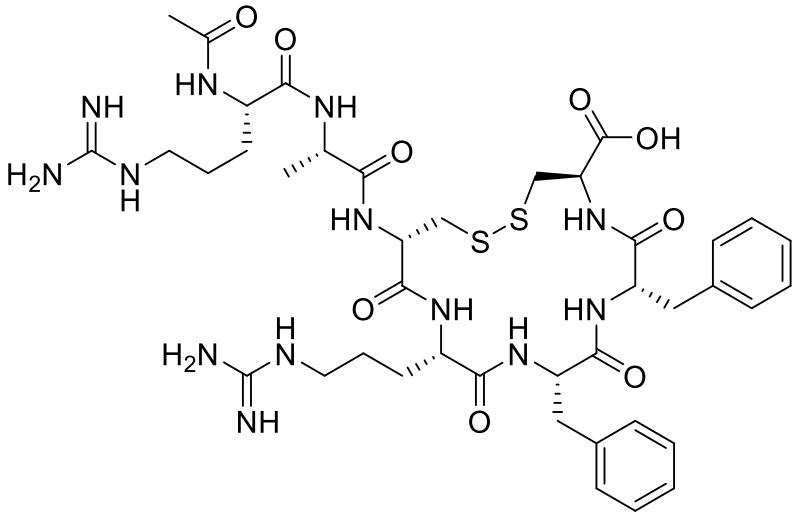

b Ac-HN-Arg-Ala-DCys-Arg-Phe-Phe-Cys-COOH

**Figure 1.17: The Structure of AZ6-2.** AZ6-2 is a seven amino acid peptide with a molecular weight of 942.13. **a)** shows the chemical structure and **b)** the amino acid sequence of AZ6-2.

## 1.15. Research Aims

Chemokines are a large family of cytokines which regulate leukocyte migration under both inflammatory and homeostatic conditions. The dysregulation of this chemokine signalling network, specifically CXCR4 signalling, enables the migration of cells which is causative to many disease states including cancer metastasis. While a vast amount of research has been conducted into describing the signalling events which govern the cellular processes downstream of CXCR4, including CXCL12-stimulated cellular migration, it is largely still unknown which downstream signalling proteins are required for the migration of different cell types. Therefore, the need to identify which of these pathways are utilised in different cancer cell lines is paramount. The identification of such pathways can be elucidated by using protein inhibitors to disrupt protein signalling in different cell types. Therefore, **CHAPTER 3** investigates the role of two therapeutic targets, PKC and PKD, in CXCL12 directed PC3 prostate cancer migration. In this chapter, PC3 cells are treated with different PKC and PKD inhibitors to determine if these two downstream signalling proteins stimulate PC3 cell migration.

Aside from inhibiting downstream signalling proteins, many clinical trials have attempted CXCR4 antagonism. However, the majority of these trials have been

unsuccessful, mainly due to off target toxicities due to multiple cells and organs expressing CXCR4. Consequently, only two CXCR4 based cancer therapies have been approved for use. Through the use of cancer cell lines that endogenously overexpress CXCR4 such as Jurkat, THP-1, MCF-7, PC3 and SKMEL28, research can be conducted to identify the ability of several novel CXCR4 therapeutics. Specifically, **CHAPTER 4** investigates the effects of the CXCR4 antagonists AMD3100, AZ3-2 and AZ6-2 in CXCL12 directed cancer cell migration. This is achieved using several cell migration assays; chemotaxis, time lapse and Oris$^{TM}$ Cell Migration assays as well as looking at the effects these compounds have upon intracellular calcium release and upon the actin cytoskeleton. Secondary to this, **CHAPTER 5** sees the development of a 'click' CXCR4 antagonist (designed at The University of East Anglia) and its effects upon CXCL12 stimulated cancer cell migration. This is again achieved using several cell migration assays: chemotaxis, time lapse and Oris$^{TM}$ Cell Migration assays as well as looking at the effects these compounds have upon intracellular calcium release and comparing these CXCR4 antagonists to those from Chapter 4. Additionally, it is determined if these CXCR4 antagonists are more stable than those from Chapter 4 and if CuAAC click chemistry can be utilised to click IS4 to a fluorescent dye.

However, CXCL12 not only binds to CXCR4 but also to ACKR3. While there is strong evidence throughout the literature that the binding of CXCL12 to CXCR4 can initiate cancer cell migration, there is controversial evidence that the binding of CXCL12 to ACKR3, can also prevent cancer cell migration. Therefore, **CHAPTER 6** investigates ACKR3 expression, internalization and influence on CXCL12 stimulated cancer migration in four cancer cell lines: MCF-7, PC3, Jurkat and THP-1 cells. The research presented here looks at the involvement of temperature upon ACKR3 expression and how this and CXCL12 can determine the method of internalisation as well as the involvement of ACKR3 in Jurkat and THP-1 cell migration.

Finally, the aim of **Chapter 7** was to design novel 3D printed materials for chemotaxis chamber for investigations into chemokine stimulated cancer cell migration and secondly to develop replacement stoppers for ORIS$^{TM}$ Cell Migration assays. The aim was to create an easy to download 3D design that could be printed anywhere and produce a cheap, accurate and reliable assay with a chemokine gradient.

# Chapter 2: Materials and Methods

**Acknowledgements**

I thank Dr M. M. D. Cominetti for synthesising AZ3-2, AZ6-2, IS3 and IS6. Additionally, I would like to thank Dr M. M. D. Cominetti for designing and synthesising IS1, IS4 and IS7 as well as supervising the production of two batches of AZ6-2. Finally, I would like to acknowledge Dr M. M. D. Cominetti for conducting the preparative and analytical HPLC, including the supervision of two analyses, as well as conducting the MALDI-TOF and NMR analyses.

I would also like to thank Dr D. Warren and Dr J. M. Courtney for their contributions to our collaborative project. Additionally, I would like to thank Dr J. M. Courtney for conducting the majority of the 3D prints as well as supervising several of these prints.

## 2.1. Cell Lines, Tissue Culture and Associated Materials

### 2.1.1. Jurkat Cell Line

The Jurkat cell line is derived from the peripheral blood of a 14-year-old male donor with acute T cell leukaemia and was originally purchased from American Type Culture Collection (ATCC) (Teddington, UK) (ATCC, 2017b). Jurkat cells have proven to be a good research model as they endogenously express high levels of the CXCR4 making this cell line susceptible for HIV entry, for which Jurkat cells are commonly used as a model (Hesselgesser et al., 1998). This cell line was cultured in 75 $cm^3$ flasks (ThermoFisher Scientific) and maintained under standard conditions: 37˚C, air 95% and 5% $CO_2$ using Roswell Park Memorial Institute (RPMI) medium (Corning, Biosera). This media was supplemented with 10% v/v foetal bovine serum (FBS) (Invitrogen), 2 mM L-glutamine (Invitrogen) and 100 µM non-essential amino acids (Gibco).

### 2.1.2. MCF-7 Cell Line

The MCF-7 cell line is derived from the mammary gland of a 69 year old, Caucasian female donor with a metastatic adenocarcinoma and was originally purchased from Merck (Merck, 2017). These cells are widely used to study epithelial cancer and is the best characterised and most widely used of all the human breast cancer cell lines (Holliday and Speirs, 2011). This cell line was cultured in 75 $cm^3$ flasks (ThermoFisher Scientific) and maintained under standard conditions: 37˚C, air 95% and 5% $CO_2$ using Dulbecco's modified Eagle medium (DMEM) (Corning, Biosera). This media was supplemented with 10% v/v FBS (Invitrogen), 2 mM L-glutamine (Invitrogen) and 100 µM non-essential amino acids (Gibco).

### 2.1.3. MDA-MB-231 Cell Line

The MDA-MB-231 cell line is derived from a metastatic adenocarcinoma from the pleural effusion of 51-year-old Caucasian female and was originally purchased from ATCC (Teddington, UK) (ATCC, 2017c). The MDA-MB-231 cell line is commonly used as a triple negative breast cancer model that is highly invasive *in vitro* (Holliday and Speirs, 2011). This cell line was cultured in 75 $cm^3$ flasks (ThermoFisher Scientific) and maintained under standard conditions: 37˚C, air 95% and 5% $CO_2$ using DMEM. This media was supplemented with 10% v/v FBS (Invitrogen), 2 mM L-glutamine (Invitrogen) and 100 µM non-essential amino acids (Gibco).

### 2.1.4. THP-1 Cell Line

The THP-1 cell line is derived from the peripheral blood of a 1-year old male donor with acute monocytic leukaemia (AML) and was originally purchased from ATCC (Teddington, UK) (ATCC, 2017e). THP-1 cells have proven to be a good research models as they endogenously express the CXCR4 human chemokine receptor (Yu et al., 2018). This cell line was cultured in 75 $cm^3$ flasks (ThermoFisher Scientific) and maintained under standard conditions: 37˚C, air 95% and 5% $CO_2$ using RPMI medium (Corning, Biosera). This media was supplemented with 10% v/v FBS (Invitrogen), 2 mM L-glutamine (Invitrogen) and 100 µM non-essential amino acids (Gibco).

### 2.1.5. PC3 Cell Line

The PC3 prostate cancer cell line is derived from a metastatic grade IV adenocarcinoma from the bone of a 62-year-old Caucasian male and was originally purchased from ATCC (Teddington, UK) (ATCC, 2017d). The PC3 cell line is both prostate specific antigen negative ($PSA^-$) and androgen receptor negative ($AR^-$) and is therefore commonly used as a model to study highly aggressive hormone therapy resistant prostate cancer (Tai et al., 2011). This cell line was cultured in 75 $cm^3$ flasks (ThermoFisher Scientific) and maintained under standard conditions: 37˚C, air 95% and 5% $CO_2$ using RPMI medium. This media was supplemented with 10% v/v FBS (Invitrogen), 2 mM L-glutamine (Invitrogen) and 100 µM non-essential amino acids (Gibco).

### 2.1.6. BT-474 Cell Line

The BT-474 breast cancer cell line is derived from the mammary glands of a 60-year-old female and was originally purchased from ATCC (Teddington, UK) (ATCC, 2017a). The BT-474 cell line is commonly used as a model to study $ER^+$ and $HER2^+$ breast cancer with high tumorigenic potential (Holliday and Speirs, 2011). This cell line was cultured in 75 $cm^3$ flasks (ThermoFisher Scientific) and maintained under standard conditions: 37˚C, air 95% and 5% $CO_2$ using DMEM medium. This media was supplemented with 10% v/v FBS (Invitrogen), 2 mM L-glutamine (Invitrogen) and 100 µM non-essential amino acids (Gibco).

### 2.1.7. SKBR3 Cell Line

The SKBR3 breast cancer cell line is derived from the pleural effusion of a metastatic mammary breast adenocarcinoma of a 43-year-old Caucasian female and was originally purchased from ATCC (Teddington, UK)(ATCC, 2016c). The SKBR3 cell line is commonly used as a model to study $ER^-$ but $HER2^+$ breast

cancer. It has subsequently proven to have limited tumorigenic potential (Holliday and Speirs, 2011). This cell line was cultured in 75 $cm^3$ flasks (ThermoFisher Scientific) and maintained under standard conditions: 37˚C, air 95% and 5% $CO_2$ using DMEM medium. This media was supplemented with 10% v/v FBS (Invitrogen), 2 mM L-glutamine (Invitrogen) and 100 µM non-essential amino acids (Gibco).

### 2.1.8. SKMEL28 Cell Line

The SKMEL28 malignant melanoma cell line is derived from the skin of a 51-year-old male and was originally purchased from ATCC (Teddington, UK) (ATCC, 2016d). SKMEL28 cells harbour the V600E mutation of B-Raf and have wild type N-Ras thus can be used as models for such tumours (Gril et al., 2011). This cell line was cultured in 75 $cm^3$ flasks (ThermoFisher Scientific) and maintained under standard conditions: 37˚C, air 95% and 5% $CO_2$ using RPMI medium. This media was supplemented with 10% v/v FBS (Invitrogen), 2 mM L-glutamine (Invitrogen) and 100 µM non-essential amino acids (Gibco).

### 2.1.9. NCI-H292 Cell Line

The NCI-H292 lung cancer cell line is derived from the lung tissue of a 32-year-old black female with a mucoepidermoid pulmonary carcinoma and was originally purchased from ATCC (Teddington, UK) (ATCC, 2016b). This cell line is commonly used as a prototype for transfecting human subgenomic fragments and to study the pathogenesis of the hepatitis B virus (HBV) and lung cancer (ATCC, 2016b). This cell line was cultured in 75 $cm^3$ flasks (ThermoFisher Scientific) and maintained under standard conditions: 37˚C, air 95% and 5% $CO_2$ using RPMI medium. This media was supplemented with 10% v/v FBS (Invitrogen), 2 mM L-glutamine (Invitrogen) and 100 µM non-essential amino acids (Gibco).

### 2.1.10. A549 Cell Line

The A549 lung cancer cell line is derived from the lung tissue of a 58-year-old Caucasian male with a lung carcinoma and was originally purchased from ATCC (Teddington, UK) (ATCC, 2016a). A549 cells are used as a model for non-small-cell lung cancer (NSCLC) and for the development of specific drug therapies (Kim et al., 2013). This cell line was cultured in 75 $cm^3$ flasks (ThermoFisher Scientific) and maintained under standard conditions: 37˚C, air 95% and 5% $CO_2$ using DMEM medium. This media was supplemented with 10% v/v FBS (Invitrogen), 2 mM L-glutamine (Invitrogen) and 100 µM non-essential amino acids (Gibco).

### 2.1.11. Routine Tissue Culture Procedure

At 80-95% confluency, the adherent MCF-7 cells were removed from the flask using 5 mM PBS/EDTA (2 mL of 0.5 M EDTA to 200 mL PBS) and incubated for 10 minutes at 37˚C, 95% air and 5% $CO_2$. Both PBS (1.5 mM potassium phosphate monobasic, 3 mM potassium phosphate dibasic, 150 mM NaCl; pH 7.2) and EDTA were obtained from ThermoFisher. After this period, the cells were agitated to remove any remaining MCF-7 cells from the bottom of the flask. Cells were then used for experimentation or passaged by reducing the cell density by 75%. All other adherent cell lines were removed from the flask using 0.25% Trypsin-EDTA (1X) (Gibco) and incubated for 1-2 minutes at 37˚C, 95% air and 5% $CO_2$. Cells were then agitated and used for experimentation or passaged.

The suspension cell lines, Jurkat and THP-1, were cultured until the cell density reached approximately $1x10^6$ $mL^{-1}$ and were not allowed to exceed approximately $3x10^6$ $mL^{-1}$. Therefore, every 2-3 days the appropriate amount of cells were split into a new flask or discarded and fresh media added.

Cells that were frozen for preservation were allowed to grow to approximately 80-95% confluency if adherent, or $1x10^6$ $mL^{-1}$ if in suspension. These cells were then harvested, centrifuged at 1200 rpm for 5 minutes then resuspended into 1 mL of 10% v/v DMSO in FBS and finally transferred to cryotubes. To enable slow freezing and to attempt to minimise damage to the cells, the cryotubes were first wrapped in tissue and chilled to -80˚C for at least 48 hours before being transferred into liquid nitrogen at -196˚C.

## 2.2. Chemokines

A complete list of chemokines, their stock and working concentrations are detailed below (Table 2.1). All chemokines except CCL3 were purchased from Peprotech (New Jersey, USA). This includes CCL5, CCL8, CXCL8, CXCL10, CXCL11 and the CXCR4 chemokine CXCL12 (SDF-1α). Stock concentrations were made up to 1 µM using purified water and subsequent working concentrations for use in chemotaxis assays were made up to 1-5 nM using working buffer (see, Chapter 2.7.1). Only CXCL12 was using in migration assays (excluding chemotaxis assays) at a concentration of 10 nM using the 1 µM stock solution. A 100 nM stock solution was made up for CXCL12 also using purified water and a working concentration of 15-25 nM for use in calcium release assays.

Czaplewski of British Biotech kindly donated the CCR1/CCR4/CCR5 chemokine CCL3. Again, stocks were made up to 1 µM using purified water,

diluted in working buffer for a 5 nM stock solution for chemotaxis assays and finally the 1 µM stock was used in calcium flux assays at a concentration of 200 nM. All concentrations were either determined by myself through dose concentration experimentation (working concentration for calcium release assay and working concentration for chemotaxis assay) or determined by previous members of the Mueller group. 10 nM of CXCL12 for use in internalisation assays was based upon evidence the literature (Hattermann et al., 2014).

**Table 2.1: Chemokines**

| Chemokine | Stock Concentration | Working Concentration Chemotaxis Assay | Migration and internalisation Assay Concentration | Stock Concentration Calcium Release Assay | Working Concentration Calcium Release Assay |
|---|---|---|---|---|---|
| **CCL3** | 1 µM | 5 nM | N/A | 1 µM | 200 nM |
| **CCL5** | 1 µM | 5 nM | N/A | 1 µM | 200 nM |
| **CCL8** | 1 µM | 5 nM | N/A | 1 µM | 200 nM |
| **CXCL8** | 1 µM | 5 nM | N/A | 1 µM | 200 nM |
| **CXCL10** | 1 µM | 5 nM | N/A | 1 µM | 200 nM |
| **CXCL11** | 1 µM | 5 nM | N/A | 1 µM | 200 nM |
| **CXCL12** | 1 µM | 1-5 nM | 10 nM | 100 nM | 15-25 nM |

## 2.3. PKC Inhibitors

A complete list of the PKC inhibitors is detailed below. Working concentrations were previously determined in the literature and reflect the concentrations used by Mills et al. (2016). Therefore, concentrations were maintained for the continuation of this work

.

**Table 2.2: PKC Inhibitors**

| Inhibitor | Supplier | Stock Concentration | Working Concentration | IC50 | Reference |
|---|---|---|---|---|---|
| **GF109203X** | Tocris | 23.5 mM in DMSO | 5 µM | α – 8.4 nM<br>β1 – 18 nM<br>ε – 132 nM | (Toullec et al., 1991) |
| **Staurosporine** | Tocris | 100 µM in water | 10 nM | α – 2 nM<br>γ – 5 nM<br>η – 4 nM | (Martiny-Baron et al., 1993) |
| **CID755673** | Tocris | 4.6 mM in ethanol | 11 µM | PKD1 – 180 nM<br>PKD2 – 280 nM<br>PKD3 – 227 nM<br>PKC < 10 µM | (Sharlow et al., 2008) |
| **PKCζ Pseudosubstrate inhibitor** | Calbio-chem | 1 mM in $H_2O$ | 10 µM | 10-20 µM | (Lee, 2011) |

## 2.4. Receptor Internalization Inhibitors

A complete list of cell surface receptor internalization inhibitors is detailed below. Working concentrations determined by previous members of the Mueller group and maintained for the continuation of work by Jacques et al. (2015).

**Table 2.3: Internalisation Inhibitors**

| Inhibitor | Supplier | Type of Inhibitor | Stock Concentration | Incubation Time | Working Concentration |
|---|---|---|---|---|---|
| **Dynasore** | Abcam | Dynamin inhibitor | 80 mM in DMSO | 2 hours | 60 µM |
| **Methyl-β-cyclodextrine (MCD)** | Sigma Aldrich | Cholesterol depleting agent | 0.5 M in $H_2O$ | 1 hour | 10 mM |
| **Filipin** | Sigma Aldrich | Cholesterol sequestering agent | 10 mg/mL in DMSO | 1 hour | 5 µg/mL |
| **PitStop 2** | Abcam | Clathrin inhibitor | 30 mM in DMSO | 30 minutes | 30 µM |
| **PitStop 2 Negative Control** | Abcam | N/A | 30 mM in DMSO | 30 minutes | 30 µM |
| **CK666** | TOCRIS Bioscience | Arp 2/3 inhibitor | 1 mM in DMSO | 30 minutes | 10 µM |

## 2.5. Antibodies

A complete list of primary and secondary antibodies is detailed below.

**Table 2.4: Primary Antibodies Used for Immunofluorescence and Flow Cytometry**

| Primary/Secondary | Antibody | Supplier | Dilution Factor |
|---|---|---|---|
| **Primary** | CXCR4 (12G5): sc-12764 | Santa Cruiz Biotechnology | 1:1000 |
| **Primary** | CXCR4 (4G10): sc-53534 | Santa Cruiz Biotechnology | 1:1000 |
| **Primary** | Human CXCR7/RDC-1 Antibody Monoclonal Mouse $IgG_1$ Clone #11G8 | R&D Systems | 10 µg/mL immunofluorescence 10 µg/mL for $1x10^6$ $mL^{-1}$ flow cytometry |
| **Secondary** | Goat anti-mouse IgG H&L (Alexa Fluor® 488) | Abcam | 1:1000 |

## 2.6. Solid Phase Peptide Synthesis of Peptides

The design of AZ3-2 and AZ6-2 is discussed in detail in Di Maro et al. (2016) as peptides ‘2’ and ‘10’, respectively. Dr M. M. D. Cominetti kindly carried out all the original synthesis of AZ3-2, AZ6-2, IS3 and IS6. Additionally, Dr M. M. D. Cominetti designed and synthesised IS1, IS4 and IS7 as well as supervising the production of two batches of AZ6-2.

### 2.6.1. Materials

*N*$^{\alpha}$-Fmoc-protected amino acids (all Cambridge Reagents excepting Fmoc-D-Cys(trt)-OH (Flurochem)), H-Cys-(trt)-2Cltrt resin with 0.63 mmol/g (Novabiochem), *O*-benzotriazole-*N*,*N*,*N*′,*N*′-tetramethyl-uroniumhexafluorophosphate (HBTU)( Cambridge Reagents), *N*,*N*-diisopropylethylamine (DIPEA) (Sigma Aldrich), triisopropylsilane (TIPS)(Sigma Aldrich), trifluoroacetic acid (TFA) (Flurochem), *N*-hydroxybenzotriazole (HOBt) (Cambridge Reagents), *N*,*N*-dimethylformamide (DMF) (Cambridge Reagents), dichloromethane (DCM) (Cambridge Reagents), N-Methyl-2-pyrrolidone (NMP) (Cambridge Reagents), piperidine (PIP) (Cambridge Reagents), acetyl chloride (AcCl) (Acros Organics),Ethanedithiol (EDT) (Fluka), Acetic acid (AcOH) (Fisher),

Chloroform ($CHCl_3$) (Fisher), Diethyl ether ($Et_2O$) (Honeywell) and methanol (MeOH) (Honeywell). All reagents and solvents were used without further purification.

### 2.6.2. Peptide Synthesis

All peptides were synthesis on a Multisyntech Syro I automated peptide synthesiser using Fmoc solid phase peptide synthesis. The synthesis was carried out using a H-Cys-(Trt)-2ClTrt resin with 0.63 mmol/g using methodology similar to that described by Di Maro et al. (2016). Batches of 100 mg of resin were swollen by shaking in DCM (~2 mL, 30 minutes) and subsequently in DMF (~2 mL, 30 minutes). Each coupling reaction was achieved by subsequent addition of a 4-fold excess of the following amino acids: alanine, cysteine, phenylalanine and arginine (0.5 M in NMP, except arginine – 0.5 M in DMF). HBTU (0.45 M, 3.9 equivalents) and HOBt (0.45 M, 4 equivalents) in DMF and DIPEA (2 M, 8 equivalents) in NMP. The mixture was shaken for 45 minutes, washed with DMF (3 mL, 40 seconds) and the coupling was repeated. Following this, the peptide was washed four times with DMF (3 mL, 40 seconds). As the peptide bare an acetyl group at the N-terminus, Fmoc group de-protection was performed by shaking the resin with 40% piperidine in DMF (2 times, 3 mL, 10 minutes). After completion of the peptide sequence, acetylation of the N-terminal was obtained by shaking the resin for 45 minutes with a solution of acetyl chloride (4 equivalents) and DIPEA (8 equivalents) in 2 mL of DMF (acetyl chloride was mixed quickly to DMF, followed by DIPEA, mixed for 10 seconds and then added to the resin). Completion of the acetylation was assessed by Kaiser Test. If the test provided positive, the acetylation was repeated. The resin was extensively washed with DMF, methanol/DCM 1/1 and DCM prior to drying under air flow.

### 2.6.3. Peptide Cleavage

The peptide was released from the solid support and all the protecting groups cleaved by shaking the resin with TFA/$H_2O$/TIPS/EDT (94/2.5/1/2.5% v/v/v/v) for 3 h (5 mL for 100 mg of resin). The cleavage cocktail was collected and the resin was washed with fresh TFA, which was added to the previous solution. The solvent was evaporated under reduced pressure and the crude linear peptide was recovered by precipitation and extensively washed with chilled diethyl ether to give a powder.

### 2.6.4. Creation of Disulphide Bond (AZ3-2 and AZ6-2)

The crude peptide from a batch of 100 mg of resin was dissolved in 32 mL of AcOH, and 8 mL of $H_2O$. Iodine (1 equivalent calculated considering the crude linear peptide as pure) was added and the mixture was stirred for 1 hour at room temperature to enable disulphide bond formation, see Figure 2.1 for mechanism. Following this, the solution was diluted with water and any iodine left was extracted from the mixture using chloroform. The aqueous phase was partially evaporated under reduced pressure and the concentrated solution was freeze dried with liquid nitrogen to yield the crude cyclised peptide.

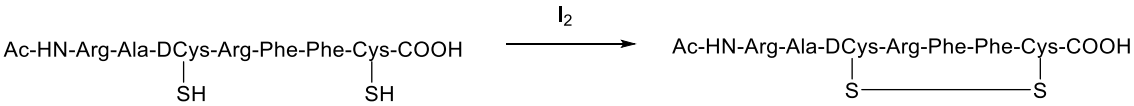


**Figure 2.1: Formation of a Disulphide Bond in AZ6-2.** Iodine was used to create the disulphide bonds in both AZ3-2 and AZ6-2.

### 2.6.5. Cyclisation by Maleimide Stapling (IS1 and IS4)

Similarly to the procedure reported in (Grison et al., 2017), the crude peptide from a batch of 300 mg of resin was dissolved in water/acetonitrile 9/1 (200 mL) at a concentration of 1.1 mg/mL. While stirring vigorously, a solution of 2,3-dibromomaleimide was used to synthesize IS1, N-propargyl-2,3-dibromomaleimide (referred to as IS3) was used to synthesize IS4 (prepared according to (Grison et al., 2017)). Acetonitrile was added slowly to IS1 or IS4 (1 equivalent to the theoretical peptide, 20 mL of acetonitrile). The solution was stirred under nitrogen for 16 hours at room temperature. The volume was reduced by evaporation under reduced pressure and the remaining solvent was freeze-dried. The yellow solid obtained was triturated with ethyl acetate, dried under reduced pressure and purified by preparative HPLC. See Figure 2.2 for mechanism.

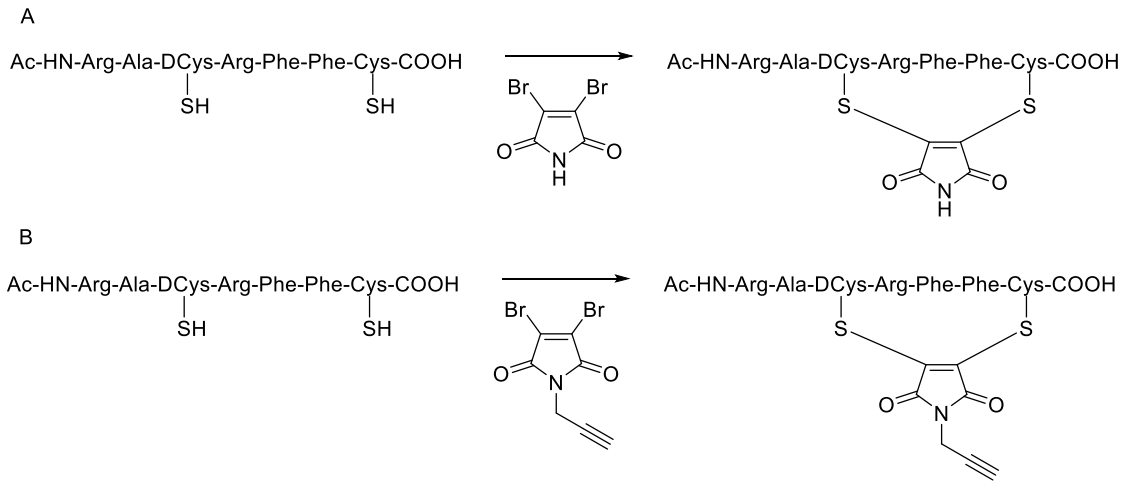


**Figure 2.2: Formation of a Maleimide Bond in IS1 and IS4.** 2, 3-dibromomaleimide or N-propargyl-2, 3-dibromomleimide (IS3) to create the maleimide bond seen in IS1 and IS4, respectively.

### 2.6.6. Purification and Analysis

Peptides were purified by preparative HPLC using an Agilent Technologies 1260 Infinity Series) equipped with an Agilent ZORBAX XDB-C18 21.2 mm × 150 mm column (5 µm pore size). Separation was obtained with a linear gradient from 5% to 95% of methanol in water over 15 min followed by 5 minutes of 95% methanol and a 3-minute gradient to return to the initial conditions (flow rate of 20 mL/min, all solvents contain 0.05% TFA).

Peptides were analysed by analytical HPLC using an Agilent Technologies 1200 Series HPLC equipped with an Agilent ZORBAX Eclipse YDB-C18 4.6 mm x 150 mm column (5 µM pore size). Samples were eluted using a linear gradient from 5% to 95% of methanol in water over 15 min followed by 5 minutes of 95% methanol and a 5-minute gradient to return to the initial conditions (flow rate of 1.0 mL/min, all solvents contain 0.05% TFA). The UV detector was set to record at 254 and 210 nm wavelengths. Integration of the traces was used to assess purity. Only samples with purity ≥ 95% were considered for biological evaluation.

Molecular weights of compounds (Table 2.5) were confirmed by MALDI-TOF on a KRATOS AXIMA-CFR using either sinapinic acid or alpha-cyano-4-hydroxycinnamic acid as matrix.

For IS3, NMR spectra were recorded on a Bruker Ultrashield Plus 400. The chemical shifts for both $^{1}H$ and $^{13}C$ spectra are reported in ppm and referenced to the residual solvent peak. Multiplicities are described as s = singlet, d =

doublet, dd = doublet of doublet, t = triplet, q = quartet, m = multiplet and br = broad. Coupling constants are reported in hertz. Data analysis and presentation was performed with Bruker TopSpin 3.5 software.

The melting point of IS3 was measured on a Stuart Scientific melting point apparatus SMP3 and were reported uncorrected as 118-120 ºC.

**Table 2.5: Molecular Weight of Synthesized Peptides**

| Peptide | Molecular Weight |
|---|---|
| **AZ3-2** | 942.13 |
| **AZ6-2** | 942.13 |
| **IS1** | 1037.18 |
| **IS4** | 1075.23 |
| **IS7** | 1708.84 |

## 2.7. Migration Assays

### 2.7.1. Chemotaxis Assay using ChemoTX Plate

Chemotaxis assays for Jurkat and THP-1 cells were conducted in a ChemoTX 5 µm pore transwell chemotaxis plate (Neuroprobe Inc, USA). Wells to be used in the assay were blocked with 31 µL of blocking buffer consisting of serum free RPMI with 1% bovine serum albumin (BSA) for up to 30 minutes at room temperature. Chemokine solutions were prepared at 1 or 5 nM in working buffer (0.1% BSA in serum free RPMI). Cells were harvested and spun down at 1200 rpm for 5 minutes, washed once in serum free RPMI containing 0.1% BSA and then re-suspended to give an approximate concentration of $25x10^4$ $mL^{-1}$ of Jurkat cells or $50x10^4$ $mL^{-1}$ of THP-1 cells. Cells were then treated with the relevant inhibitor or vehicle control and incubated at 37˚C, 95% air and 5% $CO_2$ for 30 minutes. The blocking buffer was removed from the plate after 15-30 minutes and replaced with either 31 µL of negative controls (serum free RPMI contained 0.1% BSA) or 31 µL of the relevant chemokine solution (1 nM solutions of CXCL12 for Jurkat cells, 5 nM for THP-1 cells) with duplicates of each condition being conducted. The membrane (a polyvinylpyrollidone-free polycarbonate filter with 5 µm pores) was then attached and 20 µL of cell suspension was added to the top surface. Finally, the plate was placed inside a humidified chamber and left to incubate at 100% humidity, 37˚C, air 95% and 5% $CO_2$ for 4 hours. Following these 4 hours, the remaining cells on top of the membrane were wiped off, the filter removed and 10 µL of cells within each well were counted using a

haemocytometer to assess the number of cells that had migrated into the bottom of the compartment.

### 2.7.2. Scratch Closure Assay

Sterile 24 well plates were prepared by marking the outside bottom surface of each well with two parallel lines in permanent marker to create a reference point for the scratch and subsequent scratch closure. Adherent MCF-7 cells at approximately 90-95% confluency were suspended via incubation with PBS containing 5 mM of EDTA for 10 minutes. Following this, the cells were collected and centrifuged at 1200 rpm for 5 minutes. 1 mL of DMEM was added to each well and approximately $5x10^5$ $mL^{-1}$ cells were pipetted into each of the 24 pre-marked wells and incubated for 24 hours at 37˚C, 95% air and 5% $CO_2$ to enable the cells to grow to >95% confluency. After 24 hours, the cells were washed once with DMEM with no supplements (incomplete DMEM). Three scratches per well were then made on the cell monolayer, perpendicular to the reference lines using 200 µL pipette tips. The cells were washed again in incomplete DMEM to remove any loose and now suspended cells. Finally, DMEM supplemented with only 0.5% FBS, glutamine and non-essential amino acids is used to incubate the cells. Images were taken at this point (time 0), using an inverted Leica DMIL fluorescence microscope with a Leica DFC420 camera in bright-field mode at 10X magnification so that the horizontal reference lines are visible in the images. The relevant chemokines and/or inhibitors were then added to their respective wells. Cells were then incubated for another 24 hours and again images were taken after this period (time 24). These images were analysed and the width of the wound was measured using Microsoft Excel PowerPoint using the horizontal reference lines to guide where the images should be taken at both time points. The ratio of the width of the wounds consisted of the width of the wound after 24 hours divided by the width of the wound at 0 hours.

### 2.7.3. Time Lapse Assay

Original time-lapse microscopy was conducted using a Celestron Micro 360 microscope attached to its associated camera maintained under standard conditions: 37˚C, air 95% and 5% $CO_2$. Images were taken using bright-field at a 4x objective at either 30 second or 2 minute intervals for 10 hours controlled using Debut Professional Video Capture v 3.01 (NCH Software) and for the compilations of time-lapse videos Camtasia Studio 8 was used.

Subsequent time-lapse microscopy was conducted using a Zeiss Axiovert 200M motorise inverted fluorescent/ live cell imaging microscope attached to its associated Axiocam CCD camera under standard conditions 37˚C, air 95% and 5% $CO_2$. Images were taken using bright-field at a 10x objective (5.5x overall magnification) every 4 minutes for 10 hours controlled using Carl Zeiss AxioVision Rel. 4.8.

### 2.7.3.1. Scratch Closure Time Lapse Assay

Protocol as previous scratch closure assay however, 3 $cm^3$ petri dishes were used. Additionally, once the monolayer had been scratched, washed and prepared with either 0.5%, 0.1% or 0% serum, the petri dishes were placed in an incubator and cell movement recorded using Debut Professional Video Capture v 3.01 (NCH Software) as previously described. Two recordings were created, one without the addition of chemokine and a second recording on the same pre-prepared plate with 10 nM of CXCL12. Images were taken every 2 minutes for 10 hours using a 4x objective and compiled into a time-lapse movie of collective cell migration into the wound. The acquired movies were then exported from Camtasia Studio 8 as .avi files and subsequently uncompressed. Images exported were subjected to a series of processing steps using Image J software to compare wound size at T=0 and wound size at T=10/20/30. Initially the image was transformed into an 8-bit image (Image-Type-8-bit) then the edge of the wound was defined (process-find edges, process-sharpen). To increase contrast between the wound and the cell front and an appropriate threshold was applied to each image to generate a binary image (image-adjust threshold, process-find edges). Each image was then inverted (image-lookup tables –invert LUT) and wound area was measured from the area percentage value (analyse-analyse particles). The area size change between T=0 and T=10/20/30 hours determined percentage wound closure/percentage cell coverage.

### 2.7.3.2. Single Cell Tracking Time Lapse

Adherent MCF-7, PC3 or SKMEL28 cells at approximately 90% confluency were suspended via incubation with either PBS containing 5 mM of EDTA (MCF-7 cells) for 10 minutes or with 0.25% trypsin-EDTA (1X) (Gibco) (PC3 and SKMEL28) for approximately 2 minutes. Following this, the cells were collected and centrifuged at 1200 rpm for 5 minutes. 1 mL of complete DMEM/RPMI was added to each well and approximately $1x10^4$ $mL^{-1}$ cells were pipetted into either sterile 3 $cm^3$ petri dishes or 24 well plates were and incubated for 24 hours at

37˚C, 95% air and 5% $CO_2$ to achieve ≤10% confluency. The following day MCF-7 cells were washed and the media replace with fresh complete DMEM, PC3 cells were washed and the media was replaced with fresh complete RPMI medium and finally SKMEL28 cells were washed and the media was replaced with incomplete RPMI. The relevant chemokines and/or inhibitors were then added to their respective wells. Using Image J software, single cells were manually tracked by clicking on the centre of cell nuclei throughout consecutive frames. Tracking was terminated if the cell divided as this temporarily suspended the cells migratory behaviour. 10 cells per condition were tracked unless cell density or high cell division rates prevented this. Each movie was saved as an uncompressed .avi file. Using these x-y co-ordinates, Image J measured migration distance and subsequent calculation identified each cells individual speed which could be averaged to enable comparisons between conditions. Additionally, for MCF-7 cells the number of cells that underwent proliferation during the course of the 10 hours were counted to determine the proliferative rates of basal and 10 nM CXCL12 conditions.

### 2.7.4. Boyden Chemotaxis Chamber

Adherent PC3 cells were cultured until approximately 90% confluency then incubated with 0.25% trypsin-EDTA (1X) (Gibco) for approximately 1-2 minutes. Following this, the cells were collected and centrifuged at 1200 rpm for 5 minutes. 8.0 µm cell culture inserts (Corning) were used to determine the migration of PC3 cells towards CXCL12. Inserts were placed in a 24 well plate and 600 µL of RPMI culture media containing 0.1% BSA was added to the well with the relevant concentration of chemokine. $1x10^6$ $mL^{-1}$ of cells were washed in PBS, re-suspended in RPMI culture media containing 0.1% BSA and subsequently 200 µL were seeded into the inserts. Cells were then treated with the relevant inhibitors and incubated overnight at 37˚C, 95% air and 5% $CO_2$. The following day, 4 µM of calcein AM (Cayman Chemical Company) was added to the well and left to incubate for 45 minutes. The inserts were then removed and placed in new, sterile 24 wells containing 0.5 mL of 0.25% trypsin-EDTA and incubated at 37˚C, 95% air and 5% $CO_2$ for 30 minutes with frequent agitation. Finally, 200 µL of the cell impregnated 0.25% trypsin-EDTA was added to each well of a black, opaque plate (ThermoFisher Scientific) before being analysed at an excitation/emission wavelength of 485/520 using a BMG LabTech FLUOstar

Optima Flourometer using Optima (BMG Labtech) software (BMG LabTech, Germany).

### 2.7.5. 3D Printed Boyden Chemotaxis Chamber

The original concept of chemotaxis chambers was developed by myself and Dr D. Warren while the designing of these chambers was conducted Dr J. M. Courtney, Dr D. Warren and myself. All CAD designs and the majority of the 3D prints were conducted by Dr J. M. Courtney.

Google Sketch Up Make (64 bit) 2017 version 17.1.174 (Trimble Inc.) was used to design the 3D CAD models and exported in .STL file format. CURA 2.6.2 slicing software was then used to generate the print files (as a .gcode or .3mf file). An Ultimaker 3 Extended 3D printer, printing with PLA (2.85 mm, RS Components) filament was used to print each iteration. Optimum parameters for the majority of prints were:

**Quality**

Layer height: 0.1 mm

Initial layer height: 0.27 mm

Line width: 0.35 mm

Wall line width: 0.35 mm

Outer wall line width: 0.35 mm

Inner wall(s) line width: 0.3 mm

Top/bottom line width: 0.35 mm

Infill line width: 0.35 mm

Support line width: 0.4 mm

Support interface line width: 0.5 mm

**Shell**

Wall thickness: 0.1 mm

Wall line count: 1

Top/bottom thickness: 1 mm

Top thickness: 1 mm

Top layers: 10

Top/bottom pattern: lines

Infill density: 20%

**Materials**

Printing temperature: 200˚C

Build plate temperature: 60˚C

Diameter 2.85 mm

Flow: 100 %

Enable reaction: (tick [yes])

**Speed**

Print speed: 100 mm/s

Travel speed: 250 mm/s

Print acceleration: 4000 mm/s$^2$

Travel acceleration: 5000 mm/s$^2$

Print jerk: 25 mm/s

Travel jerk: 30 mm/s

**Cooling**

Enabled print cooling: (tick [yes])

Support - not used

Build plate adhesion: not used

Once the final iteration was designed and printed, quick drying silicone (Gedeo 300g Siligum Moulding Paste, white, Amazon) was then pressed into the 3D printed mould to create a silicone cast. This silicone cast was then inserted into a 6 well plate. Molten 4% agarose in complete RPMI with 1% penicillin/streptomycin was then poured around the silicone cast and incubated for 10 minutes at 4˚C to set. Once set, the silicone cast was removed and any excess agarose was cut away. Cells were then seeded into the well and left overnight enabling the adherence of the cells. After incubation, 10 µM of CXCL12 chemokine was added to the opposite well and time-lapse microscopy ensued for 10 hours using a Zeiss Axiovert 200M motorise inverted fluorescent/ live cell imaging microscope attached to its associated Axiocam CCD camera under standard conditions 37˚C, air 95% and 5% $CO_2$. Time-lapse movies were exported as described previously to Image J and analysed.

### 2.7.6. ORIS™ Cell Migration Assay

Adherent PC3 cells at approximately 95% confluency were suspended via incubation with 0.25% trypsin-EDTA (1X) (Gibco) for 1-2 minutes. Following this, the cells were collected and centrifuged at 1200 rpm for 5 minutes. Cells at a density of $5x10^4$ mL $^{-1}$ were re-suspended in 100 µL of complete RPMI and seeded into a 96 well Oris™ Cell Migration assay black opaque, clear bottomed, stopper fitted plate (Platypus Technologies) and incubated for 24 hours at 37˚C, 95% air and 5% $CO_2$. These stoppered plates create a central cell-free detection

zone and when the stopped is removed, it allows cells to migrate into the centre. Following the 24-hour incubation period, the stoppers were removed and the required chemokines and/or inhibitors were added then incubated for a further 24 hours. Cells were washed and re-suspended in PBS with 4 µM of calcein AM (Cayman Chemical Company) and incubated for 45 minutes at 37˚C, 95% air and 5% $CO_2$. Again, cells were washed in PBS then the plate was loaded into a BMG LabTech FLUOstar Optima Flourometer (BMG Labtech, Germany) and fluorescence in the detection zone of the well was detected using excitation 430-10 and emission 510-20 nm. Optima (BMG Labtech, Germany) software data recorded fluorescence which relates to the ability of cells to migrate into the detection zone.

### 2.7.7. 3D Printed ORIS$^{TM}$ Cell Migration Assay Stoppers

The original concept of 3D printing replacement stoppers was developed by myself. All CAD drawing and 3D printing was outsourced to Dr J. M. Courtney.

Google Sketch Up Make (64 bit) 2017 version 17.1.174 (Trimble Inc.) was used to design the 3D CAD stoppers and exported in .STL file format. Slic3r (version 1.2.9) slicing software was then used to generate the print files (as a .gcode or .3mf file). These were printed using a DIY Reprap Prusa i3 (sintron) printer, printing with TPE-U (1.75 mm, FFFworld) filament.

## 2.8. Calcium Release Assay

Adherent MCF-7 cells at approximately 80% confluency were incubated with PBS containing 5 mM of EDTA for approximately 10 minutes. Following this, the cells were collected and centrifuged at 1200 rpm for 5 minutes. The same was conducted with PC3 cells aside from being incubated with 0.25% trypsin-EDTA (1X) (Gibco). Jurkat and THP-1 cells were collected and centrifuged at 1200 rpm for 5 minutes. Following this, the cells were washed twice with a calcium flux buffer (137 mM NaCl, 5 mM KCl, 1 mM $MgCl_2$, 1.5 mM $CaCl_2$, 10 mM Hepes and 25 mM D-Glucose made up to 500 mL with purified water; pH 7.4) before being re-suspended to give an approximate concentration of $2x10^6$ mL $^{-1}$ cells. Cells were then treated with the relevant concentration of inhibitor and loaded with 4 µM Fura-2 AM dye (Invitrogen) before being incubated for 30 minutes at 37˚C, air 95% and 5% $CO_2$. Fura-2 acetoxymethyl (AM) is a high affinity cell permeable, intracellular calcium indicator (ThermoFisherScientific, 2018). Upon binding to $Ca^{2+}$, Fura-2 AM shifts its peak absorbance from 340 nm to 380 nm in the $Ca^{2+}$ free state (Paredes et al., 2008). Following this, the cells are centrifuged at 1200

rpm and washed twice with 1 mL of calcium buffer. Finally, 100 µL of cells were pipetted into a black, opaque 96-well plate (ThermoFisher Scientific). This plate was loaded into a BMG LabTech FLUOstar Optima Flourometer (BMG Labtech, Germany) that injected chemokine directly in the wells contained the treated cells. The changes in the release of calcium was analysed via radiometric analyses of the changes in fluorescence at a fixed emission frequency of 510 nm. Using Optima (BMG Labtech, Germany) software data was recorded and analysed as a ratio of 340/380 nm which is directly related to the amount of intracellular calcium release. Data was expressed as a change in fluorescence ratio (340nm/380nm) where the basal fluorescence prior to the addition of chemokine is subtracted from peak fluorescence following addition of chemokine.

### 2.8.1. Calcium Release Stability Assay

Compounds were diluted in FBS to achieve a final concentration of 1 µM and incubated for 30 minutes at 37˚C, air 95% and 5% $CO_2$. THP-1 cells were collected and prepared as previous. After incubation, the FBS/compound stock was then added to the prepared cells and loaded with 4 µM Fura-2 AM dye (Invitrogen) before being incubated for a further 30 minutes at 37˚C, air 95% and 5% $CO_2$. Following this, the cells were centrifuged at 1200 rpm and washed twice with 1 mL of calcium buffer. Finally, 100 µL of cells were pipetted into a black, opaque 96-well plate (ThermoFisher Scientific). This plate was loaded into a BMG LabTech FLUOstar Optima Flourometer (BMG Labtech, Germany) and data was collected as previous.

### 2.8.2. Calcium Release Following Incubation with Triton X-100 and EDTA

THP-1 cells were collected and prepared and loaded into a black, opaque 96-well plate as previous (ThermoFisher Scientific). This plate was loaded into a BMG LabTech FLUOstar Optima Flourometer (BMG Labtech, Germany). Analysis was allowed to run for ~10 seconds before being manually stopped. The plate was then removed and 10% (10 µL) of Triton X-100 was added to the cells. The plate was reloaded into the FLUOstar Optima Flourometer and readings were taken. This was repeated using the same well of cell however after manually interrupting the readings and ejecting the plate, 10% (10 µL) EDTA was added to the cells. This was repeated twice for basal cells and twice for treated cells. No chemokine was injected during these experiments. Data was expressed as a change in fluorescence ratio (340nm/380nm) where the basal fluorescence (the

interrupted reading) was subtracted from peak fluorescence (the uninterrupted reading).

## 2.9. Internalisation Assay and Flow Cytometry Analysis

MCF-7 cells at approximately 80-90% confluency were incubated with PBS containing 5 mM of EDTA for approximately 10 minutes. Following this, the cells were collected and centrifuged at 1200 rpm for 5 minutes. MCF-7 and Jurkat cells, were resuspended in 1 mL of 0.5% BSA/PBS to give a cell density of $1x10^6$ $mL^{-1}$. Cells were treated for 30 minutes to 2 hours with inhibitors (see Table 2.3) or 1 hour with CXCL12 (15 nM) at either 37˚C and 4˚C. Following this, cells were centrifuged, washed twice with ice cold 0.5% BSA/PBS then re-suspended with 10 µg/µL of human CXCR7 (11G8, R&D Systems) or control (0.5% BSA/PBS only) and incubated for one hour at either 37˚C and 4˚C. Cells were centrifuged, washed twice with ice cold 0.5% BSA/PBS then re-suspended with anti-mouse Alexa Fluor® 488 (1:1000) and incubated for one hour at either 37˚C and 4˚C. Cells were centrifuged, washed twice with ice cold 0.5% BSA/PBS then re-suspended with 100 µL of paraformaldehyde incubated at 4˚C for 15 minutes. Finally, cells were centrifuged, washed twice with ice cold 0.5% BSA/PBS then re-suspended in a final volume of 300 µL of 0.5% BSA/PBS. Using a Beckman Coulter CytoFLEX with its associated CytExpert 1.2.11 software, cells were gated to exclude dead cells.

## 2.10. Cell Viability and Proliferation Assays

MTS assays were conducted using a CellTiter 96® AQueous Non-Radioactive Cell Proliferation Assay (Promega). Adherent cells at approximately 90% confluency were suspended via incubation with either PBS containing 5 mM of EDTA (MCF-7 cells) for 10 minutes or 0.25% trypsin-EDTA (1X) (Gibco) (all other adherent cell lines) for approximately 2 minutes. Following this, the cells were collected and centrifuged at 1200 rpm for 5 minutes. Wells in a 96-well plate were plated to contain 100 µL of cells at a density of $5x10^5$ $mL^{-1}$ in complete RPMI for suspension cells or $2x10^4$ $mL^{-1}$ in complete RPMI/DMEM (except in the negative control wells which contained complete media only). For MTS assays, the relevant inhibitors were added to their respective wells. The plate was then incubated at 37˚C, 95% air and 5% $CO_2$ for up to 72 hours. After this incubation period, cell viability or cell proliferation could be tested via the addition of 3-(4, 5-dimethylthiazol-2-yl)-5-(3-carboxymethoxyphenyl)-2-(4-sulfophenyl)-2H-tetrazolium (MTS) tetrazolium compound. This compound is bio-reduced by cells,

presumably by NADPH or NADH produced by dehydrogenase enzymes in the metabolically active cell. This reductions converts the MTS into a coloured formazan product that is soluble in tissue culture (Berridge and Tan, 1993). Therefore, aliquots of 10 µL of the CellTiter 96® Aqueous Assay Reagent were added directly to the wells and the plate was then incubated for 4-6 hours at 37˚C, 95% air and 5% $CO_2$. Following this, the plate was read using a FLUOstar Optima Flourometer and using Optima (BMG Labtech) software at an absorbance of 490 nm. The quantity of the coloured formazan product measured is directly proportional to the number of living cells.

## 2.11. Imaging Techniques

### 2.11.1. Phalloidin Actin Stain

MCF-7 cells were split at 90% confluency with PBS containing 5 mM of EDTA. Following this, cells were spun down at 1200 rpm and $1x10^5$ $mL^{-1}$ cells were cultured onto 70% ethanol washed 0.13 mm glass cover slips in a 12-well plate and incubated for 24 hours to allow cell adherence. The relevant chemokines and/or inhibitors were then added to their respective wells for one hour at 37˚C, 95% air and 5% $CO_2$. Alternatively, for PC3 cells; at approximately 90% confluency, PC3 cells were incubated with 0.25% trypsin-EDTA (1X) (Gibco) for 1-2 minutes, spun down at 1200 rpm and resuspended at a density of $1x10^5$ $mL^{-1}$ cells onto 70% ethanol washed 0.13 mm glass cover slips in a 12-well plate. Cells were incubated for approximately 6 hours to allow cell adherence and then the relevant chemokine and or PKC or PKD inhibitors added and the plate was incubated overnight. Following this all cells were washed twice with PBS and fixed for 10 minutes in 4% paraformaldehyde at room temperature. Cells were then gently washed twice with PBS then their cell membranes were permeabilised using 0.1% Triton X-100 (FisherBioTec) solution for 5 minutes. Cells were then washed twice in PBS then incubated with Phalloidin-iFluor 488 Conjugate (Abcam), 1:100 dilution in PBS, for 30 minutes in the dark at room temperature. Again, cells were washed twice with PBS then coverslips with cells were mounted onto glass coverslips using DPX mounting media (Fisher Scientific) that contains anti-oxidant to prevent fluorescent fading. Cells were visualized using an inverted Leica DMIL fluorescence microscope attached to its associated Leica DFC420 camera.

### 2.11.2. CXCR4 Receptor Stain of Adherent Cells

Adherent cells were incubation with either PBS containing 5 mM of EDTA (MCF-7 cells) for 10 minutes or 0.25% trypsin-EDTA (1X) (Gibco) (all other adherent cells) for approximately 2 minutes. Following this, the cells were collected and centrifuged at 1200 rpm for 5 minutes. Cells were grown on 70% ethanol washed 0.13 mm glass cover slips in a 12-well plate at a density of $1x10^5$ $mL^{-1}$ for 24 hours to allow cells to adhere. In the case of PC3 and SKMEL28 cells, the following day cells were washed twice with PBS then fixed with 4% paraformaldehyde for 10 minutes. Cells were washed twice with PBS then incubated with the relevant inhibitors and/or chemokines for one hour at either 4˚C or 37˚C. Following this, cells were washed twice in ice cold PBS then stained with either 12G5 or 4G10 anti-CXCR4 antibody (SantaCruz Biotechnology) (1:1000 in PBS, with PBS only used in the negative control) and incubated again for one hour at either 4°C and 37°C. Cells were washed twice in ice cold PBS then incubated in anti-mouse- Alexa Fluor® 488 secondary antibody (Sigma Alderich) (1:1000 in PBS) for another hour again at either 4°C or 37°C. Cells were washed twice with ice cold PBS then incubated with the cell nuclei stain 4', 6'-Diamidino-2-Pheylindoledihydrochloride or DAPI (Sigma) for 10 minutes. Again, cells were washed twice and all cells except PC3 or SKMEL28 were fixed with 4% paraformaldehyde for 10 minutes. Cells were washed twice then the coverslips were mounted onto glass slides using DPX mounting media (Fisher Scientific). After approximately one hour to allow the drying of the DPX, cells were visualized using an inverted Leica DMIL fluorescence microscope attached to its associated Leica DFC420 camera.

### 2.11.3. CXCR4 Receptor Stain of Suspension Cells

For suspension cells, the procedure carried out in 2.11.2 was followed however, cells were prepared in a suspension of 50 µL PBS in a 1.5 mL Eppendorf tube with a cell density of $2x10^6$ $mL^{-1}$. Cells were centrifuged and washed with ice cold PBS between treatments. Following the final incubation period, 10 µL of cells in PBS were loaded into DPX (Fisher Scientific) on a glass slide and covered with a 0.13 mm glass cover slip. After approximately 1-2 hours to allow the DPX to dry, cells were visualized using an inverted Leica DMIL fluorescence microscope attached to its associated Leica DFC420 camera.

### 2.11.4. ACKR3 Receptor Stain of Adherent and Suspension Cells

For both adherent and suspension cells, cells were prepared in a suspension of approximately $1x10^5$ $mL^{-1}$. Upon the last of the three centrifuge and washes, cells were resuspended in 10 µg/µL of human CXCR7 (11G8, R&D Systems) and incubated for one hour at either 4°C or 37°C. The cells were centrifuged and washed with ice cold PBS. PC3 cells were treated with 4% paraformaldehyde as previous, otherwise cells were then incubated with anti-mouse- Alexa Fluor® 488 secondary antibody (Sigma Alderich) (1:500 in PBS) for another hour at either 4°C or 37°C. Cells were washed twice with ice cold PBS then incubated with DAPI (Sigma) for 10 minutes. Again, all cells except PC3 cells were washed twice and fixed with 4% paraformaldehyde for 10 minutes. Following the final incubation period, 10 µL of cells were loaded into DPX (Fisher Scientific) on a glass slide and covered with a 0.13 mm glass cover slip. After approximately 1-2 hours to allow the DPX to dry, cells were visualized using an inverted Leica DMIL fluorescence microscope attached to its associated Leica DFC420 camera.

### 2.11.5. ACKR3 Receptor Internalization Inhibition of Adherent and Suspension Cells

Both adherent and suspension cells were prepared into a suspension of 250 µL in PBS in a 1.5 mL Eppendorf tube. Cells were then incubated either for 2 hours with Dynasore, 1 hour with filipin or MCD or 30 minutes with either PitStop 2, PitStop 2 negative control or CK666 at 37°C. Following incubation cells were washed three times with PBS and then protocol is conducted as in 2.11.4.

### 2.11.6. Copper-Catalysed Azide-Alkyne Cycloaddition Reaction (CuAAC)

Adherent MCF-7 cells were incubation with PBS containing 5 mM of EDTA for 10 minutes. Following this, the cells were seeded onto 0.13 mm glass cover slips in a 12-well plate at $1x10^5$ $mL^{-1}$ for up to 24 hours in DMEM culture medium. The following day, the cells were washed twice with PBS then incubated for one hour with 1 µM IS4 a 37˚C, 95% air and 5% $CO_2$. Following this, the cells were washed in ice cold PBS then incubated in a master mix of 30 mM sodium ascorbate (diluted in water), 1 mM $CuSO_4$ (diluted in water) and 0.1-0.45 mM 3-azido-7-hydroxycoumarin/IS6 (diluted in DMSO) at a volume of 500 mL for 10 to 60 minutes in the dark at room temperature. Alternatively, cells were washed twice

with PBS then incubated for one hour with 1 μM IS7 a 37˚C, 95% air and 5% $CO_2$. Then finally, cells were again washed twice with PBS then fixed with 4% paraformaldehyde for 10 minutes. Cells were then washed and mounted onto glass slides using DPX mounting media (Fisher Scientific). After approximately one hour, cells were visualized using a Leica DMIL microscope attached to its associated Leica DFC420 camera.

### 2.11.7. Microscopy

Fluorescently stained slides were all imaged using a Leica DMIL widefield epifluorescence microscope fitted with 10, 40 and 63x inverted air objectives and a colour DFC420 camera objective 0.55x. This made images taken on a 10x objective have a 5.5x overall magnification, 40x objective a 22x overall magnification and finally with a 63x objective there was an overall magnification of 35x. Leica images were captured and analysed using Leica Imaging Suite software with multi-coloured imaged overlays representing the true colours of the fluorescence dyes. All immunofluorescence was validated by using a negative control which consisted of secondary antibody only, thus would identify any non-specific staining.

Confocal images were taken using a Zeiss LSM510 META camera with Carl Zeiss LSM510 software using a monochromatic argon laser with 40% tube current and 6.7A. Images were taken using a 63x objective and Z-stacks were created to get a 3D image of cells.

### 2.11.8. Analysis of Fluorescence Intensity, Cell Area and Cell Circularity

Image J software was used to analyse fluorescence intensity or cell area and circularity by manually drawing around individual cells and from the ‘Analyse’ menu, selecting set measurements (including area, integrated density or cell area and circularity). For the analysis of background fluorescence, areas containing no cells were circled and the same protocol followed as previous. The formula; Corrected Total Cell Fluorescence (CTCF) = Integrated Density – (Area of selected cell x Mean fluorescence of background readings), can then be used to compare fluorescence intensity. A maximum of five cells were analysed per image.

## 2.12. Ethical Issues

All cell lines used were purchased from either the American Type Cell Culture (ATCC) or Merck who collected the cells in accordance with ethical regulations.

## 2.13. Statistical Analysis

All data were analysed using GraphPad Prism 6 and represents at least three independent experiments, unless otherwise stated. Statistical analyses were performed using either an unpaired Student's T-Tests or One-way ANOVA with post-hoc Tukey's or Dunnett's multiple comparison test. If data was normalised; a Wilcoxon Signed Rank Tests or Kruskal-Wallis non-parametric test with post hoc Dunn's multiple comparison test were conducted. All concentration response curves used to calculate $IC_{50}$ were fitted with a log (inhibitor) vs. response (three parameter) curve using percentage corrected data. Significance values of $p \leq 0.05$ (*) were deemed significant with a $p$ values of $p \leq 0.01$ (**), $p \leq 0.001$ (***) and $p \leq 0.0001$ (****) being highly significant. Any $p$ values of $p > 0.05$ were considered not significant (ns). All error bars represent the mean ± standard error (SEM) unless otherwise stated.

# Chapter 3: The Role of PKC and PKD in CXCL12 Directed Prostate Cancer Cell Migration

## 3.1. Introduction

Prostate cancer is the most common cancer in males in the UK and is the second most common cause of cancer deaths accounting for 14% of total cancer deaths in the UK (Cancer Research, 2017). This high death rate is not in relation to the primary cancer but due to the metastasis of the prostate cancer whereby it most commonly metastases to the bone (Chaffer and Weinberg, 2011, Thobe et al., 2011). There are several treatment options available for bone metastasis including chemotherapy and androgen ablation. However, there has been an emergence of 'castration-resistant' prostate cancers that no longer respond to these therapy (Frieling et al., 2015). An alternative approach is to look at preventing the signalling pathways that enable cancer metastasis to occur for example, protein kinase C (PKC) and protein kinase D (PKD) activation via the CXCR4/CXCL12 signalling axis (Taichman et al., 2002).

PKC and PKD are families of serine/threonine kinases of which there are nine isoforms of PKC and three isoforms of PKD, see Chapter 1.7.4. (Newton, 2009). Although not oncogenes, the overexpression of and subsequent activation of PKC and/or PKD has been related to cell transformation, tumour progression and metastasis (Martiny-Baron and Fabbro, 2007). While there has been extensive research into the involvement of different chemokines for cellular chemotaxis such as CXCL12, there is little information on which of the activated downstream signalling proteins or protein isoforms are required for chemokine cellular migration in different cancer cell types. We have previously shown that the downstream protein Rac1 is important in CXCL12 migration in both adherent and suspension cells but not in CCL3 migration (Mills et al., 2018). Moreover, we have found that different downstream signalling proteins, such as Src, are required in both leukemic Jurkat cells and MCF-7 breast cancer cells while inhibiting several PKC isoforms (PKCα, β1, δ, ε, γ, η) caused no effect on Jurkat cell migration but were required for MCF-7 cellular migration (Mills et al., 2016). The cause for these discrepancies is possibly due to different cancer cell types having different expression levels of different proteins, thus differing levels of PKC and PKD isoforms. For example; PKCα has been found to be upregulated and therefore shown to promote migration of colon, breast and lung cancers (Dowling et al., 2017, Mills et al., 2016). Based on this research, several PKCα targeted therapies including LY900003 and Aprinocarsen (ISIS 3521) amongst many others were synthesised, all of which were unsuccessful with no clinical trials featuring PKC

inhibitors currently open on www.clinicaltrials.gov (Rao et al., 2004, Villalona-Calero et al., 2004). Not only were these trials unsuccessful but some patients had worse outcomes. The cause of these failures was due to cancer-associated mutations in PKC that cause loss-of-function and subsequent tumour suppressor activity in a multitude of different cancers. This tumour suppressor activity is the consequence of the mutant PKC impairing the phosphorylation of other PKC isozymes thus reducing the steady state level of PKC (Newton, 2018). Therefore, more investigation into the roles of different PKC isoforms in different tissue types is vital for successful cancer therapeutics. This is also true for PKD as the exact role of PKD in cellular migration remains controversial with some groups suggesting that PKD acts as a negative regulator for cell migration while other suggest that PKD can drive cancer migration (Eiseler et al., 2007, Alpsoy and Gündüz, 2015, Peterburs et al., 2009). Therefore, while several PKD inhibitors have been synthesized, again there are currently no clinical trials open for these compounds (George et al., 2011).

## 3.2. Chapter Aims and Hypotheses

**Hypothesis**: That specific PKC isoforms and PKD are involved in CXCL12 driven prostate cancer migration.

**Aims:** To examine the roles of different PKC and PKD isoforms in CXCL12 stimulated PC3 prostate cancer migration using specific PKC or PKD inhibitors. Additionally, to examine intracellular calcium release and cytoskeletal changes after incubation with PKC and PKD inhibitors. This will give a pharmacological insight into the roles of these two proteins in PC3 prostate cancer migration and enable the furthering of knowledge on the intricate role of CXCL12 driven cancer progression.

## 3.3. Results

### 3.3.1. PKC and PKD are important for CXCL12-stimulated migration in prostate cancer cells

To determine the effects of PKC and PKD in prostate cancer, the androgen independent, metastatic prostate cancer cell line PC3 was treated with several specific PKC/PKD inhibitors: GF109203X for cPKCs (PKCα and PKCβ1) and nPKCs (PKCδ and PKCε); Staurosporine for cPKCs (PKCα and PKCγ) and nPKCs (PKCη); PKCζ Pseudosubstrate inhibitor and finally CID755673 for the three PKD isoforms. Expression of CXCR4 in PC3 cells was confirmed using a monoclonal antibody against CXCR4 (Figure 3.1).

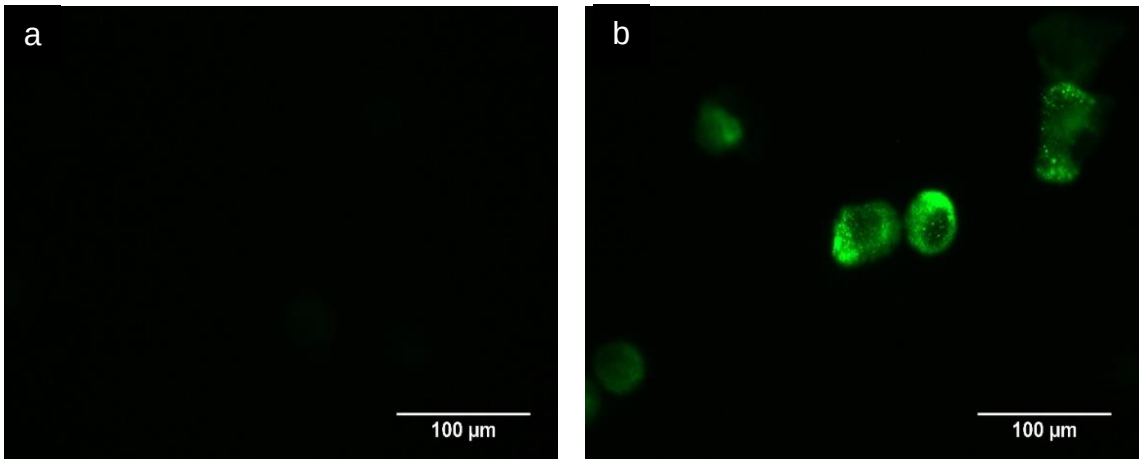


**Figure 3.1: CXCR4 expression in PC3 cells. a)** Negative control whereby PC3 cells were fixed with 4% paraformaldehyde then treated with secondary anti-mouse Alexa Fluor® 488 antibody before imaging. **b)** Positive control whereby PC3 cells fixed with 4% paraformaldehyde then CXCR4 was visualised using mouse 12G5 primary mAb and secondary anti-mouse Alexa Fluor® 488 antibody before imaging. Data shows representative cells from 7 independent experiments with similar findings. Acquired with Leica imaging suite with 63x objective, 35x overall magnification.

Inhibition of migration was examined by Oris™ Cell Migration assay and by time lapse assay. The three inhibitors GF109203X, PKCζ Pseudosubstrate inhibitor and CID755673 caused a significant reduction in migration in both assays when PC3 cells were stimulated by 10 nM CXCL12. Oris™ Cell Migration assay showed significant inhibitory effects of GF109203X, PKCζ Pseudosubstrate inhibitor and CID755673 after 24 hours (Figure 3.2).

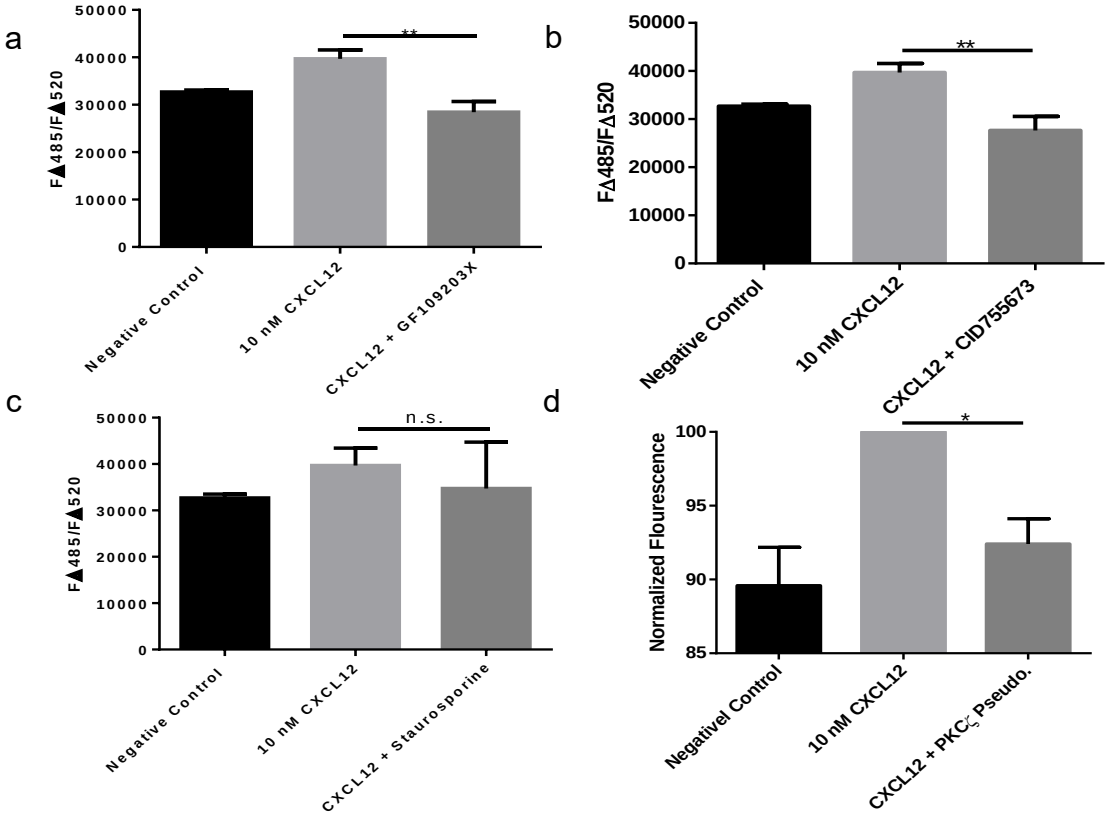


**Figure 3.2: PKC and PKD are important for CXCL12 stimulated PC3 cell migration determined using Oris™ Cell Migration assay.** PC3 cells were seeded and incubated for 24 hours before the addition of inhibitors and/or chemokine then incubated for a further 24 hours before analysis using calcein 485/520 nm. **a)** PC3 cells treated with and without 5 μM GF109203X (inhibitor of PKCα, β1, δ and ε) and stimulated with 10 nM CXCL12. **b)** PC3 cells treated with and without 11 μM CID755673 (inhibitor of PKD1, PKD2 and PKD3) and stimulated with 10 nM CXCL12. **c)** PC3 cells treated with and without 10 nM Staurosporine (inhibitor of PKCα, γ and η) and stimulated with 10 nM CXCL12. **d)** PC3 cells treated with and without 10 μM PKCζ Pseudosubstrate inhibitor then stimulated with 10 nM CXCL12. Data represents the mean ± SEM of 4-6 independent experiments. One-Way ANOVA with post hoc Dunnett's multiple comparison, or where data was normalised to CXCL12, Kruskal-Wallis non-parametric test with post hoc Dunn's multiple comparison test was conducted. N.s. = $p > 0.05$, * = $p \leq 0.05$ and ** = $p \leq 0.01$.

Time lapse assay showed the inhibitory effects of each compound over a 10-hour period (Figure 3.3). As summarised in Table 3.1, a significant decrease in migratory speeds from 46.95±4.55 μm/h to 19.19±6.442 μm/h with the addition of GF109203X and to 21.79±3.436 μm/h with CID755673 (Figure 3.3a) were found. Additionally, migratory speeds significantly decreased from 56.13±8.034 μm/h to 13.55±2.843 μm/h with the addition of PKCζ Pseudosubstrate inhibitor (Figure 3.3c). However, there was not a significant decrease in the migratory speeds of PC3 incubated with Staurosporine (untreated 46.87±6.436; treated 39.27±9.175) (Figure 3.3b). This reduced migration is not a consequence of cellular toxicity caused by the inhibitors as demonstrated by MTS assay (Appendix A1).

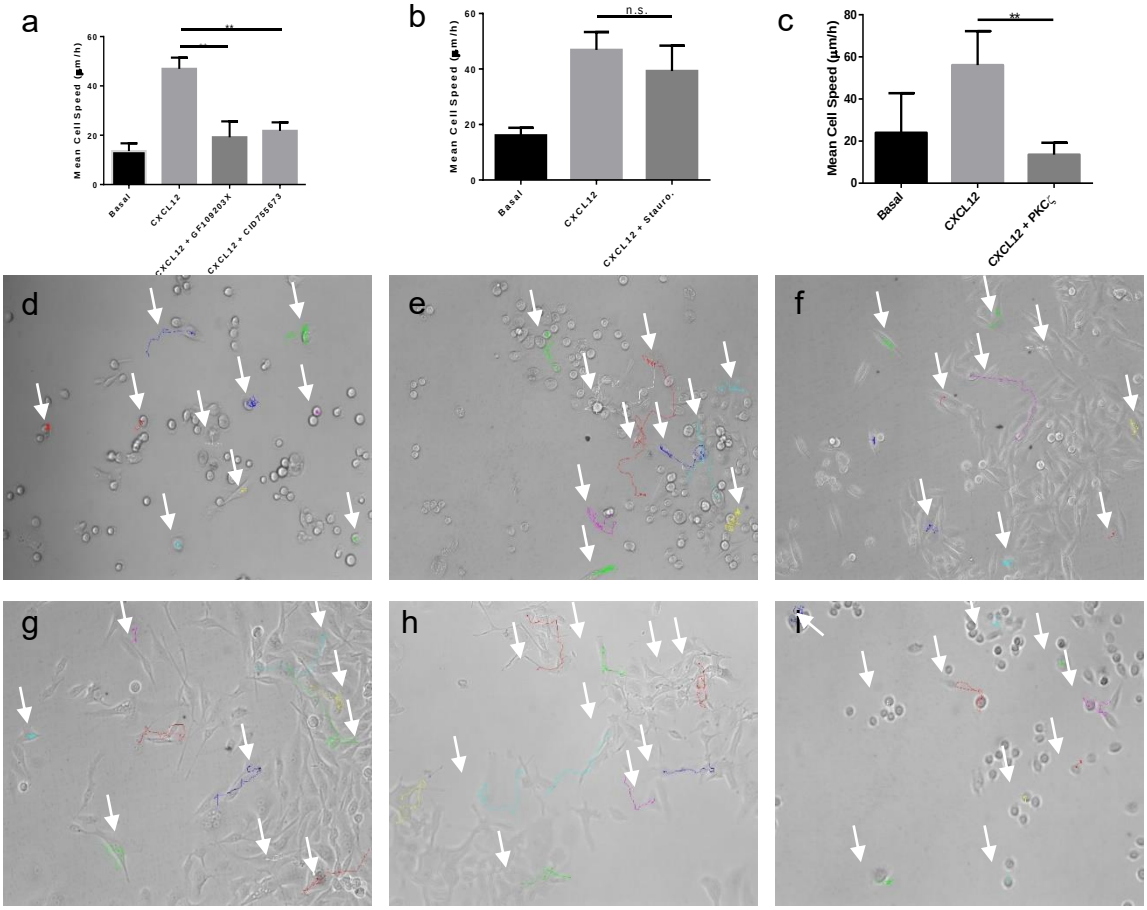


**Figure 3.3: PKC and PKD are important for CXCL12 stimulated PC3 migration determined using time lapse assay.** PC3 cells were seeded and incubated for 24 hours before the addition of inhibitors and/or chemokine then migration was tracked for 10 hours. **a)** 5 µM GF109203X (inhibitor of PKCα, β1, δ and ε) and 11 µM CID755673 (inhibitor of PKD1, PKD2 and PKD3). **b)** 10 nM Staurosporine (inhibitor of PKCα, γ and η). **c)** 10 µM PKCζ Pseudosubstrate inhibitor. **d)** Tracked basal PC3 cells. **e)** Tracked PC3 cells stimulated with 10 nM CXCL12. **f)** Tracked PC3 cells treated with 5 µM GF109203X and stimulated with 10 nM CXCL12. **g)** Tracked PC3 cells treated with 11 µM CID755673 and stimulated with 10 nM CXCL12. **h)** Tracked PC3 cells treated with 10 nM Staurosporine and stimulated with 10 nM CXCL12. **i)** Tracked PC3 cells treated with 10 µM PKCζ Pseudosubstrate inhibitor and stimulated with 10 nM CXCL12. Data shows representative cell tracks from 3-4 independent experiments with similar findings. Acquired with a Zeiss Axiovert 200M motorise inverted fluorescent/ live cell imaging microscope with 10x objective. Data represents the mean ± SEM of 3-4 independent experiments. One-Way ANOVA with post hoc Dunnett's multiple comparison n.s. = $p > 0.05$ and ** = $p \leq 0.01$.

**Table 3.1: PC3 migratory speeds when stimulated with 10 nM CXCL12 and treated with or without PKC/PKD inhibitors. Data represents the mean ± SEM of three or four independent experiments.**

| | Basal Speed (μm/h) | 10 nM CXCL12 Speed (μm/h) | Compound Speed (μm/h) |
|---|---|---|---|
| **5 μM GF109203X** | 13.58 ± 3.167 | 46.95 ± 4.551 | 19.19 ± 6.442 |
| **11 μM CID755673** | 13.58 ± 3.167 | 46.95 ± 4.551 | 21.79 ± 3.436 |
| **10 nM Staurosporine** | 16.07 ± 2.772 | 46.87 ± 6.436 | 39.27 ± 9.175 |
| **10 μM PKCζ Pseudosubstrate inhibitor** | 23.94 ± 9.427 | 56.13 ± 8.034 | 13.55 ± 2.843 |

### 3.3.2. PKC and PKD do not affect intracellular $Ca^{2+}$ release from prostate cancer cells

CXCL12 has been shown to induce a dose-dependent calcium response in adherent cells which can then utilize intracellular calcium to enhance migration (Agle et al., 2010). Owing to this, calcium release can be used to monitor ligand-receptor binding with the amount of calcium released being proportional to the amount of receptor binding thus the amount of signalling created via this binding. Therefore, the monitoring of calcium release can determine the extent of ligand binding with and without the presence of inhibitory antagonists (Grynkiewicz et al., 1985). Several PKC and PKD can be activated by $Ca^{2+}$ (Newton, 2009, Kunkel et al., 2007). Therefore, the release of $Ca^{2+}$ is upstream of PKC/PKD and so the inhibition of PKCs or PKDs should not affect calcium release. To confirm this, calcium release assays were conducted and as a result, incubation with GF109203X, CID755673, Staurosporine and PKCζ Pseudosubstrate inhibitor did not cause any significant difference in the release of $Ca^{2+}$ in PC3 cells (Figure 3.4).

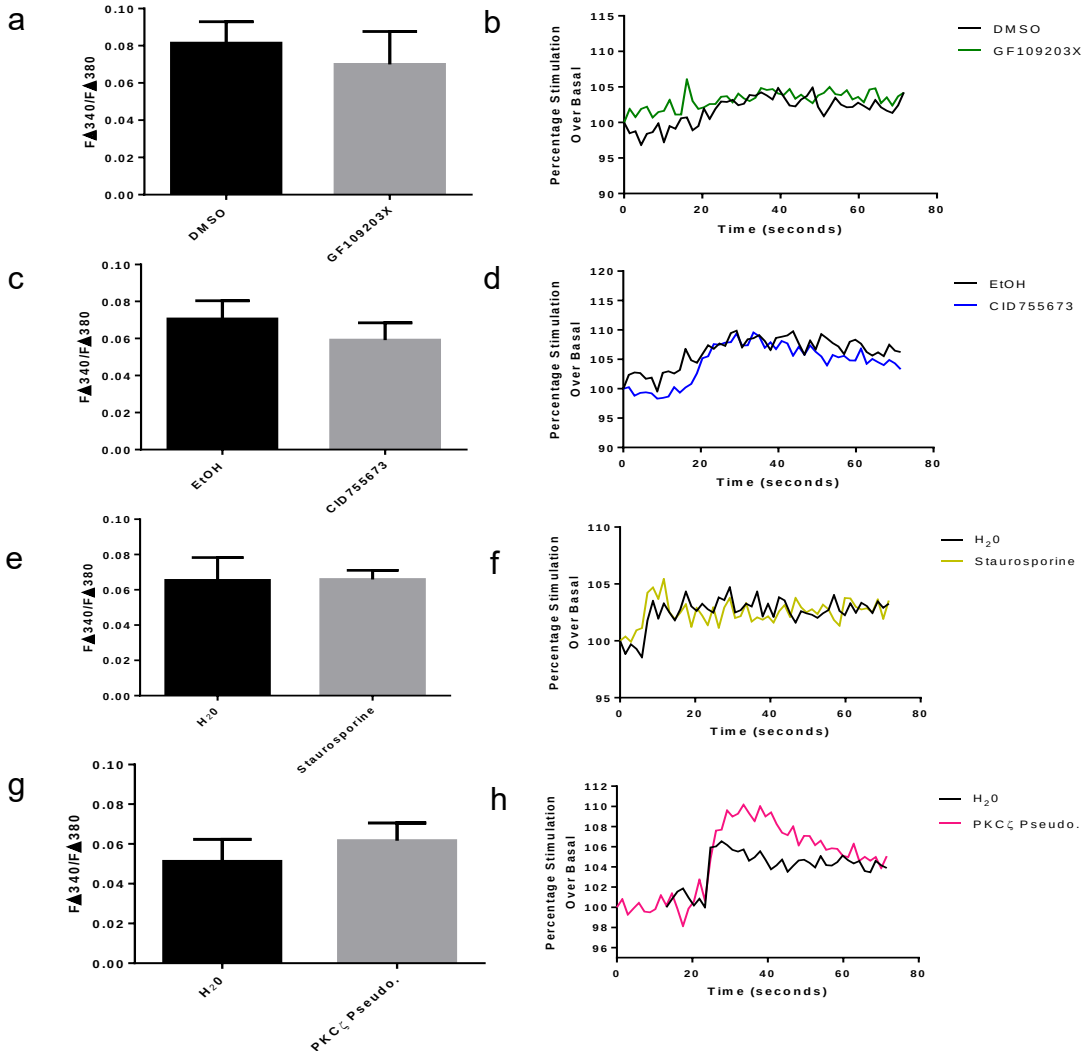


**Figure 3.4: PKC and PKD do not affect intracellular Ca2+ release from CXCL12 stimulated PC3 cells.** Cells were incubated for 30 minutes with inhibitor or vehicle control and the calcium indicator Fura-2 AM. **a)** 5 μM GF109203X (inhibitor of PKCα, β1, δ and ε) against equivalent volume DMSO vehicle. **b)** 5 μM GF109203X calcium release trace. **c)** 11 μM CID755673 (inhibitor of PKD1, PKD2 and PKD3) against equivalent volume EtOH vehicle. **d)** 11 μM CID755673 calcium release trace. **e)** 10 nM Staurosporine (inhibitor of PKCα, γ and η) against equivalent volume $H_20$ vehicle. **f)** 10 nM Staurosporine calcium release trace. **g)** 10 μM PKCζ Pseudosubstrate inhibitor against equivalent volume $H_20$ vehicle. **h)** 10 μM PKCζ Pseudosubstrate inhibitor calcium release trace. Data is expressed as a change in fluorescence ratio (340nm/380nm) where the basal fluorescence prior to the addition of 15 nM CXCL12 is subtracted from peak fluorescence following addition of CXCL12. Chemokine injected after 10 seconds. Data shows representative calcium traces from 3-4 independent experiments with similar findings. Data represents the mean ± SEM of 3-5 independent experiments. Student's T-test, results not significant.

### 3.3.3. PKC and PKD affect the cytoskeleton of prostate cancer cells

Both PKC and PKD have been implicated in cancer cell migration, thus may influence cellular cytoskeletal changes (Alpsoy and Gündüz, 2015, Mills et al., 2016). Therefore, PC3 cells were incubated with PKC/PKD inhibitors with or without 10 nM CXCL12 then subsequently stained with Phalloidin-iFluor 488 Conjugate to determine if the inhibitors cause any obvious changes to the actin cytoskeleton (Figure 3.5).

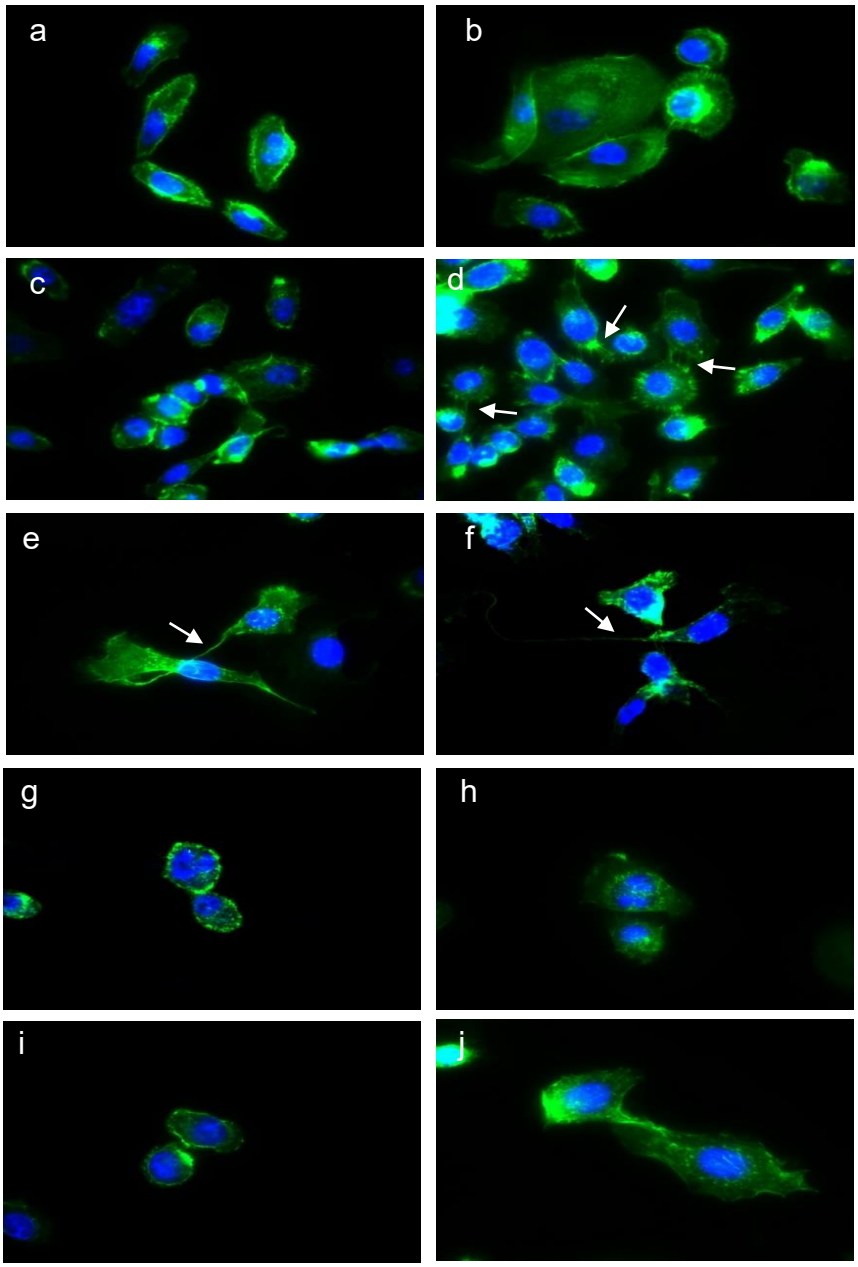


**Figure 3.5: PKC and PKD affect the cytoskeleton of PC3 cells.** PC3 cells were treated with inhibitors and/or chemokine for 24 hours then fixed with 4% paraformaldehyde for 10 minutes, permeabalised with 0.1% Triton X-100 for 5 minutes and stained with Phalloidin-iFluor 488 Conjugate (green) and DAPI (blue) before imaging. **a)** Basal. **b)** 10 nM CXCL12. **c)** 5 μM GF109203X (inhibitor of PKCα, β1, δ and ε). **d)** 5 μM GF109203X and 10 nM CXCL12. Arrows indicative of stress fibres. **e)** 11 μM CID755673 (inhibitor of PKD1, PKD2 and PKD3). Arrow indicative of cell elongation. **f)** 11 μM CID755673 and 10 nM CXCL12. Arrow indicative of cell elongation. **g)** 10 nM Staurosporine (inhibitor of PKCα, γ and η). **h)** 10 nM Staurosporine and 10 nM CXCL12. **i)** 10 μM PKCζ Pseudosubstrate inhibitor. **j)** 10 μM PKCζ Pseudosubstrate inhibitor and 10 nM CXCL12. Data shows representative cells from 5 independent experiments with similar findings. Acquired with Leica imaging suite with 63x objective, 35x overall magnification.

Specifically cell area and cell circularity were analysed (Figure 3.6 and Figure 3.7, respectively). Compared to the basal, the addition of 10 nM CXCL12 showed a trend of increased area but no overall change to cell shape (Figure 3.5a and b, 3.6a, 3.7a). Incubation with GF109203X with or without CXCL12 and Staurosporine with or without CXCL12 showed a significant decrease in cellular area (Figure 3.6b and d). CID755673 treatment showed no significant change in area (Figure 3.6c) while PC3 cells incubated with PKCζ Pseudosubstrate inhibitor and CXCL12 showed a significant increased cellular area (Figure 3.6e). In relation to cell shape, GF109203X and PKCζ Pseudosubstrate inhibitor showed no significant difference in cell shape compared to basal and incubation with 10 nM CXCL12 (Figure 3.7b and e). Incubation with GF109203X produced a noticeable increased number of stress fibres (Figure 3.5c and d). Incubation with CID755673 showed a discernible shape change with cells becoming more elongated and appearing 'sticky' due to what appear to be a lack of release of the cell tail and often cells were seen sticking to one another (Figure 3.5e and f and Figure 3.7a). While Staurosporine caused no significant change to migration, incubation with Staurosporine caused cells to significantly have a more rounded morphology (Figure 3.7d and Figure 3.5g and h).

.

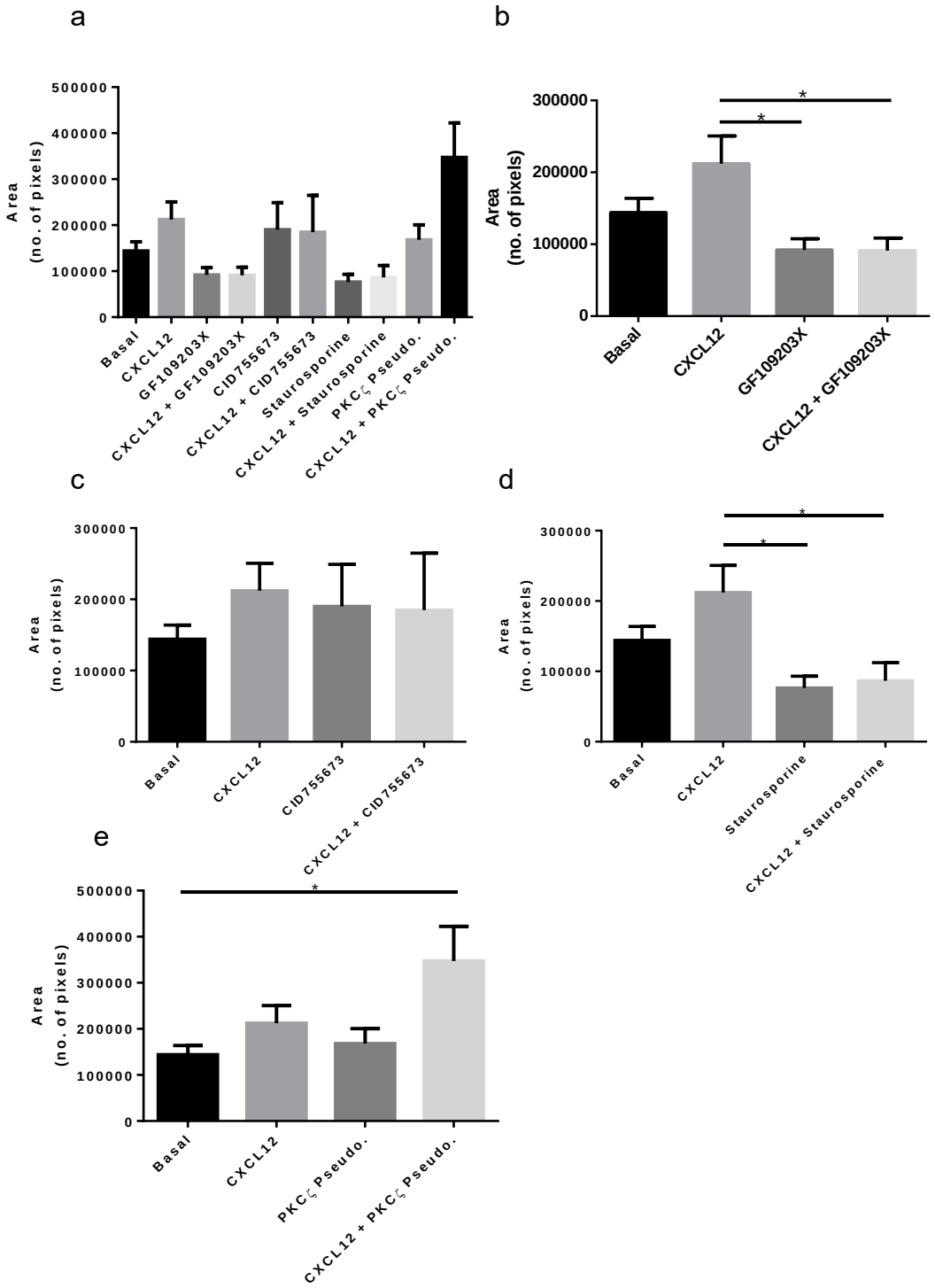


**Figure 3.6: Specific PKC inhibitors affect PC3 cell area.** Analysis of Phalloidin-iFluor 488 Conjugate stained PC3 cells from Figure 3.5 using ImageJ. **a)** Area of cells under all treatment conditions. **b)** 5 µM GF109203X (inhibitor of PKCα, β1, δ and ε) with and without 10 nM CXCL12. **c)** 11 µM CID755673 (inhibitor of PKD1, PKD2 and PKD3) with and without 10 nM CXCL12. **d)** 10 nM Staurosporine (inhibitor of PKCα, γ and η) with and without 10 nM CXCL12. **e)** 10 µM PKCζ Pseudosubstrate inhibitor with and without 10 nM CXCL12. Data represents the mean ± SEM of 4 independent experiments. One-Way ANOVA with post hoc Dunnett's multiple comparison * = p≤ 0.05.

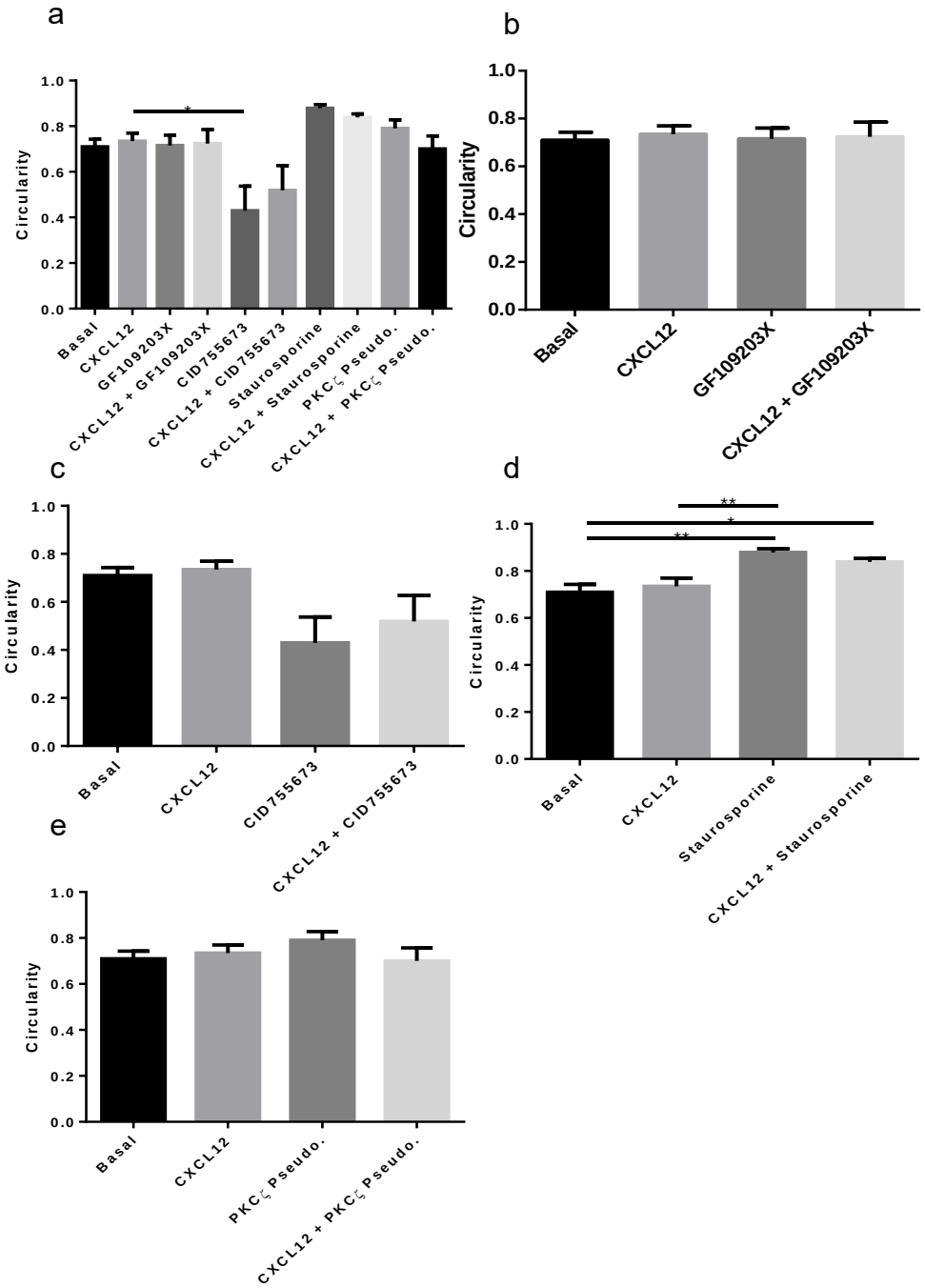


**Figure 3.7: Specific PKC and PKD inhibitors affect PC3 cell circularity.** Analysis of Phalloidin-iFluor 488 Conjugate stained PC3 cells from Figure 3.5 using ImageJ. **a)** Circularity of cells under all treatment conditions. **b)** 5 µM GF109203X (inhibitor of PKCα, β1, δ and ε) with and without 10 nM CXCL12. **c)** 11 µM CID755673 (inhibitor of PKD1, PKD2 and PKD3) with and without 10 nM CXCL12. **d)** 10 nM Staurosporine (inhibitor of PKCα, γ and η) with and without 10 nM CXCL12. **e)** 10 µM PKCζ Pseudosubstrate inhibitor with and without 10 nM CXCL12. 0 indicates more elongated, 1 indicates more rounded morphology. Data represents the mean ± SEM of 5 independent experiments. One-Way ANOVA with post hoc Dunnett's multiple comparison, * = p≤ 0.05 and ** = p≤ 0.01.

## 3.4. Discussion

Chemokine receptors are well known to be involved in cancer cell migration and specifically the CXCR4 receptor has been shown to be upregulated in a number of different cancers leading to metastasis (Borrello et al., 2005, Koshiba et al., 2000, Mehta et al., 2007, Müller et al., 2001, Singh et al., 2009). However, while there has been much investigation into different chemokines such as CXCL12, there is little information on which of the activated downstream signalling proteins are required for chemokine cellular migration in different cancer cell types. Specifically, the involvement of PKC and PKD in cancer migration has produced conflicting results due to different cancer cell lines requiring different isoforms to enable migration under different chemokine stimuli. Therefore, the aim of this chapter was to examine the role of PKC and PKD specifically in CXCL12 stimulated PC3 cell migration. This will expand upon our previous knowledge of the role of PKC as discussed in Mills et al. (2016) where it was shown that inhibiting several PKC isoforms (PKCα, β1, δ, ε, γ, η) had no effect on CXCL12 stimulated Jurkat cellular migration but were required for CXCL12 stimulated MCF-7 cellular migration.

It was confirmed that both PKCs and PKDs are required for CXCL12 stimulated migration in the PC3 metastatic prostate cancer cell line. Three inhibitors significantly reduced the speed of PC3 cells: CID755673 specific to PKD isoforms; PKCζ Pseudosubstrate inhibitor specific to PKCζ and GF109203X a less specific compound that inhibits both cPKCs (PKCα and PKCβ1) and nPKCs (PKCδ and PKCε). Staurosporine (inhibitor of cPKCs (PKCα and PKCγ) and nPKCs (PKCη)) caused no significant change to migration. However, from this it can be discerned that PKCα, inhibited by both GF109203X and Staurosporine, is likely not important for CXCL12 mediated PC3 cell migration due to the ineffectiveness of Staurosporine in reducing PC3 migratory speeds. This is contrary to evidence that PKCα is required for MCF-7 cell migration (Mills et al., 2016). However, PKCα has been found to have tumour suppressing activities in cancers such as lung cancer and has been shown to contribute to cell death in androgen-dependant prostate cancer cells (Tanaka et al., 2003, Hill et al., 2014). While PC3 cancer cells are androgen-independent, it appears that PKCα also does not affect CXCL12 mediated PC3 migration. Additionally, due to Staurosporine having no significant effect upon migration, it is possible to assume that PKCγ and PKCη do not contribute to CXCL12 mediated PC3 cellular

migration. PKCα and PKCε have previously been shown to control focal adhesion formation and activation of integrins, respectively, thus implicating a role in mesenchymal migration (Disatnik and Rando, 1999, Gimona et al., 2008). This would implicate that while PKCα may not be involved in PC3 migration, PKCε may be important in the migration of PC3 cells. This corroborates with work by Mills et al. (2016) whom found that inhibition of PKCα and PKCε in MCF-7 cells caused significantly reduced migration, while inhibition of PKCα and PKCε in Jurkat cells has no effect upon their potential to migrate. This would implicate that inhibition of PKCα and PKCε negatively effects mesenchymal migration due to preventing successful integrin formation in both MCF-7 and PC3 cells, while in Jurkat cells, which migrate via amoeboid migration thus does not require integrin formation, was unaffected. However, it cannot be concretely determined here which of the targets of GF109203X, PKCβ1, PKCδ or PKCε, are required for cellular migration. Each isoform has already been implicated in cancer migration for example; PKCδ has been linked to apoptotic cellular death in androgen-dependant prostate cancer but conversely has also been shown to enhance androgen-dependant prostate cancer invasiveness (Fujii et al., 2000, Villar et al., 2007). There is little information about the role of PKCβ1 in prostate cancer migration. However, it has been shown that PKCβ isoforms contribute to the progression of many cancers including prostate with inhibition of PKCβ1 in androgen-dependant tumours preventing tumour proliferation (Metzger et al., 2010). Finally, PKCε overexpression has been shown to enable the conversion of LNCaP androgen dependant cell to androgen-independent variants and can subsequently protect these variants against apoptotic stimuli, thus enabling prostate cancer proliferation (Meshki et al., 2010, Wu et al., 2002). Additionally, Hafeez et al. (2011) found that genetic deletion of PKCε inhibited prostate cancer development and metastasis, suggesting a role of PKCε in prostate cancer migration. Unfortunately, due to the promiscuity of GF109203X, from this data alone we cannot determine which of the three isoforms of PKC or combination of these isoforms contribute specifically to CXCL12 mediated PC3 migration. Further studies would have to be conducted using more specific PKC/PKD inhibitors such as the PKCβ inhibitor CAS 257879-35-9, PKCβII inhibitor CAS 145915-60-2, PKCη Pseudosubstrate inhibitor, PKCθ Pseudosubstrate inhibitor, PKCε translocation peptide amongst other inhibitors available from Merck. It would also have been beneficial to conduct experiments using the inhibitors

without the presence of CXCL12 to determine if they have any effect upon the basal level of migration. Additionally, siRNA knockdown studies are paramount to confirm the results obtained with these small molecule inhibitors.

We found that none of the four inhibitors affected CXCL12 mediated intracellular calcium release which was to be expected as intracellular calcium release is upstream of PKC activation (Newton, 2009). Therefore, this demonstrated that these inhibitors were not having off target effects in relation to CXCL12 stimulated calcium release.

In relation to PC3 migration, it has been found that PC3 cells can migrate via both mesenchymal and in a more rounded amoeboid form of migration (Caley et al., 2016, Morley et al., 2014, Paul et al., 2017). While amoeboid migration has previously been considered as random shape change, it has recently been found that it actually involves symmetrical changes involving G proteins and the actin cytoskeleton (van Haastert et al., 2018). This form of amoeboid migration is specifically called α-motility i.e. protrusion based amoeboid migration (Fritz-Laylin et al., 2017). Due to the involvement of protrusions and the actin cytoskeleton in both modes of migration, distinguishing which method was being utilized by PC3 was difficult to ascertain in these experiments. Therefore, future experiments such as siRNA knockdown of RhoA, Rac and FAK are paramount to determine which mode of motility is utilised by PC3 cells. However, in relation to shape change, the addition of 10 nM of CXCL12 demonstrated a trend of increased cellular area but no change in cell circularity. This is possibly due to analysing cells at the beginning of cellular division. However, it was found that 10 nM of CXCL12 did not cause an increased in cellular proliferation (Appendix A3). Therefore, it is more likely that the addition of CXCL12 enabled the capture of more cells in the process of migrating with wide pseudopodia protrusions. Incubation with GF109203X saw a reduction in the size of individual cells with little change to the cell shape but with an increased number of cellular protrusions similar in appearance to stress fibres. This indicates a loss of polarization of the cell due to the randomness of these protrusions and the decrease in cell size is indicative that migration was reduced, possibly due to loss of the pseudopodia protrusion. As discussed previously, while it cannot be ascertained which PKC isoform(s) are responsible for these cytoskeletal changes, classical and novel PKC all have roles in regulating the actin cytoskeleton (reviewed in Larsson (2006)). PKCα, PKCγ and PKCη inhibition through Staurosporine caused cells to

assume a smaller and more rounded morphology that can be confirmed to not be related to apoptosis (Appendix A1) and due to the apoptotic properties of Staurosporine only being achieved with a concentration of 200-1000 nM (Thuret et al., 2003, Zhang et al., 2004). Therefore, the change in cell size and shape is most likely to be in relation to more cells transitioning to amoeboid cellular migration. In opposition to this, PKD inhibition by CID755673 caused the PC3 cells to assume a more elongated morphology with no change to area. This is indicative of a transition from amoeboid to mesenchymal migration. Additionally, it seemed that the cells have lost the ability to detach their tails due to very elongated cells with a 'sticky' appearance, indicating a role for PKD in tail detachment. This is most likely in relation to PKD isoforms being localised to and regulating focal adhesions (FA), dynamic structures that are continuously assembled and disassembled during protrusion based cellular migration (Durand et al., 2016). It is known that PKD1 generally blocks cellular migration by localising to the leading edge and inhibits the activity of slingshot proteins thus preventing cellular migration (Eiseler et al., 2009, Eiseler et al., 2007). However, CID755673 is a non-specific PKD inhibitor, thus inhibits PKD1 but also PKD2 and PKD3 both of which have been found to promote cellular invasion by modulating NF-κB and HDAC1 expressions (Zou et al., 2012). The results presented here implicate a novel role of PKD2 and PKD3 in tail release however, more investigation into this is required as well as investigations into the cause for the transition from amoeboid to mesenchymal migration and vice versa. Finally, PKCζ inhibition demonstrated no shape or area change in cells. However, incubation with both PKCζ Pseudosubstrate inhibitor and 10 nM CXCL12 actually saw an increase in cell size. This is possibly in relation to PKCζ inhibition enabling pseudopodia protrusions therefore, increasing cellular size, but not enabling the cell to then migrate in that direction possibly due to these protrusions being unregulated and non-directional protrusions creating larger and non-functional pseudopodia. This abrogation of actin polarisation in relation to PKCζ inhibition was also seen by Petit et al. (2005) where they found that blocking PKCζ abolished CXCL12 stimulated actin polymerisation in $CD34^{+}$ and G2 human cells due to PKCζ directly associating with the cytoskeleton. While cell shape and circularity were analysed, it may be beneficial to conducted Corrected Total Cell Fluorescence (CTCF) analysis to determine the level of actin polymerisation i.e.

if these inhibitors are negatively affected the ability of PC3 cells to reorganise its cytoskeleton.

Overall, PKCζ has a very dominant role in preventing cellular migration, not only in CXCL12 driven PC3 cells, but also in CXCL12 driven THP-1, Jurkat and MCF-7 migration (Appendix A2) (Mills et al., 2016). It is possible that the broad inhibitory properties of PKCζ over other PKC isoform could be related to the proteins atypical activation or more likely related to its expression levels across these cell types. Again, this suggests the need for siRNA knockdown studies to confirm if the PKCζ isoform is the strongest target to develop novel therapeutics for the prevention of CXCL12 driven cellular migration.

## 3.5 Conclusions

It can be concluded that specific classical, novel and atypical PKC isoforms and PKD are important for CXCL12 directed migration in PC3 prostate cancer cells. Specifically, the classical isoforms PKCα and PKCγ and the novel PKC isoform PKCη are not important for CXCL12 stimulated migration in PC3 prostate cancer cells. PKC and PKD do not affect intracellular calcium release from PC3 cells. Both PKC and PKD affect the normal cytoskeletal dynamics of PC3 cells. Finally, PKCζ might possibly be the strongest target for future development of novel cancer therapies due to its inhibitory activity across several cell lines.

# Chapter 4: Effects of the CXCR4 Antagonists AMD3100, AZ3-2 and AZ6-2 on CXCL12 Directed Cancer Cell Migration

**Acknowledgements**

I thank Dr M. M. D. Cominetti for synthesising AZ3-2 and AZ6-2 as well as supervising the production of two batches of AZ6-2. I would also like to thank Dr M. M. D. Cominetti for conducting the preparative and analytical HPLC, including the supervision of two preparative and analytical HPLC analyses, as well as conducting all the MALDI-TOF and NMR analyses on both AZ3-2 and AZ6-2.

## 4.1. Introduction

CXCR4 has a major role in neutrophil homeostasis whereby expression levels of CXCR4 increase on old or senescent neutrophils, aiding in their clearance from the blood to the bone marrow (Martin et al., 2003). However, increased expression of CXCR4 has also been observed on many types of tumour cells and to date including but not limited to: acute myeloid leukaemia, breast, ovarian, melanoma, thyroid, renal, pancreatic, prostate cancer and more recently salivary gland neoplasms (Borrello et al., 2005, Koshiba et al., 2000, Mehta et al., 2007, Müller et al., 2001, Scotton et al., 2001, Singh et al., 2004, Staller et al., 2003, Vela et al., 2015, Phattarataratip and Dhanuthai, 2017). This aberrant CXCR4 signalling increases metastatic potential enabling tumours to migrate to tissue sites in the body that naturally express CXCL12 such as the bone marrow, brain, lungs, liver etc. (Johnson et al., 2004, Müller et al., 2001). Therefore, the inhibition of the CXCR4/CXCL12 migratory pathway can potential lead to the prevention of tumour metastasis. However, while multiple CXCR4-peptidic and non-peptidic antagonists have been developed, most CXCR4 antagonists never progress from pre-clinical stages. This is extensively reviewed in Domanska et al. (2013) with a comprehensive list of the more recent CXCR4/CXCL12 inhibitors in preclinical development or in clinical trials listed in Table 1.3. Two exception are Plerixafor (AMD3100) which was approved by the FDA for therapeutic use in MM and NHL in 2008 and CTCE-9908, approved for use in osteosarcoma only (Wong et al., 2014, DiPersio et al., 2009b). However, the use of AMD3100 in these cancers is not for the prevention of metastasis but for mobilizing stem cells from the bone marrow for autologous stem cell transplantation (DiPersio et al., 2009b). Therefore, the development of novel CXCR4 antagonist is paramount for the progression of personalised medicine and cancer therapeutics.

Recently, Portella et al. (2013) synthesized a CXCL12-mimetic peptide called ‘R’ that proved to successfully reduce migration in osteosarcoma and hepatocellular carcinoma cells (Fontanella et al., 2016). A modified analogue of Peptide ‘R’ called Peptide ‘R29’ was found to suppress T regulatory cells (that express high levels of CXCR4) in renal cancer (Santagata et al., 2017). Peptide ‘R’ has since been used to synthesise several disulphide-bridged cyclic peptidic antagonists. One particular analogue, ‘10’ (named throughout as AZ6-2), was effective at impairing CXCL12 directed migration in both HT29 and HCT116 colon cancer cell lines and the CCRF-CEM acute lymphoblastic leukaemia (ALL) cell

line (Di Maro et al., 2016). AZ6-2 has also been proven to be stable up to 180 minutes in human plasma at 37˚C and demonstrated limited ability to bind to CXCR7/ACKR3.

Some of these peptide analogues have progressed into clinical trials (Santagata et al., 2017). However, the initial research investigated only a limited number of cancer cell lines therefore, it is not known how broad these peptides are. Additionally, these peptides underwent limited biological investigation hence, more research is required to characterise these peptides in order to gain an insight into their broader potential.

## 4.2. Chapter Aims and Hypotheses

**Hypotheses:** The CXCL12 mimetic cyclic peptide, AZ6-2, has an antagonistic effect against multiple cancer cell line overexpressing CXCR4. AZ6-2 is more potent than the already marketed AMD3100 and more potent than analogue '3' (named throughout as AZ3-2). The only difference between AZ3-2 and AZ6-2 is the conformation of the first cysteine (AZ6-2 is in the *D* configuration creating Arg-Ala-[DCys-Arg-Phe-Phe-Cys]). Our final hypothesis is that AZ6-2 is specific for the CXCR4 receptor.

**Aims:** To identify at least two adherent and two suspension cell lines that naturally express high levels of CXCR4. To examine the antagonistic effect of AZ6-2, AZ3-2 and AMD3100 in CXCL12 stimulated cancer cell migration and upon CXCL12 stimulated intracellular calcium release. Additionally, to confirm that AZ6-2 is a CXCL12-mimetic and is CXCR4 specific. To determine the effects of these compound in relation to cell area, shape and cytoskeletal changes or if these compounds initiate receptor internalisation. Finally, to determine if AZ6-2 is specific to the CXCR4 receptor only. This will give a deeper insight into the application of these CXCR4 antagonists and enable the furthering of knowledge about the effect these antagonists have upon cancerous cells.

## 4.3. Results

### 4.3.1. Jurkat and THP-1 suspension cells express CXCR4

The Jurkat cell line is derived from the peripheral blood of a 14-year-old male donor with acute T cell leukaemia and has been proven to express high levels of the CXCR4 human chemokine receptor (ATCC, 2017b, Hesselgesser et al., 1998). This expression was confirmed using a monoclonal antibody against CXCR4 (Figure 4.1 and Table 4.1).

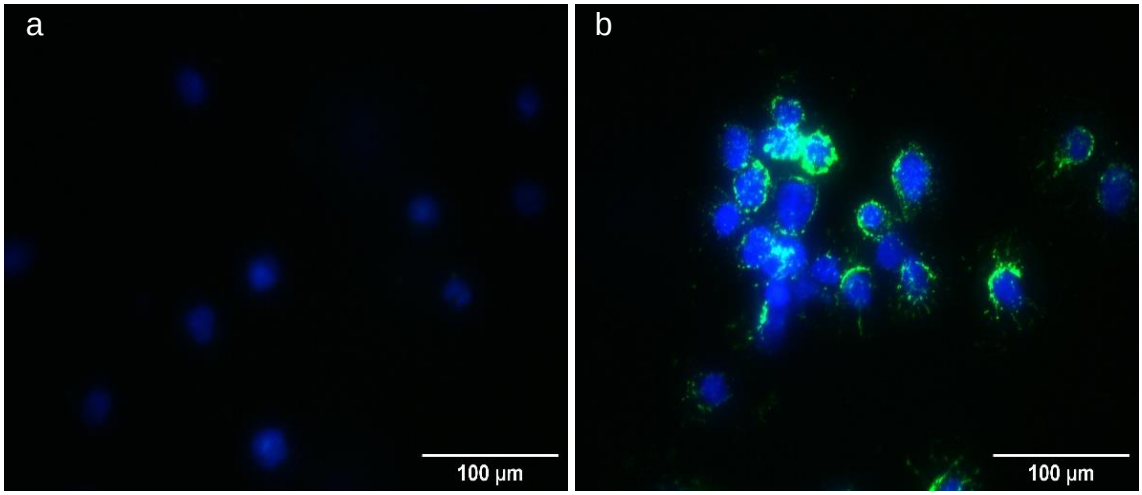


**Figure 4.1: CXCR4 expression in Jurkat cells**. **a)** Negative control treated with secondary anti-mouse Alexa Fluor® 488 antibody (green), DAPI (blue) and fixed with 4% paraformaldehyde before imaging. **b)** Positive control whereby CXCR4 was visualised on Jurkat cells using mouse 12G5 primary mAb, secondary anti-mouse Alexa Fluor® 488 antibody (green), DAPI (blue) and fixed with 4% paraformaldehyde before imaging. Data shows representative cells from 8 independent experiments with similar findings. Acquired with Leica imaging suite with 63x objective, 35x overall magnification.

**Table 4.1: Cellular Expression of CXCR4**

| Cell Line | CXCR4 Expression |
|---|---|
| **Jurkat** | ✓ |
| **THP-1** | ✓ |
| **PC3** | ✓ |
| **MCF-7** | ✓ |
| **SKMEL28** | ✓ |
| **BT-474** | × |
| **SKBR3** | × |
| **H292** | × |
| **A549** | × |
| **MDA-MB-231** | × |

The THP-1 cell line is derived from the peripheral blood of a 1-year-old male donor with AML and is a good research model due to expressing high levels of the CXCR4 human chemokine receptor (ATCC, 2017e, Yu et al., 2018) . Again, this expression was confirmed using a monoclonal antibody against CXCR4 (Figure 4.2 and Table 4.1).

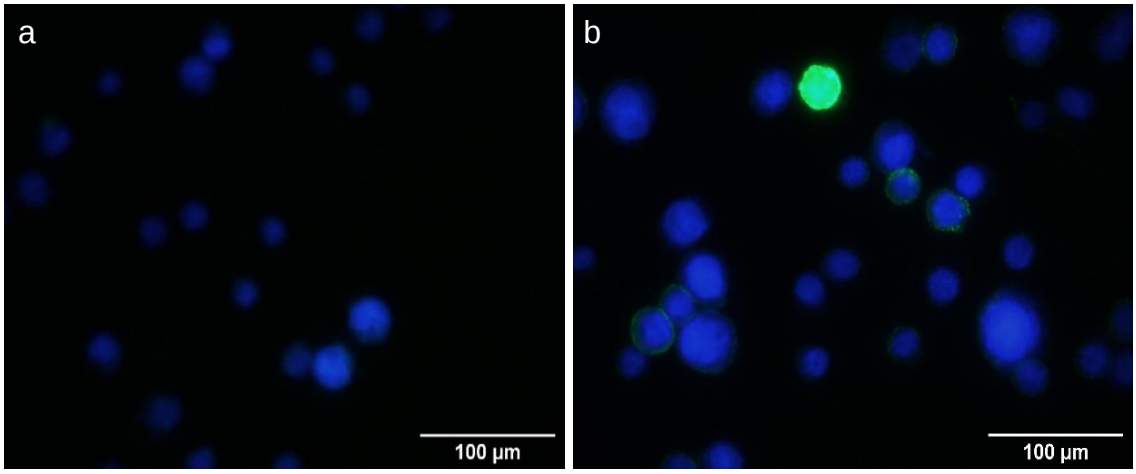


**Figure 4.2: CXCR4 expression in THP-1 cells. a)** Negative control treated with secondary anti-mouse Alexa Fluor® 488 antibody (green), DAPI (blue) and fixed with 4% paraformaldehyde before imaging. **b)** Positive control whereby CXCR4 was visualised on THP-1 cells using mouse 12G5 primary mAb, secondary anti-mouse Alexa Fluor® 488 antibody (green), DAPI (blue) and fixed with 4% paraformaldehyde before imaging. Data shows representative cells from 6 independent experiments with similar findings. Acquired with Leica imaging suite with 63x objective, 35x overall magnification.

### 4.3.2. PC3, MCF-7 and SKMEL28 adherent cells express CXCR4

PC3 cells, as investigated in Chapter 3, are metastatic prostate cancer cells that have previously been confirmed to express CXCR4 (Figure 3.1 and Table 4.1). The MCF-7 cell line is derived from the mammary glands of a patient with metastatic adenocarcinoma and has been show in the literature to express CXCR4 (Akekawatchai et al., 2005, Merck, 2017). This expression was confirmed using a monoclonal antibody against CXCR4 (Figure 4.3).

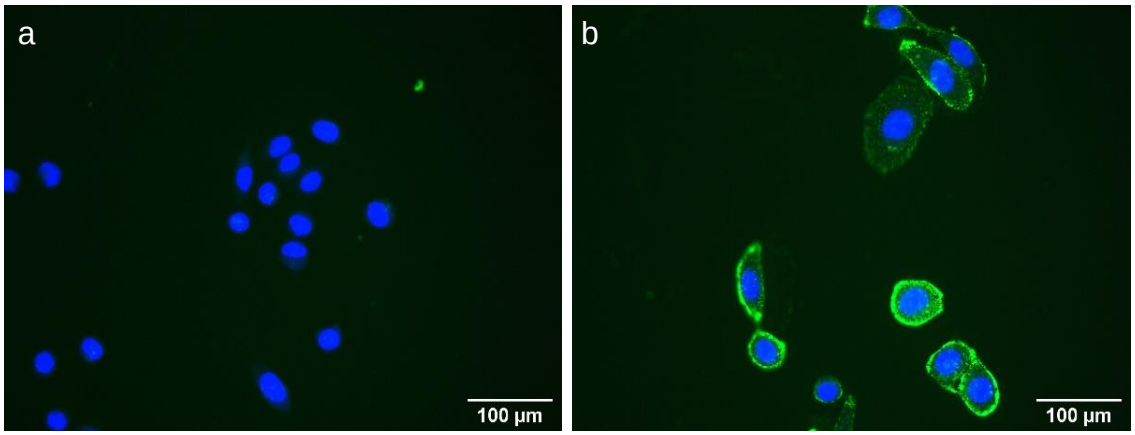


**Figure 4.3: CXCR4 expression in MCF-7 cells. a)** Negative control treated with secondary anti-mouse Alexa Fluor® 488 antibody (green), DAPI (blue) and fixed with 4% paraformaldehyde before imaging**. b)** Positive control whereby CXCR4 was visualised on MCF-7 cells using mouse 12G5 primary mAb, secondary anti-mouse Alexa Fluor® 488 antibody (green), DAPI (blue) and fixed with 4% paraformaldehyde before imaging. Data shows representative cells from 12 independent experiments with similar findings. Acquired with Leica imaging suite with 40x objective, 22x overall magnification.

SKMEL28 cells are malignant melanoma cells derived from the skin and are more commonly used for research into the V600E mutation in B-Raf. It was confirmed that this cell line also expresses CXCR4 (Figure 4.4). Other cell lines including: BT-474, H292, A549 and MDA-MB-231, were also assessed but were found to not express high enough levels of CXCR4 for future studies (Table 4.1).

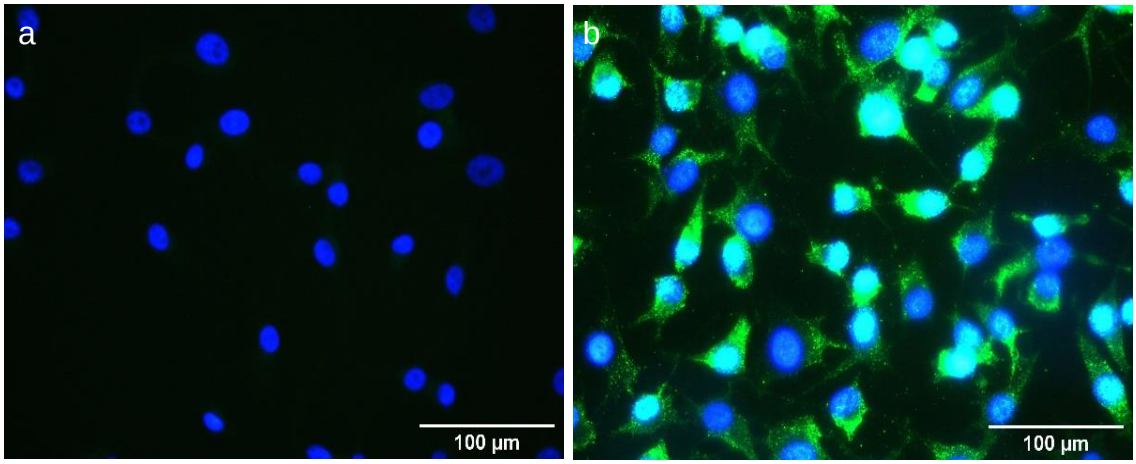


**Figure 4.4: CXCR4 expression in SKMEL28 cells. a)** Negative control SKMEL28 cells were fixed with 4% paraformaldehyde then treated with secondary anti-mouse Alexa Fluor® 488 antibody (green) and DAPI (blue) before imaging**. b)** Positive control whereby SKMEL28 cells were fixed with 4% paraformaldehyde then CXCR4 was visualised using mouse 12G5 primary mAb, secondary anti-mouse Alexa Fluor® 488 antibody (green) and DAPI (blue) before imaging. Data shows representative cells from 6 independent experiments with similar findings. Acquired with Leica imaging suite with 63x objective, 35x overall magnification.

### 4.3.3. CXCL12 directed migration in Jurkat cells is inhibited by AMD3100, AZ3-2 and AZ6-2

To enable comparisons between the two novel CXCR4 antagonists and the already marketed CXCR4 antagonist, AMD3100, chemotaxis assays were conducted using a 10-fold dose range of AMD3100 from 0.1-1000 nM. Using the raw data, AMD3100 did not significantly inhibit CXCL12 directed migration in the Jurkat cell line however there was a trend showing inhibition at 1000 nM and 100 nM (Figure 4.5).

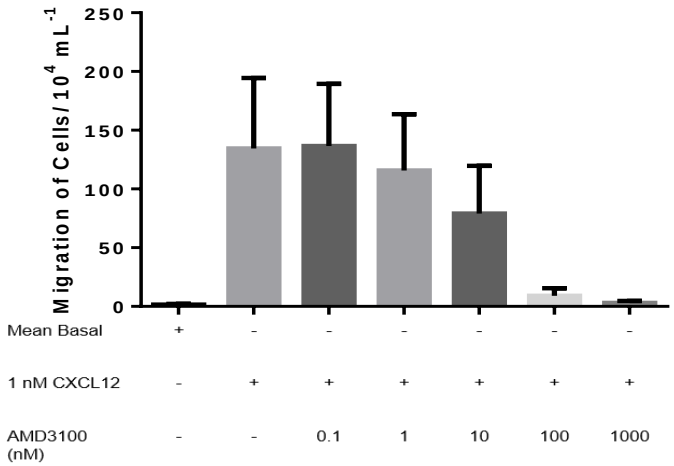


**Figure 4.5: AMD3100 shows a trend that it prevents CXCL12 directed migration in Jurkat cells using chemotaxis assays.** The migration of Jurkat cells was stimulated by 1 nM of CXCL12 in the presence and absence of AMD3100 (0.1-1000 nM) for 4 hours. Data represents the mean ± SEM of 4 independent experiments. One-Way ANOVA with post hoc Dunnett's multiple comparison, data not significant.

When this data was percentage corrected, AMD3100 significantly inhibited Jurkat cell migration in a dose dependant manner (Figure 4.6).

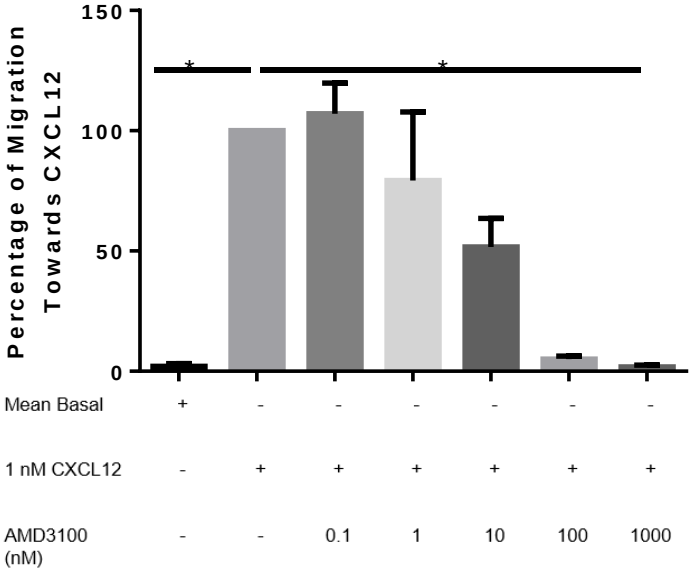


**Figure 4.6: 1000 nM of AMD3100 prevents CXCL12 directed migration in Jurkat cells using percentage corrected data from chemotaxis assays.** Normalization of data from Figure 4.5 showing the migration of Jurkat cells stimulated by 1 nM of CXCL12 in the presence and absence of AMD3100 (0.1-1000 nM) for 4 hours. Data represents the mean ± SEM of 4 independent experiments. Data normalised to CXCL12 and Kruskal-Wallis non-parametric test with post hoc Dunn's multiple comparison test conducted, * = p≤ 0.05.

Finally, AMD3100 had an $IC_{50}$ of 11.50 nM ± 4.39 nM SEM (Figure 4.7). This reduced migration is not a consequence of cellular toxicity caused by AMD3100 as demonstrated by MTS assay (Appendix A4).

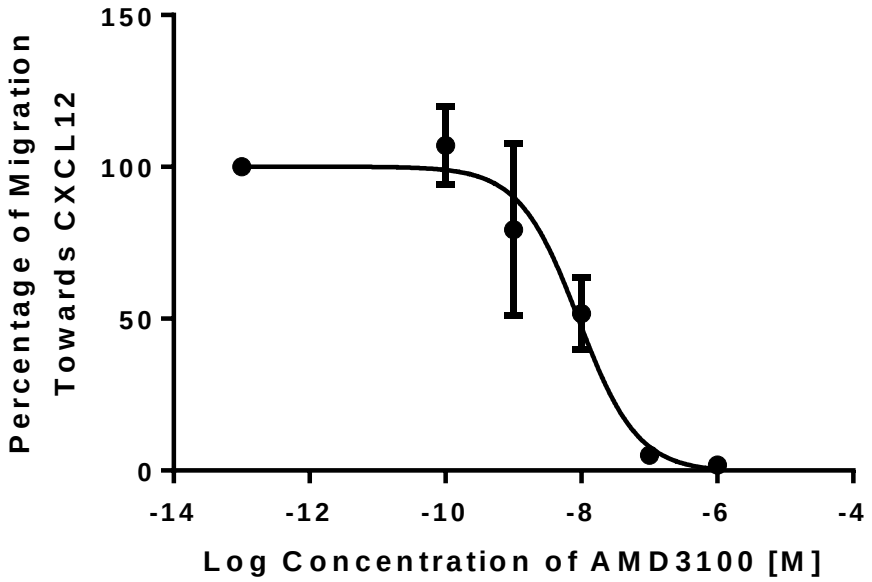


**Figure 4.7: Dose response curve of the migration of Jurkat cells when treated with a dose range of AMD3100 then stimulated by 1 nM of CXCL12.** An $IC_{50}$ of 11.50 nM ± 4.39 nM SEM was calculated using data from Figure 4.6. Data represents the mean ± SEM of 4 independent experiments. Log (inhibitor) vs. response (three parameters).

The first of the two novel CXCR4 antagonists, AZ3-2, was used in CXCL12 stimulated chemotaxis assays using a 10-fold dose range of AZ3-2 from 1-1000 nM. Using the raw data, AZ3-2 was found to have inhibitory effects at concentrations of 100 to 1000 nM (Figure 4.8).

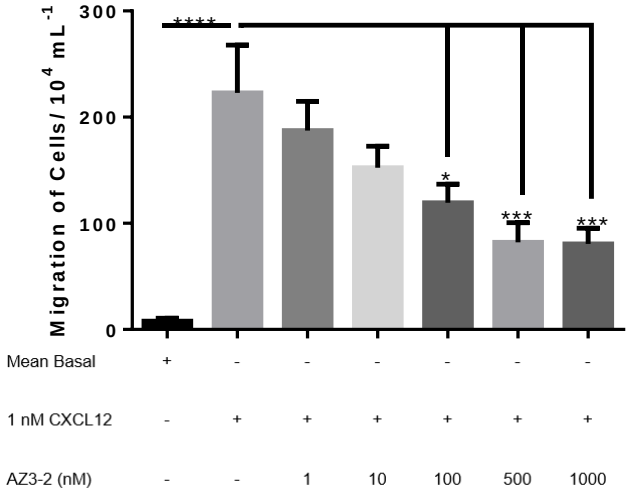


**Figure 4.8: 100-1000 nM of AZ3-2 prevents CXCL12 directed migration in Jurkat cells using chemotaxis assays**. The migration of Jurkat cells was stimulated by 1 nM of CXCL12 in the presence and absence of AZ3-2 (1-1000 nM) for 4 hours. Data represents the mean ± SEM of 7 independent experiments. One-Way ANOVA with post hoc Dunnett's multiple comparison * = p≤ 0.05, *** = p≤ 0.001 and **** = p≤ 0.0001.

Data was percentage corrected and it was confirmed that AZ3-2 significantly inhibited Jurkat cell migration at a concentration of 1000 nM (Figure 4.9).

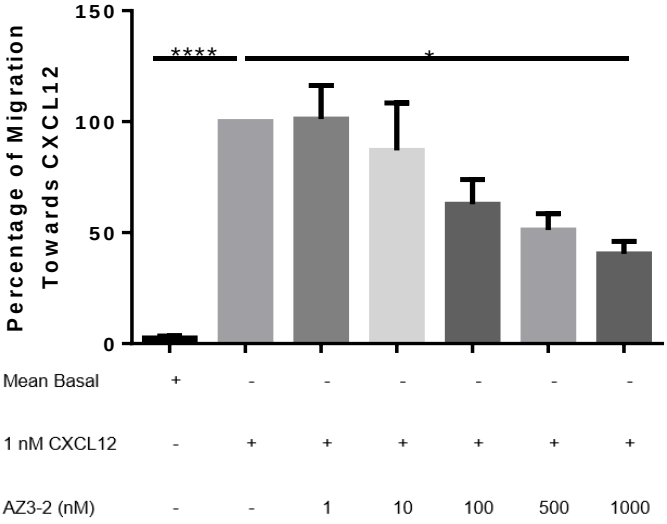


**Figure 4.9: 1000 nM of AZ3-2 prevents CXCL12 directed migration in Jurkat cells using percentage corrected data from chemotaxis assays.** Normalization of data from Figure 4.8 showing the migration of Jurkat cells stimulated by 1 nM of CXCL12 in the presence and absence of AZ3-2 (1-1000 nM) for 4 hours. Data represents the mean ± SEM of 7 independent experiments. Data normalised to CXCL12 and Kruskal-Wallis non-parametric test with post hoc Dunn's multiple comparison test was conducted, * = p≤ 0.05 and **** = p≤ 0.0001.

While inhibition with AZ3-2 never fell below 50%, an $IC_{50}$ of 259.80 nM ± 230.70 nM SEM was calculated for purpose of comparison (Figure 4.10). This reduced migration is not a consequence of cellular toxicity caused by the novel CXCR4 antagonists as demonstrated by MTS assay (Appendix A5).

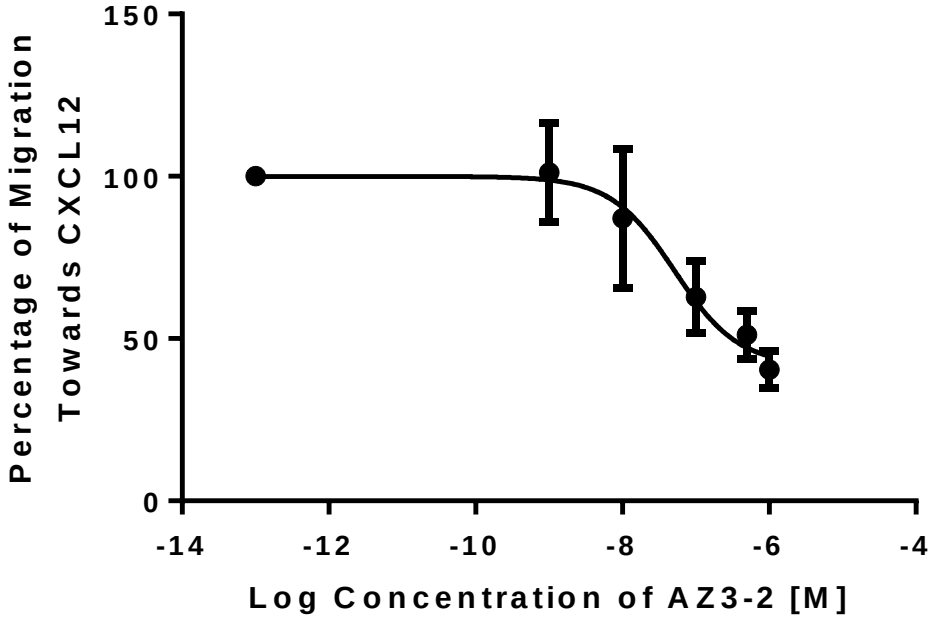


**Figure 4.10: Dose response curve of the migration of Jurkat cells when treated with a dose range of AZ3-2 then stimulated by 1 nM of CXCL12.** An $IC_{50}$ of 259.80 nM ± 230.70 nM SEM was calculated using data from Figure 4.9. Data represents the mean ± SEM of 7 independent experiments. Log (inhibitor) vs. response (three parameters).

The second novel CXCR4 antagonists, AZ6-2, was also used in CXCL12 directed chemotaxis assays using a 10-fold dose range from 0.01-1000 nM. Using the raw data, AZ6-2 was found to have inhibitory effects at concentrations of 1 to 1000 nM (Figure 4.11).

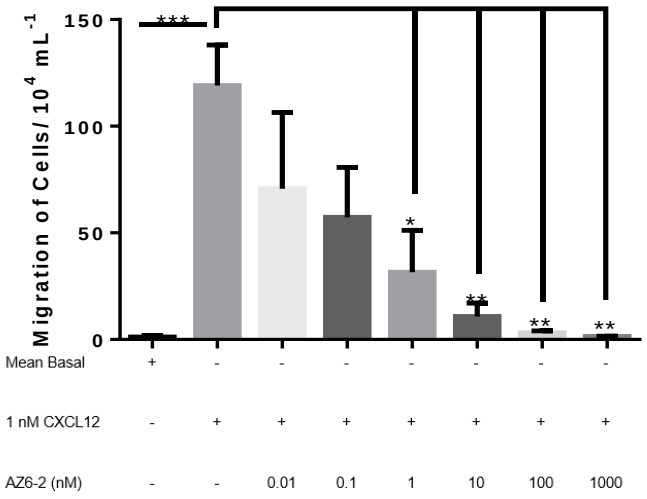


**Figure 4.11: 1-1000 nM of AZ6-2 prevents CXCL12 directed migration in Jurkat cells using chemotaxis assays.** The migration of Jurkat cells was stimulated by 1 nM of CXCL12 in the presence and absence of AZ6-2 (0.01-1000 nM) for 4 hours. Data represents the mean ± SEM of 4 independent experiments. One-Way ANOVA with post hoc Dunnett's multiple comparison, * = p≤ 0.05, ** = p≤ 0.01 and **** = p≤ 0.0001.

This data was percentage corrected which confirmed that AZ6-2 significantly inhibited Jurkat cell migration at a concentration of 1000 nM (Figure 4.12).

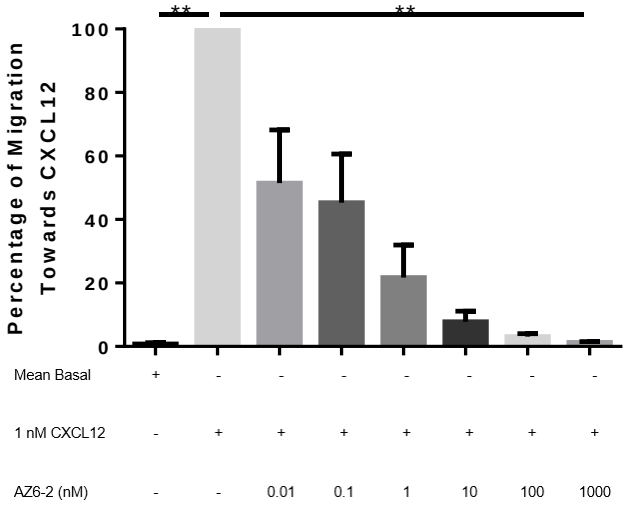


**Figure 4.12: 1000 nM of AZ6-2 prevents CXCL12 directed migration in Jurkat cells using percentage corrected data from chemotaxis assays.** Normalization of data from Figure 4.11 showing the migration of Jurkat cells stimulated by 1 nM of CXCL12 in the presence and absence of AZ6-2 (0.01-1000 nM) for 4 hours. Data represents the mean ± SEM of 4 independent experiments. Data normalised to CXCL12 and Kruskal-Wallis non-parametric test with post hoc Dunn's multiple comparison test was conducted, ** = p≤ 0.01.

AZ6-2 significantly inhibits Jurkat cells in a dose dependant manner with an $IC_{50}$ of 0.28 nM ± 0.18 nM SEM (Figure 4.13). This reduced migration is not a consequence of cellular toxicity caused by AZ6-2 as demonstrated by MTS assay (Appendix A6).

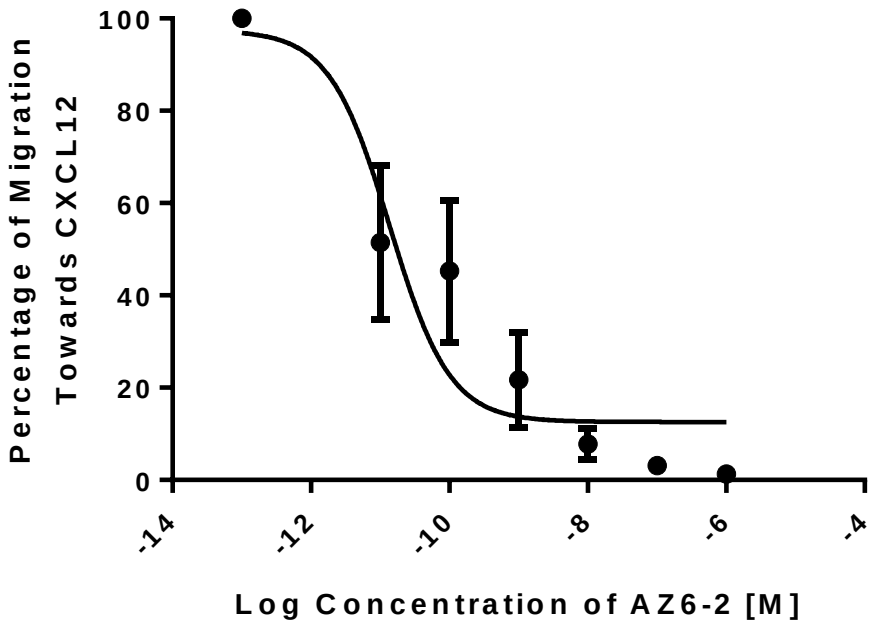


**Figure 4.13: Dose response curve of the migration of Jurkat cells when treated with a dose range of AZ6-2 then stimulated by 1 nM of CXCL12.** An $IC_{50}$ of 0.28 nM ± 0.18 nM SEM was calculated using data from Figure 4.12. Data represents the mean ± SEM of 4 independent experiments. Log (inhibitor) vs. response (three parameters).

### 4.3.4. CXCL12 directed migration in THP-1 cells is inhibited by AMD3100 and AZ6-2 but not AZ3-2

A second suspension cell line, THP-1, was also used in CXCL12 directed chemotaxis assay to determine any inhibitory effects of the two novel CXCR4 antagonists and AMD3100. These experiments help determine whether these CXCR4 antagonists are only suitable for specific cell lines or if they could be used more broadly. Chemotaxis assays were conducted using a 10-fold dose range of AMD3100 from 0.01-1000 nM. Using the raw data, AMD3100 significantly inhibits CXCL12 directed migration at a concentration of 1000 nM (Figure 4.14).

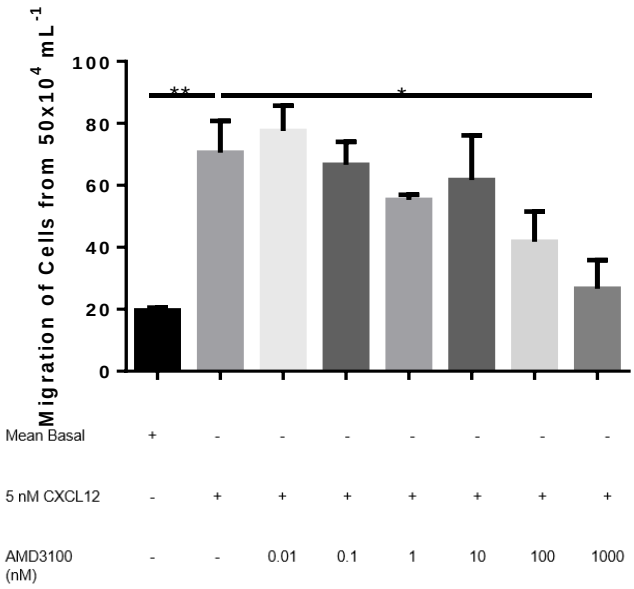


**Figure 4.14: 1000 nM of AMD3100 prevents CXCL12 directed migration in THP-1 cells using chemotaxis assays.** The migration of THP-1 cells was stimulated by 5 nM of CXCL12 in the presence and absence of AMD3100 (0.01-1000 nM) for 4 hours. Data represents the mean ± SEM of 3 independent experiments. One-Way ANOVA with post hoc Dunnett's multiple comparison, * = p≤ 0.05 and ** = p≤ 0.01.

However, when this data was percentage corrected, significance was lost (Figure 4.15).

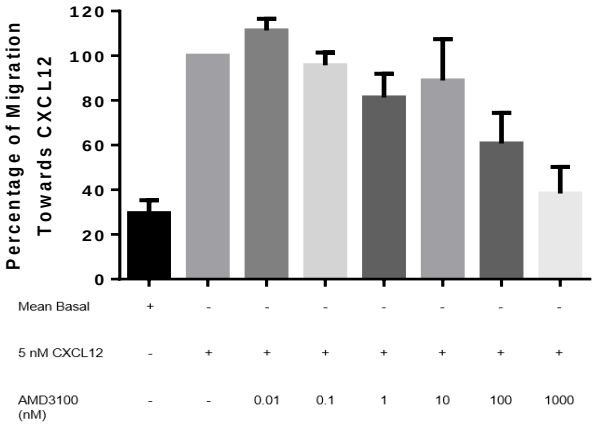


**Figure 4.15: AMD3100 shows a trend that it prevents CXCL12 directed migration in THP-1 cells using percentage corrected data from chemotaxis assays.** Normalization of data from Figure 4.14 showing the migration of THP-1 cells stimulated by 5 nM of CXCL12 in the presence and absence of AMD3100 (0.01-1000 nM) for 4 hours. Data represents the mean ± SEM of 3 independent experiments. Data normalised to CXCL12 and Kruskal-Wallis non-parametric test with post hoc Dunn's multiple comparison test was conducted, data not significant.

AMD3100 inhibited THP-1 cell migration in a dose dependant manner with an $IC_{50}$ of 59.47 nM ± 57.33 nM SEM (Figure 4.16). This reduced migration is not a consequence of cellular toxicity caused by AMD3100 in this cell line as demonstrated by MTS assay (Appendix A7).

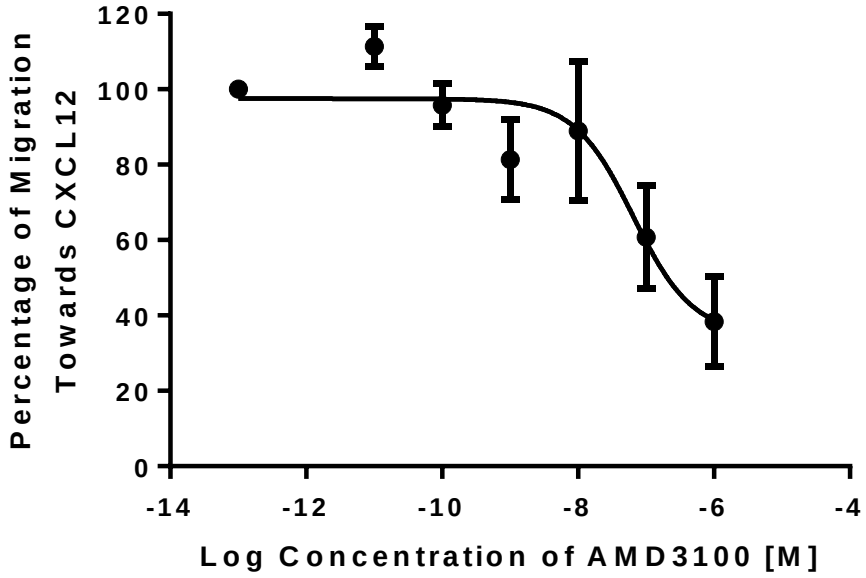


**Figure 4.16: Dose response curve of the migration of THP-1 cells when treated with a dose range of AMD3100 then when stimulated by 5 nM of CXCL12.** An $IC_{50}$ of 59.47 nM ± 57.33 nM SEM was calculated using data from Figure 4.15. Data represents the mean ± SEM of 3 independent experiments. Log (inhibitor) vs. response (three parameters).

To compare, AZ3-2 was used in CXCL12 directed chemotaxis assays using a 10-fold dose range of AZ3-2 from 0.01 to 1000 nM. Using this raw data, AZ3-2 was found to have no inhibitory effects in THP-1 cells (Figure 4.17).

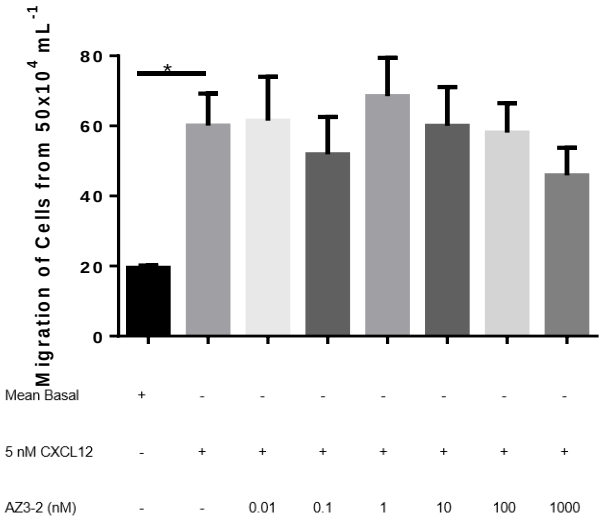


**Figure 4.17: AZ3-2 does not prevent CXCL12 directed migration in THP-1 cells using chemotaxis assays.** The migration of THP-1 cells was stimulated by 5 nM of CXCL12 in the presence and absence of AZ3-2 (0.01-1000 nM) for 4 hours. Data represents the mean ± SEM of 4 independent experiments. One-Way ANOVA with post hoc Dunnett's multiple comparison, * = p≤ 0.05.

Furthermore, when this data was percentage corrected, AZ3-2 still had no significant inhibitory effect in THP-1 cells (Figure 4.18).

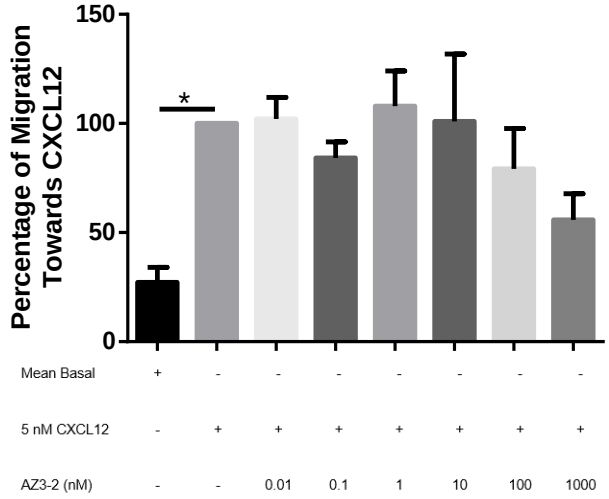


**Figure 4.18: AZ3-2 does not prevent CXCL12 directed migration in THP-1 cells using percentage corrected data from chemotaxis assays.** Normalization of data from Figure 4.17 showing the migration of THP-1 cells stimulated by 5 nM of CXCL12 in the presence and absence of AZ3-2 (0.01-1000 nM) for 4 hours. Data represents the mean ± SEM of 4 independent experiments. Data normalised to CXCL12 and Kruskal-Wallis non-parametric test with post hoc Dunn's multiple comparison test was conducted, * = p≤ 0.05.

While inhibition with AZ3-2 never fell below 50%, an $IC_{50}$ of 1212 nM ± 2424 nM SEM was calculated for purpose of comparison (Figure 4.19). These results were not a consequence of cellular toxicity caused by AZ3-2 in this cell line as demonstrated by MTS assay (Appendix A8).

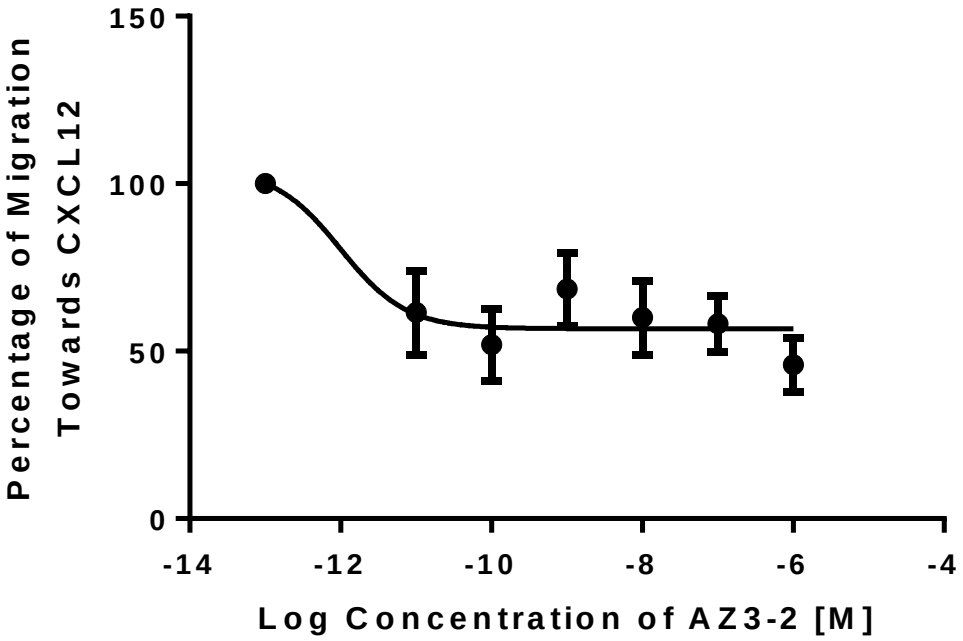


**Figure 4.19: Dose response curve of the migration of THP-1 cells when treated with a dose range of AZ3-2 then when stimulated by 5 nM of CXCL12.** An $IC_{50}$ of 1212 nM ± 2424 nM SEM was calculated using data from Figure 4.18. Data represents the mean ± SEM of 4 independent experiments. Log (inhibitor) vs. response (three parameters).

The second novel CXCR4 antagonists, AZ6-2, was also used in CXCL12 directed chemotaxis assays using a 10-fold dose range from 0.01-1000 nM. Using the raw data, AZ6-2 was found to have inhibitory effects at concentrations of 1 to 1000 nM in THP-1 cells (Figure 4.20).

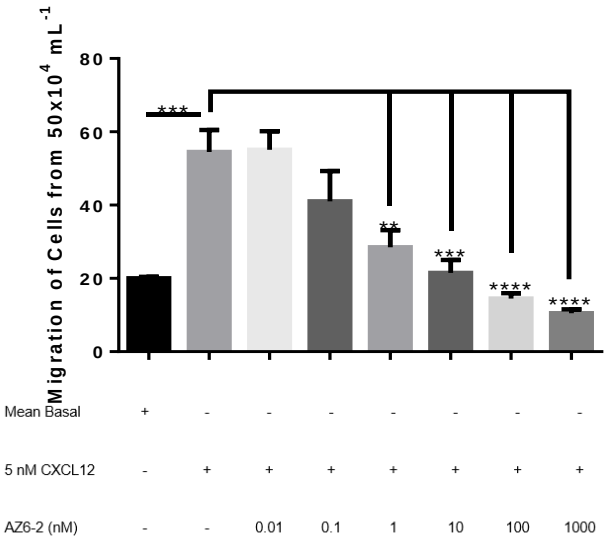


**Figure 4.20: 1-1000 nM of AZ6-2 prevents CXCL12 directed migration in THP-1 cells using chemotaxis assays.** The migration of THP-1 cells was stimulated by 5 nM of CXCL12 in the presence and absence of AZ6-2 (0.01-1000 nM) for 4 hours. Data represents the mean ± SEM of 4 independent experiments. One-Way ANOVA with post hoc Dunnett's multiple comparison, ** = p≤ 0.01 *** = p≤ 0.001 and **** = p≤ 0.0001.

When this data was percentage corrected, AZ6-2 significant inhibited THP-1 cell migration at a concentration of 100 to 1000 nM (Figure 4.21).

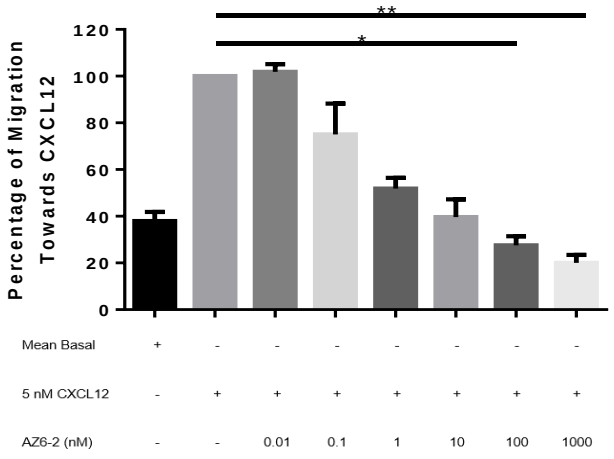


**Figure 4.21: 100-1000 nM of AZ6-2 prevents CXCL12 directed migration in THP-1 cells using percentage corrected data from chemotaxis assays.** Normalization of data from Figure 4.10 showing the migration of THP-1 cells stimulated by 5 nM of CXCL12 in the presence and absence of AZ6-2 (0.01-1000 nM) for 4 hours. Data represents the mean ± SEM of 4 independent experiments. Data normalised to CXCL12 and Kruskal-Wallis non-parametric test with post hoc Dunn's multiple comparison test was conducted, * = p≤ 0.05 and ** = p≤ 0.01.

From these results, AZ6-2 was found to significantly inhibit THP-1 cell migration in a dose dependant manner with and $IC_{50}$ of 0.56 nM ± 0.19 nM SEM (Figure 4.22). This reduced migration is not a consequence of cellular toxicity caused by AZ6-2 in this cell line as demonstrated by MTS assay (Appendix A9). The results from both Jurkat and THP-1 cell migration are summarised in Table 4.2.

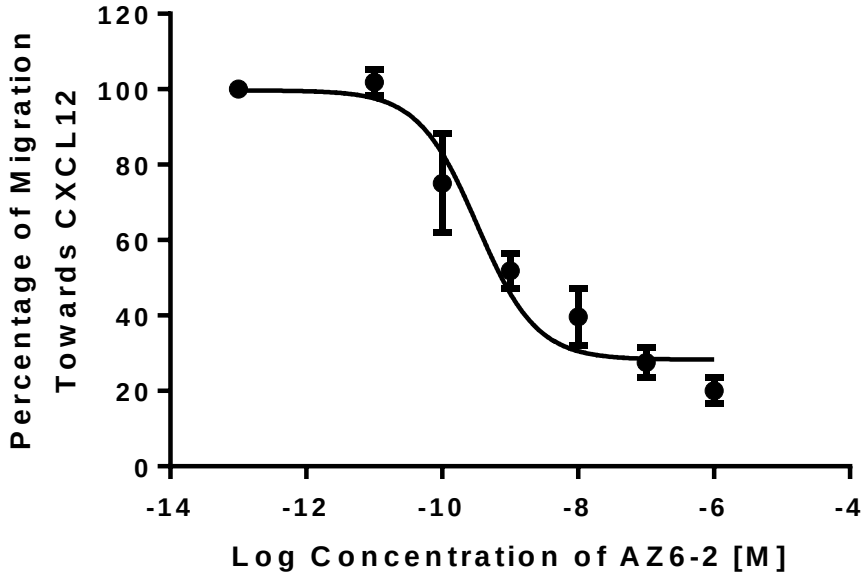


**Figure 4.22: Dose response curve of the migration of THP-1 cells when treated with a dose range of AZ6-2 then when stimulated by 5 nM of CXCL12**. An $IC_{50}$ of 0.56 nM ± 0.19 nM SEM was calculated using data from Figure 4.21. Data represents the mean ± SEM of 4 independent experiments. Log (inhibitor) vs. response (three parameters).

**Table 4.2: Summary of $IC_{50}$ values of AMD3100, AZ3-2 and AZ6-2 treated Jurkat and THP-1 cells obtained from chemotaxis assays. Data represents the mean ± SEM of at least three independent experiments.**

| Peptide | Cell Line | |
|---|---|---|
| | Jurkat | THP-1 |
| **AMD3100** | 11.50 nM ± 4.39 | 59.47 nM ± 57.33 |
| **AZ3-2** | 259.8 nM ± 230.7 | 1212 µM ± 2424 |
| **AZ6-2** | 0.28 nM ± 0.18 | 0.56 nM ± 0.19 |

### 4.3.5. AMD3100, AZ3-2 and AZ6-2 reduces intracellular $Ca^{2+}$ release from MCF-7 breast cancer cells

The intracellular release of $Ca^{2+}$ is triggered via downstream signalling of the CXCR4/CXCL12 signalling axis. Specifically, CXCR4 is associated with a G protein composed of three subunits: α, β and γ subunits (Liebmann and Bohmer, 2000, Strathmann and Simon, 1991). The binding of CXCL12 to CXCR4 causes the dissociation of GDP that is bound to the α subunit and is replaced by GTP. The α subunit can then dissociate from the receptor and from the βγ subunit thus 'activating' the G protein (Hepler and Gilman, 1992, Johnson and Dhanasekaran, 1989). Following this, both the Gα subunit and the Gβγ subunit dimer can interact with and activate different effector molecules. Specifically, for intracellular $Ca^{2+}$ release, the Gβγ subunit triggers PLCβ activation, which in turn hydrolyses PIP2 into two secondary messengers: IP3 and DAG. IP3 activation then leads to the mobilization of intracellular calcium ($Ca^{2+}$) (Goldsmith and Dhanasekaran, 2007). Therefore, as all three CXCR4 antagonists are CXCL12-mimetic compounds, they should bind CXCR4 and prevent G protein activation, thus preventing the release of intracellular calcium. To confirm this, calcium release assays were conducted and it was shown that incubation with 1 μM of AMD3100, AZ3-2 and AZ6-2 significantly reduced the release of intracellular $Ca^{2+}$ in MCF-7 cells (Figure 4.23). This reduced release of intracellular $Ca^{2+}$ is not a consequence of cellular toxicity caused by the CXCR4 antagonists in this cell line as demonstrated by MTS assay (Appendix A10-12).

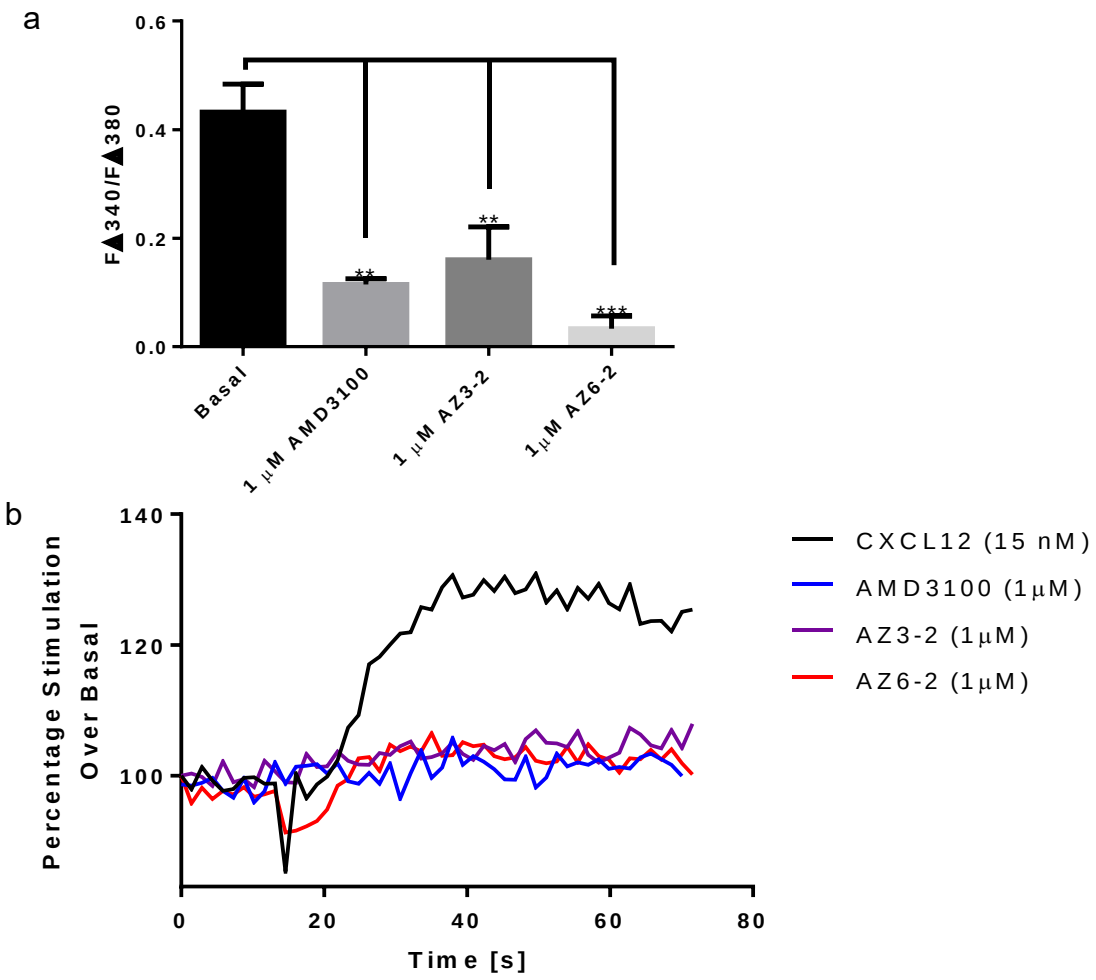


**Figure 4.23: AMD3100, AZ3-2 and AZ6-2 significantly reduces the release of intracellular $Ca^{2+}$ from MCF-7 breast cancer cells.** Cells were incubated for 30 minutes with antagonists and the calcium indicator Fura-2 AM. **a)** MCF-7 cell treated with 1 μM AMD3100, AZ3-2 or AZ6-2 then stimulated with 15 nM CXCL12. **b)** Representative intracellular calcium release traces of MCF-7 breast cancer cells treated with 1 μM AMD3100, AZ3-2 or AZ6-2 then stimulated with 15 nM CXCL12. Data is expressed as a change in fluorescence ratio (340nm/380nm) where the basal fluorescence prior to the addition of CXCL12 is subtracted from peak fluorescence following addition of CXCL12. Chemokine injected after 10 seconds. Data represents the mean ± SEM of 3 independent experiments. One-Way ANOVA with post hoc Dunnett's multiple comparison, ** = p≤ 0.01 and *** =p≤ 0.001.

### 4.3.6. Intracellular $Ca^{2+}$ release is reduced by both AMD3100 and AZ6-2 in Jurkat cells but only AZ6-2 reduces intracellular $Ca^{2+}$ release from THP-1 and PC3 cells

Further investigations into the ability of the novel peptide AZ6-2 to reduce the release of intracellular $Ca^{2+}$ were conducted with three other cell lines: Jurkat, THP-1 and PC3. Incubation with 1 µM of AZ6-2 significantly reduced the release of intracellular $Ca^{2+}$ in all cell lines cells (Figure 4.24). However, 1 µM AMD3100 only caused a significant reduction of intracellular $Ca^{2+}$ in Jurkat cells but not in THP-1 or PC3 cells (Figure 4.24). This reduced release of intracellular $Ca^{2+}$ in PC3 cells is not a consequence of cellular toxicity caused by the CXCR4 antagonists in this cell line as demonstrated by MTS assay (Appendix A13-15). It should be noted that a higher concentration of chemokine (25 nM) was used for Jurkat cells due to initial investigating using 15-20 nM not causing sufficient basal calcium release, thus a higher concentration was adopted.

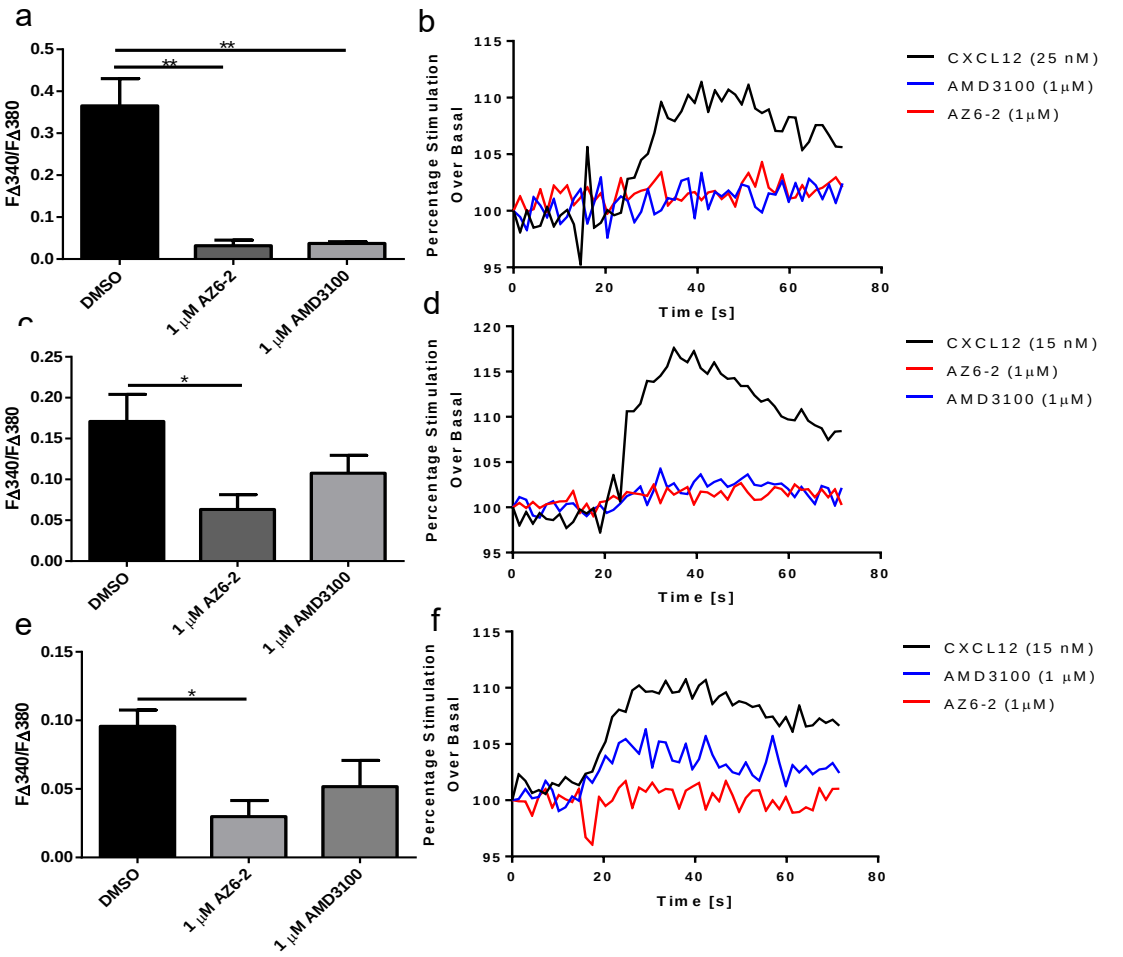


**Figure 4.24: AZ6-2 significantly reduces the release of intracellular $Ca^{2+}$ from Jurkat, THP-1 and PC3 cells but AMD3100 only significantly reduces the release of intracellular $Ca^{2+}$ from Jurkat cells.** Cells were incubated for 30 minutes with antagonist or vehicle control and the calcium indicator Fura-2 AM. **a)** Jurkat cells treated with 1 μM AMD3100 or AZ6-2 against equivalent volume DMSO vehicle then stimulated with 25 nM CXCL12. **b)** Representative intracellular calcium release traces of Jurkat cells. **c)** THP-1 cells treated with 1 μM AMD3100 or AZ6-2 against equivalent volume DMSO vehicle then stimulated with 15 nM CXCL12. **d)** Representative intracellular calcium release traces of THP-1 cells. **e)** PC3 cells treated with 1 μM AMD3100 or AZ6-2 against equivalent volume DMSO vehicle then stimulated with 15 nM CXCL12. **f)** Representative intracellular calcium release traces of PC3 cells. Data is expressed as a change in fluorescence ratio (340nm/380nm) where the basal fluorescence prior to the addition of CXCL12 is subtracted from peak fluorescence following addition of CXCL12. Chemokine injected after 10 seconds. Data represents the mean ± SEM of 3-6 independent experiments. One-Way ANOVA with post hoc Dunnett's multiple comparison, * = p≤ 0.05 and ** = p≤ 0.01.

### 4.3.7. AZ6-2 is a CXCL12-mimetic compound

Di Maro et al. (2016) states that AZ6-2 is a CXCL12-mimetic peptide but there is little visual evidence to support this. Therefore, further investigation was required. MCF-7 breast cancer cells were incubated with 1 µM of AZ6-2 or AMD3100 and 10 nM of CXCL12 prior to immunofluorescence assays using the mouse 12G5 primary mAb followed by the secondary anti-mouse Alexa Fluor® 488 antibody. 12G5 is a conformation-dependant mAb that has been confirmed to recognise determinants in ECL1 and ECL2 of CXCR4 and specifically binds to the E3 epitope in the ECL2 (Zhou et al., 2001, Baribaud et al., 2001). This 12G5-CXCR4 binding is similar to that of CXCL12-CXCR4 binding as CXCL12 binds specifically to Asp187 in the ECL2 of CXCR4. Due to these similar binding sites, 12G5 and CXCL12 has been found to competitively bind to CXCR4 (Chen et al., 2014, Pawig et al., 2015, Zhou et al., 2001). Furthermore, AMD3100 has previously been shown to block the binding of anti-ECL2 mAbs suggesting that AMD3100 itself also binds to the same site as CXCL12 and 12G5 (Carnec et al., 2005).Therefore, prior incubation with AMD3100 will bind CXCR4, hence 12G5 will not be able to bind resulting in no fluorescence. As such, AMD3100 can act as a control. Di Maro et al. (2016) suggested that AZ6-2 also binds to Asp187 and therefore, it is hypothesised that it also has the same binding site as 12G5, AMD3100 and CXCL12 all of which will bind competitively. Prior incubation with 1 µM of AMD3100 or AZ6-2 indeed failed to produce any fluorescence (Figure 4.25). This suggested that AMD3100 and AZ6-2 do bind to a similar site as 12G5. Incubation with 10 nM of CXCL12 demonstrated the presence of fluorescence (Figure 4.25c) This is likely due to the concentration of CXCL12 being too low to cause complete saturation of the CXCR4 receptors.

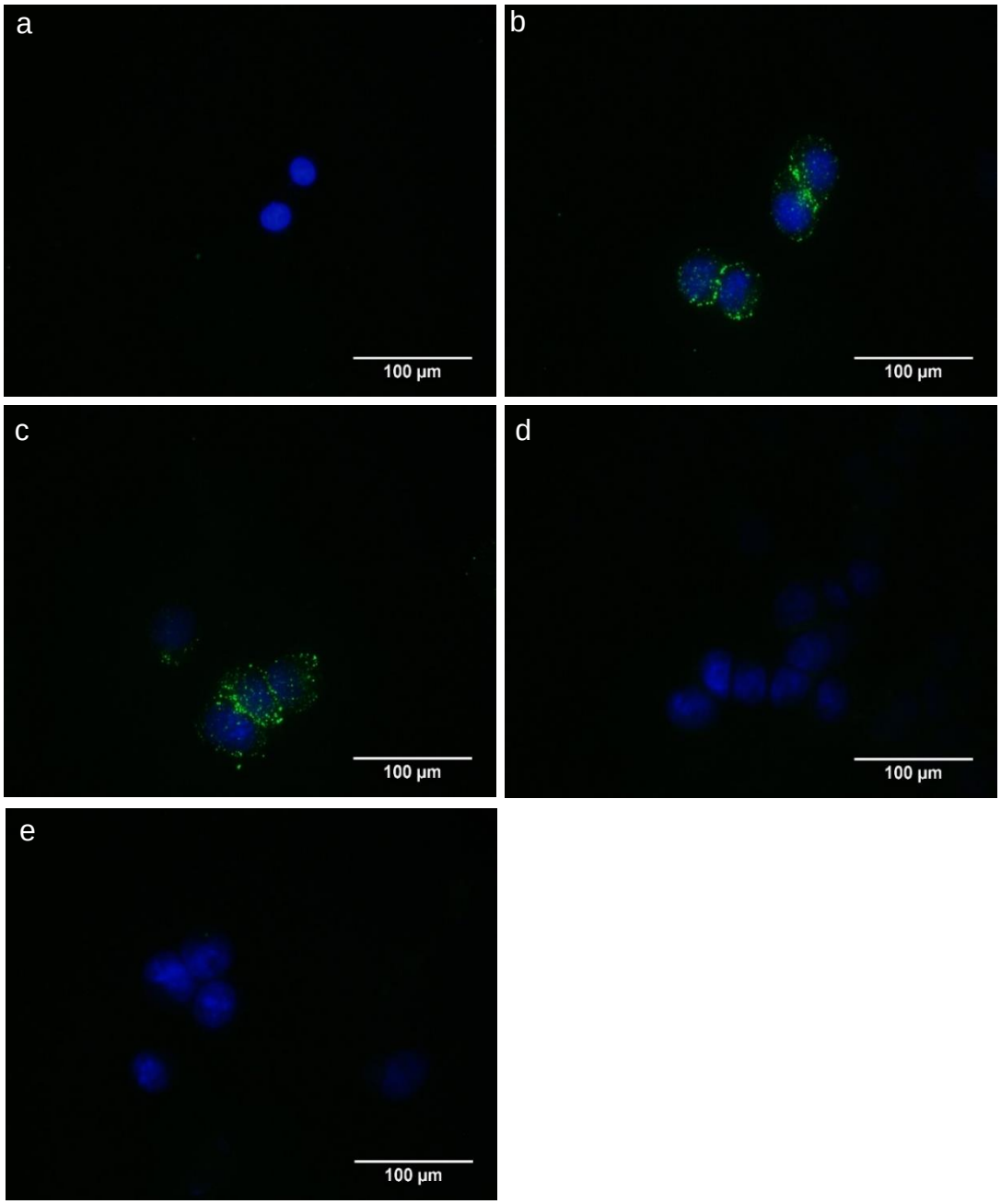


**Figure 4.25: AMD3100 and AZ6-2 prevent 12G5 mAb binding in MCF-7 breast cancer cells. a)** Negative control treated with secondary anti-mouse Alexa Fluor® 488 antibody (green), DAPI (blue) and fixed with 4% paraformaldehyde before imaging. **b)** Positive control whereby CXCR4 was visualised using mouse 12G5 primary mAb, secondary anti-mouse Alexa Fluor® 488 antibody (green), DAPI (blue) and fixed with 4% paraformaldehyde before imaging. **c)** MCF-7 cells stimulated with 10 nM of CXCL12 for 1 hour before visualising as previous. **d)** MCF-7 cells treated with 1 µM AMD3100 for 1 hour before visualising as previous**. e)** MCF-7 cells treated with 1 µM AZ6-2 for 1 hour before visualising as previous. Data shows representative cells from 10 independent experiments with similar findings. Acquired with Leica imaging suite with 63x objective, 35x overall magnification.

### 4.3.8. AMD3100 and AZ6-2 do not cause the internalisation of the CXCR4 receptor in MCF-7, Jurkat or THP-1 cells at 37˚C

In order for GPCRs to produce a signalling response of the appropriate duration and magnitude, once chemokine has bound and activated its receptor, the receptor becomes internalized from the cell surface via endocytosis (Van Hout et al., 2017). Therefore, following the confirmation that AZ6-2 has a similar binding site to 12G5, it was important to use an alternative mAb to determine the effects of AZ6-2 upon CXCR4 internalisation. Therefore, the mAb 4G10 was substituted for 12G5. 4G10 is an allosteric mAb generated against the N-terminal domain of CXCR4 and is conformation independent (Baribaud et al., 2001, Xiao et al., 2000). Briefly, MCF-7, Jurkat and THP-1 cells were incubated with 1 µM of AZ6-2 or AMD3100 and 10 nM of CXCL12 at two different temperatures (4˚C and 37˚C) prior to incubation with mouse 4G10 primary mAb followed by secondary anti-mouse Alexa Fluor® 488 antibody and fixed with 4% paraformaldehyde. AMD3100 has previously been shown to fail to trigger CXCR4 internalization (Hatse et al., 2002). Therefore, AMD3100 can be used as a control. The usage of two different incubation temperatures was conducted as the rate of cell surface receptor endocytosis at 10˚C or below should be negligible while receptor endocytosis is mostly temperature independent between 14 and 37˚C (Weigel and Oka, 1981). Therefore, there should be CXCR4 expression at an incubation temperature of 4˚C while incubation at 37˚C will determine if AZ6-2 can trigger CXCR4 internalisation. 10 nM of CXCL12, 1 µM of AMD3100 and 1 µM of AZ6-2 did not trigger CXCR4 internalisation at either 4 or 37˚C in MCF-7, Jurkat or THP-1 cells (Figure 4.26-4.31).

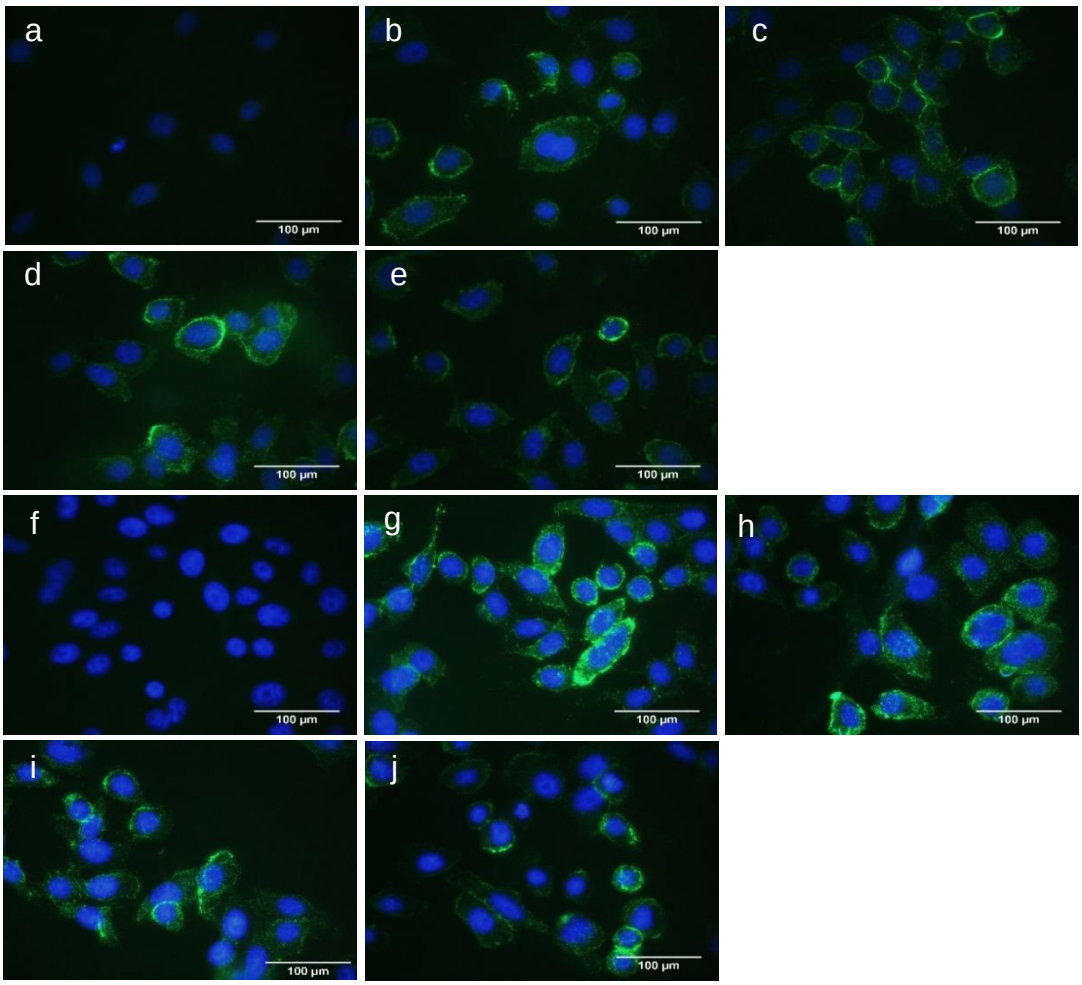


**Figure 4.26: Incubation with AMD3100 and AZ6-2 at 4˚C and 37˚C does not cause internalisation of the CXCR4 receptor in MCF-7 cells. a)** Negative control incubated at 4˚C, treated with secondary anti-mouse Alexa Fluor® 488 antibody (green), DAPI (blue) and fixed with 4% paraformaldehyde before imaging. **b)** Positive control incubated at 4˚C, whereby CXCR4 was visualised using mouse 4G10 primary mAb, secondary anti-mouse Alexa Fluor® 488 antibody (green), DAPI (blue) and fixed with 4% paraformaldehyde before imaging. **c)** MCF-7 cells stimulated with 10 nM of CXCL12 at 4˚C for 1 hour before visualisation as previous. **d)** MCF-7 cells treated with 1 µM AMD3100 at 4˚C for 1 hour before visualisation as previous. **e)** MCF-7 cells treated with 1 µM AZ6-2 at 4˚C for 1 hour before visualisation as positive control. **f)** Negative control as above, incubated at 37˚C. **g)** Positive control as above, incubated at 37˚C. **h)** MCF-7 cells stimulated with 10 nM of CXCL12 at 37˚C for 1 hour before visualisation as positive control. **i)** MCF-7 cells treated with 1 µM AMD3100 at 37˚C for 1 hour before visualisation as positive control. **j)** MCF-7 cells treated with 1 µM AZ6-2 at 37˚C for 1 hour before visualisation as positive control. Data shows representative cells from 3 independent experiments with similar findings. Acquired with Leica imaging suite with 63x objective, 35x overall magnification.

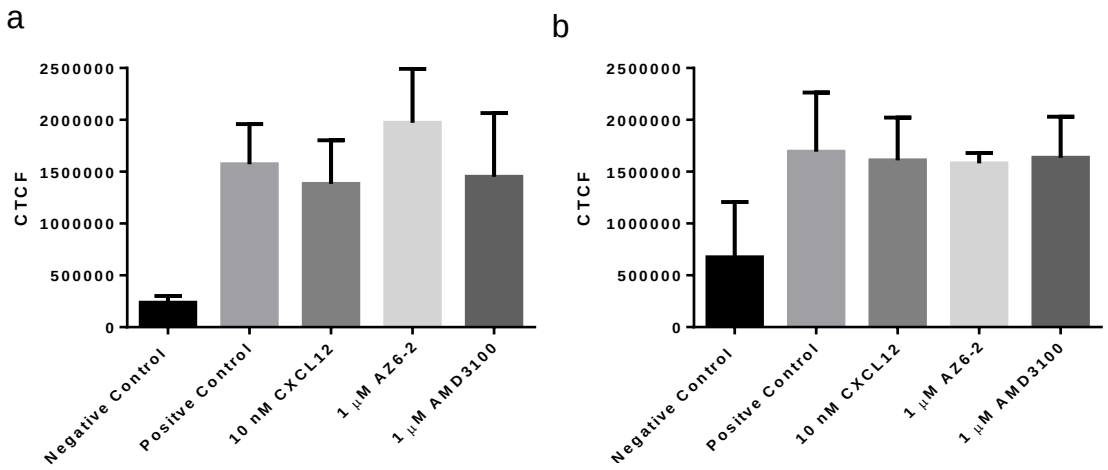


**Figure 4.27: Incubation with AMD3100 and AZ6-2 at 4˚C and 37˚C causes no significant change in the fluorescent intensity of CXCR4 receptor expression in MCF-7 cells. a)** Corrected Total Cell Fluorescence (CTCF) of MCF-7 cells from Figure 4.26 stimulated with 10 nM CXCL12 or treated with 1 μM AMD3100 or AZ6-2 at 4˚C for 1 hour. **b)** CTCF of MCF-7 cells from Figure 4.26 stimulated with 10 nM CXCL12 or treated with 1 μM AMD3100 or AZ6-2 at 37˚C for 1 hour. CTCF = Integrated Density – (Area of selected cell x Mean fluorescence of background readings). Data represents the mean ± SEM of 3 independent experiments. One-Way ANOVA with post hoc Dunnett's multiple comparison, data was not significant.

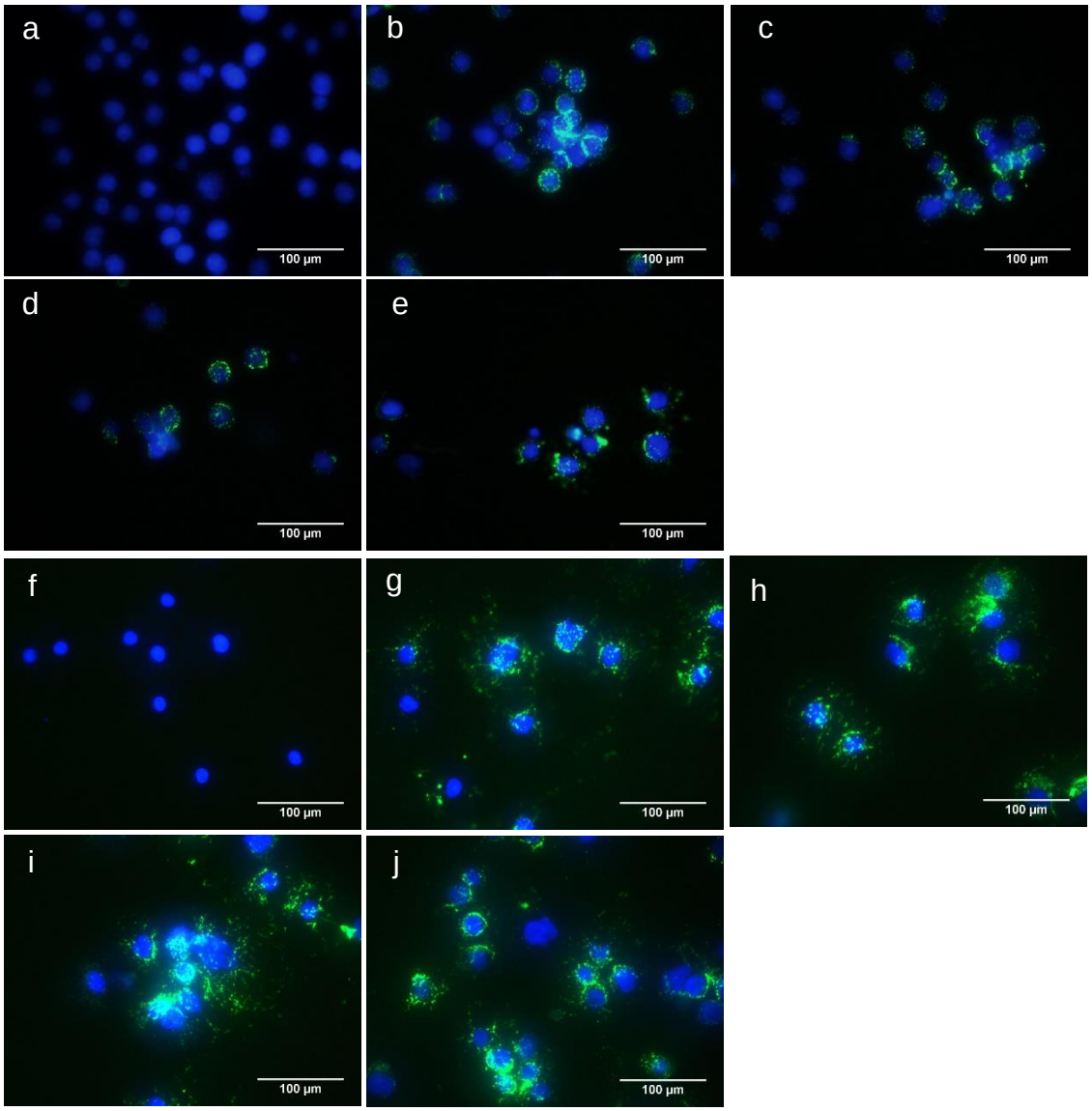


**Figure 4.28: Incubation with AMD3100 and AZ6-2 at 4˚C and 37˚C does not cause internalisation of the CXCR4 receptor in Jurkat cells. a)** Negative control as Figure 4.26 incubated at 4˚C. **b)** Positive control as Figure 4.26 incubated at 4˚C. **c)** Jurkat cells stimulated with 10 nM of CXCL12 at 4˚C for 1 hour before visualisation as Figure 4.26. **d)** Jurkat cells treated with 1 µM AMD3100 at 4˚C for 1 hour before visualisation as Figure 4.26. **e)** Jurkat cells treated with 1 µM AZ6-2 at 4˚C for 1 hour before visualisation as Figure 4.26. **f)** Negative control as Figure 4.26 incubated at 37˚C. **g)** Positive control as Figure 4.26 incubated at 37˚C. **h)** Jurkat cells stimulated with 10 nM of CXCL12 at 37˚C for 1 hour before visualisation as Figure 4.26. **i)** Jurkat cells treated with 1 µM AMD3100 at 37˚C for 1 hour before visualisation as Figure 4.26. **j)** Jurkat cells treated with 1 µM AZ6-2 at 37˚C for 1 hour before visualisation as Figure 4.26. Data shows representative cells from 3 independent experiments with similar findings. Acquired with Leica imaging suite with 63x objective, 35x overall magnification.

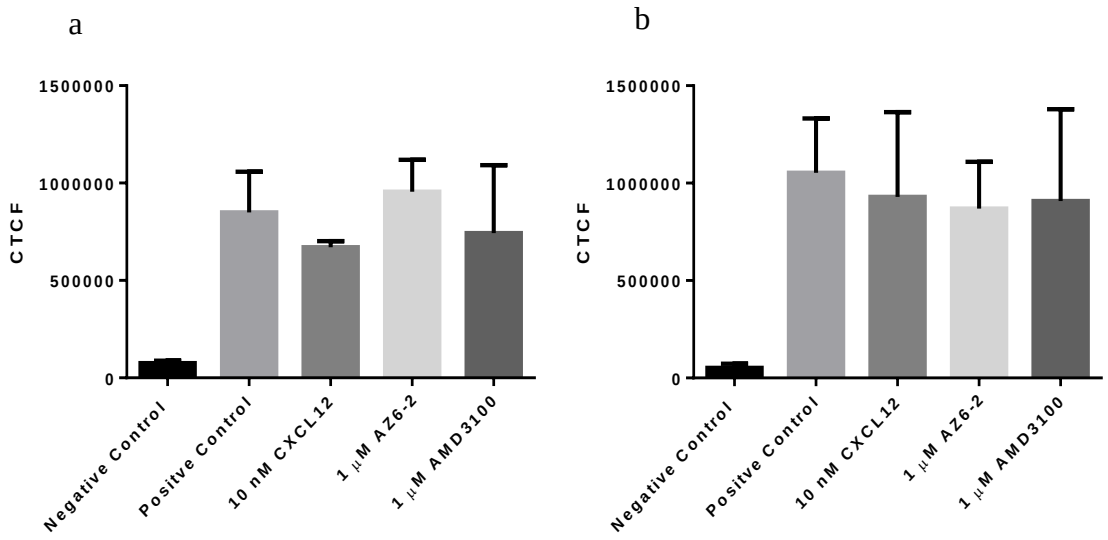


**Figure 4.29: Incubation with AMD3100 and AZ6-2 at 4˚C and 37˚C causes no significant change in the fluorescent intensity of CXCR4 receptor expression in Jurkat cells. a)** Corrected Total Cell Fluorescence (CTCF) of Jurkat cells from Figure 4.28 stimulated with 10 nM CXCL12 or treated with 1 µM AMD3100 or AZ6-2 at 4˚C for 1 hour. **b)** CTCF of Jurkat cells from Figure 4.28 stimulated with 10 nM CXCL12 or treated with 1 µM AMD3100 or AZ6-2 at 37˚C for 1 hour. CTCF = Integrated Density – (Area of selected cell x Mean fluorescence of background readings). Data represents the mean ± SEM of 3 independent experiments. One-Way ANOVA with post hoc Dunnett's multiple comparison, data was not significant.

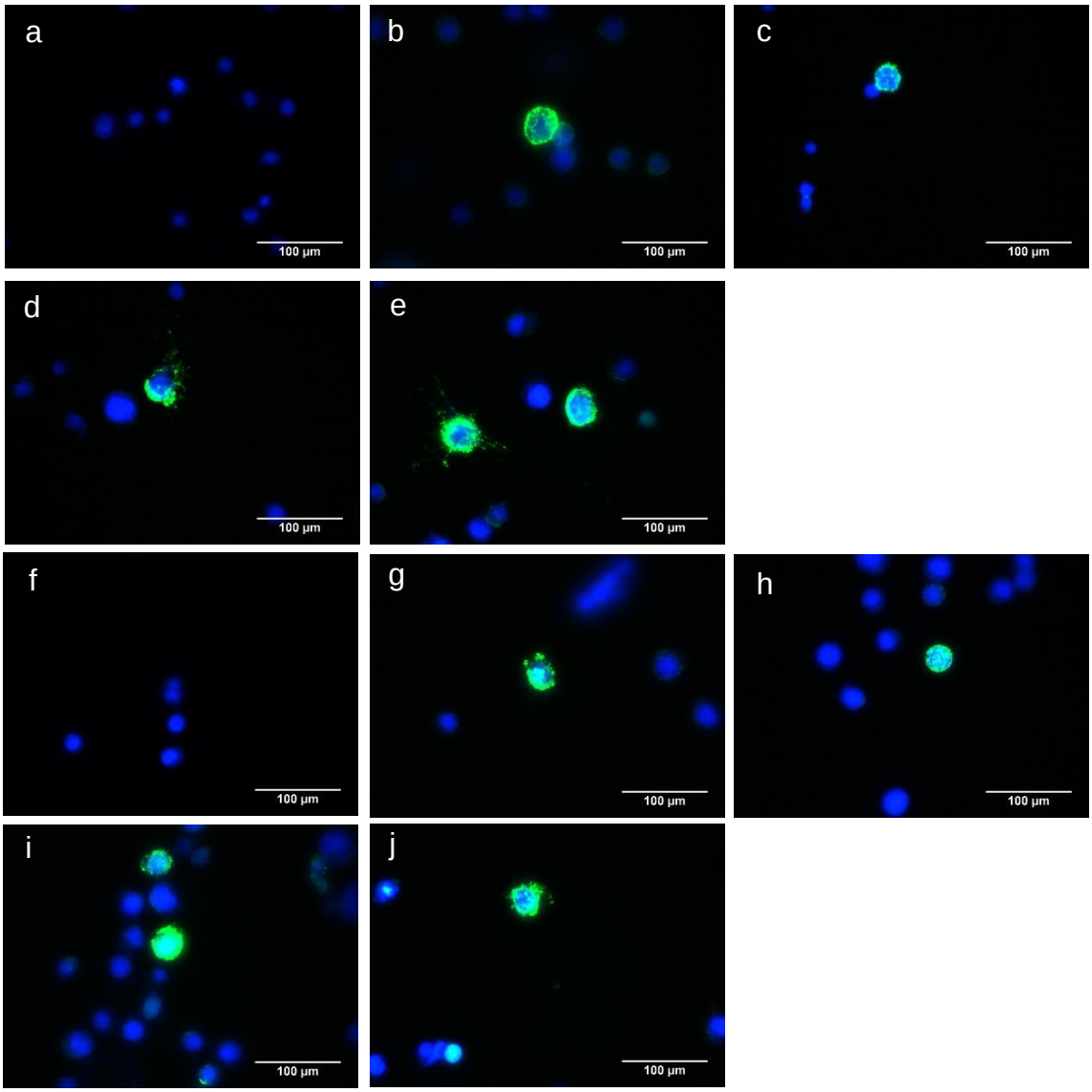


**Figure 4.30: Incubation with AMD3100 and AZ6-2 at 4˚C and 37˚C does not cause internalisation of the CXCR4 receptor in THP-1 cells. a)** Negative control as Figure 4.26 incubated at 4˚C. **b)** Positive control as Figure 4.26 incubated at 4˚C. **c)** THP-1 cells stimulated with 10 nM of CXCL12 at 4˚C for 1 hour before visualisation as Figure 4.26. **d)** THP-1 cells treated with 1 µM AMD3100 at 4˚C for 1 hour before visualisation as Figure 4.26. **e)** THP-1 cells treated with 1 µM AZ6-2 at 4˚C for 1 hour before visualisation as Figure 4.26. **f)** Negative control as Figure 4.26 incubated at 37˚C. **g)** Positive control as Figure 4.26 incubated at 37˚C. **h)** THP-1 cells stimulated with 10 nM of CXCL12 at 37˚C for 1 hour before visualisation as Figure 4.26. **i)** THP-1 cells treated with 1 µM AMD3100 at 37˚C for 1 hour before visualisation as Figure 4.26. **j)** THP-1 cells treated with 1 µM AZ6-2 at 37˚C for 1 hour before visualisation as Figure 4.26. Data shows representative cells from 3 independent experiments with similar findings. Acquired with Leica imaging suite with 63x objective, 35x overall magnification.

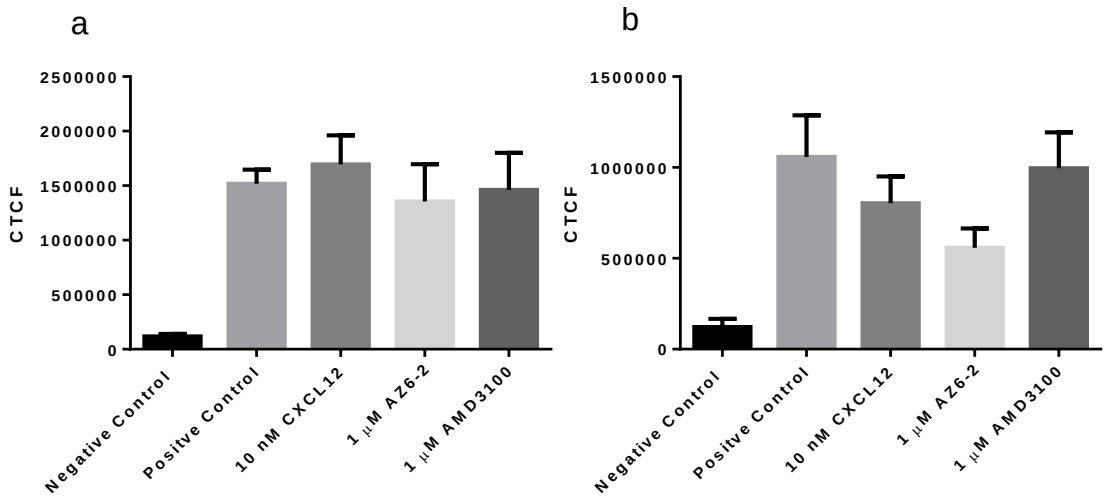


**Figure 4.31: Incubation with AMD3100 and AZ6-2 at 4˚C and 37˚C causes no significant change in the fluorescent intensity of CXCR4 receptor expression in THP-1 cells. a)** Corrected Total Cell Fluorescence (CTCF) of THP-1 cells from Figure 4.30 stimulated with 10 nM CXCL12 or treated with 1 µM AMD3100 or AZ6-2 at 4˚C for one hour. **b)** CTCF of THP-1 cells from Figure 4.30 stimulated with 10 nM CXCL12 or treated with 1 µM AMD3100 or AZ6-2 at 37˚C for 1 hour. CTCF = Integrated Density – (Area of selected cell x Mean fluorescence of background readings). Data represents the mean ± SEM of 3 independent experiments. One-Way ANOVA with post hoc Dunnett's multiple comparison, data was not significant.

### 4.3.9. AZ3-2, AZ6-2 and AMD3100 do not cause any significant changes to MCF-7 cell area or circularity but supresses actin polymerisation

The binding of CXCL12 to CXCR4 stimulates the phosphorylation of proteins such as the cytoskeletal protein, paxillin, enabling the reorganizing the actin cytoskeleton to aid cellular migration (Wang et al., 2000). Therefore, to determine if these compounds can bind to CXCR4 and prevent any cytoskeletal changes, actin staining using Phalloidin-iFluor 488 Conjugate was carried out on MCF-7 cells. It was found that there was no discernible change to either cell area or cell circularity after incubation with either 10 nM CXCL12 or 1 µM AMD3100, AZ3-2 or AZ6-2 (Figure 4.32 and 4.33).

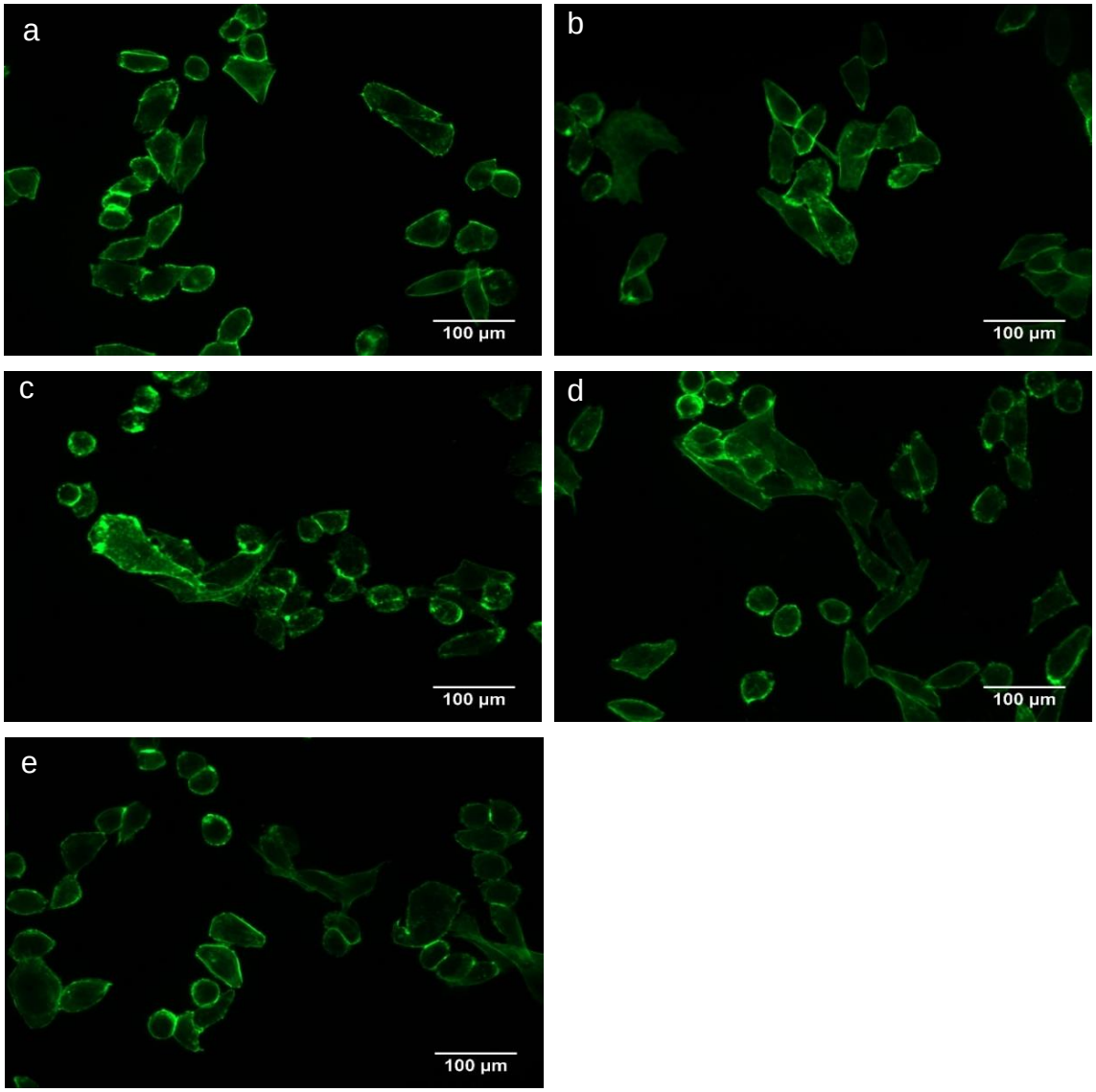


**Figure 4.32: Actin stains of MCF-7 cells.** MCF-7 cells treated with antagonists or chemokine for 1 hour then fixed with 4% paraformaldehyde for 10 minutes, permeabalised with 0.1% Triton X-100 for 5 minutes then stained with Phalloidin-iFluor 488 Conjugate (green) before imaging. **a)** Basal MCF-7 cells. **b)** MCF-7 cells stimulated with 10 nM CXCL12 for 1 hour. **c)** MCF-7 cells treated with 1 µM AMD3100 for 1 hour. **d)** MCF-7 cells treated with 1 µM AZ3-2 for 1 hour. **e)** MCF-7 cells treated with 1 µM AZ6-2 for 1 hour. Data shows representative cells from 3 independent experiments with similar findings. Acquired with Leica imaging suite with 40x objective, 22x overall magnification.

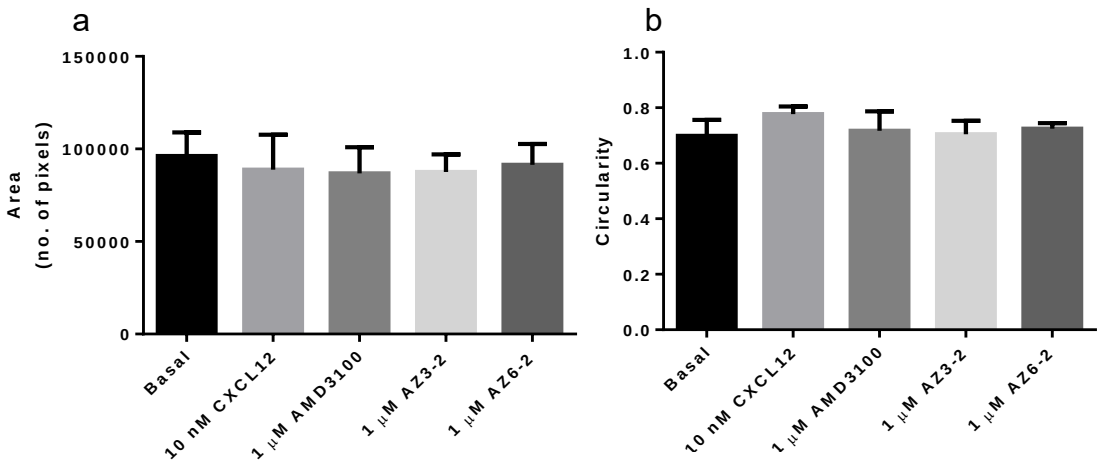


**Figure 4.33: Incubation with CXCL12, AMD3100, AZ3-2 and AZ6-2 causes no significant changed to average cell area or circularity in MCF-7 cells**. **a)** Area of MCF-7 cells from Figure 4.32. **b)** Circularity of MCF-7 cells from Figure 4.32. 0 indicates more elongated, 1 indicates more rounded morphology. Data represents the mean ± SEM of 3 independent experiments. One-Way ANOVA with post hoc Dunnett's multiple comparison, data was not significant.

However, when corrected total cell fluorescence (CTCF) was calculated, there was a significant decrease in fluorescence with the addition of all three CXCR4 antagonists, where fluorescence is equivalent to actin polymerisation (Figure 4.34).

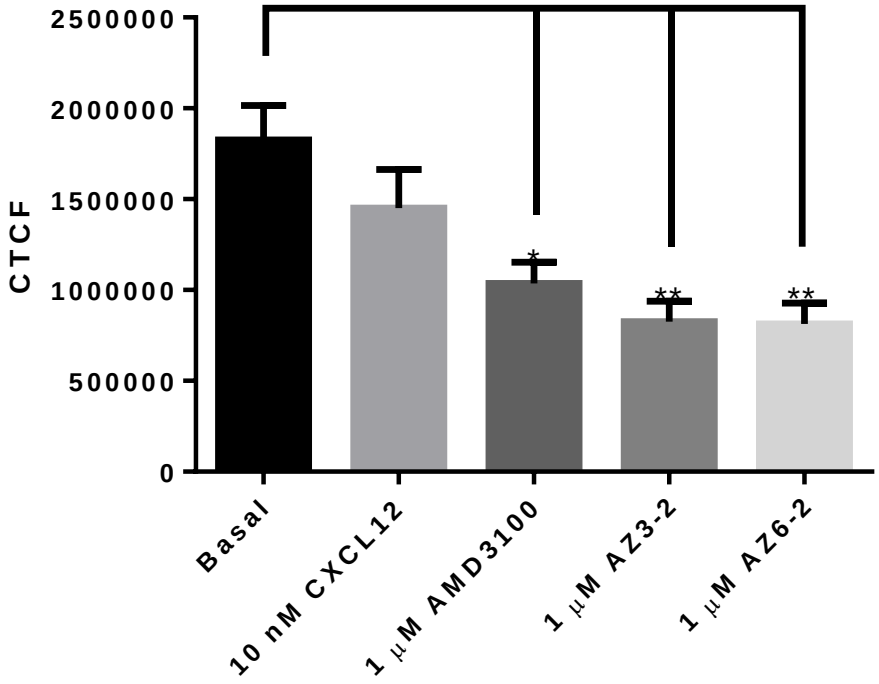


**Figure 4.34: Incubation with AMD3100, AZ3-2 and AZ6-2 causes significant decrease in the fluorescent intensity of actin.** Corrected Total Cell Fluorescence (CTCF) of MCF-7 cells from Figure 4.32 stimulated with 10 nM CXCL12 or treated with 1 µM AMD3100, AZ3-2 or AZ6-2 for 1 hours. CTCF = Integrated Density – (Area of selected cell x Mean fluorescence of background readings). Data represents the mean ± SEM of 3 independent experiments. One-Way ANOVA with post hoc Dunnett's multiple comparison, * = p≤ 0.05 and ** = p≤ 0.01.

### 4.3.10. The development of a suitable migration assay for adherent cells

Boyden chamber assays have been used extensively in the literature to examine the ability of chemokines to stimulate directional migration of cells through a membrane (Barber et al., 1999, Zang et al., 2000, Inngjerdingen et al., 2003). Therefore, PC3 prostate cancer cells were treated with 1 μM AMD3100, AZ3-2 or AZ6-2 and stimulated with 10 nM of CXCL12. Unfortunately, results produced from these Boyden chamber assays were inconclusive due to their lack of reproducibility (Figure 4.35).

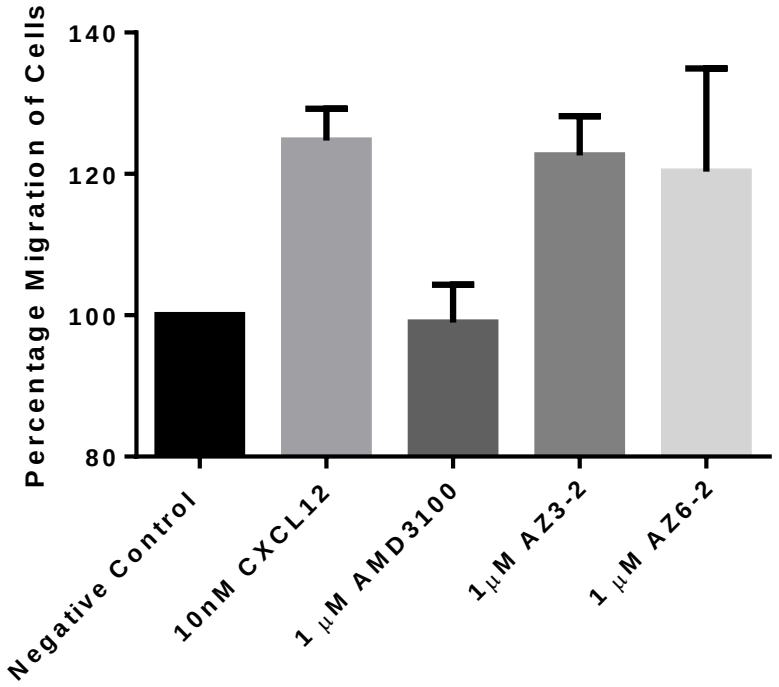


**Figure 4.35: Boyden chamber assays produced inconclusive results when using PC3 cells treated with AMD3100, AZ3-2 and AZ6-2 then stimulated with CXCL12.** PC3 prostate cancer cells seeded into Boyden chambers then treated with 1 μM of AMD3100, AZ3-2 or AZ6-2 then stimulated with 10 nM CXCL12 for 24 hours. Data represents the mean ± SEM of 3 independent experiments. Data normalised to the negative control and Kruskal-Wallis non-parametric test with post hoc Dunn's multiple comparison test was conducted, data was not significant.

MCF-7 cells had previously been used by another member of the research group who confirmed that MCF-7 migration using Boyden chamber assays was also inconclusive. This lead to the development of 3D printed materials for chemotaxis chambers that are discussed in Chapter 7. While these were in

development, an alternative method was adopted; scratch closure assays, also used extensively in the literature (Mills et al., 2016, Mills et al., 2018, Rebollo et al., 2017, Bünemann et al., 2018, Kroeze et al., 2009). PC3 cells had previously been used in scratch closure assays by another member of the research group, but these cells migrated too quickly and all scratches had closed including the negative control scratches after 24 hours. Due to this, MCF-7 breast cancer cells were used with and without 10 nM of CXCL12 to attempt scratch closure. Unfortunately, results after 24 hours showed no significant difference between the controls (Figure 4.36).

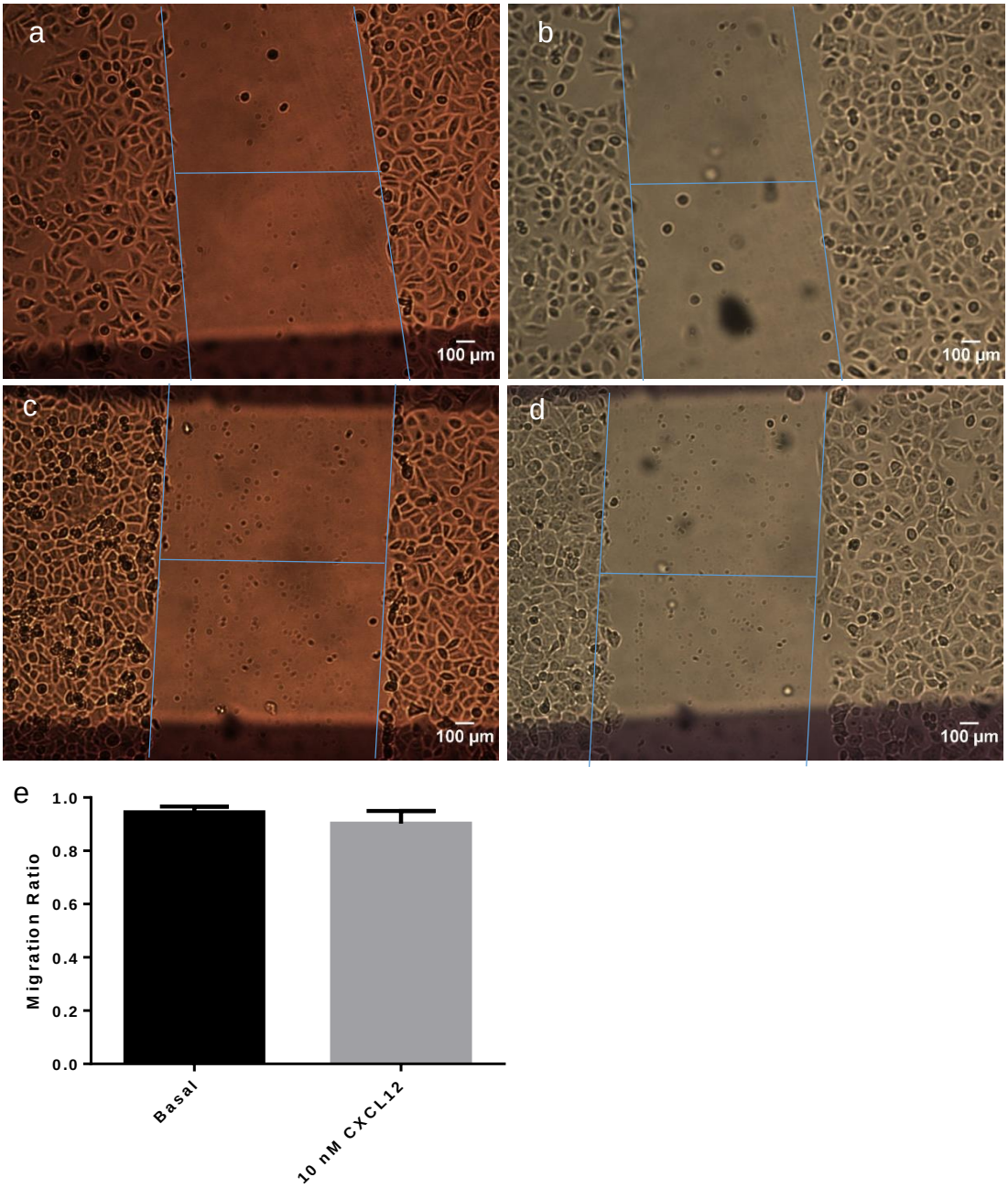


**Figure 4.36: Scratch closure assays produced inconclusive results when using MCF-7 cells stimulated with 10 nM CXCL12.** MCF-7 cells were seeded and left to grow for 24 hours, a scratch applied then stimulated with chemokine for 24 hours. **a)** Negative Control at 0 hours. **b)** Negative control at 24 hours. **c)** MCF-7 cells stimulated with 10 nM CXCL12 at 0 hours. **d)** MCF-7 cells stimulated with 10 nM CXCL12 at 24 hours. **e)** The migration ratios of basal and 10 nM CXCL12 treated scratched. Data is expressed as a change in migratory ratio (24 hours/0 hours) with 0 being a completely closed scratch. Data shows representative images from 3 independent experiments with similar findings. Acquired with Leica imaging suite with 10x objective, 5.5x overall magnification. Data represents the mean ± SEM of 3 independent experiments. Student's T-test, data not significant.

When cells were incubated for a further 24 hours, there was a negative change in scratch width as a consequence of a substantial amount of cell death (Figure 4.37).

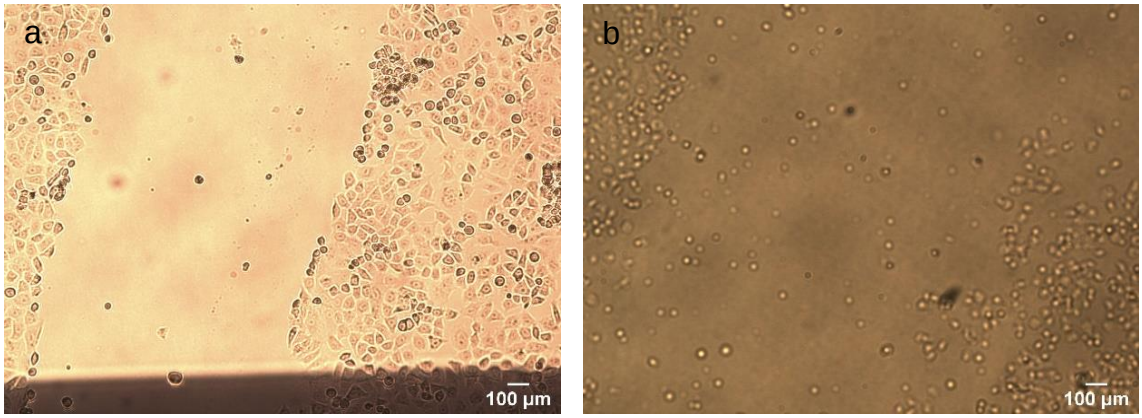


**Figure 4.37: Scratch closure assays incubated for 48-hours caused MCF-7 cell death.** MCF-7 cells were seeded and left to grow for 24 hours, a scratch applied then stimulated with chemokine for 48 hours. **a)** Negative Control at 0 hours. **b)** Negative control at 48 hours. Data shows representative images from 3 independent experiments with similar findings. Acquired with Leica imaging suite with 10x objective, 5.5x overall magnification.

In an attempt to determine a suitable time point to assess scratch closure in MCF-7 cells, the assays were conducted under time lapse using three types of FBS supplemented DMEM to find the ideal conditions that will stimulate migration but prevent cell proliferation (Table 4.3). However, after analysis there was no significant difference between the controls (refer to Figure 4.38 for an example).

**Table 4.3: Development of a suitable migration assay for adherent cells.**

| Assay | Cell Type | Time (h) | Media | Comments |
|---|---|---|---|---|
| **Scratch Closure** | MCF-7 | 10 | 0.5% FBS DMEM | Scratch failed to close |
| **Scratch Closure** | MCF-7 | 20 | 0.5% FBS DMEM | Scratch failed to close |
| **Scratch Closure** | MCF-7 | 30 | 0.5% FBS DMEM | Scratch failed to close |
| **Scratch Closure** | MCF-7 | 20 | 0.1% FBS DMEM | Scratch failed to close |
| **Scratch Closure** | MCF-7 | 20 | 0% FBS DMEM | Scratch failed to close |
| **Sparse cell seeding** | MCF-7 | 10 | 0% FBS DMEM | Poor migration |
| **Sparse cell seeding** | MCF-7 | 10 | 0.5% FBS DMEM | Poor migration |
| **Sparse cell seeding** | MCF-7 | 10 | 5% FBS DMEM | High proliferative rates |
| **Sparse cell seeding** | MCF-7 | 10 | 0.5% FBS DMEM | 10 nM CXCL12 soaked filter paper used |
| **Sparse cell seeding** | PC3 | 10 | 5% FBS RPMI | Increased cell speed with the addition of 10 nM CXCL12 |

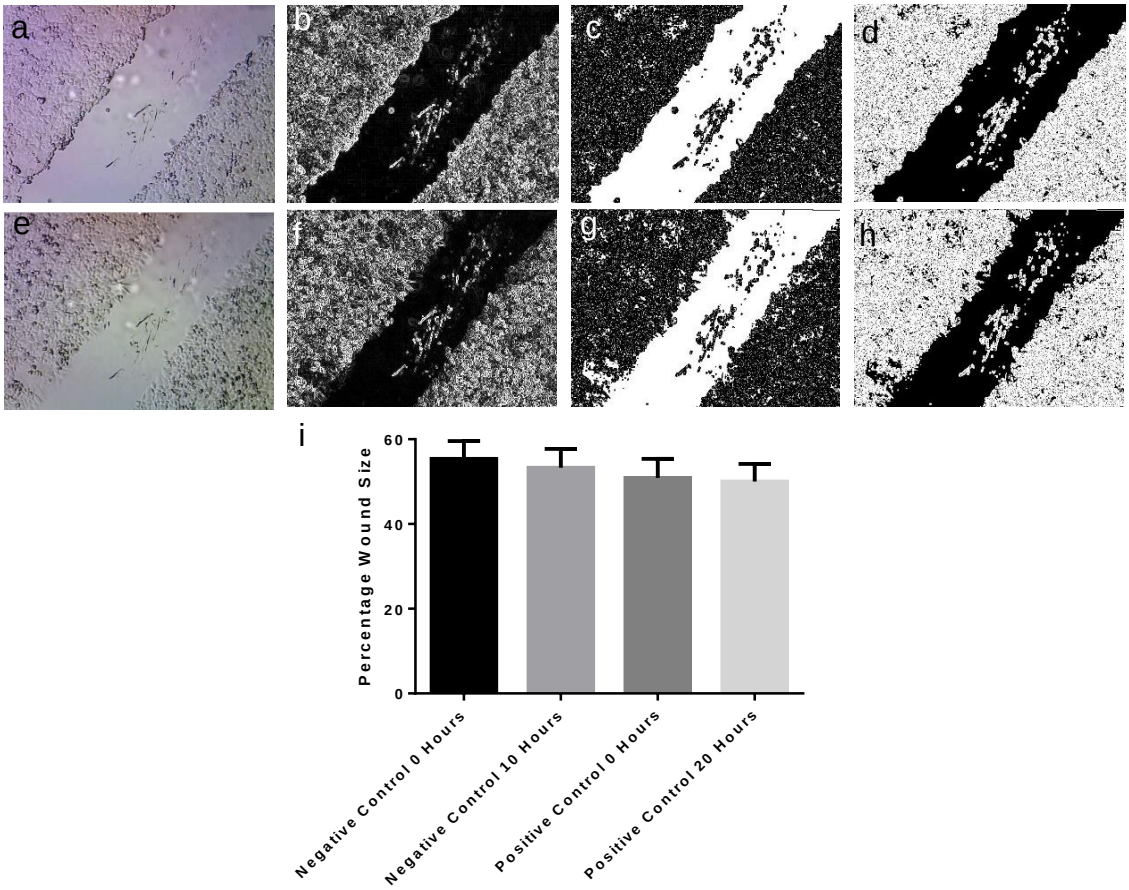


**Figure 4.38: Still images of exemplar time lapse scratch closure assay analysis of MCF-7 cells supplemented with 0.1% FBS DMEM.** MCF-7 cells were seeded and left to grow for 24 hours, a scratch applied then stimulated with chemokine for 20 hours. **a)** Scratch in monolayer of MCF-7 at 0 hours**. b)** Edge of 0-hour wound defined. **c)** Increased contrast between 0-hour wound and cell front defined. **d)** 0-hour scratch image inverted to enable measurement of wound area. **e)** Scratch in monolayer of MCF-7 at 20 hours. **f)** Edge of 20-hour wound defined. **g)** Increased contrast between 20-hour wound and cell front defined. **h)** 20-hour scratch image inverted to enable measurement of wound area**. i)** Percentage scratch size in MCF-7 monolayer with and without 10 nM of CXCL12 at 0 and 20 hours. Data shows representative images from 3 independent experiments with similar findings. Acquired with Debut Professional Video Capture v 3.01 and Camtasia Studio 8 was used to compose the image with 10x objective. Data represents the mean ± SEM of 3 independent experiments. One-Way ANOVA with post hoc Dunnett's multiple comparison, data not significant.

An alternative approach was conducted under time lapse; sparse seeding of MCF-7 cells to attempt to determine their migratory speed again using three types of FBS supplemented DMEM and by using chemokine soaked filter paper (Table 4.3). Unfortunately, MCF-7 cells migrated too slowly to get an accurate assessment of migration speed with an average basal speed of 3.76 ± 0.38 µm/h and an average speed of 2.35 ± 0.41 µm/h recorded with the addition of 10 nM CXCL12 (Figure 4.39). Consequently, MCF-7 cells were deemed unsuitable for accurate migration and migratory speed assessment.

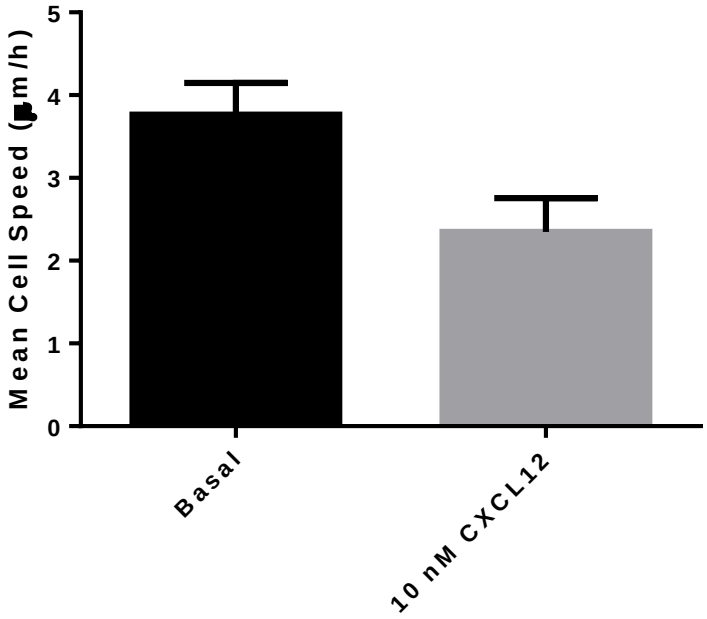


**Figure 4.39: MCF-7 cells supplemented with 0.5% FBS DMEM migrate too slowly to get accurate migratory speeds**. MCF-7 cells were seeded and incubated for 24 hours before stimulation with 10 nM CXCL12 for 10 hours. Subsequently, MCF-7 cells were tracked and basal cell speed was calculated to be 3.76 ± 0.38 µm/h. CXCL12 stimulated MCF-7 cell speed was calculated to be 2.35 ± 0.41 µm/h. Data represents the mean ± SEM of 3 independent experiments. Student's T-test, data not significant.

Therefore, PC3 cells were revisited and used for sparse cell seeded time lapse experiments. From these experiments it was found that PC3 cells has a basal speed of 50.40 ± 7.48 µm/h and when stimulated with 10 nM of CXCL12, their speeds significantly increased to 86.24 ± 7.03 µm/h (Figure 4.40). Consequently, future experimentation into CXCL12 stimulated adherent cell migration will be conducted using time lapse assay. Data represents the mean ± SEM of 3 independent experiments.

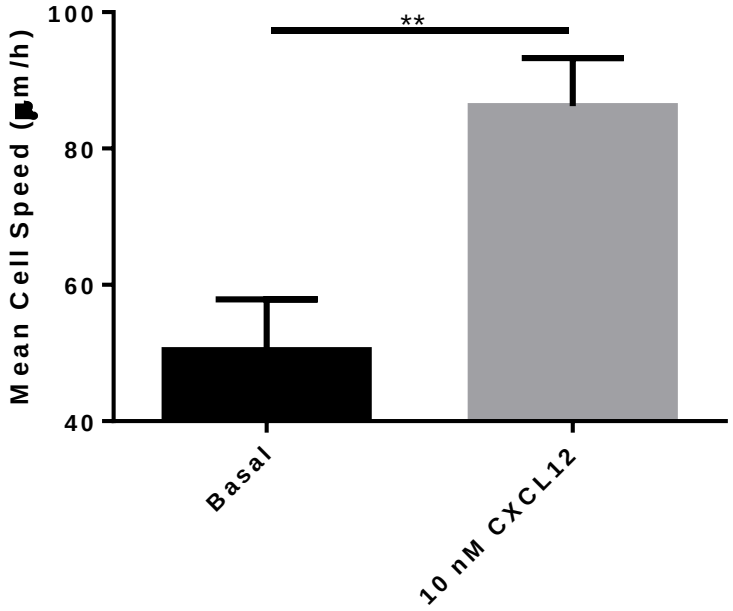


**Figure 4.40: Mean PC3 cell speed increases with the addition of CXCL12.** PC3 cells were seeded and incubated for 24 hours before stimulation with and without 10 nM CXCL12 for 10 hours. Subsequently, PC3 cells were tracked and basal cell speed was calculated to be 50.40 ± 7.48 µm/h. CXCL12 stimulated PC3 cell speed was calculated to be 86.24 ± 7.03 µm/h. Data represents the mean ± SEM of 6 independent experiments. A value of p≤ 0.01 ** was deemed significant. Student's T-test, ** = p≤ 0.01.

### 4.3.11. AZ3-2 and AZ6-2 significantly reduce PC3 and SKMEL28 cell migratory speeds, but not AMD3100

After establishing a suitable assay for adherent cell lines, comparisons were made between the two novel CXCR4 antagonists and the already marketed CXCR4 antagonist, AMD3100. Therefore, PC3 cells were treated with 1 µM of AMD3100, AZ3-2 or AZ6-2 and stimulated with 10 nM CXCL12 (Figure 4.41).

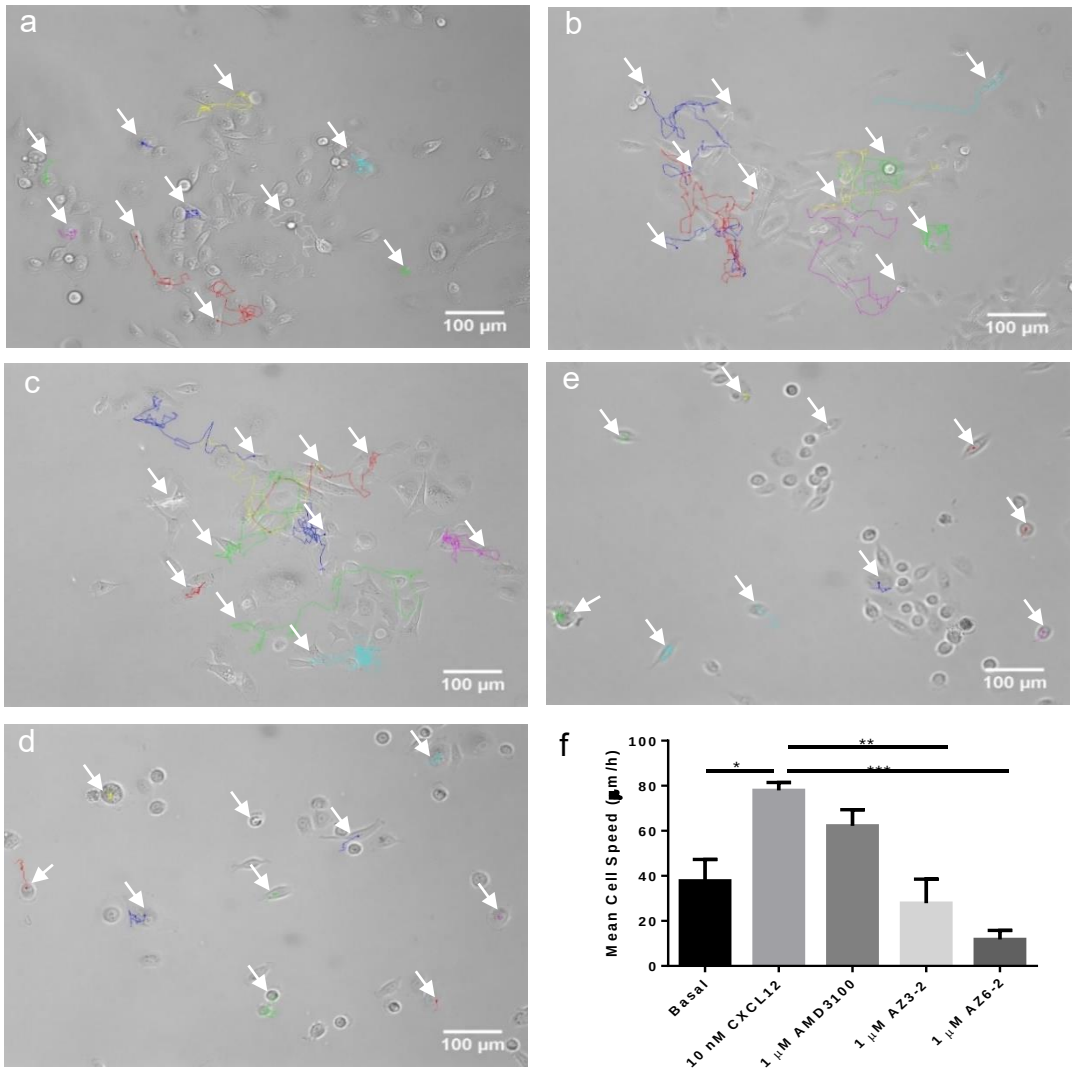


**Figure 4.41: AZ3-2 and AZ6-2 but not AMD3100 significantly decreases CXCL12 stimulated PC3 cell migratory speeds in 10-hour time lapse assays.** PC3 cells were seeded and incubated for 24 hours before the addition of antagonist and/or chemokine then migration was tracked for 10 hours. **a)** Tracked basal PC3 cell speeds. **b)** Tracked PC3 cell speeds where cells were stimulated with 10 nM CXCL12. **c)** Tracked PC3 cell speeds where cells were treated with 1 µM AMD3100 then stimulated with 10 nM CXCL12. **d)** Tracked PC3 cell speeds where cells were treated with 1 µM AZ3-2 then stimulated with 10 nM CXCL12. **e)** Tracked PC3 cell speeds where cells were treated 1 µM AZ6-2 then stimulated with 10 nM CXCL12. **f)** PC3 cells treated with 1 µM AMD3100, AZ3-2 or AZ6-2 then stimulated with 10 nM CXCL12. Data shows representative cell tracks from 3 independent experiments with similar findings. Acquired with a Zeiss Axiovert 200M motorise inverted fluorescent/ live cell imaging microscope with 10x objective. Data represents the mean ± SEM of 3 independent experiments. One-Way ANOVA with post hoc Dunnett's multiple comparison, ** = p≤ 0.01 and *** = p≤ 0.001.

Using this data, PC3 basal cell speeds were calculated to be 37. 82 ± 9.45 µm/h and rose to 77.97 ± 3.53 µm/h after being exposed to CXCL12 (Table 4.4). Incubation with AMD3100 did not significantly inhibit CXCL12 stimulated migration in PC3 cells. AZ3-2 and AZ6-2 reduced migratory speeds to 27.88 ± 10.67 µm/h and 11.76 ± 4.05 µm/h respectively.

**Table 4.4: Average Speed of PC3 cells treated with 1 µM AMD3100, AZ3-2 or AZ6-2 and stimulated by 10 nM CXCL12. Data represents the mean ± SEM of 3 independent experiments.**

| Treatment | Average Speed (µm/h) |
|---|---|
| **Basal** | 37.82 ± 9.45 |
| **10 nM CXCL12** | 77.97 ± 3.53 |
| **10 nM CXCL12 + 1 µM AMD3100** | 62.19 ± 7.19 |
| **10 nM CXCL12 + 1 µM AZ3-2** | 27.88 ± 10.67 |
| **10 nM CXCL12 + 1 µM AZ6-2** | 11.76 ± 4.05 |

Following this, a concentration range of 125 to 1000 nM of AZ6-2 was used in times lapse assays. From the raw data, it was found that concentrations of 125 nM, 500 nM and 1000 nM caused a significant decrease in PC3 migratory speeds (Figure 4.42).

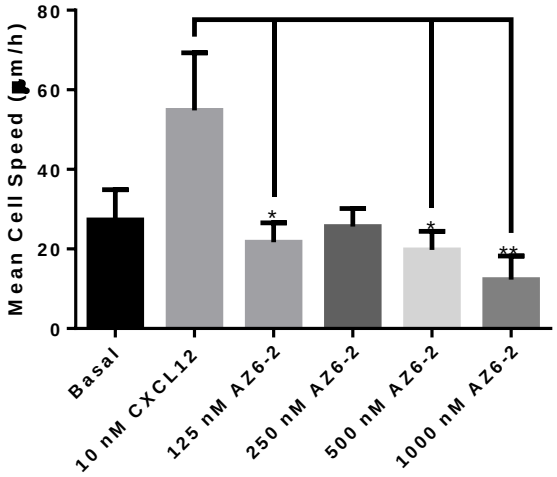


**Figure 4.42: 125-1000 nM of AZ6-2 significantly decreases CXCL12 stimulated PC3 cells migratory speeds in 10-hour time lapse assays**. PC3 cells were seeded and incubated for 24 hours before the addition of AZ6-2 (125-1000 nM) and 10 nM CXCL12 then migration was tracked for 10 hours. Data represents the mean ± SEM of 4 independent experiments. One-Way ANOVA with post hoc Dunnett's multiple comparison, * = p≤ 0.05 and ** = p≤ 0.01.

This data was percentage corrected and it was confirmed that AZ6-2 at concentrations of 500 nM and 1000 nM caused a significant decrease in PC3 cell migratory speeds (Figure 4.43).

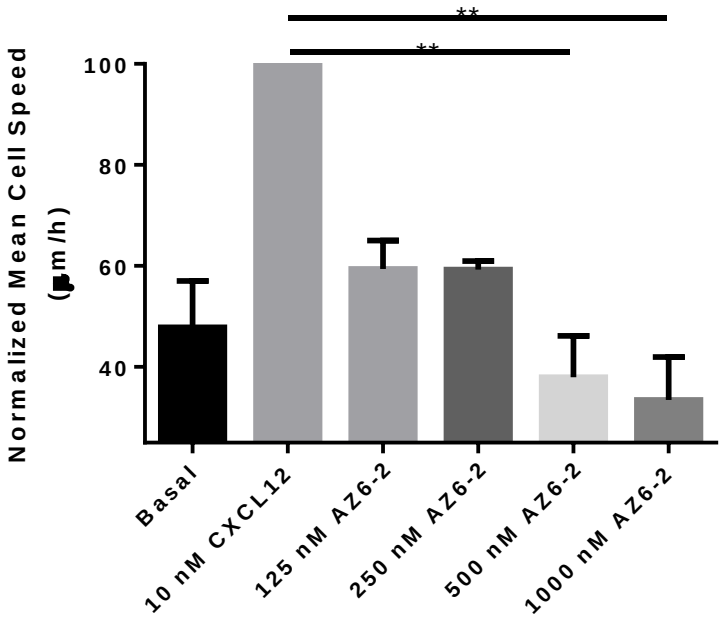


**Figure 4.43: 500-1000 nM of AZ6-2 significantly decreases CXCL12 stimulated PC3 cells migratory speeds cells using percentage corrected data from 10-hour time lapse assays.** Normalization of data from Figure 4.42 showing the migration of PC3 cells stimulated by 10 nM of CXCL12 in the presence and absence of AZ6-2 (125-1000 nM) then migration was tracked for 10 hours. Data represents the mean ± SEM of 4 independent experiments. Data normalised to CXCL12 and Kruskal-Wallis non-parametric test with post hoc Dunn's multiple comparison test was conducted, ** = p≤ 0.01.

Finally, the percentage corrected data was used to calculate an $IC_{50}$ of 128 nM ± 66.08 nM SEM (Figure 4.44).

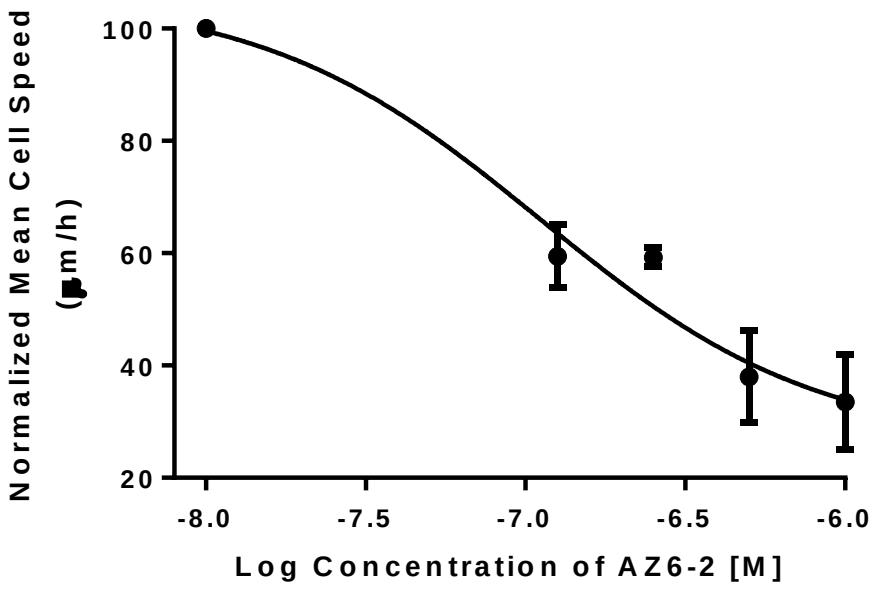


**Figure 4.44: Dose response curve of the speed of PC3 cells when treated with a dose range of AZ6-2 and stimulated by 10 nM of CXCL12.** An $IC_{50}$ of 128 nM ± 66.08 nM SEM was calculated from data from Figure 4.43. Data represents the mean ± SEM of 4 independent experiments. Log (inhibitor) vs. response (three parameters).

Similar experiments were carried out in SKMEL28 cells, where it was demonstrated that 1 μM of AMD3100 also failed to significantly reduce CXCL12 stimulated migratory speeds while AZ3-2 and AZ6-2 significantly decreased migratory speeds (Figure 4.45).

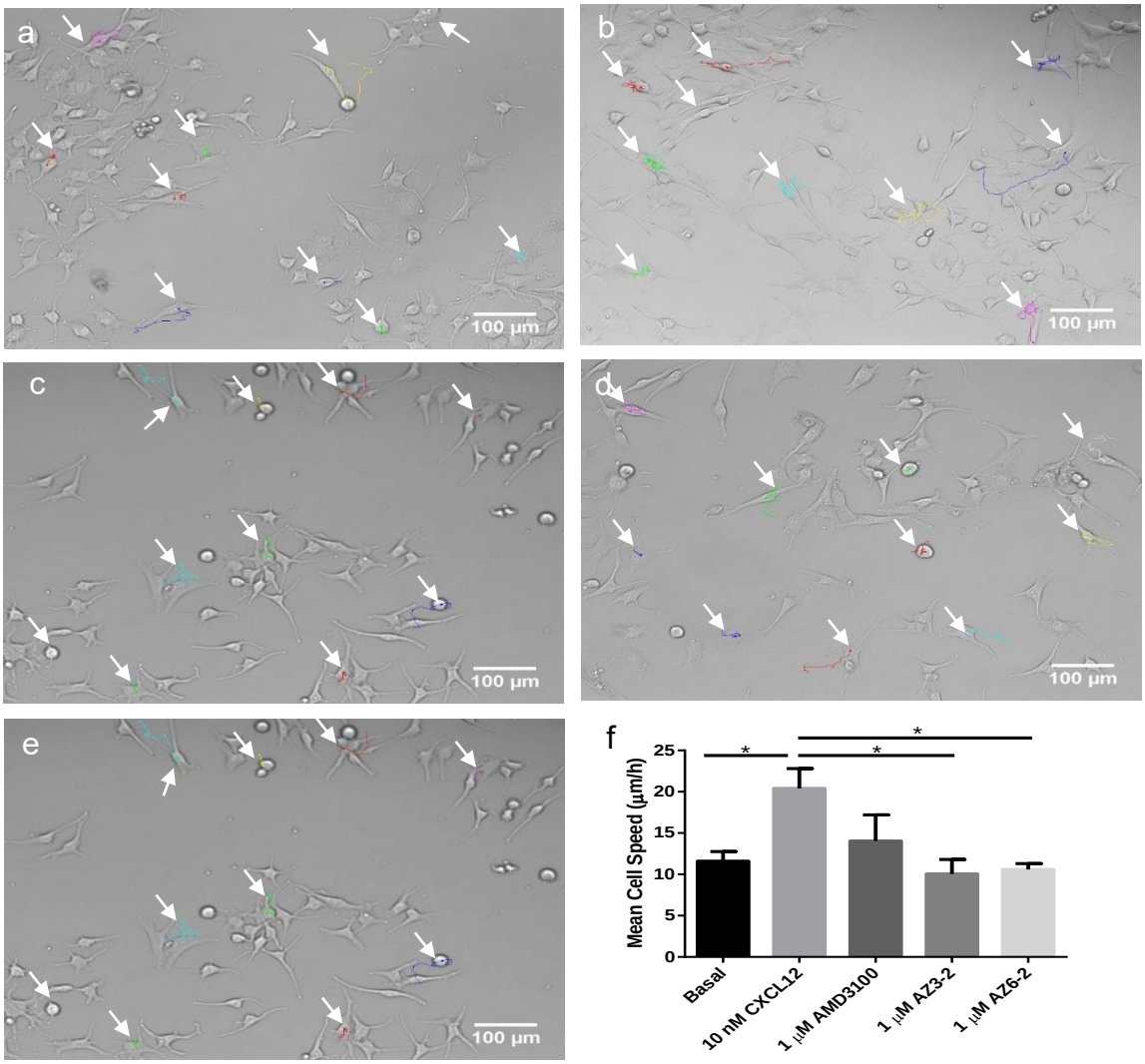


**Figure 4.45: AZ3-2 and AZ6-2 but not AMD3100 significantly decreases CXCL12 stimulated SKMEL28 cells migratory speeds in 10-hour time lapse assays.** SKMEL28 cells were seeded and incubated for 24 hours before the addition of antagonist and/or chemokine then migration was tracked for 10 hours. **a)** Tracked basal SKMEL28 cell speeds. **b)** Tracked SKMEL28 cell speeds where cells were stimulated with 10 nM CXCL12. **c)** Tracked SKMEL28 cell speeds where cells were treated with 1 µM AMD3100 then stimulated with 10 nM CXCL12. **d)** Tracked SKMEL28 cell speeds where cells were treated with 1 µM AZ3-2 then stimulated with 10 nM CXCL12. **e)** Tracked SKMEL28 cell speeds where cells were treated 1 µM AZ6-2 then stimulated with 10 nM CXCL12. **f)** SKMEL28 cells were treated with 1 µM AMD3100, AZ3-2 or AZ6-2 then stimulated with 10 nM CXCL12. Data shows representative cell tracks from 3 independent experiments with similar findings. Acquired with a Zeiss Axiovert 200M motorise inverted fluorescent/ live cell imaging microscope with 10x objective. Data represents the mean ± SEM of 3 independent experiments. One-Way ANOVA with post hoc Dunnett's multiple comparison, * = p≤ 0.05.

Compared to PC3 cells, SKMEL28 cells speeds were overall a lot slower, with an average basal speed of 11.59 ± 1.17 µm/h that increased to 20.40 ± 2.41 µm/h once stimulated with 10 nM CXCL12 (Table 4.5). Incubation with AZ3-2 and AZ6-2 reduced these speeds to 10.05 ± 1.75 µm/h and 10.59 ± 0.70 µm/h respectively.

**Table 4.5: Average speed of SKMEL28 cells treated with 1 µM AMD3100, AZ3-2 or AZ6-2 and stimulated by 10 nM CXCL12. Data represents the mean ± SEM of 3 independent experiments.**

| Treatment | Average Speed (µm/h) |
|---|---|
| **Basal** | 11.59 ± 1.17 |
| **10 nM CXCL12** | 20.40 ± 2.41 |
| **10 nM CXCL12 + 1 µM AMD3100** | 14.04 ± 1.75 |
| **10 nM CXCL12 + 1 µM AZ3-2** | 10.05 ± 0.70 |
| **10 nM CXCL12 + 1 µM AZ6-2** | 10.59 ± 3.17 |

To determine an $IC_{50}$ for AZ6-2 in SKMEL28 cells, a concentration range of 0.2-1 µM AZ6-2 was used in time lapse and these results were subsequently percentage corrected (Figure 4.46 and 4.47).

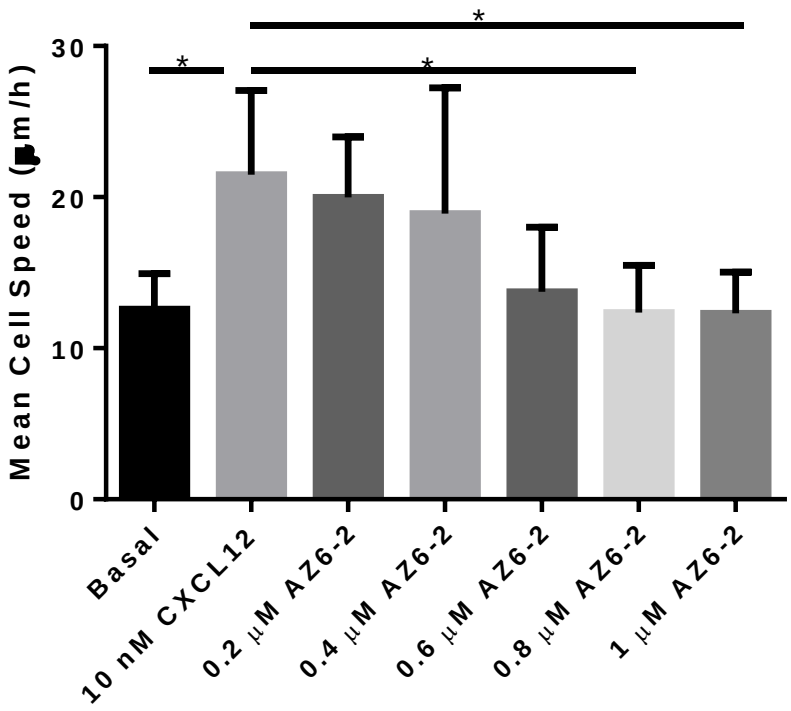


**Figure 4.46: 0.8-1 μM of AZ6-2 significantly decreases CXCL12 stimulated SKMEL28 cells migratory speeds in 10-hour time lapse assays.** SKMEL28 cells were seeded and incubated for 24 hours before the addition of AZ6-2 (0.2 - 1 μM) and 10 nM CXCL12 then migration was tracked for 10 hours. Data represents the mean ± SEM of 4 independent experiments. One-Way ANOVA with post hoc Dunnett's multiple comparison, * = p≤ 0.05 and ** = p≤ 0.01.

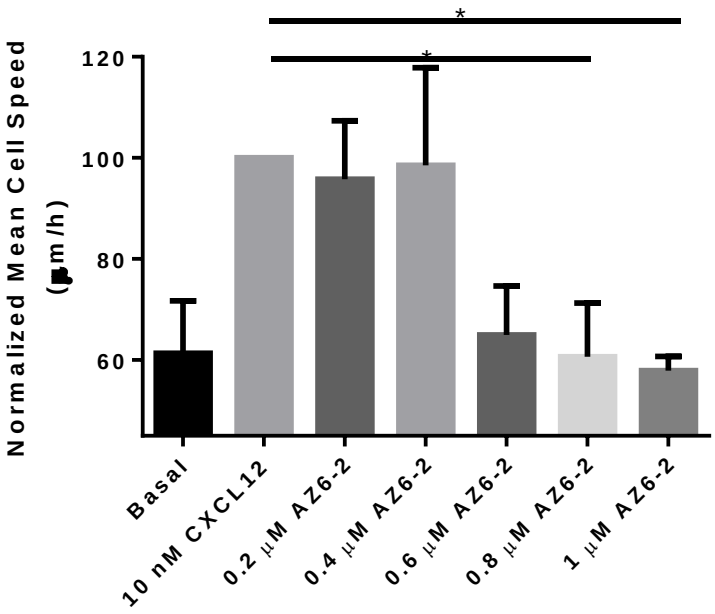


**Figure 4.47: 0.8-1 μM of AZ6-2 significantly decreases CXCL12 stimulated SKMEL28 cells migratory speeds cells using percentage corrected data from 10-hour time lapse assays.** Normalization of data from Figure 4.46 showing the migration of SKMEL28 cells stimulated by 10 nM of CXCL12 in the presence and absence of AZ6-2 (0.2-1 μM) then migration was tracked for 10 hours. Data represents the mean ± SEM of 4 independent experiments. Data normalised to CXCL12 and Kruskal-Wallis non-parametric test with post hoc Dunn's multiple comparison test was conducted, * = p≤ 0.05.

This calculated the $IC_{50}$ of AZ6-2 in SKMEL28 cells to be 266.2 nM ± 148.7 nM SEM (Figure 4.48). These reduced migratory speeds are not a consequence of cellular toxicity caused by the CXCR4 antagonists as demonstrated by MTS assay (Appendix A16-18).

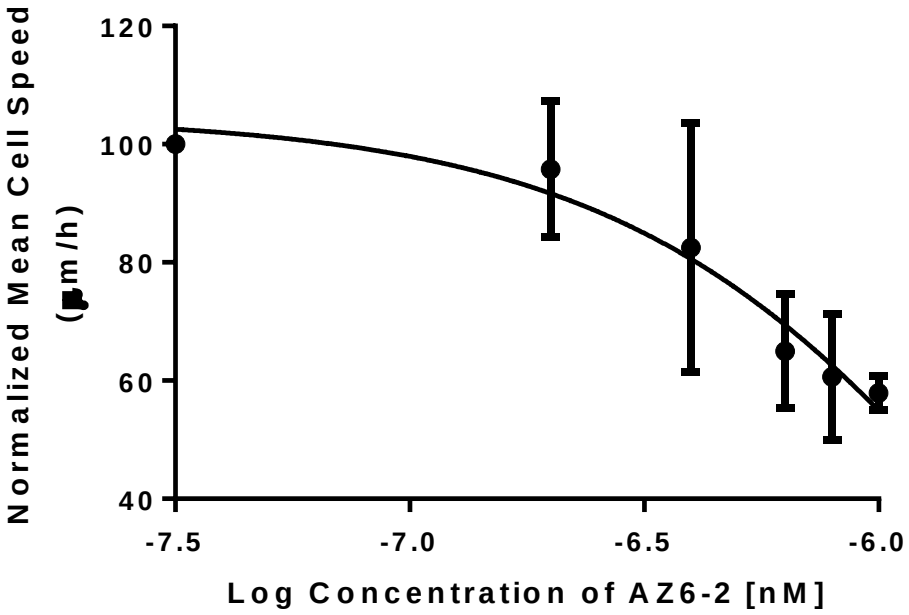


**Figure 4.48: Dose response curve of the speed of SKMEL28 cells when treated with a dose range of AZ6-2 and stimulated by 10 nM of CXCL12.** An $IC_{50}$ of 266.2 nM ± 148.7 nM SEM was calculated from data from Figure 4.47. Data represents the mean ± SEM of 4 independent experiments. Log (inhibitor) vs. response (three parameters).

Additionally, to determine if DMSO, the vehicle for AZ3-2 and AZ6-2, was causing any inhibitory effects itself, an equivalent volume of DMSO to that used to create 1 µM AZ3-2 or AZ6-2 was used in time lapse assays with both PC3 and SKMEL28 cells (Figure 4.49). This demonstrated that DMSO on its own was causing no inhibitory effects on cell speeds.

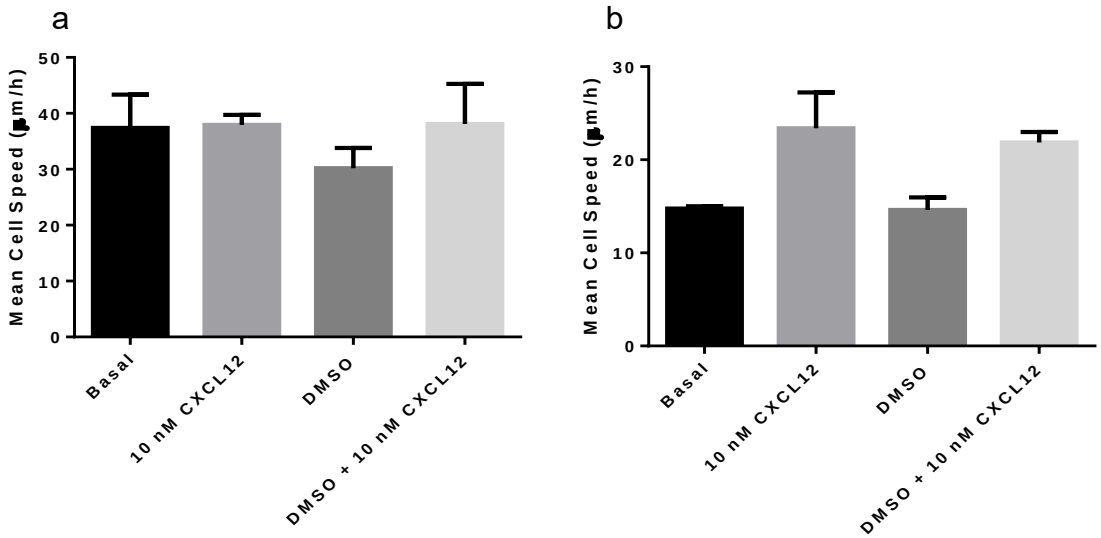


**Figure 4.49: DMSO does not have any inhibitory effects on its own in either PC3 or SKMEL28 cell lines. a)** PC3 cells were seeded and incubated for 24 hours before stimulation by 10 nM of CXCL12 in the presence and absence of an equivalent volume of DMSO vehicle then migration was tracked for 10 hours. **b)** SKMEL28 cells were seeded and incubated for 24 hours before stimulation by 10 nM of CXCL12 in the presence and absence of an equivalent volume of DMSO vehicle then migration was tracked for 10 hours. Data represents the mean ± SEM of 3 independent experiments. One-Way ANOVA with post hoc Dunnett's multiple comparison, data was not significant.

### 4.3.12. AZ6-2 significantly inhibits CXCL12 directed PC3 cell migration but not AZ3-2 and AMD3100

An additional migration assay was found to be suitable for adherent cell lines; Oris™ Cell Migration assay. Using this assay, it was determined that only AZ6-2 caused a significant decrease in CXCL12 directed migration in PC3 cells while AZ3-2 and AMD3100 caused no significant effect (Figure 4.50).

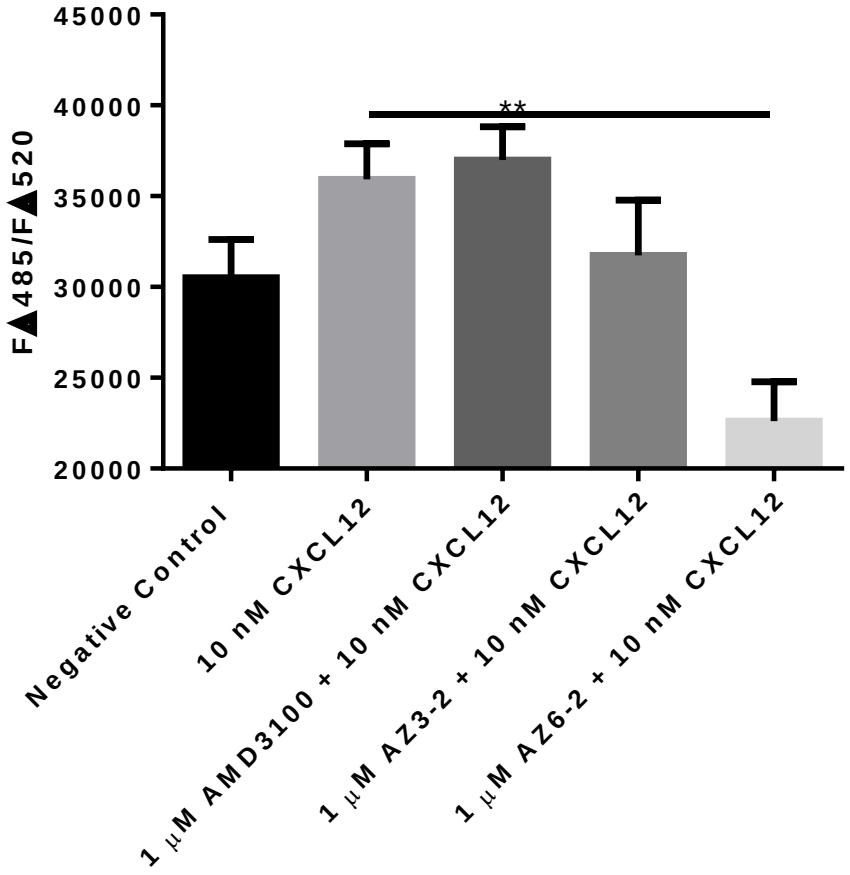


**Figure 4.50: AZ6-2 reduces CXCL12 directed migration in PC3 cells while AMD3100 and AZ3-2 do not in Oris™ Cell Migration assays.** PC3 cells were seeded and incubated for 24 hours before the addition of 1 µM AMD3100, AZ3-2 and AZ6-2 and 10 nM of CXCL12 then incubated for another for 24 hours before analysis using calcein 485/520 nm. Data represents the mean ± SEM of 4 independent experiments. One-Way ANOVA with post hoc Dunnett's multiple comparison, ** = p≤ 0.01.

Unfortunately, this assay was not sensitive enough for the slower moving SKMEL28 cell line (Figure 4.51).

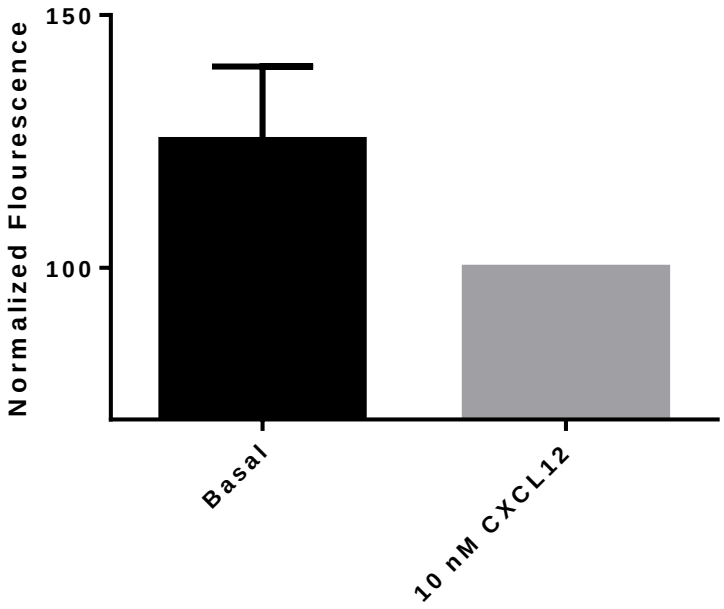


**Figure 4.51: Oris™ Cell Migration assay is not suitable for SKMEL28 cells.** SKMEL28 cells were seeded and incubated for 24 hours, stimulated with 10 nM of CXCL12 then incubated for another for 24 hours before analysis using calcein 485/520 nm. Data represents the mean ± SEM of 4 independent experiments. One-Way ANOVA with post hoc Dunnett's multiple comparison, data not significant.

### 4.3.13. AZ6-2 and AMD3100 are CXCR4 specific antagonists

In Di Maro et al. (2016) it was determined that AZ3-2 and AZ6-2 do not bind to either CXCR7 (ACKR3) nor to CXCR3. To confirm this and to further investigate the specificity of AZ6-2, two chemokines: CXCL11, which binds to CXCR3 and the 'CC' chemokine, CCL3, which binds to CCR1 and CCR5 receptors were investigated in both chemotaxis assays and calcium flux assays. From these experiments it was confirmed that AZ6-2 does not prevent CXCL11 or CCL3 stimulated THP-1 migration (Figure 4.52).

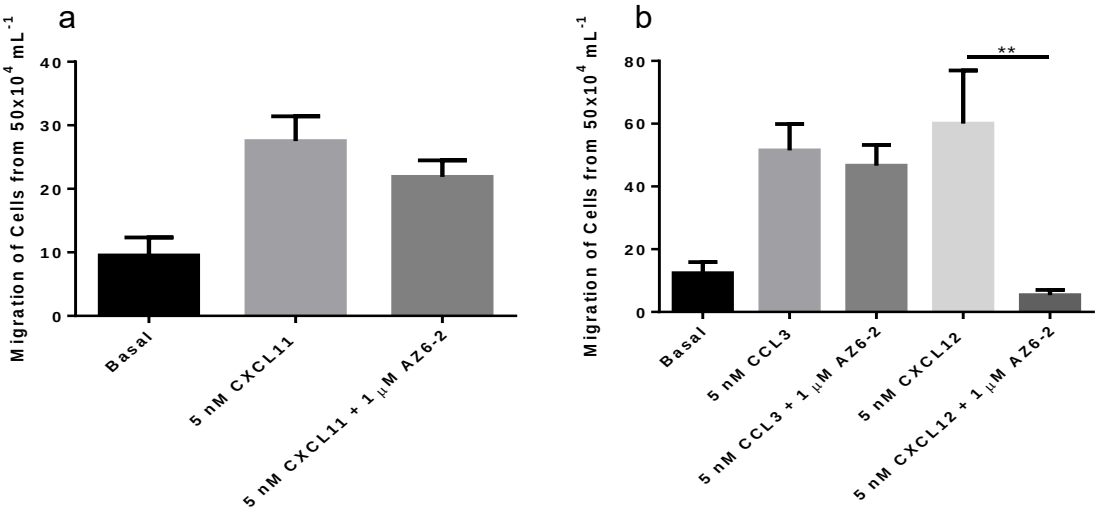


**Figure 4.52: AZ6-2 does not prevent CXCL11 or CCL3 stimulated THP-1 migration using chemotaxis assays.** The migration of THP-1 cells where cells were treated with 1 µM AZ6-2 for 30 minutes then stimulated by 5 nM of CXCL11, CCL3 or CXCL12 for 4 hours. Data represents the mean ± SEM of 3/4 independent experiments. One-Way ANOVA with post hoc Dunnett's multiple comparison,** = p≤ 0.01.

Furthermore, AMD3100 and AZ6-2 did not prevent the release of intracellular calcium from THP-1 cells stimulated with CCL3 (Figure 4.53).

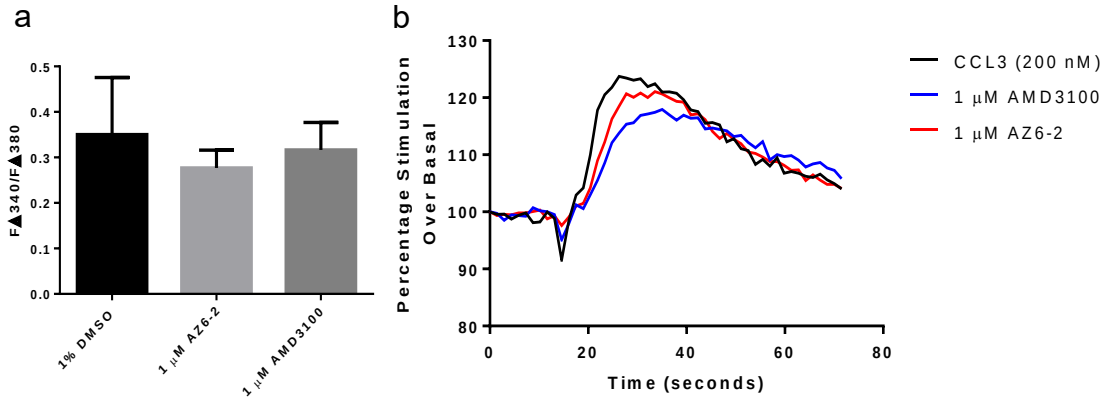


**Figure 4.53: AMD3100 and AZ6-2 do not reduce the release of intracellular Ca2+ from CCL3 stimulated THP-1 cells.** Cells were incubated for 30 minutes with antagonist or vehicle control and the calcium indicator Fura-2 AM. **a)** THP-1 cells treated with the equivalent volume of DMSO, 1 μM AMD3100 or AZ6-2 then stimulated with 200 nM CCL3. **b)** Representative intracellular calcium release traces of THP-1 cells treated with the equivalent volume of DMSO, 1 μM AMD3100 or AZ6-2 then stimulated with 200 nM CCL3. Data is expressed as a change in fluorescence ratio (340nm/380nm) where the basal fluorescence prior to the addition of CCL3 is subtracted from peak fluorescence following addition of CCL3. Chemokine injected after 10 seconds. Data represents the mean ± SEM of 3 independent experiments. One-Way ANOVA with post hoc Dunnett's multiple comparison, data not significant.

## 4.4. Discussion

CXCR4 is the most commonly overexpressed chemokine receptor in cancer, leading to more aggressive tumours due to their increased metastatic potential (Borrello et al., 2005, Koshiba et al., 2000, Mehta et al., 2007, Müller et al., 2001, Singh et al., 2009, Johnson et al., 2004). Owing to this, there has been much investigation into CXCR4 antagonists leading to the discovery of several novel agents including but not limited to: AMD3465, MSX-122, NOX-A12, POL6326. However, there has been little progression of these agents into clinical use (Bodart et al., 2009, Debnath et al., 2013, de Nigris et al., 2012, Vater et al., 2013). Therefore, the overarching aim of this chapter was to conduct some preliminary investigations into a new CXCR4 antagonist AZ6-2 (Arg-Ala-[DCys-Arg-Phe-Phe-Cys]), synthesized by Di Maro et al. (2016). The original chemical

research behind this peptide was fairly extensive and found that AZ6-2 was the most potent peptide out of the 15 synthesised and had the greatest specificity and plasma stability. However, biological investigations were limited to only one leukaemia cell line (CCRF-CEM) and two colon cancer cell lines (HT29 and HCT116). Therefore, several CXCR4 overexpressing cancer cell lines: MCF-7 (breast), Jurkat (acute T cell leukaemia), THP-1 (AML), PC3 (metastatic prostate) and SKMEL28 (skin) were used to investigate AZ6-2 in comparison to AZ3-2 (structurally identical to AZ6-2 aside from the first cysteine of the amino acid sequence being in the L-conformation) and the already approved compound, AMD3100. The use of AZ3-2 in these initial experiments was mainly to provide insight into how a small change to the peptide's structure can dramatically improve potency and/or stability, an idea which is further explored and built upon in Chapter 5.

Originally, suitable CXCR4 overexpressing cell lines had to be identified and out of the ten cell lines investigated, five were suitable (Figure 4.1-4.4 and Table 4.1). These initial experiments created questions as several of the CXCR4 negative cell lines had previously been described in the literature to express CXCR4, such as the three breast cancer cell lines: BT-474, SKBR3 and MDA-MB-231 (Akekawatchai et al., 2005, Holland et al., 2006, Salazar et al., 2014). However, this phenomenon has been seen throughout research due to the genetic instability of cancer cell lines and the development of different cell subpopulations with variations for example in their sensitivity to oestrogen and their preferential metastatic sites (Nguyen et al., 2016, Nugoli et al., 2003, Seibert et al., 1983). Therefore, it was not unusual to find these cell lines to be negative for CXCR4 expression despite evidence against this in literature. Furthermore, while it was suggested in the literature that NCI-H292 cells do not express CXCR4 and A549 cells do express CXCR4, both of these cell lines were still investigated to confirm this and both were found to express little CXCR4 (Burger et al., 2011, Murdoch et al., 1999).

These investigations identified three adherent cell lines; MCF-7, PC3 and SKMEL28 and two suspension cell lines: Jurkat and THP-1. However, while CXCR4 was homogenously expressed on the surface of most Jurkat cells, THP-1 expression of CXCR4 was heterogeneous. This was originally thought to be due to the potential for THP-1 cells to differentiate from monocytes to macrophages. Monocytes are generally abundant in CXCR4 receptor but

following differentiation to macrophages, CXCR4 expression levels have been shown to be much reduced (Lodge et al., 2018). However, in separate studies it was found that THP-1 cell differentiation did not affect CXCR4 expression levels (Konopka and Düzgüneş, 2002, Yu et al., 2018). Instead it was found that much like the breast cancer cell lines discussed above, THP-1 cells are inherently instable and possess variations in receptor expressions. In a study by Cassol et al. (2006) it was found that freshly isolated monocytes expressed high levels of CXCR4 that fell to near undetectable levels after 24 hours. Therefore, the heterogeneous expression levels of CXCR4 could be due to the individual age of the THP-1 cell and so could be strongly affected by passage numbers which were not recorded. It was observed however, that those THP-1 cells that did express CXCR4, expressed much higher quantities of CXCR4 than that seen on a given Jurkat cell. It was due to the variability in CXCR4 expression levels that two different CXCL12 concentrations were used during the chemotaxis assays; 1 nM CXCL12 for the Jurkat cell line and 5 nM CXCL12 for the THP-1 cell line as THP-1 cells required a higher concentration to obtain sufficient cellular migration. For a more concrete, quantitative determination of CXCR4 expression flow cytometry should be conducted.

From the chemotaxis assay results, it is clear to see that AZ6-2 was the most potent of the three compounds tested in the two suspension cell lines (Table 4.5). This is contrary to the results in Di Maro et al. (2016) who found that AMD3100 had the lowest $IC_{50}$ value of the tested peptides with an $IC_{50}$ of 6 nM ± 4 nM compared to AZ6-2 with 53 nM ± 4 nM. However, these results were obtained using different methods and conducted in a different suspension cell line, CCRF-CEM, demonstrating that the variability in $IC_{50}$ values is dependent upon the experimental method and the variability between cell lines. The greater potency of AZ6-2 in Jurkat cells as compared to THP-1 cells is most likely to be in relation to the amount of CXCR4 receptors present upon the cell surface. From this data, it is clear to see that the peptide AZ3-2 is the least potent of the three CXCR4 antagonists in Jurkat and THP-1 cells, confirming results by Di Maro et al. (2016). A final observation from these migration experiments is that 1 µM of AZ6-2 caused inhibition below the basal level in both Jurkat and THP-1 cells. While this is not a significant reduction, it suggests that AZ6-2 might have off target effects whereby AZ6-2 could be binding to other receptors. However, it was found that AZ6-2 does not bind to the ‘CXCR’ chemokine receptor CXCR3 nor to the ‘CCR’

chemokine receptors CCR1 and CCR5. While this investigation was limited to only three other chemokine receptors, it suggests that AZ6-2 is a highly selective CXCR4-antagonist but highlights the need for more extensive investigation into other chemokine receptors and perhaps even other cell surface receptors. Particularly for THP-1 cells, derived from monocytes, two of the major chemokine receptors they express are CCR1 and CCR2, therefore, investigations into whether AZ6-2 could bind to these receptors would be informative (Parker et al., 2004).

In calcium release assays, it was found that AZ6-2 universally prevented CXCL12 mediated intracellular calcium release from: MCF-7, Jurkat, THP-1 and PC3 cells. AMD3100 only significantly prevented CXCL12 mediated intracellular calcium release in MCF-7 and Jurkat cells. It is possible that AMD3100 was not significant due to the poor calcium release profile of THP-1 and PC3 cells in these experiments (>0.15 and <0.1, respectively) compared to MCF-7 and Jurkat cells (>0.4 and >0.3, respectively) as there is a trend of decreased intracellular calcium release after incubation with AMD3100. This difference in affinity and/or potency of the three compounds may also be related to the kinetics of the CXCR4 antagonists, specifically the speed of the peptide-protein binding, the equilibrium dissociation constant of peptide-protein complex $K_d$ (affinity) and ultimately if the compound is reversible (Berezhkovskiy, 1999). Unfortunately, kinetic experiments were not conducted and future investigations are required using similar methodology to that of Van Hout et al. (2017), where increase concentrations of CXCL12 were used to compete with the compounds to get $K_d$ values. Alternatively, surface plasmon resonance (SPR) could be conducted to determine $k_{on}$ and $k_{off}$ rates.

The origin of AZ6-2 stems from a compound called ‘R’ that was derived via a ligand-based approach using the structure of CXCL12 (Portella et al., 2013). Peptide ‘R’ or peptide ‘2’ as it is named in Di Maro et al. (2016) was then structurally altered to create AZ6-2. While AZ6-2 was determined to reduce the ability of the mAb 12G5 to bind to CXCR4, this was never shown visually. To confirm that AZ6-2 is a CXCL12-mimetic, thus able to compete with 12G5, immunofluorescence assays were conducted (Chen et al., 2014, Pawig et al., 2015, Zhou et al., 2001). As mentioned previously, AMD3100 binds to the same site as CXCL12 and 12G5 and so can be used as a control (Carnec et al., 2005). The results demonstrated that AZ6-2 did bind to CXCR4 and prevent the mAb

12G5 from binding, as expected. However, while it is reported in the literature that once CXCR4 is bound to CXCL12 it becomes internalised, the addition of 10 nM of CXCL12 did not cause the internalisation of the CXCR4 receptor in MCF-7 cells (Van Hout et al., 2017). 10 nM of CXCL12 was used in order to replicate experimental conditions as seen in Hattermann et al. (2014) however, in this case, it is most likely that CXCR4 failed to internalise due to the concentration of CXCL12 being too low. An optimum CXCL12 concentration should therefore be determine to initiate CXCR4 internalization. Alternatively, other more robust assays should be conducted to determine CXCR4 internalization including radioligand binding studies, whole cell ELISA or using the Fluorokine® receptor detection kit from R&D Systems.

The allosteric mAb 4G10 was used to determine the effect of AZ6-2 upon internalisation, where it was found that like AMD3100, AZ6-2 prevents CXCR4 internalisation in MCF-7, THP-1 and Jurkat cells, thus determining that AZ6-2 is not a CXCL12 agonist. Moreover, AMD3100, AZ3-2 and AZ6-2 caused no significant change to the MCF-7 cell area or shape. However, it was found that AMD3100, AZ3-2 and AZ6-2 did supress actin polymerisation in MCF-7 cells. As discussed in Chapter 1, the CXCR4 receptor is associated with a G protein, with most downstream signalling occurring specifically via the $G\alpha_i$ subunit (Ganju et al., 2012, Neptune and Bourne, 1997). When CXCL12 binds CXCR4, the $G\alpha_i$ subunit can activate phosphoinositide 3 kinase (PI3K), that in turn phosphorylates proteins such as the cytoskeletal protein paxillin that enable the reorganizing the actin cytoskeleton of the cell and making changes necessary for cell migration (Wang et al., 2000). The results seen here show that AMD3100, AZ3-2 and AZ6-2 are all able to significantly impede the reorganisation of the actin cytoskeleton, hence the lack of change in cell area and shape implicates the mode of action of these compounds upon preventing CXCL12 directed cellular migration. What is unusual about these results is that the addition of 10 nM of CXCL12 should stimulate the MCF-7 cells to undergo cytoskeletal changes in order to migrate however, this was not seen in these experiments. Again, this may be due to 10 nM of CXCL12 not being a high enough concentration to sufficiently stimulate all the CXCR4 receptors and produce a significant response. Alternatively, as seen in section 4.3.10., MCF-7 cells migrate very slowly and so the one-hour time frame used in these experiments is possibly not a sufficient amount of time for the CXCR4 receptors to stimulate the actin cytoskeletal rearrangements.

Therefore, there would not be enough time to witness any cellular changes stimulated by CXCL12. To get a more accurate picture, these experiments should be repeated again with an optimised concentration of CXCL12.

After optimising a suitable migration assay for adherent cells, it was determined that AZ3-2 and AZ6-2 significantly reduced PC3 and SKMEL28 migratory speeds while AMD3100 did not and only AZ6-2 prevented cell migration. While the results from these assays cannot be directly compared to the chemotaxis assays using the two suspension cell lines, it is clear to see that AZ6-2 was the most potent compound i.e. showing that it may be superior to the already marketed AMD3100 and can be used across many different cancer cell types. An alternative method of analysis, flow cytometry, could be used in place of migration assay to determine $IC_{50}$ values whereby both saturation assay and competition assays could be conducted using 12G5 and/or AMD3100. These values could then be used to determine pA2 values. This would enable direct comparisons between adherent and suspension cell lines and should be conducted in the future.

## 4.5. Conclusions

It can be concluded that AZ6-2 is the most potent CXCR4 antagonist compared to AZ3-2 and AMD3100 and is able to prevent CXCL12 stimulated migration in all CXCR4 positive cell lines tested. Additionally, AZ6-2 is able to significantly reduce intracellular calcium release in THP-1, Jurkat, MCF-7 and PC3 cells while AMD3100 is only effective in MCF-7 and Jurkat cells. AZ6-2 is a CXCL12-mimetic peptide that does not cause CXCR4 receptor internalisation, thus it is not a CXCR4 agonist. AZ6-2 prevents the reorganisation of the actin cytoskeleton, therefore prevents any changes to cell shape and area. Finally, AZ6-2 is a CXCR4 receptor specific peptide and shows great potential as a candidate for future development or for clinical trials.

# Chapter 5: The Development of a Click CXCR4 Antagonist and its Effects on CXCL12 Stimulated Cancer Cell Migration

**Acknowledgements**

I would like to thank Dr M. M. D. Cominetti for designing and synthesising IS1, IS4 and IS7. Additionally, I would like to acknowledge Dr M. M. D. Cominetti for conducting the preparative and analytical HPLC, the MALDI-TOF and NMR analyses for these antagonists.

## 5.1. Introduction

In Chapter 4 we saw the potential of AZ6-2 as a novel CXCR4 antagonist that showed both potency and specificity in a broad range of cancer cell types. However, one shortcoming of this peptide is the disulphide bond, required to stabilize the compound by limiting the unfolding or improper folding of the compound, is liable for reduction when introduced to mammalian cells. This would render the peptide inactive (Metcalfe et al., 2011). Generally, the formation and reduction of disulphide bonds are the result of reversible thiol(SH)/disulphide(SS) exchange reactions in the biological environment (Okumura et al., 2011, Sharma et al., 2016, Yi and Khosla, 2016). Glutathione, a tripeptide synthesised in the cytosol from the precursor amino acids: glutamate, cysteine and glycine (L-γ-glutamyl-L-Cysteinyl-Gly), is one of the most abundant thiol compounds found within cells (Chakravarthi et al., 2006, Okumura et al., 2011). Oxidized glutathione (GSSG) enables the formation of disulphide bonds in proteins while reduced glutathione (GSH) cleaves disulphide bonds, resulting in the formation of the thermodynamically stable conformations of proteins (Okumura et al., 2011). Within the cell, >98% of glutathione exists as GSH with cells containing up to 10 mM concentrations of GSH that are maintained in this form by cytosolic NADPH-dependant reactions catalysed by glutathione reductase (Ballatori et al., 2009, Chakravarthi et al., 2006). Protein disulphide bonds are rarely found in the cytosol due to high concentrations of GSH which reduces non-native disulphide bonds. Opposing this, there are higher levels of disulphide bonds in the lumen of the endoplasmic reticulum due to high concentrations of GSSG (Chakravarthi et al., 2006). While most of GSH remains in the cytoplasm, it can be effluxed out of the cell via glutathione transporters into the extracellular medium to serve as an antioxidant (Bachhawat et al., 2013). This would enable the reduction of AZ6-2 (Figure 5.1). Therefore, to overcome this problem, a maleimide group (2,3-dibromomaleimide) can be used to replace the disulphide bond. Not only would this prevent the reduction of the compound, but also facilitate the introduction of an alkyne group to enable the possibility for our compound to undergo ‘click’ chemistry (Kolb et al., 2001).

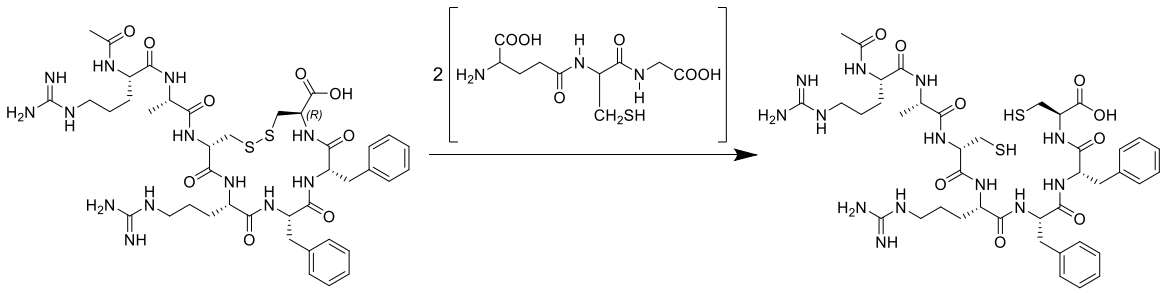

**Figure 5.1: The reduction of AZ6-2 in the presences of glutathione (GSH).**The disulphide bond in AZ6-2 is liable for reduction by GSH, a highly abundant tripeptide in mammalian cells. This would render AZ6-2 inactive.

'Click' reactions are fast, simple to use, easy to purify, versatile and give high product yields. The reaction starting materials and reagents typically use solvents that are easily removed or require a benign solvent such as water. Generally, 'click' chemistry generates minimal byproducts that can be removed by methods such as chromatography, distillation or recrystallization. 'Click' chemistry therefore has several biomedical applications such as tagging of therapeutics with fluorescent probes and loading nanoparticles with drugs for nanoscale drug delivery (Hein et al., 2008).

There are four major 'click' reactions: cycloaddition, nucleophilic ring opening, carbonyl chemistry of the non-aldol type and additions to carbon-carbon multiple bonds (Hein et al., 2008). Of the four reactions, cycloadditions, particularly 1,3-dipolar cycloadditions are the most reliable and easy to use. These reactions exclusively form small linkages that resemble amide linkages creating 1,4-substituted products (Li et al., 2017, Hein et al., 2008). 1,3-dipolar cycloaddition reactions work within a 0-160˚C temperature range, in a variety of solvents including water and work within a pH range from 5 to 12 (Hein et al., 2008, Hong et al., 2010). Unlike antibodies, alkyne and azide groups are very small, highly energetic and have narrow reactivity thus, could be used for long term antagonist experimentation (Li et al., 2010). Additionally, while fluorescent dyes or tags such as biotin could be used instead of 'click' chemistry, these often involve purification and/or multiple wash steps, with excess prelabeled reagent being hard to remove from the tissues and preventing multistep labelling. Thus, click reactions can potentially reduce background fluorescence as well as reduce the need for multiple wash steps (Sivakumar et al., 2004).

For a successful 'click' reaction, a catalyst is required. One of the most common catalysts for 1,3-dipolar cycloaddition reactions is $CuSO_4$. However, this

requires the addition of sodium ascorbate in a 3 to 10-fold excess to reduce $Cu^{II}$ to $Cu^{I}$ salts. This is due to the copper ions catalysing the production of reactive oxygen species (ROS) from oxygen in the air. The advantages of using sodium ascorbate is that it is cheap, can be used in water, is environmentally safe and enables to reaction to occur quickly with near complete reactions occurring within five minutes to an hour at room temperature (Hein et al., 2008, Li et al., 2010).

Specifically, azide-based click reactions are particularly stable and can be introduced into biomolecules without changing the properties of said biomolecule or causing cellular toxicity (Hong et al., 2010). Previously, copper-catalysed azide-alkyne cycloaddition (CuAAC) reactions have been used in fixed cells for successful enzyme inhibitor screening (Gaebler et al., 2016, Salic and Mitchison, 2008, Lallana et al., 2011). Additionally, Li et al. (2017) used the pro-fluorogenic compound 3-azido-7-hydroxycoumarin with $CuSO_4$ as the catalyst in *in situ* experiments with OVCAR5 human ovary cancer cells. This study successfully demonstrated fluorescence suggesting the potential for this method for screening cell-specific inhibitors.

Therefore, three compounds, IS1, IS4 and IS7, were kindly synthesized by Dr M. M. D. Cominetti from Professor Mark Searcey's group at The University of East Anglia. The structural differences between AZ6-2 and IS1 is caused by the addition of a maleimide group (2,3-dibromomaleimide) instead of treating the peptide with iodine to form a disulphide bond (Figure 2.2 and Figure 5.2). The R group in IS1 is hydrogen for initial proof of principle experimentation.

a

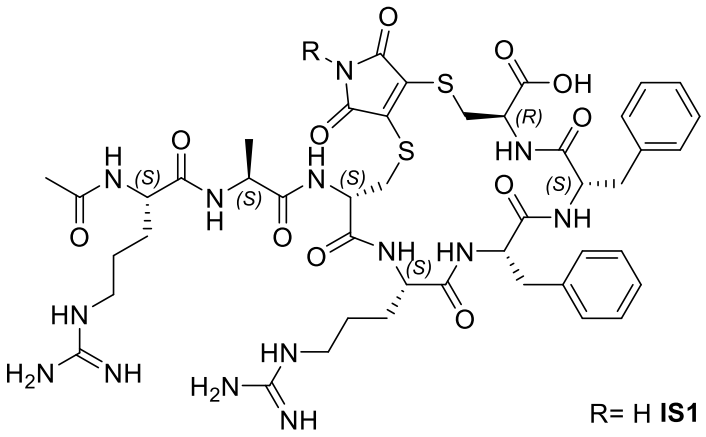


b

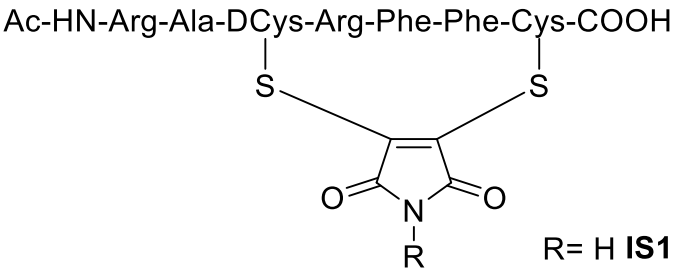


**Figure 5.2: The structure of IS1.** IS1 is a seven amino acid peptide with a molecular weight of 1037.18. **a)** shows the chemical structure and **b)** the amino acid sequence of IS1.

A different maleimide with a propargyl group (N-propargyl-2,3-dibromomaleimide referred to as IS3) was synthesised and used to cyclise the peptide to form IS4 which can be used for *in situ* CuAAC (Figure 2.2 and 5.3). Therefore, the alkyne group can serve as the linker to a number of chemical groups including: biotin, anti-cancer agents, antibodies and nanoparticles.

a

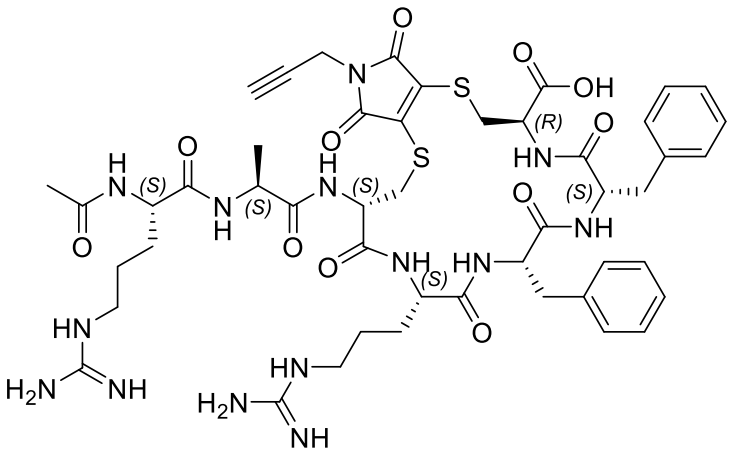

b

Ac-HN-Arg-Ala-DCys-Arg-Phe-Phe-Cys-COOH

**IS4**

**Figure 5.3: The structure of IS4.** IS4 is a seven amino acid peptide with a molecular weight of 1075.23. **a)** shows the chemical structure and **b)** the amino acid sequence of IS4.

In these experiments, the pro-fluorogenic compound, 3-azido-7-hydroxycoumarin, was used to create a CXCR4 specific fluorescence for initial proof-of-principle experimentation (Figure 5.4 and 5.5). The fluorescent coumarin dye was used due to it being small in size, biocompatible and easy to manipulate synthetically with the 3- and 7- substitutions impacting their fluorescent properties (Sivakumar et al., 2004). Specifically, 3-azido-7-hydroxycoumarin is water soluble and removes concerns of residual fluorescence as the unreacted precursors are optically inactive and so wash steps are not required (Li et al., 2010). Several CXCR4-targeting fluorescent probes have been synthesised before. For example, Khan et al. (2007) used an AMD3100 derivative with an incorporated rhodamine fluorophore to enable the production of CXCR4-targeting fluorescent probes. The AMD3100 derivative contained $Zn^{2+}$, $Ni^{2+}$, and $Cu^{2+}$ ions which yielded highly stable metal complexes with increases affinity toward CXCR4. The uncomplexed fluorophore displays no CXCR4-specific binding,

indicating that metal ions are necessary for receptor binding. Several other CXCR4-targeting fluorescent probes have been synthesized by Knight et al. (2011), Hanaoka et al. (2006), Nomura et al. (2008) and Kuil et al. (2011) amongst others. However, while many of these CXCR4-targeting fluorescent probes have proved to be successful, by using click chemistry a compound would not be limited to being a CXCR4-targeting fluorescent probe. Instead, the compound could become a multifunctional tool by replacing the fluorescent dye with a nanoparticle or a chemotherapeutic drug.

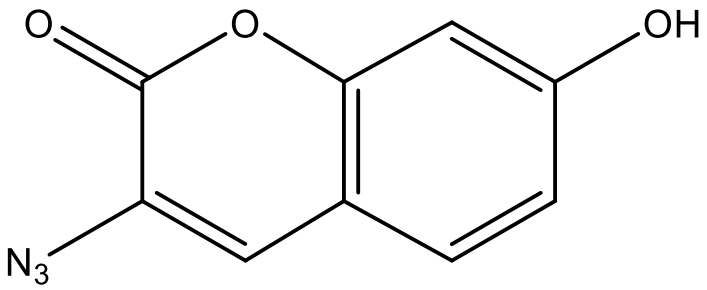


**Figure 5.4: The structure of 3-azido-7-hydroxycoumarin.** 3-azido-7-hydroxycoumarin is a fluorescent ligand that can be clicked to IS4 under a copper-catalysed azide-alkyne cycloaddition (CuAAC).

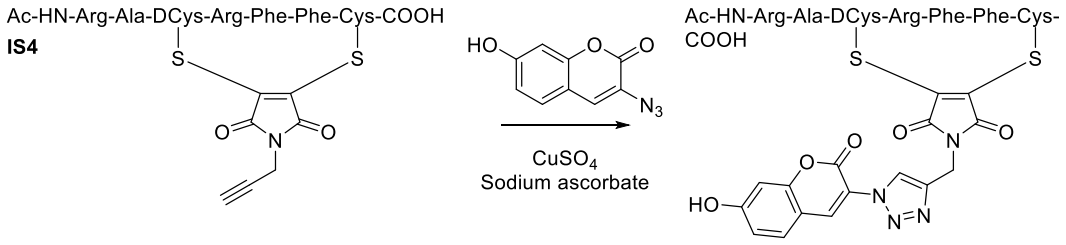


**Figure 5.5: CuAAC using IS4 and 3-azido-7-hydroxycoumarin to create the fluorescent click product, IS7.**

The final CXCR4 compound that was synthesised, IS7, is the click reaction product, i.e. it has already undergone 'click' chemistry and contains the 1,4-triazole amide isostere and is therefore bound to the 3-azido-7-hydroxycoumarin (Figure 5.6). Therefore, IS4 is for *in situ* 'click' chemistry while IS7 has been fully synthesized in the laboratory and needs only to be added to cells.

a

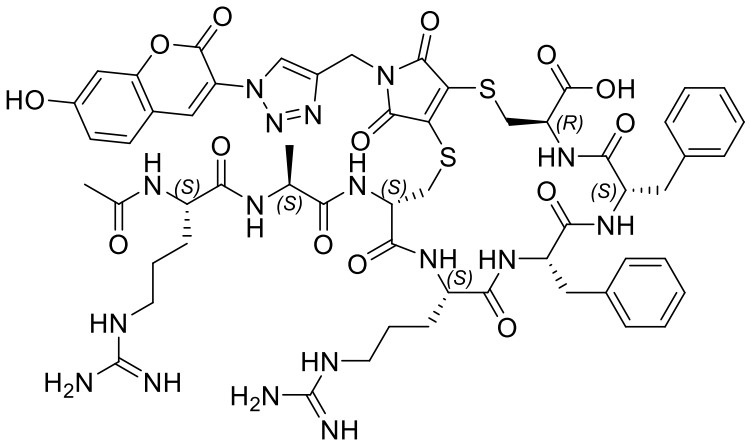

b

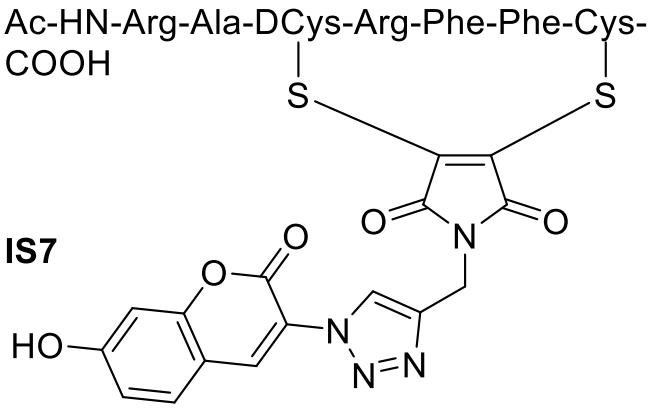


**Figure 5.6: The structure of IS7.** IS7 is a seven amino acid peptide with a molecular weight of 1708.84. **a)** shows the chemical structure of IS7 and **b)** the amino acid sequence**.**

## 5.2. Chapter Aims and Hypotheses

**Hypotheses:** The CXCL12 mimetic cyclic peptides: IS1, IS4 and IS7, will maintain their antagonistic effect against multiple cancer cell line overexpressing CXCR4. Additionally, IS4 will be more stable than AZ6-2. Using CuAAC, IS4 can be clicked to the pro-fluorogenic compound 3-azido-7-hydroxycoumarin to both label CXCR4 and prevent downstream signalling. Finally, IS7 can label CXCR4 and act as a CXCR4 antagonist.

**Aims:** To determine that antibodies are not suitable for use in long incubation experiments. To examine the antagonistic effect of IS1, IS4 and IS7 in CXCL12 directed cancer cell migration and their effects upon intracellular calcium release. Additionally, to confirm that the natural yellow colour of IS4 does not interfere with calcium release readings. To determine the effects of IS4 upon CXCR4 receptor internalisation. To discover if IS4 and IS7 are specific to the CXCR4 receptor only. To determine if IS4 can be used in CuAAC reactions and if it has superior stability over AZ6-2. Finally, to determine if IS7 has duel functionality as a CXCR4 fluorescent marker and as a CXCR4 antagonist. Overall, this will help to identify novel CXCR4 antagonists that have potential applications in competition binding assays and in ‘click’ chemistry for the development of fluorescent probes and/or drug delivery systems.

## 5.3. Results

### 5.3.1. Antibodies cannot be used in place of inhibitors for long incubation experiments

The overarching aim of this Chapter is to develop a CXCR4 antagonist that is suitable for CuAAC reactions and, as a proof of function, to click this antagonist with a fluorescence probe. However, it could be argued that this is already achievable using antibodies that are already on the market such as 12G5 (Bleul et al., 1997, Carlisle et al., 2009, van den Berg et al., 2011). There are even several monoclonal antibodies (mAbs) approved for clinical use in cancer patients including but not limited to: Rituximab, Trastuzumab and Alemtuzumab (Leget and Czuczman, 1998, Blumenthal et al., 2013, Demko et al., 2008). However, for GPCR targeting, there are only two antibodies currently on the market. The first is mogamulizumab (Poteligeo) which targets the CCR4 receptor for the treatment of CCR4-positive adult T-cell leukaemia/lymphoma (Beck and Reichert, 2012). The second is erenumab (Aimovig), a fully human antagonistic antibody against the calcitonin gene-related peptide (CGRP) receptor for

prevention of migraine (Dolgin, 2018). The limited number of currently available therapeutic antibodies that target GPCRs is related to several limitations such as their high production costs, their instability and the large amount of mAb that would have to be injected per patient to achieve the desired clinical efficacy, due to only 20% being able to reach the tumour (Chames et al., 2009, Yang et al., 2014). This limited antibody uptake is related to the large size of the mAbs making it more difficult to penetrate tissues, especially high fluid pressure tumours (Chames et al., 2009). However, much of these problems are related to animal and human models and not to tissue culture environments, with little information being available for *in vitro* use. It has also been suggested that these therapeutic antibodies might also lack specificity due to the usage of short synthetic peptide fragments. These peptide fragments lack important post-translational modifications resulting in the final antibody being promiscuous and binding to multiple antigens sharing similar linear epitopes or alternatively having poor affinity for the GPCR of interest (Bobkov et al., 2019).

Therefore, an initial experiment was conducted using 12G5 (anti-CXCR4) and 11G8 (anti-ACKR3) in the Oris™ Cell Migration assay to determine if mAbs could be used in place of inhibitors for long incubation (24 hours) experiments (Figure 5.7). In these experiments, 11G8 was used as a negative control as 11G8 does not prevent CXCL12 directed migration. Using this assay, there was a trend suggesting that 12G5 actually increased CXCL12 directed migration in PC3 cells. The cause of this result is most likely related to the lower affinity of 12G5 for CXCR4 compared to CXCL12, i.e. it is likely that 12G5 will have initially bound to CXCR4 however, over the 24-hour period it will have been competed off by CXCL12. Furthermore, comparison between Figure 5.3 and Figure 4.50, where AZ6-2 was used in the Oris™ Cell Migration assay, demonstrates that AZ6-2 successfully prevented CXCL12 directed migration over the 24-hour period where 12G5 did not. Therefore, mAbs such as 12G5 are unsuitable for use in experiments where long incubation periods are required, demonstrating a gap in the market for click CXCR4 antagonists.

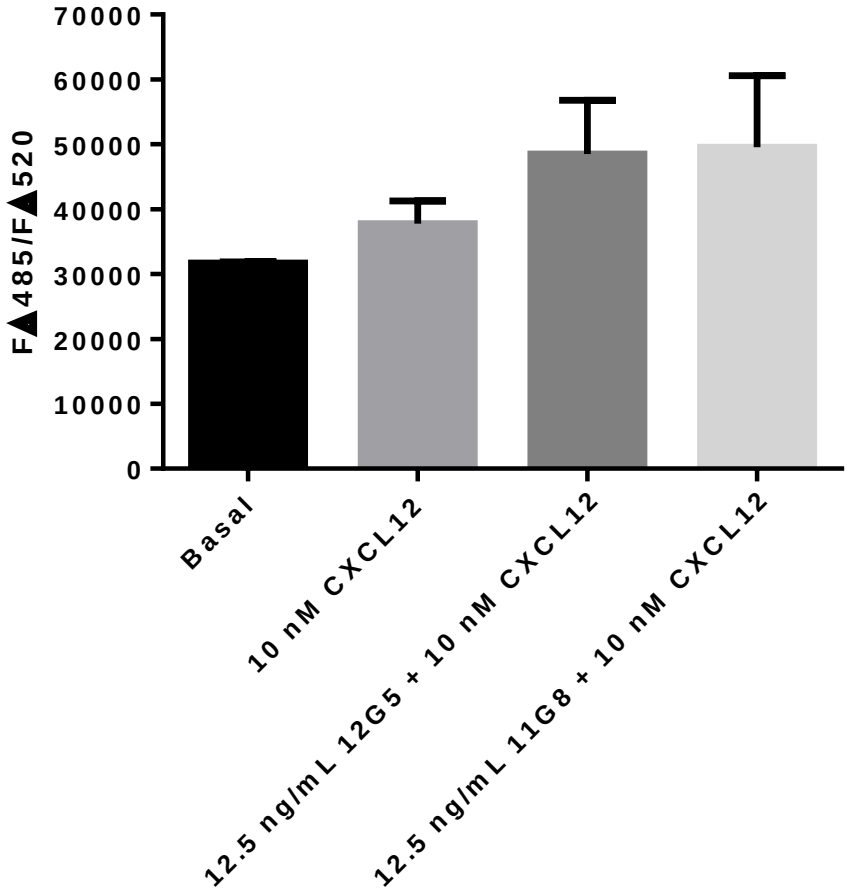


**Figure 5.7: 12G5 does not reduce CXCL12 directed migration in PC3 cells using ORIS™ Migration assays.** PC3 cell were seeded and incubated for 24 hours before the addition of 12.5 ng/mL 12G5 or 11G8 mAbs and 10 nM CXCL12 then incubated for another hour 24 hours before analysis using calcein 485/520 nm. Data represents the mean ± SEM of 3 independent experiments. One-Way ANOVA with post hoc Dunnett's multiple comparison, data not significant.

### 5.3.2. CXCL12 directed migration in Jurkat and THP-1 cells is inhibited by IS1

After it was confirmed that there was a potential application for a 'click' CXCR4 antagonist, the structure of the original peptide, AZ6-2, was altered to synthesise IS1 as previously discussed. To determine if the structural changes made to IS1 changed its affinity for CXCR4, chemotaxis assays were conducted in both Jurkat and THP-1 cells using a 10-fold dose range of IS1. Using both the raw data and the percentage corrected data it was determined that IS1 significantly inhibited CXCL12 directed migration in the Jurkat cell line at a concentration of 1000 nM (Figure 5.8 and 5.9).

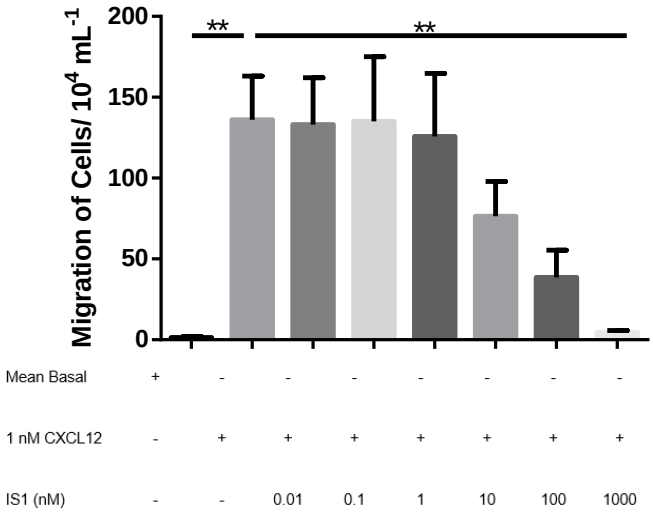


**Figure 5.8: IS1 significantly prevents CXCL12 directed migration in Jurkat cells using chemotaxis assays.** The migration of Jurkat cells was stimulated by 1 nM of CXCL12 in the presence and absence of IS1 (0.01-1000 nM) for 4 hours. Data represents the mean ± SEM of 4 independent experiments. One-Way ANOVA with post hoc Dunnett's multiple comparison, ** = p≤ 0.01 .

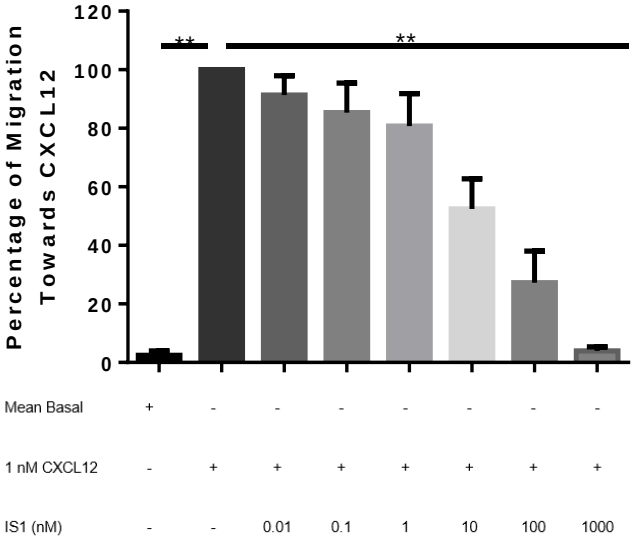


**Figure 5.9: 1000 nM of IS1 prevents CXCL12 directed migration in Jurkat cells using percentage corrected data from chemotaxis assays.** Normalization of data from Figure 5.8 showing the migration of Jurkat cells stimulated by 1 nM of CXCL12 in the presence and absence of IS1 (0.01-1000 nM) for 4 hours. Data represents the mean ± SEM of 4 independent experiments. Data normalised to CXCL12 and Kruskal-Wallis non-parametric test with post hoc Dunn's multiple comparison test conducted, ** = p≤ 0.01.

A dose response curve showed an $IC_{50}$ of 68.45 nM ± 59.24 SEM (Figure 5.10).

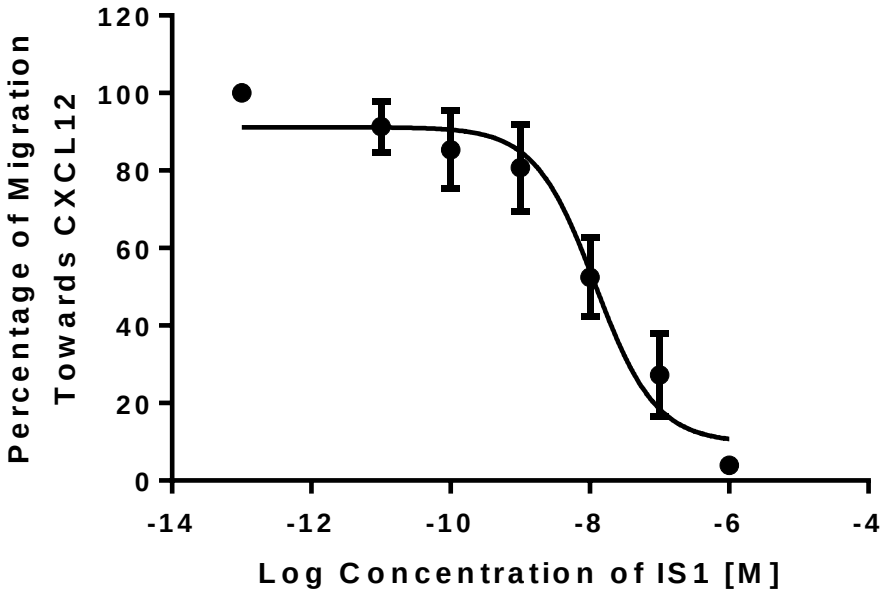


**Figure 5.10: Dose response curve of the migration of Jurkat cells when treated with a dose range of IS1 and stimulated by 1 nM of CXCL12.** An $IC_{50}$ of 68.45 nM ± 59.24 nM SEM was calculated from data from Figure 5.9. Data represents the mean ± SEM of 4 independent experiments. Log (inhibitor) vs. response (three parameters).

When these experiments were repeated in THP-1 cells, the raw data suggested that IS1 did not significantly inhibit CXCL12 directed migration however there was a trend showing inhibition at 1000 nM and 100 nM (Figure 5.11).

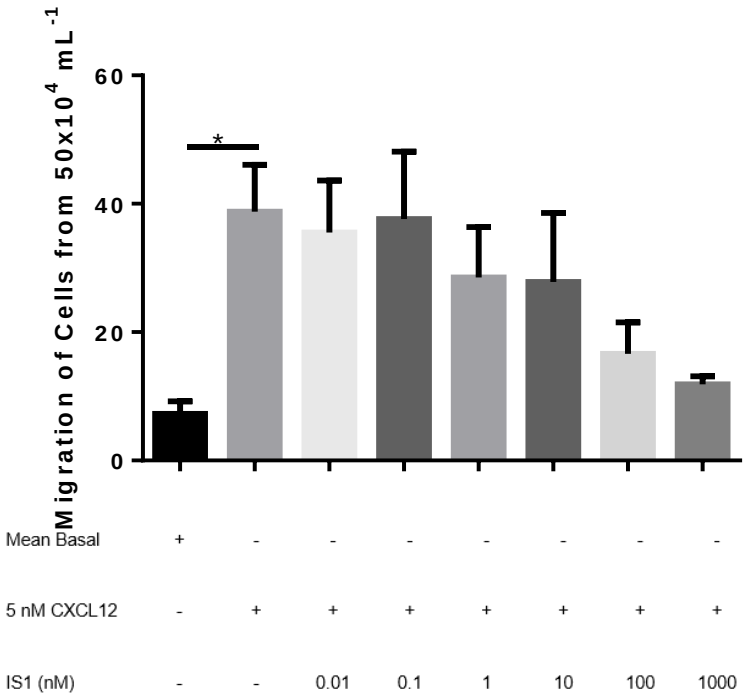


**Figure 5.11: IS1 shows a trend that it prevents CXCL12 directed migration in THP-1 cells using chemotaxis assays.** The migration of THP-1 cells was stimulated by 5 nM of CXCL12 in the presence and absence of IS1 (0.01-1000 nM) for 4 hours. Data represents the mean ± SEM of 4 independent experiments. One-Way ANOVA with post hoc Dunnett's multiple comparison, * = p≤ 0.05.

However, when this data was percentage corrected, IS1 was found to have significant inhibitory effects at concentrations of 100-1000 nM (Figure 5.12).

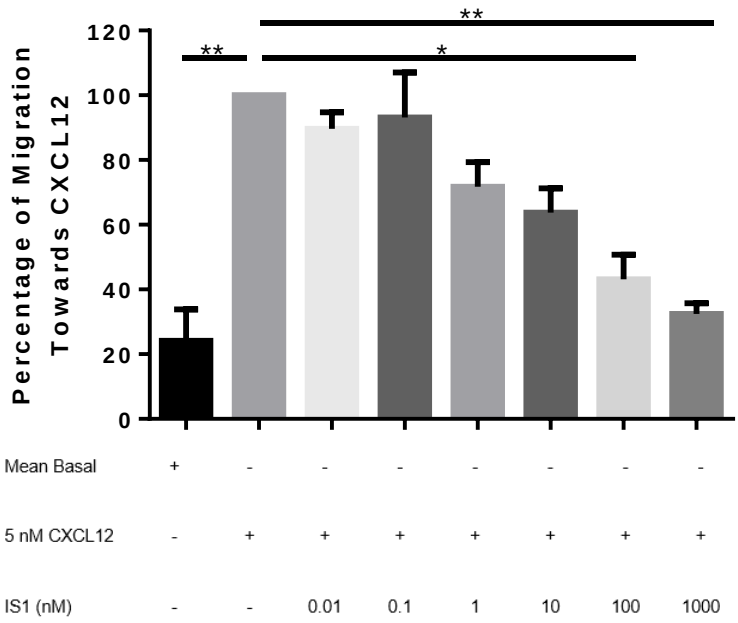


**Figure 5.12: 100-1000 nM of IS1 prevents CXCL12 directed migration in THP-1 cells using percentage corrected data from chemotaxis assays.** Normalization of data from Figure 5.11 showing the migration of THP-1 cells stimulated by 5 nM of CXCL12 in the presence and absence of IS1 (0.01-1000 nM) for 4 hours. Data represents the mean ± SEM of 4 independent experiments. Data normalised to CXCL12 and Kruskal-Wallis non-parametric test with post hoc Dunn's multiple comparison test conducted, * = p≤ 0.05 and ** = p≤ 0.01.

Dose response curves were used to calculate an $IC_{50}$ value of 19.19 nM ± 17.82 SEM (Figure 5.13). This reduced migration in the Jurkat and THP-1 cells lines is not a consequence of cellular toxicity caused by IS1 as demonstrated by MTS assays (Appendix A18 and A19). IS1 was also not toxic in MCF-7 or PC3 cells (Appendix A20 and A21).

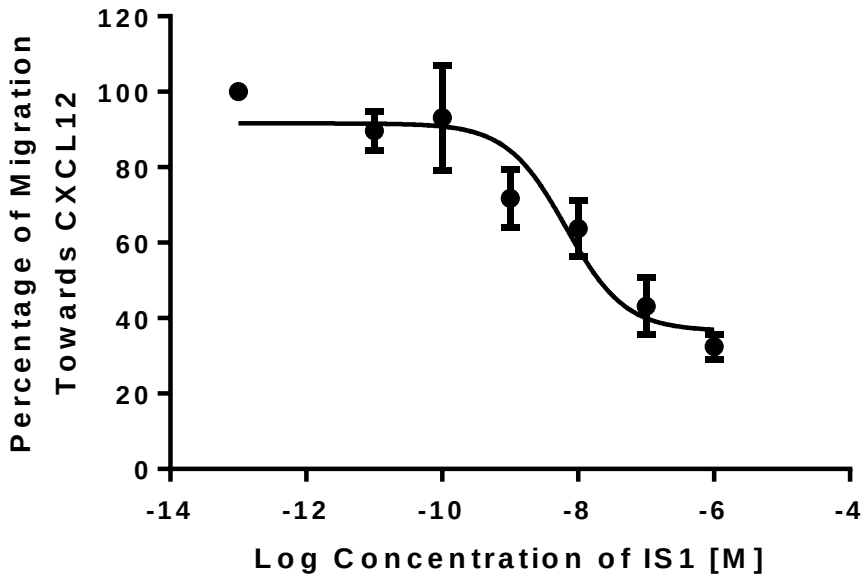


**Figure 5.13: Dose response curve of the migration of THP-1 cells when treated with a dose range of IS1 and stimulated by 5 nM of CXCL12.** An $IC_{50}$ of 19.19 nM ± 17.82 SEM was calculated from data from Figure 5.12. Data represents the mean ± SEM of 4 independent experiments. Log (inhibitor) vs. response (three parameters).

### 5.3.3. CXCL12 directed migration in Jurkat and THP-1 cells is inhibited by IS4

Once it was confirmed that the structural changes made to IS1 did not cause loss of function, IS4 (the fully functional click compound) was then used in chemotaxis assays to determine if IS4 is still as potent as the previous compound, AZ6-2. Using the raw data, IS4 significantly inhibited CXCL12 directed migration in the Jurkat cell line at concentrations of 100-1000 nM (Figure 5.14).

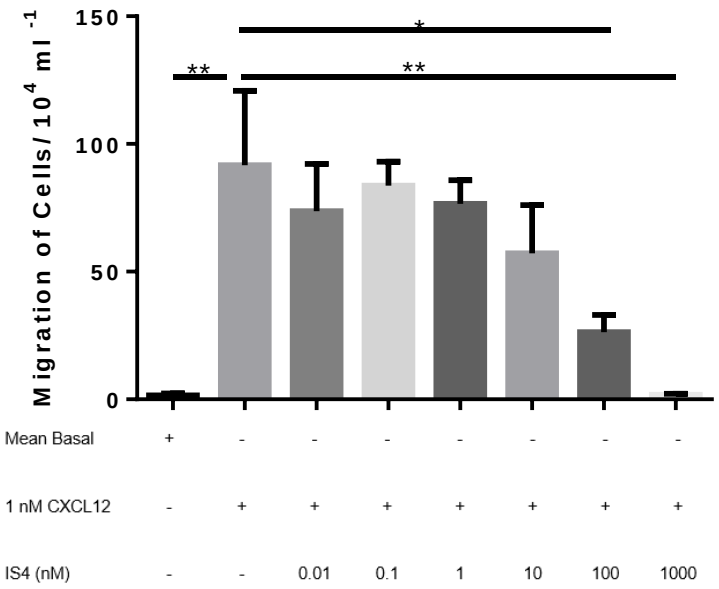


**Figure 5.14: 100-1000 nM of IS4 significantly prevents CXCL12 directed migration in Jurkat cells using chemotaxis assays.** The migration of Jurkat cells was stimulated by 1 nM of CXCL12 in the presence and absence of IS4 (0.01-1000 nM) for 4 hours. Data represents the mean ± SEM of 3 independent experiments. One-Way ANOVA with post hoc Dunnett's multiple comparison, * = p≤ 0.05 and ** = p≤ 0.01.

This data was percentage corrected and a dose response curve determined an $IC_{50}$ of 31.51 nM ± 23.36 nM SEM (Figure 5.15 and 5.16). This reduced migration is not a consequence of cellular toxicity caused by IS4 in the Jurkat cell line as demonstrated by MTS assay (Appendix A22).

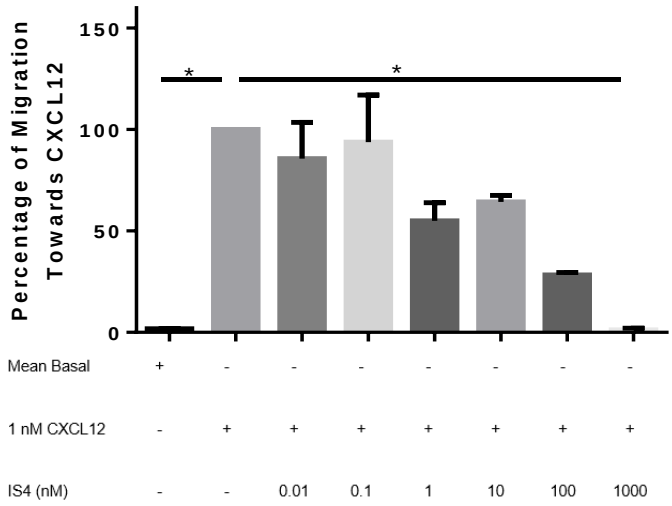


**Figure 5.15: 1000 nM of IS4 prevents CXCL12 directed migration in Jurkat cells using percentage corrected data from chemotaxis assays.** Normalization of data from Figure 5.14 showing the migration of Jurkat cells stimulated by 1 nM of CXCL12 in the presence and absence of IS4 (0.01-1000 nM) for 4 hours. Data represents the mean ± SEM of 3 independent experiments. Data normalised to CXCL12 and Kruskal-Wallis non-parametric test with post hoc Dunn's multiple comparison test conducted, * = p≤ 0.05.

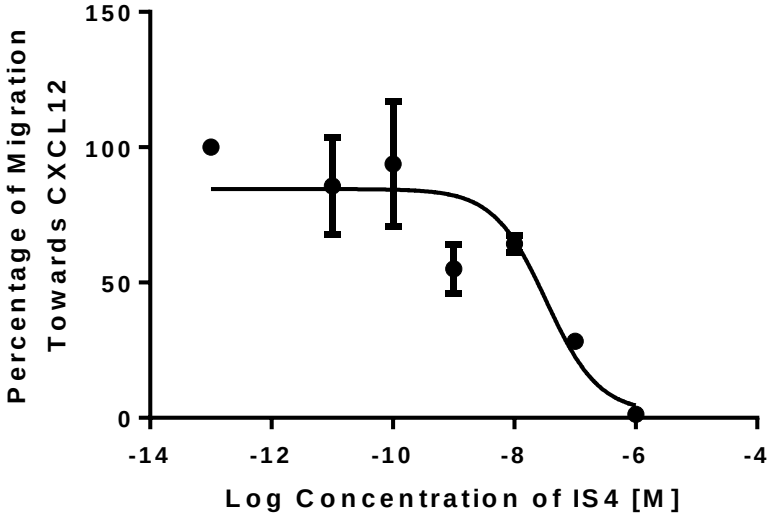


**Figure 5.16: Dose response curve of the migration of Jurkat cells when treated with a dose range of IS4 and stimulated by 1 nM of CXCL12.** An $IC_{50}$ of 31.51 nM ± 23.36 nM SEM was calculated from data from Figure 5.15. Data represents the mean ± SEM of 3 independent experiments. Log (inhibitor) vs. response (three parameters).

Raw data from the THP-1 cell line, indicated that IS4 did not significantly inhibit CXCL12 directed migration however there was a trend showing inhibition at 1000 nM to 1 nM (Figure 5.17).

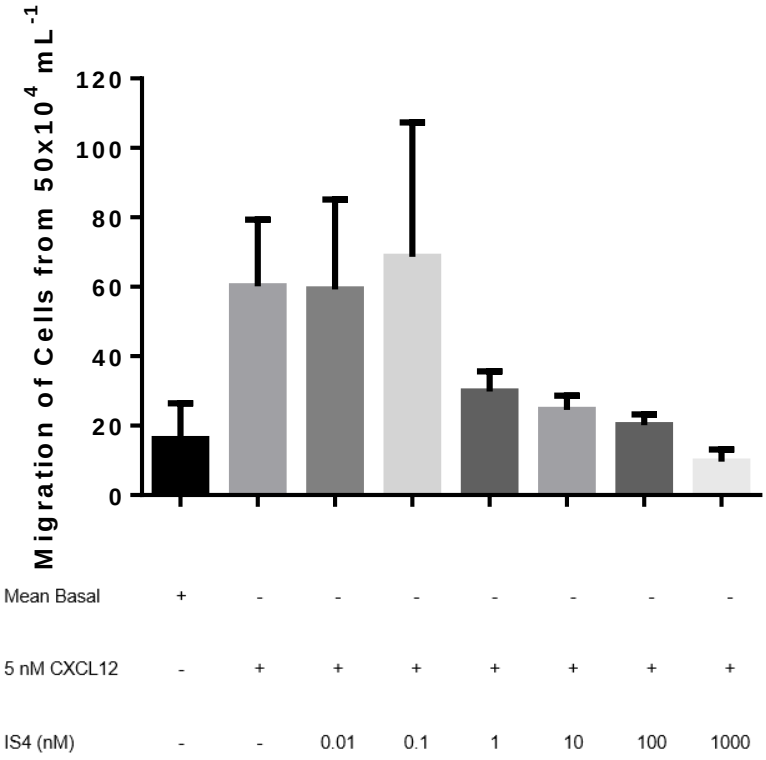


**Figure 5.17: IS4 shows a trend that it prevents CXCL12 directed migration in THP-1 cells using chemotaxis assays.** The migration of THP-1 cells was stimulated by 5 nM of CXCL12 in the presence and absence of IS4 (0.01-1000 nM) for 4 hours. Data represents the mean ± SEM of 4 independent experiments. One-Way ANOVA with post hoc Dunnett's multiple comparison, data not significant.

However, when this data was percentage corrected, IS4 was found to have significant inhibitory effects at a concentration of 1000 nM (Figure 5.18).

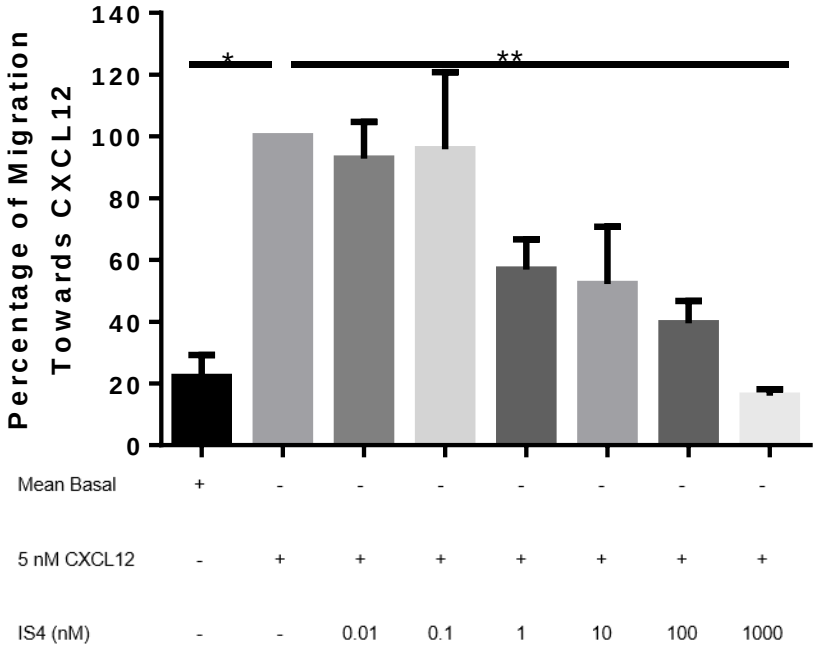


**Figure 5.18: 1000 nM of IS4 prevents CXCL12 directed migration in THP-1 cells using percentage corrected data from chemotaxis assays.** Normalization of data from Figure 5.17 showing the migration of THP-1 cells stimulated by 5 nM of CXCL12 in the presence and absence of IS4 (0.01-1000 nM) for 4 hours. Data represents the mean ± SEM of 4 independent experiments. Data normalised to CXCL12 and Kruskal-Wallis non-parametric test with post hoc Dunn's multiple comparison test conducted, * = p≤ 0.05, ** = p≤ 0.01.

Again, dose response curves were created to calculate an $IC_{50}$ value of 33.18 nM ± 32.67 nM SEM (Figure 5.19). The observed reduction in migration of the THP-1 cells line is not a consequence of cellular toxicity caused by IS4 as demonstrated by MTS assays (Appendix A23). All $IC_{50}$ values are presented in Table 5.1.

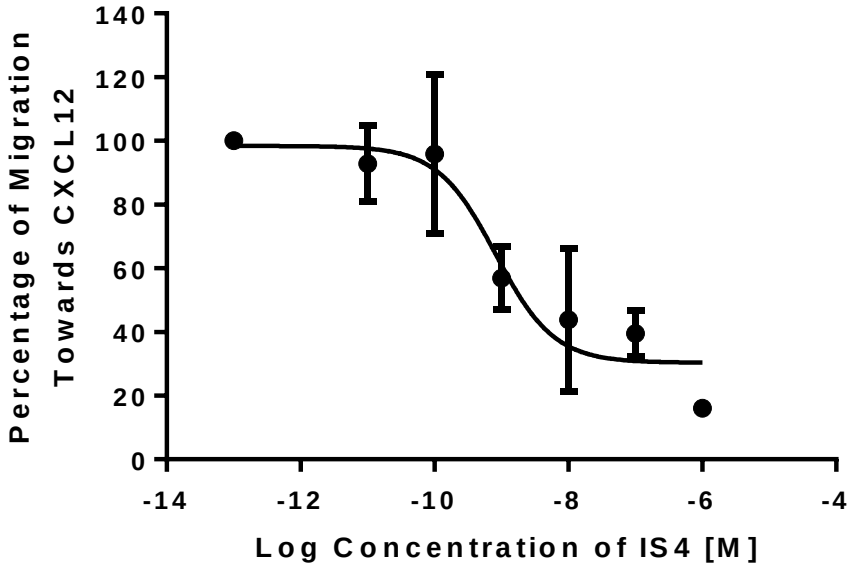


**Figure 5.19: Dose response curve of the migration of THP-1 cells when treated with a dose range of IS4 and stimulated by 5 nM of CXCL12.** An $IC_{50}$ of 33.18 nM ± 23.87 nM SEM was calculated from data from Figure 5.18. Data represents the mean ± SEM of 4 independent experiments. Log (inhibitor) vs. response (three parameters).

**Table 5.1: Summary of IC50 values of AMD3100, AZ3-2, AZ6-2, IS1 and IS4 in both Jurkat and THP-1 cells. Data represents the mean ± SEM of at least 3 independent experiments.**

| Peptide | Cell Line | |
|---|---|---|
| | Jurkat | THP-1 |
| **AMD3100** | 11.50 nM ± 4.39 | 59.47 nM ± 57.33 |
| **AZ3-2** | 259.8 nM ± 230.7 | 1212 µM ± 2424 |
| **AZ6-2** | 0.28 nM ± 0.18 | 0.56 nM ± 0.19 |
| **IS1** | 68.45 nM ± 59.24 | 19.19 nM ± 17.82 |
| **IS4** | 31.51 nM ± 23.36 | 33.18 nM ± 23.87 |

### 5.3.4. IS4 reduces intracellular $Ca^{2+}$ release from MCF-7, PC3, Jurkat and THP-1

As before, calcium release assays were undertaken. Results showed that incubation with 1 µM of IS4 significantly reduced the release of $Ca^{2+}$ in MCF-7, Jurkat, THP-1 and PC3 cells (Figure 5.20). This reduced release of intracellular $Ca^{2+}$ from MCF-7 and PC3 cells is not a consequence of cellular toxicity caused by IS4 as demonstrated by MTS assay (Appendix A24 and A25).

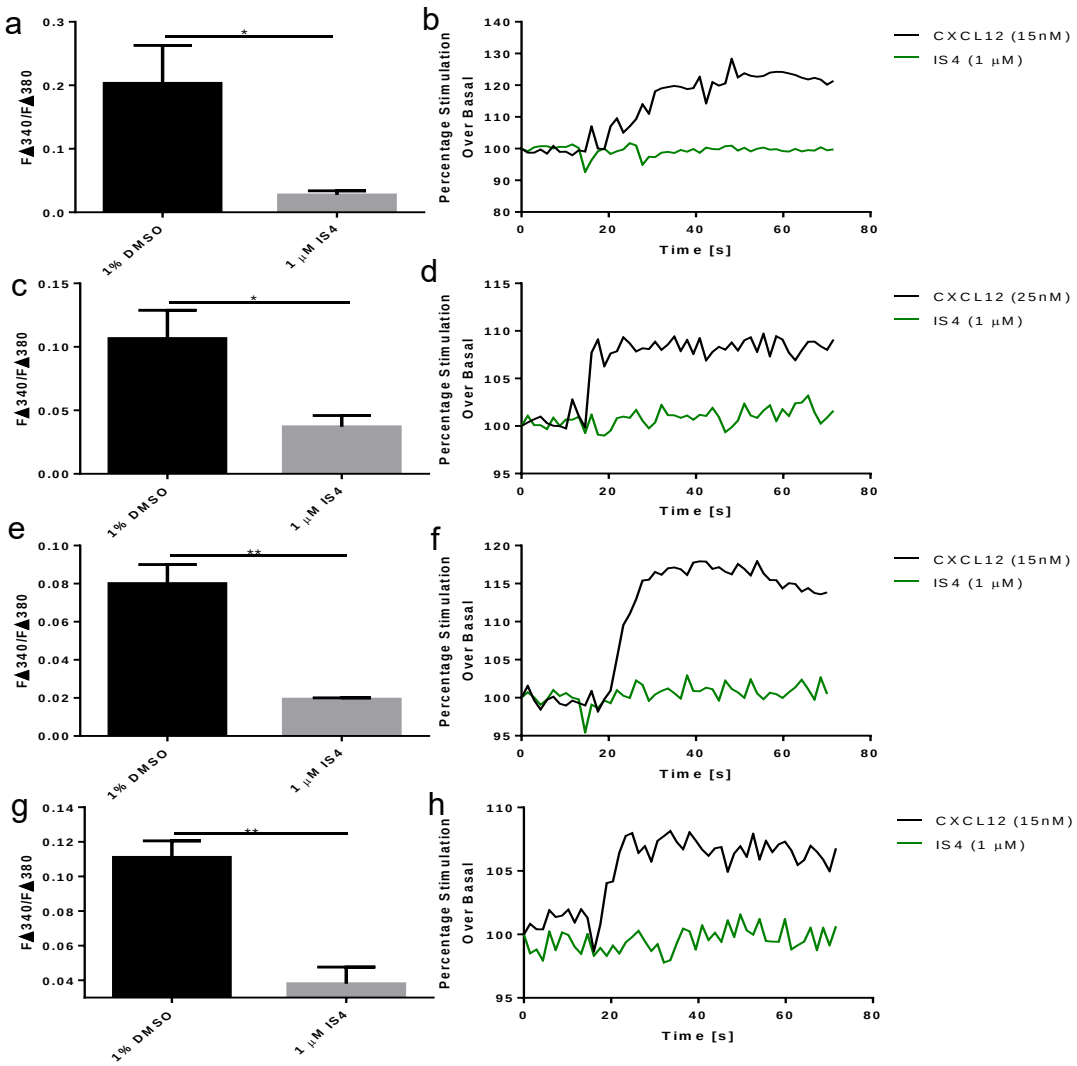


**Figure 5.20: IS4 significantly reduces the release of intracellular $Ca^{2+}$ from MCF-7, Jurkat, THP-1 and PC3 cells.** Cells were incubated for 30 minutes with antagonist or vehicle control and the calcium indicator Fura-2 AM. **a)** MCF-7 cells treated with 1 μM IS4 then stimulated with 15 nM CXCL12. **b)** Representative intracellular calcium release traces of MCF-7 cells. **c)** Jurkat cells treated with 1 μM IS4 then stimulated with 25 nM CXCL12. **d)** Representative intracellular calcium release traces of Jurkat cells. **e)** THP-1 cells treated with 1 μM IS4 then stimulated with 15 nM CXCL12. **f)** Representative intracellular calcium release traces of THP-1 cells. **g)** PC3 cells treated with 1 μM IS4 then stimulated with 15 nM CXCL12. **h)** Representative intracellular calcium release traces of PC3 cells. Data is expressed as a change in fluorescence ratio (340nm/380nm) where the basal fluorescence prior to the addition of CXCL12 is subtracted from peak fluorescence following addition of CXCL12. Chemokine injected after 10 seconds. Data represents the mean ± SEM of 3-5 independent experiments. One-Way ANOVA with post hoc Dunnett's multiple comparison, * = p≤ 0.05 and ** = p≤ 0.01.

### 5.3.5. IS4 interferes with fluorescence readings taken during calcium release assays

One observable difference between AZ6-2 and IS4 is the colour of the compounds with AZ6-2 being colourless while IS4 is yellow both as a powder and when dissolved in DMSO. Therefore, there were concerns that IS4 was interfering with the fluorescence output of the calcium release assay. To determine this, cells were prepared for calcium release assay as normal. However, during the assay, the readings were interrupted and Triton X-100 was injected onto cells. Triton X-100 is commonly used to permeabilize cell membranes, thus causing non-specific release of calcium (Jamur and Oliver, 2010). Following this, ethylenediaminetetraacetic acid (EDTA), a calcium sequestering agent was added, which depletes the levels of all calcium (Motekaitis et al., 1982). This will enable the comparison of cells incubated with and without 1 µM IS4 to determine if the colour of IS4 is effecting the fluorescence reading, as the addition of Triton X-100 should cause the same level of calcium to be released from both treated and untreated cells. THP-1 cells incubated with only the solvent, DMSO, had an average fluorescent readout of 0.67 ± 0.12 FΔ340/FΔ380 while cells incubated with 1 µM IS4 had an average fluorescent readout of 0.27 ± 0.06 FΔ340/FΔ380 (Figure 5.21). This confirmed that the colour of IS4 significantly interferes with the calcium release fluorescence readings. However, while the colour is causing a depletion in fluorescence by >50%, results in Figure 5.20 demonstrate a ~10-fold decrease in fluorescence. Therefore, while the results are compromised, IS4 can be confirmed to be causing a further decrease in calcium release. This highlights that calcium release assays are not the best method to assess the function of coloured compounds such as IS4 and alternative methods are required.

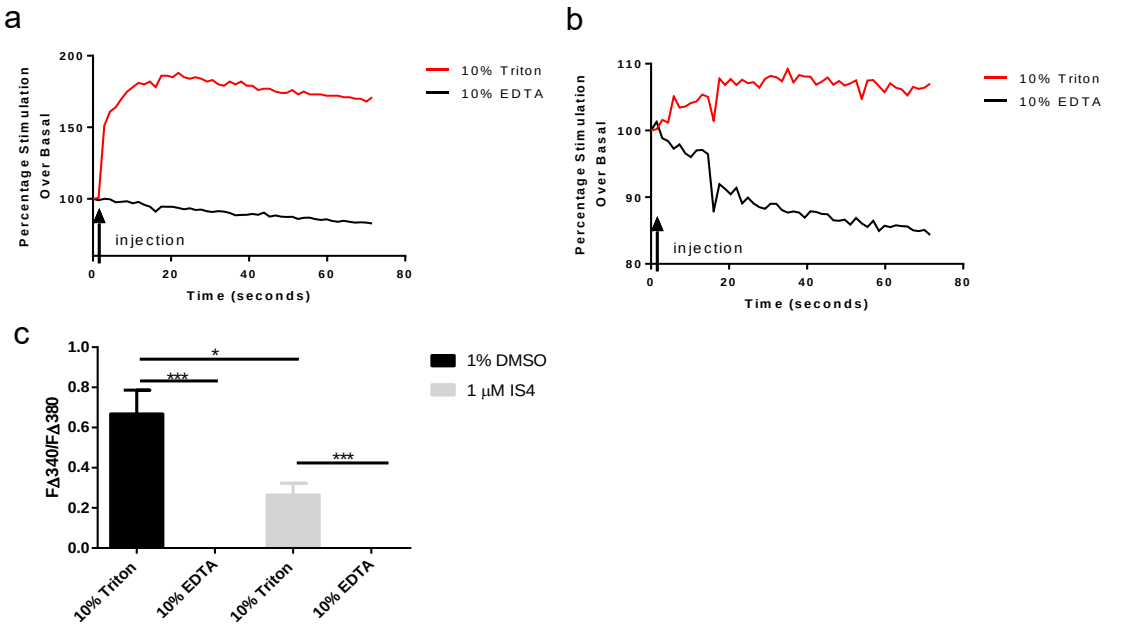


**Figure 5.21: IS4 significantly interferes with the fluorescent readings taken during calcium release assays.** Cells were incubated for 30 minutes with antagonist or vehicle control and the calcium indicator Fura-2 AM. **a)** Representative intracellular calcium release traces of THP-1 cells injected with 10% Triton X-100 and 10% EDTA. **b)** Representative intracellular calcium release traces of THP-1 cells treated with 1 μM IS4 and injected with 10% Triton X-100 and 10% EDTA. **c)** Basal THP-1 cells and THP-1 cells treated with 1 μM IS4 and injected with 10% Triton X-100 and 10% EDTA. Data is expressed as a change in fluorescence ratio (340nm/380nm) where the basal fluorescence prior to the addition of Triton X-100 or EDTA is subtracted from peak fluorescence following addition of Triton X-100 or EDTA. Data represents the mean ± SEM of 3 independent experiments. One-Way ANOVA with post hoc Dunnett's multiple comparison, * = p≤ 0.05 and *** = p≤ 0.001.

### 5.3.6. IS4 does not cause the internalisation of the CXCR4 receptor in MCF-7, Jurkat or THP-1 cells at 37˚C

Again, to determine if the structural changes made to IS4 have affected the properties of this compound, an investigation was conducted to determine if IS4 stimulated receptor internalisation. It was found that 1 μM of IS4 did not trigger CXCR4 internalisation at either 4˚C or 37˚C in any cell line (Figure 5.22-5.27).

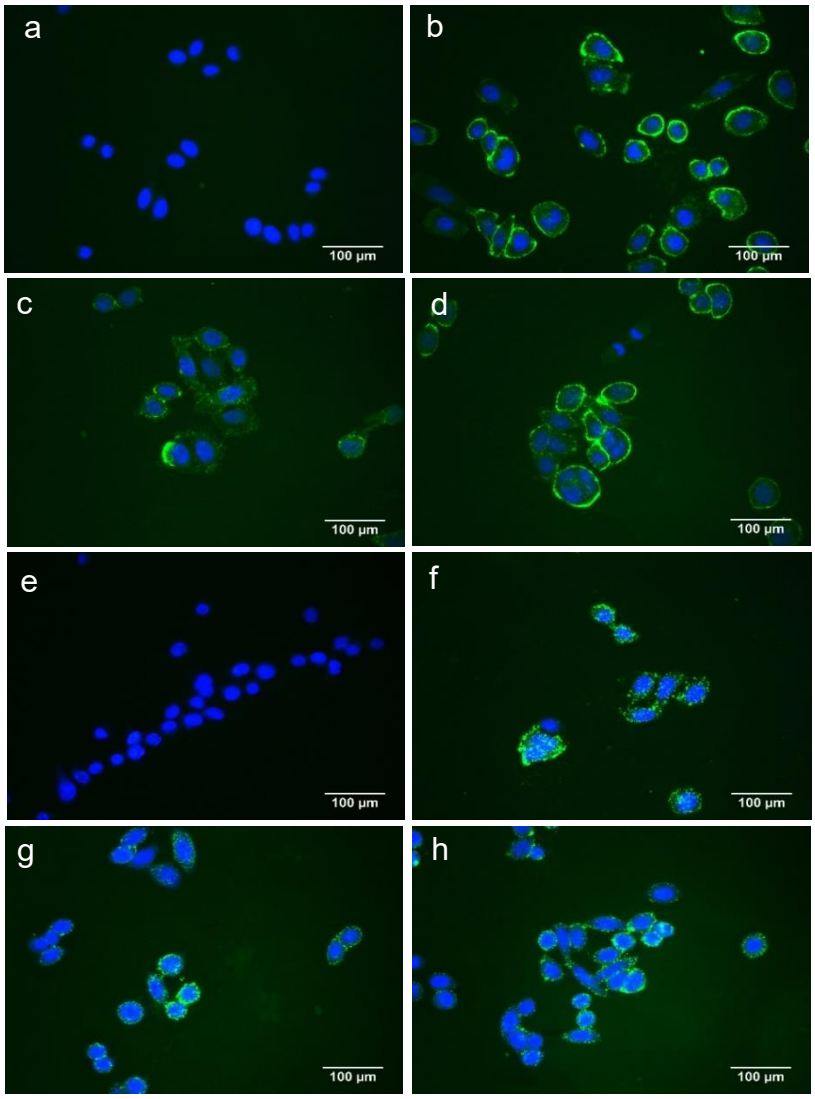


**Figure 5.22: Incubation with IS4 at 4˚C and 37˚C does not cause internalisation of the CXCR4 receptor in MCF-7 cells. a)** Negative control incubated at 4˚C, treated with secondary anti-mouse Alexa Fluor® 488 antibody (green), DAPI (blue) and fixed with 4% paraformaldehyde before imaging. **b)** Positive control incubated at 4˚C, whereby CXCR4 was visualised using mouse 4G10 primary mAb, secondary anti-mouse Alexa Fluor® 488 antibody (green), DAPI (blue) and fixed with 4% paraformaldehyde before imaging. **c)** MCF-7 cells stimulated with 10 nM of CXCL12 at 4˚C for 1 hour before visualisation as positive control. **d)** MCF-7 cells treated with 1 µM IS4 at 4˚C for 1 hour before visualisation as positive control. **e)** Negative control as above, incubated at 37˚C. **f)** Positive control as above, incubated at 37˚C. g**)** MCF-7 cells stimulated with 10 nM of CXCL12 at 37˚C for 1 hour before visualisation as positive control. **h)** MCF-7 cells treated with 1 µM IS4 at 37˚C for 1 hour before visualisation as positive control. Data shows representative cells from three independent experiments with similar findings. Acquired with Leica imaging suite with 40x objective, 22x overall magnification.

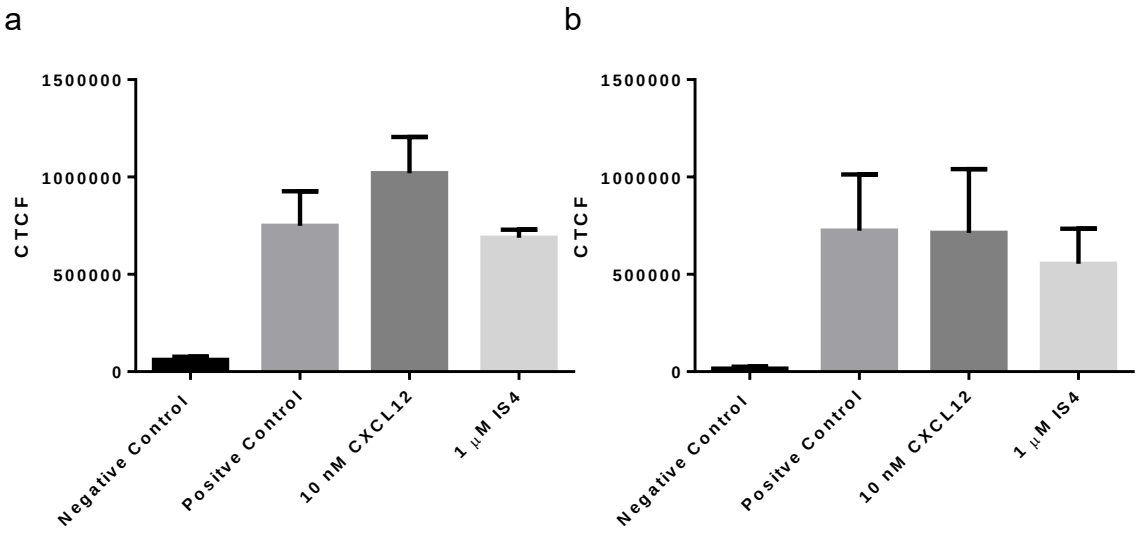


**Figure 5.23: Incubation with IS4 at 4˚C and 37˚C causes no significant change in the fluorescent intensity of CXCR4 receptor expression in MCF-7 cells. a)** Corrected Total Cell Fluorescence (CTCF) of MCF-7 cells from Figure 5.22 stimulated with 10 nM CXCL12 or treated with 1 µM IS4 at 4˚C for 1 hour. **b)** CTCF of MCF-7 cells from Figure 5.22 stimulated with 10 nM CXCL12 or treated with 1 µM IS4 at 37˚C for 1 hour. CTCF = Integrated Density – (Area of selected cell x Mean fluorescence of background readings). Data represents the mean ± SEM of 3 independent experiments. One-Way ANOVA with post hoc Dunnett's multiple comparison, data was not significant.

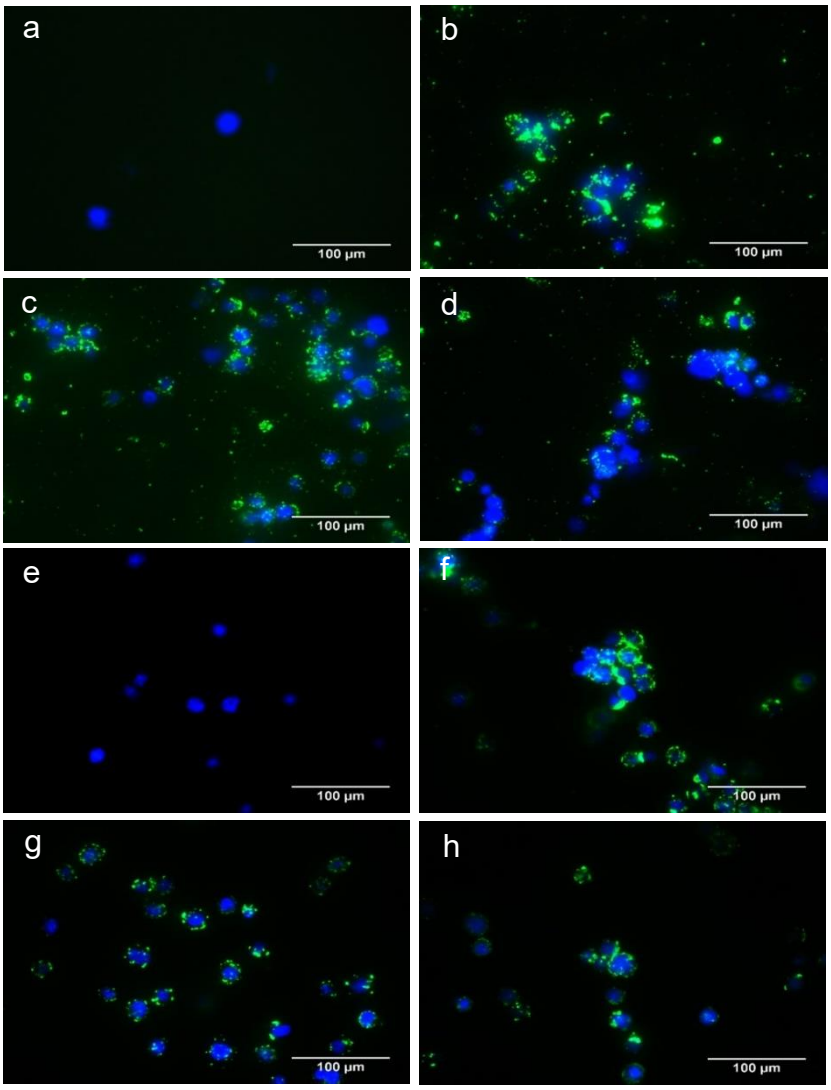


**Figure 5.24: Incubation with IS4 at 4˚C and 37˚C does not cause internalisation of the CXCR4 receptor in Jurkat cells. a)** Negative control incubated at 4˚C, treated with secondary anti-mouse Alexa Fluor® 488 antibody (green), DAPI (blue) and fixed with 4% paraformaldehyde before imaging. **b)** Positive control incubated at 4˚C, whereby CXCR4 was visualised using mouse 4G10 primary mAb, secondary anti-mouse Alexa Fluor® 488 antibody (green), DAPI (blue) and fixed with 4% paraformaldehyde before imaging. **c)** Jurkat cells stimulated with 10 nM of CXCL12 at 4˚C for 1 hour before visualisation as positive control. **d)** Jurkat cells treated with 1 µM IS4 at 4˚C for 1 hour before visualisation as positive control. **e)** Negative control as above, incubated at 37˚C. **f)** Positive control as above, incubated at 37˚C. g**)** Jurkat cells stimulated with 10 nM of CXCL12 at 37˚C for 1 hour before visualisation as positive control. **h)** Jurkat cells treated with 1 µM IS4 at 37˚C for 1 hour before visualisation as positive control. Data shows representative cells from three independent experiments with similar findings. Acquired with Leica imaging suite with 63x objective, 35x overall magnification.

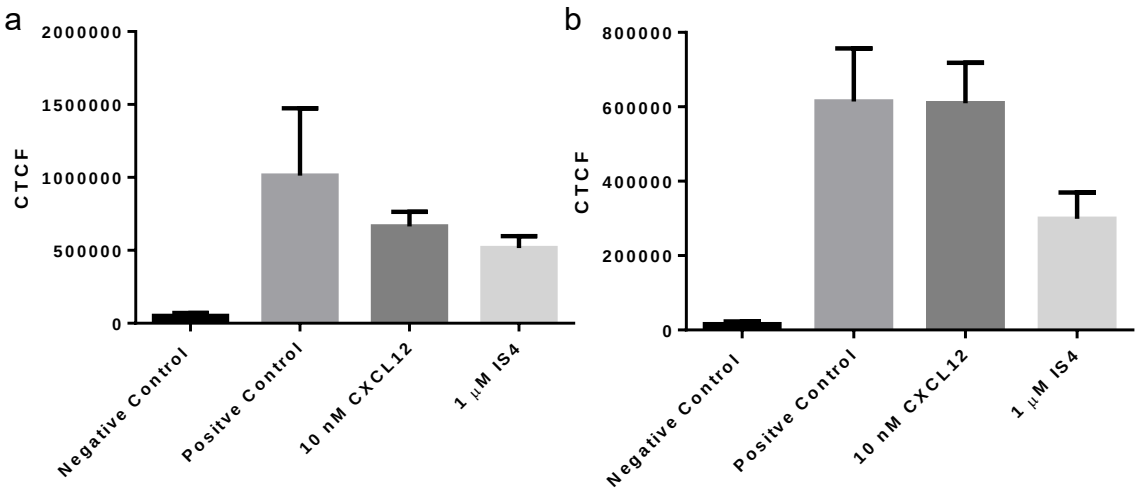


**Figure 5.25: Incubation with IS4 at 4˚C and 37˚C causes no significant change in the fluorescent intensity of CXCR4 receptor expression in Jurkat cells. a)** Corrected Total Cell Fluorescence (CTCF) of Jurkat cells from Figure 5.24 stimulated with 10 nM CXCL12 or treated with 1 μM IS4 at 4˚C for 1 hour. **b)** CTCF of Jurkat cells from Figure 5.24 stimulated with 10 nM CXCL12 or treated with 1 μM IS4 at 37˚C for 1 hour. CTCF = Integrated Density – (Area of selected cell x Mean fluorescence of background readings). Data represents the mean ± SEM of 3 independent experiments. One-Way ANOVA with post hoc Dunnett's multiple comparison, data was not significant.

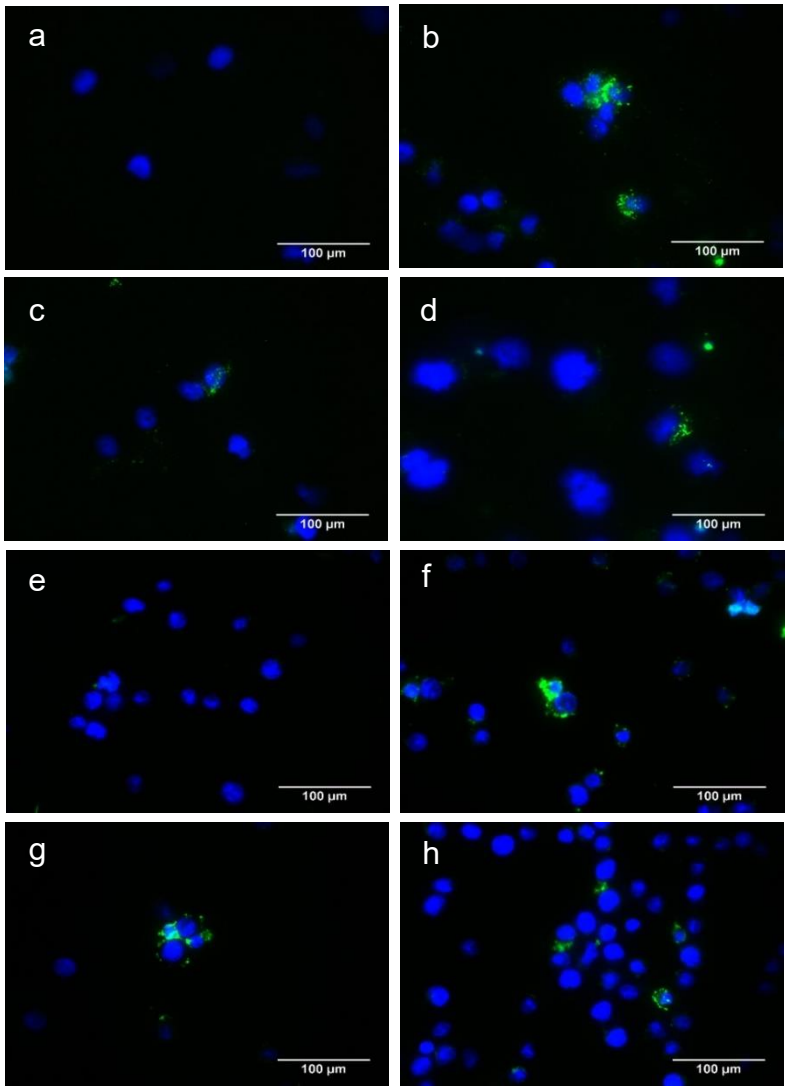


**Figure 5.26: Incubation with IS4 at 4˚C and 37˚C does not cause internalisation of the CXCR4 receptor in THP-1 cells. a)** Negative control incubated at 4˚C, treated with secondary anti-mouse Alexa Fluor® 488 antibody (green), DAPI (blue) and fixed with 4% paraformaldehyde before imaging. **b)** Positive control incubated at 4˚C, whereby CXCR4 was visualised using mouse 4G10 primary mAb, secondary anti-mouse Alexa Fluor® 488 antibody (green), DAPI (blue) and fixed with 4% paraformaldehyde before imaging. **c)** THP-1 cells stimulated with 10 nM of CXCL12 at 4˚C for 1 hour before visualisation as positive control. **d)** THP-1 cells treated with 1 µM IS4 at 4˚C for 1 hour before visualisation as positive control. **e)** Negative control as above, incubated at 37˚C. **f)** Positive control as above, incubated at 37˚C. g**)** THP-1 cells stimulated with 10 nM of CXCL12 at 37˚C for 1 hour before visualisation as positive control. **h)** THP-1 cells treated with 1 µM IS4 at 37˚C for 1 hour before visualisation as positive control. Data shows representative cells from three independent experiments with similar findings. Acquired with Leica imaging suite with 63x objective, 35x overall magnification.

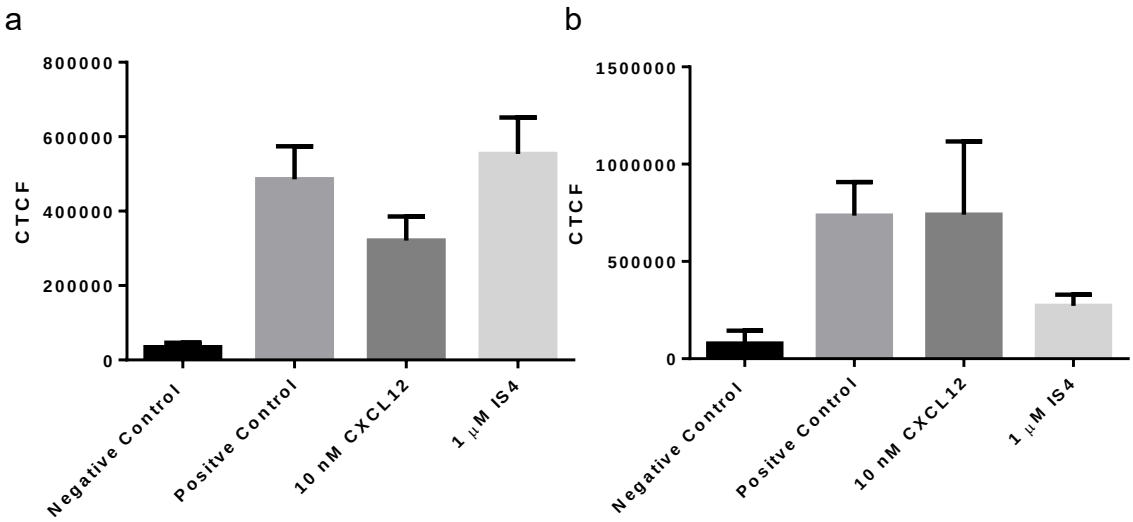


**Figure 5.27: Incubation with IS4 at 4˚C and 37˚C causes no significant change in the fluorescent intensity of CXCR4 receptor expression in THP-1 cells. a)** Corrected Total Cell Fluorescence (CTCF) of THP-1cells from Figure 5.26 stimulated with 10 nM CXCL12 or treated with 1 μM IS4 at 4˚C for 1 hour. **b)** CTCF of THP-1 cells from Figure 5.26 stimulated with 10 nM CXCL12 or treated with 1 μM IS4 at 37˚C for 1 hour. CTCF = Integrated Density – (Area of selected cell x Mean fluorescence of background readings). Data represents the mean ± SEM of 3 independent experiments. One-Way ANOVA with post hoc Dunnett's multiple comparison, data was not significant.

While it was proven that there was no statistical difference in the CTFC of the positive control compared to the IS4 treated cells, all experiments conducted at 37 ˚C demonstrated an overall trend showing decreased fluorescence in IS4 treated cells. Therefore, confocal imaging was conducted in the Jurkat cell line (Figure 5.28). Confocal imaging improves the resolution of the image taken, but more importantly for these experiments, it gives information about the depth. With the confocal images it is possible to get an idea about whole cellular CXCR4 expression from stacking images from multiple focal planes rather than just the one focal plane that you are limited to with epifluorescence imaging (Sanderson et al., 2014). While this provided a more comprehensive picture of whole cell CXCR4 expression, for a quantitative and more accurate assessment of CXCR4 expression, flow cytometry should be conducted.

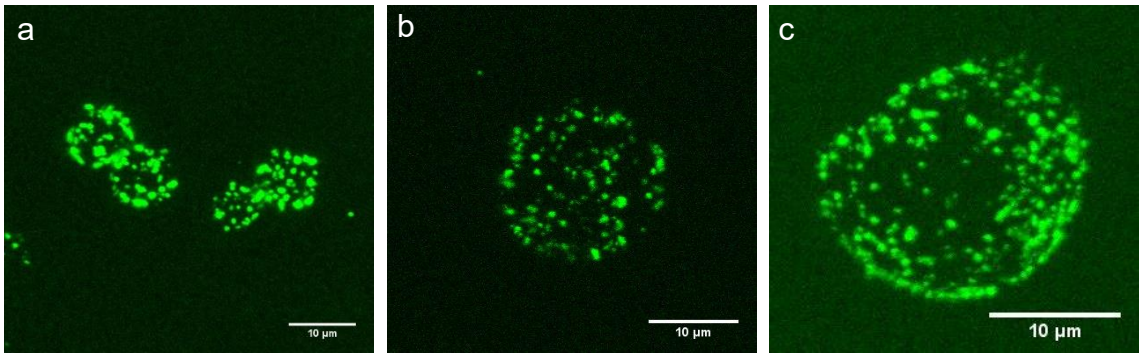


**Figure 5.28: Incubation with 10 nM CXCL12 or 1 µM IS4 at 37˚C does not cause internalisation of the CXCR4 receptor in Jurkat cells using confocal microscopy. a)** Positive control incubated at 37˚C, whereby CXCR4 was visualised using mouse 4G10 primary mAb, the secondary anti-mouse Alexa Fluor® 488 antibody (green) and fixed with 4% paraformaldehyde before imaging. **b)** Jurkat cells stimulated with 10 nM of CXCL12 at 37˚C for 1 hour before visualisation as previous. **d)** Jurkat cells treated with 1 µM IS4 at 37˚C for 1 hour before visualisation as previous. Data shows representative cells from 3 independent experiments with similar findings. Acquired with Carl Zeiss LSM510 software with 63x objective.

### 5.3.7. IS4 significantly reduce PC3 and SKMEL28 cell migratory speeds

To compare IS4 to AZ6-2, PC3 cells were stimulated with 10 nM CXCL12 and treated with 1 µM of IS4 (Figure 5.29). Using this data, PC3 basal cell speeds were calculated to be 37. 82 ± 9.45 µm/h and rose to 77.97 ± 3.53 µm/h after being stimulated with CXCL12 (Figure 4.41). Incubation with IS4 reduced migratory speeds to 11.76 ± 3.99 µm/h (Table 5.2).

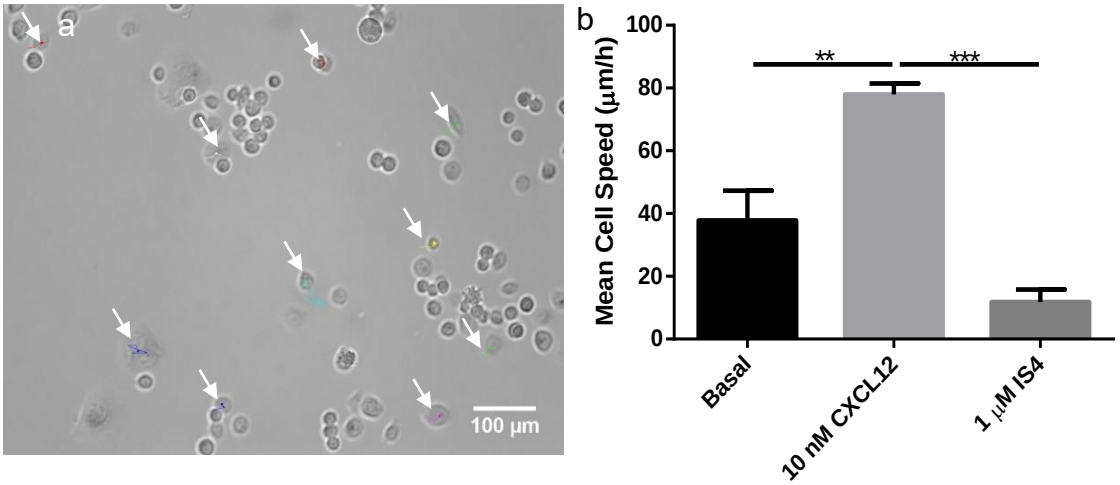


**Figure 5.29: IS4 significantly decreases CXCL12 stimulated PC3 cell migratory speeds in 10-hour time lapse assays.** PC3 cells were seeded and incubated for 24 hours before the addition of antagonist and/or chemokine then migration was tracked for 10 hours. **a)** Tracked PC3 cell speeds treated with 1 µM IS4 then stimulated with 10 nM CXCL12. **b)** PC3 cells treated with 1 µM IS4 then stimulated with 10 nM CXCL12. Data shows representative cell tracks from 3 independent experiments with similar findings. Acquired with a Zeiss Axiovert 200M motorise inverted fluorescent/ live cell imaging microscope with 10x objective. Data represents the mean ± SEM of 3 independent experiments. One-Way ANOVA with post hoc Dunnett's multiple comparison, ** = p≤ 0.01 and *** = p≤ 0.001.

**Table 5.2: Average speed of PC3 cells treated with 1 μM AMD3100, AZ3-2, AZ6-2 or IS4 and stimulated by 10 nM CXCL12. Data represents the mean ± SEM of 3 independent experiments.**

| Treatment | Average Speed (μm/h) |
|---|---|
| **Basal** | 37.82 ± 9.45 |
| **10 nM CXCL12** | 77.97 ± 3.53 |
| **10 nM CXCL12 + 1 μM AMD3100** | 62.19 ± 7.19 |
| **10 nM CXCL12 + 1 μM AZ3-2** | 27.88 ± 10.67 |
| **10 nM CXCL12 + 1 μM AZ6-2** | 11.76 ± 4.05 |
| **10 nM CXCL12 + 1 μM IS4** | 11.76 ± 3.99 |

Following this, a concentration range of 125 to 1000 nM of IS4 was used in times lapse assays then percentage corrected to calculate an $IC_{50}$ of 172 nM ± 53.65 nM SEM (Figure 5.30-5.32).

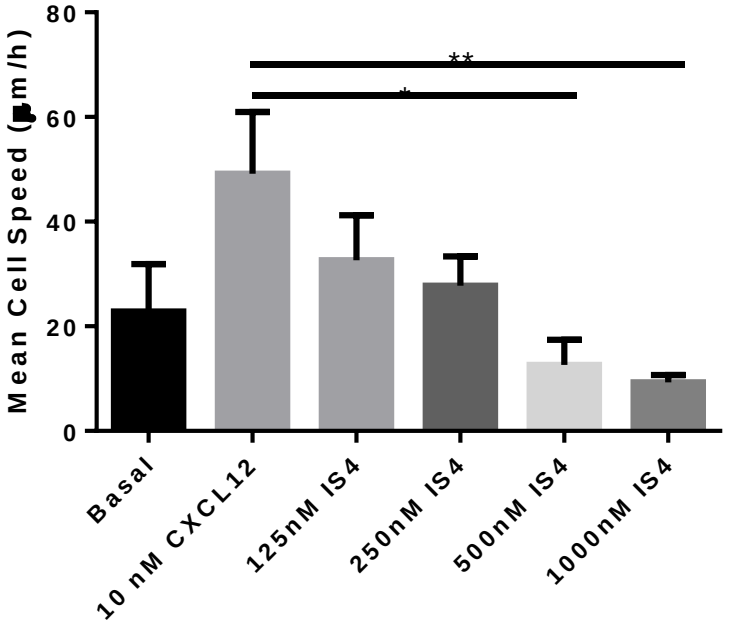


**Figure 5.30: 500-1000 nM of IS4 significantly decreases CXCL12 stimulated PC3 cell migratory speeds in 10-hour time lapse assays.** PC3 cells were seeded and incubated for 24 hours before the addition of IS4 (125-1000 nM) and 10 nM CXCL12 then migration was tracked for 10 hours. Data represents the mean ± SEM of 4 independent experiments. One-Way ANOVA with post hoc Dunnett's multiple comparison, * = p≤ 0.05 and ** = p≤ 0.01.

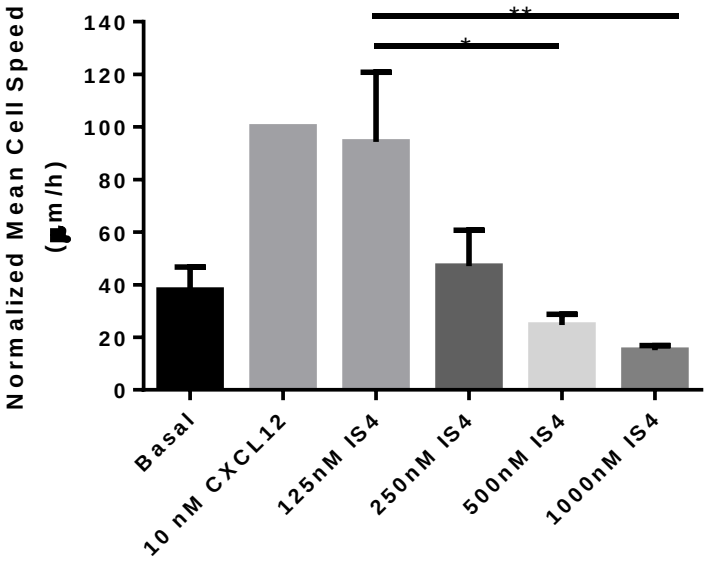


**Figure 5.31: 500-1000 nM of IS4 significantly decreases CXCL12 stimulated PC3 cell migratory speeds cells using percentage corrected data from 10-hour time lapse assays.** Normalization of data from Figure 5.30 showing the migration of PC3 cells stimulated by 10 nM of CXCL12 in the presence and absence of IS4 (125-1000 nM) then migration was tracked for 10 hours. Data represents the mean ± SEM of 4 independent experiments. Data normalised to CXCL12 and Kruskal-Wallis non-parametric test with post hoc Dunn's multiple comparison test was conducted, * = p≤ 0.05 and ** = p≤ 0.01.

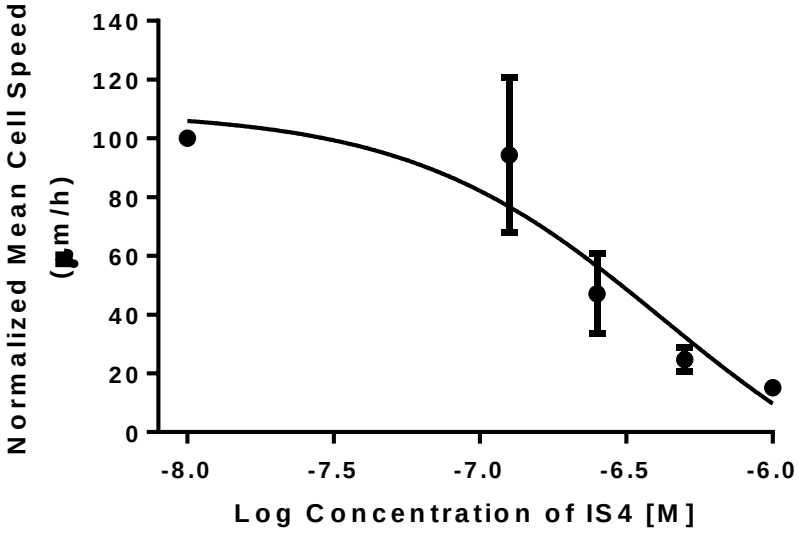


**Figure 5.32: Dose response curve of the speed of PC3 cells when treated with a dose range of IS4 and stimulated by 10 nM of CXCL12.** An $IC_{50}$ of 172 nM ± 53.65 nM SEM was calculated from data from Figure 5.31. Data represents the mean ± SEM of 4 independent experiments. Log (inhibitor) vs. response (here parameters).

Similar experiments were carried out in SKMEL28 cells which also demonstrated that 1 µM of IS4 significantly decreased migratory speeds (Figure 5.33). Average basal speed of SKMEL28 cells were 10.91 ± 1.01 µm/h that increase to 18.07 ± 1.89 µm/h once stimulated with 10 nM CXCL12 (Table 5.3). Incubation with IS4 reduced these speeds to 5.30 ± 0.26 µm/h.

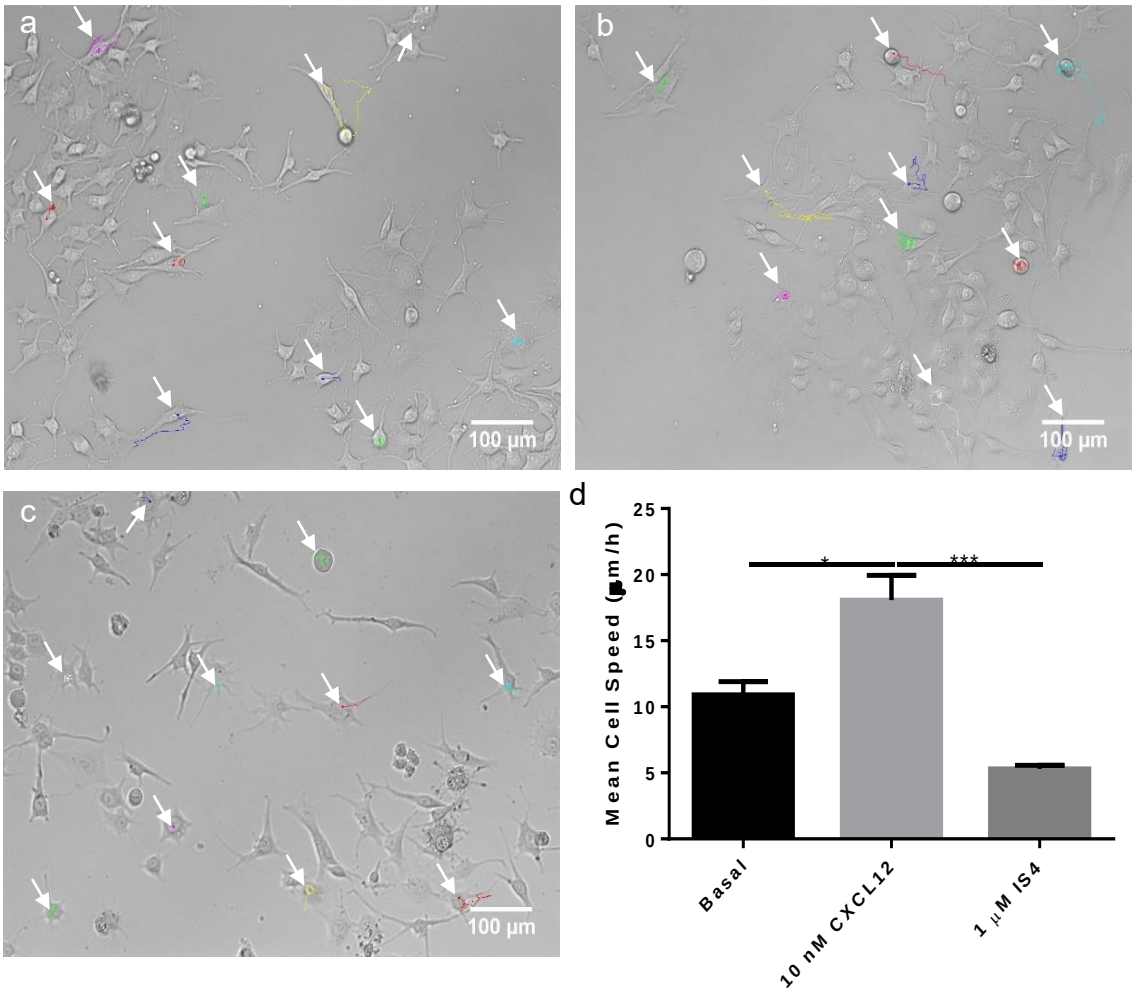


**Figure 5.33: IS4 significantly decreases CXCL12 stimulated SKMEL28 cells migratory speeds in 10-hour time lapse assays.** SKMEL28 cells were seeded and incubated for 24 hours before the addition of antagonist and/or chemokine then migration was tracked for 10 hours. **a)** Tracked basal SKMEL28 cell speeds. **b)** Tracked SKMEL28 cell speeds stimulated with 10 nM CXCL12. **c)** Tracked SKMEL28 cell speeds treated with 1 µM IS4 then stimulated with 10 nM CXCL12. **d)** SKMEL28 cells treated with 1 µM IS4 then stimulated with 10 nM CXCL12. Data shows representative cell tracks from 3 independent experiments with similar findings. Acquired with a Zeiss Axiovert 200M motorise inverted fluorescent/ live cell imaging microscope with 10x objective. Data represents the mean ± SEM of 3 independent experiments. One-Way ANOVA with post hoc Dunnett's multiple comparison, * = p≤ 0.05 and *** = p≤ 0.001.

**Table 5.3: Average speed of SKMEL28 cells treated with 1 μM IS4 and stimulated by 10 nM CXCL12. Data represents the mean ± SEM of 3 independent experiments.**

| Treatment | Average Speed (μm/h) |
|---|---|
| **Basal** | 10.91 ± 1.01 |
| **10 nM CXCL12** | 18.07 ± 1.89 |
| **10 nM CXCL12 + 1 μM IS4** | 5.30 ± 0.26 |

To determine an $IC_{50}$ for IS4 in SKMEL28 cells a concentration range of 0.125-1 μM IS4 was used in time lapse assays and subsequently percentage corrected (Figure 5.34 and 5.35).

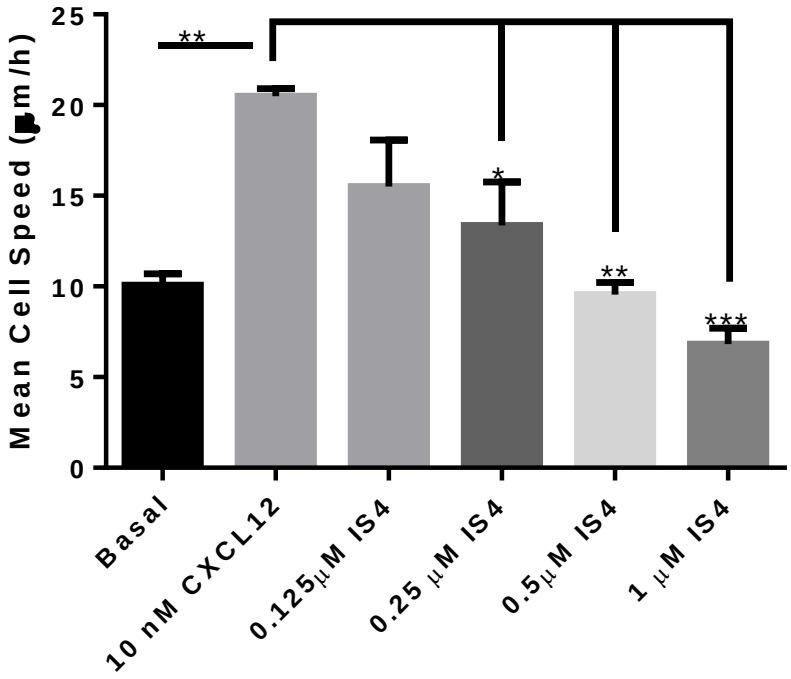


**Figure 5.34: 0.25-1 μM of IS4 significantly decreases CXCL12 stimulated SKMEL28 cells migratory speeds in 10-hour time lapse assays.** SKMEL28 cells were seeded and incubated for 24 hours before the addition of IS4 (0.125 - 1 μM) and 10 nM CXCL12 then migration was tracked for 10 hours. Data represents the mean ± SEM of 3 independent experiments. One-Way ANOVA with post hoc Dunnett's multiple comparison, * = p≤ 0.05, ** = p≤ 0.01 and *** = p≤ 0.001.

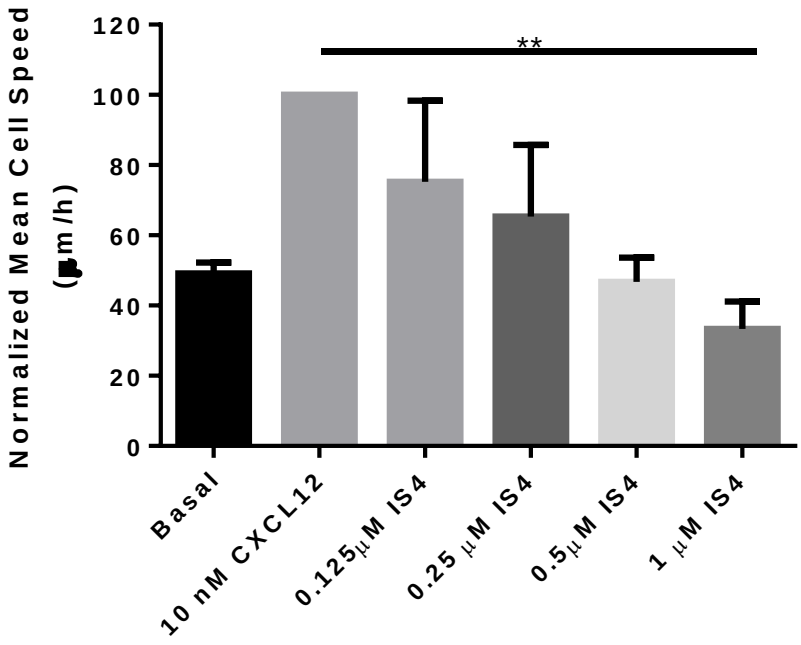


**Figure 5.35: 1 μM of IS4 significantly decreases CXCL12 stimulated SKMEL28 cells migratory speeds cells using percentage corrected data from 10-hour time lapse assays**. Normalization of data from Figure 5.34 showing the migration of SKMEL28 cells stimulated by 10 nM of CXCL12 in the presence and absence of IS4 (0.125-1 μM) then tracked for 10 hours. Data represents the mean ± SEM of 3 independent experiments. Data normalised to CXCL12 and Kruskal-Wallis non-parametric test with post hoc Dunn's multiple comparison test was conducted, ** = p≤ 0.01.

This calculated the $IC_{50}$ of IS4 in SKMEL28 cells to be 423 nM ± 229.6 nM SEM (Figure 5.36). This reduced migratory speed in SKMEL28 cells is not a consequence of cellular toxicity caused by IS4 as demonstrated by MTS assay (Appendix A26). Comparisons of $IC_{50}$ values of AZ6-2 and IS4 in both PC3 and SKMEL28 cells are compared in Table 5.4.

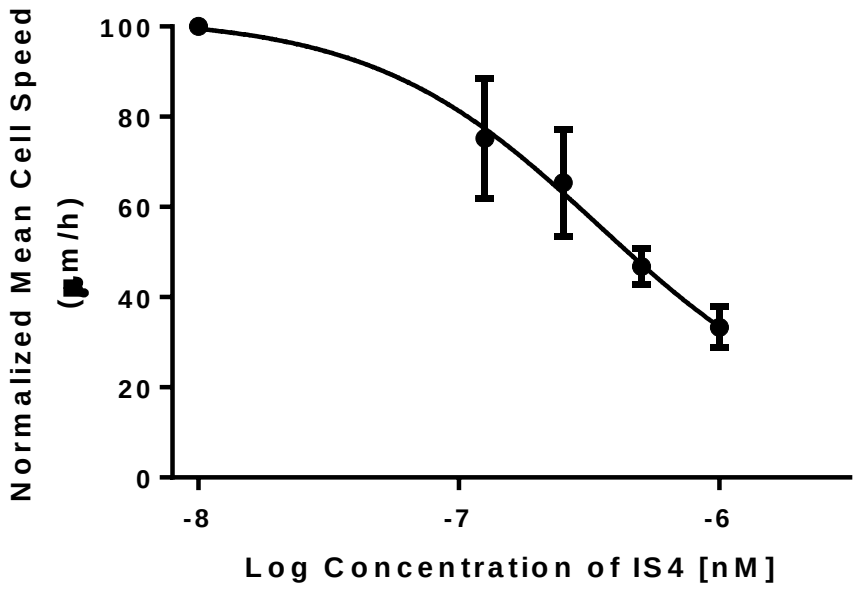


**Figure 5.36: Dose response curve of the speed of SKMEL28 cells when treated with a dose range of IS4 and stimulated by 10 nM of CXCL12.** An $IC_{50}$ of 423 nM ± 229.6 nM SEM was calculated from data from Figure 5.35. Data represents the mean ± SEM of 3 independent experiments. Log (inhibitor) vs. response (three parameters).

**Table 5.4: Summary of IC50 values of AZ6-2 and IS4 in both PC3 and SKMEL28 cells. Data represents the mean ± SEM of at least 3 independent experiments.**

| Peptide | Cell Line | |
|---|---|---|
| | PC3 | SKMEL28 |
| **AZ6-2** | 128 nM ± 66.08 | 266.2 nM ± 148.7 |
| **IS4** | 172 nM ± 53.65 | 423 nM ± 229.6 nM |

### 5.3.8. IS4 significantly inhibits CXCL12 directed PC3 cell migration

As before, Oris™ Cell Migration assays were conducted and it was determined that IS4 caused a significant decrease in CXCL12 directed migration in PC3 cells (Figure 5.37).

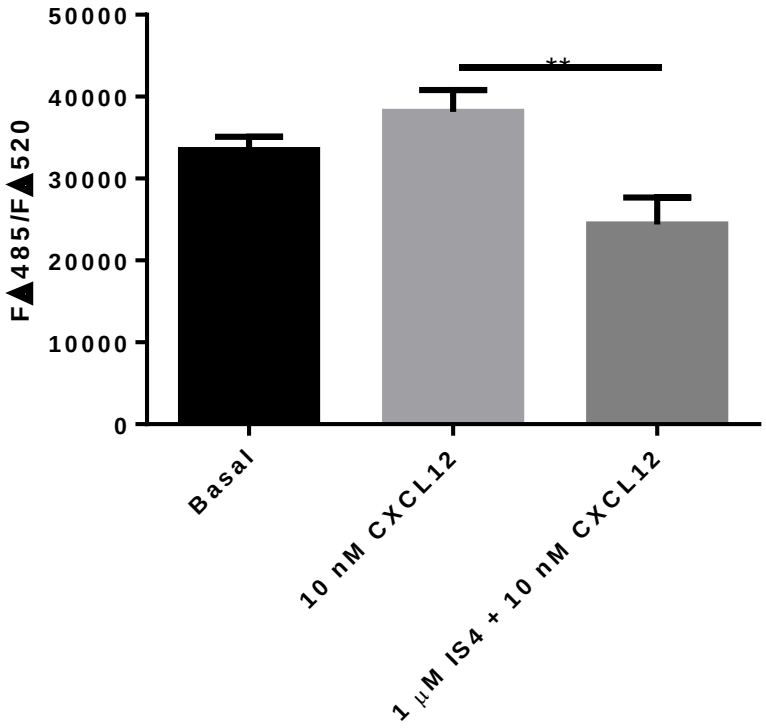


**Figure 5.37: IS4 reduces CXCL12 directed migration in PC3 cells using Oris™ Cell Migration assays.** PC3 cells were seeded and incubated for 24 hours before the addition of 1 μM IS4 and 10 nM of CXCL12 then incubated for another 24 hours before analysis using calcein 485/520 nm. Data represents the mean ± SEM of 4 independent experiments. One-Way ANOVA with post hoc Dunnett's multiple comparison, ** = p≤ 0.01.

### 5.3.9. IS4 is a CXCR4 specific antagonist

It was previously determined that AZ6-2 did not bind to CXCR3, CCR1 nor CCR5. To confirm if the structural changes made to synthesise IS4 have affected its specificity, the same two chemokines, CXCL11 and CCL3, were used plus CCL5, CCL8, CXCL8 and CXCL10 in chemotaxis assays and/or calcium flux assays to further characterise how specific IS4 is as a CXCR4 antagonist (Table 5.5). From these experiments it was confirmed that IS4 does not prevent CXCL10, CCL3, CCL5, CCL8 or CXCL8 stimulated THP-1 migration (Figure 5.38).

**Table 5.5: Chemokines used to determine IS4 specificity and their associated chemokine receptors.**

| Chemokine | Associated Receptor(s) |
|---|---|
| **CCL3** | CCR1 and CCR5 |
| **CCL5** | CCR1, CCR3, CCR4 and CCR5 |
| **CCL8** | CCR1, CCR2, CCR3 and CCR5 |
| **CXCL8** | CXCR1 and CXCR2 |
| **CXCL11** | CXCR3 |
| **CXCL10** | CXCR3 |
| **CXCL12** | CXCR4 and CXCR7(ACKR3) |

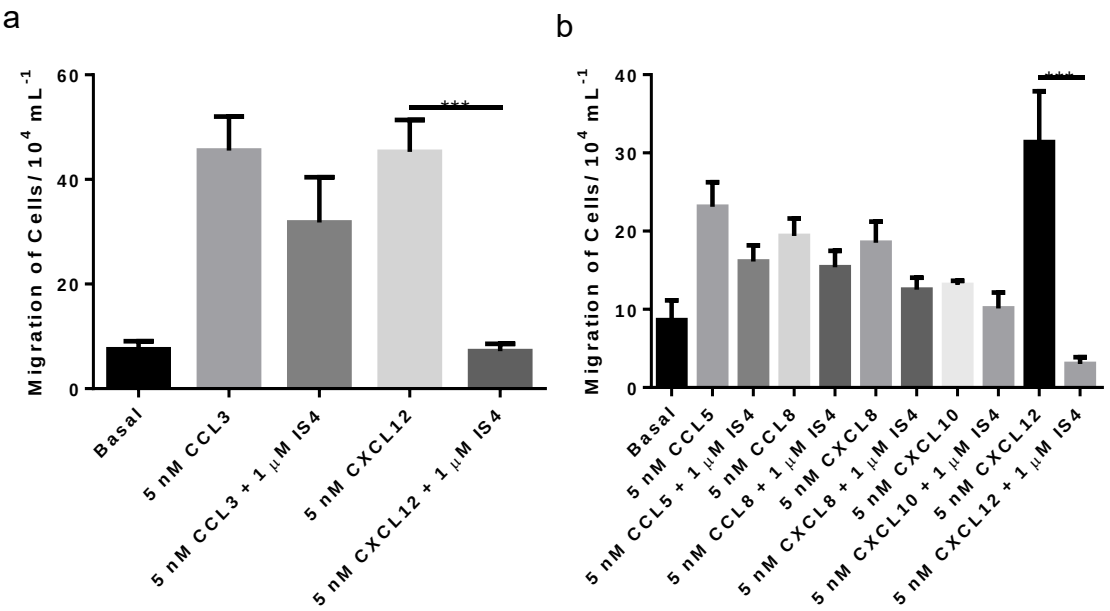


**Figure 5.38: IS4 does not prevent CCL3, CCL5, CCL8, CXCL8 or CXCL10 stimulated THP-1 migration.** Migration of THP-1 cells where cells were treated with 1 µM IS4 for 30 minutes then stimulated by 5 nM of CCL3, CCL5, CCL8, CXCL8, CXCL10 or CXCL12 for 4 hours. Data represents the mean ± SEM of 4/5 independent experiments. One-Way ANOVA with post hoc Dunnett's multiple comparison, *** = p≤ 0.001.

Furthermore, IS4 did not prevent the release of intracellular calcium from THP-1 cells stimulated with CXCL11, CCL3, CCL5, CCL8 or CXCL8 (Figure 5.39).

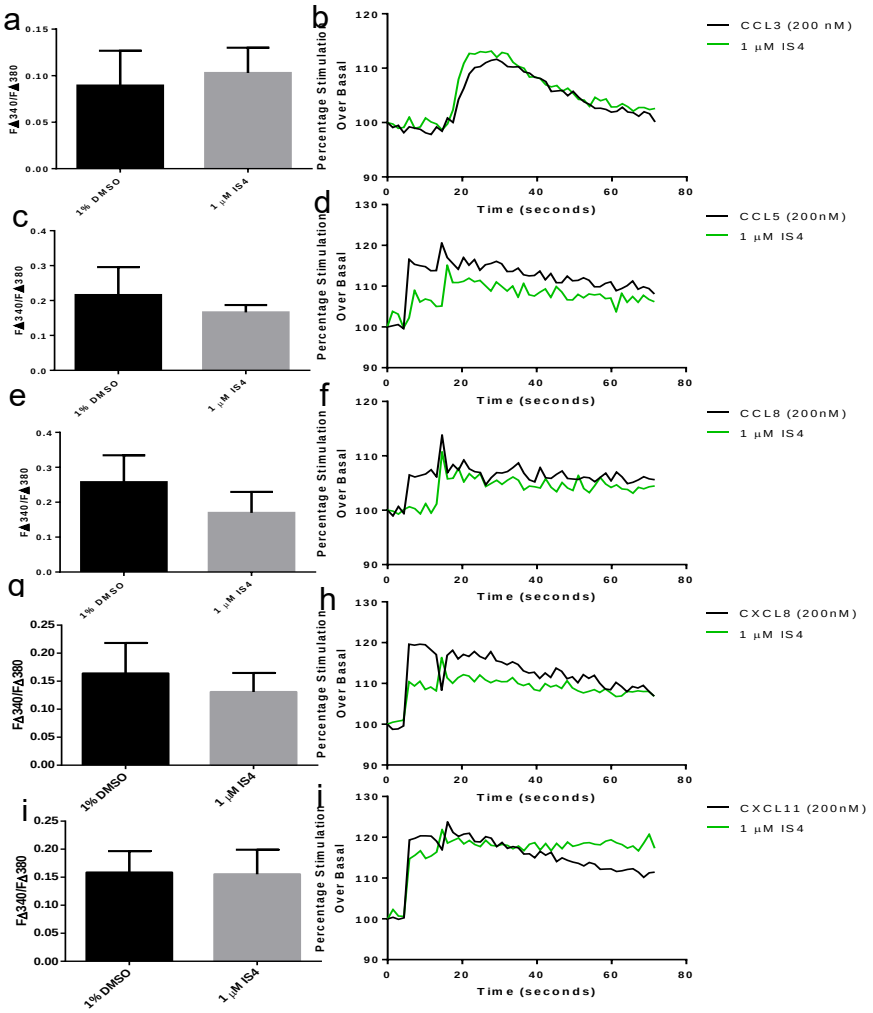


**Figure 5.39: IS4 do not reduce the release of intracellular $Ca^{2+}$ from CCL3, CCL5, CCL8, CXCL8 or CXCL11 stimulated THP-1 cells.** Cells were incubated for 30 minutes with antagonist or vehicle control and the calcium indicator Fura-2 AM. **a)** THP-1 cell were treated with 1 μM IS4 then stimulated with 200 nM CCL3. **b)** Representative intracellular calcium release traces with 200 nM CCL3. **c)** THP-1 cell treated with 1 μM IS4 then stimulated with 200 nM CCL5. **d)** Intracellular calcium release traces with 200 nM CCL5. **e)** THP-1 cell treated with 1 μM IS4 then stimulated with 200 nM CCL8. **f)** Intracellular calcium release traces with 200 nM CCL8. **g)** THP-1 cell treated with 1 μM IS4 then stimulated with 200 nM CXCL8. **h)** Intracellular calcium release traces with 200 nM CXCL8. **i)** THP-1 cell treated with 1 μM IS4 then stimulated with 200 nM CXCL11. **j)** Intracellular calcium release traces with 200 nM CXCL11. Data is expressed as a change in fluorescence ratio (340nm/380nm) where the basal fluorescence prior to the addition of chemokine is subtracted from peak fluorescence following addition of chemokine. Chemokine injected after 10 seconds. Data represents the mean ± SEM of 3-5 independent experiments. One-Way ANOVA with post hoc Dunnett's multiple comparison, data not significant.

### 5.3.10. IS4 is more stable than AZ6-2

As mentioned previously, one of the disadvantages of AZ6-2 is that the disulphide bond is liable to becoming reduced when introduced to mammalian cells, rendering the compound inactive (Chakravarthi et al., 2006, Okumura et al., 2011). Initial experiments by Di Maro et al. (2016) tested the metabolic stability of AZ6-2 via incubation in diluted human plasma at 37℃ for 30-180 minutes followed by analysis using RP-HPLC-ESI. From these results, it was stated that AZ6-2 remained stable up to 180 minutes. While the same experiment could not be conducted with IS4, FBS was substituted for the dilute human plasma and calcium release assays were conducted to determine if IS4 had improved stability over AZ6-2 i.e. if IS4 could still prevent calcium release. From these results, it was determined that after only 30 minutes incubated with FBS, AZ6-2 lost the ability to prevent calcium release while IS4 was still able to function as a CXCR4 antagonist and prevent the release of calcium in THP-1 cells (Figure 5.40).

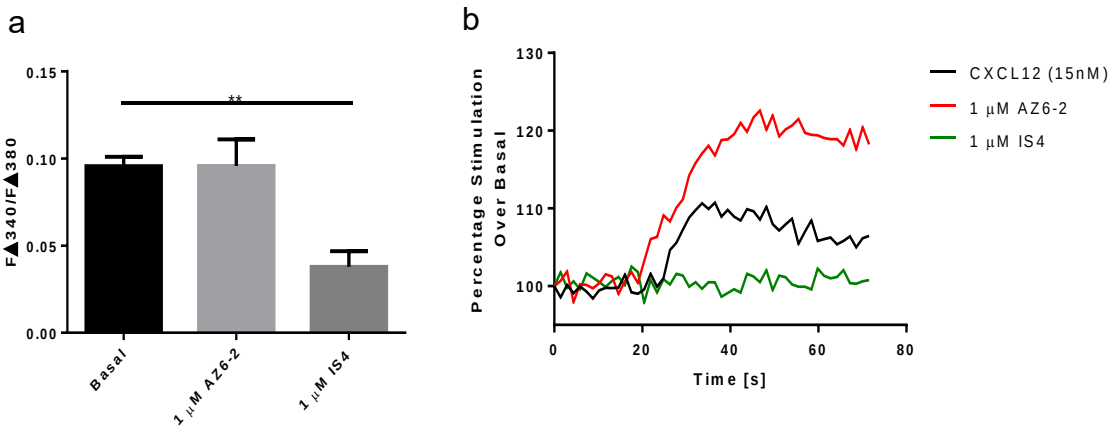


**Figure 5.40: IS4 but not AZ6-2 remained stable after 30 minutes incubated in FBS. a)** THP-1 cells treated with 30 minute FBS incubated 1 μM AZ6-2 or IS4 then stimulated with 15 nM CXCL12. **b)** Representative intracellular calcium release traces of THP-1 cells treated with 30 minute FBS incubated 1 μM AZ6-2 or IS4 then stimulated with 15 nM CXCL12. Data is expressed as a change in fluorescence ratio (340nm/380nm) where the basal fluorescence prior to the addition of CXCL12 is subtracted from peak fluorescence following addition of CXCL12. Chemokine injected after 10 seconds. Data represents the mean ± SEM of 4 independent experiments. One-Way ANOVA with post hoc Dunnett's multiple comparison, ** = p≤ 0.01.

### 5.3.11. Copper-catalysed alkyne-azide cycloaddition click chemistry with IS4 and 3-azido-7-hydroxycoumarin is not suitable for in situ experimentation

IS4 was used in CuAAC reactions where conditions followed procedure of Li et al. (2010). Figure 5.41, demonstrates that subsequent to CuAAC there were high levels of the 3-azido-7-hydroxycoumarin dye in the nucleus of the MCF-7 cell and non-specific extracellular staining. Alterations to the incubation time (10, 30, 40 and 60 minute incubations), incubation temperature (4℃, 37℃ and room temperature), fixing with 4% paraformaldehyde before or after CuAAC and alterations to concentration of the 3-azido-7-hydroxycoumarin dye (0.1- 0.45 mM) caused little change to the end result. The high amount of nuclear fluorescence is not attributed to CXCR4 internalisation as seen in Figure 5.22. Therefore, the failure of these click reactions is most likely attributed to the 3-azido-7-hydroxycoumarin dye itself. 3-azido-7-hydroxycoumarin was used by Li et al. (2010) due to it being a small molecule which is capable of penetrating the nucleus and detecting DNA for measurement of cells in the S phase. Therefore, while the small size of 3-azido-7-hydroxycoumarin was an advantage for Li et al. (2010), this proved to be a disadvantage for the labelling of external CXCR4 receptor as it appears that the 3-azido-7-hydroxycoumarin penetrated the nucleus before the CuAAC reaction can complete. Why the dye could be visualised when it had not clicked to IS4 is most likely due to 3-azido-7-hydroxycoumarin not being very stable in oxidative conditions or in DMSO, which might not have been washed sufficiently from the cell monolayer. As such, the 3-azido-7-hydroxycoumarin could have broken down to the optically active compound (Li et al., 2017). Therefore, *in situ* CuAAC using IS4 and the dye 3-azido-7-hydroxycoumarin was unsuccessful.

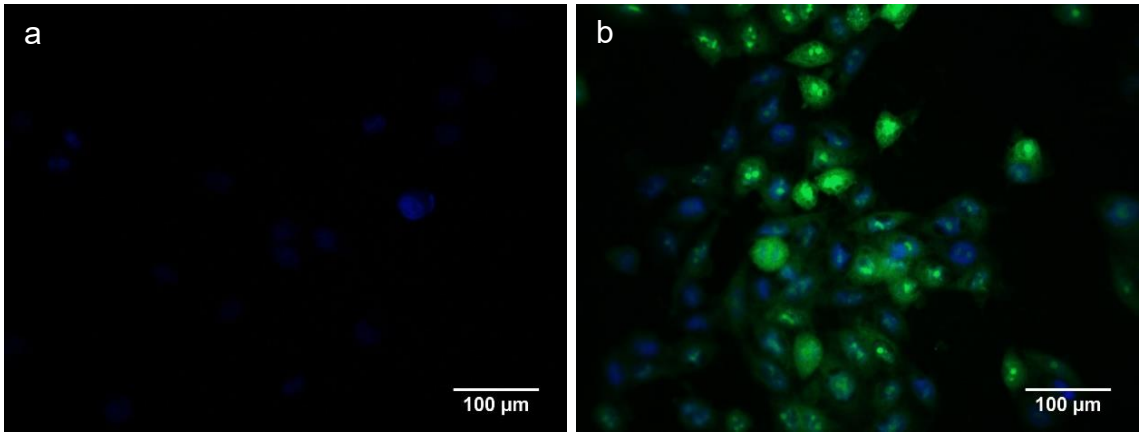


**Figure 5.41: *In situ* CuAAC click reaction with IS4 failed to fluorescently label CXCR4 receptors on MCF-7 cells. a)** Negative control incubated at room temperature, treated with DAPI (blue) and fixed with 4% paraformaldehyde before imaging. **b)** MCF-7 cells incubated with 1 µM IS4, washed with PBS and then reacted with 0.1 mM 3-azido-7-hydroxycoumarin (green), 1 mM $CuSO_4$ and 30 mM of sodium ascorbate at room temperature for 1 hour then treated with DAPI (blue). Cells were then washed with PBS and fixed with 4% paraformaldehyde for 10 minutes. Data shows representative cells from 7 independent experiments with similar findings. Acquired with Leica imaging suite with 40x objective, 22x overall magnification.

### 5.3.12. IS7 successfully binds to CXCR4

Due to the failure of the *in situ* CuAAC click reaction with IS4, IS7 was synthesised fully in the laboratory (Figure 5.3 and 5.6). Therefore, IS7 has already been clicked to 3-azido-7-hydroxycoumarin *ex situ* and was added directly to cells and incubated for an hour. It was found that IS7 fluorescently labelled CXCR4 receptors on MCF-7 cells (Figure 5.42).

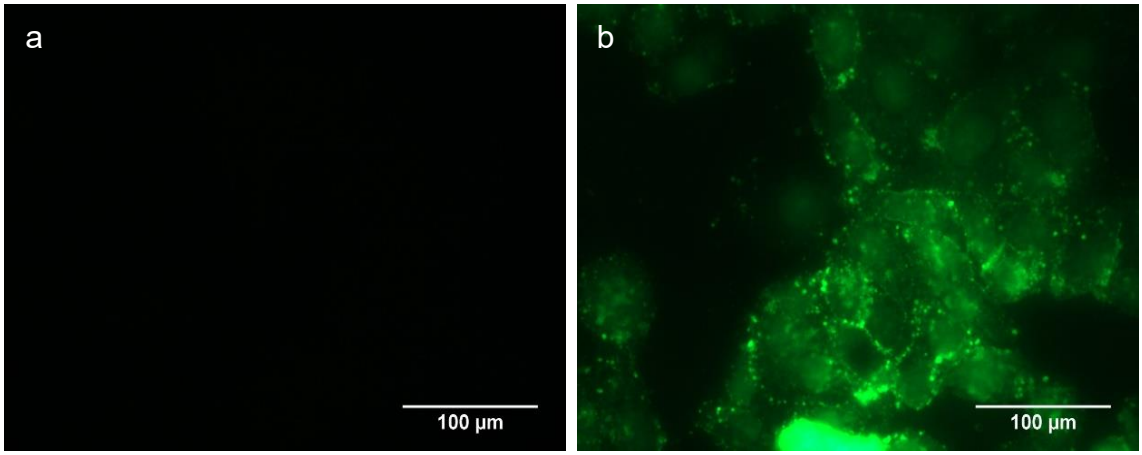


**Figure 5.42: CuAAC click reaction with IS7 fluorescently labelled CXCR4 receptors on MCF-7 cells. a)** Negative control incubated at room temperature and fixed with 4% paraformaldehyde before imaging. **b)** MCF-7 cells incubated with 1 µM IS7 (green) for 1 hour and fixed with 4% paraformaldehyde for 10 minutes. Data shows representative cells from 4 independent experiments with similar findings. Acquired with Leica imaging suite with 63x objective, 35x overall magnification.

### 5.3.13. IS7 significantly reduces intracellular $Ca^{2+}$ release from MCF-7, PC3, Jurkat and THP-1

Calcium release assays were conducted as before and results demonstrated that incubation with 1 µM of IS7 significantly reduced the release of $Ca^{2+}$ in MCF-7, Jurkat, THP-1 and PC3 cells (Figure 5.43). This reduced release of intracellular $Ca^{2+}$ in these cell lines is not a consequence of cellular toxicity caused by IS7 as demonstrated by MTS assay (Appendix A27 to A30).

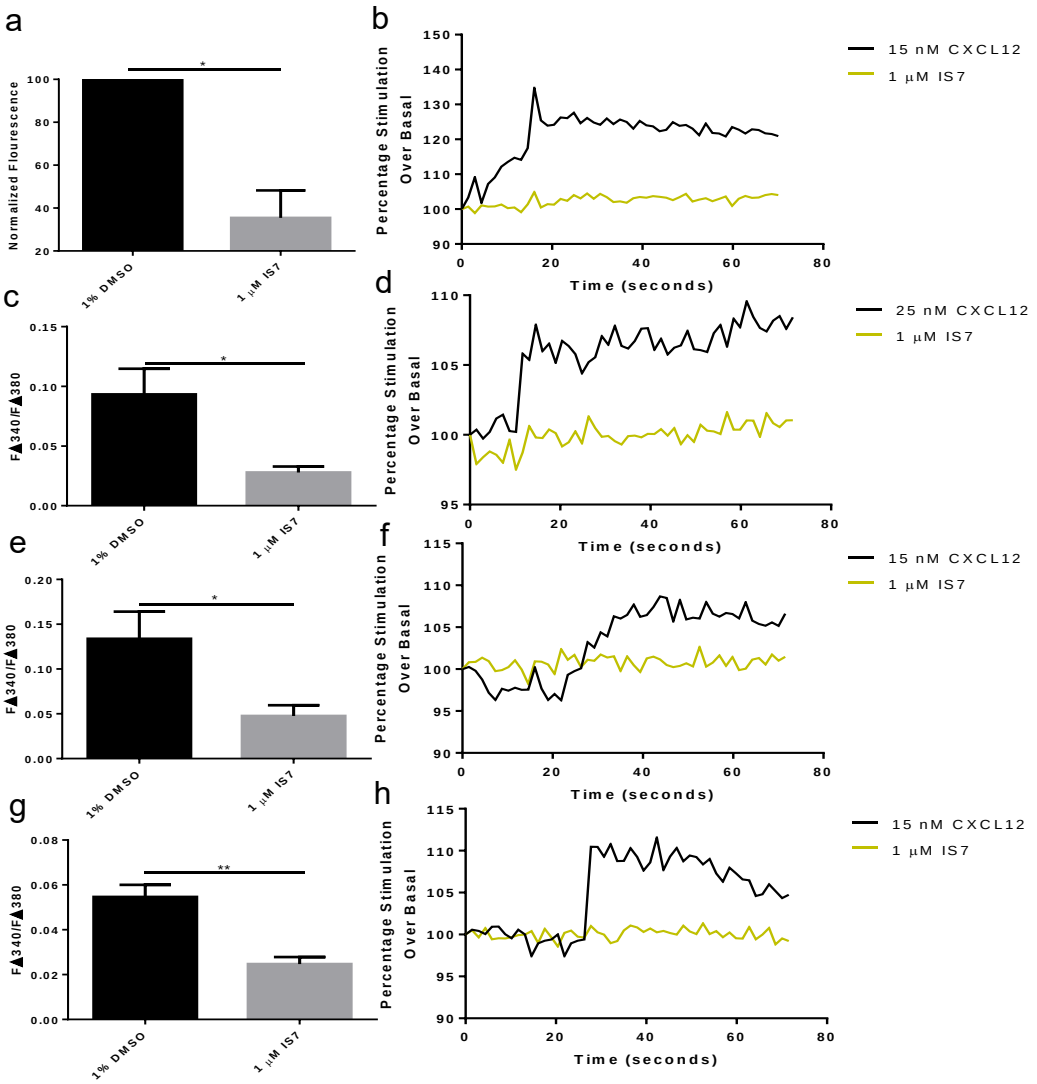


**Figure 5.43: IS7 significantly reduces the release of intracellular $Ca^{2+}$ from MCF-7, Jurkat, THP-1 and PC3 cells.** Cells were incubated for 30 minutes with antagonist or vehicle control and the calcium indicator Fura-2 AM. **a)** MCF-7 cells treated with 1 μM IS7 then stimulated with 15 nM CXCL12. **b)** Representative intracellular calcium release traces of MCF-7 cells. **c)** Jurkat cells treated with 1 μM IS7 then stimulated with 25 nM CXCL12. **d)** Representative intracellular calcium release traces of Jurkat cells. **e)** THP-1 cells treated with 1 μM IS7 then stimulated with 15 nM CXCL12. **f)** Representative intracellular calcium release traces of THP-1 cells. **g)** PC3 cells treated with 1 μM IS7 then stimulated with 15 nM CXCL12. **h)** Representative intracellular calcium release traces of PC3 cells. Data is expressed as a change in fluorescence ratio (340nm/380nm) where the basal fluorescence prior to the addition of CXCL12 is subtracted from peak fluorescence following addition of CXCL12. Chemokine injected after 10 seconds. Data represents the mean ± SEM of 3-6 independent experiments. One-Way ANOVA with post hoc Dunnett's multiple comparison, * = p≤ 0.05 and ** = p≤ 0.01.

### 5.3.14. IS7 significantly reduce PC3 cell migratory speeds

To compare IS7 to the other CXCR4 antagonists investigated, PC3 cells were stimulated with 10 nM CXCL12 and treated with 1 µM of IS7 (Figure 5.44). Using this data, PC3 basal cell speeds were calculated to be 37. 82 ± 9.45 µm/h and rose to 77.97 ± 3.53 µm/h after being stimulated with CXCL12 (Figure 4.41). Incubation with IS7 reduced migratory speeds down to 17.26 ± 7.27 µm/h. This enabled us to compare the migratory speeds for all five compounds (Table 5.6).

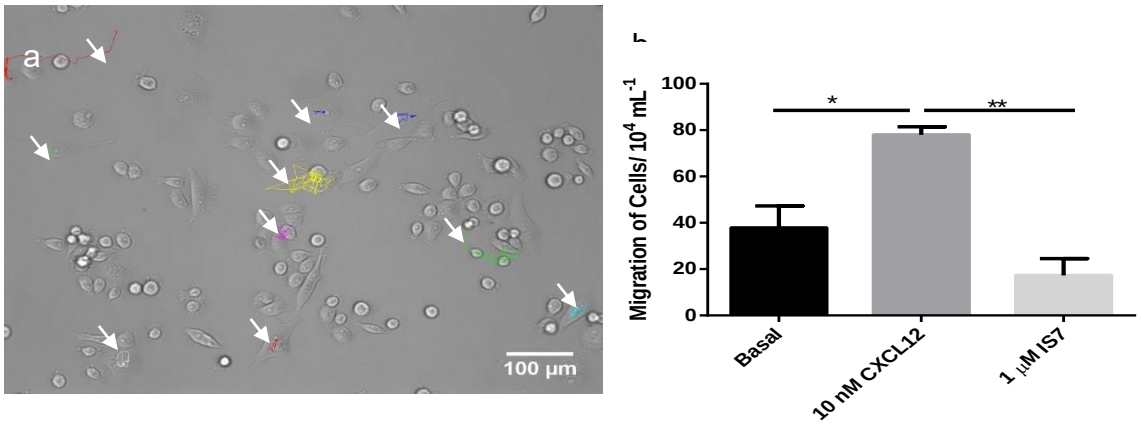


**Figure 5.44: IS7 significantly decreases CXCL12 stimulated PC3 cell migratory speeds in 10-hour time lapse assays.** PC3 cells were seeded and incubated for 24 hours before the addition of antagonist and/or chemokine then migration was tracked for 10 hours. **a)** Tracked PC3 cell speeds where cells are treated with 1 µM IS7 then stimulated with 10 nM CXCL12. **d)** PC3 cells treated with 1 µM IS7 then stimulated with 10 nM CXCL12. Data shows representative cell tracks from 3 independent experiments with similar findings. Acquired with a Zeiss Axiovert 200M motorise inverted fluorescent/ live cell imaging microscope with 10x objective. Data represents the mean ± SEM of 3 independent experiments. One-Way ANOVA with post hoc Dunnett's multiple comparison, * = p≤ 0.05 and ** = p≤ 0.01.

**Table 5.6: Average speed of PC3 cells treated with 1 µM AMD3100, AZ3-2, AZ6-2, IS4 or IS7 and stimulated with 10 nM CXCL12.**

| Treatment | Average Speed (µm/h) |
|---|---|
| **Basal** | 37.82 ± 9.45 |
| **10 nM CXCL12** | 77.97 ± 3.53 |
| **10 nM CXCL12 + 1 µM AMD3100** | 62.19 ± 7.19 |
| **10 nM CXCL12 + 1 µM AZ3-2** | 27.88 ± 10.67 |
| **10 nM CXCL12 + 1 µM AZ6-2** | 11.76 ± 4.05 |
| **10 nM CXCL12 + 1 µM IS4** | 11.76 ± 3.99 |
| **10 nM CXCL12 + 1 µM IS7** | 17.26 ± 7.27 |

## 5.3.15. IS7 significantly inhibits CXCL12 directed PC3 cell migration

Oris™ Cell Migration assays were conducted to determine if IS7 prevented CXCL12 directed migration in PC3 cells. While the raw data suggested that IS7 could not inhibit CXCL12 directed migration, when the data was normalized, IS7 was found to significantly inhibit CXCL12 directed migration (Figure 5.45).

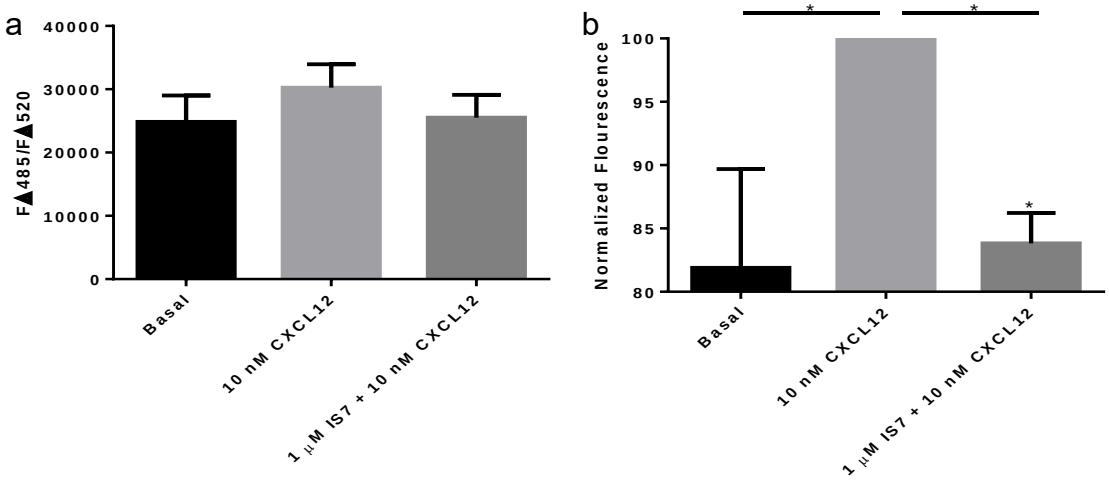


**Figure 5.45: IS7 reduces CXCL12 directed migration in PC3 cells using Oris™ Cell Migration assays.** PC3 cells were seeded and incubated for 24 hours before the addition of 1 µM IS7 and 10 nM CXCL12 then incubated for another 24 hours before analysis using calcein 485/520 nm. Data represents the mean ± SEM of 4 independent experiments. One-Way ANOVA with post hoc Dunnett's multiple comparison, or where data was normalised to CXCL12, Kruskal-Wallis non-parametric test with post hoc Dunn's multiple comparison test was conducted, * = p≤ 0.05.

### 5.3.16. IS7 is a CXCR4 specific antagonist

As before, CCL3, CCL5, CCL8, CXCL8 and CXCL11 were used in chemotaxis assays and/or calcium flux assays to determine the specificity of IS7. From these experiments it was confirmed that IS7 does not prevent CCL3 stimulated THP-1 migration (Figure 5.46).

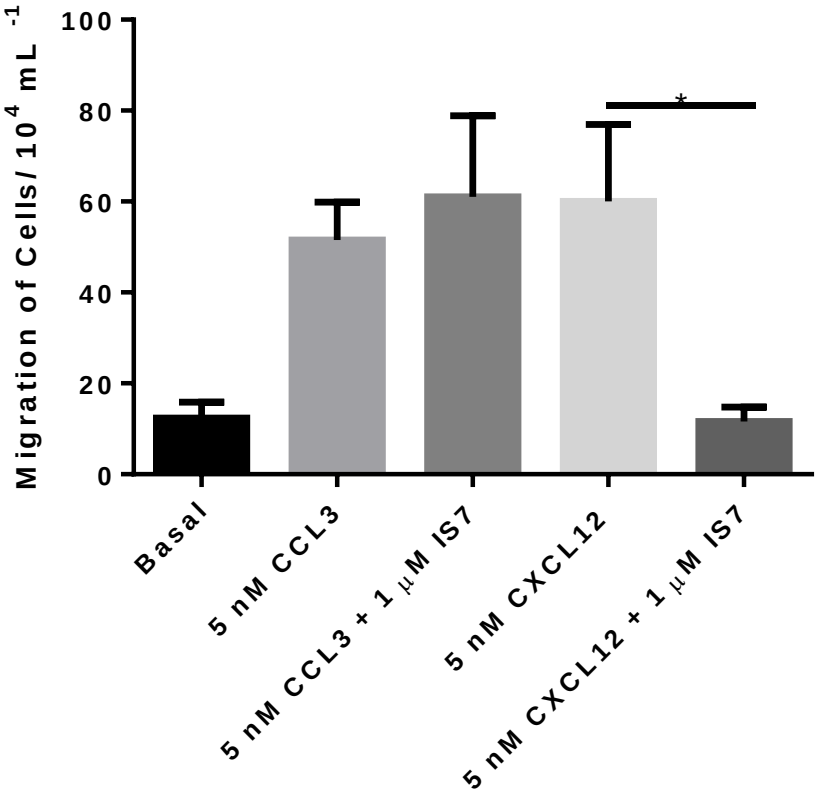


**Figure 5.46: IS7 does not prevent CCL3 stimulated THP-1 migration.** Migration of THP-1 cells where cells were treated with 1 µM IS7 for 30 minutes then stimulated by 5 nM CCL3 or CXCL12 for 4 hours. Data represents the mean ± SEM of 4 independent experiments. One-Way ANOVA with post hoc Dunnett's multiple comparison, * = p≤ 0.05.

Furthermore, IS7 did not prevent the release of intracellular calcium from THP-1 cells stimulated with CCL3, CCL5, CCL8, CXCL8 or CXCL11 (Figure 5.47).

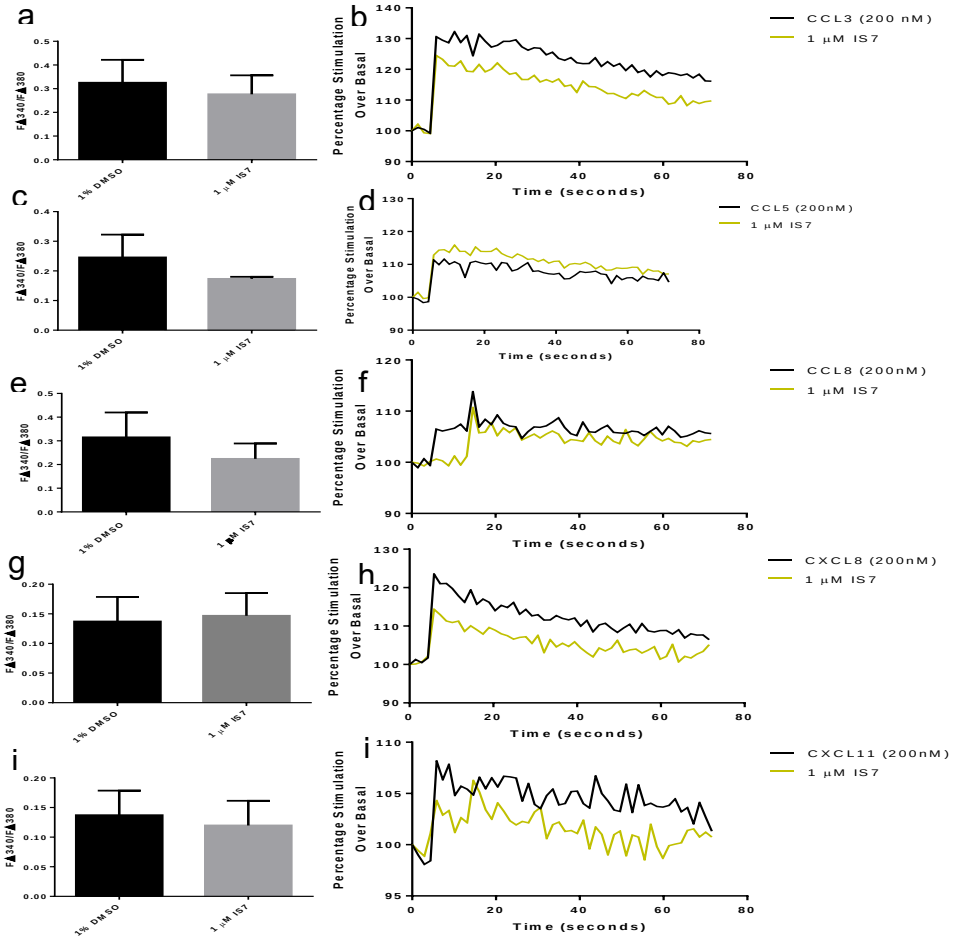


**Figure 5.47: IS7 do not reduce the release of intracellular $Ca^{2+}$ from CCL3, CCL5, CCL8, CXCL8 or CXCL11 stimulated THP-1 cells.** Cells were incubated for 30 minutes with antagonist or vehicle control and the calcium indicator Fura-2 AM. **a)** THP-1 cells treated with 1 µM IS7 then stimulated with 200 nM CCL3. **b)** Representative intracellular calcium release traces of THP-1 cells with 200 nM CCL3. **c)** THP-1 cells treated with 1 µM IS7 then stimulated with 200 nM CCL5. **d)** Intracellular calcium release traces of THP-1 cells with 200 nM CCL5. **e)** THP-1 cell treated with 1 µM IS7 then stimulated with 200 nM CCL8. **f)** Intracellular calcium release traces of THP-1 cells with 200 nM CCL8. **g)** THP-1 cell treated with 1 µM IS7 then stimulated with 200 nM CXCL8. **h)** Intracellular calcium release traces of THP-1 cells with 200 nM CXCL8. **i)** THP-1 cell treated with 1 µM IS7 then stimulated with 200 nM CXCL11. **j)** Intracellular calcium release traces of THP-1 cells with 200 nM CXCL11. Data is expressed as a change in fluorescence ratio (340nm/380nm) where the basal fluorescence prior to the addition of chemokine is subtracted from peak fluorescence following addition of chemokine. Chemokine injected after 10 seconds. Data represents the mean ± SEM of 3/4 independent experiments. One-Way ANOVA with post hoc Dunnett's multiple comparison, data not significant.

## 5.4. Discussion

The first overarching aim of this chapter was to improve the stability of the compound AZ6-2 without jeopardising the potency. Secondly, the aim was to develop a compound that acted as a CXCR4 antagonist that could also be 'clicked' to a florescent marker as a proof of principle experiment before attempting clicking other agents such as chemotherapeutics.

Initially, investigations were carried out using the CXCR4 mAb, 12G5 as this fulfils the criteria of acting as a CXCR4 antagonist and can be bound to secondary, fluorescent tagged antibodies, thus questions the need for a 'click' CXCR4 antagonist. Therefore, Oris™ Cell Migration assays were conducted due to their requirement for a 24-hour incubation period. From these experiments it was found that 12G5 was unable to prevent CXCL12 directed migration in PC3 cells. This was most likely due to 12G5 having a lower affinity for the CXCR4 receptor than CXCL12 with research from Zhukovsky et al. (2010) finding that an $IC_{50}$ of only 140 nM CXCL12 could compete with 0.25 µg/mL 12G5 in Cf2Th cells. While 12G5 was unable to prevent CXCL12 directed migration, it was shown previously (Figure 4.50) that AZ6-2 at a concentration of 1 µM was not competed from the CXCR4 receptor by 10 nM CXCL12, thus demonstrating the requirement for CXCR4 antagonists rather than antibodies. Limitations to these investigations are appreciated and would benefit from future investigations such as using AZ6-2, IS4 and 12G5 in the same experiment rather than comparing between two. Additionally, there would be considerable benefit in conducting competition assays using increased CXCL12 concentrations to compete both 12G5 and AZ6-2 from CXCR4 and doing time dependant investigations to find the maximal time that 12G5 can be used as a CXCR4 antagonist. Despite these limitations, it could be concluded that mAb are unsuitable for use as antagonists for long incubation experimentation, thus demonstrates an opportunity for the development of 'click' CXCR4 antagonists.

To enable these novel antagonists to undergo CuAAC click chemistry, structural changes had to occur to AZ6-2 to develop IS1. While IS1 itself cannot undergo CuAAC due to it missing the necessary alkyne group, it was important to determine if the structural changes made to the compound caused any detrimental effects upon its affinity for CXCR4. It was found that the $IC_{50}$ in Jurkat cells rose from 0.28 nM ± 0.18 with AZ6-2 to 68.45 nM ± 59.24 with IS1 and from 0.56 nM ± 0.19 to 19.19 nM ± 17.82 in THP-1 cells. Therefore, IS1 is less potent

than AZ6-2. However, these values remain in the nM range and so the change in the structure of IS1 was not too detrimental. Thus, synthesis of IS4 went ahead and again the $IC_{50}$ values were compared. As with IS1, there was a small decrease in potency but again only in the nM range. For adherent cells, it was found that IS4 had very similar potency to AZ6-2 regarding their ability to reduce CXCL12 stimulated PC3 migratory speeds. Speeds decreased from 77.97 ± 3.53 µm/h to 11.76 ± 4.05 µm/h with the addition of 1 µM AZ6-2 and to 11.76 ± 3.99 µm/h with the addition of 1 µM IS4. $IC_{50}$ values however demonstrated again that AZ6-2 was more potent with an $IC_{50}$ of 128 nM ± 68.88 compared to IS4 with an $IC_{50}$ of 172 nM ± 53.65 in PC3 cells. A similar trend was seen in SKMEL28 cells with AZ6-2 having an $IC_{50}$ of 266.2 nM ± 148.7 compared to IS4 with an $IC_{50}$ of 423 nM ± 229.6 nM. However, much like in the suspension cells, these values remain in the nM range. As before there is a trend that IS4 causes a decrease in migration below the basal level. This might suggest that both AZ6-2 and IS4 are potential inverse agonists and would require further investigation. Alternatively, it is possible that CXCR4 is spontaneously adopting an active conformation that is capable of regulating cellular signalling in the absence of CXCL12 that gets abrogated with the addition of IS4, hence a fall below basal levels (Berg and Clarke, 2018).

As mentioned, IS4 was developed to be an improvement of AZ6-2 and therefore experiments that were conducted on AZ6-2 were repeated with IS4 to determine whether there were any observable differences between these two CXCR4 antagonists. Similar to AZ6-2, IS4 prevented CXCL12 mediated intracellular calcium release from: MCF-7, Jurkat, THP-1 and PC3 cells. While there were initial concerns about the yellow colour of IS4 causing some interference with the calcium release results, overall the colour did not jeopardise the observed conclusion. However, it would be worthwhile to conduct calcium radioligand binding assays which would overcome the problem of background fluorescence.

Unlike AZ6-2, initial results from the internalisation assays demonstrated a trend of decreased fluorescence with the addition of IS4. Therefore, further experimentation had to be conducted using confocal microscopy, which demonstrated that IS4 did not cause CXCR4 internalisation. The most likely cause for this discrepancy is due to the fluorescent microscopy images being only on one focal plane, thus producing only a cross section of the cells and potentially

not capturing a representative image of whole cell CXCR4 that can be captured during confocal microscopy (Sanderson et al., 2014). Alternatively, flow cytometry is a high throughput technique that can compare thousands of cells rather than the tens of cells that are analysed with fluorescent microscopy and so should be conducted to give a much more accurate measurement of CXCR4 expression (Gualda et al., 2017). Alternatively, other more robust assays should be conducted to determine CXCR4 internalization including radioligand binding studies, whole cell ELISA or using the Fluorokine® receptor detection kit from R&D Systems. Finally, investigations into the specificity of AZ6-2 were limited to only two other chemokines: CXCL11 and CCL3 while five further chemokines were investigated for IS4. So many chemokines were investigated due to the promiscuous nature of chemokine receptors which demonstrate a high degree of redundancy with multiple chemokines binding to the same receptor (Bièche et al., 2007, Salazar et al., 2013). Therefore, while the original structure of AZ6-2 was modelled as a CXCL12-mimic, it was sensible to determine if IS4 interacted with other receptors. As hypothesised, IS4 only prevented calcium release or reduced migration from CXCL12 stimulated THP-1 cells. However, there was a trend that IS4 caused a slight decrease in migration of THP-1 cells when stimulated with CCL3, CCL5, CCL8, CXCL8 and CXCL10. Evidence in the literature suggests that CXCR4 can form heterodimers with CCR5, CCR2 and CXCR3 (Contento et al., 2008, Sohy et al., 2007, Watts et al., 2013). Therefore, it is possible that IS4 is inadvertently modulating these dimerized receptors migratory responses via allosteric transinhibition (Sohy et al., 2007).

After determining that the structural changes made to AZ6-2 did not cause any adverse effects to the function, potency or specificity of IS4, it was then determined that IS4 was more stable than AZ6-2 after incubation with FBS for 30 minutes. As mentioned previously, Di Maro et al. (2016) tested the metabolic stability of AZ6-2 via incubation in diluted human plasma at 37˚C for 30-180 minutes and determined that AZ6-2 remained stable up to 180 minutes. This conflicts the data collected here which found AZ6-2 was not stable after 30 minutes. These discrepancies could be due to the different experimental methods (human plasma vs. FBS) or due to the method of analysis (RP-HPLC-ESI vs. calcium release assays). Serum is the liquid portion of the blood obtained after clotting, while plasma is the liquid that remains when clotting is prevented with the addition of an anticoagulant. Therefore, there are considerable differences in

the concentration of certain metabolites. Liu et al. (2010) analysed 72 compounds and found that 36 (50%) of these compounds discriminated serum from plasma, with 29 and 7 metabolites showing a significantly higher abundance in serum and plasma, respectively. Such examples include plasma having significantly reduced levels of most amino acids, hypoxanthine, glycerol-3-phosphate, and β-hydroxybutyrate but with higher concentrations of pyruvate, citrate, glycerate, fumarate, and the nitrogen metabolites urate and hydroxylamine than serum. This suggested that serum is a better representation of whole blood, thus a better representation of how the compounds would fair inside an animal or human. However, future research would benefit from stability investigations using both FBS and human plasma. Overall, this data demonstrated that while AZ6-2 is more potent, IS4 is a more stable compound and therefore would be more suitable for clinical use. Due to AZ6-2 proving to be unstable after 30-minute incubation with FBS, no further experiments were conducted. However, it would be beneficial to conduct stability experiments up to 180 minutes to determine how long IS4 is stable for in FBS.

Despite the success of making IS4 more stable than AZ6-2, clicking IS4 to 3-azido-7-hydroxycoumarin was unsuccessful. As mentioned previously, this was possibly due to the 3-azido-7-hydroxycoumarin being too small and penetrating the nucleus, leading to large accumulations of the dye in the nucleus and only background staining on the cell surface. Investigation then moved away from *in situ* click chemistry and turned to IS7, which is synthesised fully outside of the cells. However, there is still the potential that IS4 might be suitable for *in situ* click chemistry using a different dye. Wang et al. (2012) also noted that dyes had to be large to prevent nuclear penetration during CuAAC and so were investigating a pro-fluorophore dye similar to 3-azido-7-hydroxycoumarin called BODIPY (borondipyrromethene) (Figure 5.48). Like 3-azido-7-hydroxycoumarin, when the azido group was introduced to the 3-position of BODIPY, the electron donating effect of the α-nitrogen of the azido group quenched fluorescence. The CuAAC reaction with a terminal alkyne produced a triazole ring which has a lower electron donating ability than the α-nitrogen and therefore caused the emission of fluorescence. Future research using different dyes such as BODIPY is therefore essential for the future of *in situ* click chemistry with IS4. The other main concern for CuAAC is related to the toxicity presented by the copper catalyst. MTS assays would have to be conducted by incubating cells with $CuSO_4$ and sodium

ascorbate with and without the dye to determine if the concentrations are toxic to the cells. The concentrations used for CuAAC were as described by Li et al. (2010). However, other groups have used different concentrations of both $CuSO_4$ and sodium ascorbate such as Li et al. (2017), whom used a tenfold lower dose of $CuSO_4$. Additionally, Li et al. (2017) found that the addition of *N*-ethylmaleimide (NEM) was required to deactivate intracellular GSH to prevent it complexing with $Cu^1$ and depleting the effect of the catalyst. Additionally, they found that adding DMEM reduced cellular toxicity but decreased reaction rate while adding NEM caused an increase in product yield from 0.8% to 14.9%. Other groups found that buthionine sulfoximine (BSO) can be added which inhibits GSH synthesis or the water-soluble derivatives of tris(triazolylmethyl)amine, a family of ligands that can be used to intercept the generation of ROS (De Nicola and Ghibelli, 2014, Hong et al., 2010). Additionally, it has been found that the CuAAC reaction is very fast with completion occurring after only 5-minute incubation with longer incubation giving rise to increased cytotoxicity (Hong et al., 2010). CuAAC reactions are predominantly carried out at room temperature, but due to the phenomenon of CXCR4 internalisation discussed in Chapter 4, it would be beneficial to determine if CuAAC reactions could be carried out successfully at 4˚C to prevent receptor endocytosis. Additionally, to reduce ROS production the $CuSO_4$/ligand/ sodium ascorbate mixture can be made and allowed to stand for 10 minutes to allow the catalyst to quench the ROS before application to the cells (Hong et al., 2010). This highlights the importance of identifying the optimum CuAAC conditions for future IS4 investigations.

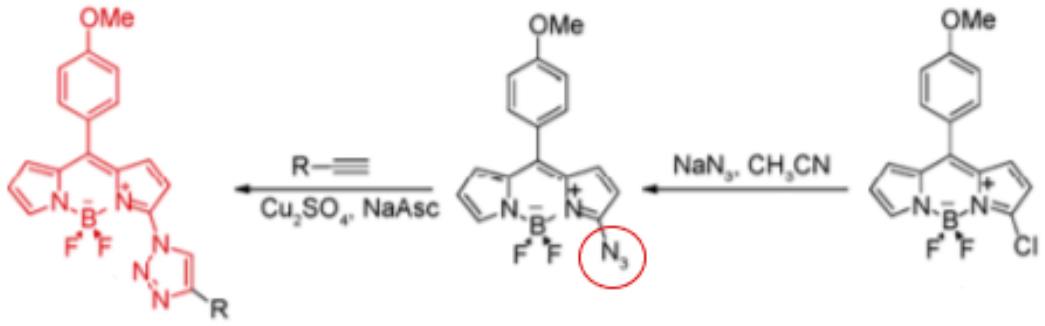


**Figure 5.48: Synthesis of the azide-BODIPY dye and CuAAC reaction (Wang et al., 2012).** Like 3-azido-7-hydroxycoumarin, when the azido group is introduced to the 3-position of BODIPY(circled), the electron donating effect of the α-nitrogen of the azido group quenches fluorescence. During the CuAAC reaction, a triazole ring is produced which has a lower electron donating ability than the α-nitrogen enabling the emission of fluorescence.

Investigations then turned to IS7. While it was shown that IS7 functioned as a click compound, these experiments should be conducted again using IS1 as a control. Again, initial experiments were conducted to determine if the growing size of the compound was effecting its potency and or specificity. Initial investigations found that IS7 prevented CXCL12 mediated intracellular calcium release from MCF-7, Jurkat, THP-1 and PC3 cells, reduced CXCL12 stimulated migratory speeds and inhibited CXCL12 stimulated PC3 cell migration. Additionally, the compound was found to be specific to the CXCR4 receptor. Therefore, IS7 was the same in its function and specificity as IS4. Unfortunately, the potency of the compound was not investigated due to limited resources, highlighting the requirement for these experiments in the future. Additionally, it is paramount to determine the stability of IS7. The most important finding was that IS7 proved to successfully bind to CXCR4 and enable fluorescence. This proves the principle that this CXCR4 antagonist can be clicked to a dye for specific CXCR4 receptor targeting and in theory could be clicked to other agents such as chemotherapeutic agents. This technique shows the potential not only for the use of this click CXCR4 antagonist for scientific investigation, but also for therapeutic use as a multifunctional tool preventing CXCL12 stimulated migration of cancer cells as well as targeting these cells for death.

## 5.5. Conclusions

Overall, the results shown here demonstrate that the structural changes made to IS4 still enabled it to function as a CXCR4 antagonist while maintaining its potency. Additionally, IS4 was proven to be a CXCR4 specific antagonist with improved stability over AZ6-2. While initial *in situ* CuAAC click chemistry reactions using IS4 and the dye 3-azido-7-hydroxycoumarin were unsuccessful, this failure is most likely related to the dye rather than IS4 with future research into alternatives dyes being paramount. The subsequent development of IS7, bound to 3-azido-7-hydroxycoumarin *ex situ*, proved that this compound can be clicked to a fluorescent dye for laboratory uses such as in competitive binding assays. More importantly, these results open up the potential for this CXCR4 antagonist to be clicked to other agents such as chemotherapeutic agents for duel function cancer therapeutics.

# Chapter 6: Investigations into ACKR3/CXCR7 Expression, Internalisation and Influence on CXCL12 Stimulated Cancer Cell Migration

## 6.1. Introduction

ACKR3 expression has been found to be up-regulated in a number of pathological conditions such as inflammatory bowel disease, encephalitis, rheumatoid arthritis, acute renal failure and in cancer such as prostate, kidney, liver, brain, lung and breast cancer (Neves et al., 2019). However, while it is agreed that ACKR3 had modulating effects upon the CXCR4/CXCL12 pathway in these cancers, there are contradictory studies into whether ACKR3 expression is associated with a positive or negative effect in cancer and/or cancer metastasis.

Wang et al. (2008) found that ACKR3 was highly expressed on the human prostate cancer cell line PCa which correlated with increased aggression of the tumour due to its ability to enhance cell proliferation, cell survival, adhesion and chemotaxis. Salazar et al. (2014) saw that in the breast cancer cell line MCF-7, the downregulation of ACKR3 caused a decrease in growth which was related to the inhibition of cell cycle progression shown via increased p21 levels and decreased levels of Cyclin B1. This group also established that down regulation of ACKR3 decreased levels of ERK1/2 activation, thus decreasing cellular proliferation. Additionally, in lung cancer it has been shown that ACKR3 expression can also lead to tumour cell survival, enhanced proliferation and the enhanced progression of lung metastasis (Miao et al., 2007). Alternatively, some research groups have noted ACKR3 to function as a decoy receptor for CXCR4. Luker et al. (2010) found that in MDA-MB-231 breast cancer cells, ACKR3 has a 10-fold higher binding affinity to CXCL12 relative to CXCR4 and once bound, ACKR3 internalizes and degrades CXCL12, removing it from the extracellular space thus regulating receptor signalling. Confirming this hypothesis, in a study by Stacer et al. (2016) mice with deleted ACKR3 receptors had elevated levels of CXCL12 which resulted in greater experimentally-stimulated breast cancer metastasis including metastatic bone cancer. This led Stacer et al. (2016) to the conclusion that endothelial ACKR3 expressions supresses tumour growth, vascular intravasation, cellular survival and proliferation of breast cancer cells.

Not only is there conflicting evidence whether ACKR3 positively or negatively affects migration in different solid tumour cell types, but there is even conflicting evidence regarding the role of ACKR3 in CXCL12-stimulated migration in suspension cells and suspension cell lines. Research by Balabanian et al. (2005) and Levoye et al. (2009) demonstrated that ACKR3 promoted CXCL12 driven

migration in peripheral blood leukocytes extracted from healthy volunteers. Furthermore, incubation with 9C4 (anti-ACKR3) and subsequent transwell assays demonstrated a reduction in migration of these cells (Balabanian et al., 2005). Another research group, Melo et al. (2014), found that the silencing of ACKR3 in Jurkat cells caused decreased CXCL12 driven migration. In THP-1 cells, Sánchez-Martín et al. (2011) saw that using both an ACKR3 inhibitor, CCX733, and via ACKR3 silencing there was a reduction in CXCL12 directed cellular migration. Opposing this, Hartmann et al. (2008) found that using the anti-ACKR3 mAb, 11G8, ACKR3 did not promote CXCL12 driven migration in peripheral blood leukocytes from healthy volunteers.

There is even conflicting data over cellular expression and cellular localization of the ACKR3 receptor. In a study by Luker et al. (2010), ACKR3 continuously cycled between the cell surface and the endosomal compartment in a ligand independent manner in MCF-7 cells with a preference for intracellular localization that was enhanced with the addition of CXCL12. Opposing this, research by Hattermann et al. (2014) saw that the localisation of the receptor could be seen clearly on the cell surface of MCF-7 cells with only the addition of CXCL12 causing ACKR3 internalisation. Additionally, Luker et al. (2010) found that the internalisation of the ACKR3 receptor was owing to clathrin mediated endocytosis in transfected MDA-MB-231 cells however, did not explore if this was the case for MCF-7 cells. There is also conflicting data about the cellular localization of ACKR3 in suspension cells. A study by Tarnowski et al. (2010) showed that expression of ACKR3 was easily detected at the cell surface of THP-1 cells. While Melo et al. (2014) and Piovan et al. (2018) found that ACKR3 expression in Jurkat cells was localised both on the cell surface and intracellularly with a predilection for intracellular localisation.

Overall, there is both conflicting and limited research into the cellular expression and internalization capabilities of ACKR3 as well as the role of ACKR3 in suspension cell migration.

## 6.2. Chapter Aims and Hypotheses

**Hypothesis**: That inhibition of ACKR3 will prevent CXCL12 stimulated migration in the two suspension cell lines: Jurkat and THP-1. Additionally, that different cell lines will have varied ACKR3 expression, varied localization of ACKR3 and varied methods of endocytosis.

**Aims:** To confirm ACKR3 expression in MCF-7, Jurkat, THP-1 and PC3 cells and determine the cellular localisation of ACKR3 in these cell lines. To examine the role of ACKR3 in CXCL12 directed Jurkat and THP-1 cancer migration using a specific ACKR3 mAb. Finally, to determine by which method ACKR3 receptor internalisation is occurring. This will give a pharmacological insight into the role of ACKR3 in suspension cell migration and provide more information on ACKR3 receptor activity at the cell surface.

## 6.3. Results

### 6.3.1. ACKR3 is expressed in MCF-7, Jurkat, THP-1 and PC3 cells

Preliminary experiments were conducted to confirm the expression of ACKR3 in two adherent cell lines (MCF-7 and PC3) and two suspension cell lines (THP-1 and Jurkat). Cell surface expression of ACKR3 in MCF-7, PC3, THP-1 and Jurkat cells had already been reported by Hattermann et al. (2014), Tarnowski et al. (2010), Melo et al. (2014), Piovan et al. (2018) and Wang et al. (2008) and was confirmed using the monoclonal antibody against ACKR3, 11G8 (Figure 6.1).

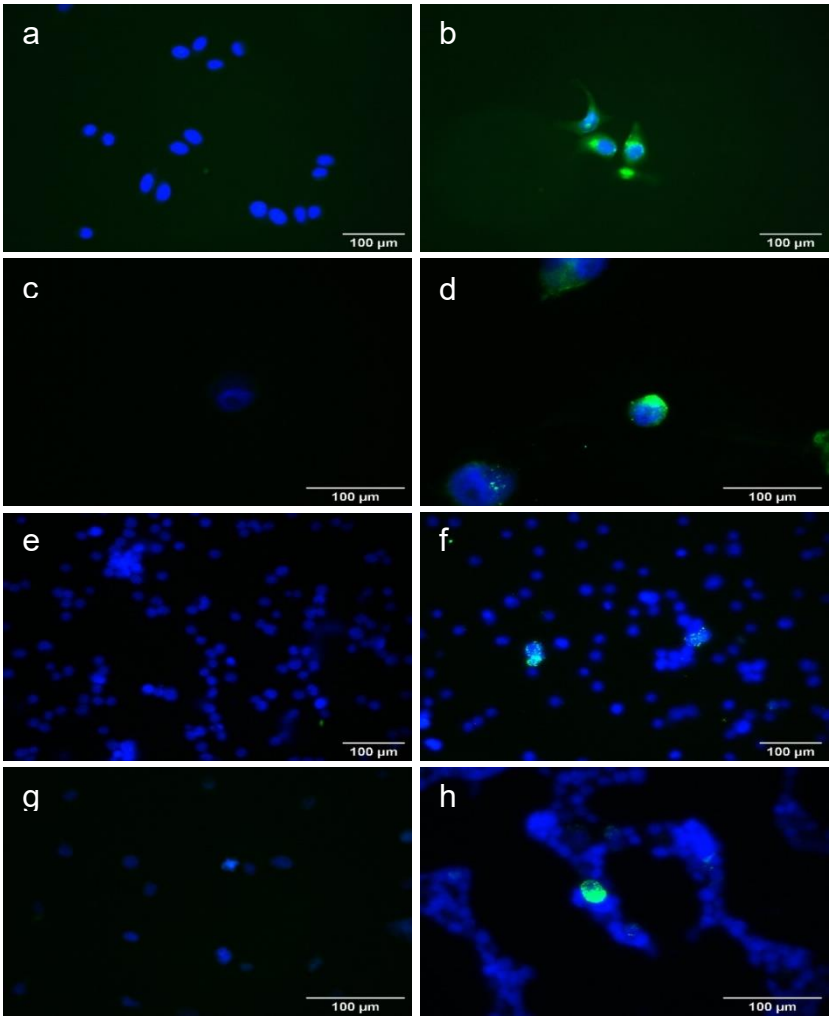


**Figure 6.1: ACKR3 expression in MCF-7, PC3, Jurkat and THP-1 cells. a)** Negative control MCF-7 cells were treated with secondary anti-mouse Alexa Fluor® 488 antibody (green), DAPI (blue) and fixed with 4% paraformaldehyde before imaging. **b)** Positive control whereby ACKR3 was visualised on MCF-7 cells using mouse 11G8 primary mAb, secondary anti-mouse Alexa Fluor® 488 antibody (green), DAPI (blue) and fixed with 4% paraformaldehyde before imaging. **c)** Negative control PC3 cells were fixed with 4% paraformaldehyde then treated with secondary anti-mouse Alexa Fluor® 488 antibody (green) and DAPI (blue). **d)** Positive control PC3 cells were fixed with 4% paraformaldehyde then ACKR3 was visualised using mouse 11G8 primary mAb, secondary anti-mouse Alexa Fluor® 488 antibody (green) and DAPI. **e)** Negative control Jurkat cells (as MCF-7 negative control). **f)** Positive control Jurkat cells (as MCF-7 positive control). **g)** Negative control THP-1 cells (as MCF-7 negative control). **h)** Positive control THP-1 cells (as MCF-7 positive control). Data shows representative cells from 3-8 independent experiments with similar findings. Acquired with Leica imaging suite with either a 40x or 63x objective with 22x or 35x overall magnification.

### 6.3.2. ACKR3 expression is lost at 37˚C in MCF-7 and Jurkat cells but not in THP-1 or PC3 cells

As shown in Figure 6.1 all four cell lines express ACKR3 with MCF-7 and PC3 cells showing homogenous expression, while the two suspension cell lines THP-1 and Jurkat cells had a more heterogeneous expression of ACKR3. However, the expression of ACKR3 at the cell surface conflicts with results from other research groups. Yet, what was not consistent between these research groups was the method of identifying ACKR3 expression. For example, Melo et al. (2014) conducted FACS at room temperature to determine ACKR3 expression and localization in Jurkat cells. As previously discussed, the rate of cell surface receptor endocytosis at 10˚C or below should be negligible while receptor endocytosis is mostly temperature independent between 14 and 37˚C (Weigel and Oka, 1981). Therefore, the experiments conducted by Melo et al. (2014) which found that ACKR3 was located both at the cell surface and intracellularly could be conflicting the results of Figure 6.1 (conducted at 4˚C in an attempt to prevent receptor internalisation) solely because of the increase in temperature. Such an investigation was conducted by Naumann et al. (2010) using Daudi B cells. Briefly, control cells were incubated at 0˚C and FACS was conducted to determine both CXCR4 and ACKR3 expression levels. Following this, the cells were warmed to 37˚C and after an hour FACS was again conducted. Results demonstrated a significant decrease in both ACKR3 and CXCR4 expression on these cells after one-hour incubation at 37˚C. Furthermore, the discrepancy between Luker et al. (2010); whom found that in MCF-7 cells, 70% of ACKR3 had internalized after 30 minutes at 37˚C and Hattermann et al. (2014); whom found that ACKR3 could clearly be seen at the cell surface of MCF-7 cells after various incubation time points at 37˚C, could simply be as a result of using different experimental methods: flow cytometry vs. immunolabeling. Additionally, comparison between their methods demonstrates that Luker et al. (2010) incubated the MCF-7 cells with the mAb 11G8 for one hour before shifted the temperature to 37 ˚C and then incubating with secondary antibodies while Hattermann et al. (2014) incubated both 11G8 and secondary antibodies at 4˚C before shifting the temperature. Therefore, the methodology conducted by Hattermann et al. (2014) could have prevented temperature triggered ACKR3 internalisation.

Owing to these conflicting studies, it seemed paramount to conduct an investigation into the effect of temperature upon the internalisation of ACKR3 in MCF-7, PC3, Jurkat and THP-1 cells. By standardising the methodology, ACKR3 expression and internalisation can be compared between these cell lines. These experiments demonstrated that incubation at 37˚C triggered the internalisation of ACKR3 in MCF-7 and Jurkat cells, but not in PC3 or THP-1 cells (Figure 6.2-6.5).

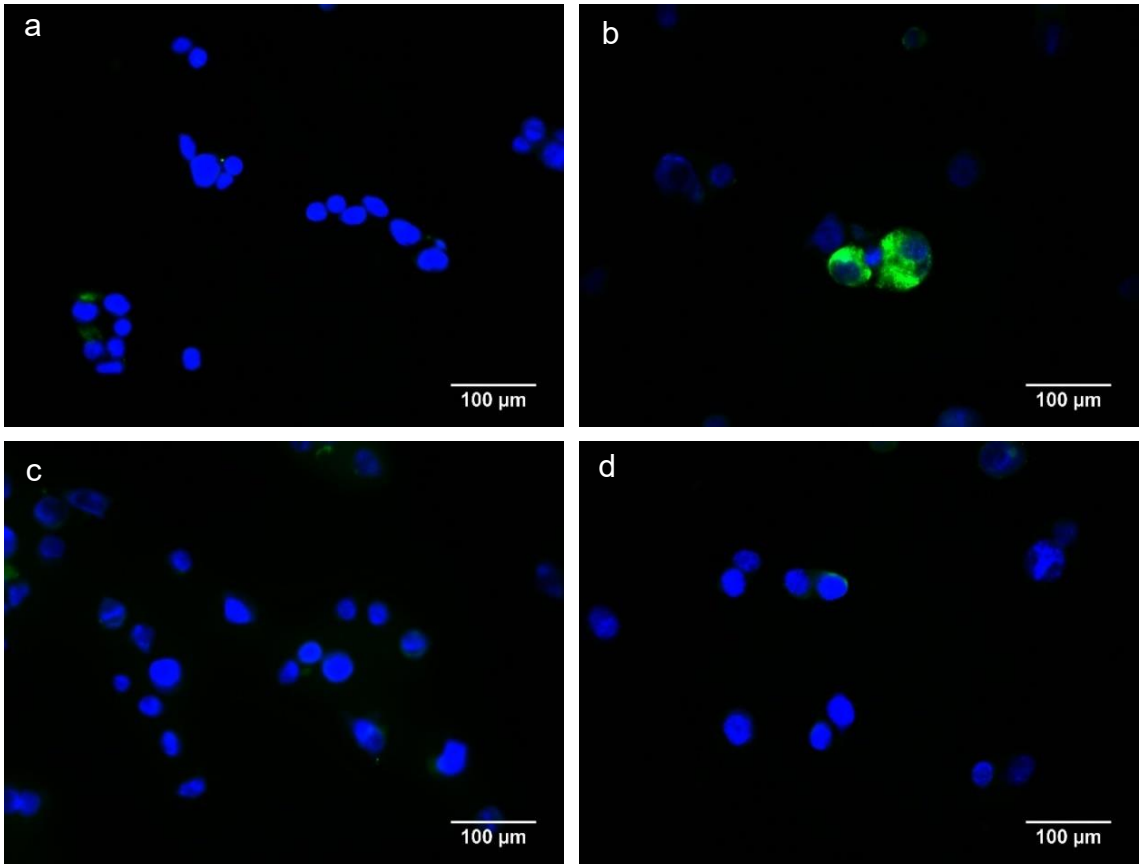


**Figure 6.2: Incubation at 37˚C causes the internalisation of the ACKR3 receptor in MCF-7 cells. a)** Negative control MCF-7 cells were treated with secondary anti-mouse Alexa Fluor® 488 antibody (green) and DAPI (blue) at 4˚C then fixed with 4% paraformaldehyde before imaging. **b)** Positive control whereby ACKR3 was visualised on MCF-7 cells using mouse 11G8 primary mAb, secondary anti-mouse Alexa Fluor® 488 antibody (green) and DAPI (blue) at 4˚C then fixed with 4% paraformaldehyde. **c)** Negative control MCF-7 cells were treated with secondary anti-mouse Alexa Fluor® 488 antibody (green) and DAPI (blue) at 37˚C then fixed with 4% paraformaldehyde before imaging. **d)** Positive control whereby ACKR3 was visualised on MCF-7 cells using mouse 11G8 primary mAb, secondary anti-mouse Alexa Fluor® 488 antibody (green) and DAPI (blue) at 37˚C then fixed with 4% paraformaldehyde. Data shows representative cells from 8 independent experiments with similar findings. Acquired with Leica imaging suite with 40x objective, 22x overall magnification.

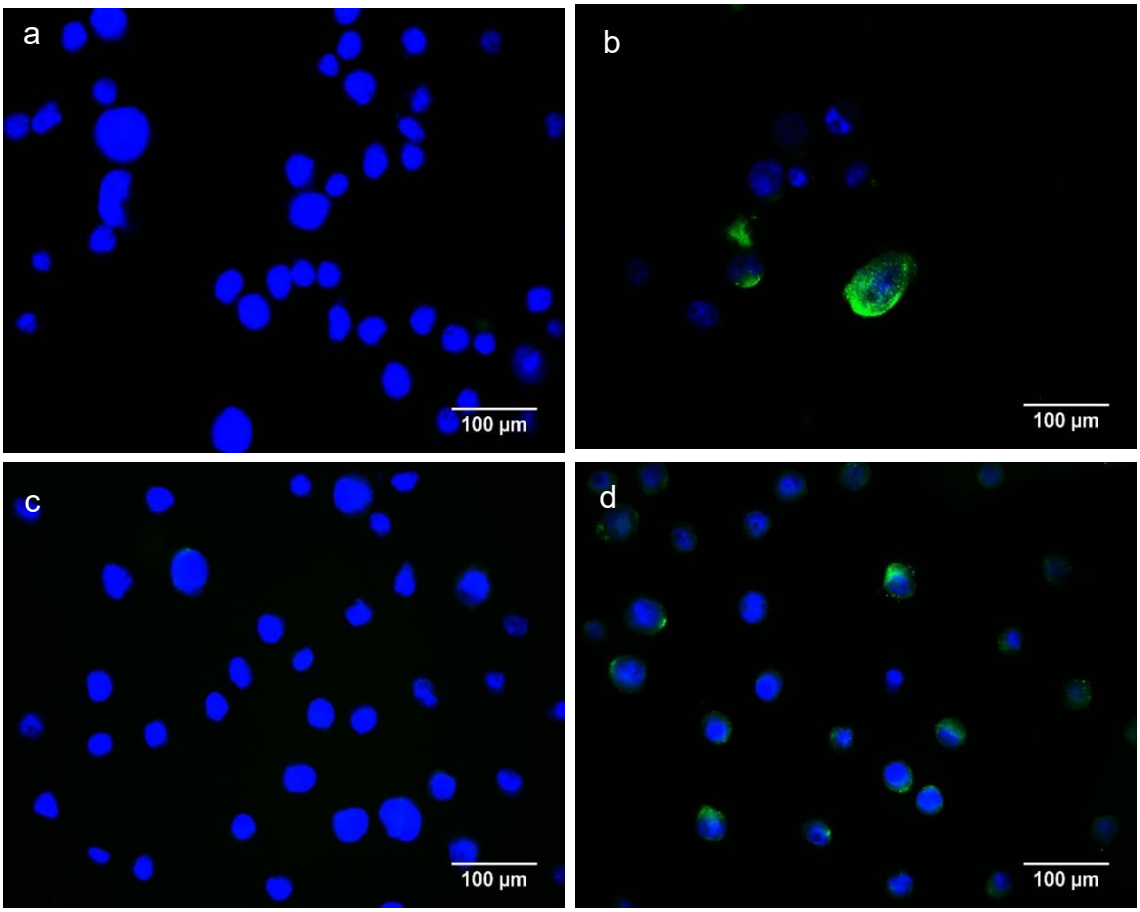


**Figure 6.3: Incubation at 37˚C does not cause the internalisation of the ACKR3 receptor in PC3 cells. a)** Negative control PC3 cells were fixed with 4% paraformaldehyde then treated with secondary anti-mouse Alexa Fluor® 488 antibody (green) and DAPI (blue) at 4˚C. **b)** Positive control whereby PC3 cells were fixed with 4% paraformaldehyde then ACKR3 was visualised using mouse 11G8 primary mAb, secondary anti-mouse Alexa Fluor® 488 antibody (green) and DAPI at 4˚C. **c)** Negative control PC3 cells were fixed with 4% paraformaldehyde then treated with secondary anti-mouse Alexa Fluor® 488 antibody (green) and DAPI (blue) at 37˚C. **d)** Positive control whereby PC3 cells were fixed with 4% paraformaldehyde then ACKR3 was visualised using mouse 11G8 primary mAb, secondary anti-mouse Alexa Fluor® 488 antibody (green) and DAPI at 37˚C. Data shows representative cells from 3 independent experiments with similar findings. Acquired with Leica imaging suite with 40x objective, 22x overall magnification.

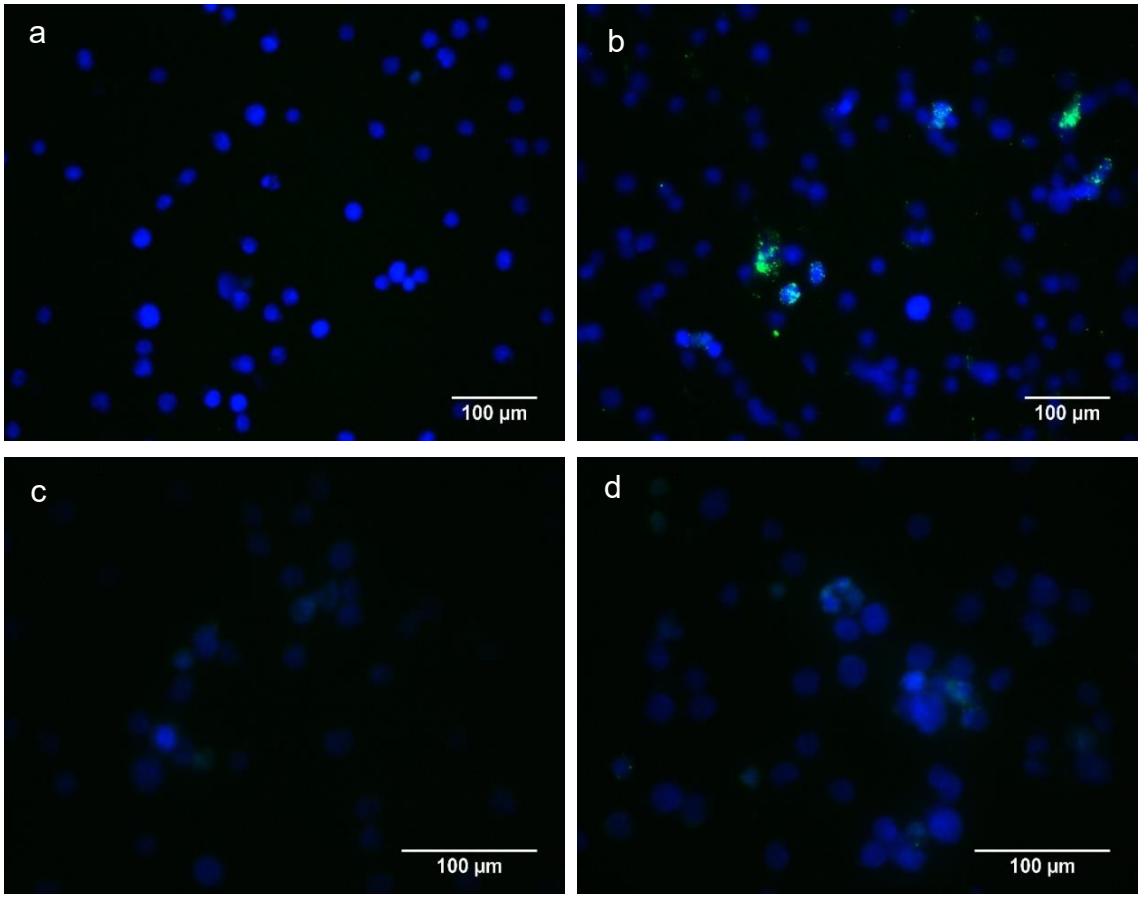


**Figure 6.4: Incubation at 37˚C causes the internalisation of the ACKR3 receptor in Jurkat cells**. **a)** Negative control Jurkat cells were treated with secondary anti-mouse Alexa Fluor® 488 antibody (green) and DAPI (blue) at 4˚C then fixed with 4% paraformaldehyde before imaging. **b)** Positive control whereby ACKR3 was visualised on Jurkat cells using mouse 11G8 primary mAb, secondary anti-mouse Alexa Fluor® 488 antibody (green) and DAPI (blue) at 4˚C then fixed with 4% paraformaldehyde. **c)** Negative control Jurkat cells were treated with secondary anti-mouse Alexa Fluor® 488 antibody (green) and DAPI (blue) at 37˚C then fixed with 4% paraformaldehyde before imaging. **d)** Positive control whereby ACKR3 was visualised on Jurkat cells using mouse 11G8 primary mAb, secondary anti-mouse Alexa Fluor® 488 antibody (green) and DAPI (blue) at 37˚C then fixed with 4% paraformaldehyde. Data shows representative cells from 5 independent experiments with similar findings. Acquired with Leica imaging suite with 40x or 63x objective, 22x or 35x overall magnification.

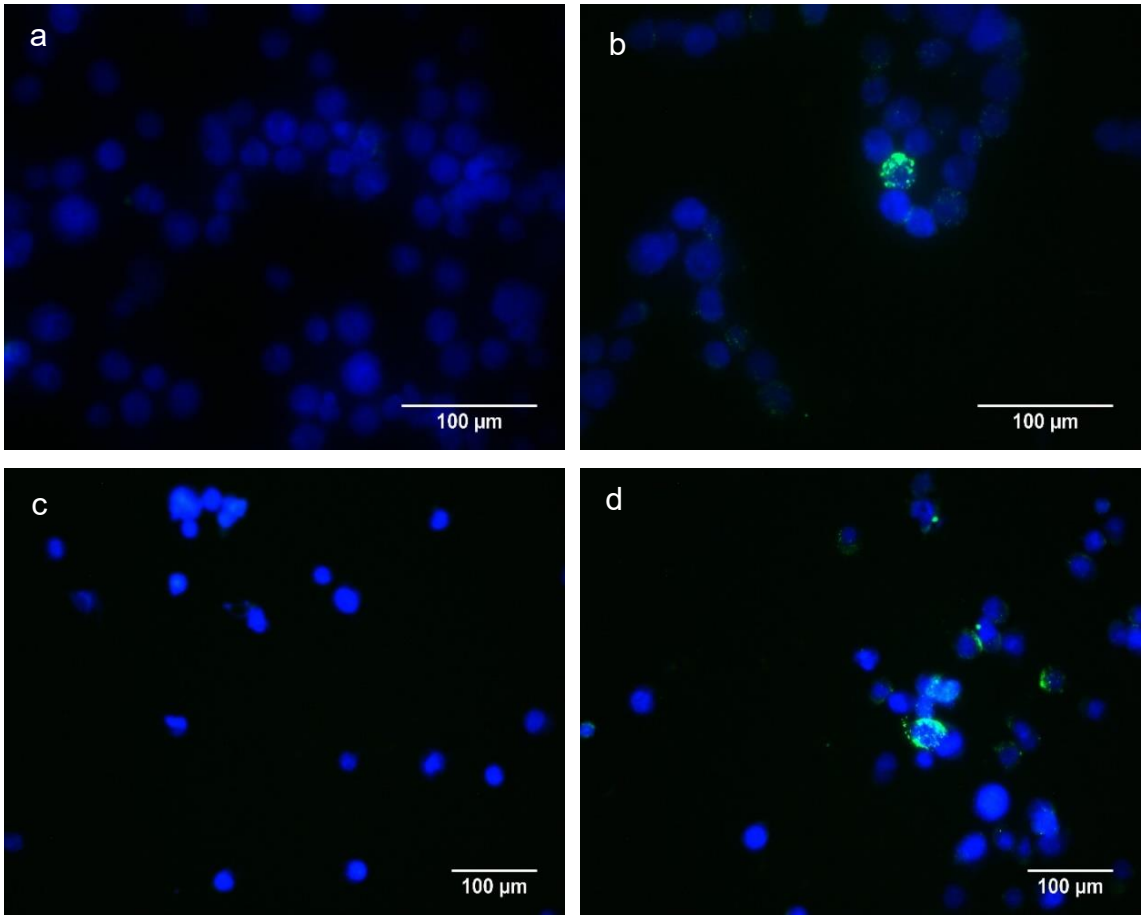


**Figure 6.5: Incubation at 37˚C does not cause the internalisation of the ACKR3 receptor in THP-1 cells. a)** Negative control THP-1 cells were treated with secondary anti-mouse Alexa Fluor® 488 antibody (green) and DAPI (blue) at 4˚C then fixed with 4% paraformaldehyde before imaging. **b)** Positive control whereby ACKR3 was visualised on THP-1 cells using mouse 11G8 primary mAb, secondary anti-mouse Alexa Fluor® 488 antibody (green) and DAPI (blue) at 4˚C then fixed with 4% paraformaldehyde. **c)** Negative control THP-1 cells were treated with secondary anti-mouse Alexa Fluor® 488 antibody (green) and DAPI (blue) at 37˚C then fixed with 4% paraformaldehyde before imaging. **d)** Positive control whereby ACKR3 was visualised on THP-1 cells using mouse 11G8 primary mAb, secondary anti-mouse Alexa Fluor® 488 antibody (green) and DAPI (blue) at 37˚C then fixed with 4% paraformaldehyde. Data shows representative cells from 5 independent experiments with similar findings. Acquired with Leica imaging suite with 63x or 40x objective, 35x or 22x overall magnification.

Preliminary results with flow cytometry conducted on Jurkat cells also confirmed quantitatively that at 4˚C there was expression of ACKR3 that was lost when these cells were incubated at 37˚C or incubated with 15 nM of CXCL12 (Figure 6.6.)

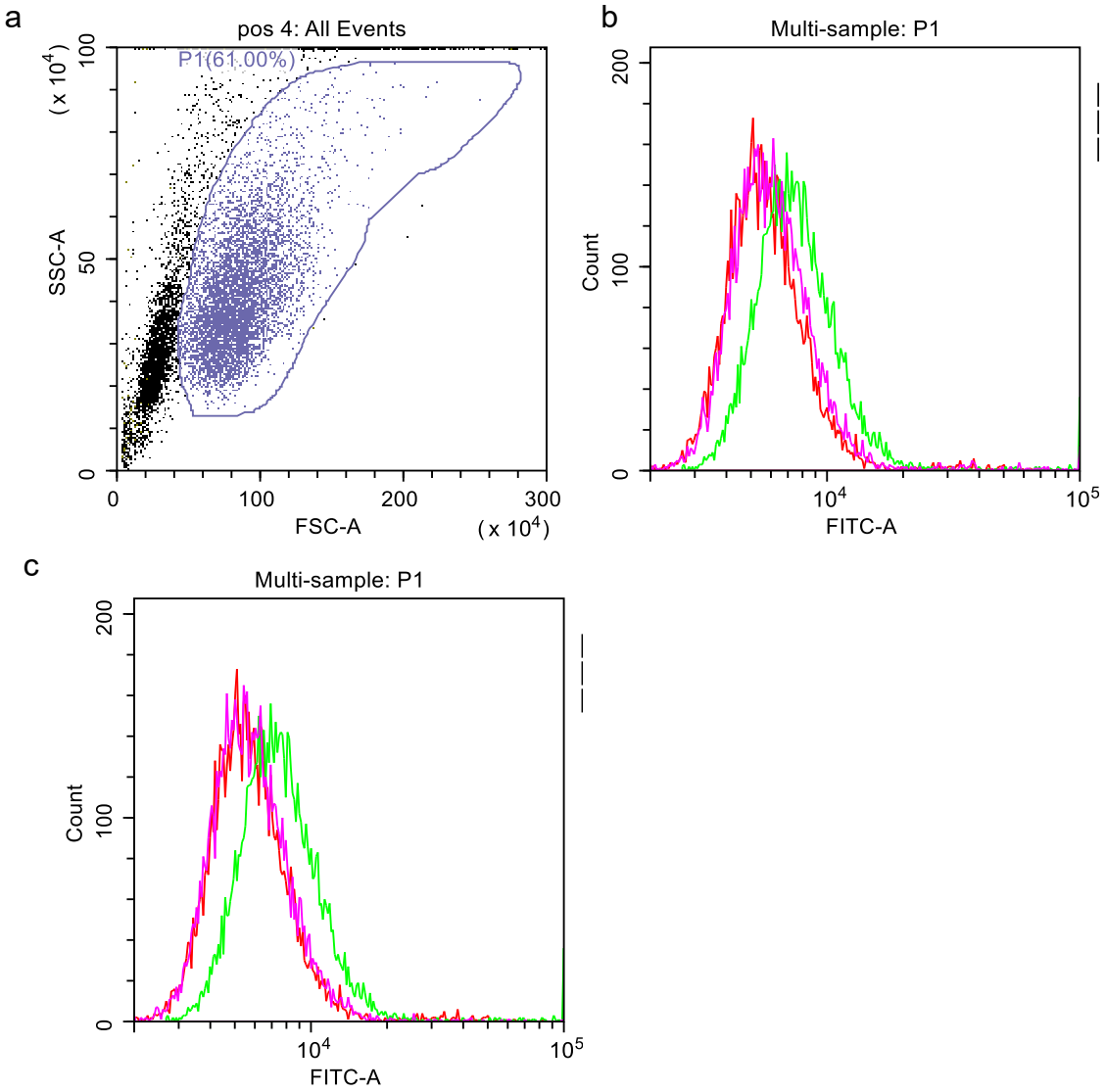


**Figure 6.6: Incubation for 1 hour at 37˚C and incubation with 15 nM CXCL12 causes the internalisation of the ACKR3 receptor in Jurkat cells.** Jurkat cells were incubated for 1 hour with or without CXCL12, 1 hour with primary 11G8 mAb (except negative control cells) and 1 hour with secondary anti-mouse Alexa Fluor® 488 antibody before analysis. **a)** P1 gate shows live Jurkat cell population incubated at 4˚C. **b)** Shift in fluorescence of P1 gated Jurkat cells from negative control (red) to positive control at 4˚C (green), and cells incubated at 37˚C (pink). **c)** Shift in fluorescence of P1 gated Jurkat cells from negative control (red) to positive control at 4˚C (green), induction with 15 nM CXCL12 (pink). Preliminary results from 1 experiment.

### 6.3.3. ACKR3 internalisation in MCF-7 cells occurs via caveolin-dependent endocytosis

Endocytosis is a cellular process whereby molecules are transported into the cell via cell membrane engulfment (Xu et al., 2017). There are two major classifications of endocytosis: phagocytosis and pinocytosis, the distinction between the two being the size of the ingestible particle (Figure 6.7, Table 6.1).

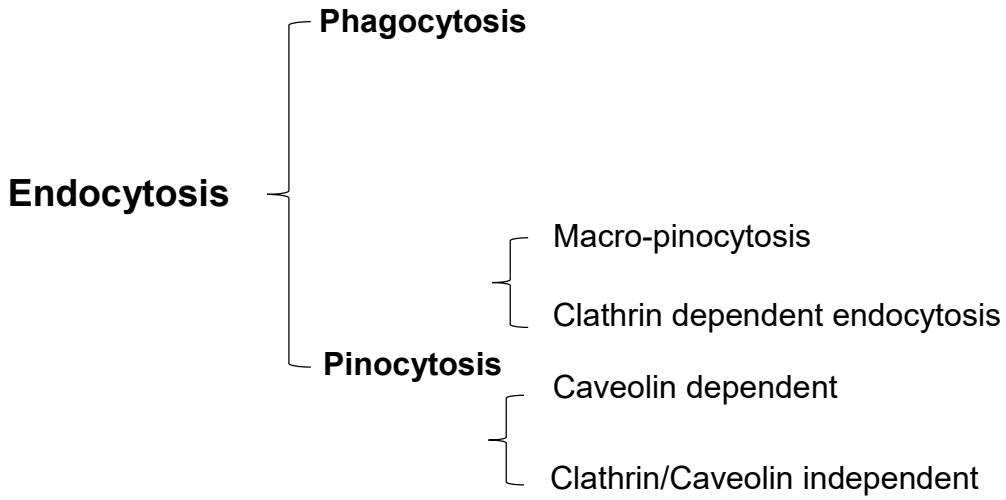


**Figure 6.7: Overview of endocytosis (adapted from (Xu et al., 2017).** Endocytosis is a cellular process whereby molecules are transported into the cell via cell membrane engulfment. Endocytosis is classified into phagocytosis and pinocytosis. Pinocytosis can be further classified into four subtypes: macropinocytosis, clathrin-dependent endocytosis (CDE), caveolin-dependent endocytosis, and clathrin/caveolae-independent endocytosis**.**

**Table 6.1: Features of endocytosis (adapted from (Xu et al., 2017).** Features of endocytosis are summarised in relation to the size of the internalised particle, the membrane domain localization and the internalisation cargo.

| Endocytosis Class | Phagocytosis | Pincocytosis | | | |
|---|---|---|---|---|---|
| | | Macro-pinocytosis | Clathrin-dependent endocytosis (CDE) | Caveolin-dependent endocytosis | Clathrin/caveolin independent endocytosis |
| Vesicle Size | 0.5-10 µm | 0.1-5 µm | <120 nm | <80 nm | <50 nm |
| Membrane Domain Localization | Lipid and non-lipid raft | Lipid and non-lipid raft | Non-lipid raft | Lipid raft | Lipid raft |
| Internalisation Cargo | Pathogens Apoptotic remnants | Fluids bacteria | GPCR Toxins Receptor Tyrosine Kinase Transferrin receptor | Insulin-like growth factor I receptor | Interleukin 2 receptor β |

Phagocytosis generally involves the ingestion of large and solid particles such as pathogens or apoptotic remnants while pinocytosis refers to the internalization of liquids via endocytic vesicles. Pinocytosis can be further classified into four subtypes: macropinocytosis, clathrin-dependent endocytosis (CDE), caveolin-dependent endocytosis, and clathrin/caveolae-independent endocytosis (Xu et al., 2017).

Briefly, CDE requires the assembly of a protein complex on the cytosolic side of the plasma membrane in order to induce curvature and the formation of a vesicle that can become pinched off, internalizing the surface cargo (Figure 6.8) (Tourdot and Radhakrishnan, 2013). This protein complex consists of FCHo1/2, Eps15, Intersectin-1 and enables AP-2 and Epsin to be recruited to the plasma membrane and initiates curvature (Benmerah et al., 1998, Henne et al., 2010, Lundmark and Carlsson, 2010). Specifically, $PIP_2$ in the plasma membrane anchors these proteins and protein complexes and coordinates curvature (Lundmark and Carlsson, 2010). AP-2 then recruits clathrin, a triskelion scaffolding protein that has three ‘legs’ all of which can bind to AP-2, polymerise and form a basket-like lattice (Rappoport et al., 2006). Curvature continues and a budding vesicle begins to emerge from the membrane with a tubular neck that is uncovered by clathrin and has high amounts of $PIP_2$ (Ringstad et al., 1999). Dynamin is then recruited and forms a helical collar around the neck which pinches off the vesicle (Fournier et al., 2003). The clathrin coat is then disassembled by several proteins including; Rab5, Auxillin and HSC70 and the vesicle can then fuse with an endosome for sorting and recycling or, if the endosome fuses to a lysosome, vesicle degradation (Tourdot and Radhakrishnan, 2013).

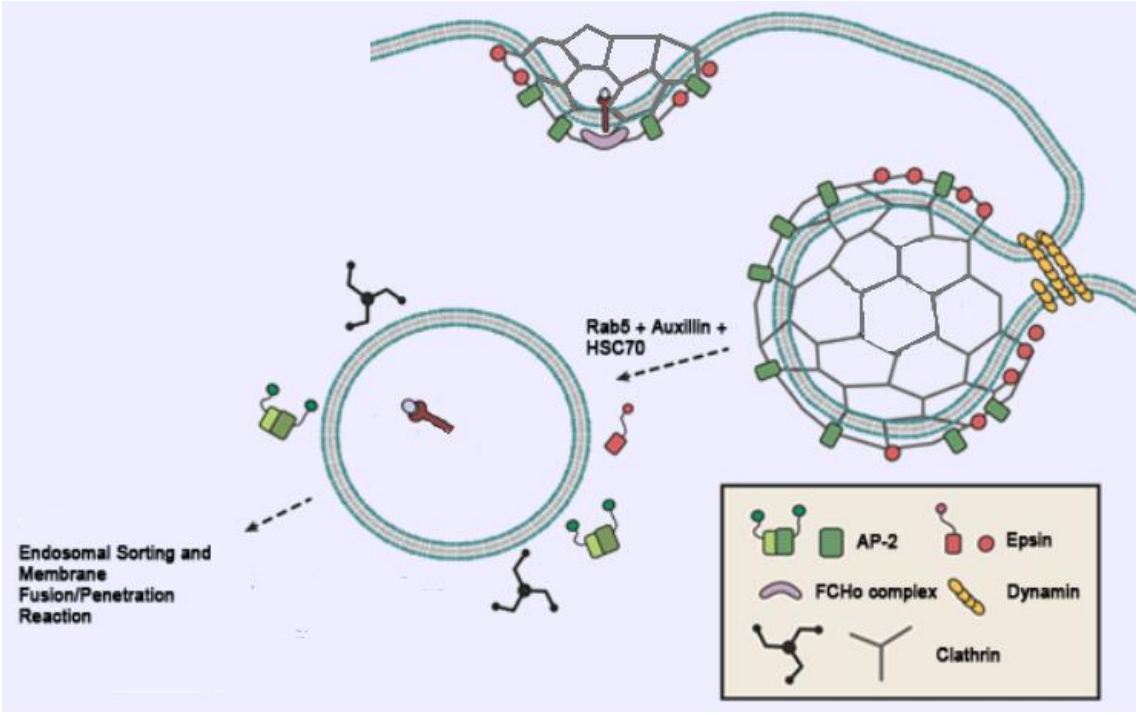


**Figure 6.8: Clathrin dependant endocytosis (CDE) adapted from (Tourdot and Radhakrishnan, 2013)**. CDE requires the assembly of the FCHo protein complex on the cytosolic side of the plasma membrane which in turn recruits AP-2 and Epsin. AP-2 then recruits clathrin which forms a basket-like lattice and initiates the curvature of the membrane. Curvature continues creating a budding vesicle that dynamin forms a helical collar around to pinch off the vesicle. The clathrin coat is then disassembled by several proteins including; Rab5, Auxillin and HSC70 and the vesicle can then fuse with an endosome for sorting.

Less is known about caveolin-dependent endocytosis except that the main structural protein caveolin -1, which inserts in the bilayer like a hairpin, is anchored to the plasma membrane by the cytoskeleton. Endocytosis then depends upon caveolin-1 phosphorylation, cytoskeletal reorganisation and the recruitment of dynamin to pinch off the vesicle (Kiss and Botos, 2009). The major factor discriminating CDE and caveolin-dependent endocytosis is that CDE occurs on a more fluid membrane while caveolin-dependent endocytosis occurs in specific, more rigid regions of the membrane called lipid rafts (Pike, 2003, Xu et al., 2017). Lipid rafts are areas of the membrane that are rich in sphingolipids, glycosysylphosphatidylinositol (GPI)-anchored proteins, cholesterol and caveolins amongst other components and are resistant to detergents such as Triton X-100 (Pike, 2003). While the exact roles of lipid rafts in the membrane are still to be fully elucidated, it has been suggested that they have major roles in enhancing signal transductions as well as organising, sorting and trafficking

signalling molecules due to the accumulation of receptors to this location including CXCR4 (Brown and London, 1998, Alonso and Millán, 2001, Simons and Sampaio, 2011).

Generally, GPCRs including the CXCR4 receptor undergo CDE (Table 6.1) (DeNies et al., 2019, Xu et al., 2017, Ferreira et al., 2012). Despite ACKR3 no longer being classified as a GPCR, it was still hypothesised that all ACKR3 internalization must occur through CDE due to ACKR3 associating with β-arrestin 2 which mediates CDE (Shenoy and Lefkowitz, 2003, Luker et al., 2010, Zabel et al., 2009). Supporting this, Luker et al. (2010) found that ACKR3 internalisation in MDA-MB-231 breast cancer cells occurred via CDE. However, a recent study by Montpas et al. (2018) demonstrated that β-arrestins are not always required for chemokine scavenging by ACKR3 and internalisation could be triggered by other, unknown, scaffolding proteins. Therefore, some preliminary experiments were conducted in MCF-7 cells using Pitstop 2, an inhibitor of CDE; Methyl-β-cyclodextrin (MCD) and filipin, inhibitors of caveolin-dependent endocytosis and finally CK666 and Dynasore, two non-specific endocytosis inhibitors. Incubation with the Pitstop 2, CK666 and Dynasore failed to prevent ACKR3 internalisation in MCF-7 cells. However, incubation with the two caveolin-dependent endocytosis inhibitors prevented ACKR3 internalisation (Figure 6.9). This suggests that the internalisation of ACKR3 in MCF-7 cells is likely to occur via caveolin-dependent endocytosis.

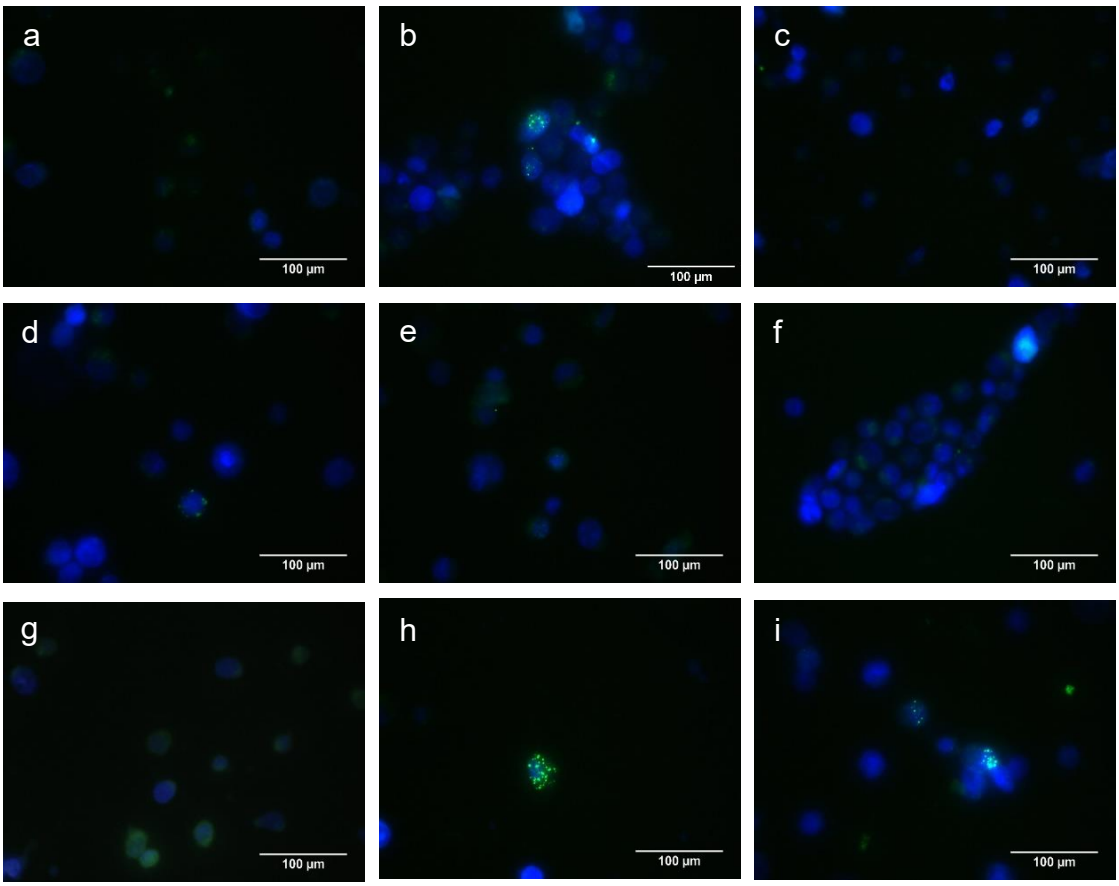


**Figure 6.9: Incubation with filipin and MCD prevents the internalisation of ACKR3 in MCF-7 cells**. **a)** Negative control MCF-7 cells were treated with secondary anti-mouse Alexa Fluor® 488 antibody (green) and DAPI (blue) at 4˚C then fixed with 4% paraformaldehyde before imaging. **b)** Positive control whereby ACKR3 was visualised on MCF-7 cells using mouse 11G8 primary mAb, secondary anti-mouse Alexa Fluor® 488 antibody (green) and DAPI (blue) at 4˚C then fixed with 4% paraformaldehyde. **c)** MCF-7 cells treated with mouse 11G8 primary mAb, secondary anti-mouse Alexa Fluor® 488 antibody (green) and DAPI (blue) at 37˚C then fixed with 4% paraformaldehyde. **d)** MCF-7 cells incubated with 30 µM Pitstop 2 then treated with mouse 11G8 primary mAb, secondary anti-mouse Alexa Fluor® 488 antibody (green) and DAPI (blue) at 37˚C then fixed with 4% paraformaldehyde. **e)** MCF-7 cells incubated with 30 µM Pitstop 2 negative control. ACKR3 visualised as d). **f)** MCF-7 cells incubated with 10 µM CK666. ACKR3 visualised as d). **g)** MCF-7 cells incubated with 60 µM Dynasore. ACKR3 visualised as d). **h)** MCF-7 cells incubated with 5 µg/mL filipin. ACKR3 visualised as d). **i)** MCF-7 cells incubated with 10 mM MCD. ACKR3 visualised as d). Data shows representative cells from 3 independent experiments with similar findings. Acquired with Leica imaging suite with 63x objective, 35x overall magnification.

### 6.3.4. In the absence of CXCL12, ACKR3 internalisation in Jurkat cells occurs via caveolin-dependent endocytosis while in the presence of CXCL12 ACKR3 internalisation occurs via clathrin/caveolin independent endocytosis

Immunofluorescence experiments in Jurkat cells were conducted as outlined previously using the aforementioned inhibitors of endocytosis. The only inhibitor that appeared to prevent the internalisation of ACKR3 was Dynasore, suggesting that the internalisation of ACKR3 in Jurkat cells occurs via clathrin/caveolin independent endocytosis (Figure 6.10).

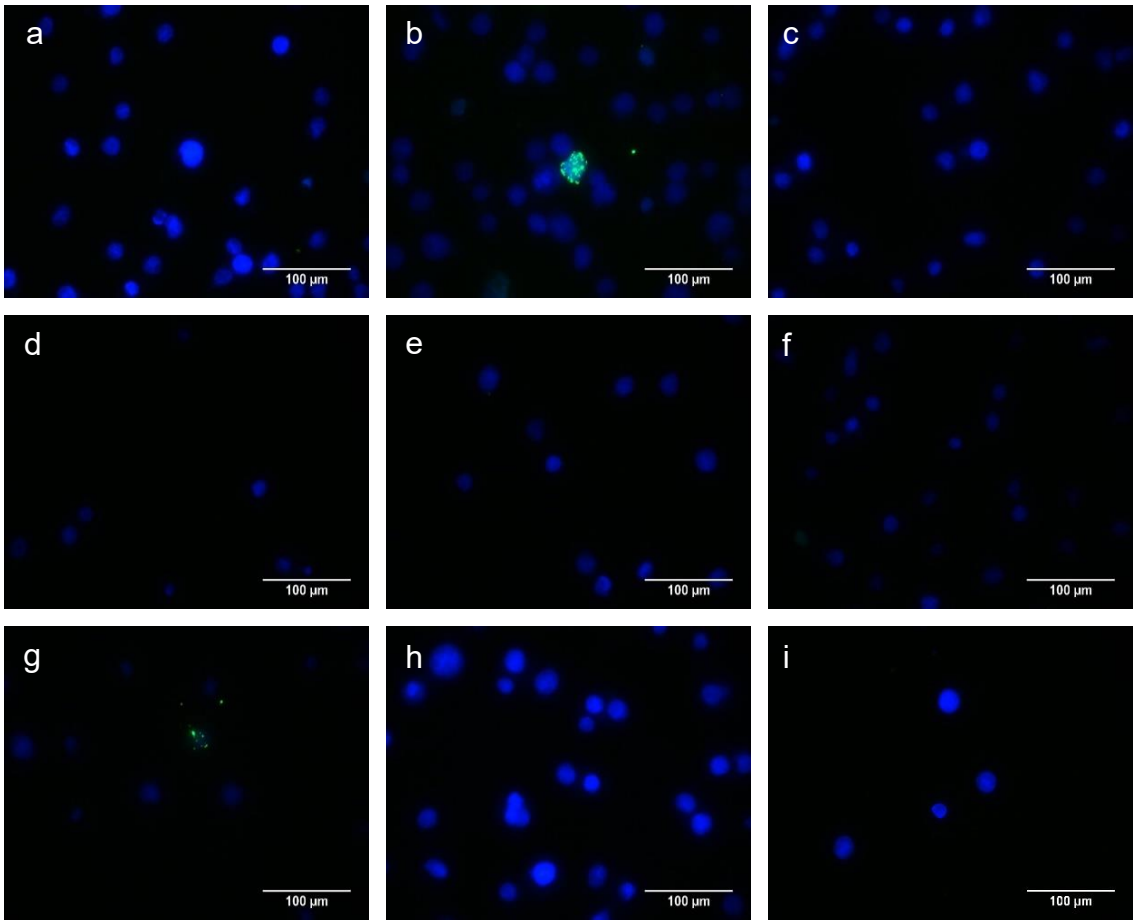


**Figure 6.10: Incubation with Dynasore prevents the internalisation of ACKR3 in Jurkat cells**. **a)** Negative control Jurkat cells were treated with secondary anti-mouse Alexa Fluor® 488 antibody (green) and DAPI (blue) at 4˚C then fixed with 4% paraformaldehyde before imaging. **b)** Positive control whereby ACKR3 was visualised on Jurkat cells using mouse 11G8 primary mAb, secondary anti-mouse Alexa Fluor® 488 antibody (green) and DAPI (blue) at 4˚C then fixed with 4% paraformaldehyde. **c)** Jurkat cells treated with mouse 11G8 primary mAb, secondary anti-mouse Alexa Fluor® 488 antibody (green) and DAPI (blue) at 37˚C then fixed with 4% paraformaldehyde. **d)** Jurkat cells incubated with 30 µM Pitstop 2 then treated with mouse 11G8 primary mAb, secondary anti-mouse Alexa Fluor® 488 antibody (green) and DAPI (blue) at 37˚C then fixed with 4% paraformaldehyde. **e)** Jurkat cells incubated with 30 µM Pitstop 2 negative control. ACKR3 visualised as d). **f)** Jurkat cells incubated with 10 µM CK666. ACKR3 visualised as d). **g)** Jurkat cells incubated with 60 µM Dynasore. ACKR3 visualised as d). **h)** Jurkat cells incubated with 5 µg/mL filipin. ACKR3 visualised as d). **i)** Jurkat cells incubated with 10 mM MCD. ACKR3 visualised as d). Data shows representative cells from 3 independent experiments with similar findings. Acquired with Leica imaging suite with 63x objective, 35x overall magnification.

However, due to the heterogeneous expression of ACKR3 in Jurkat cells and very few positive control cells expressing ACKR3 (Figure 6.10b), immunofluorescence alone did not provide an accurate assessment of ACKR3 internalisation in Jurkat cells. Therefore, flow cytometry was adopted (Figure 6.6 and 6.11). MCD and Pitstop 2 were excluded from flow cytometry experiments as MTS assays indicated that these inhibitors were significant cytotoxic (MCD, Appendix A32) or demonstrated a trend towards toxicity (Pitstop 2 Appendix 32 and 33) in Jurkat cells. Additionally, CK666 did not appear to contribute any inhibiting effect to receptor endocytosis in either Jurkat or MCF-7 cell lines, thus this agent was also excluded. Therefore, only two agents: filipin and Dynasore with and without incubation with 15 nM CXCL12 were used during flow cytometry. It was demonstrated that filipin prevented ACKR3 from internalising however, when Jurkat cells were incubated with 15 nM of CXCL12 and filipin, ACKR3 was internalised (Figure 6.11b). Opposing the immunofluorescence results, when Jurkat cells were incubated with Dynasore, ACKR3 internalised. However, when Jurkat cells were incubated with 15 nM of CXCL12 and Dynasore, ACKR3 did not internalise (Figure 6.11d). This is indicative that in Jurkat cells, ACKR3 endocytosis occurs via two different mechanisms depending upon the presence of CXCL12. Specifically, during normal turnover of ACKR3 at 37˚C, endocytosis occurs via caveolin-dependent endocytosis however, in the presence of CXCL12, ACKR3 internalization occurs via clathrin/caveolin independent endocytosis.

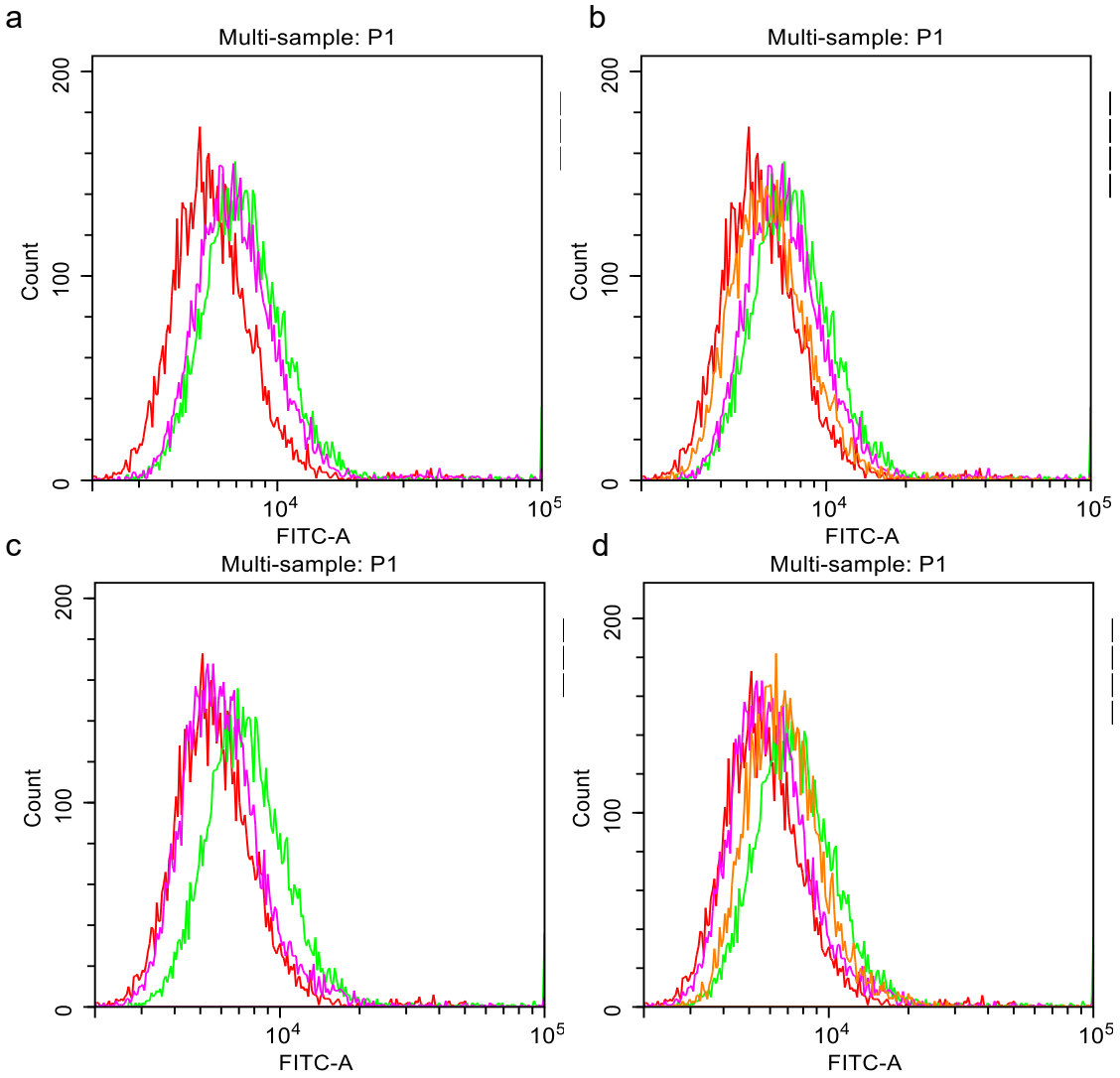


**Figure 6.11: Incubation with filipin and incubation with Dynasore and CXCL12 prevents ACKR3 internalisation in Jurkat cells.** Jurkat cells were incubated for 1 hour with or without CXCL12, filipin or Dynasore, 1 hour with primary 11G8 mAb (except negative control cells) and 1 hour with secondary anti-mouse Alexa Fluor® 488 antibody before analysis. **a)** Shift in fluorescence of P1 gated Jurkat cells from negative control (red) to positive control at 4˚C (green), and cells incubated with filipin (pink). **b)** Shift in fluorescence of P1 gated Jurkat cells from negative control (red) to positive control at 4˚C (green), cells incubated with filipin (pink) and cells incubated with 15 nM CXCL12 and filipin (orange). **c)** Shift in fluorescence of P1 gated Jurkat cells from negative control (red) to positive control at 4˚C (green), and cells incubated with Dynasore (pink). **b)** Shift in fluorescence of P1 gated Jurkat cells from negative control (red) to positive control at 4˚C (green), cells incubated with Dynasore (pink) and cells incubated with 15 nM CXCL12 and Dynasore (orange). Preliminary results from 1 experiment.

### 6.3.5. ACKR3 does not promote CXCL12 stimulated cellular migration in Jurkat and THP-1 cells

As mentioned previously, there is conflicting research on the capability of ACKR3 to promote CXCL12 stimulated cell migration in suspension cells with the majority of literature supporting the ability of ACKR3 to promote migration. One group that conflicted this hypothesis was Hattermann et al. (2014) whom used the ACKR3 mAb 11G8 while other research groups used ACKR3 inhibitors such as CCX771, CCX733 and 9C4 or used gene silencing (Balabanian et al., 2005, Sánchez-Martín et al., 2011, Zabel et al., 2009, Zabel et al., 2011). Therefore, the ACKR3 mAb 11G8 was used in chemotaxis assays to determine if ACKR3 does promote CXCL12-stimulated migration in THP-1 and Jurkat cells (Figure 6.12). A concentration of 12.5 ng/mL of 12G5 was found to successfully prevent CXCL12 stimulated migration in chemotaxis assays by previous members of the research group. Therefore, this concentration was used for both 12G5 and 11G8 to bind to and prevent downstream signalling in CXCR4 and ACKR3 receptors, respectively. Data collected from these experiments suggested that ACKR3 does not promote CXCL12 stimulated migration. This corroborates findings by Hattermann et al. (2014) but opposes findings by Melo et al. (2014) and Sánchez-Martín et al. (2011) whom found that ACKR3 did promote CXCL12 stimulated migration in Jurkat and THP-1 cells, respectively. Therefore, it is possible that the cause for these opposing results is a result of using the mAb 11G8 to inhibit ACKR3.

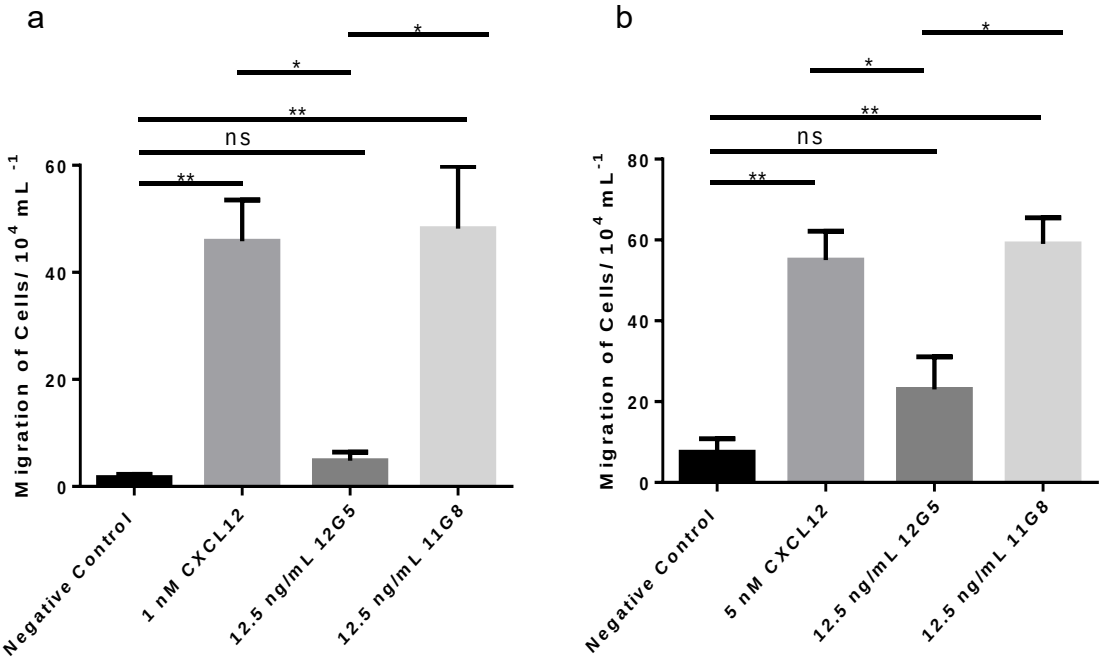


**Figure 6.12: Blocking CXCR4 receptors using the mAb 12G5 prevents CXCL12 directed migration while blocking ACKR3 using the mAb 11G8 does not prevent CXCL12 directed migration. a)** Migration of Jurkat cells was stimulated by 1 nM of CXCL12 in the presence and absence of 12.5 ng/mL 12G5 or 11G8. **b)** Migration of THP-1 cells was stimulated by 5 nM of CXCL12 in the presence and absence of 12.5 ng/mL 12G5 or 11G8. Data representative of the mean ± SEM of 3 independent experiments.

## 6.4. Discussion

Research into the ACKR3 receptor has been growing rapidly since its discovery by Shimizu et al. (2000). However, there still remains much controversy over the role ACKR3 has in CXCL12 stimulated migration, cellular expression of ACKR3 and the cellular localization of ACKR3 in different cell types.

Therefore, initial experiments focused upon determining ACKR3 expression in four cell lines, MCF-7, PC3, Jurkat and THP-1 cells. After confirming that all these cells lines expressed ACKR3, the cellular localisation of ACKR3 was investigated. Cells were warmed to 37˚C whereupon ACKR3 internalised in MCF-7 and Jurkat cells but not in PC3 or THP-1 cells. This corroborated research conducted by Luker et al. (2010) into ACKR3 expression on MCF-7 cells but opposed research conducted by Hattermann et al. (2014) and Melo et al. (2014). However, what was noted across these studies, was that there is no standardisation of the methods used for ACKR3 identification. Differences in the incubation temperatures, antibodies used, methodology (flow cytometry and

immunofluorescence) and even variations in when antibodies are added to the cells (i.e. before or after raising the incubation temperature) all contributed to variations in the results. Therefore, by standardising a method ACKR3 expression could be compared across these four cell lines. From these results, it can be hypothesised that MCF-7 and Jurkat cells have slower ACKR3 turnover compared to PC3 and THP-1 cells, hence that above 10˚C the cellular localisation of ACKR3 in MCF-7 and Jurkat cells is likely to be intracellular while in THP-1 and PC3 cells the ACKR3 receptor is localised to the cell surface possibly due to faster ACKR3 receptor turnover (Weigel and Oka, 1981).

Owing to these observations, the method by which ACKR3 was internalising was investigated in both MCF-7 and Jurkat cells. It was found that at 37˚C, the ACKR3 receptor on MCF-7 and Jurkat cells was internalising via caveolin-dependent endocytosis. However, when Jurkat cells were stimulated with CXCL12, there appeared to be a switch to clathrin/caveolin independent endocytosis. Changes to the method of endocytosis in relation to temperature has been observed before by Pastuszka et al. (2014) whom found that prior to thermal stimulation, Angiotensin II receptors on Cho cells were being internalised via CDE. However, by raising the temperature, CDE was effectively 'switched off' preventing the internalisation of Angiotensin II receptors. Unfortunately, it was not investigated whether binding the cognate ligand to Angiotensin II receptors could then cause a switch to an alternative mechanism of endocytosis. There is much debate as to why there are different mechanisms by which receptor internalization can occur. However, it has been suggested that clathrin-independent endocytosis such as via caveolins, is linked to receptor degradation (Di Guglielmo et al., 2003, Sigismund et al., 2008). This indeed is the case for the EGF receptor where it was found that high concentrations of EGF resulted in clathrin-independent endocytosis and subsequent degradation while lower concentrations of EGF caused a switch to CDE and subsequent prolonged intracellular signalling (Sigismund et al., 2008). This would suggest that different types of endocytosis have different functional consequences related to receptor signalling. Such appears to be the case with ACKR3 which demonstrates that with an increase in temperature, ACKR3 internalises via caveolin-dependent endocytosis possibly to degrade the receptor while incubation with CXCL12 and the switch to clathrin/caveolin independent endocytosis may be linked to receptor signalling and/or recycling. However, opposing this theory and opposing Sigismund et al.

(2008), research conducted by Kazazic et al., (2006) found that using even higher concentrations of EGF triggered internalisation via CDE. While this could simply be implicating that a high concentration of EGF may trigger a different intracellular signalling pathway, it also highlights that it is still unclear why the EGF receptor, or any other receptor, may switch between endocytosis pathways (Hansen and Nichols, 2009).

One of the downfalls of these experiments is the use of endocytosis inhibitors only. While MCD and filipin have shown to either remove or bind to cholesterol, respectively, thus implicate that they would disrupt lipid rafts and therefore inhibit caveolin-dependent endocytosis only, there have been reports that they are promiscuous inhibitors. Specifically, it has been found that while they do not directly inhibit CDE, MCD can cause the flattening of clathrin pits or in the case of filipin can impeach the surrounding membrane, thus these two agents can indirectly inhibit CDE (McGookey et al., 1983, Montesano et al., 1979, Rodal et al., 1999). This also appears to be the case with the CDE agent Pitstop 2, whereby a study by Dutta et al. (2012) found that the effects of Pitstop 2 were not limited to the inhibition of CDE as knockdown of clathrin failed to rescue the inhibition of clathrin independent endocytosis proteins. Therefore, they concluded that Pitstop 2 had cellular targets outside the terminal domain of clathrin and could not be used to distinguish between clathrin-dependent and clathrin-independent endocytosis. Lastly, Dynasore which targets dynamin can also be regarded as a promiscuous endocytosis inhibitor due to dynamin being required for both CDE and caveolin mediated endocytosis (Henley et al., 1998). However, dynamin-independent endocytosis is possible through the use of actin filament polymerisation (Mayor et al., 2014). Therefore, a solid conclusion cannot be reached from these experiments alone and future experiments are paramount to give a definitive answer as to which mechanism of endocytosis is occurring in these cell lines. Such experiments could include the staining of more specific markers of endocytosis including staining for clathrin and/or caveolin. Alternatively, knockdown of these two marker followed by flow cytometry would provide more concrete information as to which method of endocytosis is occurring under these different conditions.

Overall, future research relies on more in depth investigations into all four of the cell lines. Flow cytometry was never conducted in MCF-7 cells and due to ACKR3 not being internalised in THP-1 nor PC3 cells, these cell lines were not

considered for endocytosis investigations. However, it would be interesting to determine the effect upon ACKR3 receptor internalisation in these cells when they are incubated with CXCL12. Furthermore, investigations could be carried out to determine if the switch in endocytosis mechanisms indicate changes in relation to ACKR3 signalling, recycling and/or degradation. Such investigations, could involve studies into the effects of temperature and/or CXCL12 incubation in relation to expression levels of β-arrestin, Akt and/or ERK. Additionally, in relation to receptor degradation, makers such as LysoTracker, a red fluorescent dye that specifically accumulates in lysosomes could be used. Furthermore, to determine ACKR3 receptor recycling capabilities when cells are incubated at 37˚C, time-point experiments with flow cytometry analysis could be conducted to determine how long it takes ACKR3 to become internalized and subsequently how long it takes for ACKR3 to recycle back to the surface, or indeed if this is even occurring at all. Alternatively, other more robust assays should be conducted to determine CXCR4 internalization including radioligand binding studies, whole cell ELISA or using the Fluorokine® receptor detection kit from R&D Systems. Finally, it would be interesting to compare ACKR3 and CXCR4 internalisation across these four cell lines after incubation with CXCL12 as there has been evidence that ACKR3 receptor recycling occurs much faster than CXCR4, possibly in relation to mediating the degradation of CXCL12 via ACKR3 (Naumann et al., 2010). This would therefore provide more insight into if ACKR3 plays a role in promoting or inhibiting cancer progression in these four cell lines.

ACKR3 signalling occurs atypically via β-arrestin which predominantly causes ACKR3 receptor internalisation. However, ACKR3 can complex with CXCR4 to form heterodimers which could induce chemotaxis and it has been hypothesized that the recycling machinery cannot cope with the ACKR3 expression levels that are seen on several cancer cell types, thus causing a switch from receptor internalisation to signalling via Akt and ERK (Sánchez-Martín et al., 2011). However, in this research it was found that ACKR3 did not promote cancer migration in Jurkat or THP-1 cells, corroborating research by Hartmann et al. (2008) and Zabel et al. (2009) but opposing research by Melo et al. (2014) and Sánchez-Martín et al. (2011). While Hartmann et al. (2008) used the mAb 11G8, Zabel et al. (2009) used the ACKR3 inhibitor, CCX771, to prevent CXCL12 binding and found this to have no effect upon the migration of NC-37 cells in bare filter chemotaxis assays. However, when CCX771 was used to inhibit ACKR3 in

a more physiological TEM assay, it was found that CCX771 was a very potent inhibitor of CXCL12 stimulated migration of NC-37 cells with an $IC_{50}$ of 49 nM (Zabel et al., 2009). Additionally, the ACKR3-specific antagonist CCX771 was 20-fold more potent than the CXCR4 specific antagonist AMD3100 in blocking NC-37 cell migration to CXCL12 in TEM assays. Zabel et al. (2011) found that CXCL12 mediated migration was abrogated with the use of ACKR3 inhibitors and even went on to suggest that inhibiting ACKR3 could be a more effective therapeutic intervention than CXCR4 antagonists. However, it was also suggested that to prevent lymph node metastasis, the use of both ACKR3 and CXCR4 antagonists would be required. Supporting the requirement for more physiological experiments to determine the effect of ACKR3 in migration, mice studies found that blocking the ACKR3 receptor reduced the homing of $CD34^+$ cells to bone marrow of NOD/SCID mice (Melo et al., 2018). Therefore, while it is possible that in Jurkat and THP-1 cells lines, the ACKR3 receptor has no involvement in CXCL12-stimulated migration it is also possible that chemotaxis assays are not a viable method for determining if ACKR3 promotes CXCL12 stimulated migration. Overall, there appears to be more evidence in the literature supporting the hypothesis that ACKR3 can promote cancer cell migration (Gao et al., 2015, Li et al., 2015, Miao et al., 2007, Zabel et al., 2009, Zabel et al., 2011, Melo et al., 2014, Melo et al., 2018, Wang et al., 2008, Salazar et al., 2014, Sánchez-Martín et al., 2011). Therefore, it is possible that use of the mAb 11G8 may not be suitable for chemotaxis experiments. This is demonstrated as although research has been conducted using the mAb 11G8, Hartmann et al. (2008) found that this did not prevent CXCL12-stimulated migration when Melo et al. (2018) found that using 11G8 did effectively prevent CXCL12-stimulated migration. It is possible that this discrepancy could be in relation to the function of ACKR3 varying dependent upon the cell type/mouse models used, but also could be in relation to what has been previously discussed in Chapter 5.3.1., that in that long-term incubation with antibodies is not viable as they are quite unstable. Therefore, while Melo et al. (2018) successfully inhibited migration using 11G8, it is possible that 11G8 could have degraded in the chemotaxis results shown here, despite the CXCR4-mAb 12G5 not degrading. Otherwise, it is possible that higher concentration of 11G8 mAb may be required to effectively block the ACKR3 receptor as the concentrations used by Melo et al. (2018) were not available and so could have been much higher than the concentration used

in these experiments. Therefore, future research would benefit from using ACKR3-specific antagonists such as CCX771, CCX733, CCX754, TC14012 or 9C4 (Watanabe et al., 2010, Zabel et al., 2009, Ödemis et al., 2010, Balabanian et al., 2005, Cao et al., 2016). ACKR3 inhibition can even be achieved using AMD3100 at concentrations >10 µM (Kalatskaya et al., 2009). Additionally, to support results obtained using the inhibitors, knockdown experiments should be conducted.

## 6.5. Conclusions

Overall, ACKR3 is expressed in MCF-7, PC3, Jurkat and THP-1 cells. When the incubation temperature is raised to 37°C ACKR3 become internalised in both MCF-7 and Jurkat cells. This implicates a slow turnover of ACKR3 in these two cell lines while PC3 and THP-1 have a faster turnover of ACKR3. The internalisation of ACKR3 in the absence of CXCL12 occurs via caveolin-dependent endocytosis in both MCF-7 and Jurkat cells. In the presence of CXCL12, ACKR3 is internalised by clathrin/caveolin independent endocytosis in Jurkat cells. Finally, using 11G8 as an inhibitor of ACKR3, ACKR3 was found to not promote CXCL12-stimulated migration in Jurkat or THP-1 cells.

# Chapter 7: The Development of 3D Printed Materials for Investigations into Chemokine Stimulated Cancer Cell Migration

**Acknowledgments**

I would like to thank Dr D. Warren and Dr J. M. Courtney for their contributions to this collaborative project. I would also like to thank Dr J. M. Courtney for conducting the majority of the 3D prints and for supervising several of these prints.

## 7.1. Introduction

Boyden assays have been used extensively throughout the literature to determine the ability of cells to migrate through a membrane towards chemokines (Barber et al., 1999, Zang et al., 2000, Inngjerdingen et al., 2003). Boyden assays are a commonly used technique to study cell migration due to their simplicity and relatively quick incubation period. However, there is a tendency for these assays to fail to produce a gradient across the membrane due to fluid level imbalances nominally attributed to pipetting errors. Even slight changes in fluid levels can cause the failure of the porous membrane of the insert to not come into contact with the media below, or to be submerged in it (Keenan and Folch, 2008) It is likely that a failure to produce a gradient caused the results seen in Chapter 4 where PC3 cells were stimulated with CXCL12 chemokine and treated with specific CXCR4 antagonists (Figure 4.35). The results produced showed no significant increase in cell migration with the addition of CXCL12, nor any significant inhibition with the addition of the CXCR4 antagonists previously proven to cause significant inhibition (Figure 4.23). Therefore, it was determined that these results were due to the limited reproducibility of each Boyden assay experiment, thus in this context, Boyden assays were not a reliable enough method. With these findings in mind, efforts were devoted to developing an alternative chemotaxis chamber using 3D printed materials and later producing replacement stoppers for the Oris™ Cell Migration assay.

3D printing, also known as additive manufacturing is a process whereby material is built up layer upon layer to make a 3D model. There are numerous methods of 3D printing such as: Stereolithography (SLA), bioprinter, Digital Light Processing (DLP), Selective Laser Sintering (SLS), Selective Laser Melting (SLM), Laminated Object Manufacturing (LOM), Binder Jetting (BJ), Material Jetting (MJ), Fused Deposition Method (FDM) and Electron Beam Melting (EBM) (Ho et al., 2015, Lee et al., 2017). Selecting a method is dependent upon several factors including but not limited to: costs, print quality, print speeds and availability. In this project FDM was conducted due to having the expertise available, its relatively cheap production costs compared to SLA, rapid filament solidification thus rapid printing capabilities, very little waste materials, favourable toxicity and SHE requirements compared to SLA, having the ability to produce complex parts in a single print and easily reproducible at little cost.

3D printing is a multistep process. Firstly, computer aided design (CAD) using software such as Google Sketch Up Make 2017 or Blender is used to create a 3D model. Following this, slicing software is utilised such as CURA 2.6.2 to generate files that can be processed by computer aided manufacture (CAM) devices, in this case, 3D printers, where the design is rebuilt layer-by-layer based on the 2D slices. Specifically, in FDM 3D printing a solid filament, in this case PLA filament (and later TPE-U), is fed into the printer to a heated element where it becomes molten or semi-molten. This is then fed through a nozzle and using X-Y coordinates, the material is deposited onto the partially constructed 3D object where it fuses and hardens. After one layer, the platform holding the 3D object moves vertically in the Z direction to enable a new layer to be deposited on top of the previous layer. This continues until there is a full representation of the developed CAD file. The 3D object can then be removed from the platform and cleaned (Dudek, 2013).

Since it was first described by Charles W. Hill in 1986, 3D printing technology has developed dramatically in many sectors including in the biological sector (Hull, 1986). Such an example is the development of scaffold guides for tissue regeneration whereby scaffolds were composed of biodegradable materials such as poly-glycolic acid (PGA) or poly-lactic acid (PLA). These scaffolds were then cultured to allow cell attachment and finally implanted *in vivo*. These attached cells, along with cells in the host that migrate to the scaffold, proliferate and differentiate to replenish the tissue. Over time, the 3D scaffold biodegrades and is absorbed (Hutmacher, 2001, Hutmacher et al., 2004, Peter et al., 1998, Evans, 2000). However, there were limitations to this approach, the major limitation being the difficulty in engineering a whole major organ from random cell seeding to the scaffolds. Therefore, 3D bioprinting was developed whereby living cells, biochemicals and other biological materials could be printed layer upon layer to create a 3D structure for eventual 3D printing of tissues and organs (Nakamura et al., 2010, Mironov et al., 2003, Zopf et al., 2013). While this technology is available it has yet to be perfected, but demonstrates the potential of 3D printing. Additionally, 3D printing has been used for the development of biological devices such as microfluidic devices to enable the study of biological systems in a precise and controlled manner at a micrometre scale. These microfluidic devices enables small volumes of fluids to pass over the devices for uses in cytotoxicity assays, cellular stress assays and single cell behaviour studies amongst other assays

(Ho et al., 2015, Kitson et al., 2012). Other biological tools have been developed using 3D printing such as 3D printed microscope chambers. These were created to facilitate the 3D imaging of hundreds of living objects in 20 hours irrespective of the shape of the sample or the type of microscopy used (Alessandri et al., 2017). Therefore, the use of 3D printing in the biological sector is growing and these examples demonstrate the applicability of using 3D printing for the development of novel chemotaxis chambers.

This 3D printing project was in collaboration with Dr D. Warren who co-designed the chambers and with Dr J. M. Courtney who aided with CAD and facilitated the 3D printing.

## 7.2. Chapter Aims and Hypotheses

**Hypothesis**: That 3D printing can be utilised to develop 3D printed materials for the production of chemotaxis chambers that possess a chemokine gradient for *in vitro* use. Additionally, that 3D printing can be used to develop cheap replacement stoppers for the Oris™ Cell Migration assay.

**Aims:** The overarching aim of this project was to develop a suitable CAD design for 3D printed materials that can be readily downloaded for free. This would enable access to cheap and reproducible chemotaxis chambers with only the small expense of renting time on a FDM 3D printer. This would enable real time observations of single cells towards a chemokine gradient to be reproduced at very little cost in any laboratory. For the successful development of such 3D printed materials, there were several requirements that the chemotaxis chamber must adhere to:

1. The chamber must fit inside a 3 $cm^2$ Petri dish and/or 6-well plate.
2. Each chamber requires two wells and a separating channel.
3. Each well must be a set volume (500 µL).
4. The separating channel must have a minimum width of 1 mm and 10 mm length.
5. If an insert is to be included, it must be watertight, removable and fit across the width of the channel.
6. Materials used must be nontoxic to cells.
7. The lid of the Petri dish or 6-well plate must be able to fit flush over the mould.
8. The materials used should withstand a minimum of 37°C and a humid environment without disfigurement.

9. The separating channel must permit light and camera entry.
10. Cells must not leak into or under the mould materials.

Additionally, it would be desirable if:

1. The 3D printed moulds fitted into multiple brands of petri dish and/or 6-well plates.
2. The 3D printed moulds were reusable.
3. If multiple 'potting' materials could be used to create the desired chemotaxis chambers.

Finally, the aim was to develop replacement stoppers for the Oris™ Cell Migration Assay that could be used in place of buying a whole new plate.

## 7.3. Results

### 7.3.1. First generation development of 3D material for silicone casts for 3 $cm^2$ petri dishes

Initial development went into designing 3D PLA moulds into which silicone could be inserted. Once dried the silicone could be removed creating a silicone cast. These casts could then be inserted into 3 $cm^2$ petri dishes (ThermoFisher Scientific) and cell infused media could be added directly into the space created by the silicone cast. Figure 7.1 shows the initial CAD of the 3D PLA mould, the subsequent 3D printed mould and finally, the silicone cast. While the CAD was simple to construct and the subsequent 3D PLA mould printed well with few imperfections, it was found that the PLA mould fitted too tightly to the edges of the petri dish which caused several dishes to crack and deform. This was partially due to the use of several different brands of petri dish with the 3 $cm^2$ petri dishes from Corning being slightly smaller than 3 $cm^2$ petri dishes petri dishes from ThermoFisher Scientific or from Nunclon™ Delta Surface. Therefore, all future designs were conducted based on 3 $cm^2$ petri dishes from ThermoFisher Scientific.

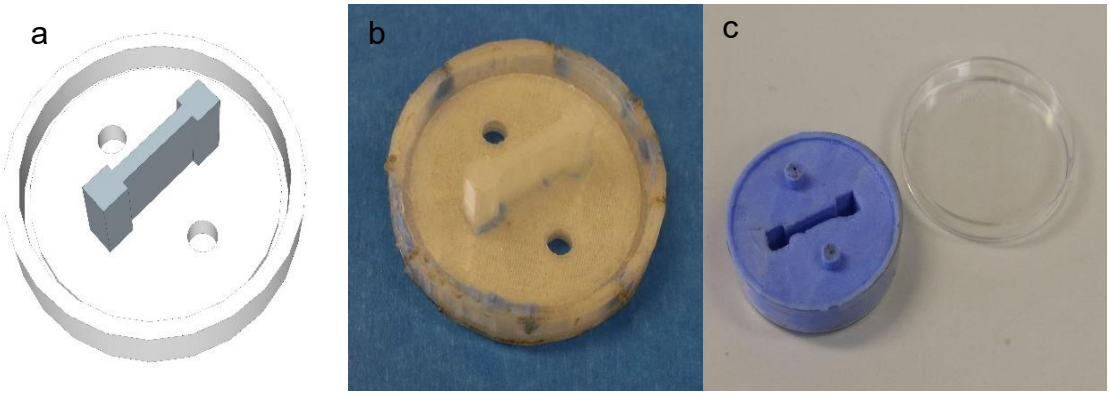


**Figure 7.1: Original PLA mould design, 3D printed PLA mould and silicone cast. a)** CAD design created in Google Sketch Up (64 bit) 2017 for the PLA mould. **b)** 3D printed PLA mould printed using Ultimaker 3 extended. **c)** Silicone cast created from the 3D printed PLA mould. Results representative of the production of 5 silicone casts.

Multiple different techniques were used to create the silicone casts as the silicone used (Gedeo 300g Siligum Moulding Paste, white, Amazon) began to harden within 5 minutes of moulding. Such techniques included filling the 3D mould with the silicone before pushing into the petri dish, filling the petri dish with silicone and pushing the 3D mould into the dish and a combination of the two. The final of these methods was found to produce the best results as well as using an implement to force the silicone into the edges of the 3D mould to get maximal silicone coverage. This technique was then employed for all subsequent silicone casts. Despite finding this optimum method, cracking of the petri dishes continued to occur which suggested that the CAD needed to have more clearance. Additionally, the wells designed were too small for sufficient cell seeding and the channel between these two wells was too large. Consequently, while the original design and the creation of silicone casts proved technically that the concept was achievable, further development was required.

Subsequently, the size of the wells was increased to 100 $mm^2$ and the channel size was lengthened to 13 mm and width decreased to 1 mm creating an overall volume of 218 $mm^2$. While this was still a simplistic design, the size of the channel was on the borderline of the capabilities of the CAD software (Figure 7.2.). However, the design remained within the parameters of the 3D printer and produced a well printed PLA mould.

Unfortunately, it was found that there was always a thin layer of silicone coating the bottom of the wells and channel due to imperfect silicone cast production which prevented a complete seal of the cast to the bottom of the petri dish. This

problem was due to the holes for the removal of excess silicone being too small, thus excess silicone could not be completely escape before it solidified.

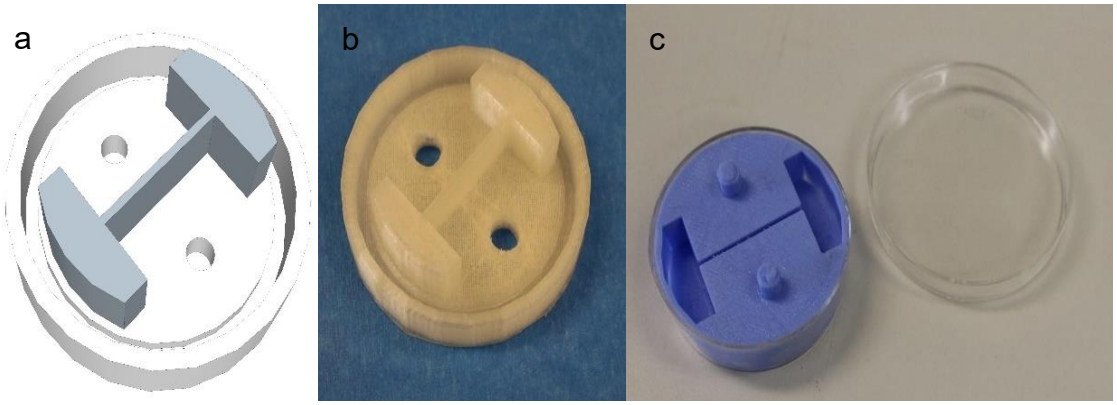


**Figure 7.2: Second PLA mould design, 3D printed PLA mould and silicone cast. a)** CAD design created in Google Sketch Up (64 bit) 2017 for the PLA mould. **b)** 3D printed PLA mould printed using Ultimaker 3 extended. **c)** Silicone cast created from the 3D printed PLA mould. Results representative of the production of 3 silicone casts.

Therefore, the third design saw the enlargement of these silicone removal holes. Additionally, the third design tested the capabilities of a Teflon insert (Teflon sheet, 1 mm, Direct Plastics.co.uk) (Figure 7.3). This insert was designed to section off one well to enable cell seeding to occur in only that well by preventing leakage of these cells into the channel. After cells had adhered, this insert could be removed, more media and chemokines added and cell migration to the non-seeded well could then be observed. The enlargement of the silicone removal holes was an improvement but still required more enlargement in the next design. Also, there was still an issue with silicone coating the bottom of the wells and channel. Therefore, the silicone was removed by scraping the bottom of the cast with a scalpel. Unfortunately, this caused ragged edges of the silicone at the bottom of the well that impeached the seal of the silicone to the petri dish and demonstrated the need for a new method of removing excess silicone. Finally, to enable the insertions of the Teflon insert, the silicone was sliced with a scalpel and the Teflon insert pushed in.

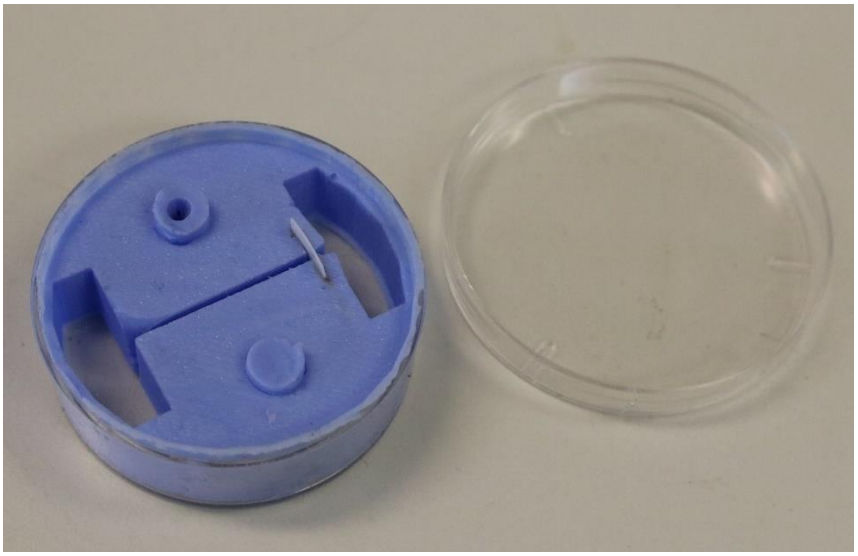

**Figure 7.3: Third silicone cast design with Teflon insert.** Silicone cast with enlarged silicone release holes. Wells were created by cutting away excess silicone from the wells with a scalpel and slicing into the silicone to insert the Teflon insert. Results representative of the production of three silicone casts. Silicone casts tested for leakage in 3 independent experiments.

However, this did not prevent the leakage of fluid due to the Teflon not sitting flush to the bottom of the petri dish and so moulds for silicone inserts were designed using CAD (Figure 7.4). This design was a two-part mould with a silicone release hole that printed well and the silicone inserts created were moulded well with few flaws. There was an again issues with excess silicone, however, this was resolved by removing the excess silicone with a scalpel.

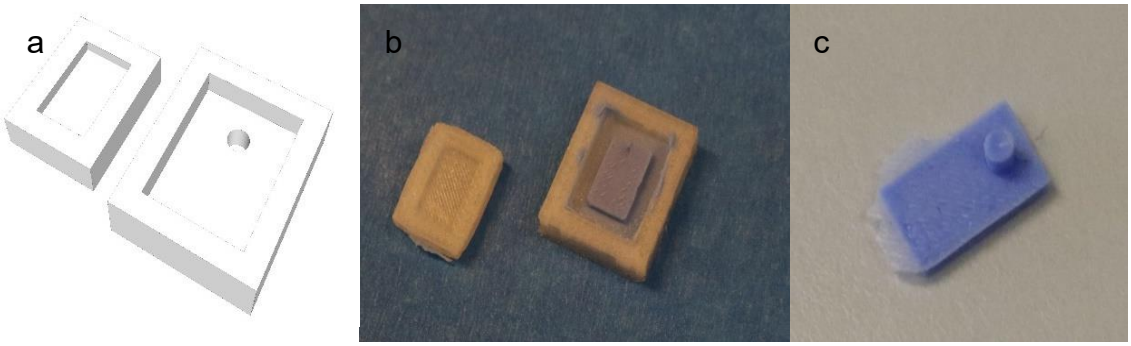


**Figure 7.4: PLA mould design for a silicone insert, 3D printed PLA mould for insert and silicone insert. a)** CAD design created in Google Sketch Up (64 bit) 2017 for the PLA mould for the insert. **b)** 3D printed PLA mould printed using Ultimaker 3 extended. **c)** Silicone insert created from the 3D printed PLA mould. Results representative of the production of over 10 silicone casts.

To incorporate the enlargement of the silicone release holes and incorporate the silicone insert, a fourth PLA mould design was created (Figure 7.5).

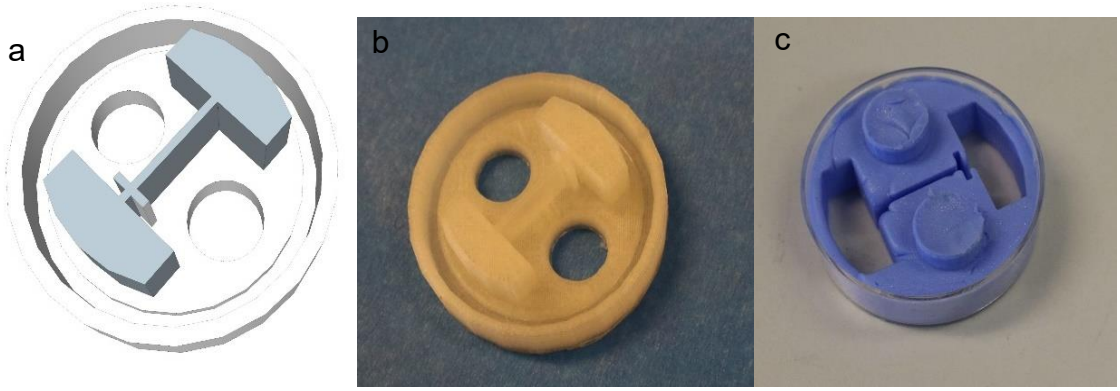


**Figure 7.5: Fourth PLA mould design, 3D printed PLA mould and silicone cast. a)** CAD design created in Google Sketch Up (64 bit) 2017 for the PLA mould. **b)** 3D printed PLA mould printed using Ultimaker 3 extended. **c)** Silicone cast created from the 3D printed PLA mould. Results representative of the production of three silicone casts. Silicone casts tested for leakage in 3 independent experiments.

Again, the CAD for the fourth PLA mould was on the limit of the 1 mm design parameters for Google Sketch Up (64 bit) 2017. This highlights that other software would have to be consider if future, more intricate changes were required. Also, the initial 3D prints were poor due to the set parameters of the printer. Therefore, changes had to be made to the CURA slicer where 1 mm outliers were required to produce better 3D prints. This highlights that the printing parameters of these designs were starting to have effects upon the printed moulds. Despite the limitations noted in both the CAD and the 3D prints, the silicone casts formed well from the 3D printed moulds. However, when these casts were put into the 3 $cm^2$ petri dishes and were tested with water there was still significant fluid leakage form the chambers into the surrounding petri dish. It is possible that this leakage was due to the low quality of the moulding silicone and could be solved by using a liquid silicone. This however was not tested. Instead, a lid was designed to compress the set silicone cast into the petri dish (Figure 7.6).

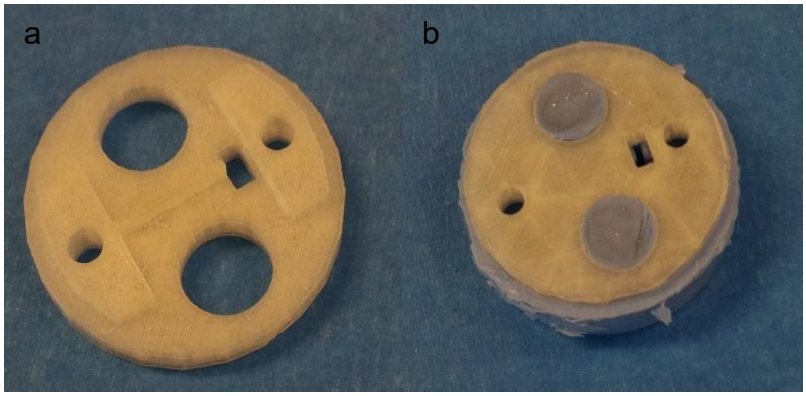


**Figure 7.6: 3D printed lid to compress the solid silicone cast into the petri dish**. **a)** 3D printed lid to compress the set silicone casts. **b)** the compression of the silicone cast into the 3 $cm^2$ petri dishes. Results representative of the production of 1 compression lid.

While this printed well it was unsuitable for microscopic usage as the camera was unable to penetrate through the plastic lid designed. Therefore, attempts were made to improve the seal to the bottom of the petri dish by improving the removal of excess silicone from the bottom of the wells (Figure 7.7). This was achieved by keeping the set silicone cast in the PLA mould and using a scalpel to gently cut away the excess silicone from the wells and channels. When the silicone cast was removed and pushed into the petri dish it was found that a water tight seal was achievable but several casts still suffered from leakage.

**Figure 7.7: Removal of silicone from well and channel using scalpel to improve water tight seal.** An improved seal was created by leaving the silicone cast in the PLA mould and using a scalpel to gently cut away the excess silicone. The silicone cast was then removed and pushed into 3 $cm^2$ petri dishes where tests demonstrated a water tight seal. Results representative of the production of 3 water tight silicone casts.

Therefore, as an alternative to the PLA lid shown in Figure 7.6, a PLA topper was designed in CAD to again, push the set silicone cast into the petri dish to form a watertight seal. Several toppers were assessed with the final design to be bonded in place with epoxied glue on top of the silicone casts in the petri dishes (Figure 7.8c). Unfortunately, these designs prevented the lids of the petri dishes to sit flush which would prevent sterile conditions within the petri dish. Additionally, when the topper was compressed, the channel underwent crushing which would prevent visibility into the channel under the microscope and would prevent cell migration. Therefore, it was suggested that the channel size should be increased from 1 mm to 2 mm in order to maintain visibility when looking down the microscope and to enable the migration of cells down this channel. This would also resolve the issues discussed earlier with the CAD and the limitations related to the 3D printer.

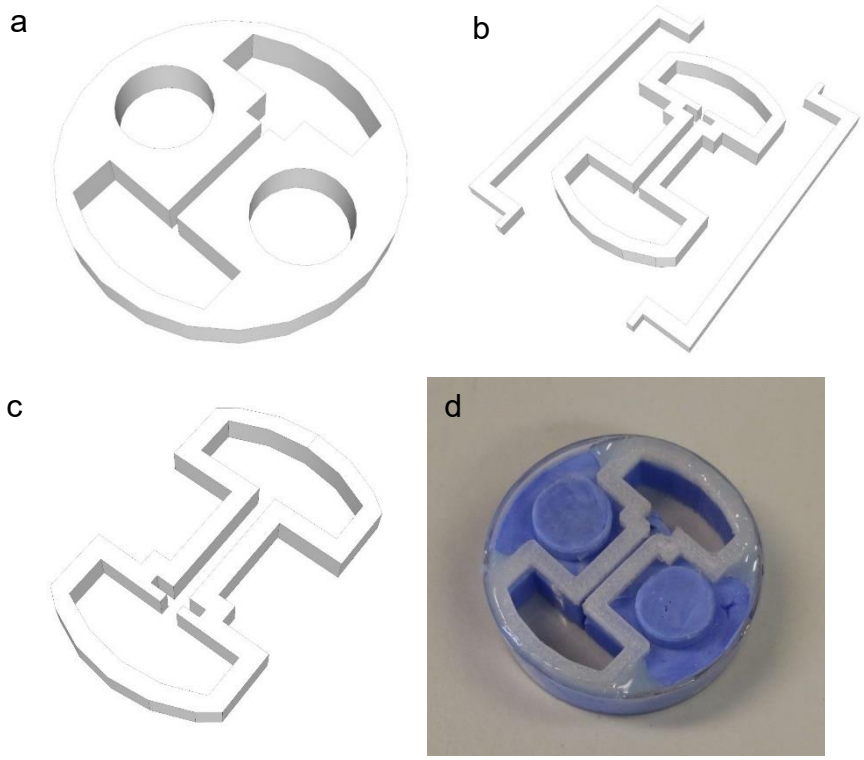


**Figure 7.8: PLA topper designs and final topper for silicone casts**. **a), b)** and **c)** are example of three CAD for silicone toppers created in Google Sketch Up (64 bit) 2017 for the PLA mould. **d)** Final PLA topper epoxied into place atop a silicone cast. Results representative of the production of 3 water tight silicone casts.

### 7.3.2. Second and third generation development of 3D material for silicone casts for 3 $cm^2$ petri dishes

The development of a second generation of the 3D PLA moulds was based upon the first generation but saw an enlargement of the channel from 1 mm to 2 mm (Figure 7.9). This overcame the issues seen previously relating to the compression of the channels and removed the issue of both designing and printing something as small as 1 mm. Using CAD and CAM, making this adjustment was quick and the printed PLA mould was well formed.

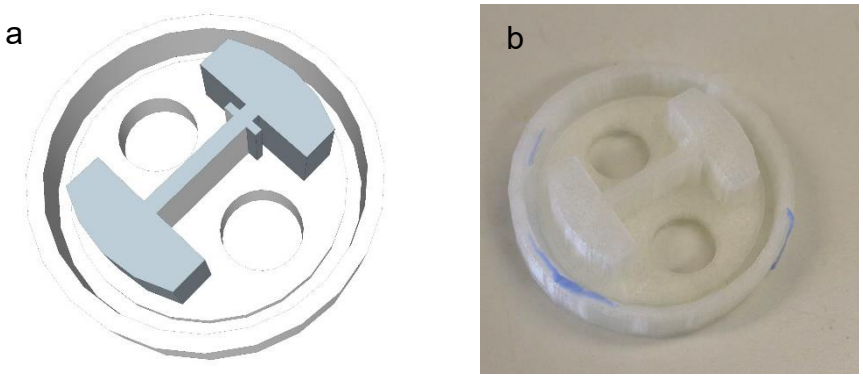


**Figure 7.9: Second generation PLA mould CAD and 3D printed PLA mould. a)** CAD design created in Google Sketch Up (64 bit) 2017 for the second generation PLA mould. **b)** 3D printed PLA mould printed using Ultimaker 3 extended. Results representative of the production of 3 printed PLA moulds.

It was found that these designs enabled the creation of well-formed silicone casts that were easy to reproduce (Figure 7.10). However, there were still leakage issues.

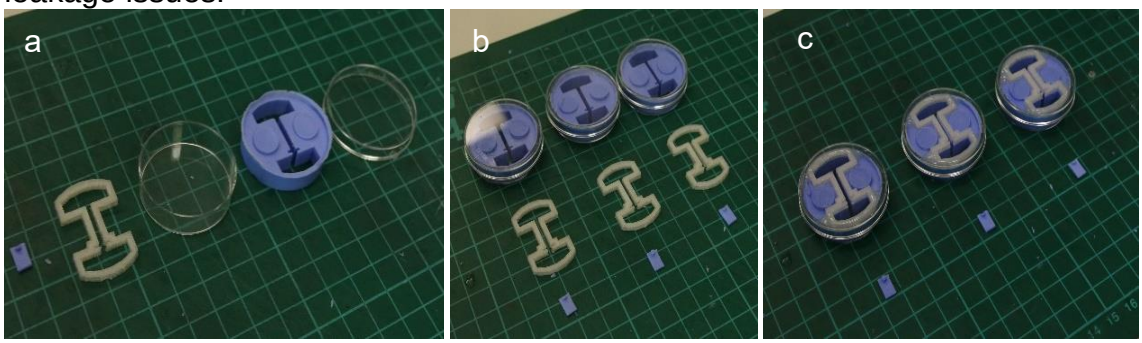


**Figure 7.10: Second generation silicone cast with PLA toppers and silicone inserts. a)** and **b)** silicone cast created from the 3D printed PLA mould with PLA printed topper and silicone insert. **c)** Final PLA topper epoxied into place atop a silicone cast with inserts. Results representative of the production of 3 printed PLA moulds that were all tested for fluid leakage.

A third generation of 3D printed PLA moulds were created (Figure 7.11). The aim of this generation of PLA moulds was to design a mould that could create silicone casts outside of the petri dish as a separate single unit. This would enable better compression of the silicone casts while helping to prevent the issue of cracking the plastic petri dishes when trying to form the silicone casts which had been a problem throughout these early developmental stages. To create this mould, the original CAD was modified to create flared insert holes in order to slot the upper and lower parts of the mould together to enable compression of the silicone to form the silicone casts. Additionally, a fourth PLA topper was designed to cover more area of the silicone cast to try to improve the compression of the silicone cast when inside the petri dish. These moulds printed well and produced well-formed silicone casts. Despite all these design changes, there was still leakage of fluid from the wells into the surrounding petri dish. Poly-L-lysine Solution (Sigma Alderich), was used in an attempt to adhere the silicone casts to the bottom, however this proved unsuccessful.

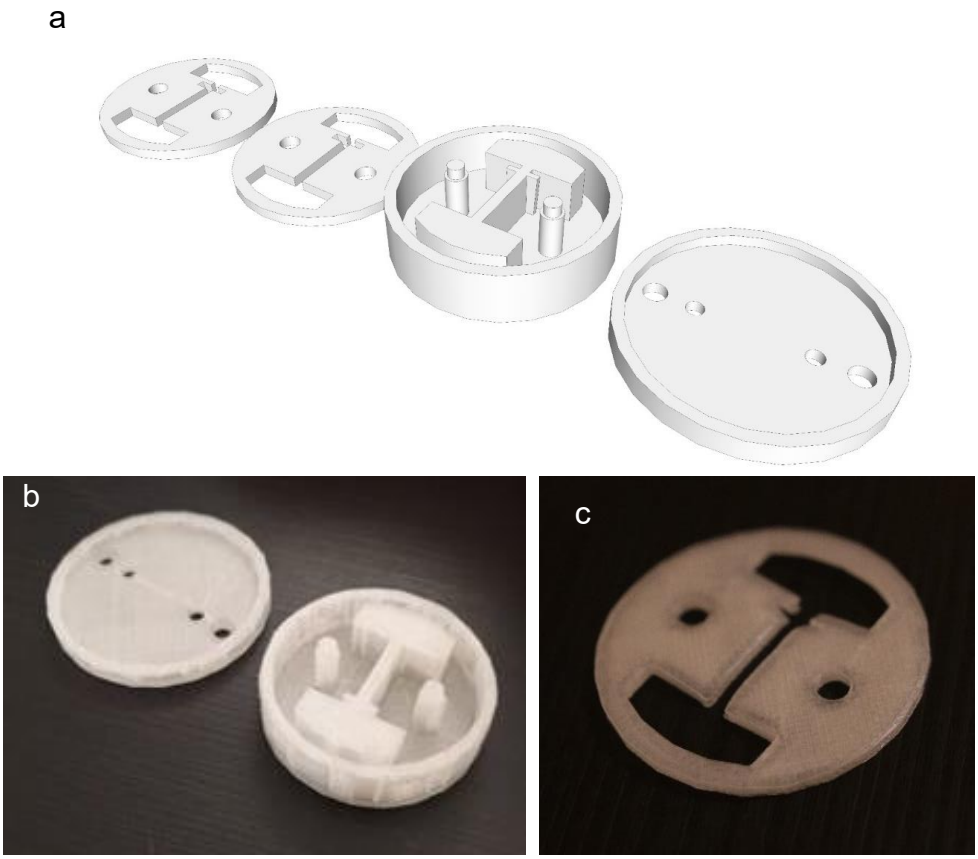


**Figure 7.11: Third generation PLA mould, CAD and 3D printed PLA mould**. **a)** CAD design created in Google Sketch Up (64 bit) 2017 for the third generation PLA mould. **b)** 3D printed PLA mould printed using Ultimaker 3 extended. **c)** 3D printed fourth generation PLA topper. Results representative of the production of 3 printed PLA moulds and topper that were all tested for fluid leakage.

A final design for the chambers was created (Figure 7.12). This involved drilling holes into a 6-well plate from StarLab into which the silicone casts were inserted. A PLA topper was added to the top of these silicone casts and to the outside of the bottom of the 6-well plate to provide extra strength for the plastic and to aid in compression of the silicone cast into the well. These three parts were then tightly screwed into place. Despite this design successfully making the wells water tight, several other issues arose. The first being that the 6-well plates were selected over the petri dishes as the 6-well plates had thicker plastic and so would withstand the drilling process better. Despite this, several of the wells cracked which caused fluid leakage from the well. Additionally, the drilling of holes often breached the airtight seal of the plate, preventing sterile conditions inside the plate. Thirdly, it was found that the screws were susceptible to rust due to the humid atmosphere that the plates were exposed to. Finally, when this design was used to seed PC3 cells, it was found that the cells failed to adhere to the plate, most likely related to toxicity issues in relation to the silicone used. Ultimately, it was decided that an alternative design had to be established for the chemotaxis chambers.

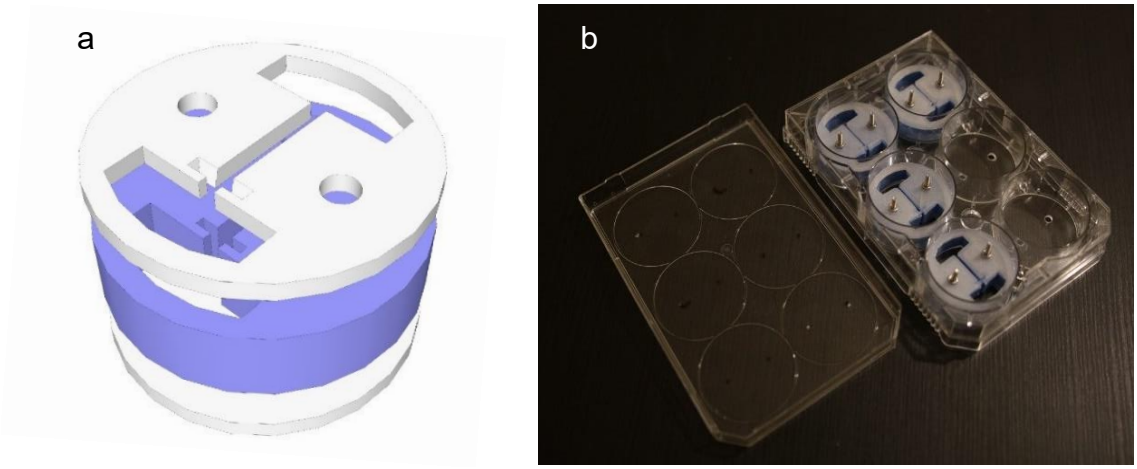


**Figure 7.12: CAD design for silicone casts inserted into a 6-well plate with toppers and the final product. a)** CAD design created in Google Sketch Up (64 bit) 2017 for the silicone casts with two toppers. **c)** Silicone casts inserted into a 6-well plate with 2 printed PLA topper and screwed into place. Results representative of the production of eight printed PLA moulds and toppers in 3 separate 6-well plates that were all tested for fluid leakage. Cellular adherence results representative of 5 individual experiments.

### 7.3.3. First generation development of 3D material for 3 $cm^2$ petri dish epoxy chemotaxis chambers

The aim for this new design was to produce a new 3D PLA mould that silicone could be inserted into to create a silicone cast. Once dried the silicone could be removed and the cast can be inserted into a 3 $cm^2$ petri dishes (ThermoFisher Scientific). Liquid epoxy could then be poured around the silicone cast whereupon the epoxy will solidify creating a two welled chemotaxis chamber. Figure 7.13 shows the initial CAD of this new 3D PLA mould, the subsequent 3D printed mould, the silicone cast and the epoxy chemotaxis chamber. The CAD for this new mould required a lot of development but the final design produced a well printed 3D PLA mould that was within the parameters of the 3D printer. From this PLA mould, the silicone cast was produced well. Due to the depth of the mould it proved difficult to remove the cast. However, after several trial and error methods of removing the cast, it was found that it could be removed with no ill effects upon the cast. This silicone cast was inserted into a petri dish and vice clamps were used to push the cast flush to the bottom of the dish. Following this, liquid epoxy was inserted and left to set. The first epoxy assessed (Araldite Rapid, Huntsman Advanced Materials, RS components) was a quick set epoxy that set within five minutes. This epoxy saw significant distortion of the connecting channel between the wells due to the pressure put upon the petri dish by the clamps. Therefore, the creation of the epoxy chambers was repeated with less pressure. However, there was still significant distortion of the channels until too little pressure was put upon the petri dish and the chambers failed to form.

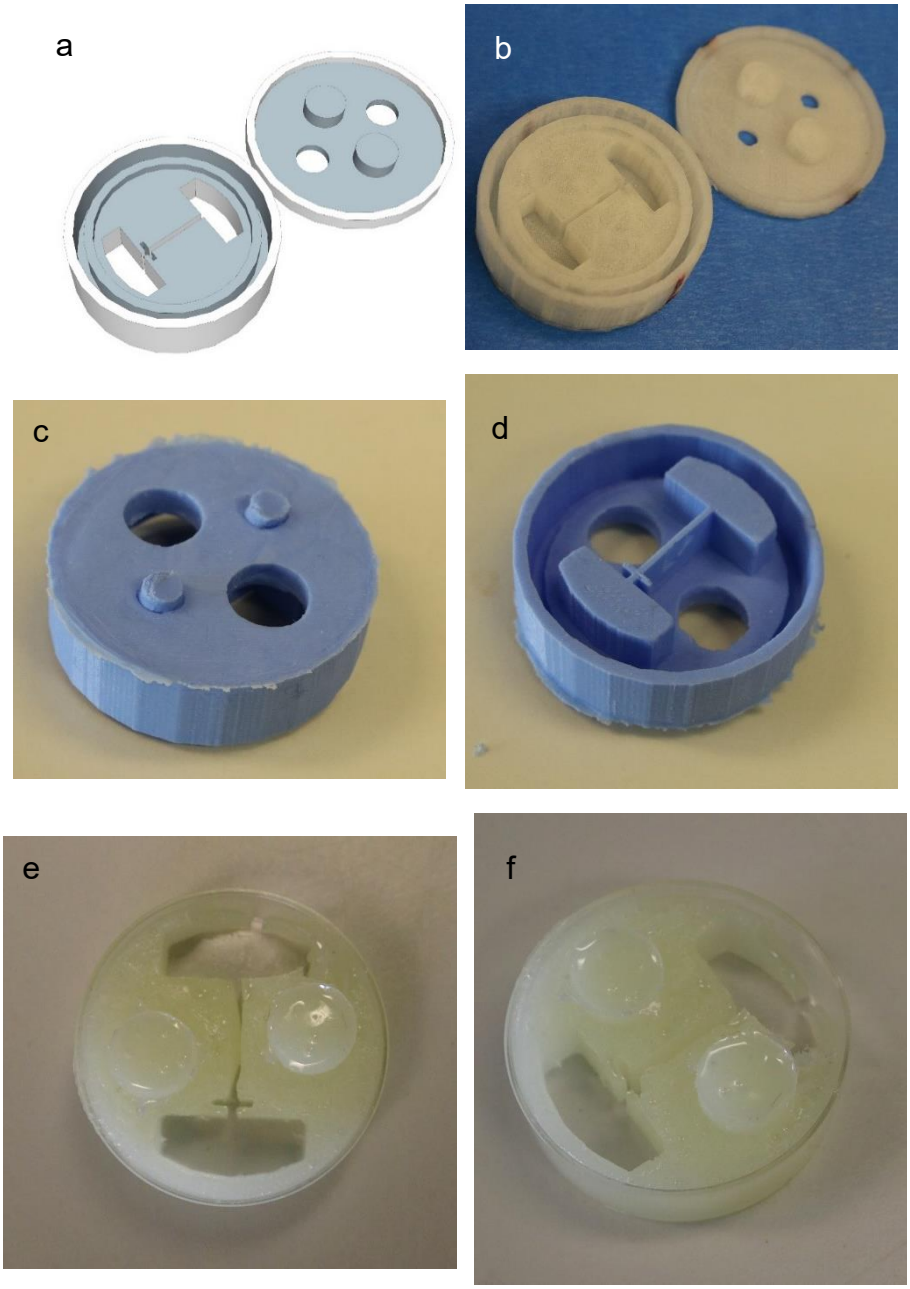


**Figure 7.13: CAD for epoxy chemotaxis chambers, the 3D printed PLA mould, the silicone cast and the fast set epoxy chemotaxis chamber. a)** CAD design created in Google Sketch Up (64 bit) 2017 for the epoxy chemotaxis chambers. **b)** 3D printed PLA mould printed using Ultimaker 3 extended. **c)** and **d)** The silicone cast created from the PLA mould. **e)** and **f)** The epoxy cast created using Araldite Rapid Epoxy from Huntsman Advanced Materials. Results representative of the production of 6 epoxy chemotaxis chambers.

Therefore, a second mid-set standard epoxy was assessed (Araldite Standard, Huntsman Advanced Materials, RS components). This epoxy took up to two hours to set but again it was found that the channel was still distorting due to the pressure of the clamps with less pressure again leading to the leaking of the epoxy and the failure of the chemotaxis chamber to form (Figure 7.14).

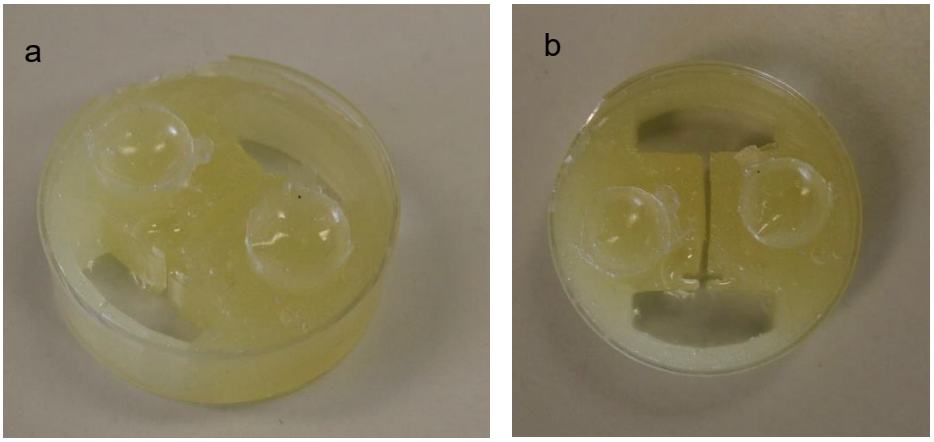


**Figure 7.14: Epoxy chemotaxis chamber made from standard set epoxy. a)** and **b)** The epoxy cast created using Araldite Standard from Huntsman Advanced Materials, RS, Components. Results representative of the production of 3 epoxy chemotaxis chambers.

In place of epoxy, a long cure clear resin was assessed (Crystal resin, Gedeo, Pebeo) to determine if a change in material and drying time prevented distortion (Figure 7.15).

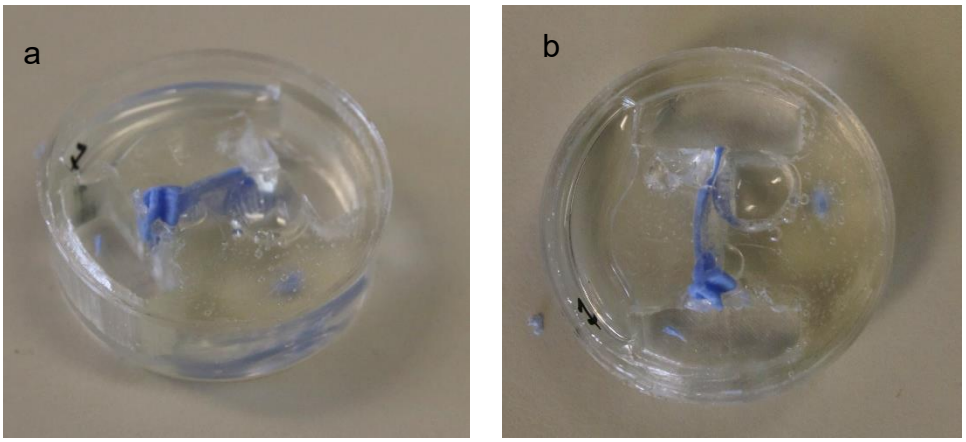


**Figure 7.15: Resin chemotaxis chamber made from long cure clear resin. a)** and **b)** The resin cast created using Crystal resin from Gedeo, Pebeo. Results representative of the production of 3 epoxy chemotaxis chambers.

However, after the 24-hour drying time it was found that the chambers were still distorting. It was concluded that to prevent this channel distortion an insert would have to be added to the silicone cast to create a 'backbone' that would prevent the cast flexing under pressure from the clamps and thus prevent the distorting of the channel (Figure 7.16). It was found that these Teflon supports were easy to incorporate and co-mould into place when making the silicone casts. Additionally, when these adapted silicone casts were used to create the epoxy chemotaxis chambers using the original quick dry epoxy, it was found that there

was no distortion of the channel (Figure 7.16 c and d). Therefore, it was concluded that the next generation of epoxy chemotaxis chambers were to include a 3D printed support for better incorporation into the silicone casts.

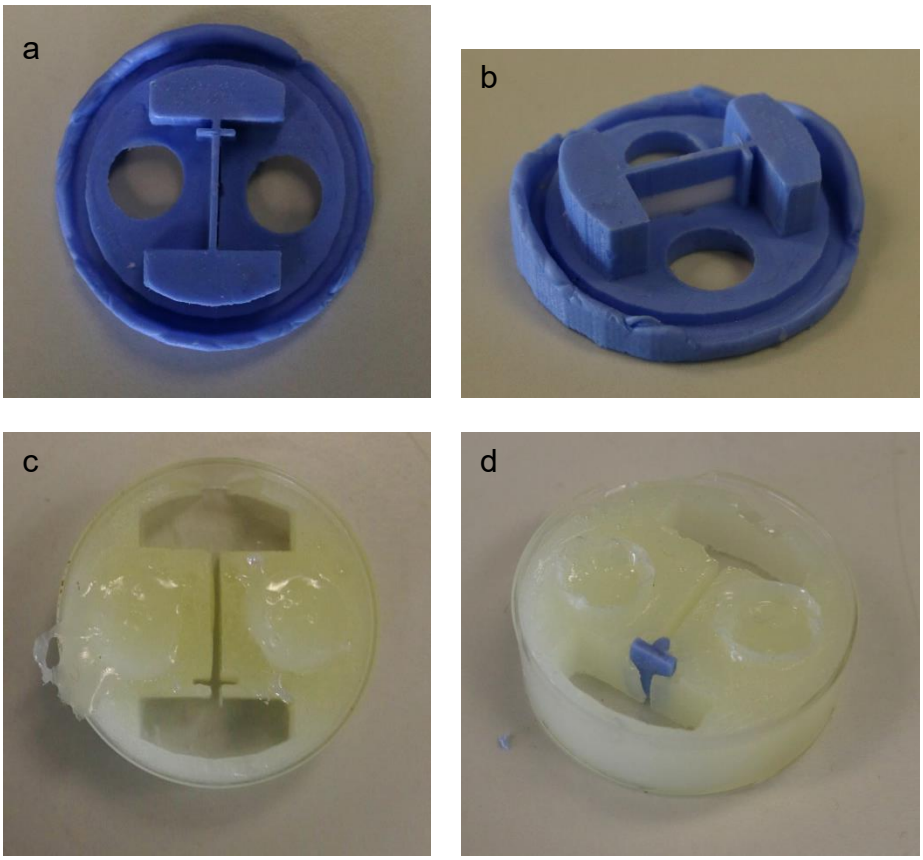


**Figure 7.16: Silicone cast and with Teflon support and the subsequent epoxy chemotaxis chamber. a)** and **b)** Silicone cast with added Teflon support. **c)** and **d)** Quick dry epoxy cast created using Araldite Rapid Epoxy from Huntsman Advanced Materials. Results representative of the production of 3 epoxy chemotaxis chambers.

### 7.3.4. Second and third generation development of 3D material for 3 $cm^2$ petri dish epoxy chemotaxis chambers

This second generation of PLA moulds was based upon the first generation design with the addition of enlarging the channel to 2 mm and printing a PLA support (Figure 7.17). This change was easily modifiable with CAD and the PLA moulds printed well. When making the silicone cast, the PLA support was easily incorporated and the casts were well formed. The PLA support is incorporated into the silicone cast with a 0.5 mm gap either side and a 2 mm gap at the bottom enabling the epoxy/resin to flush to the bottom.

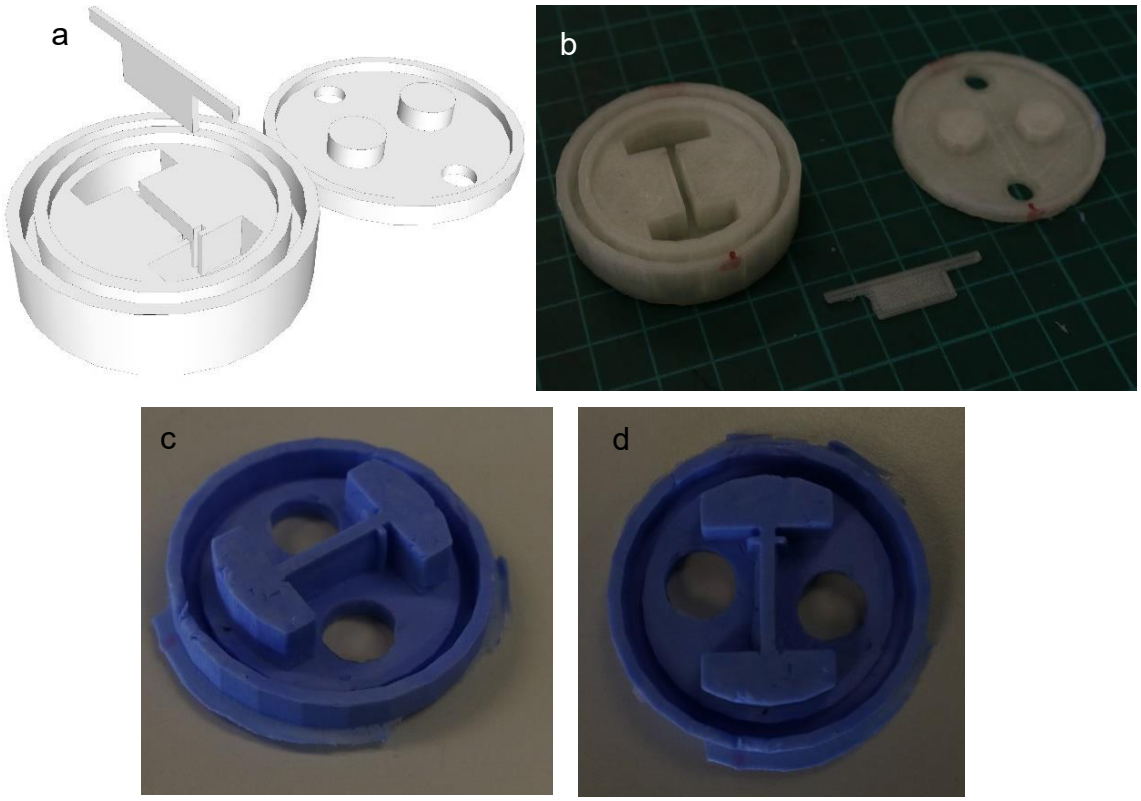


**Figure 7.17: CAD for the second generation epoxy chemotaxis chambers moulds, the 3D printed PLA mould with the 3D printed PLA support and the silicone cast produced. a)** CAD design created in Google Sketch Up (64 bit) 2017 for the second generation epoxy chemotaxis chamber moulds. **b)** 3D printed PLA mould and PLA support printed using Ultimaker 3 extended. **c)** and **d)** The silicone cast created from the PLA mould. Results representative of the production of one 3D printed PLA moulds and 4 silicone casts.

The quick dry and standard epoxy as well as the long cure resin were used to form chemotaxis chambers to determine which material was the most proficient (Figure 7.18). It was found that the standard epoxy and the resin created the cleanest, best formed chemotaxis chambers while the fast drying epoxy often

formed occlusions in the chemotaxis chambers. Testing these chemotaxis chambers with water found that all three materials created water tight chambers. Therefore, it was decided to modify the design slightly so that the silicone casts could fit into a 6-well plate which have a deeper gauge. This would enable the analysis of 6 chemotaxis chambers at any one time rather than using just the one petri dish.

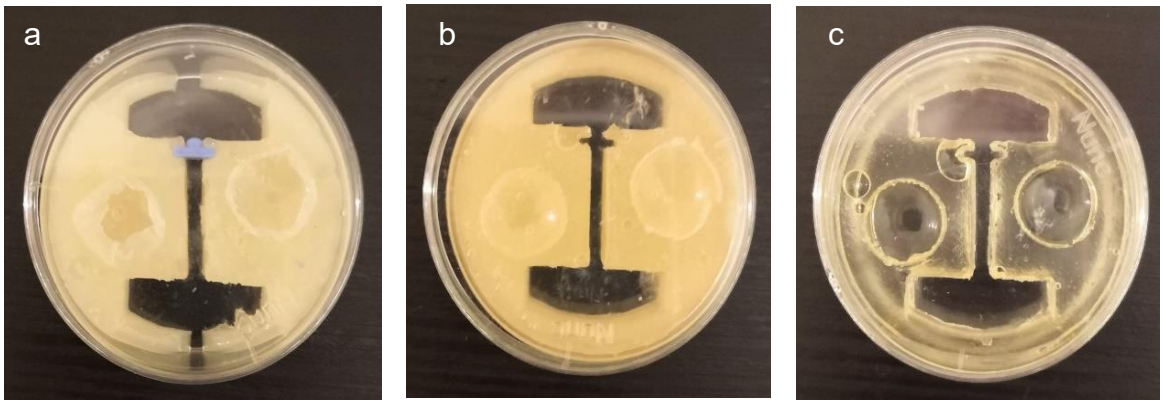


**Figure 7.18: Chemotaxis chambers created with quick dry epoxy, standard epoxy and resin. a)** Quick dry epoxy chemotaxis chamber created using Araldite Rapid Epoxy from Huntsman Advanced Materials. **b)** Standard epoxy chemotaxis chamber created using Araldite Standard epoxy from Huntsman Advanced Materials. **c)** Resin chemotaxis chamber created using Crystal resin from Gedeo, Pebeo. Results representative of the production of 3 of each chemotaxis chambers all of which did not leak when tested with water.

Therefore, the CAD for this third generation was similar to the second generation but had a deeper gauge that was easily modifiable in Google Sketch Up (Figure 7.19). The subsequent 3D printed materials were well printed with few flaws and created well-formed silicone casts. These silicone casts could then be inserted into a 6-well plate from StarLab and epoxy or resin poured around these casts. The epoxy and resin chemotaxis chambers were assessed for fluid leakage and it was determined that the chambers were water tight. Therefore, this design was taken forward for biological assessment.

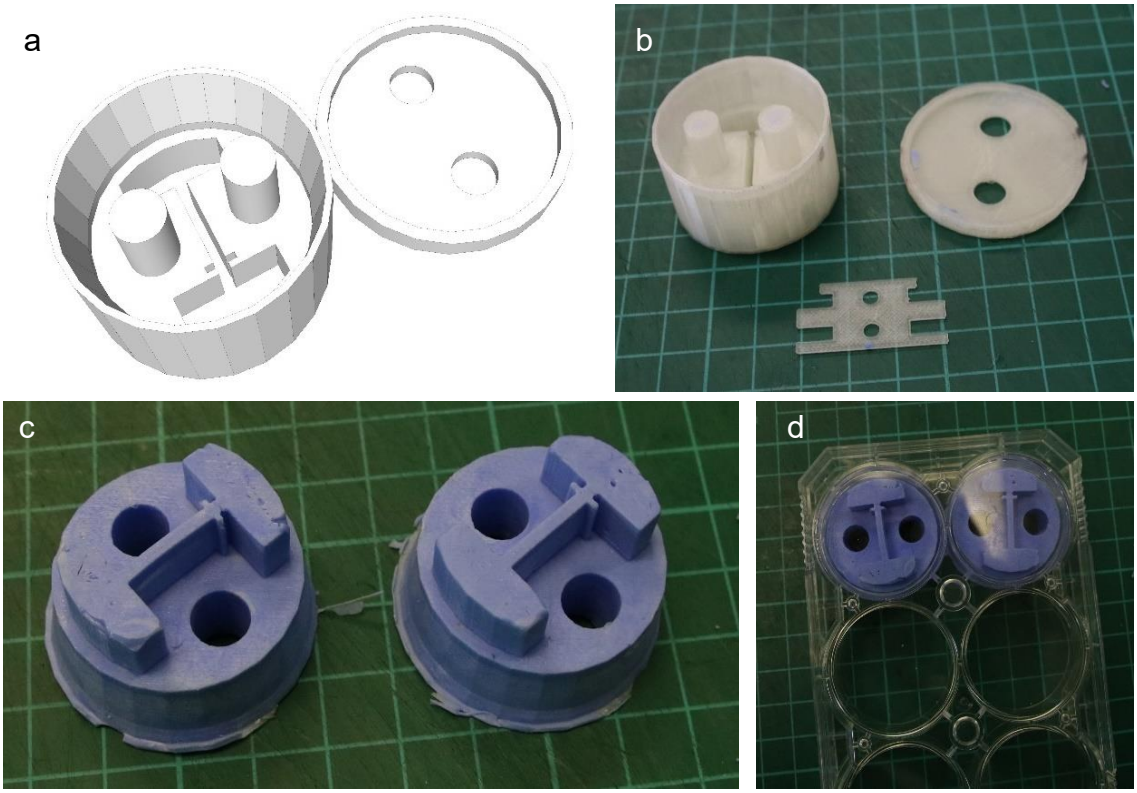


**Figure 7.19: CAD for the third generation epoxy chemotaxis chambers moulds, the 3D printed PLA mould with the 3D printed PLA support and the silicone cast produced**. **a)** CAD design created in Google Sketch Up (64 bit) 2017 for the third generation epoxy chemotaxis chamber moulds. **b)** 3D printed PLA mould and PLA support printed using Ultimaker 3 extended. **c)** The silicone cast created from the PLA mould. **d)** The silicone casts inserted into 6-well plates. Results representative of the production of 1 3D printed PLA moulds and 6 silicone casts.

### 7.3.5. Biological assessment of chemotaxis chambers

Once the final design had been achieved, it had to be determined if the materials and the design would be suitable for its biological purpose.

Similar to the silicone chemotaxis chambers, both the fast and standard epoxy and the resin caused substantial cellular toxicity in PC3 cells with a high rate of contamination. Additionally, it was noted that the fast dry epoxy underwent a colour change due to the media used which was not observed with the standard set epoxy. Therefore, no further tests were conducted using the fast dry epoxy chemotaxis chambers. In an attempt to improve cellular adhesion, the epoxy or resin chemotaxis chambers were coated with collagen and incubated up to 30 minutes prior to cell seeding. However, this collagen coat failed to improve cellular adhesion and it was determined that the epoxy and the resin were not

compatible with human cells. Therefore, a known compatible material, agarose, was assessed. Initially a 2% agarose in PBS was used. It was found that the agarose formed a thin layer across the bottom of the wells and channel and so, much like the original silicone chambers, these agarose chambers had to be removed from the well and trimmed before placing into a fresh well. These agarose chambers were found to not be water tight and again the cells did not adhere to the plate. One observation was that it seemed that the agarose was decomposing after 24-hour incubation with there being microscopic spherical agarose particles in the media that appeared to coat the seeded cells which may be preventing their adhesion. Additionally, there were high contamination issues. To solve these problems, 4% agarose in PBS was made and underwent UV sterilisation for 30 minutes to one hour. This agarose was then used to create chemotaxis chambers and then the chambers underwent an hour of UV sterilisation. When this failed to resolve the contamination issue, the agarose was autoclaved then UV sterilised as previous. This adequately prevented further contamination however, it again appeared that the agarose was decomposing over the 24-hour period and cells were failing to adhere. In an attempt to resolve this, the agarose chambers were made and media was added without cells. This was then left for a 24-hour period, media was removed and replaced with fresh media and cells were seeded. When this failed to enable cellular adhesion, a 4% agarose in RPMI was created. Again contamination was still an issue and the agarose was subject to the same autoclaving and UV treatments as previous. When this failed to prevent contamination, after autoclaving the agarose, it was left to cool and 1% penicillin/streptomycin was added before casting the chambers. It was found that this method caused the least amount of infection to occur, however contamination still remained a prevalent issue throughout this developmental process. Despite this, the 4% agarose in RPMI was found to be a well-tolerated potting material and PC3 cells were able to adhered successfully to the plates.

Secondly, it was found that due to the small amount of media in these chambers (500-1000 µL) that after a 24-hour incubation period, the media would completely evaporate. Therefore, 3 mL of sterile water had to be added to one of the wells in the 6-well plate to create more humidity. This was an issue as it decreases the number of experimental conditions you can use per plate and caused a significant amount of condensation inside the plate. However, the

condensation did not jeopardise the recordings taken of the cells and it resolved the problem of the media evaporating.

Another issue arose in that the silicone inserts failed to prevent the leakage of cells from the well seeded into the rest of the chemotaxis chamber. This occurred via cells compressing and squeezing under the insert due to it not being flush to the bottom of the plate. Therefore, cells were seen throughout the chemotaxis chamber and even under the agarose chamber. The use of these silicone inserts themselves was questionable as it was previously seen that the silicone caused toxicity in PC3 cells. Additionally, the agarose chambers themselves were also found to not be flush to the bottom of the plate and cells were seen under the agarose. In an attempt to resolve these problems, the inserts were abandoned and instead cells were seeded onto the dry plate and incubated for 6 to 24 hours to enable cells to adhere before media being added throughout the chamber. This method of cell seeding failed due to the small amount of media evaporating before the cells had adhered. This evaporation still occurred even with the addition of sterile water to one of the wells. Alternatively, cells were seeded onto glass slides in separate plates before being transferred into the 6 well plate and the agarose chamber placed over the top. While this did successfully retain the cells to one side of the chamber, the size of the glass slides was too large and therefore, cells were again present under the agarose. Attempts to reduce the size of the glass slides manually were unsuccessful. This problem might have been resolved by purchasing smaller glass slides that would fit inside the 100 $mm^2$ well however, the cells may still have migrated off the glass and under the agarose. It is possible that by using clamps as with the epoxy chambers, the agarose could have formed a complete seal to the bottom of the plates, removing the necessity of cutting away the excess agarose, which required a lot of handling and is the most likely cause for the high contamination rates. However, the use of clamps was not assessed and so all experiments saw cells seeding under the agarose chambers.

The final problem that arose was in relation to the creation of a chemokine gradient that the PC3 cells could migrate to. It was originally confirmed by Dr D. Warren that a gradient could be achieved using the epoxy chambers filled with sterile water and dye being added to one well (data unavailable). The dye was able to filter through the water creating a gradient that was still present after 8 hours. However, this was achieved by keeping the plate stationary for the 8-hour

time period. The time-lapse camera available (Zeiss Axiovert 200M motorise inverted fluorescent/ live cell imaging microscope attached to a Axiocam CCD camera) had a stationary camera and a motorised plate platform. Therefore, to analyse multiple wells, the plate underwent X, Y and Z movements which would mix the chemokine into the media, thus any chemokine gradient was lost. Therefore, this limited analysis to just one well of the six well plate, massively reducing the output that could be achieved per plate. Additionally, the plate had to be moved from under the sterile environment of the laminar flow hood, to being placed onto the microscope plate platform, which despite efforts also saw the loss of a gradient. In an attempt to create a gradient, the amount of CXCL12 chemokine was increased from 1 µM up to 50 µM. It was found that at 50 µM there was a high rate of cellular toxicity. Additionally, such high concentrations of chemokine negated the original aim of creating a cheap migration assay. Therefore, subsequent experiments were conducted using 10 µM of CXCL12, still a very high concentration of chemokine and hugely increasing the costs the of assay.

Despite these changes, a gradient was never achieved as demonstrated in Figure 7.20 whereby the tracked PC3 cells are shown to not be migrating towards the ‘higher’ concentration of chemokine. Following this, chemokine was soaked into filter paper which was then added to one well of the chemotaxis chamber. Again, this failed to produce a gradient. Lastly, a chemokine agarose spot was created as described in Ahmed et al. (2017) and Wiggins and Rappoport (2010). However, it was found that the agarose spot did not adhere to the plastic and the addition of media caused the spot to lift off from the plastic and float in the media. Therefore, in the future an alternative method would have to be assessed such as the development of a 3D cast into which biological hydrogels made from agarose, collagen or fibrin could be made with chemokine subsequently added to this hydrogel.

Overall, two issues remained unresolved; the lack of gradient and cells seeding under the agarose chamber. These two issues negated the use of the chamber, as cells could simple be seeded into a plate and chemokine added. Therefore, the design was deemed a failure and attention was instead diverted to alternative 3D printed materials.

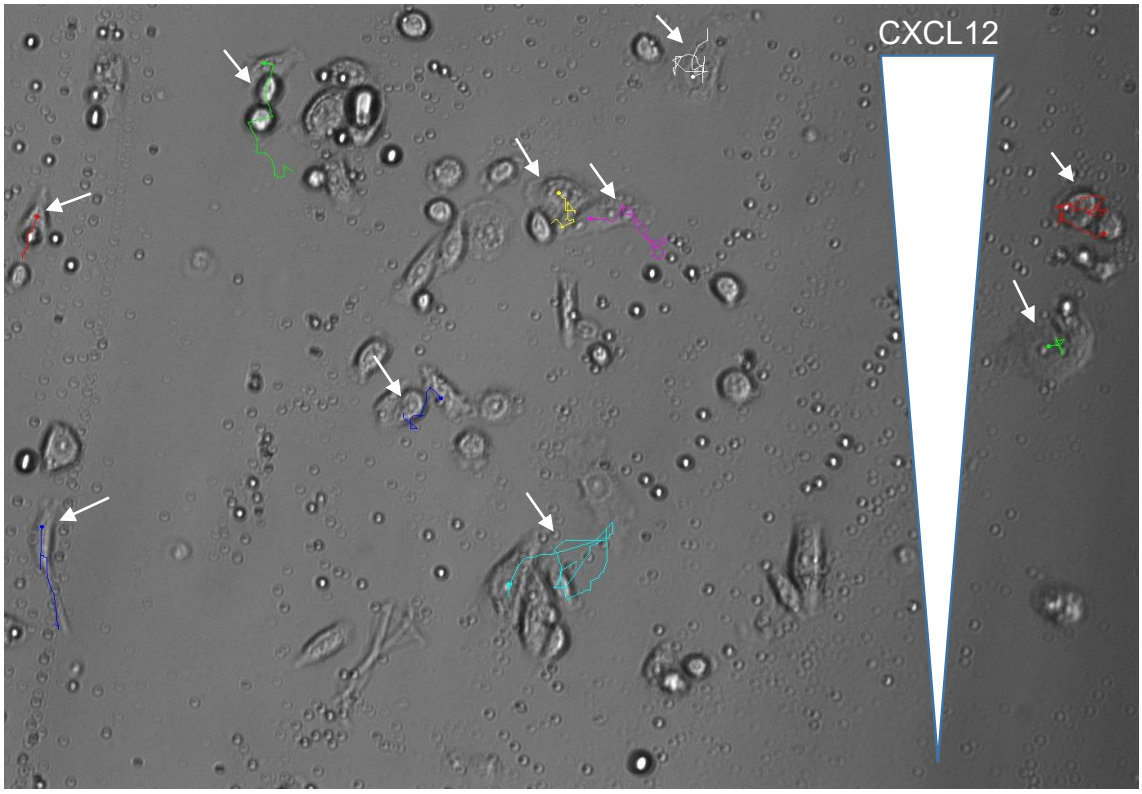


**Figure 7.20: PC3 cells did not migrate towards CXCL12 in a 10-hour time lapse assay.** Tracked PC3 cell speeds stimulated with a 10 µM CXCL12 gradient. Data shows representative cell tracks from 3 independent experiments with similar findings. Acquired with a Zeiss Axiovert 200M motorise inverted fluorescent/ live cell imaging microscope with 10x objective.

### 7.3.6. Development of 3D printed Oris™ Cell Migration assay stoppers

After initial development of the 3D printed chemotaxis chambers proved unsuccessful, time lapse assays and Oris™ Cell Migration assays were used as alternatives (Figure 7.21). Both of these assays proved to be successful assays in determining the response of cells when stimulated with CXCL12 and treated with CXCR4 antagonists (Figure 4.40 through to 4.48). Each assays had pros and cons. For example, while time lapse assays were simple and cheap assays with the ability to assess changes in the migratory speeds of individual cells in real time these assays could not determine directional migration. Alternatively, Oris™ Cell Migration assays proved to be accurate and effective at determining changes in chemokine directed migration, but could not assess single cell migration capabilities in real time. Thereby, combining both the time lapse assays and the Oris™ Cell Migration assays both migratory speeds and directed migration could be assessed. However, the Oris™ Cell Migration assays were

expensive to run, costing $299 per plate. Therefore, efforts went into designing replacement stoppers for the Oris™ Cell Migration assay plates.

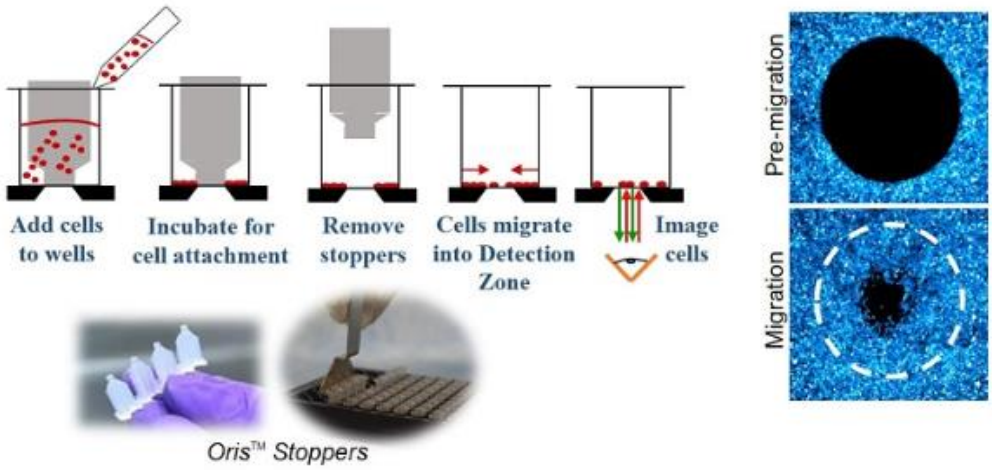


**Figure 7.21: The Oris™ Cell Migration assay (adapted from Platypus Technologies Website).** The Oris™ Cell Migration assay consists of a 96-well plate with removable stoppers. Cells can then be seeded into these wells and after leaving to incubate for up to 24 hours, these stoppers can be removed creating a cell free Detection Zone in the centre of the well. Cells can then be treated with agonists and/or antagonists and incubated again for up to 24 hours. Wells can then be imaged directly, or a fluorescent dye added. Only the cells that have migrated into the Detection Zone will be analysed, creating a research tool that is highly reproducible and accurate whilst using very low concentrations of agonists and/or antagonists.

A more flexible material than PLA was required for these stoppers. However, due to the cytotoxic effects of silicone, epoxy and resin seen previously, it was decided that the replacement stoppers should be printed directly with TPE-U (a polyurethane flexible filament material) (Figure 7.22). While the CAD of the stoppers were bordering the capabilities of Google Sketch Up 2017 due to their small size, the stoppers printed well. However, when these stoppers were used in the ORIS™ Cell Migration assay 96-well plate it was found that the space between the stoppers was too large, preventing the stoppers from smoothly inserting into the plates (Figure 7.22c). Additionally, the stoppers were too short, therefore did not come into contact with the bottom of the well, which would prevent the formation of the exclusion zone seen in Figure 7.21. Therefore, for the future successful development of these TPE-U printed stoppers several CAD changes would be required:

1. Lengthening of the stoppers from 1.1 cm to 1.4 cm.

2. Shortening of the space between the stoppers from 2 mm to 1 mm.
3. The stopper tips need to be made smaller from 3 mm to 1 mm.
4. The width of the stopper needs to be decreased from 7 mm to 6 mm as currently they form too tight a fit in the well.

Following these CAD corrections, the 3D printing of the stoppers might then have to be improved by changing the parameters of the 3D printer in order to print well-formed stoppers as several of the original prints had residual material that had to be trimmed. It has yet to be determined if TPE-U is toxic to the PC3 cells. Additionally, these TPE-U stoppers are much more ridged than the original ORIS™ Cell Migration assay stoppers which may have an effect upon the behaviour of the PC3 cells. Finally, biological assessment would have to be conducted to determine if these stoppers are suitable replacements for the ORIS™ Cell Migration assay stoppers.

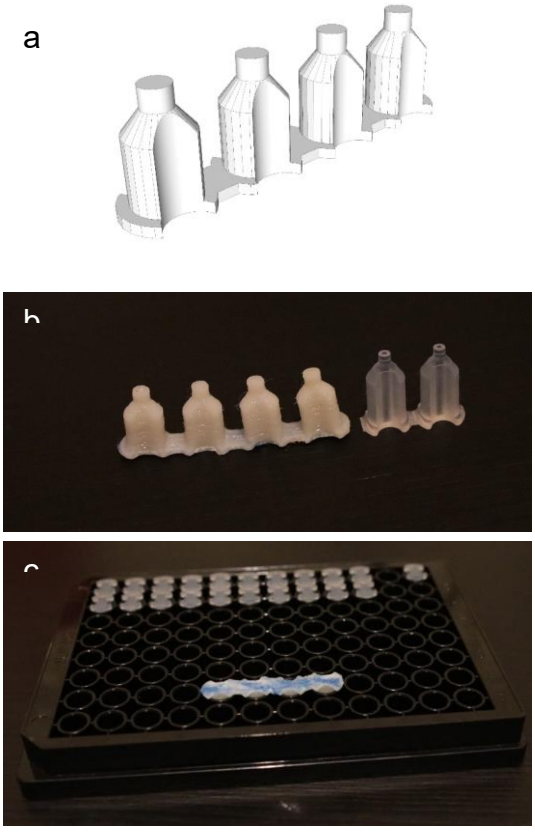


**Figure 7.22: CAD for the ORIS™ Cell Migration assay 96-well replacement stoppers and the 3D printed TPE-U stoppers. a)** CAD design created in Google Sketch Up (64 bit) 2017 for the 96-well plate stoppers. **b)** 3D printed TPE-U stoppers for use in the ORIS™ Cell Migration assay 96-well plate. **c)** Insertion of the TPE-U stoppers into the ORIS™ Cell Migration assay plate. Results representative of the production of 3 sets of 4 3D printed stoppers.

## 7.4. Discussion

Biological gradients are highly important for several mechanisms such as growth, guided migration and cellular differentiation. Specifically, biological gradients are critical for the development of metastatic cancer (Eccles, 2005). This has led to the development of several *in vitro* methodologies that would enable cells to be exposed to a biochemical gradient (Keenan and Folch, 2008). One commonly used method to assess cellular migration towards a chemokine is the Boyden chamber originally designed in 1962 by Stephen Boyden (Boyden, 1962). However, while this method is simplistic, its use in experiments with PC3 cells incubated with CXCL12 and various CXCR4 antagonists failed to produced accurate, reproducible results. The cause of this lack of reproducibility is possibly due to the failure of a gradient to form across the membrane due to fluid level imbalances caused by pipetting errors. Even slight changes in fluid levels can cause the failure of the porous membrane of the insert to not come into contact with the media below, or to be submerged in it. Additionally, the gradient cannot be controlled in a Boyden chambers due to the presence of the membrane. Finally, Boyden chambers cannot be used to observe single cells, nor can they be used for real time analysis (Keenan and Folch, 2008). Not only was it found that this assay was not reproducible, but there was the added imprudence that these assays were expensive. Therefore, a collaboration with Dr D. Warren and Dr J. M. Courtney saw the development of 3D printed materials to create chemotaxis chambers. The overarching aim of these chambers was to create a CAD that could be downloaded for free for cheap reproduction in laboratories worldwide. However, after several modifications it was found that ultimately the produced chemotaxis chambers failed to meet the required aims and so further investigations were discontinued.

One such failure was that, despite great efforts there were high levels of cellular toxicity in relation to the materials used: silicone, epoxy and resin. While silicone is used safely in medicine, such as in implants, the silicone that was used for this project was a cheap, non-biologically tested silicone that was not produced or moulded in a sterile environment. Therefore, for the continuation of this project a sterile, laboratory approved silicone would have to be purchased. While this was not possible at the time, alternative materials were explored: epoxy and resin. These materials were also cheap and easy to use for initial design development however, both have been found to have inhibitory or cytotoxic

effects upon cancer cells throughout the literature (Subash-Babu et al., 2017, Yuniarti et al., 2018, Zhang et al., 2013, Ni et al., 2012). Therefore, the final material PLA was the only material not assessed. The reasoning behind this was that while PLA is cheap and theoretically the chemotaxis chamber could have been directly printed into a petri dish, this would have increased production times significantly as it takes approximately 40 minutes to print 1 fourth generation PLA topper alone while it took only 5-10 minutes for the silicone to set and one to 24 hours for the epoxy or resin to set. Therefore, once you have printed multiple casts, production time would be relatively small and several chambers could be created at once. While PLA was never assessed for cytotoxicity, PLA has been used successfully in the literature and suggests that using this material or a coated version (see hydrogels below) might be the best material for future application, if the 6-well plates that were being printed into could withstand the high melting temperatures of the PLA (Xiang et al., 2017a, Goudarzi et al., 2018).

Another problem that occurred throughout the developmental process was in relation to high levels of contamination, no matter which generation of chemotaxis chamber was used. This was most likely to be due to the production of these chemotaxis chambers not implicating good manufacturing practise (GMP) therefore failing to produce sterile products. Due to its size and the ownership rights of the 3D printer, it was unable to be placed inside a laminar flow hood. Therefore, all PLA moulds were created in a non-sterile environment using non sterile materials. While these moulds could then be UV treated and cleaned using ethanol and/or detergents, they are unable to be heat treated as this could the plastic to warp or decompose. As mentioned previously, the silicone, epoxy and resins used were all cheap non-laboratory materials that had not been produced in a sterile environment. Additionally, the original aim was to produce cheap materials and so both the PLA moulds and the silicon casts were reused multiple times. Again, while the individual component could be sterilised using UV, alcohol and detergents and the produced chambers sterilised using UV, these two factors enabled the final chambers to carry contaminants. While every attempt was used to create sterile chambers such as using a clean and sterile laminar flow hood, the hood itself was not in a clean room and full personal protective equipment was not worn. For example; while gloves and a laboratory coat were worn, hair covers, overshoes and facemasks were not used and so contaminates could still have be introduced. Additionally, the final design for these chambers required a

lot of manual handling and while every precaution was taken to achieve sterility, this required equipment that was not always stored in a sterile environment. For example, to trim the excess agarose, tweezers and a scalpel were used that were stored and used outside of the laminar flow hood. While these were cleaned each time before use with 70% ethanol, this could have introduced contamination. Finally, when the chambers were placed inside the 6-well plates, they were occasionally stored overnight at 4˚C. While these plates were taped shut, they were no longer being stored inside a sterile package or in a sterile environment and so this may have allowed contaminates to enter the plate. Therefore, future production would require much stricter application of GMP for successful mass production of these chemotaxis chambers.

The final two major problems of the chemotaxis chambers were that the chambers failed to produce a chemotactic gradient for the cells to migrate to and the seeded cells did not remain inside the chemotaxis chamber but instead slipped under the inserts and under the agarose. To try to amend this, it would be possible to use clamps to attempt to form a complete seal of the agarose chemotaxis chamber to the bottom of the plates similar to how the epoxy chambers were created. Additionally, the chambers could be directly print into the petri dish however, this has the lengthy production times discussed previously. Alternatively, CAD could be used to produce a framework for casting biological hydrogels made from agarose, collagen or fibrin into which the chemokine could be added.

Biological hydrogels have been commonly used throughout the literature to create gradients by seeding cells either into or on top of the gel (Heit et al., 2002, Chen et al., 1998, Foxman et al., 1999, Foxman et al., 1997). To then create the gradient a void could be made in the gel before being filled with chemokine or simply by dropping the chemokine onto the surface of the hydrogel and letting it diffuse into the gel. Due to the cheap materials required for hydrogels as well as the benefit of hydrogels being theoretically similar to *in vivo* tissues, enabling free diffusion of chemokine through the gel and enabling control over the position and orientation of the gradient, the creation of 3D printed materials to form hydrogels would be the next logical step in this particular development process. Despite this, hydrogels themselves have issues developing biochemical gradients leading to poor reproducibility due to variable biochemical concentrations (Keenan and Folch, 2008). This variability is related to the inability to control the gradient once

the chemokine is loaded which can be related to the porosity of the gel and the formation of the gel matrix which cannot be exactly replicated experiment to experiment. Additionally, the placement of the cells and or the chemokine can cause huge variation in results even with a slight deviation of a millimetre. This is due to cells being sensitive to changes in their environment at distances 1000 times smaller than the millimetre variation (Goodhill and Baier, 1998).

Therefore, due to the main failures highlighted above, alternative methodologies that enable the observation of the chemokines upon cellular migration such as: Zigmond chambers, Dunn chamber, the use of micropipetting and the use of microfluidics could be investigated for alternative cheap 3D printed materials. However, the Oris™ Cell Migration assay was selected for development due to the reasons discussed previously and that only very small volumes of agonists and/or antagonists are required for this assay. Therefore, after the initial expense of buying the plate, the assay is cheap to run.

Initially, the development of the stoppers saw problems relating to scale, with the TPE-U stoppers being shorter and spaced further apart than the original stoppers. These issues were largely due to now having to outsource the CAD and 3D printing to Dr J. M. Courtney upon his leaving The University of East Anglia. Therefore, failure in the CAD reconstructions of the stoppers was based upon miscommunications and limited resources rather than any failure of the CAD or 3D printing capabilities. Therefore, while the development of the stoppers was incomplete and biological assessment was not conducted, it is likely that these stoppers will be more successful than attempting to development 3D printed materials for hydrogels as the Oris™ Cell Migration assay has already been validated to be reproducible using the PC3 cells line with the CXCL12 chemokine and various CXCR4 antagonists (Figure 4.50).

## 7.5. Conclusion

The development of 3D printed materials for chemotaxis chambers was unsuccessful and while efforts could be put into further developing this design, overall it would be more applicable to look into alternatives such as developing hydrogels for real time observation of single cell migration towards a chemokine gradient. Alternatively, there may be an application for 3D printing replacement stoppers for the Oris™ Cell Migration assay 96-well plate to reduce the cost of buying replacement plates. While the development of these stoppers was in its early stages, there is potential for these stoppers to be biological viable.

# Chapter 8: Final Discussion and Thesis Conclusions

There were several overarching aims of this thesis including: understanding the roles of the downstream proteins PKC and PKD in CXCL12-stimulated migration of prostate cancer, investigating novel CXCR4 antagonists in several CXCR4 overexpressing cell lines including the development of an antagonist to be used in click chemistry, characterising ACKR3 expression, internalisation and its effects on CXCL12- stimulated migration and finally to explore 3D printing for the development of novel research tools.

The overarching conclusions from this research are as follow:

1. The classical PKC isoforms, PKCα and PKCγ and the novel PKC isoform PKCη, are not important for CXCL12 stimulated migration in PC3 prostate cancer cells.
2. PKC and PKD do not affect intracellular calcium release from PC3 cells when stimulated with CXCL12.
3. Both PKC and PKD have effects upon the cytoskeleton of PC3 cells.
4. The novel CXCR4 antagonist AZ6-2 is the most potent CXCR4-antagonist compared to AMD3100, AZ3-2, IS4 and IS7.
5. AZ6-2, IS4 and IS7 significantly reduce intracellular calcium release in THP-1, Jurkat, MCF-7 and PC3 cells while the already marketed CXCR4 antagonist AMD3100 is only effective in MCF-7 and Jurkat cells.
6. AZ6-2 prevents the reorganisation of the actin cytoskeleton, thus prevents any changes to cell shape and area.
7. AZ6-2, IS4 and IS7 are CXCR4 receptor specific antagonist.
8. IS4 has improved stability over AZ6-2.
9. IS7 successfully bound to 3-azido-7-hydroxycoumarin *ex situ*, demonstrating its use as both a laboratory tools and for cancer therapeutics.
10. ACKR3 is expressed in MCF-7, PC3, Jurkat and THP-1 cells at 4˚C however, when the incubation temperature is raised to 37˚C, ACKR3 become internalised in both MCF-7 and Jurkat cells.
11. The internalisation of ACKR3 in the absence of CXCL12 occurs via caveolin-dependant endocytosis in both MCF-7 and Jurkat cells. In the presence of CXCL12, ACKR3 is internalised via clathrin/caveolin independent endocytosis in Jurkat cells.
12. Using 11G8, ACKR3 was found to not promote CXCL12-stimulated migration in Jurkat or THP-1 cells.

13. It is possible that 3D printing replacement stoppers for the Oris™ Cell Migration assay 96-well plate will reduce the cost of this assay.

## 8.1. The Role of PKC and PKD in CXCL12 Directed Prostate Cancer Migration

Prostate cancer is the most common cancer in males in the UK and is the second most common cause of cancer deaths accounting for 13% of total cancer deaths. This high morbidity is attributable not to the primary tumour but due to the metastasis of the prostate cancer (Cancer Research, 2017, Chaffer and Weinberg, 2011, Thobe et al., 2011). While there are several treatment options available, many prostate cancers become resistant to these therapy (Frieling et al., 2015). Therefore, there is a requirement for alternative therapies such as targeting the CXCR4 receptor and/or its downstream signalling proteins (Taichman et al., 2002). CXCR4 is the most commonly overexpressed chemokine receptor on tumour cells including prostate cancer. It is this aberrant CXCR4 signalling that enables many tumours, including prostate tumours, to have increased metastatic potential (Johnson et al., 2004). While there has been extensive research into developing CXCR4 antagonists, their success had been limited. Therefore, an alternative approach is to determine which of the downstream signalling proteins of CXCR4 are important for CXCL12 stimulated prostate cancer migration.

This work determined that two downstream signalling proteins, PKC and PKD, are important for CXCL12-stimulated migration in PC3 prostate cancer. While it could not be confirmed which specific PKC or PKD isoforms were important in this migration, it was confirmed that several isoforms were not important for CXCL12 stimulated migration including the classical isoforms PKCα and PKCγ and the novel PKC isoform PKCη. It was confirmed that PKC and PKD do not affect intracellular calcium release from PC3 cells, which was to be expected due to these two proteins being downstream of calcium release. Additionally, inhibition of PKC and PKD affected the cytoskeleton of the PC3 cells. Specifically, the inhibitors GF109203X (inhibitor of PKCα, PKCβ1, PKCδ and PKCε) and Staurosporine (inhibitor of PKCα, PKCγ and PKCη) caused a reduction in the size of the cell with GF109203X causing an increase in the number of protrusion while Staurosporine caused cells to assume a more rounded morphology. However, PKD inhibition by CID755673 caused the PC3 cells to assume a more elongated morphology with no change to area. Indicating the different, but equally important,

roles PKC and PKD have in cell migration via changes to the actin cytoskeleton. Overall, this work highlights the potential for targeting PKC and PKD for novel prostate cancer therapeutic purposes.

Due to several of the inhibitors used not being PKC or PKD isoform specific, it was unable to determine which isoform(s) were specifically involved in reducing CXCL12 stimulated migration or which isoforms were involved in the actin cytoskeletal rearrangement of the PC3 cells. Therefore, to further this work it is necessary to use more specific PKC/PKD inhibitors or alternative approaches like protein knockdowns. Additionally, the elongation of the PC3 cells after inhibition by the PKD inhibitor CID755673 implicated a novel role of PKD in tail release. Therefore, further studies should be carried out to determine which isoform(s) are involved in tail release. Additional investigations are required to determine the cause for the transition from amoeboid to mesenchymal migration and vice versa.

## 8.2. Effects of the CXCR4 Antagonists AMD3100, AZ3-2 and AZ6-2 on CXCL12 Directed Cancer Cell Migration

As mentioned previously, CXCR4 overexpression has been detected in more than 30 human cancers including: acute myeloid leukaemia, breast, ovarian, melanoma, thyroid, renal, pancreatic and prostate cancer and more recently salivary gland neoplasms (Borrello et al., 2005, Koshiba et al., 2000, Mehta et al., 2007, Müller et al., 2001, Scotton et al., 2001, Singh et al., 2004, Staller et al., 2003, Vela et al., 2015, Phattarataratip and Dhanuthai, 2017). This aberrant CXCR4 signalling increases metastatic potential enabling tumours to migrate to tissue sites in the body that naturally express CXCL12 such as the bone marrow, brain, lungs and liver (Johnson et al., 2004, Müller et al., 2001). Therefore, the inhibition of the CXCR4/CXCL12 migratory pathway can potential lead to the prevention of tumour metastasis. While multiple CXCR4 antagonists have been developed only two have so far been approved for use in cancer, AMD3100 and CTCE-9908 (DiPersio et al., 2009b, Wong et al., 2014). However, the use of these CXCR4 antagonists is limited as AMD3100 is only approved for use in MM and NHL and CTCE-9908 is only approved for use in osteosarcoma. Additionally, AMD3100 is not used for the prevention of metastasis but for mobilizing stem cells from the bone marrow for autologous stem cell transplantation (DiPersio et al., 2009b). Therefore, the development of novel CXCR4 antagonist is paramount for the progression of personalised medicine and cancer therapeutics. Di Maro et al. (2016) synthesised two novel CXCL12-mimetic peptides, named throughout

as AZ3-2 and AZ6-2, which impaired CXCL12 stimulated migration in both HT29 and HCT116 colon cancer cell lines and the CCRF-CEM ALL cancer cell line (Di Maro et al., 2016). Therefore, these two novel peptides were tested in five other cell lines: Jurkat (acute T cell leukaemia), THP-1 (AML), MCF-7 (breast), PC3 (metastatic prostate) and SKMEL28 (melanoma) and compared to the already marketed compound, AMD3100.

AZ6-2 was the most potent CXCR4-antagonist compared to AZ3-2 and AMD3100 and was able to prevent CXCL12 stimulated migration in all CXCR4 positive cell lines tested. Additionally, AZ6-2 significantly reduced intracellular calcium release in THP-1, Jurkat, MCF-7 and PC3 cells while AMD3100 was only effective in MCF-7 and Jurkat cells. AZ6-2 was found to be a CXCL12-mimetic peptide that did not cause CXCR4 receptor internalisation. Also, AZ6-2 prevented the reorganisation of the actin cytoskeleton and finally, it was determined that AZ6-2 is a CXCR4 receptor specific peptide.

It was observed that 1 μM of AZ6-2 caused inhibition below the basal level of migration in Jurkat, THP-1 and PC3 cells. While this was not a significant reduction, it suggests that AZ6-2 might have off target effects whereby AZ6-2 could be binding to other receptors. While other chemokine receptors were investigated (CXCR3, CCR1 and CCR5) to determine if AZ6-2 also inhibited these receptors, future investigations would require a more extensive investigation into other chemokine receptors and other cell surface receptors. Additionally, compound kinetics were never investigated therefore it would be beneficial to determine the speed of the peptide-protein binding, the equilibrium dissociation constant of peptide-protein complex Kd (affinity) and ultimately if the compound is reversible. While all three CXCR4 antagonists prevented cytoskeletal changes, it was observed that the addition of 10 nM of CXCL12 did not stimulate MCF-7 cells to undergo cytoskeletal changes in order to migrate. This is likely due to the 10 nM concentration of CXCL12 not being high enough to sufficiently stimulate all the CXCR4 receptors and produce a significant response. Alternatively, it is possible that the one-hour time frame used in these experiment is not long enough for CXCL12 to stimulate migration thus not long enough to stimulate any actin cytoskeletal changes in MCF-7 cells. Therefore, these experiments should be repeated again with an optimised concentration of CXCL12 and an optimised time for MCF-7 cell migration.

## 8.3. The Development of a ‘Click’ CXCR4 Antagonist and its Effects upon CXCL12 Stimulated Cancer Cell Migration

While AZ6-2 was both a potent and a specific CXCR4 antagonist, the disulphide bond in its structure is liable for reduction when introduce to mammalian cells. Therefore, a new CXCR4 antagonist, IS4 was synthesised replacing the disulphide bond with a maleimide group. This would prevent the reduction of the compound, but also facilitate the introduction of an alkyne group to enable the possibility for our compound to undergo ‘click’ chemistry (Kolb et al., 2001). Specifically, the addition of the maleimide group creates an opportunity for a CuAAC click chemistry. This is a particularly stable click reaction that does not change the properties of the original compound or cause cellular toxicity (Hong et al., 2010). This clickable CXCR4 antagonist could then be used for scientific investigation by clicking biotin, fluorescent markers, antibodies and drugs amongst other biomolecules. Additionally, these clickable compounds could be used for therapeutic use as a multifunctional tool preventing CXCL12 stimulated migration of cancer cells as well as targeting these cells for death.

Overall, it was shown that the structural changes made to IS4 still enabled it to function as a CXCR4 antagonist and maintain its potency. Additionally, IS4 proved to be a CXCR4 specific antagonist with improved stability over AZ6-2*. In situ* CuAAC click chemistry using IS4 and the dye 3-azido-7-hydroxycoumarin was unsuccessful however, it is likely that this is related to the dye used. The subsequent development of IS7, bound to 3-azido-7-hydroxycoumarin *ex situ*, proved that this compound can be clicked to a fluorescent dye for use as a laboratory tool.

Initially, investigations were carried out using the CXCR4 mAb, 12G5 as a CXCR4 antagonist. These investigations demonstrated that 12G5 cannot be used for long term incubation, thus demonstrating a gap in the market for click CXCR4 compounds, it would be beneficial to conduct future investigations using AZ6-2, IS4 and 12G5 in the same experiment rather than comparing between two experiments. Additionally, there would be considerable benefit in conducting competition assays using increased CXCL12 concentrations to compete 12G5, AZ6-2, IS4 and IS7 from CXCR4 and doing time dependant investigations to find the maximal time that 12G5 can be used as a CXCR4 antagonist. It was found that the yellow colour of IS4 caused interference with the calcium release results. Although these observations were concluded to not jeopardise the results, it

would be worthwhile to conduct alternative experiments that do not require fluorescence such as radioligand binding assays. During internalisation assays, IS4 demonstrated a trend of decreased fluorescence i.e. it suggested that IS4 may be causing internalisation of CXCR4. Therefore, to confirm that IS4 does not cause CXCR4 internalisation, quantitative methods such as flow cytometry, ELISA, radioligand binding or Fluorokine® Receptor Detection Kits should be conducted. Similar to what was seen with AZ6-2, it was observed that 1 µM of IS4 or IS7 caused inhibition below the basal level of migration in Jurkat, THP-1 and PC3 cells. This suggests that IS4 (and indeed AZ6-2) may be acting as inverse agonists and would require further investigation. While more chemokine receptors were analysed to determine antagonist specificity (CCR1, CCR2, CCR3, CCR4, CCR5, CXCR1, CXCR2, CXCR3), it was found that IS4 and IS7 did not have any significant inhibitory effects on these receptors however, there was a trend indicating slight inhibition. This is possibly due to the formation of CXCR4 heterodimers and warrants future research. Similar to AZ6-2, it would also be beneficial to conduct kinetic profile assay on IS4 and IS7 to determine if this compound is reversible and able to compete with CXCL12. It was determined that IS4 was more stable the AZ6-2 after 30-minute incubation with FBS. This conflicted results by Di Maro et al. (2016) who used human plasma and found that AZ6-2 was stable up to 180 minutes. Therefore, future research would benefit from stability investigations using both FBS and human plasma. Additionally, it would be beneficial to conduct stability experiments up to 180 minutes to determine how long IS4 is stable for in FBS and/or human plasma. *In situ* click chemistry with IS4 was unsuccessful however, this was most likely due to 3-azido-7-hydroxycoumarin being small enough to penetrate the nucleus, preventing cell surface staining of CXCR4. Therefore, future research using different dyes such as BODIPY is essential. Additionally, MTS assays need to be conducted, incubating cells with $CuSO_4$ and sodium ascorbate with and without the dye to determine if the concentrations use are toxic to the cells. Other groups have used significantly different concentrations of both $CuSO_4$ and sodium ascorbate as well as using additionally reactants such as NEM or BSO and using different incubation times (De Nicola and Ghibelli, 2014, Hong et al., 2010). Therefore, future work needs to be carried out to find the optimum conditions for CuAAC in cancer cells as well as determining if CuAAC can occur at 4˚C to prevent receptor endocytosis. Finally, due to a limited amount of IS7, very few

investigations were conducted with it. Future work should focus upon determining the potency and stability of this compound, if it is toxic and if it can successfully bind to CXCR4 and enable fluorescence in multiple cancer cell types, not just MCF-7 cells. More long term future work, should determine if IS4/IS7 can be clicked to other biomolecules and not just a fluorescent dye. This will determine if this clickable CXCR4 antagonist could become a valuable laboratory tool or possible even as a duel functioning cancer therapeutic.

## 8.4. Investigations into ACKR3 Expression, Internalization and Influence on CXCL12 Stimulated Cancer Migration

This thesis largely focuses on CXCL12 stimulated cancer migration. However, CXCL12 binds to both CXCR4 and ACKR3. The ACKR3 receptor cannot bind to G-proteins, thus cannot induce calcium mobilization or other signals via the classical GPCR pathway. Therefore, ACKR3 was originally regarded only as a CXCL12 scavenger, sequestering CXCL12 for gradient control (Boldajipour et al., 2008, Salazar et al., 2014, Zabel et al., 2009, Coggins et al., 2014). However, ACKR3 was found to be able to both positively and negatively modulate CXCR4 signalling by forming CXCR4/ACKR3 heterodimers (Levoye et al., 2009, Sierro et al., 2007). Additionally, ACKR3 can bind CXCL12 and activate Akt and ERK via β-arrestin (Coggins et al., 2014, Gravel et al., 2010, Rajagopal et al., 2010). While it is agreed that ACKR3 had modulating effects upon the CXCR4/CXCL12 pathway, there are contradictory studies as to whether ACKR3 expression causes positive or negative outcomes in cancer and/or cancer metastasis. Additionally, there is conflicting research regarding cellular expression and cellular localization of the ACKR3 receptor. Therefore, the aim of this chapter was to try and answer some of these questions.

ACKR3 was found to be expressed in MCF-7, PC3, Jurkat and THP-1 cells. However, when the incubation temperature was raised to 37˚C ACKR3 internalized in both MCF-7 and Jurkat cells. This suggested that Jurkat and MCF-7 cells have a slow turnover of ACKR3 while PC3 and THP-1 have a faster turnover. The internalisation of ACKR3 in the absence of CXCL12 occurs via caveolin-dependent endocytosis in both MCF-7 and Jurkat cells. In the presence of CXCL12, ACKR3 is internalised via clathrin/caveolin independent endocytosis in Jurkat cells. Finally, using 11G8 as an inhibitor of ACKR3, ACKR3 was found to not promote CXCL12-stimulated migration in Jurkat or THP-1 cells.

One of the limitations of these experiments is the use of endocytosis inhibitors only as research has found these inhibitors were not very specific and could in fact impeach both CDE and caveolin-dependent endocytosis (McGookey et al., 1983, Montesano et al., 1979, Rodal et al., 1999, Dutta et al., 2012, Henley et al., 1998). Therefore, future experiments are paramount to give a definitive answer as to which mechanism of endocytosis is occurring in these cell lines. Such experiments could include the staining of more specific markers of endocytosis including clathrin and/or caveolin. Alternatively, knockdown of these two marker followed by flow cytometry would provide more concrete information as to which method of endocytosis is occurring under these different conditions. Repeats of these experiments were not completed and are paramount for a definitive conclusion. Additionally, flow cytometry was never conducted in MCF-7, THP-1 nor PC3 cells. Therefore, it would be interesting to determine ACKR3 receptor internalisation in these cells at different temperatures and when they are incubated with CXCL12. Furthermore, investigations could be carried out to determine if the switch in endocytosis mechanisms indicate changes in relation to ACKR3 signalling, recycling and/or degradation. Such investigations, could involve studies into the effects of temperature and/or CXCL12 incubation in relation to expression levels of β-arrestin, Akt and/or ERK. Additionally, in relation to receptor degradation, makers such as LysoTracker, a red fluorescent dye that specifically accumulates in lysosomes could be used. To determine ACKR3 receptor recycling capabilities when cells are incubated at 37˚C, time-point experiments with flow cytometry analysis could be conducted to determine how long it takes ACKR3 to become internalized and subsequently how long it takes for ACKR3 to recycle back to the surface, or indeed if this is even occurring at all. It would be interesting to compare ACKR3 and CXCR4 internalisation across these four cell lines after incubation with CXCL12 as there has been evidence that ACKR3 receptor recycling occurs much faster than CXCR4, possibly in relation to mediating the degradation of CXCL12 via ACKR3 (Naumann et al., 2010). Finally, using 11G8 as an ACKR3 inhibitor may not be applicable. Therefore future research would require using ACKR3-specific antagonists such as CCX771, CCX733, CCX754, TC14012 and 9C4 or using AMD3100 at concentrations >10 μM (Watanabe et al., 2010, Zabel et al., 2009, Ödemis et al., 2010, Balabanian et al., 2005, Cao et al., 2016, Kalatskaya et al., 2009).

## 8.5. The Development of 3D Printed Materials for Investigations into Chemokine Stimulated Cancer Cell Migration

Boyden assays are used extensively throughout the literature to determine the ability of cells to migrate through a membrane towards chemokines (Barber et al., 1999, Zang et al., 2000, Inngjerdingen et al., 2003). However, there is a tendency for these assays to fail to produce a gradient across the membrane. Therefore, efforts went into developing alternative methods using 3D printed materials. 3D printing has been used successfully for biological purposes including the development of microfluidic devices, 3D printed microscope chambers and biodegradable 3D printed cell scaffolds (Alessandri et al., 2017, Ho et al., 2015, Kitson et al., 2012, Hutmacher, 2001, Hutmacher et al., 2004). Therefore, this collaborative project designed novel 3D printed chemotaxis chambers and 3D printed replacement ORIS™ Cell Migration assay stoppers.

The overall outcome demonstrated that the designed 3D printed materials for chemotaxis chambers was unsuccessful. However, there may be an application for 3D printing replacement stoppers for the Oris™ Cell Migration assay 96-well plate to reduce the cost of buying replacement plates.

One of the problems found during this project was that the 3D printed materials were not produced in a sterile environment and subsequently, there was a major issue with contamination. Therefore, in the future it would be worthwhile to purchase sterile, laboratory approved materials and conduct all the 3D printing in a sterile environment using strict application of GMP. The purchasing of laboratory approved materials will also resolve problems with cellular toxicity seen with the epoxy, resin and silicone materials. ORIS™ Cell Migration assay replacement stoppers are to be printed with TPE-U and due to the cytotoxicity seen with the other materials, it is important to determine if TPE-U would also cause cytotoxicity. Two other problem that arose were the lack of a chemotactic gradient and that the seeded cells did not remain inside the chemotaxis chamber but instead slipped under the inserts and under the agarose. To try to amend this, it would be possible to use clamps to attempt to formed a complete seal of the agarose chemotaxis chamber to the bottom of the plates. The chemotaxis chambers could in theory be printed directly into the petri dish and this is something to try in the future, however, this would increase production times. An alternative idea was to design and 3D print a framework for casting biological hydrogels made from agarose, collagen or fibrin into which the chemokine could

be added as is something that could be designed in the future. Therefore, the project took a different turn and began the development of ORIS™ Cell Migration assay replacement stoppers. This project was in the very early stages of development and while it was demonstrated that 3D printing could be used to make these stoppers, several adjustments to the size of these stoppers is required. Additionally, it is essential to then test these stoppers in the ORIS™ Cell Migration assay 96-well plate to determine if they are applicable replacements. If these replacement stoppers are found to be good replacements for the original stoppers, the CAD file could be made available to the public as a cheaper alternative for buying replacement plates.

# REFERENCES


ABRAHAM, M., AL-RAWI, A., PEREG, Y., KLEIN, S., WALD, H., EIZENBERG, O., BULVIK, B., RUSSOVSKY, L., VAINSTEIN, A., AHARON, A., MCQUEEN, T., PEMMARAJU, N., CORTES, J., PELED, A., BORTHAKUR, G. & ANDREEF, M. 2015. BL-8040, A novel CXCR4 inhibitor, affects AML blasts survival and induces their terminal differentiation. *Clinical Lymphoma Myeloma and Leukemia,* 15**,** S12.

ADACHI, T., CUI, C.-H., KANDA, A., KAYABA, H., OHTA, K. & CHIHARA, J. 2004. Activation of epidermal growth factor receptor via CCR3 in bronchial epithelial cells. *Biochemical and biophysical research communications,* 320**,** 292-296.

AGLE, K. A., VONGSA, R. A. & DWINELL, M. B. 2010. Calcium mobilization triggered by the chemokine CXCL12 regulates migration in wounded intestinal epithelial monolayers. *Journal of Biological Chemistry,* 285**,** 16066-16075.

AHMED, M., BASHEER, H. A., AYUSO, J. M., AHMET, D., MAZZINI, M., PATEL, R., SHNYDER, S. D., VINADER, V. & AFARINKIA, K. 2017. Agarose spot as a comparative method for in situ analysis of simultaneous chemotactic responses to multiple chemokines. *Scientific reports,* 7**,** 1075.

AIUTI, A., TAVIAN, M., CIPPONI, A., FICARA, F., ZAPPONE, E., HOXIE, J., PEAULT, B. & BORDIGNON, C. 1999. Expression of CXCR4, the receptor for stromal cell-derived factor-1 on fetal and adult human lymphohematopoietic progenitors. *European journal of immunology,* 29**,** 1823-1831.

AIUTI, A., WEBB, I., BLEUL, C., SPRINGER, T. & GUTIERREZ-RAMOS, J. 1997. The chemokine SDF-1 is a chemoattractant for human CD34+ hematopoietic progenitor cells and provides a new mechanism to explain the mobilization of CD34+ progenitors to peripheral blood. *Journal of Experimental Medicine,* 185**,** 111-120.

AKASHI, T., KOIZUMI, K., TSUNEYAMA, K., SAIKI, I., TAKANO, Y. & FUSE, H. 2008. Chemokine receptor CXCR4 expression and prognosis in patients with metastatic prostate cancer. *Cancer science,* 99**,** 539-542.

AKEKAWATCHAI, C., HOLLAND, J. D., KOCHETKOVA, M., WALLACE, J. C. & MCCOLL, S. R. 2005. Transactivation of CXCR4 by the insulin-like growth factor-1 receptor (IGF-1R) in human MDA-MB-231 breast cancer epithelial cells. *Journal of Biological Chemistry,* 280**,** 39701-39708.

ALESSANDRI, K., ANDRIQUE, L., FEYEUX, M., BIKFALVI, A., NASSOY, P. & RECHER, G. 2017. All-in-one 3D printed microscopy chamber for multidimensional imaging, the UniverSlide. *Scientific reports,* 7**,** 42378.

ALISON, M. R., CHINERY, R., POULSOM, R., ASHWOOD, P., LONGCROFT, J. M. & WRIGHT, N. A. 1995. Experimental ulceration leads to sequential expression of spasmolytic polypeptide, intestinal trefoil factor, epidermal growth factor and transforming growth factor alpha mRNAs in rat stomach. *The Journal of pathology,* 175**,** 405-414.

ALKHATIB, G. 2009. The biology of CCR5 and CXCR4. *Current Opinion in HIV and AIDS,* 4**,** 96-103.

ALLEN, S. J., CROWN, S. E. & HANDEL, T. M. 2007. Chemokine: receptor structure, interactions, and antagonism. *Annual review of immunology,* 25**,** 787-820.

ALONSO, M. A. & MILLÁN, J. 2001. The role of lipid rafts in signalling and membrane trafficking in T lymphocytes. *Journal of cell science,* 114**,** 3957-3965.
ALPSOY, A. & GÜNDÜZ, U. 2015. Protein kinase D2 silencing reduced motility of doxorubicin-resistant MCF7 cells. *Tumor Biology,* 36**,** 4417-4426.
ALQAWI, O., WANG, H. P., ESPIRITU, M. & SINGH, G. 2007. Chronic hypoxia promotes an aggressive phenotype in rat prostate cancer cells. *Free radical research,* 41**,** 788-797.
AMARA, A., LORTHIOIR, O., VALENZUELA, A., MAGERUS, A., THELEN, M., MONTES, M., VIRELIZIER, J.-L., DELEPIERRE, M., BALEUX, F., LORTAT-JACOB, H. & ARENZANA-SEISDEDOS, F. 1999. Stromal cell-derived factor-1α associates with heparan sulfates through the first β-strand of the chemokine. *Journal of Biological Chemistry,* 274**,** 23916-23925.
ASSEMAN, C., PANCRÉ, V., DELANOYE, A., CAPRON, A. & AURIAULT, C. 1994. A radioimmunoassay for the quantification of human ubiquitin in biological fluids: application to parasitic and allergic diseases. *Journal of immunological methods,* 173**,** 93-101.
ATCC. 2016a. *A549 (ATCC® CCL-185™)* [Online]. [Accessed 13/2/2018].
ATCC. 2016b. *NCI-H292 [H292] (ATCC® CRL-1848™)* [Online]. [Accessed 13/2/2018].
ATCC. 2016c. *SK-BR-3 [SKBR3] (ATCC® HTB-30™)* [Online]. [Accessed 13/2/2018].
ATCC. 2016d. *SK-MEL-28 (ATCC® HTB-72™)* [Online]. [Accessed 13/2/2018].
ATCC. 2017a. *BT-474 (ATCC® HTB-20™)* [Online]. [Accessed 13/2/2018].
ATCC. 2017b. *Jurkat, Clone E6-1 (ATCC® TIB-152™)* [Online]. [Accessed 13/2/2018].
ATCC. 2017c. *MDA-MB-231 (ATCC® HTB-26™)* [Online]. [Accessed 13/2/2018].
ATCC. 2017d. *PC-3 (ATCC® CRL-1435™)* [Online]. [Accessed 13/2/2018].
ATCC. 2017e. *THP-1 (ATCC® TIB-202™)* [Online]. [Accessed 13/2/2018].
ATTWOOD, T. & FINDLAY, J. 1994. Fingerprinting G-protein-coupled receptors. *Protein Engineering, Design and Selection,* 7**,** 195-203.
AUGSTEN, M., HÄGGLÖF, C., OLSSON, E., STOLZ, C., TSAGOZIS, P., LEVCHENKO, T., FREDERICK, M. J., BORG, Å., MICKE, P., EGEVAD, L. & OSTMAN, A. 2009. CXCL14 is an autocrine growth factor for fibroblasts and acts as a multi-modal stimulator of prostate tumor growth. *Proceedings of the National Academy of Sciences,* 106**,** 3414-3419.
BACHELERIE, F., BEN-BARUCH, A., BURKHARDT, A. M., COMBADIERE, C., FARBER, J. M., GRAHAM, G. J., HORUK, R., SPARRE-ULRICH, A. H., LOCATI, M., LUSTER, A. D., MANTOVANI, A., MATSUSHIMA, K., MURPHY, P. M., NIBBS, R., ROSENKILDE, M. M., ROT, A., SOZZANI, S., THELEN, M., YOSHIE, O. & ZLOTNIK, A. 2014. International Union of Pharmacology. LXXXIX. Update on the extended family of chemokine receptors and introducing a new nomenclature for atypical chemokine receptors. *Pharmacological reviews,* 66**,** 1.
BACHHAWAT, A. K., THAKUR, A., KAUR, J. & ZULKIFLI, M. 2013. Glutathione transporters. *Biochimica et Biophysica Acta (BBA)-General Subjects,* 1830**,** 3154-3164.
BAGGIOLINI, M. 2001. Chemokines in pathology and medicine. *Journal of internal medicine,* 250**,** 91-104.
BAGGIOLINI, M. & DAHINDEN, C. A. 1994. CC chemokines in allergic inflammation. *Immunology today,* 15**,** 127-133.

BALABANIAN, K., LAGANE, B., INFANTINO, S., CHOW, K. Y., HARRIAGUE, J., MOEPPS, B., ARENZANA-SEISDEDOS, F., THELEN, M. & BACHELERIE, F. 2005. The chemokine SDF-1/CXCL12 binds to and signals through the orphan receptor RDC1 in T lymphocytes. *Journal of Biological Chemistry,* 280**,** 35760-35766.

BALKWILL, F. R., CAPASSO, M. & HAGEMANN, T. 2012. The tumor microenvironment at a glance. *Journal of Cell Science,* 125**,** 5591-5596.

BALLATORI, N., KRANCE, S. M., MARCHAN, R. & HAMMOND, C. L. 2009. Plasma membrane glutathione transporters and their roles in cell physiology and pathophysiology. *Molecular aspects of medicine,* 30**,** 13-28.

BANISADR, G., SKRZYDELSKI, D., KITABGI, P., ROSTÈNE, W. & PARSADANIANTZ, S. M. 2003. Highly regionalized distribution of stromal cell-derived factor-1/CXCL12 in adult rat brain: constitutive expression in cholinergic, dopaminergic and vasopressinergic neurons. *European Journal of Neuroscience,* 18**,** 1593-1606.

BARBER, M. R., PANTSCHENKO, A. G., HINCKLEY, L. S. & YANG, T. 1999. Inducible and constitutive in vitro neutrophil chemokine expression by mammary epithelial and myoepithelial cells. *Clinical and Diagnostic Laboratory Immunology,* 6**,** 791-798.

BARIBAUD, F., EDWARDS, T. G., SHARRON, M., BRELOT, A., HEVEKER, N., PRICE, K., MORTARI, F., ALIZON, M., TSANG, M. & DOMS, R. W. 2001. Antigenically distinct conformations of CXCR4. *Journal of virology,* 75**,** 8957-8967.

BARKER, H. E., PAGET, J. T., KHAN, A. A. & HARRINGTON, K. J. 2015. The tumour microenvironment after radiotherapy: mechanisms of resistance and recurrence. *Nature reviews Cancer,* 15**,** 409-425.

BEAR, J. E. & HAUGH, J. M. 2014. Directed migration of mesenchymal cells: where signaling and the cytoskeleton meet. *Current opinion in cell biology,* 30**,** 74-82.

BECK, A. & REICHERT, J. M. 2012. Marketing approval of mogamulizumab: a triumph for glyco-engineering. *MAbs,* 4**,** 419-425.

BENMERAH, A., LAMAZE, C., BÈGUE, B., SCHMID, S. L., DAUTRY-VARSAT, A. & CERF-BENSUSSAN, N. 1998. AP-2/Eps15 interaction is required for receptor-mediated endocytosis. *The Journal of cell biology,* 140**,** 1055-1062.

BEREZHKOVSKIY, L. M. 1999. The analysis of peptide affinity and its binding kinetics to DR1DW1 major histocompatibility complex protein. *Biophysical chemistry,* 77**,** 183-194.

BERG, K. A. & CLARKE, W. P. 2018. Making sense of pharmacology: inverse agonism and functional selectivity. *International Journal of Neuropsychopharmacology,* 21**,** 962-977.

BERNHAGEN, J., KROHN, R., LUE, H., GREGORY, J. L., ZERNECKE, A., KOENEN, R. R., DEWOR, M., GEORGIEV, I., SCHOBER, A., LENG, L., KOOISTRA, T., FINGERLE-ROWSON, G., GHEZZI, P., KLEEMANN, R., MCCOLL, S. R., BUCALA, R., HICKEY, M. & WEBER, C. 2007. MIF is a noncognate ligand of CXC chemokine receptors in inflammatory and atherogenic cell recruitment. *Nature medicine,* 13**,** 587-596.

BERRIDGE, M. V. & TAN, A. S. 1993. Characterization of the cellular reduction of 3-(4, 5-dimethylthiazol-2-yl)-2, 5-diphenyltetrazolium bromide (MTT): subcellular localization, substrate dependence, and involvement of mitochondrial electron transport in MTT reduction. *Archives of biochemistry and biophysics,* 303**,** 474-482.

BERTHEBAUD, M., RIVIERE, C., JARRIER, P., FOUDI, A., ZHANG, Y., COMPAGNO, D., GALY, A., VAINCHENKER, W. & LOUACHE, F. 2005. RGS16 is a negative regulator of SDF-1–CXCR4 signaling in megakaryocytes. *Blood,* 106**,** 2962-2968.

BIÈCHE, I., CHAVEY, C., ANDRIEU, C., BUSSON, M., VACHER, S., LE CORRE, L., GUINEBRETIÈRE, J.-M., BURLINCHON, S., LIDEREAU, R. & LAZENNEC, G. 2007. CXC chemokines located in the 4q21 region are up-regulated in breast cancer. *Endocrine-related cancer,* 14**,** 1039-1052.

BLEUL, C. C., FARZAN, M., CHOE, H., PAROLIN, C., CLARK-LEWIS, I., SODROSKI, J. & SPRINGER, T. A. 1996. The lymphocyte chemoattractant SDF-1 is a ligand for LESTR/fusin and blocks HIV-1 entry. *Nature,* 382**,** 829-833.

BLEUL, C. C., WU, L., HOXIE, J. A., SPRINGER, T. A. & MACKAY, C. R. 1997. The HIV coreceptors CXCR4 and CCR5 are differentially expressed and regulated on human T lymphocytes. *Proceedings of the National Academy of Sciences,* 94**,** 1925-1930.

BLUMENTHAL, G. M., SCHER, N. S., CORTAZAR, P., CHATTOPADHYAY, S., TANG, S., SONG, P., LIU, Q., RINGGOLD, K., PILARO, A. M., TILLEY, A., KING, K., GRAHAM, L., RELLAHAN, B., WEINBERG, W., CHI, B., THOMAS, C., HUGHES, P., IBRAHIM, A., JUSTICE, R. & PAZDUR, R. 2013. First FDA approval of dual anti-HER2 regimen: pertuzumab in combination with trastuzumab and docetaxel for HER2-positive metastatic breast cancer. *Clinical cancer research,* 19**,** 4911-4916.

BOBKOV, V., ARIMONT, M., ZARCA, A., DE GROOF, T. W., VAN DER WONING, B., DE HAARD, H. & SMIT, M. J. 2019. Antibodies targeting chemokine receptors CXCR4 and ACKR3. *Molecular pharmacology,* 96**,** 753-764.

BODART, V., ANASTASSOV, V., DARKES, M. C., IDZAN, S. R., LABRECQUE, J., LAU, G., MOSI, R. M., NEFF, K. S., NELSON, K. L., RUZEK, M. C., PATEL, K., SANTUCCI, Z., SCARBOROUGH, R., WONG, R. S., BRIDGER, G. J., MACFARLAND, R. T. & FRICKER, S. P. 2009. Pharmacology of AMD3465: a small molecule antagonist of the chemokine receptor CXCR4. *Biochemical pharmacology,* 78**,** 993-1000.

BOLDAJIPOUR, B., MAHABALESHWAR, H., KARDASH, E., REICHMAN-FRIED, M., BLASER, H., MININA, S., WILSON, D., XU, Q. & RAZ, E. 2008. Control of chemokine-guided cell migration by ligand sequestration. *Cell,* 132**,** 463-473.

BORRELLO, M. G., ALBERTI, L., FISCHER, A., DEGL'INNOCENTI, D., FERRARIO, C., GARIBOLDI, M., MARCHESI, F., ALLAVENA, P., GRECO, A., COLLINI, P., PILOTTI, S., CASSINELLI, G., BRESSAN, P., FUGAZZOLA, L., MANTOVANI, A. & PIEROTTI, M. A. 2005. Induction of a proinflammatory program in normal human thyrocytes by the RET/PTC1 oncogene. *Proceedings of the National Academy of Sciences of the United States of America,* 102**,** 14825-14830.

BOURBON, N. A., YUN, J. & KESTER, M. 2000. Ceramide directly activates protein kinase C ζ to regulate a stress-activated protein kinase signaling complex. *Journal of Biological Chemistry,* 275**,** 35617-35623.

BOYDEN, S. 1962. The chemotactic effect of mixtures of antibody and antigen on polymorphonuclear leucocytes. *Journal of Experimental Medicine,* 115**,** 453-466.

BROWN, D. & LONDON, E. 1998. Functions of lipid rafts in biological membranes. *Annual review of cell and developmental biology,* 14**,** 111-136.

BROXMEYER, H. E., SHERRY, B., LU, L., COOPER, S., OH, K.-O., TEKAMP-OLSON, P., KWON, B. S. & CERAMI, A. 1990. Enhancing and suppressing effects of recombinant murine macrophage inflammatory proteins on colony formation in vitro by bone marrow myeloid progenitor cells. *Blood,* 76**,** 1110-1116.

BÜNEMANN, E., HOFF, N.-P., BUHREN, B. A., WIESNER, U., MELLER, S., BÖLKE, E., MÜLLER-HOMEY, A., KUBITZA, R., RUZICKA, T., ZLOTNIK, A., HOMEY, B. & GERBER, P. A. 2018. Chemokine ligand–receptor interactions critically regulate cutaneous wound healing. *European journal of medical research,* 23**,** 4.

BURGER, J. A., STEWART, D. J., WALD, O. & PELED, A. 2011. Potential of CXCR4 antagonists for the treatment of metastatic lung cancer. *Expert review of anticancer therapy,* 11**,** 621-630.

BUSILLO, J. M. & BENOVIC, J. L. 2007. Regulation of CXCR4 signaling. *Biochimica et Biophysica Acta (BBA)-Biomembranes,* 1768**,** 952-963.

CALEY, M. P., KING, H., SHAH, N., WANG, K., RODRIGUEZ-TEJA, M., GRONAU, J. H., WAXMAN, J. & STURGE, J. 2016. Tumor-associated Endo180 requires stromal-derived LOX to promote metastatic prostate cancer cell migration on human ECM surfaces. *Clinical & experimental metastasis,* 33**,** 151-165.

CAMPS, M., CAROZZI, A., SCHNABEL, P., SCHEER, A., PARKER, P. J. & GIERSCHIK, P. 1992. Isozyme-selective stimulation of phospholipase C-β2 by G protein βγ-subunits. *Nature,* 360**,** 684-686.

CANCER RESEARCH. 2017. *Prostate Cancer Statistics* [Online]. Cancer Research UK. [Accessed 1/4/2020].

CAO, X., ZHANG, W., WAN, T., HE, L., CHEN, T., YUAN, Z., MA, S., YU, Y. & CHEN, G. 2000. Molecular cloning and characterization of a novel CXC chemokine macrophage inflammatory protein-2γ chemoattractant for human neutrophils and dendritic cells. *The Journal of Immunology,* 165**,** 2588-2595.

CAO, Z., LIS, R., GINSBERG, M., CHAVEZ, D., SHIDO, K., RABBANY, S. Y., FONG, G.-H., SAKMAR, T. P., RAFII, S. & DING, B.-S. 2016. Targeting of the pulmonary capillary vascular niche promotes lung alveolar repair and ameliorates fibrosis. *Nature medicine,* 22**,** 154-162.

CARLISLE, A. J., LYTTLE, C. A., CARLISLE, R. Y. & MARIS, J. M. 2009. CXCR4 expression heterogeneity in neuroblastoma cells due to ligand-independent regulation. *Molecular cancer,* 8**,** 126.

CARNEC, X., QUAN, L., OLSON, W. C., HAZAN, U. & DRAGIC, T. 2005. Anti-CXCR4 monoclonal antibodies recognizing overlapping epitopes differ significantly in their ability to inhibit entry of human immunodeficiency virus type 1. *Journal of virology,* 79**,** 1930-1933.

CASSOL, E., ALFANO, M., BISWAS, P. & POLI, G. 2006. Monocyte-derived macrophages and myeloid cell lines as targets of HIV-1 replication and persistence. *Journal of leukocyte biology,* 80**,** 1018-1030.

CERADINI, D. J., KULKARNI, A. R., CALLAGHAN, M. J., TEPPER, O. M., BASTIDAS, N., KLEINMAN, M. E., CAPLA, J. M., GALIANO, R. D., LEVINE, J. P. & GURTNER, G. C. 2004. Progenitor cell trafficking is regulated by hypoxic gradients through HIF-1 induction of SDF-1. *Nature medicine,* 10**,** 858-864.

CHAFFER, C. L. & WEINBERG, R. A. 2011. A perspective on cancer cell metastasis. *Science,* 331**,** 1559-1564.

CHAKRAVARTHI, S., JESSOP, C. E. & BULLEID, N. J. 2006. The role of glutathione in disulphide bond formation and endoplasmic-reticulum-generated oxidative stress. *EMBO reports,* 7**,** 271-275.
CHAMES, P., VAN REGENMORTEL, M., WEISS, E. & BATY, D. 2009. Therapeutic antibodies: successes, limitations and hopes for the future. *British journal of pharmacology,* 157**,** 220-233.
CHATTERJEE, S., AZAD, B. B. & NIMMAGADDA, S. 2014. The intricate role of CXCR4 in cancer. *Advances in cancer research,* 124**,** 31-82.
CHEN, G., WANG, W., MENG, S., ZHANG, L., WANG, W., JIANG, Z., YU, M., CUI, Q. & LI, M. 2014. CXC chemokine CXCL12 and its receptor CXCR4 in tree shrews (Tupaia belangeri): structure, expression and function. *PloS one,* 9**,** e98231.
CHEN, H., HE, Z., BAGRI, A. & TESSIER-LAVIGNE, M. 1998. Semaphorin–neuropilin interactions underlying sympathetic axon responses to class III semaphorins. *Neuron,* 21**,** 1283-1290.
CHENG, Y., QU, J., CHE, X., XU, L., SONG, N., MA, Y., GONG, J., QU, X. & LIU, Y. 2017. CXCL12/SDF-1α induces migration via SRC-mediated CXCR4-EGFR cross-talk in gastric cancer cells. *Oncology letters,* 14**,** 2103-2110.
CHENG, Z.-J., ZHAO, J., SUN, Y., HU, W., WU, Y.-L., CEN, B., WU, G.-X. & PEI, G. 2000. β-arrestin differentially regulates the chemokine receptor CXCR4-mediated signaling and receptor internalization, and this implicates multiple interaction sites between β-arrestin and CXCR4. *Journal of Biological Chemistry,* 275**,** 2479-2485.
CHEUNG, K. J. & EWALD, A. J. 2016. A collective route to metastasis: Seeding by tumor cell clusters. *Science,* 352**,** 167-169.
CHIA, C. M., WINSTON, R. & HANDYSIDE, A. H. 1995. EGF, TGF-alpha and EGFR expression in human preimplantation embryos. *Development,* 121**,** 299-307.
CHRISTOPHERSON, K. & HROMAS, R. 2001. Chemokine regulation of normal and pathologic immune responses. *Stem Cells,* 19**,** 388-396.
CHRISTOPHERSON, K. W., HANGOC, G. & BROXMEYER, H. E. 2002. Cell surface peptidase CD26/dipeptidylpeptidase IV regulates CXCL12/stromal cell-derived factor-1α-mediated chemotaxis of human cord blood CD34+ progenitor cells. *The Journal of Immunology,* 169**,** 7000-7008.
CLAING, A., LAPORTE, S. A., CARON, M. G. & LEFKOWITZ, R. J. 2002. Endocytosis of G protein-coupled receptors: roles of G protein-coupled receptor kinases and ß-arrestin proteins. *Progress in neurobiology,* 66**,** 61-79.
CLORE, G. & GRONENBORN, A. 1995. Three-dimensional structures of alpha and beta chemokines. *The FASEB Journal,* 9**,** 57-62.
COGGINS, N. L., TRAKIMAS, D., CHANG, S. L., EHRLICH, A., RAY, P., LUKER, K. E., LINDERMAN, J. J. & LUKER, G. D. 2014. CXCR7 controls competition for recruitment of β-arrestin 2 in cells expressing both CXCR4 and CXCR7. *PloS one,* 9**,** e98328.
COJOC, M., PEITZSCH, C., TRAUTMANN, F., POLISHCHUK, L., TELEGEEV, G. D. & DUBROVSKA, A. 2013. Emerging targets in cancer management: role of the CXCL12/CXCR4 axis. *OncoTargets and therapy,* 6**,** 1347-1361.
COLLINS, P. J., MCCULLY, M. L., MARTÍNEZ-MUÑOZ, L., SANTIAGO, C., WHEELDON, J., CAUCHETEUX, S., THELEN, S., CECCHINATO, V., LAUFER, J. M., PURVANOV, V., MONNEAU, Y. R., LORTAT-JACOB,

H., LEGLER, D. F., UGUCCIONI, M., THELEN, M., PIGUET, V., MELLADO, M. & MOSER, B. 2017. Epithelial chemokine CXCL14 synergizes with CXCL12 via allosteric modulation of CXCR4. *The FASEB Journal,* 31**,** 3084-3097.

CONDEELIS, J. & SEGALL, J. E. 2003. Intravital imaging of cell movement in tumours. *Nature Reviews Cancer,* 3**,** 921-930.

CONKLIN, B. R. & BOURNE, H. R. 1993. Structural elements of Gα subunits that interact with Gβγ, receptors, and effectors. *Cell,* 73**,** 631-641.

CONTENTO, R. L., MOLON, B., BOULARAN, C., POZZAN, T., MANES, S., MARULLO, S. & VIOLA, A. 2008. CXCR4–CCR5: a couple modulating T cell functions. *Proceedings of the National Academy of Sciences,* 105**,** 10101-10106.

COUSSENS, L., PARKER, P. J., RHEE, L., YANG-FENG, T. L., CHEN, E., WATERFIELD, M. D., FRANCKE, U. & ULLRICH, A. 1986. Multiple, distinct forms of bovine and human protein kinase C suggest diversity in cellular signaling pathways. *Science,* 233**,** 859-866.

CROWTHER-SWANEPOEL, D., QURESHI, M., DYER, M. J., MATUTES, E., DEARDEN, C., CATOVSKY, D. & HOULSTON, R. S. 2009. Genetic variation in CXCR4 and risk of chronic lymphocytic leukemia. *Blood,* 114**,** 4843-4846.

CRUMP, M. P., GONG, J. H., LOETSCHER, P., RAJARATHNAM, K., AMARA, A., ARENZANA-SEISDEDOS, F., VIRELIZIER, J. L., BAGGIOLINI, M., SYKES, B. D. & CLARK-LEWIS, I. 1997. Solution structure and basis for functional activity of stromal cell-derived factor-1; dissociation of CXCR4 activation from binding and inhibition of HIV-1. *The EMBO journal,* 16**,** 6996-7007.

CURNOCK, A. P., LOGAN, M. K. & WARD, S. G. 2002. Chemokine signalling: pivoting around multiple phosphoinositide 3-kinases. *Immunology,* 105**,** 125-136.

D'ALTERIO, C., NASTI, G., POLIMENO, M., OTTAIANO, A., CONSON, M., CIRCELLI, L., BOTTI, G., SCOGNAMIGLIO, G., SANTAGATA, S., DE DIVITIIS, C., NAPPI, A., NAPOLITANO, M., TANTANGELO, F., PACELLI, R., IZZO, F., VUTTARIELLO, F., BOTTI, G. & SCALA, S. 2016. CXCR4–CXCL12–CXCR7, TLR2–TLR4, and PD-1/PD-L1 in colorectal cancer liver metastases from neoadjuvant-treated patients. *Oncoimmunology,* 5**,** e1254313.

D'APUZZO, M., ROLINK, A., LOETSCHER, M., HOXIE, J. A., CLARK-LEWIS, I., MELCHERS, F., BAGGIOLINI, M. & MOSER, B. 1997. The chemokine SDF-1, stromal cell-derived factor 1, attracts early stage B cell precursors via the chemokine receptor CXCR4. *European journal of immunology,* 27**,** 1788-1793.

DAI, C., BASILICO, P., CREMONA, T. P., COLLINS, P., MOSER, B., BENARAFA, C. & WOLF, M. 2015. CXCL14 displays antimicrobial activity against respiratory tract bacteria and contributes to clearance of Streptococcus pneumoniae pulmonary infection. *The Journal of Immunology,* 194**,** 5980-5989.

DAR, A., KOLLET, O. & LAPIDOT, T. 2006. Mutual, reciprocal SDF-1/CXCR4 interactions between hematopoietic and bone marrow stromal cells regulate human stem cell migration and development in NOD/SCID chimeric mice. *Experimental hematology,* 34**,** 967-975.

DAVIS, D. A., SINGER, K. E., SIERRA, M. D. L. L., NARAZAKI, M., YANG, F., FALES, H. M., YARCHOAN, R. & TOSATO, G. 2005. Identification of carboxypeptidase N as an enzyme responsible for C-terminal cleavage

of stromal cell-derived factor-1α in the circulation. *Blood,* 105**,** 4561-4568.
DE CLERCQ, E. 2009. The AMD3100 story: the path to the discovery of a stem cell mobilizer (Mozobil). *Biochemical pharmacology,* 77**,** 1655-1664.
DE MUNNIK, S. M., SMIT, M. J., LEURS, R. & VISCHER, H. F. 2015. Modulation of cellular signaling by herpesvirus-encoded G protein-coupled receptors. *Frontiers in pharmacology,* 6.
DE NICOLA, M. & GHIBELLI, L. 2014. Glutathione depletion in survival and apoptotic pathways. *Frontiers in pharmacology,* 5**,** 267.
DE NIGRIS, F., SCHIANO, C., INFANTE, T. & NAPOLI, C. 2012. CXCR4 inhibitors: tumor vasculature and therapeutic challenges. *Recent patents on anti-cancer drug discovery,* 7**,** 251-264.
DEBNATH, B., XU, S., GRANDE, F., GAROFALO, A. & NEAMATI, N. 2013. Small molecule inhibitors of CXCR4. *Theranostics,* 3**,** 47-75.
DELGADO, M. B., CLARK-LEWIS, I., LOETSCHER, P., LANGEN, H., THELEN, M., BAGGIOLINI, M. & WOLF, M. 2001. Rapid inactivation of stromal cell-derived factor-1 by cathepsin G associated with lymphocytes. *European journal of immunology,* 31**,** 699-707.
DEMKO, S., SUMMERS, J., KEEGAN, P. & PAZDUR, R. 2008. FDA drug approval summary: alemtuzumab as single-agent treatment for B-cell chronic lymphocytic leukemia. *The Oncologist,* 13**,** 167-174.
DENIES, M. S., ROSSELLI-MURAI, L. K., SCHNELL, S. & LIU, A. P. 2019. Clathrin heavy chain knockdown impacts CXCR4 signaling and post-translational modification. *Frontiers in cell and developmental biology,* 7.
DI GUGLIELMO, G. M., LE ROY, C., GOODFELLOW, A. F. & WRANA, J. L. 2003. Distinct endocytic pathways regulate TGF-β receptor signalling and turnover. *Nature cell biology,* 5**,** 410-421.
DI MARO, S., TROTTA, A. M., BRANCACCIO, D., DI LEVA, F. S., LA PIETRA, V., IERANO, C., NAPOLITANO, M., PORTELLA, L., D'ALTERIO, C., SICILIANO, R. A., SEMENTA, D., TOMASSI, S., CAROTENUTO, A., NOVELLINO, E., SCALA, S. & MARINELLI, L. 2016. Exploring the N-terminal region of CXC motif chemokine 12 (CXCL12): Identification of plasma-stable cyclic peptides as novel, potent CXC chemokine receptor type 4 (CXCR4) antagonists. *Journal of Medicinal Chemistry,* 59**,** 8369-8380.
DIPERSIO, J. F., MICALLEF, I. N., STIFF, P. J., BOLWELL, B. J., MAZIARZ, R. T., JACOBSEN, E., NADEMANEE, A., MCCARTY, J., BRIDGER, G. & CALANDRA, G. 2009a. Phase III prospective randomized double-blind placebo-controlled trial of plerixafor plus granulocyte colony-stimulating factor compared with placebo plus granulocyte colony-stimulating factor for autologous stem-cell mobilization and transplantation for patients with non-Hodgkin's lymphoma. *Journal of Clinical Oncology,* 27**,** 4767-4773.
DIPERSIO, J. F., STADTMAUER, E. A., NADEMANEE, A., MICALLEF, I. N., STIFF, P. J., KAUFMAN, J. L., MAZIARZ, R. T., HOSING, C., FRÜEHAUF, S., HORWITZ, M., COOPER, D., BRIDGER, G. & CALANDRA, G. 2009b. Plerixafor and G-CSF versus placebo and G-CSF to mobilize hematopoietic stem cells for autologous stem cell transplantation in patients with multiple myeloma. *Blood,* 113**,** 5720-5726.
DISATNIK, M.-H. & RANDO, T. A. 1999. Integrin-mediated Muscle Cell Spreading THE ROLE OF PROTEIN KINASE C IN OUTSIDE-IN AND INSIDE-OUT SIGNALING AND EVIDENCE OF INTEGRIN CROSS-TALK. *Journal of Biological Chemistry,* 274**,** 32486-32492.

DOLGIN, E. 2018. First GPCR-directed antibody passes approval milestone. *Nature Reviews Drug Discovery,* 17**,** 457-459.
DOMANSKA, U. M., KRUIZINGA, R. C., NAGENGAST, W. B., TIMMER-BOSSCHA, H., HULS, G., DE VRIES, E. G. & WALENKAMP, A. M. 2013. A review on CXCR4/CXCL12 axis in oncology: no place to hide. *European journal of cancer,* 49**,** 219-230.
DOMANSKA, U. M., TIMMER-BOSSCHA, H., NAGENGAST, W. B., MUNNINK, T. H. O., KRUIZINGA, R. C., ANANIAS, H. J., KLIPHUIS, N. M., HULS, G., DE VRIES, E. G., DE JONG, I. J. & WALENKAMP, A. M. 2012. CXCR4 inhibition with AMD3100 sensitizes prostate cancer to docetaxel chemotherapy. *Neoplasia,* 14**,** 709-718.
DOWLING, C. M., HAYES, S. L., PHELAN, J. J., CATHCART, M. C., FINN, S. P., MEHIGAN, B., MCCORMICK, P., COFFEY, J. C., O'SULLIVAN, J. & KIELY, P. A. 2017. Expression of protein kinase C gamma promotes cell migration in colon cancer. *Oncotarget,* 8**,** 72096-72107.
DUBEYKOVSKAYA, Z., DUBEYKOVSKIY, A., SOLAL-COHEN, J. & WANG, T. C. 2009. Secreted trefoil factor 2 activates the CXCR4 receptor in epithelial and lymphocytic cancer cell lines. *Journal of Biological Chemistry,* 284**,** 3650-3662.
DUDEK, P. 2013. FDM 3D printing technology in manufacturing composite elements. *Archives of Metallurgy and Materials,* 58**,** 1415-1418.
DURAND, N., BASTEA, L. I., LONG, J., DÖPPLER, H., LING, K. & STORZ, P. 2016. Protein Kinase D1 regulates focal adhesion dynamics and cell adhesion through Phosphatidylinositol-4-phosphate 5-kinase type-I γ. *Scientific reports,* 6**,** 35963.
DUTTA, D., WILLIAMSON, C. D., COLE, N. B. & DONALDSON, J. G. 2012. Pitstop 2 is a potent inhibitor of clathrin-independent endocytosis. *PloS one,* 7**,** e45799.
ECCLES, S. A. 2005. Targeting key steps in metastatic tumour progression. *Current opinion in genetics & development,* 15**,** 77-86.
ECK, S. M., CÔTÉ, A. L., WINKELMAN, W. D. & BRINCKERHOFF, C. E. 2009. CXCR4 and matrix metalloproteinase-1 are elevated in breast carcinoma–associated fibroblasts and in normal mammary fibroblasts exposed to factors secreted by breast cancer cells. *Molecular Cancer Research,* 7**,** 1033-1044.
EISELER, T., DÖPPLER, H., YAN, I. K., KITATANI, K., MIZUNO, K. & STORZ, P. 2009. Protein kinase D1 regulates cofilin-mediated F-actin reorganization and cell motility through slingshot. *Nature cell biology,* 11**,** 545-556.
EISELER, T., SCHMID, M. A., TOPBAS, F., PFIZENMAIER, K. & HAUSSER, A. 2007. PKD is recruited to sites of actin remodelling at the leading edge and negatively regulates cell migration. *FEBS letters,* 581**,** 4279-4287.
ENDO, K., OKI, E., BIEDERMANN, V., KOJIMA, H., YOSHIDA, K., JOHANNES, F.-J., KUFE, D. & DATTA, R. 2000. Proteolytic cleavage and activation of protein kinase C μ by caspase-3 in the apoptotic response of cells to 1-β-d-arabinofuranosylcytosine and other genotoxic agents. *Journal of Biological Chemistry,* 275**,** 18476-18481.
EVANS, G. R. 2000. Challenges to nerve regeneration. *Seminars in surgical oncology,* 19**,** 312-318.
FALASCA, M., LOGAN, S., LEHTO, V., BACCANTE, G., LEMMON, M. & SCHLESSINGER, J. 1998. Activation of phospholipase Cγ by PI 3-kinase-induced PH domain-mediated membrane targeting. *The EMBO journal,* 17**,** 414-422.

FEDERSPPIEL, B., MELHADO, I. G., DUNCAN, A. M., DELANEY, A., SCHAPPERT, K., CLARK-LEWIS, I. & JIRIK, F. R. 1993. Molecular cloning of the cDNA and chromosomal localization of the gene for a putative seven-transmembrane segment (7-TMS) receptor isolated from human spleen. *Genomics,* 16**,** 707-712.

FERREIRA, F., FOLEY, M., COOKE, A., CUNNINGHAM, M., SMITH, G., WOOLLEY, R., HENDERSON, G., KELLY, E., MUNDELL, S. & SMYTHE, E. 2012. Endocytosis of G protein-coupled receptors is regulated by clathrin light chain phosphorylation. *Current Biology,* 22**,** 1361-1370.

FOGH, B. S., MULTHAUPT, H. A. & COUCHMAN, J. R. 2014. Protein kinase C, focal adhesions and the regulation of cell migration. *Journal of Histochemistry & Cytochemistry,* 62**,** 172-184.

FONTANELLA, R., PELAGALLI, A., NARDELLI, A., D'ALTERIO, C., IERANÒ, C., CERCHIA, L., LUCARELLI, E., SCALA, S. & ZANNETTI, A. 2016. A novel antagonist of CXCR4 prevents bone marrow-derived mesenchymal stem cell-mediated osteosarcoma and hepatocellular carcinoma cell migration and invasion. *Cancer letters,* 370**,** 100-107.

FOURNIER, J.-B., DOMMERSNES, P. G. & GALATOLA, P. 2003. Dynamin recruitment by clathrin coats: a physical step? *Comptes rendus biologies,* 326**,** 467-476.

FOXMAN, E. F., CAMPBELL, J. J. & BUTCHER, E. C. 1997. Multistep navigation and the combinatorial control of leukocyte chemotaxis. *The Journal of cell biology,* 139**,** 1349-1360.

FOXMAN, E. F., KUNKEL, E. J. & BUTCHER, E. C. 1999. Integrating conflicting chemotactic signals: the role of memory in leukocyte navigation. *The Journal of cell biology,* 147**,** 577-588.

FREDERICK, M. J., HENDERSON, Y., XU, X., DEAVERS, M. T., SAHIN, A. A., WU, H., LEWIS, D. E., EL-NAGGAR, A. K. & CLAYMAN, G. L. 2000. In vivo expression of the novel CXC chemokine BRAK in normal and cancerous human tissue. *The American journal of pathology,* 156**,** 1937-1950.

FREDRIKSSON, R., LAGERSTRÖM, M. C., LUNDIN, L.-G. & SCHIÖTH, H. B. 2003. The G-protein-coupled receptors in the human genome form five main families. Phylogenetic analysis, paralogon groups, and fingerprints. *Molecular pharmacology,* 63**,** 1256-1272.

FRICKER, S. P., ANASTASSOV, V., COX, J., DARKES, M. C., GRUJIC, O., IDZAN, S. R., LABRECQUE, J., LAU, G., MOSI, R. M., NELSON, K. L., QIN, L., SANTUCCI, Z. & WONG, R. S. 2006. Characterization of the molecular pharmacology of AMD3100: a specific antagonist of the G-protein coupled chemokine receptor, CXCR4. *Biochemical pharmacology,* 72**,** 588-596.

FRIEDL, P. & MAYOR, R. 2017. Tuning collective cell migration by cell–cell junction regulation. *Cold Spring Harbor perspectives in biology,* 9**,** a029199.

FRIEDL, P. & WOLF, K. 2003. Tumour-cell invasion and migration: diversity and escape mechanisms. *Nature Reviews Cancer,* 3**,** 362-374.

FRIEDL, P. & WOLF, K. 2008. Tube travel: the role of proteases in individual and collective cancer cell invasion. *Cancer research,* 68**,** 7247-7249.

FRIELING, J. S., BASANTA, D. & LYNCH, C. C. 2015. Current and emerging therapies for bone metastatic castration-resistant prostate cancer. *Cancer Control,* 22**,** 109-120.

FRITZ-LAYLIN, L. K., LORD, S. J. & MULLINS, R. D. 2017. WASP and SCAR are evolutionarily conserved in actin-filled pseudopod-based motility. *Journal of Cell Biology,* 216**,** 1673-1688.
FRUGTNIET, B., JIANG, W. G. & MARTIN, T. A. 2015. Role of the WASP and WAVE family proteins in breast cancer invasion and metastasis. *Breast Cancer: Targets and Therapy,* 7**,** 99-109.
FUJII, T., GARCÍA-BERMEJO, M. A. L., BERNABÓ, J. L., CAAMAÑO, J., OHBA, M., KUROKI, T., LI, L., YUSPA, S. H. & KAZANIETZ, M. G. 2000. Involvement of Protein Kinase C δ (PKCδ) in Phorbol Ester-induced Apoptosis in LNCaP Prostate Cancer Cells LACK OF PROTEOLYTIC CLEAVAGE OF PKCδ. *Journal of Biological Chemistry,* 275**,** 7574-7582.
GAEBLER, A., PENNO, A., KUERSCHNER, L. & THIELE, C. 2016. A highly sensitive protocol for microscopy of alkyne lipids and fluorescently tagged or immunostained proteins. *Journal of lipid research,* 57**,** 1934-1947.
GAMBARYAN, N., PERROS, F., MONTANI, D., COHEN-KAMINSKY, S., MAZMANIAN, M., RENAUD, J., SIMONNEAU, G., LOMBET, A. & HUMBERT, M. 2011. Targeting of c-kit+ haematopoietic progenitor cells prevents hypoxic pulmonary hypertension. *European Respiratory Journal,* 37**,** 1392-1399.
GAN, C. P., PATEL, V., MIKELIS, C. M., ZAIN, R. B., MOLINOLO, A. A., ABRAHAM, M. T., TEO, S.-H., RAHMAN, Z. A. A., GUTKIND, J. S. & CHEONG, S. C. 2014. Heterotrimeric G-protein alpha-12 (Gα12) subunit promotes oral cancer metastasis. *Oncotarget,* 5**,** 9626-9640.
GANJU, R. K., DEOL, Y. S. & NASSER, M. W. 2012. *Signaling pathways and molecular mediators in metastasis,* Dordrecht, Springer Science & Business Media.
GAO, W., MEI, X., WANG, J., ZHANG, X. & YUAN, Y. 2015. ShRNA-mediated knock-down of CXCR7 increases TRAIL-sensitivity in MCF-7 breast cancer cells. *Tumor Biology,* 36**,** 7243-7250.
GAUR, P., VERMA, V., GUPTA, S., SORANI, E., VAINSTEIN HARAS, A., OBERKOVITZ, G., PELED, A. & KHLEIF, S. 2018. CXCR4 antagonist (BL-8040) to enhance antitumor effects by increasing tumor infiltration of antigen-specific effector T-cells. *Journal of Clinical Oncology,* 36**,** 73-73.
GEORGE, K. M., FRANTZ, M.-C., BRAVO-ALTAMIRANO, K., LAVALLE, C. R., TANDON, M., LEIMGRUBER, S., SHARLOW, E. R., LAZO, J. S., WANG, Q. J. & WIPF, P. 2011. Design, synthesis, and biological evaluation of PKD inhibitors. *Pharmaceutics,* 3**,** 186-228.
GILMAN, A. G. 1987. G proteins: transducers of receptor-generated signals. *Annual review of biochemistry,* 56**,** 615-649.
GILMORE, A. P. & BURRIDGE, K. 1996. Molecular mechanisms for focal adhesion assembly through regulation of protein–protein interactions. *Structure,* 4**,** 647-651.
GIMONA, M., BUCCIONE, R., COURTNEIDGE, S. A. & LINDER, S. 2008. Assembly and biological role of podosomes and invadopodia. *Current opinion in cell biology,* 20**,** 235-241.
GIORGIONE, J. R., LIN, J.-H., MCCAMMON, J. A. & NEWTON, A. C. 2006. Increased membrane affinity of the C1 domain of protein kinase Cδ compensates for the lack of involvement of its C2 domain in membrane recruitment. *Journal of Biological Chemistry,* 281**,** 1660-1669.
GLEICHMANN, M., GILLEN, C., CZARDYBON, M., BOSSE, F., GREINER-PETTER, R., AUER, J. & MÜLLER, H. W. 2000. Cloning and characterization of SDF-1γ, a novel SDF-1 chemokine transcript with

developmentally regulated expression in the nervous system. *European Journal of Neuroscience,* 12**,** 1857-1866.
GOLDSMITH, Z. & DHANASEKARAN, D. 2007. G protein regulation of MAPK networks. *Oncogene,* 26**,** 3122-3142.
GOODHILL, G. J. & BAIER, H. 1998. Axon guidance: stretching gradients to the limit. *Neural computation,* 10**,** 521-527.
GOUDARZI, F., ASADI, A., AFSHARPOUR, M. & JAMADI, R. H. 2018. In vitro characterization and evaluation of the cytotoxicity effects of nisin and nisin-loaded PLA-PEG-PLA nanoparticles on gastrointestinal (AGS and KYSE-30), hepatic (HepG2) and blood (K562) cancer cell lines. *AAPS PharmSciTech,* 19**,** 1554-1566.
GRAVEL, S., MALOUF, C., BOULAIS, P. E., BERCHICHE, Y. A., OISHI, S., FUJII, N., LEDUC, R., SINNETT, D. & HEVEKER, N. 2010. The peptidomimetic CXCR4 antagonist TC14012 recruits β-arrestin to CXCR7 roles of receptor domains. *Journal of Biological Chemistry,* 285**,** 37939-37943.
GRIFFITHS, K., DOLEZAL, O., CAO, B., NILSSON, S. K., SEE, H. B., PFLEGER, K. D., ROCHE, M., GORRY, P. R., POW, A., VIDUKA, K., LIM, K., LU, B. G., CHANG, D. H., MURRAY-RUST, T., KVANSAKUL, M., OPERUGINI, M. A., DOGOVSKI, C., DOERFLINGER, M., ZHANG, Y., PARISI, K., CASEY, J. L., NUTTALL, S. D. & FOLEY, M. 2016. i-bodies, human single domain antibodies that antagonize chemokine receptor CXCR4. *Journal of Biological Chemistry,* 291**,** 12641-12657.
GRIL, B., PALMIERI, D., QIAN, Y., ANWAR, T., ILEVA, L., BERNARDO, M., CHOYKE, P., LIEWEHR, D. J., STEINBERG, S. M. & STEEG, P. S. 2011. The B-Raf status of tumor cells may be a significant determinant of both antitumor and anti-angiogenic effects of pazopanib in xenograft tumor models. *PloS one,* 6**,** e25625.
GRISON, C. M., BURSLEM, G. M., MILES, J. A., PILSL, L. K., YEO, D. J., IMANI, Z., WARRINER, S. L., WEBB, M. E. & WILSON, A. J. 2017. Double quick, double click reversible peptide “stapling”. *Chemical science,* 8**,** 5166-5171.
GRYNKIEWICZ, G., POENIE, M. & TSIEN, R. Y. 1985. A new generation of Ca2+ indicators with greatly improved fluorescence properties. *Journal of Biological Chemistry,* 260**,** 3440-3450.
GUALDA, E. J., PEREIRA, H., MARTINS, G. G., GARDNER, R. & MORENO, N. 2017. Three-dimensional imaging flow cytometry through light-sheet fluorescence microscopy. *Cytometry Part A,* 91**,** 144-151.
GUREVICH, E. V., TESMER, J. J., MUSHEGIAN, A. & GUREVICH, V. V. 2012. G protein-coupled receptor kinases: more than just kinases and not only for GPCRs. *Pharmacology & therapeutics,* 133**,** 40-69.
GURUMURTHY, C. B. & LLOYD, K. C. K. 2019. Generating mouse models for biomedical research: technological advances. *Disease models & mechanisms,* 12**,** dmm029462.
GUSTAVSSON, M., WANG, L., VAN GILS, N., STEPHENS, B. S., ZHANG, P., SCHALL, T. J., YANG, S., ABAGYAN, R., CHANCE, M. R. & KUFAREVA, I. 2017. Structural basis of ligand interaction with atypical chemokine receptor 3. *Nature communications,* 8**,** 14135.
HAFEEZ, B. B., ZHONG, W., WEICHERT, J., DRECKSCHMIDT, N. E., JAMAL, M. S. & VERMA, A. K. 2011. Genetic ablation of PKC epsilon inhibits prostate cancer development and metastasis in transgenic mouse model of prostate adenocarcinoma. *Cancer research,* 71**,** 2318-2327.

HALKS-MILLER, M., HESSELGESSER, J., JMIKO, I. & HORUK, R. 1997. Chemokine receptors in developing human brain. *Methods in enzymology,* 288**,** 27-38.
HAMSHAW, I., AJDARIRAD, M. & MUELLER, A. 2019. The role of PKC and PKD in CXCL12 directed prostate cancer migration. *Biochemical and biophysical research communications,* 519**,** 86-92.
HANAOKA, H., MUKAI, T., TAMAMURA, H., MORI, T., ISHINO, S., OGAWA, K., IIDA, Y., DOI, R., FUJII, N. & SAJI, H. 2006. Development of a 111In-labeled peptide derivative targeting a chemokine receptor, CXCR4, for imaging tumors. *Nuclear medicine and biology,* 33**,** 489-494.
HANSEN, C. G. & NICHOLS, B. J. 2009. Molecular mechanisms of clathrin-independent endocytosis. *Journal of cell science,* 122**,** 1713-1721.
HARIBABU, B., RICHARDSON, R. M., FISHER, I., SOZZANI, S., PEIPER, S. C., HORUK, R., ALI, H. & SNYDERMAN, R. 1997. Regulation of human chemokine receptors CXCR4 Role of phosphorylation in desensitization and internalization. *Journal of Biological Chemistry,* 272**,** 28726-28731.
HARTMANN, T. N., GRABOVSKY, V., PASVOLSKY, R., SHULMAN, Z., BUSS, E. C., SPIEGEL, A., NAGLER, A., LAPIDOT, T., THELEN, M. & ALON, R. 2008. A crosstalk between intracellular CXCR7 and CXCR4 involved in rapid CXCL12-triggered integrin activation but not in chemokine-triggered motility of human T lymphocytes and CD34+ cells. *Journal of leukocyte biology,* 84**,** 1130-1140.
HASSAN, S., BUCHANAN, M., JAHAN, K., AGUILAR-MAHECHA, A., GABOURY, L., MULLER, W. J., ALSAWAFI, Y., MOURSKAIA, A. A., SIEGEL, P. M., SALVUCCI, O. & BASIK, M. 2011. CXCR4 peptide antagonist inhibits primary breast tumor growth, metastasis and enhances the efficacy of anti-VEGF treatment or docetaxel in a transgenic mouse model. *International journal of cancer,* 129**,** 225-232.
HATSE, S., PRINCEN, K., BRIDGER, G., DE CLERCQ, E. & SCHOLS, D. 2002. Chemokine receptor inhibition by AMD3100 is strictly confined to CXCR4. *FEBS letters,* 527**,** 255-262.
HATTERMANN, K., HOLZENBURG, E., HANS, F., LUCIUS, R., HELD-FEINDT, J. & MENTLEIN, R. 2014. Effects of the chemokine CXCL12 and combined internalization of its receptors CXCR4 and CXCR7 in human MCF-7 breast cancer cells. *Cell and tissue research,* 357**,** 253-266.
HAYASAKA, H., KOBAYASHI, D., YOSHIMURA, H., NAKAYAMA, E. E., SHIODA, T. & MIYASAKA, M. 2015. The HIV-1 Gp120/CXCR4 axis promotes CCR7 ligand-dependent CD4 T cell migration: CCR7 homo- and CCR7/CXCR4 hetero-oligomer formation as a possible mechanism for up-regulation of functional CCR7. *PLoS One,* 10**,** e0117454.
HAYASHI, A., SEKI, N., HATTORI, A., KOZUMA, S. & SAITO, T. 1999. PKCν, a new member of the protein kinase C family, composes a fourth subfamily with PKCμ. *Biochimica et Biophysica Acta (BBA)-Molecular Cell Research,* 1450**,** 99-106.
HEIN, C. D., LIU, X.-M. & WANG, D. 2008. Click chemistry, a powerful tool for pharmaceutical sciences. *Pharmaceutical research,* 25**,** 2216-2230.
HEIT, B., TAVENER, S., RAHARJO, E. & KUBES, P. 2002. An intracellular signaling hierarchy determines direction of migration in opposing chemotactic gradients. *The Journal of cell biology,* 159**,** 91-102.
HENLEY, J. R., KRUEGER, E. W., OSWALD, B. J. & MCNIVEN, M. A. 1998. Dynamin-mediated internalization of caveolae. *The Journal of cell biology,* 141**,** 85-99.

HENNE, W. M., BOUCROT, E., MEINECKE, M., EVERGREN, E., VALLIS, Y., MITTAL, R. & MCMAHON, H. T. 2010. FCHo proteins are nucleators of clathrin-mediated endocytosis. *Science,* 328**,** 1281-1284.
HEPLER, J. R. & GILMAN, A. G. 1992. G proteins. *Trends in biochemical sciences,* 17**,** 383-387.
HERSHKO, A. & CIECHANOVER, A. 1998. The ubiquitin system. *Annual review of biochemistry,* 67**,** 425-479.
HESSELGESSER, J., LIANG, M., HOXIE, J., GREENBERG, M., BRASS, L. F., ORSINI, M. J., TAUB, D. & HORUK, R. 1998. Identification and characterization of the CXCR4 chemokine receptor in human T cell lines: ligand binding, biological activity, and HIV-1 infectivity. *The Journal of Immunology,* 160**,** 877-883.
HEUNINCK, J., VICIANO, C. P., IŞBILIR, A., CASPAR, B., CAPOFERRI, D., BRIDDON, S. J., DURROUX, T., HILL, S. J., LOHSE, M. J., MILLIGAN, G., PIN, J. P. & HOFFMANN, C. 2019. Context-Dependent Signaling of CXC Chemokine Receptor 4 and Atypical Chemokine Receptor 3. *Molecular Pharmacology,* 96**,** 778-793.
HEVEZI, P., MOYER, B. D., LU, M., GAO, N., WHITE, E., ECHEVERRI, F., KALABAT, D., SOTO, H., LAITA, B., LI, C., YEH, S. A., ZOLLER, M. & ZLOTNIK, A. 2009. Genome-wide analysis of gene expression in primate taste buds reveals links to diverse processes. *PloS one,* 4**,** e6395.
HEYDTMANN, M. & ADAMS, D. 2002. Understanding selective trafficking of lymphocyte subsets. *Gut,* 50**,** 150-152.
HILL, K., ERDOGAN, E., KHOOR, A., WALSH, M., LEITGES, M., MURRAY, N. R. & FIELDS, A. P. 2014. Protein kinase Cα suppresses Kras-mediated lung tumor formation through activation of a p38 MAPK-TGFβ signaling axis. *Oncogene,* 33**,** 2134-2144.
HIRAI, T. & CHIDA, K. 2003. Protein kinase Cζ (PKCζ): activation mechanisms and cellular functions. *Journal of biochemistry,* 133**,** 1-7.
HITCHON, C., WONG, K., MA, G., REED, J., LYTTLE, D. & EL-GABALAWY, H. 2002. Hypoxia-induced production of stromal cell–derived factor 1 (CXCL12) and vascular endothelial growth factor by synovial fibroblasts. *Arthritis & Rheumatism,* 46**,** 2587-2597.
HO, C. M. B., NG, S. H., LI, K. H. H. & YOON, Y.-J. 2015. 3D printed microfluidics for biological applications. *Lab on a Chip,* 15**,** 3627-3637.
HOFFMANN, F., MÜLLER, W., SCHÜTZ, D., PENFOLD, M. E., WONG, Y. H., SCHULZ, S. & STUMM, R. 2012. Rapid uptake and degradation of CXCL12 depend on CXCR7 carboxyl-terminal serine/threonine residues. *Journal of Biological Chemistry,* 287**,** 28362-28377.
HOFFMANN, W. & JAGLA, W. 2002. Cell type specific expression of secretory TFF peptides: colocalization with mucins and synthesis in the brain. *International review of cytology,* 213**,** 147-181.
HOLLAND, J. D., KOCHETKOVA, M., AKEKAWATCHAI, C., DOTTORE, M., LOPEZ, A. & MCCOLL, S. R. 2006. Differential functional activation of chemokine receptor CXCR4 is mediated by G proteins in breast cancer cells. *Cancer research,* 66**,** 4117-4124.
HOLLIDAY, D. L. & SPEIRS, V. 2011. Choosing the right cell line for breast cancer research. *Breast cancer research,* 13**,** 215-222.
HONG, V., STEINMETZ, N. F., MANCHESTER, M. & FINN, M. 2010. Labeling live cells by copper-catalyzed alkyne− azide click chemistry. *Bioconjugate chemistry,* 21**,** 1912-1916.
HORUK, R. 2009. Chemokine receptor antagonists: overcoming developmental hurdles. *Nature reviews Drug discovery,* 8**,** 23-33.

HROMAS, R., BROXMEYER, H. E., KIM, C., NAKSHATRI, H., CHRISTOPHERSON II, K., AZAM, M. & HOU, Y.-H. 1999. Cloning of BRAK, a novel divergent CXC chemokine preferentially expressed in normal versus malignant cells. *Biochemical and biophysical research communications,* 255**,** 703-706.

HU, T.-H., YAO, Y., YU, S., HAN, L.-L., WANG, W.-J., GUO, H., TIAN, T., RUAN, Z.-P., KANG, X.-M., WANG, J., WANG, S. H. & NAN, K. J. 2014. SDF-1/CXCR4 promotes epithelial–mesenchymal transition and progression of colorectal cancer by activation of the Wnt/β-catenin signaling pathway. *Cancer letters,* 354**,** 417-426.

HUISING, M. O., VAN DER MEULEN, T., FLIK, G. & VERBURG-VAN KEMENADE, B. 2004. Three novel carp CXC chemokines are expressed early in ontogeny and at nonimmune sites. *European Journal of Biochemistry,* 271**,** 4094-4106.

HULL, C. W. 1986. Apparatus for production of three-dimensional objects by stereolithography. 19**,** 1-16.

HUNTER, Z. R., YANG, G., XU, L., LIU, X., CASTILLO, J. J. & TREON, S. P. 2017. Genomics, signaling, and treatment of Waldenström macroglobulinemia. *Journal of Clinical Oncology,* 35**,** 994-1001.

HUTMACHER, D. W. 2001. Scaffold design and fabrication technologies for engineering tissues—state of the art and future perspectives. *Journal of Biomaterials Science, Polymer Edition,* 12**,** 107-124.

HUTMACHER, D. W., SITTINGER, M. & RISBUD, M. V. 2004. Scaffold-based tissue engineering: rationale for computer-aided design and solid free-form fabrication systems. *TRENDS in Biotechnology,* 22**,** 354-362.

IGLESIAS, T., MATTHEWS, S. & ROZENGURT, E. 1998a. Dissimilar phorbol ester binding properties of the individual cysteine-rich motifs of protein kinase D. *FEBS letters,* 437**,** 19-23.

IGLESIAS, T. & ROZENGURT, E. 1998. Protein kinase D activation by mutations within its pleckstrin homology domain. *Journal of Biological Chemistry,* 273**,** 410-416.

IGLESIAS, T. & ROZENGURT, E. 1999. Protein kinase D activation by deletion of its cysteine-rich motifs. *FEBS letters,* 454**,** 53-56.

IGLESIAS, T., WALDRON, R. T. & ROZENGURT, E. 1998b. Identification of in vivo phosphorylation sites required for protein kinase D activation. *Journal of Biological Chemistry,* 273**,** 27662-27667.

ILINA, O. & FRIEDL, P. 2009. Mechanisms of collective cell migration at a glance. *Journal of cell science,* 122**,** 3203-3208.

INNGJERDINGEN, M., ROLSTAD, B. & RYAN, J. C. 2003. Activating and inhibitory Ly49 receptors modulate NK cell chemotaxis to CXC chemokine ligand (CXCL) 10 and CXCL12. *The Journal of Immunology,* 171**,** 2889-2895.

IRETON, K. 2013. Molecular mechanisms of cell–cell spread of intracellular bacterial pathogens. *Open biology,* 3**,** 130079.

JAAKOLA, V.-P. 2005. Functional and Structural Studies on Heptahelical Membrane Proteins.

JACQUEMET, G., HAMIDI, H. & IVASKA, J. 2015. Filopodia in cell adhesion, 3D migration and cancer cell invasion. *Current opinion in cell biology,* 36**,** 23-31.

JACQUES, R. O., MILLS, S. C., CAZZONATTO ZERWES, P., FAGADE, F. O., GREEN, J. E., DOWNHAM, S., SEXTON, D. W. & MUELLER, A. 2015. Dynamin function is important for chemokine receptor-induced cell migration. *Cell biochemistry and function,* 33**,** 407-414.

JÄHNICHEN, S., BLANCHETOT, C., MAUSSANG, D., GONZALEZ-PAJUELO, M., CHOW, K. Y., BOSCH, L., DE VRIEZE, S., SERRUYS, B., ULRICHTS, H., VANDEVELDE, W., SAUNDERS, M., DE HAARD, H. J., SCHOLS, D., LEURS, R., VANLANDSCHOOT, P., VERRIPS, T. & SMIT, M. J. 2010. CXCR4 nanobodies (VHH-based single variable domains) potently inhibit chemotaxis and HIV-1 replication and mobilize stem cells. *Proceedings of the National Academy of Sciences,* 107**,** 20565-20570.

JAMORA, C., YAMANOUYE, N., VAN LINT, J., LAUDENSLAGER, J., VANDENHEEDE, J. R., FAULKNER, D. J. & MALHOTRA, V. 1999. Gβγ-mediated regulation of Golgi organization is through the direct activation of protein kinase D. *Cell,* 98**,** 59-68.

JAMUR, M. C. & OLIVER, C. 2010. Permeabilization of cell membranes. *Methods in Moleculr Biology,* 588**,** 63-66.

JANOWSKI, M. 2009. Functional diversity of SDF-1 splicing variants. *Cell adhesion & migration,* 3**,** 243-249.

JANSSENS, R., BOFF, D., RUYTINX, P., MORTIER, A., VANHEULE, V., LARSEN, O., DAUGVILAITE, V., ROSENKILDE, M. M., NOPPEN, S. & LIEKENS, S. 2018a. Peroxynitrite exposure of CXCL12 impairs monocyte, lymphocyte and endothelial cell chemotaxis, lymphocyte extravasation in vivo and anti-HIV-1 activity. *Frontiers in immunology,* 9.

JANSSENS, R., STRUYF, S. & PROOST, P. 2018b. Pathological roles of the homeostatic chemokine CXCL12. *Cytokine & growth factor reviews,* 44**,** 51-68.

JIMÉNEZ-SAINZ, M. C., MURGA, C., KAVELAARS, A., JURADO-PUEYO, M., KRAKSTAD, B. F., HEIJNEN, C. J., MAYOR, F. & ARAGAY, A. M. 2006. G protein-coupled receptor kinase 2 negatively regulates chemokine signaling at a level downstream from G protein subunits. *Molecular biology of the cell,* 17**,** 25-31.

JO, D.-Y., RAFII, S., HAMADA, T. & MOORE, M. A. 2000. Chemotaxis of primitive hematopoietic cells in response to stromal cell–derived factor-1. *The Journal of clinical investigation,* 105**,** 101-111.

JOHANNES, F.-J., PRESTLE, J., EIS, S., OBERHAGEMANN, P. & PFIZENMAIER, K. 1994. PKCu is a novel, atypical member of the protein kinase C family. *Journal of Biological Chemistry,* 269**,** 6140-6148.

JOHNSON, G. L. & DHANASEKARAN, N. 1989. The G-protein family and their interaction with receptors. *Endocrine reviews,* 10**,** 317-331.

JOHNSON, Z., POWER, C., WEISS, C., RINTELEN, F., JI, H., RUCKLE, T., CAMPS, M., WELLS, T., SCHWARZ, M., PROUDFOOT, A. & ROMMEL, C. 2004. Chemokine inhibition–why, when, where, which and how? *Biochemical Society Transactions,* 32**,** 366-377.

JOOST, P. & METHNER, A. 2002. Phylogenetic analysis of 277 human G-protein-coupled receptors as a tool for the prediction of orphan receptor ligands. *Genome biology,* 3**,** 1-16.

KAHLER, A. & STICHT, H. 2016. A modeling strategy for G-protein coupled receptors. *AIMS Biophysics,* 3**,** 211-231.

KALATSKAYA, I., BERCHICHE, Y. A., GRAVEL, S., LIMBERG, B. J., ROSENBAUM, J. S. & HEVEKER, N. 2009. AMD3100 is a CXCR7 ligand with allosteric agonist properties. *Molecular pharmacology,* 75**,** 1240-1247.

KANG, N., CHOI, S. Y., KIM, B. N., YEO, C. D., PARK, C. K., KIM, Y. K., KIM, T.-J., LEE, S.-B., LEE, S. H. & PARK, J. Y. 2019. Hypoxia-induced

cancer stemness acquisition is associated with CXCR4 activation by its aberrant promoter demethylation. *BMC cancer,* 19**,** 148-159.
KASAMA, T., OHTSUKA, K., SATO, M., TAKAHASHI, R., WAKABAYASHI, K. & KOBAYASHI, K. 2011. Macrophage migration inhibitory factor: a multifunctional cytokine in rheumatic diseases. *Arthritis,* 2010.
KASAMA, T., STRIETER, R. M., LUKACS, N. W., LINCOLN, P. M., BURDICK, M. D. & KUNKEL, S. L. 1995. Interleukin-10 expression and chemokine regulation during the evolution of murine type II collagen-induced arthritis. *Journal of Clinical Investigation,* 95**,** 2868-2676.
KATO, M., KITAYAMA, J., KAZAMA, S. & NAGAWA, H. 2003. Expression pattern of CXC chemokine receptor-4 is correlated with lymph node metastasis in human invasive ductal carcinoma. *Breast Cancer Research,* 5**,** 144-150.
KATZ, A., WU, D. & SIMON, M. I. 1992. Subunits βγ of heterotrimeric G protein activate β2 isoform of phospholipase C. *Nature,* 360**,** 686-689.
KAZAZIC, M., ROEPSTORFF, K., JOHANNESSEN, L. E., PEDERSEN, N. M., VAN DEURS, B., STANG, E. & MADSHUS, I. H. 2006. EGF-induced activation of the EGF receptor does not trigger mobilization of caveolae. *Traffic,* 7**,** 1518-1527.
KEENAN, T. M. & FOLCH, A. 2008. Biomolecular gradients in cell culture systems. *Lab on a Chip,* 8**,** 34-57.
KHAN, A., SILVERSIDES, J. D., MADDEN, L., GREENMAN, J. & ARCHIBALD, S. J. 2007. Fluorescent CXCR4 chemokine receptor antagonists: metal activated binding. *Chemical communications,* 28**,** 416-418.
KIKKAWA, U., OGITA, K., SHEARMAN, M., ASE, K., SEKIGUCHI, K., NAOR, Z., KISHIMOTO, A., NISHIZUKA, Y., SAITO, N., TANAKA, C., ONO, Y., FUJII, T. & IGARASHI, K. 1988. The family of protein kinase C: its molecular heterogeneity and differential expression. *Cold Spring Harbor symposia on quantitative biology,* 53**,** 97-102.
KIM, B.-Y., LEE, J., PARK, S. J., BANG, O.-S. & KIM, N. S. 2013. Gene expression profile of the A549 human non-small cell lung carcinoma cell line following treatment with the seeds of Descurainia sophia, a potential anticancer drug. *Evidence-Based Complementary and Alternative Medicine,* 2013**,** 1-13.
KIM, Y.-N., KOO, K. H., SUNG, J. Y., YUN, U.-J. & KIM, H. 2012. Anoikis resistance: an essential prerequisite for tumor metastasis. *International journal of cell biology,* 2012.
KIRUI, J. K., XIE, Y., WOLFF, D. W., JIANG, H., ABEL, P. W. & TU, Y. 2010. Gβγ signaling promotes breast cancer cell migration and invasion. *Journal of Pharmacology and Experimental Therapeutics,* 333**,** 393-403.
KISS, A. L. & BOTOS, E. 2009. Endocytosis via caveolae: alternative pathway with distinct cellular compartments to avoid lysosomal degradation? *Journal of cellular and molecular medicine,* 13**,** 1228-1237.
KITSON, P. J., ROSNES, M. H., SANS, V., DRAGONE, V. & CRONIN, L. 2012. Configurable 3D-Printed millifluidic and microfluidic 'lab on a chip'reactionware devices. *Lab on a Chip,* 12**,** 3267-3271.
KLEEMANN, P., PAPA, D., VIGIL-CRUZ, S. & SEIFERT, R. 2008. Functional reconstitution of the human chemokine receptor CXCR4 with G i/G o-proteins in Sf9 insect cells. *Naunyn-Schmiedeberg's archives of pharmacology,* 378**,** 261-274.
KNIGHT, J. C., HALLETT, A. J., BRANCALE, A., PAISEY, S. J., CLARKSON, R. W. & EDWARDS, P. G. 2011. Evaluation of a Fluorescent Derivative

of AMD3100 and its Interaction with the CXCR4 Chemokine Receptor. *ChemBioChem,* 12**,** 2692-2698.
KO, S., SHIM, G., KIM, J. & OH, Y.-K. 2018. Chemokine-mimetic plerixafor derivative for tumor-specific delivery of nanomaterials. *Nano Research,* 11**,** 2159-2172.
KOLB, H. C., FINN, M. & SHARPLESS, K. B. 2001. Click chemistry: diverse chemical function from a few good reactions. *Angewandte Chemie International Edition,* 40**,** 2004-2021.
KONOPKA, K. & DÜZGÜNEŞ, N. 2002. Expression of CD4 controls the susceptibility of THP-1 cells to infection by R5 and X4 HIV type 1 isolates. *AIDS research and human retroviruses,* 18**,** 123-131.
KOSHIBA, T., HOSOTANI, R., MIYAMOTO, Y., IDA, J., TSUJI, S., NAKAJIMA, S., KAWAGUCHI, M., KOBAYASHI, H., DOI, R., HORI, T., FUJII, N. & IMAMURA, M. 2000. Expression of stromal cell-derived factor 1 and CXCR4 ligand receptor system in pancreatic cancer: a possible role for tumor progression. *Clinical cancer research,* 6**,** 3530-3535.
KROEZE, K. L., JURGENS, W. J., DOULABI, B. Z., VAN MILLIGEN, F. J., SCHEPER, R. J. & GIBBS, S. 2009. Chemokine-mediated migration of skin-derived stem cells: predominant role for CCL5/RANTES. *Journal of Investigative Dermatology,* 129**,** 1569-1581.
KRUPNICK, J. G. & BENOVIC, J. L. 1998. The role of receptor kinases and arrestins in G protein–coupled receptor regulation. *Annual review of pharmacology and toxicology,* 38**,** 289-319.
KUHNE, M. R., MULVEY, T., BELANGER, B., CHEN, S., PAN, C., CHONG, C., CAO, F., NIEKRO, W., KEMPE, T., HENNING, K. A., COHEN, L. J., KORMAN, A. J. & CARDARELLI, P. M. 2013. BMS-936564/MDX-1338: a fully human anti-CXCR4 antibody induces apoptosis in vitro and shows antitumor activity in vivo in hematologic malignancies. *Clinical cancer research,* 19**,** 357-366.
KUIL, J., BUCKLE, T., YUAN, H., VAN DEN BERG, N. S., OISHI, S., FUJII, N., JOSEPHSON, L. & VAN LEEUWEN, F. W. 2011. Synthesis and evaluation of a bimodal CXCR4 antagonistic peptide. *Bioconjugate chemistry,* 22**,** 859-864.
KUKIELKA, G. L., YOUKER, K. A., MICHAEL, L. H., KUMAR, A. G., BALLANTYNE, C. M., SMITH, C. W. & ENTMAN, M. L. 1995. Role of early reperfusion in the induction of adhesion molecules and cytokines in previously ischemic myocardium. *Molecular and cellular biochemistry,* 147**,** 5-12.
KUNKEL, M. T., TOKER, A., TSIEN, R. Y. & NEWTON, A. C. 2007. Calcium-dependent regulation of protein kinase D revealed by a genetically encoded kinase activity reporter. *Journal of Biological Chemistry,* 282**,** 6733-6742.
KUROSAKA, S. & KASHINA, A. 2008. Cell biology of embryonic migration. *Birth Defects Research Part C: Embryo Today: Reviews,* 84**,** 102-122.
KURTH, I., WILLIMANN, K., SCHAERLI, P., HUNZIKER, T., CLARK-LEWIS, I. & MOSER, B. 2001. Monocyte selectivity and tissue localization suggests a role for breast and kidney–expressed chemokine (BRAK) in macrophage development. *Journal of Experimental Medicine,* 194**,** 855-862.
L MOHAN, M., T VASUDEVAN, N., K GUPTA, M., E MARTELLI, E. & V NAGA PRASAD, S. 2012. G-protein coupled receptor resensitization-appreciating the balancing act of receptor function. *Current molecular pharmacology,* 5**,** 350-361.

LAFAVE, L. M. & LEVINE, R. L. 2012. JAK2 the future: therapeutic strategies for JAK-dependent malignancies. *Trends in pharmacological sciences,* 33**,** 574-582.
LAING, K. J. & SECOMBES, C. J. 2004. Chemokines. *Developmental & Comparative Immunology,* 28**,** 443-460.
LALLANA, E., RIGUERA, R. & FERNANDEZ-MEGIA, E. 2011. Reliable and efficient procedures for the conjugation of biomolecules through Huisgen azide–alkyne cycloadditions. *Angewandte Chemie International Edition,* 50**,** 8794-8804.
LAMBEIR, A.-M., PROOST, P., DURINX, C., BAL, G., SENTEN, K., AUGUSTYNS, K., SCHARPÉ, S., VAN DAMME, J. & DE MEESTER, I. 2001. Kinetic investigation of chemokine truncation by CD26/dipeptidyl peptidase IV reveals a striking selectivity within the chemokine family. *Journal of Biological Chemistry,* 276**,** 29839-29845.
LAPA, C., LÜCKERATH, K., RUDELIUS, M., SCHMID, J.-S., SCHOENE, A., SCHIRBEL, A., SAMNICK, S., PELZER, T., BUCK, A. K., KROPF, S., WESTER, H. J. & HERRMANN, K. 2016. [68Ga] Pentixafor-PET/CT for imaging of chemokine receptor 4 expression in small cell lung cancer-initial experience. *Oncotarget,* 7**,** 9288-9295.
LAPA, C., SCHREDER, M., SCHIRBEL, A., SAMNICK, S., KORTÜM, K. M., HERRMANN, K., KROPF, S., EINSELE, H., BUCK, A. K., WESTER, H.-J., KNOP, S. & LÜCKERATH, K. 2017. [68Ga] Pentixafor-PET/CT for imaging of chemokine receptor CXCR4 expression in multiple myeloma-Comparison to [18F] FDG and laboratory values. *Theranostics,* 7**,** 205-212.
LAROCCA, T. J., ALTMAN, P., JARRAH, A. A., GORDON, R., WANG, E., HADRI, L., BURKE, M. W., HADDAD, G. E., HAJJAR, R. J. & TARZAMI, S. T. 2019. CXCR4 Cardiac Specific Knockout Mice Develop a Progressive Cardiomyopathy. *International journal of molecular sciences,* 20**,** 1-15.
LARSSON, C. 2006. Protein kinase C and the regulation of the actin cytoskeleton. *Cellular signalling,* 18**,** 276-284.
LE, Y., ZHOU, Y., IRIBARREN, P. & WANG, J. 2004. Chemokines and chemokine receptors: their manifold roles in homeostasis and disease. *Cell Mol Immunol,* 1**,** 95-104.
LEE, A. W. 2011. The role of atypical protein kinase C in CSF-1-dependent Erk activation and proliferation in myeloid progenitors and macrophages. *PloS one,* 6.
LEE, J.-Y., AN, J. & CHUA, C. K. 2017. Fundamentals and applications of 3D printing for novel materials. *Applied Materials Today,* 7**,** 120-133.
LEGET, G. A. & CZUCZMAN, M. S. 1998. Use of rituximab, the new FDA-approved antibody. *Current opinion in oncology,* 10**,** 548-551.
LEOPOLDT, D., HANCK, T., EXNER, T., MAIER, U., WETZKER, R. & NÜRNBERG, B. 1998. Gβγ stimulates phosphoinositide 3-kinase-γ by direct interaction with two domains of the catalytic p110 subunit. *Journal of Biological Chemistry,* 273**,** 7024-7029.
LEVOYE, A., BALABANIAN, K., BALEUX, F., BACHELERIE, F. & LAGANE, B. 2009. CXCR7 heterodimerizes with CXCR4 and regulates CXCL12-mediated G protein signaling. *Blood,* 113**,** 6085-6093.
LI, J.-T., JIA, L.-T., LIU, N.-N., ZHU, X.-S., LIU, Q.-Q., WANG, X.-L., YU, F., LIU, Y.-L., YANG, A.-G. & GAO, C.-F. 2015. MiRNA-101 inhibits breast cancer growth and metastasis by targeting CX chemokine receptor 7. *Oncotarget,* 6**,** 30818-30830.

LI, K., LEE, L. A., LU, X. & WANG, Q. 2010. Fluorogenic “click” reaction for labeling and detection of DNA in proliferating cells. *Biotechniques,* 49**,** 525-527.
LI, S., WANG, L., YU, F., ZHU, Z., SHOBAKI, D., CHEN, H., WANG, M., WANG, J., QIN, G., ERASQUIN, U. J., REN, L., WANG, Y. & CHENGZHI, C. 2017. Copper-catalyzed click reaction on/in live cells. *Chemical science,* 8**,** 2107-2114.
LIANG, Z., BROOKS, J., WILLARD, M., LIANG, K., YOON, Y., KANG, S. & SHIM, H. 2007. CXCR4/CXCL12 axis promotes VEGF-mediated tumor angiogenesis through Akt signaling pathway. *Biochemical and biophysical research communications,* 359**,** 716-722.
LIANG, Z., YOON, Y., VOTAW, J., GOODMAN, M. M., WILLIAMS, L. & SHIM, H. 2005. Silencing of CXCR4 blocks breast cancer metastasis. *Cancer research,* 65**,** 967-971.
LIEBMANN, C. & BOHMER, F. 2000. Signal Transduction Pathways of G Protein-coupled Receptors and Their Cross-Talk with Receptor Tyrosine Kinases Lessons from Bradykinin Signaling. *Current medicinal chemistry,* 7**,** 911-943.
LILES, W. C., BROXMEYER, H. E., RODGER, E., WOOD, B., HÜBEL, K., COOPER, S., HANGOC, G., BRIDGER, G. J., HENSON, G. W., CALANDRA, G. & DALE, D. C. 2003. Mobilization of hematopoietic progenitor cells in healthy volunteers by AMD3100, a CXCR4 antagonist. *Blood,* 102**,** 2728-2730.
LING, K., WANG, P., ZHAO, J., WU, Y.-L., CHENG, Z.-J., WU, G.-X., HU, W., MA, L. & PEI, G. 1999. Five-transmembrane domains appear sufficient for a G protein-coupled receptor: functional five-transmembrane domain chemokine receptors. *Proceedings of the National Academy of Sciences,* 96**,** 7922-7927.
LIU, L., AA, J., WANG, G., YAN, B., ZHANG, Y., WANG, X., ZHAO, C., CAO, B., SHI, J., LI, M., ZHENG, T., ZHENG, Y., HAO, G., ZHOU, F., SUN, J. & WU, Z. 2010. Differences in metabolite profile between blood plasma and serum. *Analytical biochemistry,* 406**,** 105-112.
LIU, W., YIN, L., CHEN, C. & DAI, Y. 2011. Function modification of SR-PSOX by point mutations of basic amino acids. *Lipids in health and disease,* 10**,** 1-8.
LODGE, R., GILMORE, J., FERREIRA BARBOSA, J., LOMBARD-VADNAIS, F. & COHEN, É. 2018. Regulation of CD4 Receptor and HIV-1 Entry by MicroRNAs-221 and-222 during Differentiation of THP-1 Cells. *Viruses,* 10**,** 1-18.
LOETSCHER, M., GEISER, T., O'REILLY, T., ZWAHLEN, R., BAGGIOLINI, M. & MOSER, B. 1994. Cloning of a human seven-transmembrane domain receptor, LESTR, that is highly expressed in leukocytes. *Journal of Biological Chemistry,* 269**,** 232-237.
LORENZO, M., TERUEL, T., HERNANDEZ, R., KAYALI, A. G. & WEBSTER, N. J. 2002. PLCγ participates in insulin stimulation of glucose uptake through activation of PKCζ in brown adipocytes. *Experimental cell research,* 278**,** 146-157.
LUKER, K. E., STEELE, J. M., MIHALKO, L. A., RAY, P. & LUKER, G. D. 2010. Constitutive and chemokine-dependent internalization and recycling of CXCR7 in breast cancer cells to degrade chemokine ligands. *Oncogene,* 29**,** 4599-4610.

LUNDMARK, R. & CARLSSON, S. R. Driving membrane curvature in clathrin-dependent and clathrin-independent endocytosis. Seminars in cell & developmental biology, 2010. Elsevier, 363-370.
LUO, J., BUSILLO, J. M., STUMM, R. & BENOVIC, J. L. 2017. G Protein-Coupled Receptor Kinase 3 and Protein Kinase C phosphorylate the distal C-terminal tail of the chemokine receptor CXCR4 and mediate recruitment of β-Arrestin. *Molecular pharmacology,* 91**,** 554-566.
MA, Q., JONES, D., BORGHESANI, P. R., SEGAL, R. A., NAGASAWA, T., KISHIMOTO, T., BRONSON, R. T. & SPRINGER, T. A. 1998. Impaired B-lymphopoiesis, myelopoiesis, and derailed cerebellar neuron migration in CXCR4-and SDF-1-deficient mice. *Proceedings of the National Academy of Sciences,* 95**,** 9448-9453.
MAERKI, C., MEUTER, S., LIEBI, M., MÜHLEMANN, K., FREDERICK, M. J., YAWALKAR, N., MOSER, B. & WOLF, M. 2009. Potent and broad-spectrum antimicrobial activity of CXCL14 suggests an immediate role in skin infections. *The Journal of Immunology,* 182**,** 507-514.
MAJETSCHAK, M., KREHMEIER, U., BARDENHEUER, M., DENZ, C., QUINTEL, M., VOGGENREITER, G. & OBERTACKE, U. 2003. Extracellular ubiquitin inhibits the TNF-α response to endotoxin in peripheral blood mononuclear cells and regulates endotoxin hyporesponsiveness in critical illness. *Blood,* 101**,** 1882-1890.
MAJETSCHAK, M., ZEDLER, S., HOSTMANN, A., SORELL, L. T., PATEL, M. B., NOVAR, L. T., KRAFT, R., HABIB, F., DE MOYA, M. A., ERTEL, W., FAIST, E. & SCHADE, U. 2008. Systemic ubiquitin release after blunt trauma and burns: association with injury severity, posttraumatic complications, and survival. *Journal of Trauma and Acute Care Surgery,* 64**,** 586-598.
MANTOVANI, A. 1999. The chemokine system: redundancy for robust outputs. *Immunology today,* 20**,** 254-257.
MANTOVANI, A., MARCHESI, F., MALESCI, A., LAGHI, L. & ALLAVENA, P. 2017. Tumour-associated macrophages as treatment targets in oncology. *Nature reviews Clinical oncology,* 14**,** 399.
MARCHESE, A., CHEN, C., KIM, Y.-M. & BENOVIC, J. L. 2003. The ins and outs of G protein-coupled receptor trafficking. *Trends in biochemical sciences,* 28**,** 369-376.
MARCHESE, A., PAING, M. M., TEMPLE, B. R. & TREJO, J. 2008. G protein–coupled receptor sorting to endosomes and lysosomes. *Annual review of pharmacology and toxicology,* 48**,** 601-629.
MARCHESI, F., MONTI, P., LEONE, B. E., ZERBI, A., VECCHI, A., PIEMONTI, L., MANTOVANI, A. & ALLAVENA, P. 2004. Increased survival, proliferation, and migration in metastatic human pancreatic tumor cells expressing functional CXCR4. *Cancer research,* 64**,** 8420-8427.
MAROTTA, L. L., ALMENDRO, V., MARUSYK, A., SHIPITSIN, M., SCHEMME, J., WALKER, S. R., BLOUSHTAIN-QIMRON, N., KIM, J. J., CHOUDHURY, S. A., MARUYAMA, R., WU, Z., M, G., MULVEY, L. A., BESSARABOVA, M. O., HUH, S. J., SILVER, S. J., KIM, S. Y., PARK, S. Y., LEE, H. E., ANDERSON, K. S., RICHARDSON, A. L., NIKOLSKAYA, T., LIU, X. S., ROOT, D. E., HAHN, W. C., FRANK, D. A. & POLYAK, K. 2011. The JAK2/STAT3 signaling pathway is required for growth of CD44+ CD24–stem cell–like breast cancer cells in human tumors. *The Journal of clinical investigation,* 121**,** 2723-2735.
MARQUEZ-CURTIS, L., JALILI, A., DEITEREN, K., SHIRVAIKAR, N., LAMBEIR, A. M. & JANOWSKA-WIECZOREK, A. 2008.

Carboxypeptidase M Expressed by Human Bone Marrow Cells Cleaves the C-Terminal Lysine of Stromal Cell-Derived Factor-1α: Another Player in Hematopoietic Stem/Progenitor Cell Mobilization? *Stem cells,* 26**,** 1211-1220.

MARTIN, C., BURDON, P. C., BRIDGER, G., GUTIERREZ-RAMOS, J.-C., WILLIAMS, T. J. & RANKIN, S. M. 2003. Chemokines acting via CXCR2 and CXCR4 control the release of neutrophils from the bone marrow and their return following senescence. *Immunity,* 19**,** 583-593.

MARTIN, S. K., DIAMOND, P., WILLIAMS, S. A., TO, L. B., PEET, D. J., FUJII, N., GRONTHOS, S., HARRIS, A. L. & ZANNETTINO, A. C. 2010. Hypoxia-inducible factor-2 is a novel regulator of aberrant CXCL12 expression in multiple myeloma plasma cells. *Haematologica,* 95**,** 776-784.

MARTINY-BARON, G. & FABBRO, D. 2007. Classical PKC isoforms in cancer. *Pharmacological research,* 55**,** 477-486.

MARTINY-BARON, G., KAZANIETZ, M. G., MISCHAK, H., BLUMBERG, P. M., KOCHS, G., HUG, H., MARME, D. & SCHÄCHTELE, C. 1993. Selective inhibition of protein kinase C isozymes by the indolocarbazole Gö 6976. *Journal of Biological Chemistry,* 268**,** 9194-9197.

MAUDSLEY, S., MARTIN, B. & LUTTRELL, L. M. 2005. The origins of diversity and specificity in G protein-coupled receptor signaling. *Journal of Pharmacology and Experimental Therapeutics,* 314**,** 485-494.

MAYOR, S., PARTON, R. G. & DONALDSON, J. G. 2014. Clathrin-independent pathways of endocytosis. *Cold Spring Harbor perspectives in biology,* 6**,** a016758.

MCGOOKEY, D. J., FAGERBERG, K. & ANDERSON, R. 1983. Filipin-cholesterol complexes form in uncoated vesicle membrane derived from coated vesicles during receptor-mediated endocytosis of low density lipoprotein. *The Journal of cell biology,* 96**,** 1273-1278.

MCQUIBBAN, G. A., BUTLER, G. S., GONG, J.-H., BENDALL, L., POWER, C., CLARK-LEWIS, I. & OVERALL, C. M. 2001. Matrix metalloproteinase activity inactivates the CXC chemokine stromal cell-derived factor-1. *Journal of Biological Chemistry,* 276**,** 43503-43508.

MEHRAD, B., KEANE, M. P. & STRIETER, R. M. 2007. Chemokines as mediators of angiogenesis. *Thrombosis and Haemostasis* 97**,** 755-762.

MEHTA, S., CHRISTOPHERSON, K., BHAT-NAKSHATRI, P., GOULET, R., BROXMEYER, H., KOPELOVICH, L. & NAKSHATRI, H. 2007. Negative regulation of chemokine receptor CXCR4 by tumor suppressor p53 in breast cancer cells: implications of p53 mutation or isoform expression on breast cancer cell invasion. *Oncogene,* 26**,** 3329-3337.

MELLADO, M., RODRÍGUEZ-FRADE, J. M., MAÑES, S. & MARTÍNEZ-A, C. 2001. Chemokine signaling and functional responses: the role of receptor dimerization and TK pathway activation. *Annual review of immunology,* 19**,** 397-421.

MELLER, N., ELITZUR, Y. & ISAKOV, N. 1999. Protein kinase C-θ (PKCθ) distribution analysis in hematopoietic cells: proliferating T cells exhibit high proportions of PKCθ in the particulate fraction. *Cellular immunology,* 193**,** 185-193.

MELO, R. D. C. C., FERRO, K. P. V., DUARTE, A. D. S. S. & SAAD, S. T. O. 2018. CXCR7 participates in CXCL12-mediated migration and homing of leukemic and normal hematopoietic cells. *Stem cell research & therapy,* 9**,** 1-5.

MELO, R. D. C. C., LONGHINI, A. L., BIGARELLA, C. L., BARATTI, M. O., TRAINA, F., FAVARO, P., DE MELO CAMPOS, P. & SAAD, S. T. O. 2014. CXCR7 is highly expressed in acute lymphoblastic leukemia and potentiates CXCR4 response to CXCL12. *PLoS One,* 9**,** e85926.
MERCK. 2017. *MCF7 Cell Line human* [Online]. [Accessed].
MESHKI, J., CAINO, M. C., VON BURSTIN, V. A., GRINER, E. & KAZANIETZ, M. G. 2010. Regulation of prostate cancer cell survival by protein kinase Cϵ involves bad phosphorylation and modulation of the TNFα/JNK pathway. *Journal of Biological Chemistry,* 285**,** 26033-26040.
METCALFE, C., CRESSWELL, P., CIACCIA, L., THOMAS, B. & BARCLAY, A. N. 2011. Labile disulfide bonds are common at the leucocyte cell surface. *Open biology,* 1.
METZGER, E., IMHOF, A., PATEL, D., KAHL, P., HOFFMEYER, K., FRIEDRICHS, N., MÜLLER, J. M., GRESCHIK, H., KIRFEL, J., JI, S., KUNOWSKA, N., BEISENHERZ-HUSS, C., GÜNTHER, T., BUETTNER, R. & SCHÜLE, R. 2010. Phosphorylation of histone H3T6 by PKCβ I controls demethylation at histone H3K4. *Nature,* 464**,** 792-796.
MEUTER, S. & MOSER, B. 2008. Constitutive expression of CXCL14 in healthy human and murine epithelial tissues. *Cytokine,* 44**,** 248-255.
MIAO, Z., LUKER, K. E., SUMMERS, B. C., BERAHOVICH, R., BHOJANI, M. S., REHEMTULLA, A., KLEER, C. G., ESSNER, J. J., NASEVICIUS, A., LUKER, G. D., HOWARD, M. C. & SCHALL, T. J. 2007. CXCR7 (RDC1) promotes breast and lung tumor growth in vivo and is expressed on tumor-associated vasculature. *Proceedings of the National Academy of Sciences,* 104**,** 15735-15740.
MILLS, S. C., GOH, P. H., KUDATSIH, J., NCUBE, S., GURUNG, R., MAXWELL, W. & MUELLER, A. 2016. Cell migration towards CXCL12 in leukemic cells compared to breast cancer cells. *Cellular signalling,* 28**,** 316-324.
MILLS, S. C., HOWELL, L., BEEKMAN, A., STOKES, L. & MUELLER, A. 2018. Rac1 plays a role in CXCL12 but not CCL3-induced chemotaxis and Rac1 GEF inhibitor NSC23766 has off target effects on CXCR4. *Cellular signalling,* 42**,** 88-96.
MIRONOV, V., BOLAND, T., TRUSK, T., FORGACS, G. & MARKWALD, R. R. 2003. Organ printing: computer-aided jet-based 3D tissue engineering. *TRENDS in Biotechnology,* 21**,** 157-161.
MISHRA, R. K., SHUM, A. K., PLATANIAS, L. C., MILLER, R. J. & SCHILTZ, G. E. 2016. Discovery and characterization of novel small-molecule CXCR4 receptor agonists and antagonists. *Scientific Reports,* 6.
MITHAL, D. S., BANISADR, G. & MILLER, R. J. 2012. CXCL12 signaling in the development of the nervous system. *Journal of Neuroimmune Pharmacology,* 7**,** 820-834.
MO, W., CHEN, J., PATEL, A., ZHANG, L., CHAU, V., LI, Y., CHO, W., LIM, K., XU, J., LAZAR, A. J., CREIGHTON, C., BOLSHAKOV, S., MCKAY, R., LEV, D., LE, L. & PARADA, L. 2013. CXCR4/CXCL12 mediate autocrine cell-cycle progression in NF1-associated malignant peripheral nerve sheath tumors. *Cell,* 152**,** 1077-1090.
MODING, E. J., KASTAN, M. B. & KIRSCH, D. G. 2013. Strategies for optimizing the response of cancer and normal tissues to radiation. *Nature reviews Drug discovery,* 12**,** 526- 542.
MONTANER, S., KUFAREVA, I., ABAGYAN, R. & GUTKIND, J. S. 2013. Molecular Mechanisms Deployed by Virally Encoded G Protein–Coupled

Receptors in Human Diseases. *Annual review of pharmacology and toxicology,* 53**,** 331-354.
MONTESANO, R., PERRELET, A., VASSALLI, P. & ORCI, L. 1979. Absence of filipin-sterol complexes from large coated pits on the surface of culture cells. *Proceedings of the National Academy of Sciences,* 76**,** 6391-6395.
MONTIEL, M., DE LA BLANCA, E. P. & JIMÉNEZ, E. 2006. P2Y receptors activate MAPK/ERK through a pathway involving PI3K/PDK1/PKC-ζ in human vein endothelial cells. *Cellular Physiology and Biochemistry,* 18**,** 123-134.
MONTPAS, N., ST-ONGE, G., NAMA, N., RHAINDS, D., BENREDJEM, B., GIRARD, M., HICKSON, G., PONS, V. & HEVEKER, N. 2018. Ligand-specific conformational transitions and intracellular transport are required for atypical chemokine receptor 3–mediated chemokine scavenging. *Journal of Biological Chemistry,* 293**,** 893-905.
MORLEY, S., HAGER, M. H., POLLAN, S. G., KNUDSEN, B., DI VIZIO, D. & FREEMAN, M. R. 2014. Trading in your spindles for blebs: the amoeboid tumor cell phenotype in prostate cancer. *Asian journal of andrology,* 16**,** 530-535.
MOTEKAITIS, R. J., COX III, X., TAYLOR, P., MARTELL, A. E., MILES, B. & TVEDT JR, T. J. 1982. Thermal degradation of EDTA chelates in aqueous solution. *Canadian Journal of Chemistry,* 60**,** 1207-1213.
MUELLER, W., SCHÜTZ, D., NAGEL, F., SCHULZ, S. & STUMM, R. 2013. Hierarchical organization of multi-site phosphorylation at the CXCR4 C terminus. *PloS one,* 8**,** e64975.
MÜLLER, A., HOMEY, B., SOTO, H., GE, N., CATRON, D., BUCHANAN, M. E., MCCLANAHAN, T., MURPHY, E., YUAN, W., WAGNER, S. N., BARRERA, J., MOHAR, A., VERASTEGUI, E. & ZLOTNIK, A. 2001. Involvement of chemokine receptors in breast cancer metastasis. *Nature,* 410**,** 50-56.
MURDOCH, C. & FINN, A. 2000. Chemokine receptors and their role in inflammation and infectious diseases. *Blood,* 95**,** 3032-3043.
MURDOCH, C., MONK, P. & FINN, A. 1999. Functional expression of chemokine receptor CXCR4 on human epithelial cells. *Immunology,* 98**,** 36-41.
MURGA, C., FUKUHARA, S. & GUTKIND, J. S. 2000. A novel role for phosphatidylinositol 3-kinase β in signaling from G protein-coupled receptors to Akt. *Journal of Biological Chemistry,* 275**,** 12069-12073.
MURPHY, D. A. & COURTNEIDGE, S. A. 2011. The'ins' and'outs' of podosomes and invadopodia: characteristics, formation and function. *Nature reviews Molecular cell biology,* 12**,** 413-426.
MURPHY, J. W., CHO, Y., SACHPATZIDIS, A., FAN, C., HODSDON, M. E. & LOLIS, E. 2007. Structural and functional basis of CXCL12 (stromal cell-derived factor-1α) binding to heparin. *Journal of Biological Chemistry,* 282**,** 10018-10027.
MURPHY, P. M. 2019. 10 - Chemokines and Chemokine Receptors. *In:* ROBERT R. RICH, W. T. S., A. J. FREW, THOMAS A. FLEISHER, HARRY, W. SCHROEDER, CORNELIA M. WEYAND (ed.) *Clinical Immunology Principles and Practice.* 5th ed.: ELSEVIER.
NAGASAWA, T., HIROTA, S., TACHIBANA, K., TAKAKURA, N., NISHIKAWA, S.-I., KITAMURA, Y., YOSHIDA, N., KIKUTANI, H. & KISHIMOTO, T. 1996. Defects of B-cell lymphopoiesis and bone-marrow myelopoiesis in mice lacking the CXC chemokine PBSF/SDF-1. *Nature,* 382**,** 635-638.

NAGASAWA, T., KIKUTANI, H. & KISHIMOTO, T. 1994. Molecular cloning and structure of a pre-B-cell growth-stimulating factor. *Proceedings of the National Academy of Sciences,* 91**,** 2305-2309.

NAKAMURA, M., IWANAGA, S., HENMI, C., ARAI, K. & NISHIYAMA, Y. 2010. Biomatrices and biomaterials for future developments of bioprinting and biofabrication. *Biofabrication,* 2**,** 1-7.

NAMEN, A. E., SCHMIERER, A. E., MARCH, C. J., OVERELL, R. W., PARK, L. S., URDAL, D. L. & MOCHIZUKI, D. Y. 1988. B cell precursor growth-promoting activity. Purification and characterization of a growth factor active on lymphocyte precursors. *Journal of Experimental Medicine,* 167**,** 988-1002.

NAUMANN, U., CAMERONI, E., PRUENSTER, M., MAHABALESHWAR, H., RAZ, E., ZERWES, H.-G., ROT, A. & THELEN, M. 2010. CXCR7 functions as a scavenger for CXCL12 and CXCL11. *PloS one,* 5**,** e9175.

NEDOSZYTKO, B., SOKOŁOWSKA-WOJDYŁO, M., RUCKEMANN-DZIURDZIŃSKA, K., ROSZKIEWICZ, J. & NOWICKI, R. J. 2014. Chemokines and cytokines network in the pathogenesis of the inflammatory skin diseases: atopic dermatitis, psoriasis and skin mastocytosis. *Postepy Dermatologii Alergologii,* 31**,** 84-91.

NEPTUNE, E. R. & BOURNE, H. R. 1997. Receptors induce chemotaxis by releasing the βγ subunit of Gi, not by activating Gq or Gs. *Proceedings of the National Academy of Sciences,* 94**,** 14489-14494.

NEVES, M., FUMAGALLI, A., VAN DEN BOR, J., MARIN, P., SMIT, M. J. & MAYOR, F. 2019. The role of ACKR3 in breast, lung and brain cancer. *Molecular pharmacology,* 1.

NEWTON, A. C. 2009. Protein kinase C: poised to signal. *American Journal of Physiology-Endocrinology And Metabolism,* 298**,** 395-402.

NEWTON, A. C. 2018. Protein kinase C as a tumor suppressor. *Seminars in cancer biology,* 48**,** 18-26.

NGUYEN, A., YOSHIDA, M., GOODARZI, H. & TAVAZOIE, S. F. 2016. Highly variable cancer subpopulations that exhibit enhanced transcriptome variability and metastatic fitness. *Nature communications,* 7**,** 1-13.

NI, X., SUHAIL, M. M., YANG, Q., CAO, A., FUNG, K.-M., POSTIER, R. G., WOOLLEY, C., YOUNG, G., ZHANG, J. & LIN, H.-K. 2012. Frankincense essential oil prepared from hydrodistillation of Boswellia sacra gum resins induces human pancreatic cancer cell death in cultures and in a xenograft murine model. *BMC complementary and alternative medicine,* 12**,** 1-14.

NIMMAGADDA, S., PULLAMBHATLA, M., STONE, K., GREEN, G., BHUJWALLA, Z. M. & POMPER, M. G. 2010. Molecular imaging of CXCR4 receptor expression in human cancer xenografts with [64Cu] AMD3100 positron emission tomography. *Cancer research,* 70**,** 3935-3944.

NISHIKAWA, K., TOKER, A., JOHANNES, F.-J., SONGYANG, Z. & CANTLEY, L. C. 1997. Determination of the specific substrate sequence motifs of protein kinase C isozymes. *Journal of Biological Chemistry,* 272**,** 952-960.

NOMURA, W., TANABE, Y., TSUTSUMI, H., TANAKA, T., OHBA, K., YAMAMOTO, N. & TAMAMURA, H. 2008. Fluorophore labeling enables imaging and evaluation of specific CXCR4− ligand interaction at the cell membrane for fluorescence-based screening. *Bioconjugate chemistry,* 19**,** 1917-1920.

NUGOLI, M., CHUCHANA, P., VENDRELL, J., ORSETTI, B., URSULE, L., NGUYEN, C., BIRNBAUM, D., DOUZERY, E. J., COHEN, P. & THEILLET, C. 2003. Genetic variability in MCF-7 sublines: evidence of rapid genomic and RNA expression profile modifications. *BMC cancer,* 3.

O'CALLAGHAN, K., LEE, L., NGUYEN, N., HSIEH, M.-Y., KANEIDER, N. C., KLEIN, A. K., SPRAGUE, K., VAN ETTEN, R. A., KULIOPULOS, A. & COVIC, L. 2012. Targeting CXCR4 with cell-penetrating pepducins in lymphoma and lymphocytic leukemia. *Blood,* 119**,** 1717-1725.

OBERLIN, E., AMARA, A., BACHELERIE, F., BESSIA, C., VIRELIZIER, J.-L., ARENZANA-SEISDEDOS, F., SCHWARTZ, O., HEARD, J., CLARK-LEWIS, I., LEGLER, D. F., LOETSCHER, M., BAGGIOLINI, M. & MOSER, B. 1996. The CXC chemokine SDF-1 is the ligand for LESTR/fusin and prevents infection by T-cell-line-adapted HIV-1. *Nature,* 382**,** 833-835.

ÖDEMIS, V., BOOSMANN, K., HEINEN, A., KÜRY, P. & ENGELE, J. 2010. CXCR7 is an active component of SDF-1 signalling in astrocytes and Schwann cells. *Journal of cell science,* 123**,** 1081-1088.

OERTEL, M., GRANESS, A., THIM, L., BUHLING, F., KALBACHER, H. & HOFFMANN, W. 2001. Trefoil Factor Family–Peptides Promote Migration of Human Bronchial Epithelial Cells: Synergistic Effect with Epidermal Growth Factor. *American journal of respiratory cell and molecular biology,* 25**,** 418-424.

OFFERMANNS, S. & SCHULTZ, G. 1994. Complex information processing by the transmembrane signaling system involving G proteins. *Naunyn-Schmiedeberg's archives of pharmacology,* 350**,** 329-338.

OKUMURA, M., SAIKI, M., YAMAGUCHI, H. & HIDAKA, Y. 2011. Acceleration of disulfide-coupled protein folding using glutathione derivatives. *The FEBS journal,* 278**,** 1137-1144.

OLSON, M. F. & SAHAI, E. 2009. The actin cytoskeleton in cancer cell motility. *Clinical & experimental metastasis,* 26**,** 273-287.

OO, Y. H. & ADAMS, D. H. 2010. The role of chemokines in the recruitment of lymphocytes to the liver. *Journal of autoimmunity,* 34**,** 45-54.

OPPERMANN, M., MACK, M., PROUDFOOT, A. E. & OLBRICH, H. 1999. Differential effects of CC chemokines on CC chemokine receptor 5 (CCR5) phosphorylation and identification of phosphorylation sites on the CCR5 carboxyl terminus. *Journal of Biological Chemistry,* 274**,** 8875-8885.

OZAWA, S., KATO, Y., KOMORI, R., MAEHATA, Y., KUBOTA, E. & HATA, R.-I. 2006. BRAK/CXCL14 expression suppresses tumor growth in vivo in human oral carcinoma cells. *Biochemical and biophysical research communications,* 348**,** 406-412.

PALCZEWSKI, K., KUMASAKA, T., HORI, T., BEHNKE, C. A., MOTOSHIMA, H., FOX, B. A., LE TRONG, I., TELLER, D. C., OKADA, T., STENKAMP, R. E., YAMAMOTO, N. & MIYANO, M. 2000. Crystal structure of rhodopsin: AG protein-coupled receptor. *Science,* 289**,** 739-745.

PALLERIA, C., DI PAOLO, A., GIOFRÈ, C., CAGLIOTI, C., LEUZZI, G., SINISCALCHI, A., DE SARRO, G. & GALLELLI, L. 2013. Pharmacokinetic drug-drug interaction and their implication in clinical management. *Journal of research in medical sciences: the official journal of Isfahan University of Medical Sciences,* 18**,** 601-610.

PAŇKOVÁ, K., RÖSEL, D., NOVOTNÝ, M. & BRÁBEK, J. 2010. The molecular mechanisms of transition between mesenchymal and amoeboid

invasiveness in tumor cells. *Cellular and molecular life sciences,* 67**,** 63-71.
PARAMESWARAN, R., YU, M., LIM, M., GROFFEN, J. & HEISTERKAMP, N. 2011. Combination of drug therapy in acute lymphoblastic leukemia with a CXCR4 antagonist. *Leukemia,* 25**,** 1314-1323.
PAREDES, R. M., ETZLER, J. C., WATTS, L. T., ZHENG, W. & LECHLEITER, J. D. 2008. Chemical calcium indicators. *Methods,* 46**,** 143-151.
PARKER, L. C., WHYTE, M. K., VOGEL, S. N., DOWER, S. K. & SABROE, I. 2004. Toll-like receptor (TLR) 2 and TLR4 agonists regulate CCR expression in human monocytic cells. *The Journal of Immunology,* 172**,** 4977-4986.
PARRI, M. & CHIARUGI, P. 2010. Rac and Rho GTPases in cancer cell motility control. *Cell Communication and Signaling,* 8.
PASTUSZKA, M. K., OKAMOTO, C. T., HAMM-ALVAREZ, S. F. & MACKAY, J. A. 2014. Flipping the switch on clathrin-mediated endocytosis using thermally responsive protein microdomains. *Advanced functional materials,* 24**,** 5340-5347.
PAUL, C. D., MISTRIOTIS, P. & KONSTANTOPOULOS, K. 2017. Cancer cell motility: lessons from migration in confined spaces. *Nature Reviews Cancer,* 17**,** 131-140.
PAWIG, L., KLASEN, C., WEBER, C., BERNHAGEN, J. & NOELS, H. 2015. Diversity and inter-connections in the CXCR4 chemokine receptor/ligand family: molecular perspectives. *Frontiers in immunology,* 6.
PEASE, J. & HORUK, R. 2012. Chemokine receptor antagonists. *Journal of medicinal chemistry,* 55**,** 9363-9392.
PELED, A., WALD, O. & BURGER, J. 2012. Development of novel CXCR4-based therapeutics. *Expert opinion on investigational drugs,* 21**,** 341-353.
PENG, S.-B., ZHANG, X., PAUL, D., KAYS, L. M., YE, M., VAILLANCOURT, P., DOWLESS, M., STANCATO, L. F., STEWART, J., UHLIK, M. T., LONG, H., CHU, S. & OBUNGU, V. H. 2016. Inhibition of CXCR4 by LY2624587, a fully humanized anti-CXCR4 antibody induces apoptosis of hematologic malignancies. *PloS one,* 11**,** e0150585.
PERRY, S. J. & LEFKOWITZ, R. J. 2002. Arresting developments in heptahelical receptor signaling and regulation. *Trends in cell biology,* 12**,** 130-138.
PETER, S., MILLER, M. J., YASKO, A., YASZEMSKI, M. J. & MIKOS, A. 1998. Polymer concepts in tissue engineering. *Journal of biomedical materials research,* 43**,** 422-427.
PETERBURS, P., HEERING, J., LINK, G., PFIZENMAIER, K., OLAYIOYE, M. A. & HAUSSER, A. 2009. Protein kinase D regulates cell migration by direct phosphorylation of the cofilin phosphatase slingshot 1 like. *Cancer research,* 69**,** 5634-5638.
PETIT, I., GOICHBERG, P., SPIEGEL, A., PELED, A., BRODIE, C., SEGER, R., NAGLER, A., ALON, R. & LAPIDOT, T. 2005. Atypical PKC-ζ regulates SDF-1–mediated migration and development of human CD34+ progenitor cells. *The Journal of clinical investigation,* 115**,** 168-176.
PEVERI, P., WALZ, A., DEWALD, B. & BAGGIOLINI, M. 1988. A novel neutrophil-activating factor produced by human mononuclear phagocytes. *The Journal of experimental medicine,* 167**,** 1547-1559.
PHATTARATARATIP, E. & DHANUTHAI, K. 2017. Expression of CXC motif chemokine receptors 4 and 7 in salivary gland neoplasms. *Archives of Oral Biology,* 83**,** 136-144.

PIKE, L. J. 2003. Lipid rafts bringing order to chaos. *Journal of lipid research,* 44**,** 655-667.
PIOVAN, E., TOSELLO, V., AMADORI, A. & ZANOVELLO, P. 2018. Chemotactic cues for NOTCH1-dependent leukemia. *Frontiers in immunology,* 9.
POLLARD, T. D. & BORISY, G. G. 2003. Cellular motility driven by assembly and disassembly of actin filaments. *Cell,* 112**,** 453-465.
PORCILE, C., BAJETTO, A., BARBIERI, F., BARBERO, S., BONAVIA, R., BIGLIERI, M., PIRANI, P., FLORIO, T. & SCHETTINI, G. 2005. Stromal cell-derived factor-1α (SDF-1α/CXCL12) stimulates ovarian cancer cell growth through the EGF receptor transactivation. *Experimental cell research,* 308**,** 241-253.
PORTELLA, L., VITALE, R., DE LUCA, S., D'ALTERIO, C., IERANO, C., NAPOLITANO, M., RICCIO, A., POLIMENO, M. N., MONFREGOLA, L. & BARBIERI, A. 2013. Preclinical development of a novel class of CXCR4 antagonist impairing solid tumors growth and metastases. *PloS one,* 8**,** e74548.
POTTER, D. A., TIRNAUER, J. S., JANSSEN, R., CROALL, D. E., HUGHES, C. N., FIACCO, K. A., MIER, J. W., MAKI, M. & HERMAN, I. M. 1998. Calpain regulates actin remodeling during cell spreading. *The Journal of cell biology,* 141**,** 647-662.
PUNEET, P., MOOCHHALA, S. & BHATIA, M. 2005. Chemokines in acute respiratory distress syndrome. *American Journal of Physiology-Lung Cellular and Molecular Physiology,* 288**,** L3-L15.
QIN, L., KUFAREVA, I., HOLDEN, L. G., WANG, C., ZHENG, Y., ZHAO, C., FENALTI, G., WU, H., HAN, G. W., CHEREZOV, V., ABAGYAN, R., STEVENS, R. C. & HANDEL, T. M. 2015. Crystal structure of the chemokine receptor CXCR4 in complex with a viral chemokine. *Science,* 347**,** 1117-1122.
QIU, R.-G., ABO, A. & MARTIN, G. S. 2000. A human homolog of the C. elegans polarity determinant Par-6 links Rac and Cdc42 to PKCζ signaling and cell transformation. *Current biology,* 10**,** 697-707.
QUOYER, J., JANZ, J. M., LUO, J., REN, Y., ARMANDO, S., LUKASHOVA, V., BENOVIC, J. L., CARLSON, K. E., HUNT, S. W. & BOUVIER, M. 2013. Pepducin targeting the CXC chemokine receptor type 4 acts as a biased agonist favoring activation of the inhibitory G protein. *Proceedings of the National Academy of Sciences,* 110**,** E5088-E5097.
RAFTOPOULOU, M. & HALL, A. 2004. Cell migration: Rho GTPases lead the way. *Developmental biology,* 265**,** 23-32.
RAJAGOPAL, S., KIM, J., AHN, S., CRAIG, S., LAM, C. M., GERARD, N. P., GERARD, C. & LEFKOWITZ, R. J. 2010. β-arrestin-but not G protein-mediated signaling by the "decoy" receptor CXCR7. *Proceedings of the National Academy of Sciences,* 107**,** 628-632.
RAMAN, D., SOBOLIK-DELMAIRE, T. & RICHMOND, A. 2011. Chemokines in health and disease. *Experimental cell research,* 317**,** 575-589.
RAMSEY, D. M. & MCALPINE, S. R. 2013. Halting metastasis through CXCR4 inhibition. *Bioorganic & medicinal chemistry letters,* 23**,** 20-25.
RAO, S., WATKINS, D., CUNNINGHAM, D., DUNLOP, D., JOHNSON, P., SELBY, P., HANCOCK, B., FEGAN, C., CULLIGAN, D., SCHEY, S., MORRIS, T. C. M., LISSITCHKOV, T., OLIVER, J. W. & HOLMLUND, J. T. 2004. Phase II study of ISIS 3521, an antisense oligodeoxynucleotide to protein kinase C alpha, in patients with previously treated low-grade non-Hodgkin's lymphoma. *Annals of oncology,* 15**,** 1413-1418.

RAPPOPORT, J. Z., KEMAL, S., BENMERAH, A. & SIMON, S. M. 2006. Dynamics of clathrin and adaptor proteins during endocytosis. *American Journal of Physiology-Cell Physiology,* 291**,** C1072-C1081.
RATAJCZAK, M., ZUBA-SURMA, E., KUCIA, M., RECA, R., WOJAKOWSKI, W. & RATAJCZAK, J. 2006. The pleiotropic effects of the SDF-1–CXCR4 axis in organogenesis, regeneration and tumorigenesis. *Leukemia,* 20**,** 1915-1924.
RAWLINGS, J. S., ROSLER, K. M. & HARRISON, D. A. 2004. The JAK/STAT signaling pathway. *Journal of cell science,* 117**,** 1281-1283.
REBECCHI, M. J. & PENTYALA, S. N. 2000. Structure, function, and control of phosphoinositide-specific phospholipase C. *Physiological reviews,* 80**,** 1291-1335.
REBOLLO, J., GELIEBTER, J. & REYES, N. 2017. ESM-1 siRNA knockdown decreased migration and expression of CXCL3 in prostate cancer cells. *International journal of biomedical science: IJBS,* 13**,** 35-42.
REITER, E. & LEFKOWITZ, R. J. 2006. GRKs and β-arrestins: roles in receptor silencing, trafficking and signaling. *Trends in endocrinology & metabolism,* 17**,** 159-165.
RETTIG, M. P., ANSSTAS, G. & DIPERSIO, J. F. 2012. Mobilization of hematopoietic stem and progenitor cells using inhibitors of CXCR4 and VLA-4. *Leukemia,* 26**,** 34-53.
RIDLEY, A. J., SCHWARTZ, M. A., BURRIDGE, K., FIRTEL, R. A., GINSBERG, M. H., BORISY, G., PARSONS, J. T. & HORWITZ, A. R. 2003. Cell migration: integrating signals from front to back. *Science,* 302**,** 1704-1709.
RINGSTAD, N., GAD, H., LÖW, P., DI PAOLO, G., BRODIN, L., SHUPLIAKOV, O. & DE CAMILLI, P. 1999. Endophilin/SH3p4 is required for the transition from early to late stages in clathrin-mediated synaptic vesicle endocytosis. *Neuron,* 24**,** 143-154.
RODAL, S. K., SKRETTING, G., GARRED, Ø., VILHARDT, F., VAN DEURS, B. & SANDVIG, K. 1999. Extraction of cholesterol with methyl-β-cyclodextrin perturbs formation of clathrin-coated endocytic vesicles. *Molecular biology of the cell,* 10**,** 961-974.
ROMMEL, C., CAMPS, M. & JI, H. 2007. PI3Kδ and PI3Kγ: partners in crime in inflammation in rheumatoid arthritis and beyond? *Nature Reviews Immunology,* 7**,** 191-201.
ROSSI, D. & ZLOTNIK, A. 2000. The biology of chemokines and their receptors. *Annual review of immunology,* 18**,** 217-242.
ROT, A. 1992. Endothelial cell binding of NAP-1/IL-8: role in neutrophil emigration. *Immunology today,* 13**,** 291-294.
ROT, A. & VON ANDRIAN, U. H. 2004. Chemokines in innate and adaptive host defense: basic chemokinese grammar for immune cells. *Annual review of immunology,* 22**,** 891-928.
ROZENGURT, E. 2011. Protein kinase D signaling: multiple biological functions in health and disease. *Physiology,* 26**,** 23-33.
ROZENGURT, E., REY, O. & WALDRON, R. T. 2005. Protein kinase D signaling. *Journal of Biological Chemistry,* 280**,** 13205-13208.
ROZENGURT, E., SINNETT-SMITH, J., VAN LINT, J. & VALVERDE, A. M. 1995. Protein kinase D (PKD): a novel target for diacylglycerol and phorbol esters. *Mutation Research/Fundamental and Molecular Mechanisms of Mutagenesis,* 333**,** 153-160.
RUEDA, P., BALABANIAN, K., LAGANE, B., STAROPOLI, I., CHOW, K., LEVOYE, A., LAGURI, C., SADIR, R., DELAUNAY, T., IZQUIERDO, E.,

PABLOS, J. L., LENDINEZ, E., CARUZ, A., FRANCO, D., BALEAUX, F., LORTAT-JACOB, H. & ARENZANA-SEISDEDOS, F. 2008. The CXCL12γ chemokine displays unprecedented structural and functional properties that make it a paradigm of chemoattractant proteins. *PloS one,* 3**,** e2543.

RYKX, A., DE KIMPE, L., MIKHALAP, S., VANTUS, T., SEUFFERLEIN, T., VANDENHEEDE, J. R. & VAN LINT, J. 2003. Protein kinase D: a family affair. *FEBS letters,* 546**,** 81-86.

SAHAI, E. & MARSHALL, C. J. 2003. Differing modes of tumour cell invasion have distinct requirements for Rho/ROCK signalling and extracellular proteolysis. *Nature cell biology,* 5**,** 711-719.

SAINI, V., MARCHESE, A. & MAJETSCHAK, M. 2010. CXC chemokine receptor 4 is a cell surface receptor for extracellular ubiquitin. *Journal of Biological Chemistry,* 285**,** 15566-15576.

SALAZAR, N., CASTELLAN, M., SHIRODKAR, S. S. & LOKESHWAR, B. L. 2013. Chemokines and chemokine receptors as promoters of prostate cancer growth and progression. *Critical Reviews™ in Eukaryotic Gene Expression,* 23**,** 77-91.

SALAZAR, N., MUÑOZ, D., KALLIFATIDIS, G., SINGH, R. K., JORDÀ, M. & LOKESHWAR, B. L. 2014. The chemokine receptor CXCR7 interacts with EGFR to promote breast cancer cell proliferation. *Molecular cancer,* 13.

SALIC, A. & MITCHISON, T. J. 2008. A chemical method for fast and sensitive detection of DNA synthesis in vivo. *Proceedings of the National Academy of Sciences,* 105**,** 2415-2420.

SÁNCHEZ-MARTÍN, L., ESTECHA, A., SAMANIEGO, R., SÁNCHEZ-RAMÓN, S., VEGA, M. Á. & SÁNCHEZ-MATEOS, P. 2011. The chemokine CXCL12 regulates monocyte-macrophage differentiation and RUNX3 expression. *Blood,* 117**,** 88-97.

SANDERSON, M. J., SMITH, I., PARKER, I. & BOOTMAN, M. D. 2014. Fluorescence microscopy. *Cold Spring Harbor Protocols,* 2014.

SANTAGATA, S., NAPOLITANO, M., D'ALTERIO, C., DESICATO, S., DI MARO, S., MARINELLI, L., FRAGALE, A., BUONCERVELLO, M., PERSICO, F., GABRIELE, L., NOVELLINO, E., LONGO, N., PIGNATA, S., PERDONA, S. & SCALA, S. 2017. Targeting CXCR4 reverts the suppressive activity of T-regulatory cells in renal cancer. *Oncotarget,* 8**,** 77110-77120.

SANTIAGO, B., CALONGE, E., DEL REY, M. J., GUTIERREZ-CAÑAS, I., IZQUIERDO, E., USATEGUI, A., GALINDO, M., ALCAMÍ, J. & PABLOS, J. L. 2011. CXCL12 gene expression is upregulated by hypoxia and growth arrest but not by inflammatory cytokines in rheumatoid synovial fibroblasts. *Cytokine,* 53**,** 184-190.

SARVAIYA, P. J., GUO, D., ULASOV, I., GABIKIAN, P. & LESNIAK, M. S. 2013. Chemokines in tumor progression and metastasis. *Oncotarget,* 4**,** 2171-2185.

SAXENA, N. K., SHARMA, D., DING, X., LIN, S., MARRA, F., MERLIN, D. & ANANIA, F. A. 2007. Concomitant activation of the JAK/STAT, PI3K/AKT, and ERK signaling is involved in leptin-mediated promotion of invasion and migration of hepatocellular carcinoma cells. *Cancer research,* 67**,** 2497-2507.

SCHAERLI, P., WILLIMANN, K., EBERT, L. M., WALZ, A. & MOSER, B. 2005. Cutaneous CXCL14 targets blood precursors to epidermal niches for Langerhans cell differentiation. *Immunity,* 23**,** 331-342.

SCHIÖTH, H. B. & FREDRIKSSON, R. 2005. The GRAFS classification system of G-protein coupled receptors in comparative perspective. *General and comparative endocrinology,* 142**,** 94-101.
SCHOLTEN, D., CANALS, M., MAUSSANG, D., ROUMEN, L., SMIT, M., WIJTMANS, M., DE GRAAF, C., VISCHER, H. & LEURS, R. 2012. Pharmacological modulation of chemokine receptor function. *British journal of pharmacology,* 165**,** 1617-1643.
SCHWARZE, S. R., LUO, J., ISAACS, W. B. & JARRARD, D. F. 2005. Modulation of CXCL14 (BRAK) expression in prostate cancer. *The Prostate,* 64**,** 67-74.
SCOTTON, C. J., WILSON, J. L., MILLIKEN, D., STAMP, G. & BALKWILL, F. R. 2001. Epithelial cancer cell migration. *Cancer Research,* 61**,** 4961-4965.
SEIBERT, C., VELDKAMP, C. T., PETERSON, F. C., CHAIT, B. T., VOLKMAN, B. F. & SAKMAR, T. P. 2008. Sequential tyrosine sulfation of CXCR4 by tyrosylprotein sulfotransferases. *Biochemistry,* 47**,** 11251-11262.
SEIBERT, K., SHAFIE, S. M., TRICHE, T. J., WHANG-PENG, J. J., O'BRIEN, S. J., TONEY, J. H., HUFF, K. K. & LIPPMAN, M. E. 1983. Clonal variation of MCF-7 breast cancer cells in vitro and in athymic nude mice. *Cancer Research,* 43**,** 2223-2239.
SELBIE, L. A. & HILL, S. J. 1998. G protein-coupled-receptor cross-talk: the fine-tuning of multiple receptor-signalling pathways. *Trends in pharmacological sciences,* 19**,** 87-93.
SHARLOW, E. R., GIRIDHAR, K. V., LAVALLE, C. R., CHEN, J., LEIMGRUBER, S., BARRETT, R., BRAVO-ALTAMIRANO, K., WIPF, P., LAZO, J. S. & WANG, Q. J. 2008. Potent and selective disruption of protein kinase D functionality by a benzoxoloazepinolone. *Journal of Biological Chemistry,* 283**,** 33516-33526.
SHARMA, S. V., VAN LAER, K., MESSENS, J. & HAMILTON, C. J. 2016. Thiol Redox and pKa Properties of Mycothiol, the Predominant Low-Molecular-Weight Thiol Cofactor in the Actinomycetes. *ChemBioChem,* 17**,** 1689-1692.
SHELLENBERGER, T. D., WANG, M., GUJRATI, M., JAYAKUMAR, A., STRIETER, R. M., BURDICK, M. D., IOANNIDES, C. G., EFFERSON, C. L., EL-NAGGAR, A. K., ROBERTS, D., CLAYMAN, G. L. & FREDERICK, M. J. 2004. BRAK/CXCL14 is a potent inhibitor of angiogenesis and a chemotactic factor for immature dendritic cells. *Cancer research,* 64**,** 8262-8270.
SHENOY, S. K. & LEFKOWITZ, R. J. 2003. Multifaceted roles of β-arrestins in the regulation of seven-membrane-spanning receptor trafficking and signalling. *Biochemical Journal,* 375**,** 503-515.
SHIMIZU, N., SODA, Y., KANBE, K., LIU, H.-Y., MUKAI, R., KITAMURA, T. & HOSHINO, H. 2000. A putative G protein-coupled receptor, RDC1, is a novel coreceptor for human and simian immunodeficiency viruses. *Journal of virology,* 74**,** 619-626.
SHIROZU, M., NAKANO, T., INAZAWA, J., TASHIRO, K., TADA, H., SHINOHARA, T. & HONJO, T. 1995. Structure and chromosomal localization of the human stromal cell-derived factor 1 (SDF1) gene. *Genomics,* 28**,** 495-500.
SHUKLA, A. K., XIAO, K. & LEFKOWITZ, R. J. 2011. Emerging paradigms of β-arrestin-dependent seven transmembrane receptor signaling. *Trends in biochemical sciences,* 36**,** 457-469.

SHURIN, G. V., FERRIS, R., TOURKOVA, I. L., PEREZ, L., LOKSHIN, A., BALKIR, L., COLLINS, B., CHATTA, G. S. & SHURIN, M. R. 2005. Loss of new chemokine CXCL14 in tumor tissue is associated with low infiltration by dendritic cells (DC), while restoration of human CXCL14 expression in tumor cells causes attraction of DC both in vitro and in vivo. *The Journal of Immunology,* 174**,** 5490-5498.

SIERRA, M. D. L. L., YANG, F., NARAZAKI, M., SALVUCCI, O., DAVIS, D., YARCHOAN, R., ZHANG, H. H., FALES, H. & TOSATO, G. 2004. Differential processing of stromal-derived factor-1α and stromal-derived factor-1β explains functional diversity. *Blood,* 103**,** 2452-2459.

SIERRO, F., BIBEN, C., MARTÍNEZ-MUÑOZ, L., MELLADO, M., RANSOHOFF, R. M., LI, M., WOEHL, B., LEUNG, H., GROOM, J., BATTEN, M., HARVEY, R. P., MARTINEZ, C. R., MACKAY, C. R. & MACKAY, F. 2007. Disrupted cardiac development but normal hematopoiesis in mice deficient in the second CXCL12/SDF-1 receptor, CXCR7. *Proceedings of the National Academy of Sciences of the United States of America,* 104**,** 14759-14764.

SIGISMUND, S., ARGENZIO, E., TOSONI, D., CAVALLARO, E., POLO, S. & DI FIORE, P. P. 2008. Clathrin-mediated internalization is essential for sustained EGFR signaling but dispensable for degradation. *Developmental cell,* 15**,** 209-219.

SIMON, M. I., STRATHMANN, M. P. & GAUTAM, N. 1991. Diversity of G proteins in signal transduction. *Science,* 252**,** 802-808.

SIMONS, K. & SAMPAIO, J. L. 2011. Membrane organization and lipid rafts. *Cold Spring Harbor perspectives in biology,* 3.

SINGH, S., NANNURU, K., SADANANDAM, A., VARNEY, M. & SINGH, R. 2009. CXCR1 and CXCR2 enhances human melanoma tumourigenesis, growth and invasion. *British journal of cancer,* 100**,** 1638-1646.

SINGH, S., SINGH, U. P., GRIZZLE, W. E. & LILLARD, J. W. 2004. CXCL12–CXCR4 interactions modulate prostate cancer cell migration, metalloproteinase expression and invasion. *Laboratory investigation,* 84**,** 1666-1676.

SISON, E. A. R. & BROWN, P. 2011. The bone marrow microenvironment and leukemia: biology and therapeutic targeting. *Expert review of hematology,* 4**,** 271-283.

SIVAKUMAR, K., XIE, F., CASH, B. M., LONG, S., BARNHILL, H. N. & WANG, Q. 2004. A fluorogenic 1, 3-dipolar cycloaddition reaction of 3-azidocoumarins and acetylenes. *Organic letters,* 6**,** 4603-4606.

SLATER, S. J., SEIZ, J. L., COOK, A. C., BUZAS, C. J., MALINOWSKI, S. A., KERSHNER, J. L., STAGLIANO, B. A. & STUBBS, C. D. 2002. Regulation of PKCα activity by C1-C2 domain interactions. *Journal of Biological Chemistry,* 277**,** 15277-15285.

SLEEMAN, M. A., FRASER, J. K., MURISON, J. G., KELLY, S. L., PRESTIDGE, R. L., PALMER, D. J., WATSON, J. D. & KUMBLE, K. D. 2000. B cell-and monocyte-activating chemokine (BMAC), a novel non-ELR α-chemokine. *International immunology,* 12**,** 677-689.

SOBOLIK, T., SU, Y.-J., WELLS, S., AYERS, G. D., COOK, R. S. & RICHMOND, A. 2014. CXCR4 drives the metastatic phenotype in breast cancer through induction of CXCR2 and activation of MEK and PI3K pathways. *Molecular biology of the cell,* 25**,** 566-582.

SOHNI, A. & VERFAILLIE, C. M. 2013. Mesenchymal stem cells migration homing and tracking. *Stem cells international,* 2013.

SOHY, D., PARMENTIER, M. & SPRINGAEL, J.-Y. 2007. Allosteric transinhibition by specific antagonists in CCR2/CXCR4 heterodimers. *Journal of Biological Chemistry,* 282**,** 30062-30069.
SOSSEY-ALAOUI, K., SAFINA, A., LI, X., VAUGHAN, M. M., HICKS, D. G., BAKIN, A. V. & COWELL, J. K. 2007. Down-regulation of WAVE3, a metastasis promoter gene, inhibits invasion and metastasis of breast cancer cells. *The American journal of pathology,* 170**,** 2112-2121.
SPINARDI, L. & MARCHISIO, P. C. 2006. Podosomes as smart regulators of cellular adhesion. *European journal of cell biology,* 85**,** 191-194.
SPOO, A. C., LÜBBERT, M., WIERDA, W. G. & BURGER, J. A. 2007. CXCR4 is a prognostic marker in acute myelogenous leukemia. *Blood,* 109**,** 786-791.
SPRINGER, T. A. 1994. Traffic signals for lymphocyte recirculation and leukocyte emigration: the multistep paradigm. *Cell,* 76**,** 301-314.
SPRINGER, T. A. 1995. Traffic signals on endothelium for lymphocyte recirculation and leukocyte emigration. *Annual review of physiology,* 57**,** 827-872.
STACER, A. C., FENNER, J., CAVNAR, S. P., XIAO, A., ZHAO, S., CHANG, S. L., SALOMONNSON, A., LUKER, K. E. & LUKER, G. D. 2016. Endothelial CXCR7 regulates breast cancer metastasis. *Oncogene,* 35**,** 1716-1724.
STALLER, P., SULITKOVA, J., LISZTWAN, J., MOCH, H., OAKELEY, E. J. & KREK, W. 2003. Chemokine receptor CXCR4 downregulated by von Hippel–Lindau tumour suppressor pVHL. *Nature,* 425**,** 307-311.
STARNES, T., RASILA, K. K., ROBERTSON, M. J., BRAHMI, Z., DAHL, R., CHRISTOPHERSON, K. & HROMAS, R. 2006. The chemokine CXCL14 (BRAK) stimulates activated NK cell migration: implications for the downregulation of CXCL14 in malignancy. *Experimental hematology,* 34**,** 1101-1105.
STAUDT, N. D., AICHER, W. K., KALBACHER, H., STEVANOVIC, S., CARMONA, A. K., BOGYO, M. & KLEIN, G. 2010. Cathepsin X is secreted by human osteoblasts, digests CXCL-12 and impairs adhesion of hematopoietic stem and progenitor cells to osteoblasts. *haematologica,* 95**,** 1452-1460.
STEAGALL, R. J., DANIELS, C. R., DALAL, S., JOYNER, W. L., SINGH, M. & SINGH, K. 2014. Extracellular ubiquitin increases expression of angiogenic molecules and stimulates angiogenesis in cardiac microvascular endothelial cells. *Microcirculation,* 21**,** 324-332.
STEEN, A., LARSEN, O., THIELE, S. & ROSENKILDE, M. M. 2014. Biased and g protein-independent signaling of chemokine receptors. *Frontiers in immunology,* 5.
STEINBERG, S. F. 2008. Structural basis of protein kinase C isoform function. *Physiological reviews,* 88**,** 1341-1378.
STONE, M. J., HAYWARD, J. A., HUANG, C., E HUMA, Z. & SANCHEZ, J. 2017. Mechanisms of regulation of the chemokine-receptor network. *International journal of molecular sciences,* 18.
STORZ, P. & TOKER, A. 2003. Protein kinase D mediates a stress-induced NF-κB activation and survival pathway. *The EMBO journal,* 22**,** 109-120.
STRATHMANN, M. & SIMON, M. I. 1990. G protein diversity: a distinct class of alpha subunits is present in vertebrates and invertebrates. *Proceedings of the National Academy of Sciences,* 87**,** 9113-9117.

STRATHMANN, M. P. & SIMON, M. I. 1991. G alpha 12 and G alpha 13 subunits define a fourth class of G protein alpha subunits. *Proceedings of the National Academy of Sciences,* 88**,** 5582-5586.
STRIETER, R. M., POLVERINI, P. J., KUNKEL, S. L., ARENBERG, D. A., BURDICK, M. D., KASPER, J., DZUIBA, J., VAN DAMME, J., WALZ, A., MARRIOTT, D., CHAN, S.-Y., ROCZNIAK, S. & SHANAFELT, A. B. 1995. The functional role of the ELR motif in CXC chemokine-mediated angiogenesis. *Journal of Biological Chemistry,* 270**,** 27348-27357.
STRUYF, S., NOPPEN, S., LOOS, T., MORTIER, A., GOUWY, M., VERBEKE, H., HUSKENS, D., LUANGSAY, S., PARMENTIER, M., GEBOES, K., SCHOLS, D., VAN DAMME, J. & PROOST, P. 2009. Citrullination of CXCL12 differentially reduces CXCR4 and CXCR7 binding with loss of inflammatory and anti-HIV-1 activity via CXCR4. *The Journal of Immunology,* 182**,** 666-674.
STUMM, R. K., RUMMEL, J., JUNKER, V., CULMSEE, C., PFEIFFER, M., KRIEGLSTEIN, J., HÖLLT, V. & SCHULZ, S. 2002. A dual role for the SDF-1/CXCR4 chemokine receptor system in adult brain: isoform-selective regulation of SDF-1 expression modulates CXCR4-dependent neuronal plasticity and cerebral leukocyte recruitment after focal ischemia. *Journal of Neuroscience,* 22**,** 5865-5878.
STURANY, S., VAN LINT, J., MÜLLER, F., WILDA, M., HAMEISTER, H., HÖCKER, M., BREY, A., GERN, U., VANDENHEEDE, J., GRESS, T., ALDER, T. G. & SEUFFERLEIN, T. 2001. Molecular cloning and characterization of the human protein kinase D2 a novel member of the protein kinase D family of serine threonine kinases. *Journal of Biological Chemistry,* 276**,** 3310-3318.
SUBASH-BABU, P., ALSHAMMARI, G. M., IGNACIMUTHU, S. & ALSHATWI, A. A. 2017. Epoxy clerodane diterpene inhibits MCF-7 human breast cancer cell growth by regulating the expression of the functional apoptotic genes Cdkn2A, Rb1, mdm2 and p53. *Biomedicine & Pharmacotherapy,* 87**,** 388-396.
SUN, X., CHENG, G., HAO, M., ZHENG, J., ZHOU, X., ZHANG, J., TAICHMAN, R. S., PIENTA, K. J. & WANG, J. 2010. CXCL12/CXCR4/CXCR7 chemokine axis and cancer progression. *Cancer and Metastasis Reviews,* 29**,** 709-722.
SUZUKI, N., HAJICEK, N. & KOZASA, T. 2009. Regulation and physiological functions of G12/13-mediated signaling pathways. *Neurosignals,* 17**,** 55-70.
SZPAKOWSKA, M., MEYRATH, M., REYNDERS, N., COUNSON, M., HANSON, J., STEYAERT, J. & CHEVIGNÉ, A. 2018. Mutational analysis of the extracellular disulphide bridges of the atypical chemokine receptor ACKR3/CXCR7 uncovers multiple binding and activation modes for its chemokine and endogenous non-chemokine agonists. *Biochemical pharmacology,* 153**,** 299-309.
TAI, S., SUN, Y., SQUIRES, J. M., ZHANG, H., OH, W. K., LIANG, C. Z. & HUANG, J. 2011. PC3 is a cell line characteristic of prostatic small cell carcinoma. *The Prostate,* 71**,** 1668-1679.
TAICHMAN, R. S., COOPER, C., KELLER, E. T., PIENTA, K. J., TAICHMAN, N. S. & MCCAULEY, L. K. 2002. Use of the stromal cell-derived factor-1/CXCR4 pathway in prostate cancer metastasis to bone. *Cancer research,* 62**,** 1832-1837.
TALKENBERGER, K., CAVALCANTI-ADAM, E. A., VOSS-BÖHME, A. & DEUTSCH, A. 2017. Amoeboid-mesenchymal migration plasticity

promotes invasion only in complex heterogeneous microenvironments. *Scientific reports,* 7.
TAN, W., MARTIN, D. & GUTKIND, J. S. 2006. The Gα13-Rho signaling axis is required for SDF-1-induced migration through CXCR4. *Journal of Biological Chemistry,* 281**,** 39542-39549.
TANAKA, Y., GAVRIELIDES, M. V., MITSUUCHI, Y., FUJII, T. & KAZANIETZ, M. G. 2003. Protein kinase C promotes apoptosis in LNCaP prostate cancer cells through activation of p38 MAPK and inhibition of the Akt survival pathway. *Journal of Biological Chemistry,* 278**,** 33753-33762.
TANEGASHIMA, K., SUZUKI, K., NAKAYAMA, Y., TSUJI, K., SHIGENAGA, A., OTAKA, A. & HARA, T. 2013a. CXCL14 is a natural inhibitor of the CXCL12–CXCR4 signaling axis. *FEBS letters,* 587**,** 1731-1735.
TANEGASHIMA, K., TSUJI, K., SUZUKI, K., SHIGENAGA, A., OTAKA, A. & HARA, T. 2013b. Dimeric peptides of the C-terminal region of CXCL14 function as CXCL12 inhibitors. *FEBS letters,* 587**,** 3770-3775.
TARNOWSKI, M., LIU, R., WYSOCZYNSKI, M., RATAJCZAK, J., KUCIA, M. & RATAJCZAK, M. Z. 2010. CXCR7: a new SDF-1-binding receptor in contrast to normal CD34+ progenitors is functional and is expressed at higher level in human malignant hematopoietic cells. *European journal of haematology,* 85**,** 472-483.
TASHIRO, K., TADA, H., HEIKER, R., SHIROZU, M., NAKANO, T. & HONJO, T. 1993. Signal sequence trap: a cloning strategy for secreted proteins and type I membrane proteins. *Science,* 261**,** 600-604.
TEICHER, B. A. & FRICKER, S. P. 2010. CXCL12 (SDF-1)/CXCR4 pathway in cancer. *Clinical cancer research,* 16**,** 2927-2931.
THAM, T. N., LAZARINI, F., FRANCESCHINI, I. A., LACHAPELLE, F., AMARA, A. & DUBOIS-DALCQ, M. 2001. Developmental pattern of expression of the alpha chemokine stromal cell-derived factor 1 in the rat central nervous system. *European Journal of Neuroscience,* 13**,** 845-856.
THERMOFISHERSCIENTIFIC. 2018. *Fura-2, AM, cell permeant* [Online]. [Accessed].
THIERY, J. P. & SLEEMAN, J. P. 2006. Complex networks orchestrate epithelial–mesenchymal transitions. *Nature reviews Molecular cell biology,* 7**,** 131-142.
THOBE, M. N., CLARK, R. J., BAINER, R. O., PRASAD, S. M. & RINKER-SCHAEFFER, C. W. 2011. From prostate to bone: key players in prostate cancer bone metastasis. *Cancers,* 3**,** 478-493.
THURET, G., CHIQUET, C., HERRAG, S., DUMOLLARD, J., BOUDARD, D., BEDNARZ, J., CAMPOS, L. & GAIN, P. 2003. Mechanisms of staurosporine induced apoptosis in a human corneal endothelial cell line. *British Journal of Ophthalmology,* 87**,** 346-352.
TITUS, M. A. & GOODSON, H. V. 2017. An evolutionary perspective on cell migration: Digging for the roots of amoeboid motility. *The Journal of cell biology,* 216**,** 1509-1511.
TOULLEC, D., PIANETTI, P., COSTE, H., BELLEVERGUE, P., GRAND-PERRET, T., AJAKANE, M., BAUDET, V., BOISSIN, P., BOURSIER, E. & LORIOLLE, F. 1991. The bisindolylmaleimide GF 109203X is a potent and selective inhibitor of protein kinase C. *Journal of Biological Chemistry,* 266**,** 15771-15781.
TOURDOT, R. & RADHAKRISHNAN, R. 2013. Clathrin Mediated Endocytosis and its Role in Viral Entry. *Atlas of Genetics and Cytogenetics in Oncology and Haematology*.

TRENDOWSKI, M. 2015. The inherent metastasis of leukaemia and its exploitation by sonodynamic therapy. *Critical reviews in oncology/hematology,* 94**,** 149-163.
ULVMAR, M. H., HUB, E. & ROT, A. 2011. Atypical chemokine receptors. *Experimental cell research,* 317**,** 556-568.
URANO, D., CHEN, J.-G., BOTELLA, J. R. & JONES, A. M. 2013. Heterotrimeric G protein signalling in the plant kingdom. *Open biology,* 3.
UY, G., RETTIG, M., STONE, R., KONOPLEVA, M., ANDREEFF, M., MCFARLAND, K., SHANNON, W., FLETCHER, T., REINECK, T., EADES, W., STOCKERL-GOLDSTEIN, K., ABBOUD, C., JACOBY, M., WESTERVELT, P. & DIPERSIO, J. F. 2017. A phase 1/2 study of chemosensitization with plerixafor plus G-CSF in relapsed or refractory acute myeloid leukemia. *Blood cancer journal,* 7.
VALVERDE, A. M., SINNETT-SMITH, J., VAN LINT, J. & ROZENGURT, E. 1994. Molecular cloning and characterization of protein kinase D: a target for diacylglycerol and phorbol esters with a distinctive catalytic domain. *Proceedings of the National Academy of Sciences,* 91**,** 8572-8576.
VAN DEN BERG, N. S., BUCKLE, T., KUIL, J., WESSELING, J. & VAN LEEUWEN, F. W. 2011. Immunohistochemical Detection of the CXCR4 Expression in Tumour Tissue Using the Flourescent Peptide Antagonist Ac-TZ14011-FITC. *Translational Oncology,* 4**,** 234-240.
VAN HAASTERT, P. J., KEIZER-GUNNINK, I. & KORTHOLT, A. 2018. The cytoskeleton regulates symmetry transitions in moving amoeboid cells. *The Journal of cell science,* 131.
VAN HOUT, A., D'HUYS, T., OEYEN, M., SCHOLS, D. & VAN LOY, T. 2017. Comparison of cell-based assays for the identification and evaluation of competitive CXCR4 inhibitors. *PloS one,* 12**,** e0176057.
VATER, A., SAHLMANN, J., KRÖGER, N., ZÖLLNER, S., LIOZNOV, M., MAASCH, C., BUCHNER, K., VOSSMEYER, D., SCHWOEBEL, F., PURSCHKE, W., VONHOFF, S., KRUSCHINSKI, A., HUBEL, K., HUMPHREY, M., KLUSSMANN, S. & FLIEGERT, F. 2013. Hematopoietic stem and progenitor cell mobilization in mice and humans by a first-in-class mirror-image oligonucleotide inhibitor of CXCL12. *Clin Pharmacol Ther,* 94**,** 150-157.
VAUPEL, P. 2008. Hypoxia and aggressive tumor phenotype: implications for therapy and prognosis. *The oncologist,* 13**,** 21-26.
VELA, M., ARIS, M., LLORENTE, M., GARCIA-SANZ, J. A. & KREMER, L. 2015. Chemokine receptor-specific antibodies in cancer immunotherapy: achievements and challenges. *Frontiers in immunology,* 6.
VELDKAMP, C. T., SEIBERT, C., PETERSON, F. C., NORBERTO, B., HAUGNER, J. C., BASNET, H., SAKMAR, T. P. & VOLKMAN, B. F. 2008. Structural basis of CXCR4 sulfotyrosine recognition by the chemokine SDF-1/CXCL12. *Science Signalling,* 1.
VIADANA, E., BROSS, I. & PICKREN, J. 1978. An autopsy study of the metastatic patterns of human leukemias. *Oncology,* 35**,** 87-96.
VILA-CORO, A. J., RODRÍGUEZ-FRADE, J. M., DE ANA, A. M., MORENO-ORTÍZ, M. C., MARTÍNEZ-A, C. & MELLADO, M. 1999. The chemokine SDF-1α triggers CXCR4 receptor dimerization and activates the JAK/STAT pathway. *The FASEB Journal,* 13**,** 1699-1710.
VILLALONA-CALERO, M. A., RITCH, P., FIGUEROA, J. A., OTTERSON, G. A., BELT, R., DOW, E., GEORGE, S., LEONARDO, J., MCCACHREN, S., MILLER, G. L., MODIANO, M., VALDIVESO, M., GEARY, R. S., OLIVER, J. W. & HOLMLUND, J. T. 2004. A Phase I/II study of

LY900003, an antisense inhibitor of protein kinase C-α, in combination with cisplatin and gemcitabine in patients with advanced non–small cell lung cancer. *Clinical Cancer Research,* 10**,** 6086-6093.
VILLAR, J., ARENAS, M. I., MACCARTHY, C. M., BLÁNQUEZ, M. J., TIRADO, O. M. & NOTARIO, V. 2007. PCPH/ENTPD5 Expression Enhances the Invasiveness of Human Prostate Cancer Cells by a Protein Kinase Cδ–Dependent Mechanism. *Cancer research,* 67**,** 10859-10868.
VOLPE, S., CAMERONI, E., MOEPPS, B., THELEN, S., APUZZO, T. & THELEN, M. 2012. CCR2 acts as scavenger for CCL2 during monocyte chemotaxis. *PloS one,* 7**,** e37208.
VON ZASTROW, M. & WILLIAMS, J. T. 2012. Modulating neuromodulation by receptor membrane traffic in the endocytic pathway. *Neuron,* 76**,** 22-32.
WALD, O., SHAPIRA, O. M. & IZHAR, U. 2013. CXCR4/CXCL12 axis in non small cell lung cancer (NSCLC) pathologic roles and therapeutic potential. *Theranostics,* 3**,** 26-33.
WALDRON, R. T. & ROZENGURT, E. 2000. Oxidative stress induces protein kinase D activation in intact cells involvement of Src and dependence on protein kinase C. *Journal of Biological Chemistry,* 275**,** 17114-17121.
WALENKAMP, A. M., LAPA, C., HERRMANN, K. & WESTER, H.-J. 2017. CXCR4 ligands: the next big hit? *Journal of Nuclear Medicine,* 58**,** 77S-82S.
WANG, C., XIE, F., SUTHIWANGCHAROEN, N., SUN, J. & WANG, Q. 2012. Tuning the optical properties of BODIPY dye through Cu (I) catalyzed azide-alkyne cycloaddition (CuAAC) reaction. *Science China Chemistry,* 55**,** 125-130.
WANG, J.-F., PARK, I.-W. & GROOPMAN, J. E. 2000. Stromal cell-derived factor-1α stimulates tyrosine phosphorylation of multiple focal adhesion proteins and induces migration of hematopoietic progenitor cells: roles of phosphoinositide-3 kinase and protein kinase C. *Blood,* 95**,** 2505-2513.
WANG, J., SHIOZAWA, Y., WANG, J., WANG, Y., JUNG, Y., PIENTA, K. J., MEHRA, R., LOBERG, R. & TAICHMAN, R. S. 2008. The role of CXCR7/RDC1 as a chemokine receptor for CXCL12/SDF-1 in prostate cancer. *Journal of Biological Chemistry,* 283**,** 4283-4294.
WANG, Y., XIE, Y. & OUPICKÝ, D. 2016. Potential of CXCR4/CXCL12 chemokine axis in cancer drug delivery. *Current pharmacology reports,* 2**,** 1-10.
WATANABE, K., PENFOLD, M. E., MATSUDA, A., OHYANAGI, N., KANEKO, K., MIYABE, Y., MATSUMOTO, K., SCHALL, T. J., MIYASAKA, N. & NANKI, T. 2010. Pathogenic role of CXCR7 in rheumatoid arthritis. *Arthritis & Rheumatism,* 62**,** 3211-3220.
WATTS, A., VAN LIPZIG, M., JAEGER, W., SEEBER, R., VAN ZWAM, M., VINET, J., VAN DER LEE, M., SIDERIUS, M., ZAMAN, G. & BODDEKE, H. 2013. Identification and profiling of CXCR3–CXCR4 chemokine receptor heteromer complexes. *British journal of pharmacology,* 168**,** 1662-1674.
WEAVER, A. M. 2006. Invadopodia: specialized cell structures for cancer invasion. *Clinical & experimental metastasis,* 23**,** 97-105.
WEIDT, C., NIGGEMANN, B., KASENDA, B., DRELL, T. L., ZANKER, K. S. & DITTMAR, T. 2007. Stem cell migration: a quintessential stepping stone to successful therapy. *Current stem cell research & therapy,* 2**,** 89-103.
WEIGEL, P. & OKA, J. 1981. Temperature dependence of endocytosis mediated by the asialoglycoprotein receptor in isolated rat hepatocytes.

Evidence for two potentially rate-limiting steps. *Journal of Biological Chemistry,* 256**,** 2615-2617.
WENTE, M. N., MAYER, C., GAIDA, M. M., MICHALSKI, C. W., GIESE, T., BERGMANN, F., GIESE, N. A., BÜCHLER, M. W. & FRIESS, H. 2008. CXCL14 expression and potential function in pancreatic cancer. *Cancer letters,* 259**,** 209-217.
WESCOTT, M. P., KUFAREVA, I., PAES, C., GOODMAN, J. R., THAKER, Y., PUFFER, B. A., BERDOUGO, E., RUCKER, J. B., HANDEL, T. M. & DORANZ, B. J. 2016. Signal transmission through the CXC chemokine receptor 4 (CXCR4) transmembrane helices. *Proceedings of the National Academy of Sciences,* 113**,** 9928-9933.
WIGGINS, H. L. & RAPPOPORT, J. Z. 2010. An agarose spot assay for chemotactic invasion. *Biotechniques,* 48**,** 121-124.
WOLF, K., MAZO, I., LEUNG, H., ENGELKE, K., VON ANDRIAN, U. H., DERYUGINA, E. I., STRONGIN, A. Y., BRÖCKER, E.-B. & FRIEDL, P. 2003. Compensation mechanism in tumor cell migration. *The Journal of cell biology,* 160**,** 267-277.
WOLF, K., WU, Y. I., LIU, Y., GEIGER, J., TAM, E., OVERALL, C., STACK, M. S. & FRIEDL, P. 2007. Multi-step pericellular proteolysis controls the transition from individual to collective cancer cell invasion. *Nature cell biology,* 9**,** 893-904.
WOLF, S. & GRÜNEWALD, S. 2015. Sequence, structure and ligand binding evolution of rhodopsin-like G protein-coupled receptors: a crystal structure-based phylogenetic analysis. *PloS one,* 10.
WONG, D., KANDAGATLA, P., KORZ, W. & CHINNI, S. R. 2014. Targeting CXCR4 with CTCE-9908 inhibits prostate tumor metastasis. *BMC urology,* 14.
WONG, M., XIN, W. & DUMAN, R. 1996. Rat LCR1: cloning and cellular distribution of a putative chemokine receptor in brain. *Molecular psychiatry,* 1**,** 133-140.
WU, B., CHIEN, E. Y., MOL, C. D., FENALTI, G., LIU, W., KATRITCH, V., ABAGYAN, R., BROOUN, A., WELLS, P., BI, F. C., HAMEL, D. J., KUHN, P., HANDEL, T. M., CHEREZOV, V. & STEVENS, R. C. 2010. Structures of the CXCR4 chemokine GPCR with small-molecule and cyclic peptide antagonists. *Science,* 330**,** 1066-1071.
WU, D., FOREMAN, T. L., GREGORY, C. W., MCJILTON, M. A., WESCOTT, G. G., FORD, O. H., ALVEY, R. F., MOHLER, J. L. & TERRIAN, D. M. 2002. Protein kinase Cε has the potential to advance the recurrence of human prostate cancer. *Cancer research,* 62**,** 2423-2429.
XIANG, H., MU, Y., HU, C. & LUO, X. 2017a. Biocompatibility and Toxicity of Polylactic Acid/Ferrosoferric Oxide Nanomagnetic Microsphere. *Journal of Nanomaterials,* 2017.
XIANG, Z., ZHOU, Z., XIA, G., ZHANG, X., WEI, Z., ZHU, J., YU, J., CHEN, W., HE, Y., SCHWARZ, R., BREKKEN, R. A., AWASTHI, N. & ZHANG, C. 2017b. A positive crosstalk between CXCR4 and CXCR2 promotes gastric cancer metastasis. *Oncogene,* 36**,** 5122-5133.
XIAO, X., NORWOOD, D., FENG, Y.-R., MORIUCHI, M., JONES-TROWER, A., STANTCHEV, T. S., MORIUCHI, H., BRODER, C. C. & DIMITROV, D. S. 2000. Inefficient Formation of a Complex among CXCR4, CD4 and gp120 in U937 Clones Resistant to X4 gp120–gp41-Mediated Fusion. *Experimental and molecular pathology,* 68**,** 139-146.
XU, J., WANG, F., VAN KEYMEULEN, A., HERZMARK, P., STRAIGHT, A., KELLY, K., TAKUWA, Y., SUGIMOTO, N., MITCHISON, T. & BOURNE,

H. R. 2003. Divergent signals and cytoskeletal assemblies regulate self-organizing polarity in neutrophils. *Cell,* 114**,** 201-214.
XU, Y., LIU, S., XIA, J., STEIN, S., RAMON, C., XI, H., WANG, L., XIONG, X., ZHANG, L., HE, D., YANG, W., ZHAO, X., CHENG, X., YANG, X. & WANG, H. 2017. Endocytosis and membrane receptor internalization: Implication of F-BAR protein carom. *Frontiers in bioscience (Landmark edition),* 22**,** 1439-1457.
YAGI, H., TAN, W., DILLENBURG-PILLA, P., ARMANDO, S., AMORNPHIMOLTHAM, P., SIMAAN, M., WEIGERT, R., MOLINOLO, A. A., BOUVIER, M. & GUTKIND, J. S. 2011. A synthetic biology approach reveals a CXCR4-G13-Rho signaling axis driving transendothelial migration of metastatic breast cancer cells. *Science Signalling,* 4.
YAMAMOTO, Y., IBUSUKI, M., OKUMURA, Y., KAWASOE, T., KAI, K., IYAMA, K. & IWASE, H. 2008. Hypoxia-inducible factor 1α is closely linked to an aggressive phenotype in breast cancer. *Breast cancer research and treatment,* 110**,** 465-475.
YANG, Y., ZHANG, Q., GAO, M., YANG, X., HUANG, Z. & AN, J. 2014. A novel CXCR4-selective high-affinity fluorescent probe and its application in competitive binding assays. *Biochemistry,* 53**,** 4881-4883.
YI, M. C. & KHOSLA, C. 2016. Thiol–Disulfide exchange reactions in the mammalian extracellular environment. *Annual review of chemical and biomolecular engineering,* 7**,** 197-222.
YILMAZ, M. & CHRISTOFORI, G. 2010. Mechanisms of motility in metastasizing cells. *Molecular Cancer Research,* 8**,** 629-642.
YOKOTA, J. 2000. Tumor progression and metastasis. *Carcinogenesis,* 21**,** 497-503.
YOSHIDA, R., NAGIRA, M., KITAURA, M., IMAGAWA, N., IMAI, T. & YOSHIE, O. 1998. Secondary lymphoid-tissue chemokine is a functional ligand for the CC chemokine receptor CCR7. *Journal of Biological Chemistry,* 273**,** 7118-7122.
YU, L., CECIL, J., PENG, S.-B., SCHREMENTI, J., KOVACEVIC, S., PAUL, D., SU, E. W. & WANG, J. 2006. Identification and expression of novel isoforms of human stromal cell-derived factor 1. *Gene,* 374**,** 174-179.
YU, L., YU, L., PHAM, Q. & WANG, T. T. 2018. Transcriptional and translational-uncoupling in regulation of the CXCL12 and its receptors CXCR4, 7 in THP-1 monocytes and macrophages. *Immunity, inflammation and disease,* 6**,** 106-116.
YUN, H.-J. & JO, D.-Y. 2003. Production of stromal cell-derived factor-1 (SDF-1) and expression of CXCR4 in human bone marrow endothelial cells. *Journal of Korean medical science,* 18**,** 679-685.
YUNIARTI, L., MUSTOFA, M., ARYANDONO, T. & HARYANA, S. M. 2018. Synergistic Action of 1, 2-Epoxy-3 (3-(3, 4-dimethoxyphenyl)-4H-1-benzopiyran-4-on) Propane with Doxorubicin and Cisplatin through Increasing of p53, TIMP-3, and MicroRNA-34a in Cervical Cancer Cell Line (HeLa). *Asian Pacific journal of cancer prevention: APJCP,* 19**,** 2955-2962.
ZABEL, B. A., LEWÉN, S., BERAHOVICH, R. D., JAÉN, J. C. & SCHALL, T. J. 2011. The novel chemokine receptor CXCR7 regulates trans-endothelial migration of cancer cells. *Molecular cancer,* 10.
ZABEL, B. A., WANG, Y., LEWÉN, S., BERAHOVICH, R. D., PENFOLD, M. E., ZHANG, P., POWERS, J., SUMMERS, B. C., MIAO, Z., ZHAO, B., JALILI, A., JANOWSKA-WIECZOREK, A., JAEN, J. C. & SCHALL, T. J. 2009. Elucidation of CXCR7-mediated signaling events and inhibition of

CXCR4-mediated tumor cell transendothelial migration by CXCR7 ligands. *The Journal of Immunology,* 183**,** 3204-3211.
ZANG, Y. C., SAMANTA, A. K., HALDER, J. B., HONG, J., TEJADA-SIMON, M. V., RIVERA, V. M. & ZHANG, J. Z. 2000. Aberrant T cell migration toward RANTES and MIP-1α in patients with multiple sclerosis: overexpression of chemokine receptor CCR5. *Brain,* 123**,** 1874-1882.
ZHANG, A., HITOMI, M., BAR-SHAIN, N., DALIMOV, Z., ELLIS, L., VELPULA, K. K., FRAIZER, G. C., GOURDIE, R. G. & LATHIA, J. D. 2015a. Connexin 43 expression is associated with increased malignancy in prostate cancer cell lines and functions to promote migration. *Oncotarget,* 6**,** 11640-11651.
ZHANG, C., LI, J., HAN, Y. & JIANG, J. 2015b. A meta-analysis for CXCR4 as a prognostic marker and potential drug target in non-small cell lung cancer. *Drug design, development and therapy,* 9**,** 3267-3278.
ZHANG, G., PANIGRAHY, D., MAHAKIAN, L. M., YANG, J., LIU, J.-Y., LEE, K. S. S., WETTERSTEN, H. I., ULU, A., HU, X., TAM, S., HWANG, S. H., INGHAM, E. S., KIERAN, M. W., WEISS, R. H., FERRARA, K. W. & HAMMOCK, B. D. 2013. Epoxy metabolites of docosahexaenoic acid (DHA) inhibit angiogenesis, tumor growth, and metastasis. *Proceedings of the National Academy of Sciences,* 110**,** 6530-6535.
ZHANG, X. D., GILLESPIE, S. K. & HERSEY, P. 2004. Staurosporine induces apoptosis of melanoma by both caspase-dependent and-independent apoptotic pathways. *Molecular cancer therapeutics,* 3**,** 187-197.
ZHANG, Z., NI, C., CHEN, W., WU, P., WANG, Z., YIN, J., HUANG, J. & QIU, F. 2014. Expression of CXCR4 and breast cancer prognosis: a systematic review and meta-analysis. *BMC cancer,* 14.
ZHOU, N., LUO, Z., LUO, J., LIU, D., HALL, J. W., POMERANTZ, R. J. & HUANG, Z. 2001. Structural and functional characterization of human CXCR4 as a chemokine receptor and HIV-1 co-receptor by mutagenesis and molecular modeling studies. *Journal of Biological Chemistry,* 276**,** 42826-42833.
ZHUGE, Y. & XU, J. 2001. Rac1 mediates type I collagen-dependent MMP-2 activation role in cell invasion across collagen barrier. *Journal of Biological Chemistry,* 276**,** 16248-16256.
ZHUKOVSKY, M. A., BASMACIOGULLARI, S., PACHECO, B., WANG, L., MADANI, N., HAIM, H. & SODROSKI, J. 2010. Thermal stability of the human immunodeficiency virus type 1 (HIV-1) receptors, CD4 and CXCR4, reconstituted in proteoliposomes. *PloS one,* 5**,** e13249.
ZLOTNIK, A. & YOSHIE, O. 2000. Chemokines: a new classification system and their role in immunity. *Immunity,* 12**,** 121-127.
ZOPF, D. A., HOLLISTER, S. J., NELSON, M. E., OHYE, R. G. & GREEN, G. E. 2013. Bioresorbable airway splint created with a three-dimensional printer. *The New England Journal of Medicine,* 368**,** 2043-2045.
ZOU, Y.-R., KOTTMANN, A. H., KURODA, M., TANIUCHI, I. & LITTMAN, D. R. 1998. Function of the chemokine receptor CXCR4 in haematopoiesis and in cerebellar development. *Nature,* 393**,** 595-599.
ZOU, Z., ZENG, F., XU, W., WANG, C., KE, Z., WANG, Q. J. & DENG, F. 2012. PKD2 and PKD3 promote prostate cancer cell invasion by modulating NF-κB-and HDAC1-mediated expression and activation of uPA. *Journal of cell science,* 125**,** 4800-4811.
ZOUGHLAMI, Y., VOERMANS, C., BRUSSEN, K., VAN DORT, K. A., KOOTSTRA, N. A., MAUSSANG, D., SMIT, M. J., HORDIJK, P. L. & VAN HENNIK, P. B. 2012. Regulation of CXCR4 conformation by the

small GTPase Rac1: implications for HIV infection. *Blood,* 119**,** 2024-2032.

ZUGAZA, J. L., SINNETT-SMITH, J., VAN LINT, J. & ROZENGURT, E. 1996. Protein kinase D (PKD) activation in intact cells through a protein kinase C-dependent signal transduction pathway. *The EMBO journal,* 15**,** 6220-6230.

ZUNDER, E. R., KNIGHT, Z. A., HOUSEMAN, B. T., APSEL, B. & SHOKAT, K. M. 2008. Discovery of drug-resistant and drug-sensitizing mutations in the oncogenic PI3K isoform p110α. *Cancer cell,* 14**,** 180-192.

## Appendix 1

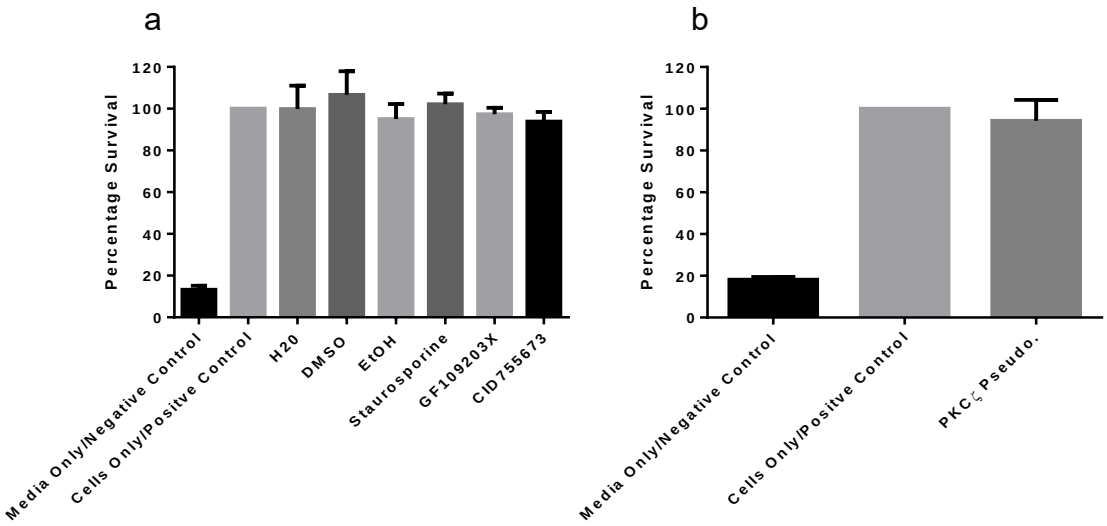


**Figure A1: PKC and PKD small molecule inhibitors were not toxic in PC3 prostate cancer cells. a)** PC3 cells were incubated with 10 nM Staurosporine, 5 μM GF109203X and 11 μM CID755673 along with the equivalent concentrations of their vehicles for 72 hours and percentage survival was subsequently calculated. **b)** PC3 cells were incubated with 10 μM PKCζ Pseudosubstrate inhibitor for 72 hours and percentage survival was subsequently calculated. Data representative of the mean ± SEM of 3 independent experiments.

## Appendix 2

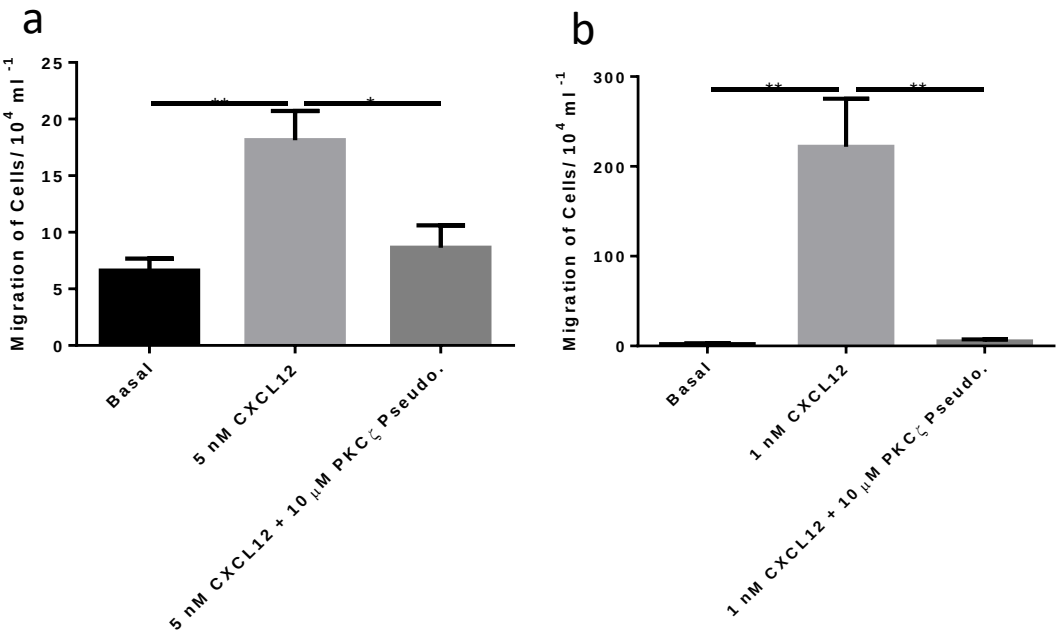


**Figure A2: PKCζ prevents CXCL12 stimulated migration in both THP-1 and Jurkat leukemic cell lines in chemotaxis assays. a)** THP-1 cells stimulated with 5 nM CXCL12 with and without 10 μM PKCζ Pseudosubstrate inhibitor. **b)** Jurkat cells stimulated with 1 nM CXCL12 with and without 10 μM PKCζ Pseudosubstrate inhibitor. Data representative of the mean ± SEM of 3 or 4 independent experiments.

## Appendix 3

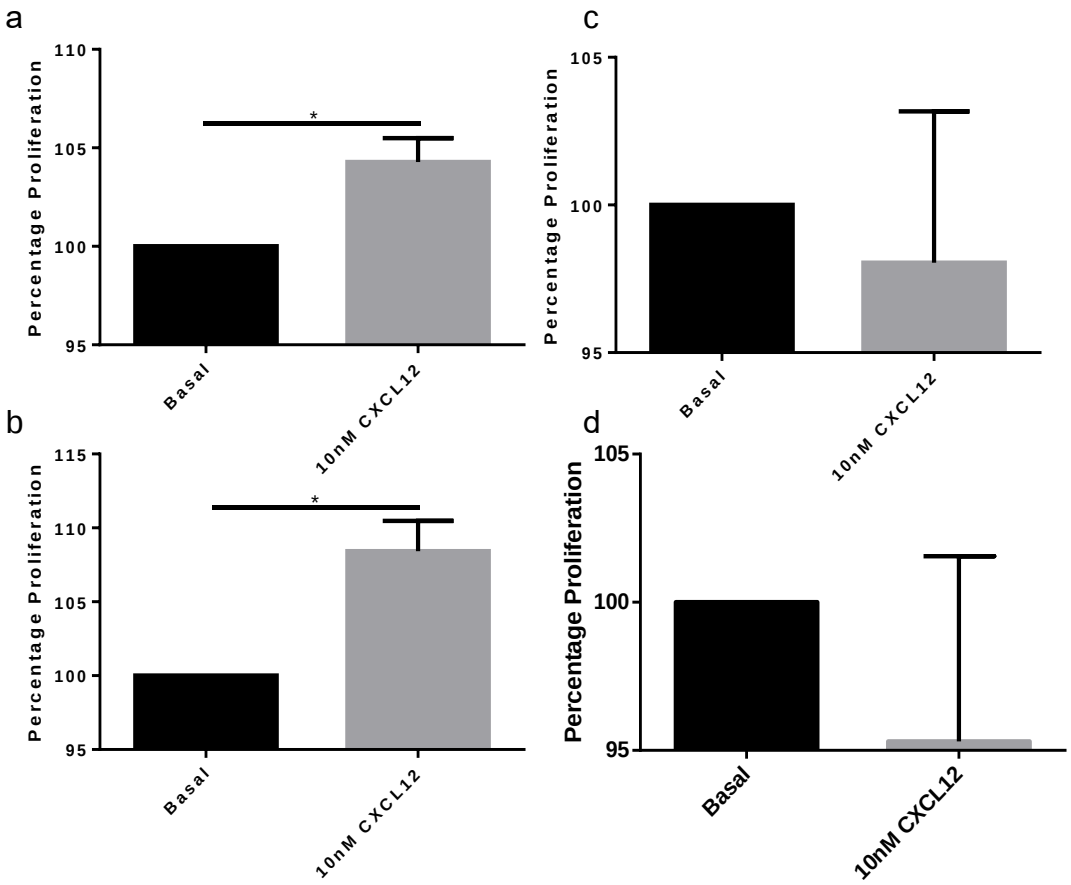


**Figure A3: Proliferation of MCF-7 and Jurkat cells is stimulates by 10 nM CXCL12 while THP-1 and PC3 cells are not. a)** MCF-7 cells were incubated with and without 10 nM CXCL12 for 72 hours and percentage proliferation was subsequently calculated. **b)** Jurkat cells were incubated with and without 10 nM CXCL12 for 72 hours and percentage proliferation was subsequently calculated. c**)** THP-1 cells were incubated with and without 10 nM CXCL12 for 72 hours and percentage proliferation was subsequently calculated. **b)** PC3 cells were incubated with and without 10 nM CXCL12 for 72 hours and percentage proliferation was subsequently calculated. Data representative of the mean ± SEM of 7 independent experiments.

## Appendix 4

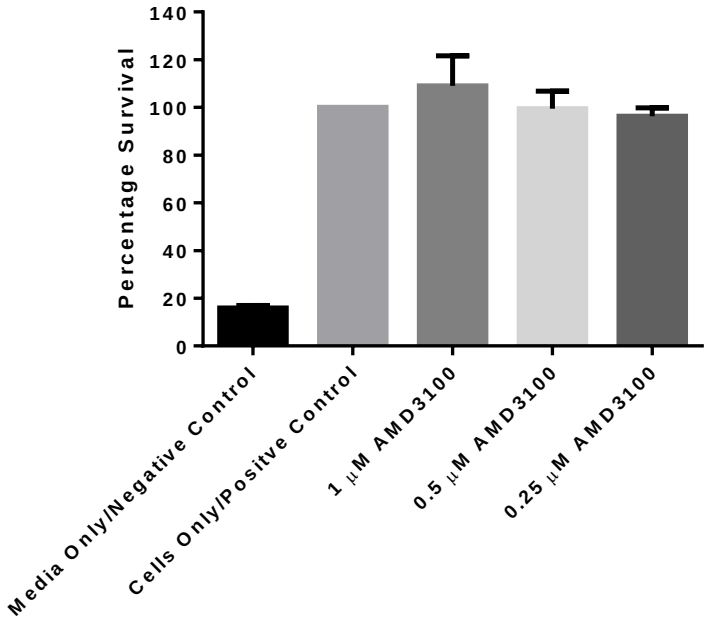


**Figure A4: AMD3100 is not toxic in Jurkat cells.** Jurkat cells were incubated with 0.25-1 μM of AMD3100 for 72 hours and percentage survival was subsequently calculated. Data representative of the mean ± SEM of 3 independent experiments.

## Appendix 5

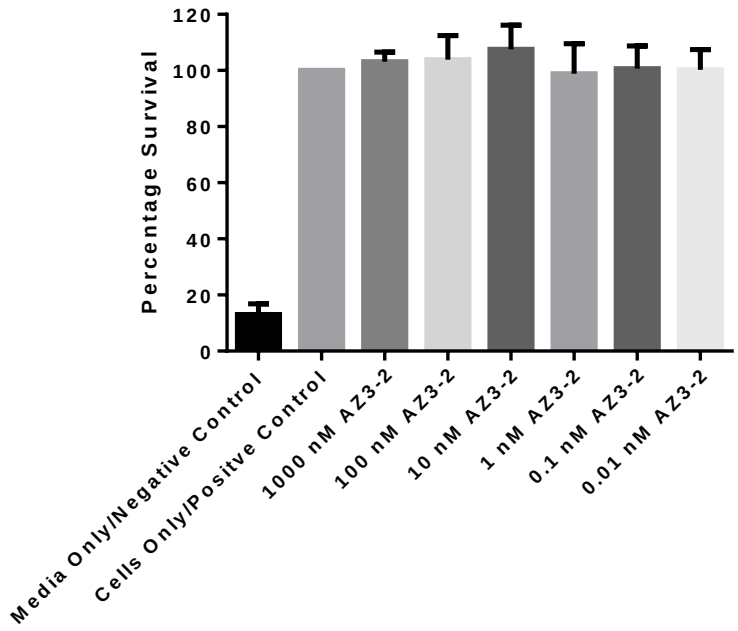


**Figure A5: AZ3-2 is not toxic in Jurkat cells.** Jurkat cells were incubated with 0.01-1000 nM of AZ3-2 for 72 hours and percentage survival was subsequently calculated. Data representative of the mean ± SEM of 3 independent experiments.

## Appendix 6

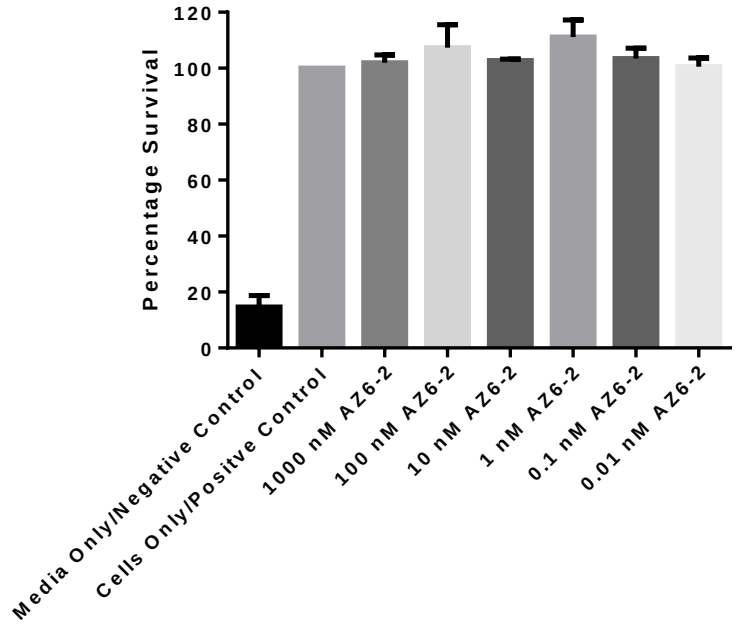


**Figure A6: AZ6-2 is not toxic in Jurkat cells.** Jurkat cells were incubated with 0.01-1000 nM of AZ6-2 for 72 hours and percentage survival was subsequently calculated. Data representative of the mean ± SEM of 3 independent experiments.

## Appendix 7

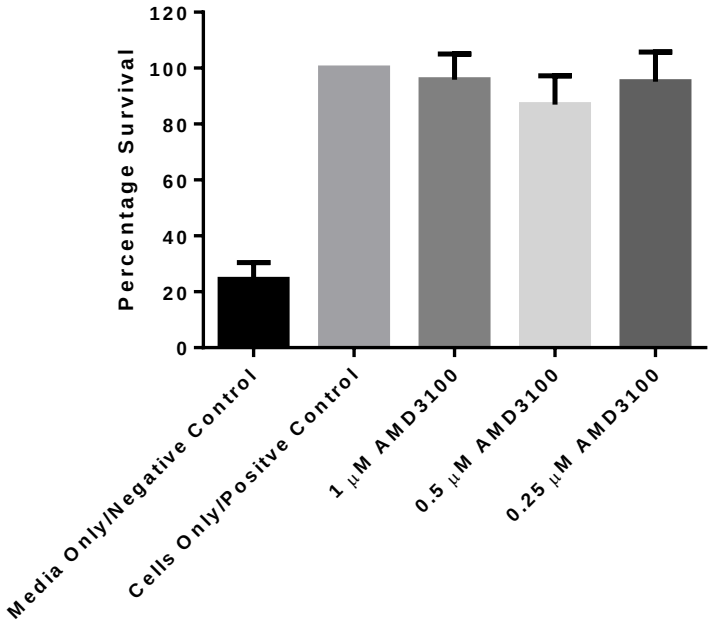


**Figure A7: AMD3100 is not toxic in THP-1 cells.** THP-1 cells were incubated with 0.25-1 μM of AMD3100 for 72 hours and percentage survival was subsequently calculated. Data representative of the mean ± SEM of 3 independent experiments.

## Appendix 8

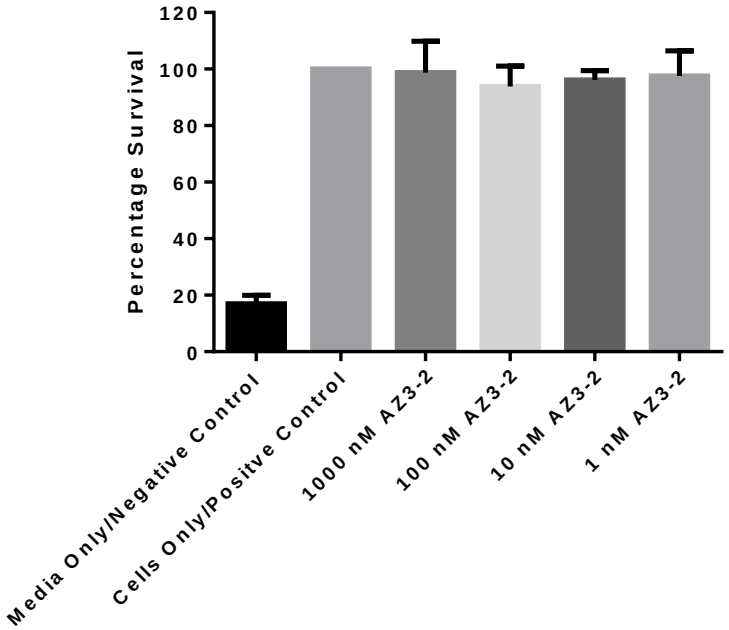


**Figure A8: AZ3-2 is not toxic in THP-1 cells.** THP-1 cells were incubated with 1-1000 nM of AZ3-2 for 72 hours and percentage survival was subsequently calculated. Data representative of the mean ± SEM of 3 independent experiments.

## Appendix 9

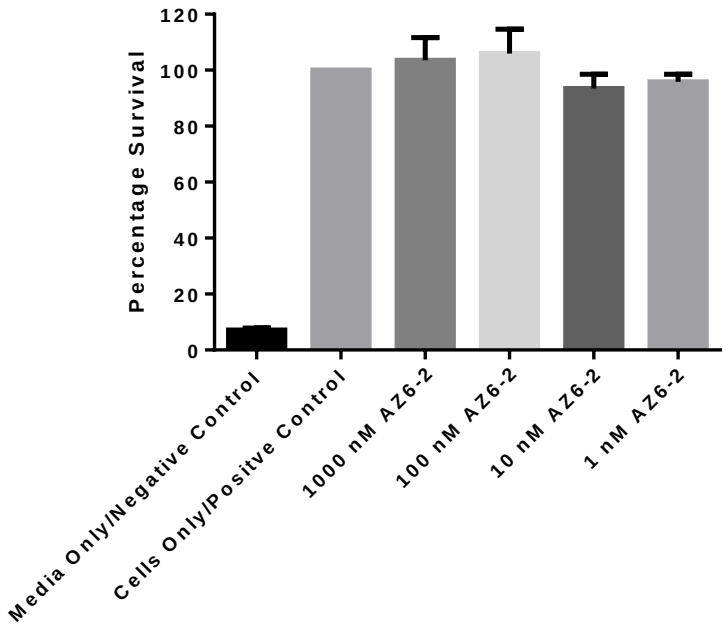


**Figure A9: AZ6-2 is not toxic in THP-1 cells.** THP-1 cells were incubated with 1-1000 nM of AZ6-2 for 72 hours and percentage survival was subsequently calculated. Data representative of the mean ± SEM of 3 independent experiments.

## Appendix 10

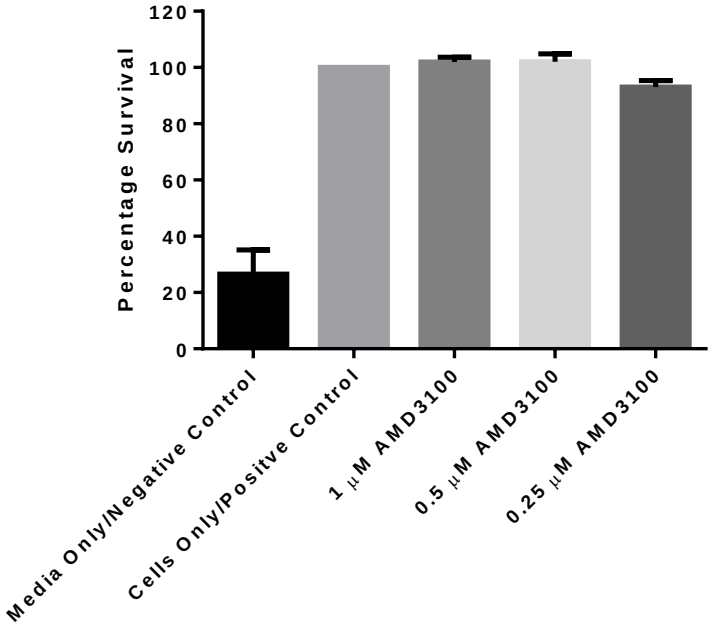


**Figure A10: AMD3100 is not toxic in MCF-7 cells.** MCF-7 cells were incubated with 0.25-1 μM of AMD3100 for 72 hours and percentage survival was subsequently calculated. Data representative of the mean ± SEM of 3 independent experiments.

## Appendix 11

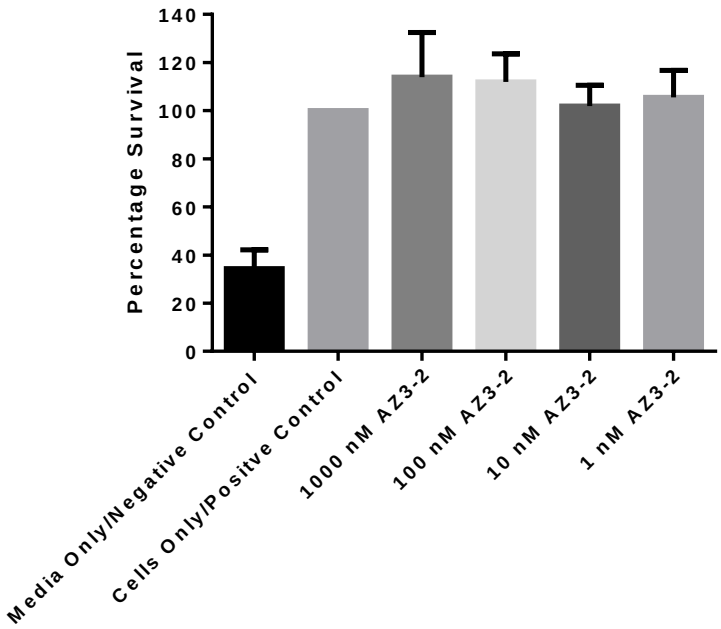


**Figure A11: AZ3-2 is not toxic in MCF-7 cells.** MCF-7 cells were incubated with 1-1000 nM of AZ3-2 for 72 hours and percentage survival was subsequently calculated. Data representative of the mean ± SEM of 3 independent experiments.

## Appendix 12

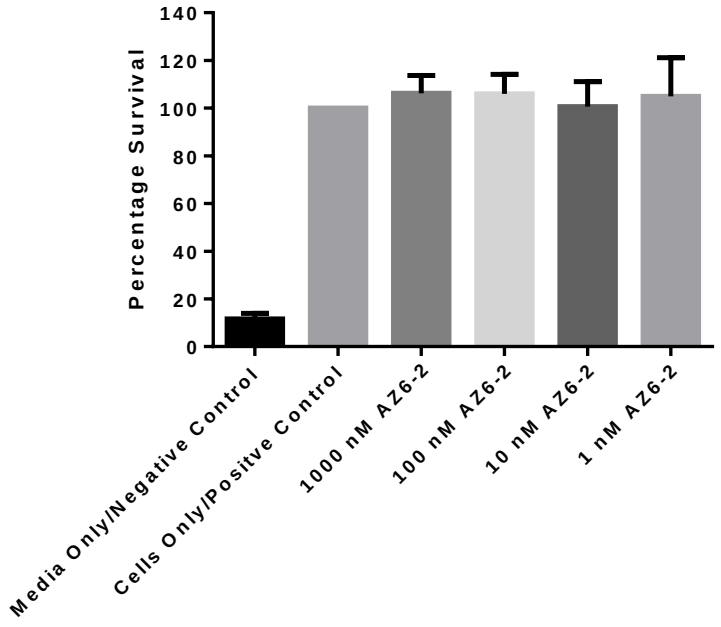


**Figure A12: AZ6-2 is not toxic in MCF-7 cells.** MCF-7 cells were incubated with 1-1000 nM of AZ6-2 for 72 hours and percentage survival was subsequently calculated. Data representative of the mean ± SEM of 3 independent experiments.

## Appendix 13

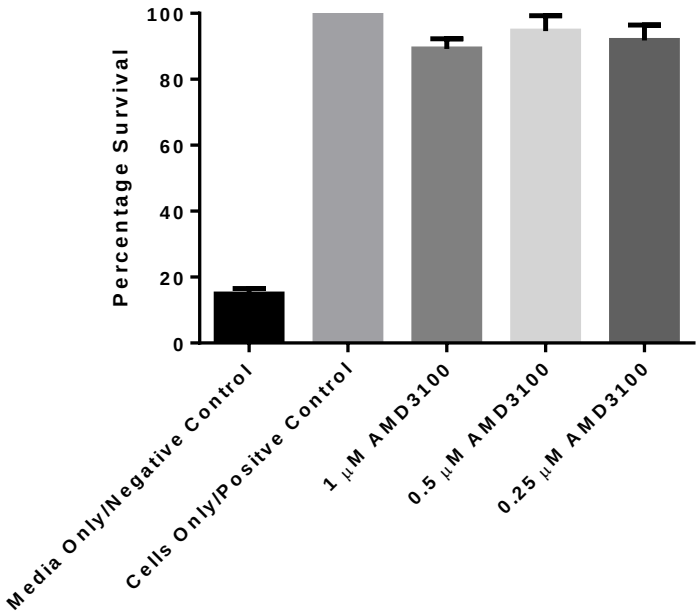


**Figure A13: AMD3100 is not toxic in PC3 cells.** PC3 cells were incubated with 0.25-1 µM of AMD3100 for 72 hours and percentage survival was subsequently calculated. Data representative of the mean ± SEM of 3 independent experiments.

## Appendix 14

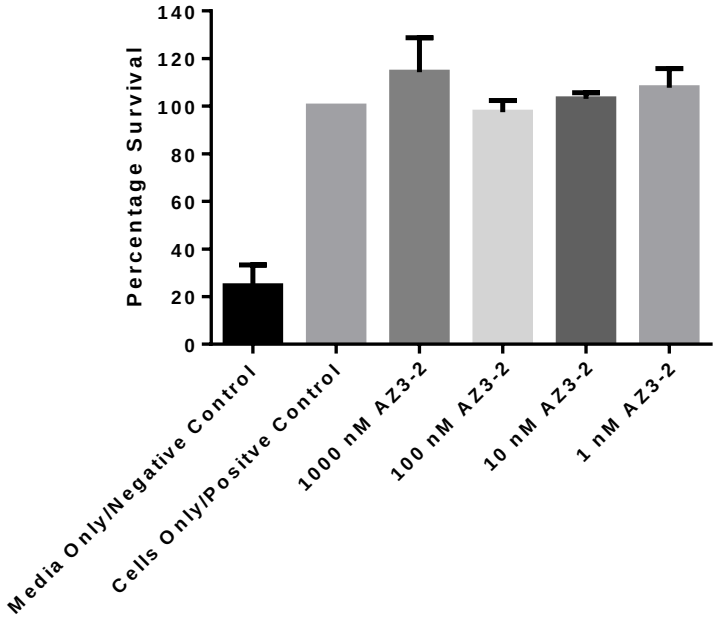


**Figure A14: AZ3-2 is not toxic in PC3 cells.** PC3 cells were incubated with 1-1000 nM of AZ3-2 for 72 hours and percentage survival was subsequently calculated. Data representative of the mean ± SEM of 3 independent experiments.

## Appendix 15

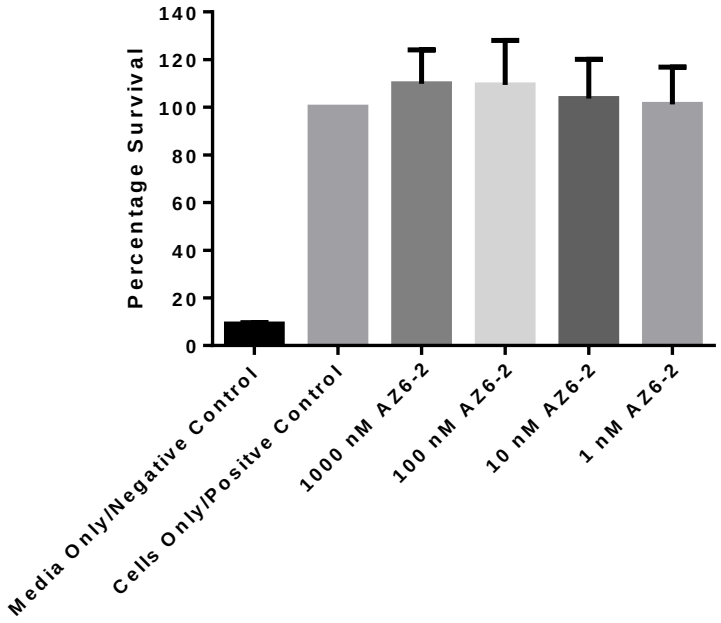


**Figure A15: AZ6-2 is not toxic in PC3 cells.** PC3 cells were incubated with 1-1000 nM of AZ6-2 for 72 hours and percentage survival was subsequently calculated. Data representative of the mean ± SEM of 3 independent experiments.

## Appendix 16

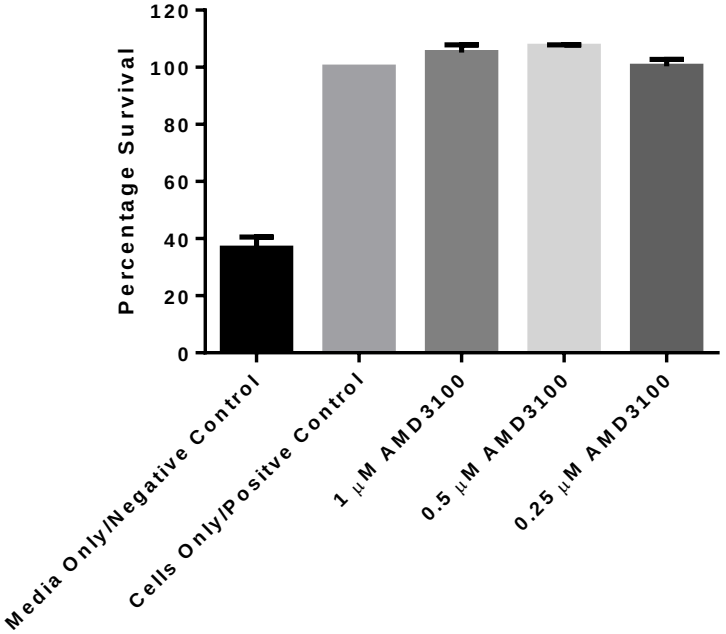


**Figure A16: AMD3100 is not toxic in SKMEL28 cells.** SKMEL28 cells were incubated with 0.25-1 µM of AMD3100 for 72 hours and percentage survival was subsequently calculated. Data representative of the mean ± SEM of 3 independent experiments.

## Appendix 17

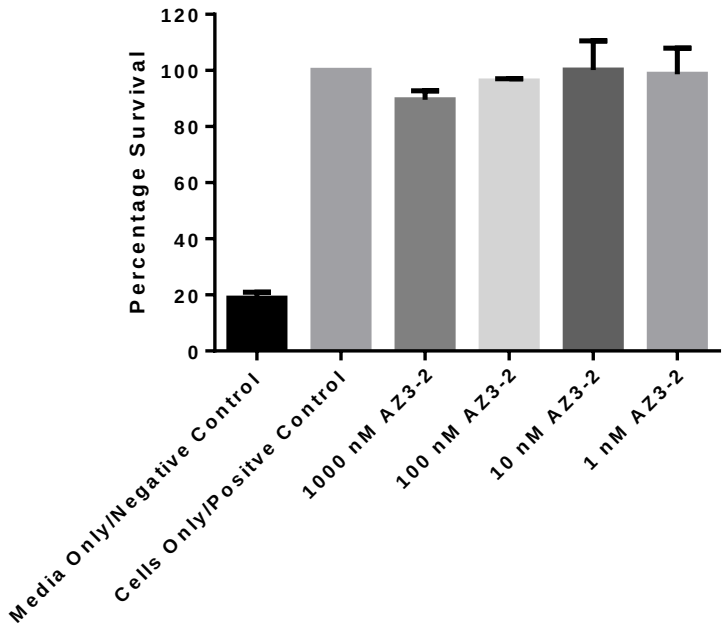


**Figure A17: AZ3-2 is not toxic in SKMEL28 cells.** SKMEL28 cells were incubated with 1-1000 nM of AZ3-2 for 72 hours and percentage survival was subsequently calculated. Data representative of the mean ± SEM of 3 independent experiments.

## Appendix 18

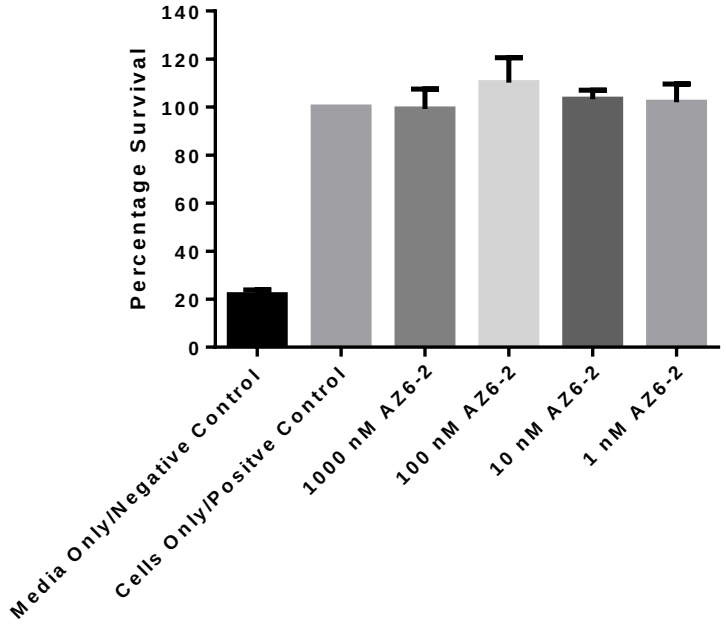


**Figure A18: AZ6-2 is not toxic in SKMEL28 cells.** SKMEL28 cells were incubated with 1-1000 nM of AZ6-2 for 72 hours and percentage survival was subsequently calculated. Data representative of the mean ± SEM of 3 independent experiments.

## Appendix 19

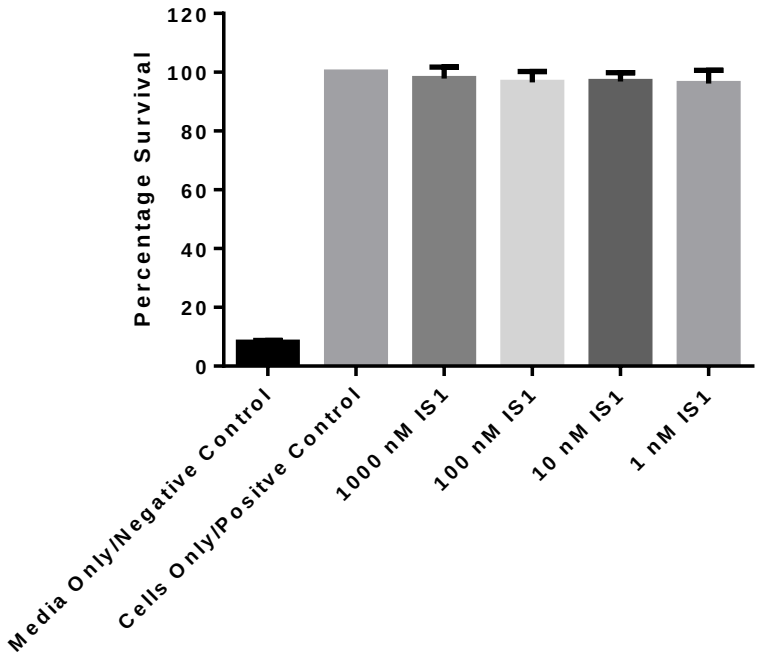


**Figure A19: IS1 is not toxic in Jurkat cells.** Jurkat cells were incubated with 1-1000 nM of IS1 for 72 hours and percentage survival was subsequently calculated. Data representative of the mean ± SEM of 3 independent experiments.

## Appendix 20

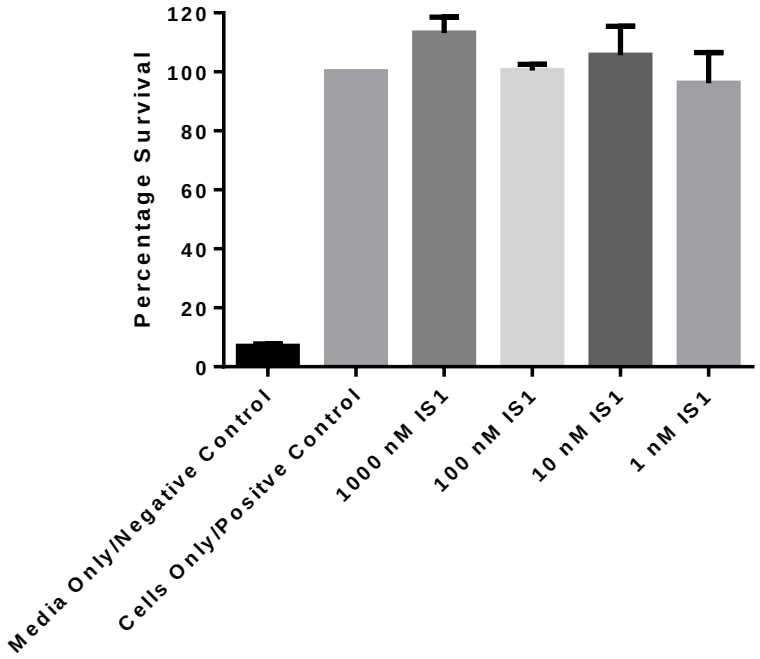


**Figure A20: IS1 is not toxic in THP-1 cells.** THP-1 cells were incubated with 1-1000 nM of IS1 for 72 hours and percentage survival was subsequently calculated. Data representative of the mean ± SEM of 3 independent experiments.

## Appendix 21

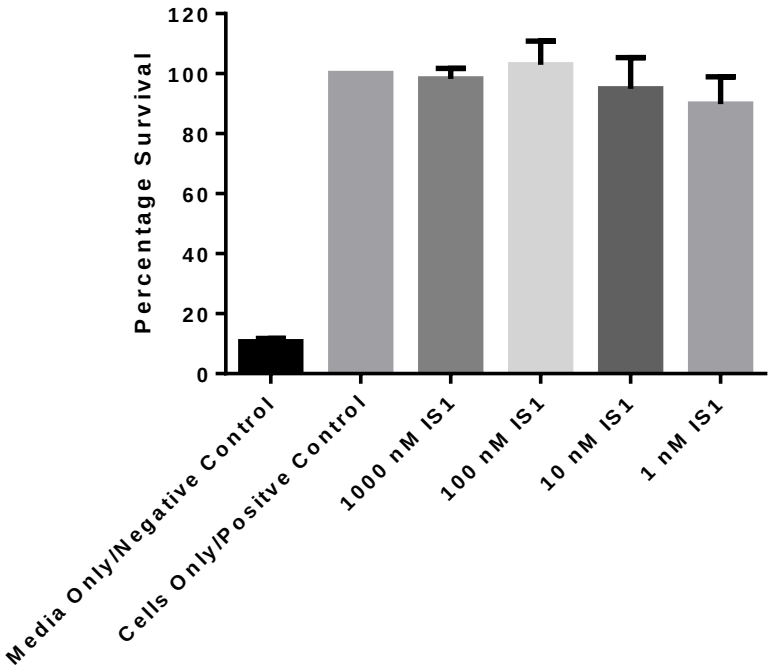


**Figure A21: IS1 is not toxic in MCF-7 cells.** MCF-7 cells were incubated with 1-1000 nM of IS1 for 72 hours and percentage survival was subsequently calculated. Data representative of the mean ± SEM of 3 independent experiments.

## Appendix 22

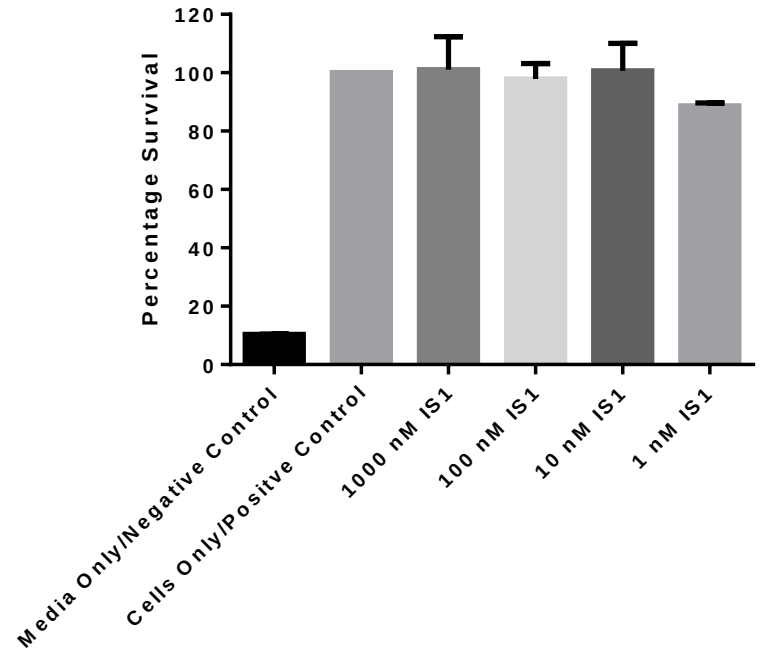


**Figure A22: IS1 is not toxic in PC3 cells.** PC3 cells were incubated with 1-1000 nM of IS1 for 72 hours and percentage survival was subsequently calculated. Data representative of the mean ± SEM of 3 independent experiments.

## Appendix 23

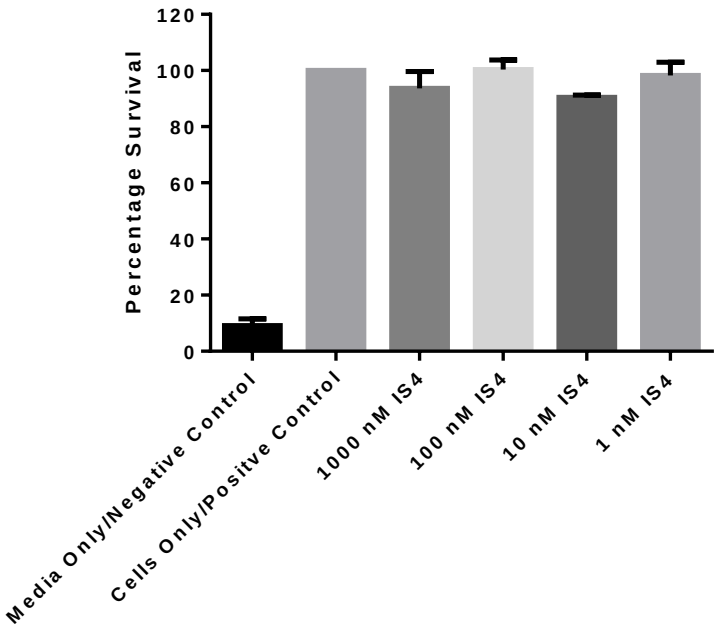


**Figure A23: IS4 is not toxic in Jurkat cells.** Jurkat cells were incubated with 1-1000 nM of IS4 for 72 hours and percentage survival was subsequently calculated. Data representative of the mean ± SEM of 3 independent experiments.

## Appendix 24

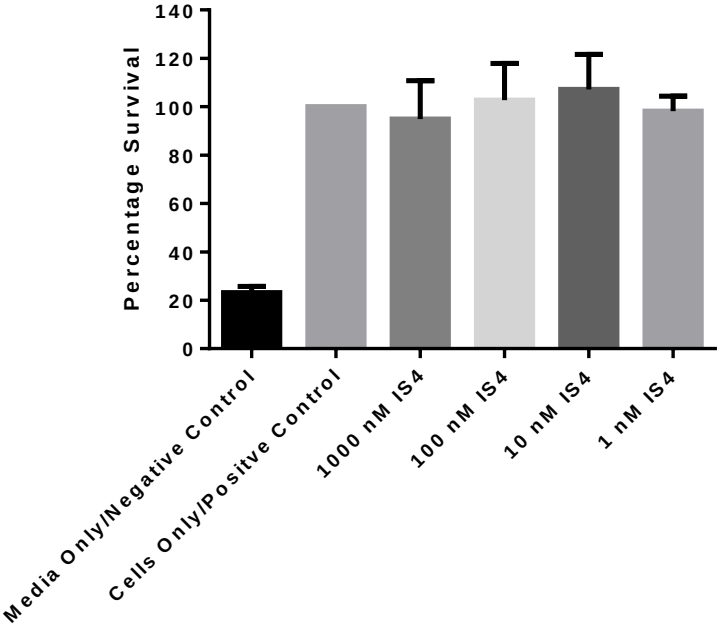


**Figure A24: IS4 is not toxic in THP-1 cells.** THP-1 cells were incubated with 1-1000 nM of IS4 for 72 hours and percentage survival was subsequently calculated. Data representative of the mean ± SEM of 3 independent experiments.

## Appendix 25

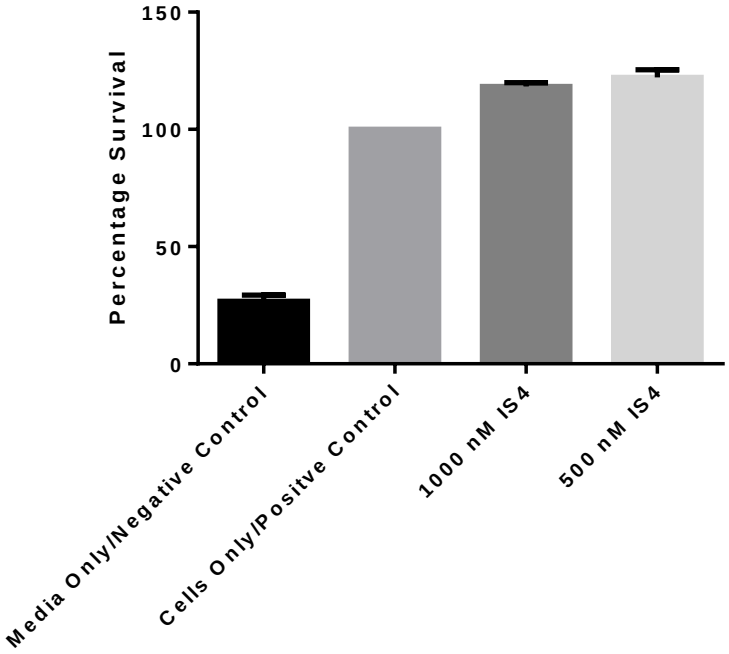


**Figure A25: IS4 is not toxic in MCF-7 cells.** MCF-7 cells were incubated with 500-1000 nM of IS4 for 72 hours and percentage survival was subsequently calculated. Data representative of the mean ± SEM of 3 independent experiments.

## Appendix 26

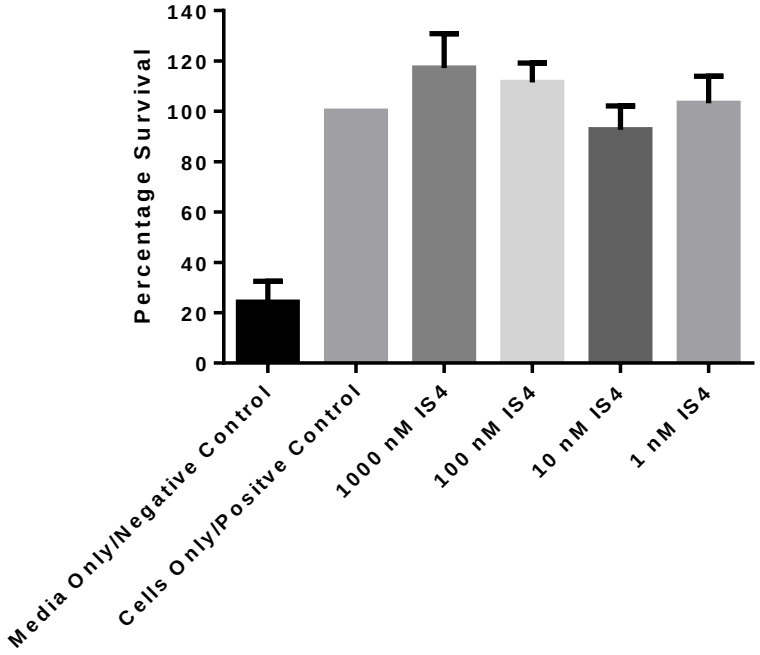


**Figure A26: IS4 is not toxic in PC3 cells.** PC3 cells were incubated with 1-1000 nM of IS4 for 72 hours and percentage survival was subsequently calculated. Data representative of the mean ± SEM of 3 independent experiments.

## Appendix 27

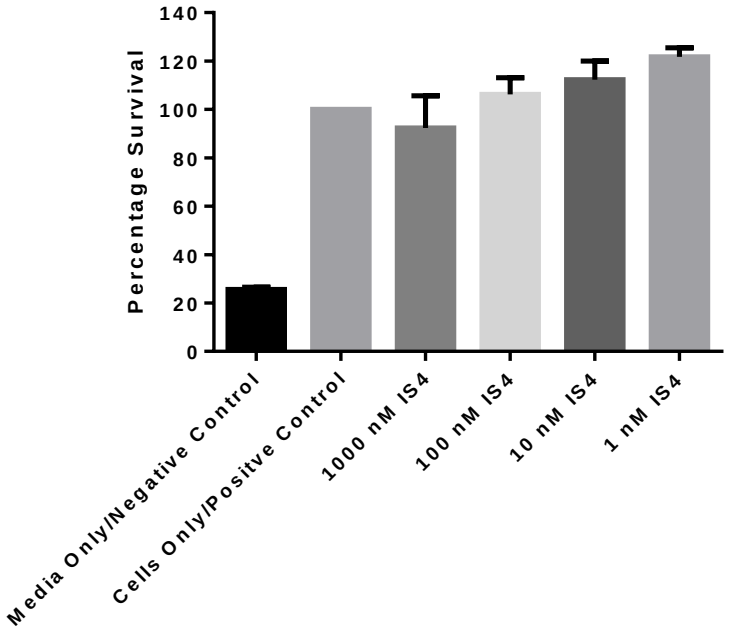


**Figure A27: IS4 is not toxic in SKMEL28 cells.** SKMEL28 cells were incubated with 1-1000 nM of IS4 for 72 hours and percentage survival was subsequently calculated. Data representative of the mean ± SEM of 3 independent experiments.

## Appendix 28

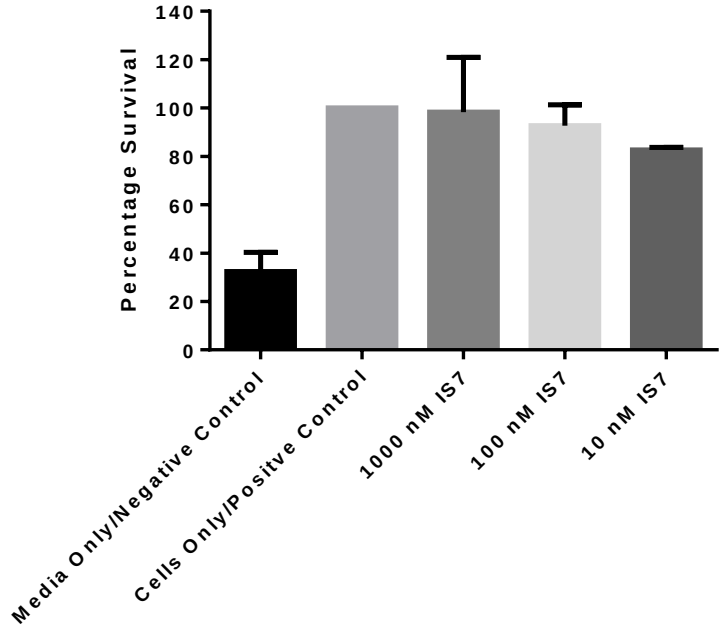


**Figure A28: IS7 is not toxic in MCF-7 cells.** MCF-7 cells were incubated with 10-1000 nM of IS7 for 72 hours and percentage survival was subsequently calculated. Data representative of the mean ± SEM of 3 independent experiments.

## Appendix 29

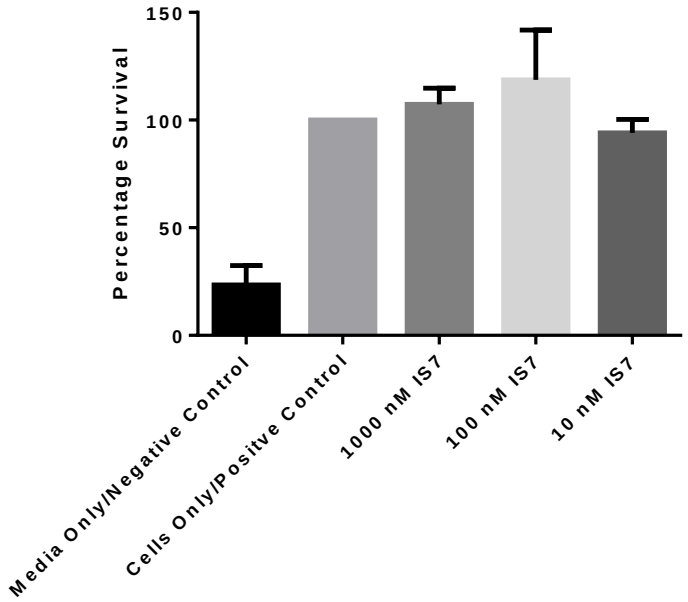


**Figure A29: IS7 is not toxic in Jurkat cells.** Jurkat cells were incubated with 10-1000 nM of IS7 for 72 hours and percentage survival was subsequently calculated. Data representative of the mean ± SEM of 3 independent experiments

## Appendix 30

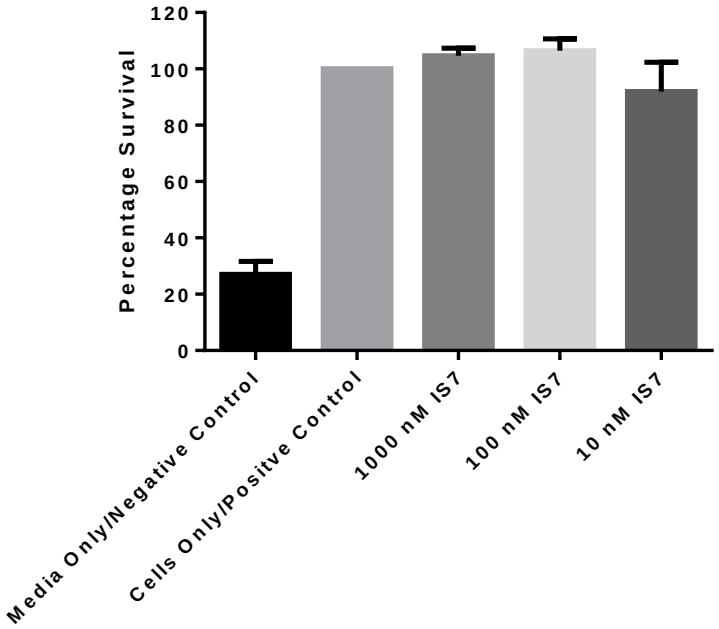


**Figure A30: IS7 is not toxic in THP-1 cells.** THP-1 cells were incubated with 10-1000 nM of IS7 for 72 hours and percentage survival was subsequently calculated. Data representative of the mean ± SEM of 3 independent experiments.

## Appendix 31

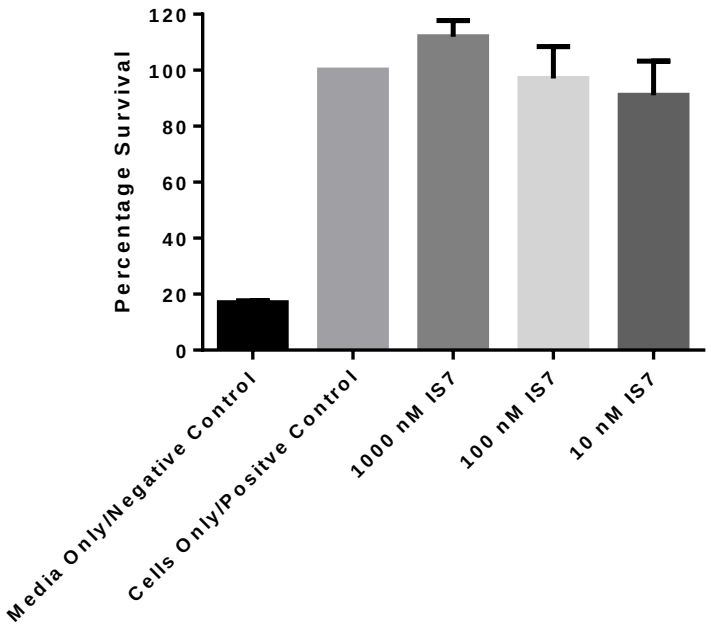


**Figure A31: IS7 is not toxic in PC3 cells.** PC3 cells were incubated with 10-1000 nM of IS7 for 72 hours and percentage survival was subsequently calculated. Data representative of the mean ± SEM of 3 independent experiments.

## Appendix 32

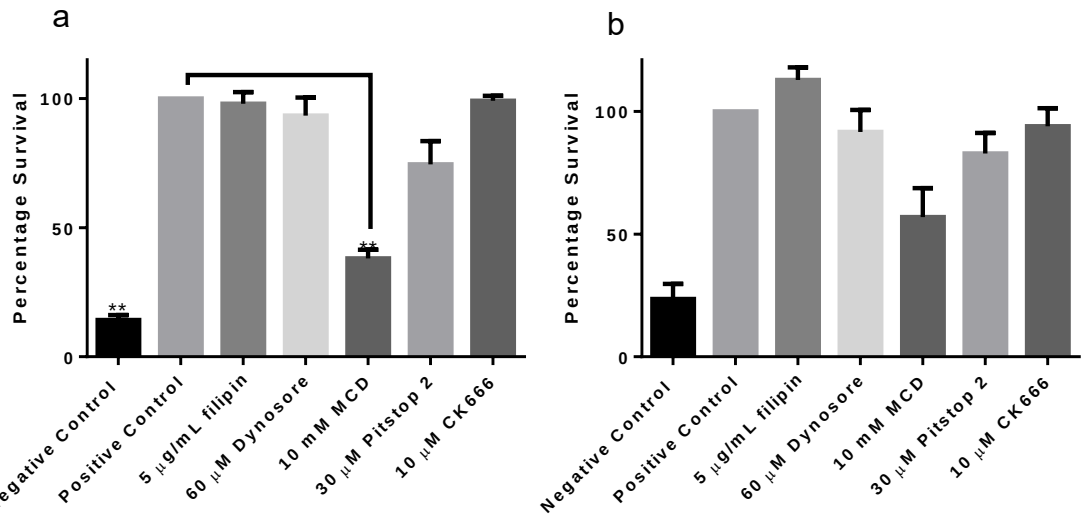


**Figure A32: The endocytosis inhibitor MCD was toxic in Jurkat cells with a trend suggesting toxicity in MCF-7 cells. a)** Jurkat cells were incubated with 5 µg/mL filipin, 60 µM Dynasore, 10 mM MCD, 30 µM Pitstop 2 and 10 µM CK666 for 2 hours and percentage survival was subsequently calculated. **b)** MCF-7 cells were incubated with 5 µg/mL filipin, 60 µM Dynasore, 10 mM MCD, 30 µM Pitstop 2 and 10 µM CK666 for 2 hours and percentage survival was subsequently calculated. Data representative of the mean ± SEM of 6 independent experiments.

## Appendix 33

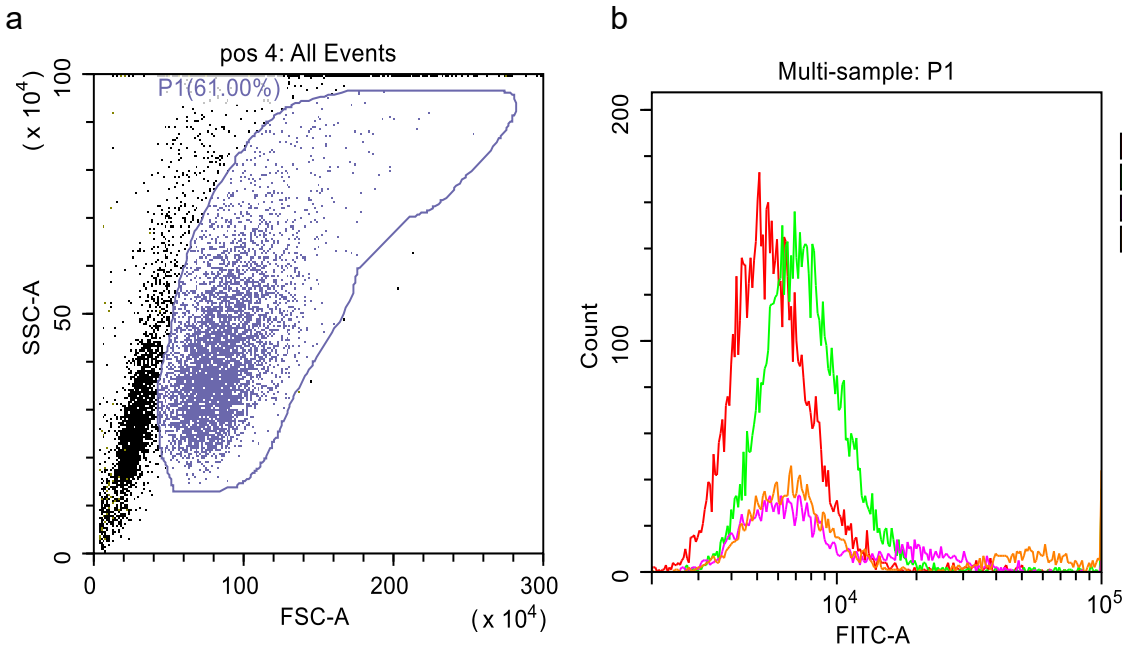


**Figure A33: The endocytosis inhibitor Pitstop 2 was toxic in Jurkat cells. a)** P1 gate shows live Jurkat cell population incubated at 4˚C. **b)** Shift in fluorescence of P1 gated Jurkat cells from negative control (red) to positive control at 4˚C (green), cells incubated with Pitstop 2 (pink) and cells incubated with 15 nM and Pitstop 2 (orange). Preliminary results from 1 experiment.